



## Thermodynamic and Process Modelling of Gas Hydrate Systems in CO<sub>2</sub> Capture Processes

Herslund, Peter Jørgensen

*Publication date:*  
2013

*Document Version*  
Publisher's PDF, also known as Version of record

[Link back to DTU Orbit](#)

*Citation (APA):*  
Herslund, P. J. (2013). *Thermodynamic and Process Modelling of Gas Hydrate Systems in CO<sub>2</sub> Capture Processes*. Technical University of Denmark, Department of Chemical and Biochemical Engineering.

---

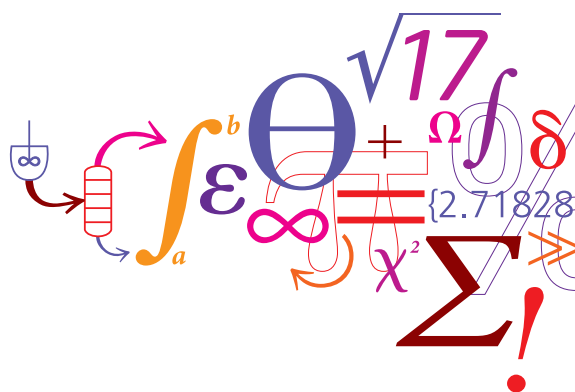
### General rights

Copyright and moral rights for the publications made accessible in the public portal are retained by the authors and/or other copyright owners and it is a condition of accessing publications that users recognise and abide by the legal requirements associated with these rights.

- Users may download and print one copy of any publication from the public portal for the purpose of private study or research.
- You may not further distribute the material or use it for any profit-making activity or commercial gain
- You may freely distribute the URL identifying the publication in the public portal

If you believe that this document breaches copyright please contact us providing details, and we will remove access to the work immediately and investigate your claim.

# Thermodynamic and Process Modelling of Gas Hydrate Systems in CO<sub>2</sub> Capture Processes



**Peter Jørgensen Herslund**

Ph.D. Thesis

October 2013

# Thermodynamic and Process Modelling of Gas Hydrate Systems in CO<sub>2</sub> Capture Processes

*Ph.d. Thesis*

Peter Jørgensen Herslund

Center for Energy Resources Engineering (CERE)

Department of Chemical and Biochemical Engineering

Technical University of Denmark

October 2013

Supervisor: Nicolas von Solms (CERE, DTU)

Co-Supervisors: Jens Abildskov (CAPEC, DTU)

Kaj Thomsen (CERE, DTU)



A part of the iCap CO<sub>2</sub> Capture project

Copyright©: **Peter Jørgensen Herslund**  
October 2013

Address: Center for Energy Resources Engineering  
**Department of Chemical and  
Biochemical Engineering  
Technical University of Denmark**  
Søltofts Plads, Building 229  
DK-2800 Kgs. Lyngby  
Denmark

Phone: +45 4525 2800

Fax: +45 4525 4588

Web: [www.cere.dtu.dk](http://www.cere.dtu.dk)

Print: **J&R Frydenberg A/S**  
København  
December 2014

ISBN: 978-87-93054-54-7

# Title sheet

**Project title:**

Thermodynamic and Process Modelling of Gas Hydrate Systems in CO<sub>2</sub> Capture Processes

**Type:**

Ph.d. Thesis.

**Supervisors at DTU:**

Main Supervisor: Nicolas von Solms (DTU, CERE)

Co-Supervisors: Kaj Thomsen (DTU, CERE)

Jens Abildskov (DTU, CAPEC)

**Department:**

Department of Chemical and Biochemical Engineering

**In Cooperation with:**

The European iCap project ([www.icapco2.org](http://www.icapco2.org))

**Author of the present report:**

Peter Jørgensen Herslund

**Delivery Date:**

October, 2013

**Date and signature:**

---

Peter Jørgensen Herslund



## Abstract

A novel gas separation technique based on gas hydrate formation (solid precipitation) is investigated by means of thermodynamic modeling and experimental investigations. This process has previously been proposed for application in post-combustion carbon dioxide capture from power station flue gases. Prior to this study it has been shown that formation of gas hydrates from mixtures of carbon dioxide and nitrogen may create a solid hydrate phase in which the carbon dioxide content is higher than the original concentration in the gas phase. Separation of carbon dioxide from flue gases by hydrate formation may be performed at pressures of approximately 20 MPa and temperatures below 280 K. Thermodynamic promoters are needed, to reduce the pressure requirement of the process, thereby making it competitive to existing capture technologies.

A literature study is presented focusing mainly on thermodynamic gas hydrate promotion by hydrate formers stabilising the classical gas clathrate hydrate structures (sI, sII and sH) at low to moderate pressures. Much literature is available on this subject. Both experimental and theoretical studies presented in the literature have pointed out cyclopentane and tetrahydrofuran as the two most efficient pressure reducing additives in classical hydrate forming systems.

The thermodynamic promoting effects reported in the literature for the two classical sII hydrate formers, tetrahydrofuran and cyclopentane are experimentally confirmed in the present work. Data presented in this work compares well with other data available in the literature for similar systems.

It is shown experimentally that the addition of tetrahydrofuran to the ternary system of water-cyclopentane-carbon dioxide provides an enhanced thermodynamic promotion of the gas hydrate phase. Hydrate equilibrium pressures are reduced by approximately 20 percent compared to the cyclopentane promoted system. The mixed promoter system thereby represents a new state-of-the-art within thermodynamic promotion of gas hydrates in the framework of the classical hydrate structures.

A thermodynamic model based on the Cubic-Plus-Association equation of state and the van der Waals-Platteeuw hydrate model is presented. This model enables the performance of a thermodynamic evaluation of gas hydrate forming systems relevant for post-combustion carbon dioxide capture. All model details and complete lists of model parameters are provided. Three simplified carbon dioxide capture processes are simulated by use of the model. Three to four capture stages are needed in all processes to obtain a product stream richer than 95 mole percent in terms of carbon dioxide.

The modeling results presented here are discouraging for the post-combustion carbon dioxide capture process under development. The present study points out several drawbacks of using tetrahydrofuran or cyclopentane as thermodynamic

hydrate promoters, when applied in low-pressure processes. Due to their high volatilities (cyclopentane in particular), they readily transfer to the vapour phases. Furthermore, they lower the process selectivity towards carbon dioxide, compared to the unpromoted system.

Finally it is concluded that separation of carbon dioxide from nitrogen by gas hydrate formation at near-atmospheric pressure provides too low gas uptakes in the hydrate phase for this process to become feasible at these conditions.



## Resumé

Denne Ph.d. afhandling præsenterer et studie i røggasrensning for kuldioxid fra kul- eller gas fyrede kraftværker. En ny metode til gasfaseseparation af kuldioxid fra nitrogen undersøges dels ved hjælp af termodynamisk modellering af relevante kemiske systemer, dels ved eksperimentelle undersøgelser foretaget på laboratorieskala. Denne separationsmetode udnytter at kuldioxid, nitrogen og vand kan danne faste stoffer med højt gasindhold – såkaldte gashydrater - ved betingelser af højt tryk og lave temperaturer. Ved dannelsen af gashydratet kan kuldioxiden fra røggassen opkoncentreres som en fysisk adsorberet gasfase i de faste partikler. Herved kan den transporteres, eller frigives efterfølgende under kontrollerede betingelser. Som udgangspunkt kan denne separation foretages ved tryk over 200 bar og temperaturer under 7 grader C.

Et litteraturstudie, foretaget som en del af dette arbejde, udpeger to additiver der ved tilførsel i systemet kan sænke de høje trykbetingelser for denne proces. Disse additiver er cyklopentan og tetrahydrofuran, hhv. en cyklisk oliekomponent og en cyklisk æter. Begge stoffer kan danne såkaldte struktur II gashydrater med vand ved atmosfærisk tryk og temperaturer over vands normale frysepunkt. Dermed er det muligt at danne de faste partikler uden at skulle komprimere røggassen. Komprimering af gas er en energikrævende enhedsoperation. Denne alternative proces til røggasrensning anses for at være urentabel, hvis det konkluderes at komprimering af røggassen bliver nødvendig i vid udstrækning.

Ved hjælp af laboratorieskalaforsøg er det i nærværende studie blevet bekræftet, at tilførslen af tetrahydrofuran, cyklopentan eller deres blandinger kan sænke ligevægtstrykket for gashydrater i systemer med kuldioxid. De målte data stemmer godt overens med andre data tilgængelige i litteraturen for tilsvarende kemiske systemer. Cyklopentan har i litteraturen været anset som et reference additiv, da denne komponent har den største trykreducerende påvirkning på disse typer af systemer. Dette studie har vist, at samtidig tilførsel af cyklopentan og tetrahydrofuran til gashydratsystemer med kuldioxid kan reducere trykkravene med yderligere 20 procent i forhold til cyklopentan systemet. Dette nye system af ”blandede additiver” repræsenterer dermed en ny reference i feltet af trykreducerende additiver.

En termodynamisk model er blevet opstillet, baseret på en avanceret tilstandsligning (Cubic-Plus-Association) samt en kendt model for gashydratfasen (van der Waals-Platteeuw). Alle modelparametre præsenteres i denne afhandling, således at de præsenterede resultater kan genskabes. Tre simplificerede røggasrensningsprocesser er blevet simuleret ved brug af den udviklede model. Det konkluderes at 3-4 oprensningstrin er nødvendige for at opnå en renhed højere end 95 molprocent i det endelige kuldioxid produkt.

Den udviklede model forudsiger en række udfordringer for den undersøgte proces, hvis additiver såsom tetrahydrofuran eller cyklopentan benyttes. Disse komponenter er flygtige og vil derfor overføres til gasfasen i store mængder ved de ønskede procesbetingelser. Dette anses som et problem ikke blot for processens økonomiske rentabilitet men i lige så høj grad pga. de miljømæssige påvirkninger disse komponenter vil forårsage i naturen. Det forventes derfor, at cyklopentan og tetrahydrofuran må re-genereres efterfølgende fra den nitrogenholdige restgas, før denne kan lukkes ud i atmosfæren. Andre problemstillinger ved ovennævnte additiver er, at de sænker processens overordnede selektivitet mod kuldioxid. Endeligt konkluderes det, at gasoptaget i hydratfasen dannet ved nær-atmosfærisk tryk bliver så lavt, at separationsprocessen næppe vil blive realiserbar i stor skala ved lave trykbetingelser.

## Acknowledgements

*Some things in this world are better left unsaid.  
Gratitude does not belong among these.*

Therefore, I would like to express my gratitude to the persons, who have stood behind me, helped me or just lend me ears during the course of performing this study.

To my main supervisor, Nicolas von Solms, I wish to direct my sincere respect and gratitude. Thank you for your help, your scientific inputs and for your easy-going personality.

Likewise, my co-supervisors Kaj Thomsen and Jens Abildskov, I am grateful for your help and for your inputs to this work.

Hélène, the love of my life. I thank you for your support and understanding and for listening patiently to me. You have given me the two most precious gifts of life, and for that I am you forever grateful.

My family, including those lost on the path of life, thank you all for supporting me in times, when needed.

My daily colleagues at CERE, DTU. I thank you all for making every day at work something to look forward to. My office mate and friend, Xiaodong Liang, thank you for our fruitful discussions on both professional and personal levels. Nagu Daraboina, thank you for providing your experimental expertise to strengthen this study.

My colleagues and friends at Centre SPIN, Ecole des Mines de Saint-Etienne, France. Prof. Jean-Michel Herri, Matthias Kwaterski, Aurélie Galfré, Pedro Brântuas and Duyen Le Quang. Thank you all for making my external research visit in Centre SPIN, ENSM-SE, Saint-Etienne a pleasant and educational experience.

Claus Maarup, thank you for your friendship and for our many meetings at various coffee machines.

Finally, I would like to acknowledge the iCap Consortium, the Department of Chemical and Biochemical Engineering, DTU and the Otto Mønsted Foundation

for their financial support of this work. In this context, I wish to thank Erling H. Stenby and Philip L. Fosbøl for the initiative and work they put into establishing the funding for DTU, as part of the iCap project.

## Preface

This thesis is submitted as partial fulfillment for obtaining the degree of ph.d. from the Technical University of Denmark.

The presented work has been carried out mainly at the Center for Energy Resources Engineering (CERE), Department of Chemical and Biochemical Engineering, DTU, Denmark.

The present study, “*Thermodynamic and Process Modelling of Gas Hydrate Systems for CO<sub>2</sub> Capture*” represents a contribution to the European research project on innovative carbon dioxide capture processes (iCap).

*“iCap is an R&D project whose objective is to develop new CO<sub>2</sub> capture technologies that individually and combined will enable highly efficient and cost effective production of electrical power from fossil fuels with near zero emissions. The target is to reduce the CO<sub>2</sub> capture energy penalty to 4-5% points, about half of the penalty today, and to reduce the associated CO<sub>2</sub> avoidance cost to 15€/tonne CO<sub>2</sub>. iCap focuses on post combustion technologies that can be used both for retrofit and for green field plants*

...

*iCap is a 4 years projects consisting of a consortium of 15 partnters, including European R&D organisations, an industrial group, and partners from Australia and China. The project is supported by the European Commission under the 7th Framework Program Contract No: 241393 and is coordinated by the Norwegian University of Science and Technology.”*

[www.icapco2.org/news\\_1.html](http://www.icapco2.org/news_1.html) (September 2013)

This work was financially supported by the iCap project, the Department of Chemical and Biochemical Engineering (DTU) and the OTTO MØNSTED Foundation.



## Table of Contents

<b>1</b>	<b>Guide to Reader .....</b>	<b>1</b>
<b>2</b>	<b>Introduction .....</b>	<b>1</b>
2.1	Carbon Dioxide Capture .....	1
2.1.1	Chemical Absorption Based Processes .....	2
2.1.2	Membrane Based Separation .....	3
2.1.3	Separation by Clathrate Hydrate Formation.....	4
2.2	Gas Clathrate Hydrates .....	6
2.2.1	Gas Hydrate Structures.....	7
2.2.2	Cavities .....	7
2.3	Motivation and Purpose of This Work.....	9
2.4	Cited Literature.....	10
<b>3</b>	<b>Literature Survey on Gas Hydrate Promotion .....</b>	<b>13</b>
3.1	The Concept of Gas Hydrate Promotion .....	13
3.2	The Mechanisms .....	14
3.3	Thermodynamic Promoters Studied in the Literature .....	16
3.3.1	Tetrahydrofuran (THF) .....	27
3.3.2	Cyclopentane (CP) .....	29
3.4	Experimental Observations on Kinetics .....	30
3.5	Studies on CO <sub>2</sub> Capture by Hydrate Formation.....	33
3.6	Summary.....	39
3.7	Cited Literature.....	42
<b>4</b>	<b>Experimental Work .....</b>	<b>51</b>
4.1	Experimental Set-up and Procedure #1 .....	52
4.2	Experimental Set-up and Procedure #2 .....	54
4.3	Discussion of Experimental Procedures.....	56
4.4	Cited Literature.....	57
<b>5</b>	<b>Thermodynamic Model .....</b>	<b>59</b>
5.1	The van der Waals-Platteeuw Hydrate Model .....	60
5.2	Attempts of Improving the Hydrate Model Theory .....	67
5.3	The Cubic-Plus-Association Equation of State .....	70
5.4	Algorithm Applied in the Present Work .....	73
5.5	Model Parameters .....	75
5.5.1	Hydrate Model .....	75
5.5.2	Equation of State (CPA) .....	77
5.6	The Gibbs Phase Rule .....	79
5.7	Cited Literature.....	81

<b>6</b>	<b>Experimental Results.....</b>	<b>85</b>
6.1	The Tetrahydrofuran Promoted System .....	85
6.2	The Cyclopentane Promoted System.....	87
6.3	The Mixed Promoter System.....	89
6.4	Summary of Experimental Results.....	92
6.5	Cited Literature .....	92
<b>7</b>	<b>Modeling Results .....</b>	<b>95</b>
7.1	Fluid Phase Modeling .....	96
7.1.1	Water-Carbon dioxide .....	97
7.1.2	Water-Nitrogen .....	98
7.1.3	Water-Tetrahydrofuran.....	100
7.1.4	Water-Cyclopentane.....	103
7.1.5	Tetrahydrofuran-Carbon dioxide .....	104
7.1.6	Tetrahydrofuran-Nitrogen .....	105
7.1.7	Cyclopentane-Carbon dioxide .....	106
7.1.8	Cyclopentane-Nitrogen .....	107
7.1.9	Carbon dioxide-Nitrogen .....	108
7.1.10	Water-Tetrahydrofuran-Cyclopentane .....	109
7.1.11	Water-Tetrahydrofuran-Carbon dioxide .....	110
7.2	The Un-promoted Gas Hydrate System .....	114
7.3	Tetrahydrofuran Promoted Gas Hydrate Systems.....	120
7.3.1	The Tetrahydrofuran Promoted Capture Process .....	129
7.4	Cyclopentane Promoted Gas Hydrate Systems .....	134
7.4.1	The Cyclopentane Promoted Capture Process.....	138
7.5	Mixed Promoter Gas Hydrate Systems .....	144
7.6	Summary of Modeling Results.....	148
7.7	Cited Literature .....	151
<b>8</b>	<b>Conclusion and Perspectives .....</b>	<b>159</b>
<b>9</b>	<b>List of Symbols and Abbreviations.....</b>	<b>165</b>
<b>Appendix 1.....</b>	<b>A</b>	
<b>Appendix 2.....</b>	<b>C</b>	
<b>Appendix 3.....</b>	<b>E</b>	
<b>Appendix 4.....</b>	<b>G</b>	
<b>Appendix 5.....</b>	<b>I</b>	







# 1 Guide to Reader

The present report presents the outcome of a three-year ph.d. study performed at the Technical University of Denmark.

Three peer-reviewed journal manuscripts have been published at the time of writing this thesis. These manuscripts have been appended the present thesis (as published) in Appendix 1, Appendix 2 and Appendix 3. Furthermore two manuscripts have been prepared for publication and are appended as Appendix 4 and Appendix 5.

This thesis presents the main results of the work and the reader is sometimes referred to the appendices for the full details. The journal articles represented by appendices 1, 2 and 3 in particular, contain much detail that may not be found in the main thesis chapters and the reader is therefore encouraged to read these carefully.

## **STRUCTURE of the thesis**

This report is constructed in the form of 8 main chapters:

### **Chapter 1:**

Chapter 1 is the present chapter, giving a short introduction to the report and describes how to read it in order to extract the most of this work.

### **Chapter 2:**

Contains an introduction to carbon dioxide capture, gas hydrates and presents the motivation and purpose of the present study.

### **Chapter 3:**

Presents a literature survey on gas hydrate promotion focussing mainly on thermodynamic properties, however some kinetic aspects are covered as well. At the end of the chapter, two lists of authors presenting thermodynamic hydrate data for gas hydrate systems relevant to this study are provided.

### **Chapter 4:**

Two experimental studies have been conducted as part of this work. Chapter 4 describes the experimental set-up's and procedures applied in these studies as well as discusses the strengths and weaknesses of the two experimental procedures.

### **Chapter 5:**

Chapter 5 presents the chosen approach for modelling gas hydrate equilibria. The Cubic-Plus-Association equation of state and the van der Waals-Platteeuw hydrate

model are presented. Models, algorithms and some numerical methods are described. Modifications to the models are briefly discussed. All parameters for the complete model are presented in the form of tables in this chapter.

#### **Chapter 6:**

Presents results from the experimental studies. Here, the reader is referred to Appendix 2 for the full details of one of the studies. Hydrate equilibrium pressures are presented for carbon dioxide hydrates promoted by tetrahydrofuran, cyclopentane or their mixtures.

#### **Chapter 7:**

Chapter 7 presents the majority of the modelling results obtained in this study. Modeling results of fluid phase equilibria in subsystems related to the system of water, tetrahydrofuran, cyclopentane, carbon dioxide and nitrogen are presented. Finally, hydrate modelling results are presented covering a large range of systems and varying phase behaviours. Three simplified carbon dioxide capture processes (based on gas hydrate formation) are simulated and their strengths and drawbacks are discussed.

#### **Chapter 8:**

Chapter 8 presents a complete summary as well as discusses how to interpret and apply the results obtained in this study.

### **SYMBOLS and ABBREVIATIONS**

A list of symbols and abbreviations used in the present report is presented in chapter 9.

### **GRAPHICAL ILLUSTRATIONS**

The present report contains several graphical illustrations. No list of captions is provided separately. Experimental data are always represented by separated markers while model results are presented in the form of lines.

### **DISCUSSION**

All results are discussed while presented. No separate section is included for the purpose of discussion.

### **LITERATURE CITED**

When citing the literature, the source is provided in the form of first author(s) and publication year. Separate lists of cited literature are provided at the end of each main chapter.

## APPENDICES

The present report includes a total of 5 appendices, appended in the final section of the report. All of these appendices represent journal manuscripts already published or ready for submission.

### Appendix 1:

Peer-reviewed journal paper published in the *Journal of Chemical Thermodynamics*.

Peter Jørgensen Herslund, Kaj Thomsen, Jens Abildskov, Nicolas von Solms\*, *Phase equilibrium modeling of gas hydrate systems for CO<sub>2</sub> capture*, J. Chem. Thermodynamics, 48 (2012), 13-27.

*This paper presents the initial model set-up and some preliminary modelling results for fluid phase equilibria and hydrate equilibria in the ternary system of water, carbon dioxide and nitrogen.*

**NOTE** that the modelled systems have been re-visited and the model accuracy has been improved in more recent work presented in main thesis.

### Appendix 2:

Peer-reviewed journal paper published in the *International Journal of Greenhouse Gas Control*.

Peter Jørgensen Herslund, Kaj Thomsen, Jens Abildskov, Nicolas von Solms\*, Aurélie Galfré, Pedro Brântuas, Matthias Kwaterski, Jean-Michel Herri, *Thermodynamic promotion of carbon dioxide-clathrate hydrate formation by tetrahydrofuran, cyclopentane and their mixtures*, Int. J. Greenhouse Gas Control, 17 (2013), 13-27.

*This paper presents the results obtained in an experimental study of the thermodynamic promoting effects of tetrahydrofuran, cyclopentane and their mixtures on the formation of mixed hydrates with carbon dioxide. It is shown that a synergistic effect occurs in the system including both promoters simultaneously. Enhanced pressure reduction is observed in the mixed promoter system compared to the individual promoter systems.*

### **Appendix 3:**

Peer-reviewed journal paper published in *Fluid Phase Equilibria*.

Peter Jørgensen Herslund, Kaj Thomsen, Jens Abildskov, Nicolas von Solms\*,  
*Application of the cubic-plus-association (CPA) equation of state to model the fluid phase behaviour of binary mixtures of water and tetrahydrofuran*, *Fluid Phase Equilibria*, 356 (2013), 209-222.

*This paper presents a thorough study on the fluid phase modelling of binary systems of water and tetrahydrofuran using CPA. Several modelling approaches are tested for their ability to simultaneously describe azeotropic vapour-liquid equilibrium (VLE) and closed-loop liquid-liquid equilibrium (LLE) in this binary system. It is found that assuming tetrahydrofuran is non self-associating but cross-associates (solvates) with water, provides accurate descriptions of both VLE and LLE.*

### **Appendix 4:**

Manuscript ready for submission.

Peter Jørgensen Herslund, Kaj Thomsen, Jens Abildskov, Nicolas von Solms\*,  
*Modelling of Tetrahydrofuran Promoted Gas Hydrate Systems for Carbon Dioxide Capture Processes*, Ready for submission, October 2013.

*This manuscript presents a complete modelling study of all systems and subsystems relevant to carbon dioxide capture using gas hydrate formation promoted by the presence of tetrahydrofuran. Both fluid phase and hydrate phase modelling results are presented.*

**NOTE** that this work updates and improves the modelling results and parameters presented in Appendix 1. The majority of results presented in this manuscript are included in Chapter 7 of the present report.

### **Appendix 5:**

Manuscript ready for submission.

Peter Jørgensen Herslund, Kaj Thomsen, Jens Abildskov, Nicolas von Solms\*,  
*Modelling of Cyclopentane Promoted Gas Hydrate Systems for Carbon Dioxide Capture Processes*, Ready for submission, October 2013.

*This manuscript presents a modelling study of all systems and subsystems relevant to carbon dioxide capture using gas hydrate formation promoted by the presence*

*of cyclopentane. Both fluid phase and hydrate phase modelling results are presented.*

*The majority of results presented in this manuscript are included in Chapter 7 of the present report.*





## 2 Introduction

Carbon dioxide is a greenhouse gas. It absorbs and re-emits long-wave (infrared) radiation in the atmosphere of this planet. Part of this re-emitted radiation is sent back to the surface of the planet, helping to retain thermal balance.

During the last 200 years, the amount of carbon dioxide present in the atmosphere has increased from 280 ppm to a level of about 390 ppm in 2010 [Garnier et al. (2011), Li et al. (2011)].

Though ambiguously shown, there is growing consensus that our climate is changing due to anthropogenic emissions of greenhouse gases. Carbon dioxide coming from anthropogenic sources is suspected a main contributor to the observed climate change [Figuerola et al. (2008)].

Sources of carbon dioxide emitted to the atmosphere are generally divided into two main sources. The first source is the naturally occurring processes that produce carbon dioxide. These processes account for the majority of the carbon dioxide emission to the atmosphere but are however counter-balanced by natural sinks over longer periods of time [Thiruvengkatachari et al. (2009)]. The second source of carbon dioxide emission is explained by human activity, hereunder combustion of fossil fuels and industrial processes related to energy- oil/gas-, cement and iron/steel production [Songolzadeh et al. (2012)].

### 2.1 Carbon Dioxide Capture

To lower the anthropogenic contribution to global warming, the Kyoto Protocol was formed in 1997. This protocol urged the included parties (37 industrialised nations and the European Union) to reduce their emission of greenhouse gases to a level approximately 5.2 percent, on average, below the carbon dioxide emission level of the year 1990 (the exact base level year varied for some countries). The goals of the protocol should be realised in the time period from 2008-2012 [Yu et al. (2012)].

Even though the protocol considered greenhouse gases in general, much focus has recently been on reducing carbon dioxide emissions from centralised locations such as e.g. fossil fuel (coal, oil and gas) fired power stations. The International Energy Agency (IEA) estimated the global carbon dioxide emission from fossil fuel fired heat- and energy production to 8.2 gigaton per year in 2001. This corresponded to approximately 35 percent of the total carbon dioxide emission related to combustion of fossil fuels that year [IEA 2003].

The Copenhagen Agreement was founded in 2009. Even though not legally binding, it encouraged all parties to limit greenhouse gas emission such that the

global temperature increase by the year 2100 would be no higher than 2 degrees compared to the pre-industrial level.

Carbon Capture and Sequestration (CCS) has been pointed out by IEA as an important technological challenge for the future, if this requirement should be met [Yu et al. (2012)].

Separation of carbon dioxide from vapour phases has been done on industrial level the last 70 years or more [Anderson and Newell (2004)]. Specialised chemical solvents were developed in the oil and gas industry to remove carbon dioxide from impure natural gases. Other applications of carbon dioxide removal are found in the food-processing or energy production industry, where similar solvents are used to recover carbon dioxide [Anderson and Newell (2004)]. Despite these technologies being considered relatively mature, they are energy and process equipment demanding and not yet ready for application in large scale post-combustion carbon dioxide capture [Yu et al. (2012)]. Among the available technologies are physical- and chemical absorption, membrane separation, cryogenic separation. More recently, a gas clathrate hydrate based process has been proposed, exploiting physical adsorption of gases into solid, crystalline formations of water.

Carbon dioxide capture is typically divided into two sections, pre- and post-combustion. In pre-combustion, a fossil fuel is contacted with air or oxygen to form hydrogen and carbon monoxide. The gas is hereafter contacted with steam, whereby the carbon monoxide is further oxidised to form carbon dioxide and more hydrogen. After this stage, the pre-combustion carbon dioxide capture stage is placed to remove carbon dioxide, thereby purifying the fuel (hydrogen) [Yu et al. (2012)]. Post-combustion implies removing carbon dioxide from flue gases after combustion, before the flue gas is released to the atmosphere. The post-combustion technology offers the advantage of being easier to retro-fit to existing plants without making significant changes to the combustion technology [Wang et al. (2011)].

The following sections describe three of the technologies currently being investigated for use in post-combustion carbon dioxide capture. These are the chemical absorption process using alkanolamines, the membrane based separation technology and finally the gas clathrate hydrate based technology, which forms the basis for the present study.

### **2.1.1 Chemical Absorption Based Processes**

Chemical absorption using alkanolamines is considered the most mature technology for use in post-combustion carbon dioxide capture [Rochelle 2009].

The alkanolamine based processes are suitable for separating carbon dioxide from flue gases with low to moderate concentrations of this compound. Such flue gases are found in coal- or gas fired power stations, where the carbon dioxide content typically ranges from 10 to 15 percent, depending on the fuel [Yu et al. (2012)].

Alkanolamines such as monoethanolamine (MEA) are used in aqueous solutions, which are contacted with the flue gas in an absorber tower. Carbon dioxide is an acid gas and can form a chemical bond with the amine group on MEA. The chemical reaction is reversible and by supplying heat at higher temperatures, a carbon dioxide rich vapour may subsequently be stripped from the loaded MEA solution.

Optimal conditions for absorption are low temperatures and high pressures, whereas for desorption, they are low pressure and high temperature. Chemical absorption is typically performed at atmospheric pressure and temperatures around 313 K - 333 K. The carbon dioxide stripper operates at slightly elevated temperatures [Yu et al. (2012)]. The released carbon dioxide rich vapour phase from the stripper is cooled, compressed and finally transferred to storage.

The advantage of this process is that it is fairly selective towards carbon dioxide (often above 95 percent carbon dioxide in the captured gas). The disadvantages are however high equipment corrosion rates, high energy consumption in the solvent regeneration stage (stripping) and large volumes required in the absorption stage. Another significant disadvantage is the low chemical stability and activity of the alkanolamines at the presence of impurities such as fly ash, NO<sub>x</sub>, SO<sub>x</sub> etc. in the flue gas [Aaron and Tsouris (2005)].

It is estimated that temperature manipulations, mainly the solvent regeneration/stripping, account for 70-80 percent of the total operating costs of this capture process [Aaron and Tsouris (2005)].

### **2.1.2 Membrane Based Separation**

Membranes may be used to allow a selective separation of carbon dioxide from vapour phases. Several types of membranes, inorganic, polymeric, solid-liquid, exist for this purpose [Aaron and Tsouris (2005)].

The separation is typically caused by size exclusion in porous membranes or by chemical interactions (e.g. by incorporating amine groups in the membrane material). Polymeric membranes are often very selective since these may be designed to optimise chemical interactions with specific molecules. In these cases, the separation occurs by solid diffusion or absorption-diffusion mechanisms [Aaron and Tsouris (2005)].

If a selective transfer across the membrane is performed, and the flue gas is supplied at a pressure of 1 atm., a significant pressure gradient is created across the membrane. For a typical coal fired power station flue gas, the pressure may be lowered to approximately 1/10 of the supply pressure down-stream of the membrane. This sets high requirements to the mechanical strength of the membrane material. Since membrane permeability most often decreases with increasing membrane thickness, the strength of the membrane cannot simply be adapted by increasing the membrane thickness.

The greatest advantage of the membrane based separation technology is its simplicity. Only the membrane and fans are needed in typical configurations [Aaron and Tsouris (2005)]. The main disadvantages are often low selectivity, low permeability or low mechanical strength of the membrane materials.

### **2.1.3 Separation by Clathrate Hydrate Formation**

The gas clathrate hydrate based separation technology forms the basis for the present study. This process has been proposed as an alternative to the existing gas separation technologies.

Gas clathrate hydrates are solid inclusions of sufficiently small molecules physically adsorbed into an ice-like, crystalline lattice of hydrogen bonded water. For further details of gas clathrate hydrates, please see section 2.2.

Carbon dioxide may form gas hydrates with water at a pressure of approximately 1.2 MPa and temperature of 273 K [Sloan and Koh (2007)]. The crystalline structure formed by the hydrogen bonded water molecules creates a total of 8 vacancies, so-called cavities, for each 46 water molecules. Assuming single occupancy of carbon dioxide in each of these cavities allow for a maximum carbon dioxide mole fraction of 0.15 in the solid phase. This corresponds to a mass fraction of carbon dioxide in the solid phase of approximately 0.31. Since gas hydrates are non-stoichiometric phases, full occupancy of carbon dioxide in the hydrate structure is however rarely achievable at moderate conditions of temperature and pressure.

Nitrogen and oxygen, like carbon dioxide, may form gas hydrates. However, these compounds form hydrates at significantly higher pressures. The formation pressure of the nitrogen hydrate at 273 K is approximately 16 MPa [Sloan and Koh (2007)]. Gas mixtures of nitrogen, oxygen and carbon dioxide will form hydrates at conditions in between those of the pure gases. The hydrates formed from these mixtures will enclathrate all gas phase components with appropriate sizes. Since carbon dioxide forms hydrates at the lowest pressures of the three main constituents of the flue gas, the formed hydrates are expected to be rich in carbon dioxide.

Assuming liquid carbon dioxide is the end-product, the hydrate based process, like the chemical absorption process, will contain two sections, capture and release. In the capture part, the flue gas is compressed, cooled and mixed with water, whereby hydrates may form by crystallisation. A carbon dioxide-rich hydrate slurry is hereafter transferred to the release section, where the solid particles are dissociated (melted) by either heating or pressure release. The captured gas is released at conditions of moderate to high pressure and low temperature. The aqueous liquid phase may be re-cycled to the capture section.

Figure 2.1 illustrates a simplified schematic of a suggested process configuration.

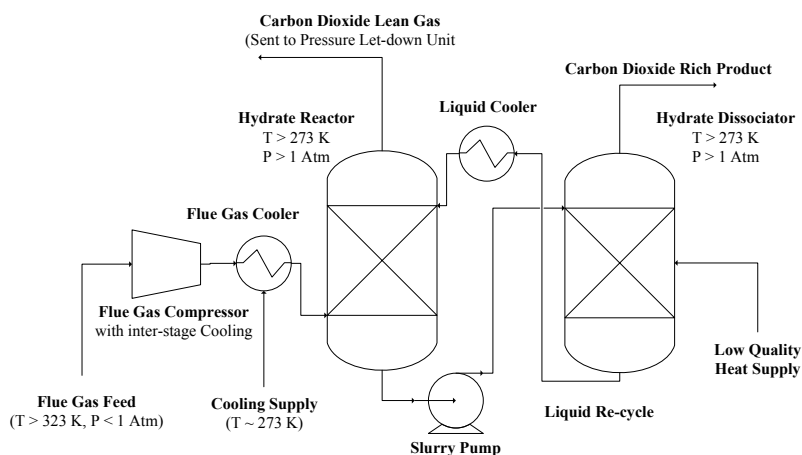


**Figure 2.1.** Simplified Schematic of a suggested configuration for the gas clathrate hydrate-based post-combustion carbon dioxide capture technology. Note that the suggested conditions for temperature and pressure are not necessarily actual conditions of the process.

One of the main advantages of the hydrate based separation technology is that it operates at temperatures, where low-quality heat can be used in the release section of the process. Also, a smaller amount of excess liquid is heated in the release part, since the hydrate slurry may be concentrated before heated. Finally, the captured gas is delivered at high pressure and low temperature, reducing costs for liquefaction of the final carbon dioxide product.

The main drawback of this process is the high pressure/low temperature requirement in the capture part. Large amounts of flue gas must be compressed in multi-stage compressor trains. A large amount of nitrogen is basically compressed just to be let down in pressure after the capture stage. By introducing a turbine generator downstream of the capture stage, some energy may be recovered from the carbon dioxide lean flue gas before emission to the atmosphere. This will however increase the capital cost of the capture plant. Other challenges with this

process are the slow kinetics of the hydrate crystallisation, low water conversions as well as handling of the particle suspension. With solid particles in the system, a high risk of plugging of process equipment is expected due to agglomeration of particles.

Recent attempts of improving this technology have looked into ways of lowering the pressure requirement in the capture stage. It has been found that the addition of low pressure/high temperature gas hydrate stabilisers, so-called thermodynamic gas hydrate promoters, may significantly lower the pressure requirement of this process. A thermodynamic gas hydrate promoter is a gas hydrate former that stabilises the hydrate structure at low pressures/high temperatures, thereby allowing for gas phase components to enter the hydrate phase at milder conditions. The result is a hydrate phase that enclathrates both the promoter and the desired gas phase constituents. If the additive is a liquid at the operating conditions of the process, it does not pollute the final gas product since it will remain with the liquid phase when the hydrates are dissociated. One disadvantage of adding these promoters is that they lower the gas storage capacity of the solid phase. Thus, a lot of research has gone into finding the ideal gas hydrate promoter that allows for hydrate formation at near-atmospheric pressure with high gas uptake capacity. More information on this may be found in Chapter 3.

Tetrahydrofuran, a five-sided cyclic ether, has been suggested as one potential thermodynamic gas hydrate promoter for the hydrate based carbon dioxide capture process.

## **2.2 Gas Clathrate Hydrates**

Gas clathrate hydrates, more commonly known as gas hydrates, are solid compounds of sufficiently small molecules and water. These solid compounds form when the constituents come into contact at conditions of low temperature and/or high pressure [Sloan and Koh (2007)].

Gas hydrates are often referred to as non-stoichiometric solid inclusion bodies, where water (host) form a lattice by hydrogen bonding [Sloan (2003), Koh et al. (2009), Sum et al. (2009)]. The lattice formation generates a number of empty cavities, in which small gas molecules (guests) may be enclathrated. The water lattice itself is a thermodynamically unstable structure, however attractive and repulsive interactions between the water and guest molecules stabilise the lattice [Sum et al. (2009)].

Gas clathrate hydrates were first discovered by Sir Humphrey Davy in 1810. Sir Humphrey Davy documented his discovery by publishing results from repeated experiments in 1811. Before Davy's discovery, Joseph Priestley stated,

in 1778, that SO<sub>2</sub> dissolved in water could cause the water to solidify under certain physical conditions, where HCl and SiF<sub>4</sub> would not [Sloan and Koh (2007)]. Since Priestley's discovery was poorly documented, and because Priestley's gas temperature was below that of the normal freezing point of water, it was never officially accepted that Priestley's solid material was clathrate hydrates and not simply pure ice [Koh et al. (2009)].

Sir Humphrey Davy's clathrate hydrates were formed by an aqueous solution of chlorine. As this solution was cooled to temperatures below 282 K, a solid compound occurred. Faraday later confirmed this discovery and suggested that the solid compound consisted of 1 part of chlorine to 10 parts of water [Englezos (1993)].

### 2.2.1 Gas Hydrate Structures

In the 1940's and 1950's, two gas clathrate hydrate crystal structures were defined. These were named structure 1 (sI) and structure 2 (sII), and both belonged to the cubic unit cell lattice type. Both structures were investigated by x-ray diffraction experiments at the University of Bonn [Sloan and Koh (2007), Englezos (1993)].

In 1987, a third crystal structure was discovered. This structure belonged to the hexagonal unit cell lattice type and was named structure H (sH) [Sloan and Koh (2007)].

More structures have been proposed since then, however as most of the naturally occurring gas hydrates belong to the three structures, sI, sII and sH, these structures are most frequently presented in the literature.

The size of the guest molecule is often what defines the structure of a formed hydrate. Guest molecules of diameter size 4.2 – 6 Å, such as methane (CH<sub>4</sub>), carbon dioxide (CO<sub>2</sub>) and hydrogen sulfide (H<sub>2</sub>S) all form structure I hydrates. Some guest molecules with diameters smaller than 4.2 Å form structure II hydrates when present as single guests. These include nitrogen (N<sub>2</sub>) and hydrogen (H<sub>2</sub>). Larger molecules with diameter 6 – 7 Å also form structure II. Propane (C<sub>3</sub>H<sub>8</sub>) and iso-butane (C<sub>4</sub>H<sub>10</sub>) are the most common among these.

Structure H hydrates are typically formed by large molecules of diameter 7 – 9 Å accompanied by smaller molecules such as methane, hydrogen sulfide or nitrogen [Sloan and Koh (2007)].

### 2.2.2 Cavities

Hydrate cavities are hydrogen bonded formations of cyclic water clusters. Computer simulations have suggested that pentamers, hexamers and squares are

the most likely cyclic cluster structures to arise naturally in water. Closed ring clusters are more stable than linear chains due to the extra hydrogen bond [Sloan and Koh (2007)]. These discoveries help explain the structure of the most common hydrate cavities.

Hydrate cavities are so-called polyhedra (poly=many, hedra=faces) crystalline structures. In the following these polyhedra will be named according to their number of faces ( $m_i$ ) with  $n_i$  edges. Cavity nomenclature becomes  $n_i^{m_i}$ . One of the simplest cavities in common hydrate structures is the dodecahedron, a 12-faced cavity composed solely of five-legged (five edges) faces all with equal side lengths. With the above nomenclature this cavity is named the  $5^{12}$  cavity. This cavity is the basic building block of the common hydrate structures and often represents the “small” cavity in a hydrate structure.

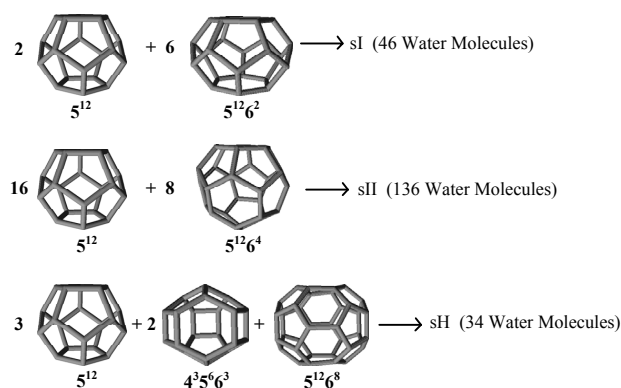


**Figure 2.2.** Hydrogen bonded water clusters forming the three most common gas clathrate hydrate structures, sI, sII and sH. Each three-leg intersection point represents an oxygen molecule [Modified from Appendix 1].

Figure 2.2 illustrates the five cavities found in the three most common hydrate structures, sI, sII and sH. The 14 sided  $5^{12}6^2$  cavity has 12 pentagonal faces and two hexagonal faces. All cavity structures are expanded relative to the hexagonal ice structure. It is the repulsive forces from the guest molecule that stabilises the expanded structures of the hydrate cavities. It has been shown that the mean volumes of the cavities vary with temperature as well as guest size and shape [Sloan and Koh (2007)].

An inspection of the shown cavities shows that the  $5^{12}6^2$ ,  $4^35^66^3$  and the  $5^{12}6^8$  cavities are non-spherical. The  $5^{12}6^8$  cavity is the most non-spherical structure of the five cavities. For this reason the physical shape of the guest molecule becomes more important in this cavity than the others [Sloan and Koh (2007)].



The sI hydrate belongs to the cubic unit cell family. The unit cell contains 46 water molecules in the shape of eight polyhedra.

The sII hydrate belongs to the face centered cubic unit cell family. The unit cell contains  $5^{12}$  and  $5^{12}6^4$  cavities in the ratio 16:8. This adds up to a total of 136 water molecules inside the unit cell.

Structure H belongs to the hexagonal unit cell type. sH comprises three cavity types,  $4^35^66^3$ ,  $5^{12}6^8$  and  $5^{12}$ . The theoretical sH unit cell composition is  $3(5^{12}) \cdot 2(4^35^66^3) \cdot 1(5^{12}6^8)$ , adding up to a total of 34 water molecules per unit cell [Sloan and Koh (2007)].

One important difference, when the sH hydrate is compared to sI and sII, is that a minimum of two different sizes of guest molecules are required to stabilise the sH hydrate. Small guest molecules may stabilise the  $5^{12}$  and the  $4^35^66^3$  cavities, while larger molecules are required to stabilise the large  $5^{12}6^8$  cavity. No single occupant has been found to stabilise the sH hydrate structure [Sloan and Koh (2007)].

### **2.3 Motivation and Purpose of This Work**

In order to evaluate the efficacy of CO<sub>2</sub> removal in the hydrate-based post-combustion carbon dioxide capture process, accurate thermodynamic models are required. One of the important first steps in process design is the performance of a thermodynamic evaluation of the proposed process. Thermodynamics will tell, if the desired process conditions are favourable or not. If thermodynamics are unfavourable, the process should be either re-designed or discarded.

A generic thermodynamic model should cover wide ranges of temperature and pressure and include descriptions of both fluid and solid phases occurring in the process.

The present study focuses on the capture part of the process only. Important information and parameters here are the hydrate formation conditions (temperature and pressure) in both the un-promoted and the promoted hydrate scenarios. The formation pressure in the capture part is the falling point of this process. If the flue gas pressure requirement becomes significant, this process is likely to be considered unsuited for carbon dioxide capture from power station flue gasses. Compression of gas phases is an energy consuming unit operation. Considering the fact that power station flue gases are generally delivered at low pressure and high temperature, and hydrates form at high pressure and low temperature, this process is challenged already at this point.

Thermodynamics will provide an indication of the minimum pressure requirement of the process. For hydrates to form in the actual process, a driving force for hydrate formation must be applied. This driving force is typically

established by either cooling to low temperatures or by pressurising to conditions above the thermodynamic equilibrium pressure.

Moreover, since gas hydrates are non-stoichiometric phases, estimates of the hydrate composition and thereby the composition of the captured gas phase is desired for various process conditions.

The developed model should include not only water, and the main flue gas constituents. Other complex components, such as gas hydrate promoters, should also be accounted for in the model. The main objectives of this work become:

- **Identify the key chemical components** of the gas clathrate hydrate based post-combustion carbon dioxide capture process.
- **Identify possible additives** to be used as thermodynamic gas hydrate promoters.
- **Identify suitable models** for these kinds of chemical systems.
- If necessary, **implement the models in a suitable form and algorithm** for the performance of a thermodynamic process evaluation.
- **Optimise model performance** to match existing data for known systems.
- **Estimate pressure requirements** for both the un-promoted and promoted hydrate capture processes.
- **Estimate the selectivity of the process.** Is the gas hydrate phase sufficiently selective towards carbon dioxide?
- **Analyse different scenarios** of process conditions.

Mainly process thermodynamics are considered in this work.

## 2.4 Cited Literature

D. Aaron, C. Tsouris, *Separation of CO<sub>2</sub> from Flue Gas: A Review*, Separation Science and Technology, 40 (2005), 321-348.

S. Anderson, R. Newell, *Prospects for Carbon Capture and Storage Technologies*, *Annu. Rev. Environ. Resour.*, 29 (2004), 109-142.

P. Englezos, *Clathrate Hydrates*, *Ind. Eng. Chem. Res.*, 32 (1993), 1251-1274.

J. D. Figueroa, T. Fout, S. Plasynski, H. McIlvried, R. D. Srivastava, *Advances in CO<sub>2</sub> capture technology – The U.S. Department of Energy’s Carbon Sequestration Program*, *Int. J. Greenhouse Gas Control*, 2 (2008), 9-20.

C. Garnier, G. Finqueneisel, T. Zimny, Z. Pokryszka, S. Lafortune, P. D. C. Défossez, E. C. Gaucher, *Selection of coals of different maturities for CO<sub>2</sub> storage by modelling of CH<sub>4</sub> and CO<sub>2</sub> adsorption isotherms*, *Int. J. Coal Geology*, 87, 2 (2011), 80-86.

IEA, *CO<sub>2</sub> emissions from fuel combustion, 1971–2001*, OECD/IEA, Paris, 2003.

C. A. Koh, A. K. Sum, E. D. Sloan, *Gas hydrates: Unlocking the energy from icy cages*, *Journal of Applied Physics*, 106 (2009), 061101.

J.-R. Li, Y. Ma, M. C. McCarthy, J. Sculley, J. Yu, J.-K. Jeong, P. B. Balbuena, H.-C. Zhou, *Carbon dioxide capture-related gas adsorption and separation in metal-organic frameworks*, *Coordination Chemistry Reviews*, 255, 15-16 (2011), 1791-1823.

G. T. Rochelle, *Amine Scrubbing for CO<sub>2</sub> Capture*, *Science*, 325 (2009), 1652-1654.

E. D. Jr Sloan, *Fundamental principles and applications of natural gas hydrates*, *Nature*, 426 (2003), 353-363.

E. D. Sloan, C. A. Koh, *Clathrate Hydrates of Natural Gases*, 3<sup>rd</sup> Ed., CRC Press, Boca Raton, 2007.

M. Songolzadeh, M. T. Ravanchi, M. Soleimani, *Carbon Dioxide Capture and Storage: A General Review on Adsorbents*, *World Academy of Science, Engineering and Technology*, 70 (2012) 225-232.

A. K. Sum, C. A. Koh, E. D. Sloan, *Clathrate Hydrates: From Laboratory Science to Engineering Practice*, *Ind. Chem. Res.*, 48 (2009), 7457-7465.

R. Thiruvenkatachari, S. Su, H., An, X. X. Yu, *Post combustion co<sub>2</sub> capture by carbon fibre monolithic adsorbents*, *Progress in Energy and Combustion Science*, 35, 5 (2009), 438-455.

M. Wang, A. Lawal, P. Stephenson, J. Sidders, C. Ramshaw, *Post-combustion co<sub>2</sub> capture with chemical absorption: A state-of-the-art review*, Chem. Eng. Res. Design, 89, 9 (2011), 1609-1624.

C.-H. Yu, C.-H. Huang, C.-S. Tan, *A Review of CO<sub>2</sub> Capture by Absorption and Adsorption*, Aerosol and Air Quality Research, 12 (2012), 745-769.

### **3 Literature Survey on Gas Hydrate Promotion**

Gas hydrates have received an increasing interest due to their relatively high gas/energy density. Whereas most previous efforts were directed toward looking for ways to avoid hydrate formation (hydrate inhibition), the focus is now also on finding ways to promote their formation at moderate temperatures and pressures (hydrate promotion). Sun et al. (2011) and Eslamimanesh et al. (2012) have reviewed recent advances in gas hydrate research including applications of promoted gas hydrate formation in processes for methane/natural gas storage, fuel gas (hydrogen) storage, and gas separation (e.g. carbon dioxide capture).

A thermodynamic promoter is defined as a component that participates actively in the hydrate formation process and stabilises a hydrate structure at higher temperature and/or lower pressure.

#### **3.1 The Concept of Gas Hydrate Promotion**

Whereas the mechanism for thermodynamic inhibition of hydrate formation is a consequence of a lowering of the liquid water activity due to hydrogen bonding between hydrate inhibitors (mainly methanol, monoethylene glycol or diethylene glycol) and water, thermodynamic promotion of gas hydrates is a consequence of the active formation of mixed promoter/gas hydrates at moderate conditions of temperature and pressure. The hydrates formed in that way serve as a storage medium for gas-like components but may also contain significant amounts of the added promoter.

Figure 3.1 illustrates, graphically, the concept of gas hydrate promotion. The specific example of carbon dioxide hydrates is shown. The promoter is tetrahydrofuran, which is a water-soluble, cyclic ether known to show significant thermodynamic promotion in these kinds of systems.

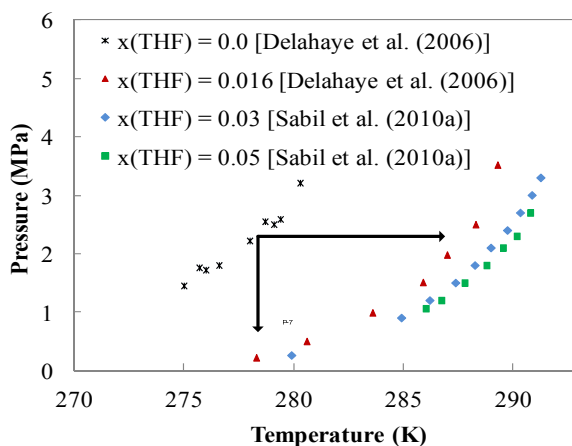


**Figure 3.1.** The principle of thermodynamic gas hydrate promotion. Markers indicate the phase boundaries of the gas hydrate formed from the ternary system of water-tetrahydrofuran-carbon dioxide.  $x(\text{THF})$  denotes concentration of tetrahydrofuran in the aqueous phase. With  $x(\text{THF}) = 0.0$ , the hydrates are pure carbon dioxide hydrates. As  $x(\text{THF})$  becomes larger than 0.0, mixed hydrates form, and the phase boundary shifts to milder conditions (higher temperatures and/or lower pressures)

Eslamimanesh et al. (2012) reviewed advances in gas hydrate research including applications of promoted gas hydrate formation in processes for methane/natural gas storage, fuel gas (hydrogen) storage, and gas separation (e.g. carbon dioxide capture). Their work provides an overview of investigated systems.

For the specific case of carbon dioxide separation from flue- or fuel gases, tetrahydrofuran (THF) and TBAB are mentioned as some of the most extensively studied promoters. THF is however stated to have the disadvantage of being volatile, unlike TBAB, which due to its nature as an electrolyte is expected to stay in the aqueous liquid phase.

### 3.2 The Mechanisms

By the use of molecular simulations, Alavi and Ripmeester (2012) investigated the phenomenon of hydrogen bonding between gas hydrate guests and host water in the sII hydrate lattice. An example of the sII hydrate of tetrahydrofuran was considered. Both the pure sII hydrate of THF and mixed sII hydrates with THF and “help” gases (CO<sub>2</sub>, CH<sub>4</sub>, H<sub>2</sub>S, Xe) were simulated at five temperatures ranging from 183 K to 263 K.

Hydrogen bonding between THF and water molecules in the large cavities was investigated. Hydrogen bonds were defined as taking place if the distance between

the oxygen atom on THF and a hydrogen atom on a surrounding water molecule became less than 2.1 Å. As a result of this hydrogen bond a Bjerrum L-defect occurs in the hydrate structure between the two water molecules that were previously hydrogen bonded.

It was shown that the THF/water hydrogen bonding was a thermally activated process. The probability of hydrogen bonds increased with increasing temperature. Interestingly, the presence of carbon dioxide in the small cavities increased the probability of hydrogen bonding between THF and water in the large cavities dramatically, whereas the presence of the three other gasses inhibited the hydrogen formation compared to the case of the pure sII hydrate of THF.

It was concluded that nearest neighbour guest-guest interactions do occur in the sII hydrate with THF filling all the large cavities. For the specific case of CO<sub>2</sub> in the small cavities it was suggested that the enhanced hydrogen bonding could be due to the physical tension on the water lattice caused by the relatively large carbon dioxide molecule present in the small cavities.

The results indicated that the basic assumptions in the original van der Waals-Platteeuw hydrate theory, regarding the water lattice being independent of the individual guests and the ignored guest-guest interactions may need reconsideration for this type of gas hydrates.

Atamas et al. (2013) applied Monte Carlo simulations to investigate the influence of physical and chemical hydrate promoter properties (such as e.g. size, dipole moment, hydrogen bonding capabilities etc.), which were assumed important for stabilising the sII hydrate at the simultaneous presence of hydrogen in the small cavities.

By calculating Gibbs free energies of the hydrate phase with varying promoter concentration in the large cavities (THF was used as an example), it was shown that the stability of the hydrate phase was linearly dependent on the THF occupancy. The lowest Gibbs free energies were found at full occupation of the large cavity by THF, independently of the cavity occupancy of hydrogen in the small cavities. This indicated the THF hydrates are the most stable when incorporating THF in all large cavities.

Atamas et al. (2013) argued that the linear dependence of THF occupation indicated that THF does not distort the sII hydrate water lattice significantly by its presence in the large cavities. The simulations were performed at a temperature of 253 K and a pressure of 101 MPa.

A total number of 19 heavy hydrocarbon sII hydrate formers (including: tetrahydropyran, cyclopentane, cyclopentene, 1,1-dichlorofluoroethane, 1,2-dichlorofluoroethane, fluorocyclopentane, tetrahydrofuran, cyclobutanone, 2,5-dihydrofuran, propanol, 2-propanol, 1,1,1,2-tetrafluoroethane, acetone, 1,3-

dioxolane, bromotrifluoromethane, dichlorofluoromethane, furan, 1,1-difluoroethane, dimethyl ether) were investigated for their stabilising effect on the mixed sII hydrate with full occupancy of promoter in the large cavities and full (single) occupancy of hydrogen in the small cavities. Simulations were performed at 101 MPa and temperatures ranging from 233 K to 293 K. Generally the lowest Gibbs free energies were found for tetrahydrofuran, 1,3-dioxolane, acetone, cyclopentane, cyclobutanone and tetrahydropyran. At 233 K the two most stabilising compounds were cyclobutanone and tetrahydrofuran. At the highest investigated temperature, 293 K, the most stable hydrates were found for cyclobutanone and cyclopentane.

No clear trends were observed relating the Gibbs free energy with the van der Waals volumes, dipole moments or the shape of the promoters. Atamas et al. (2013) concluded that the stability of the sII hydrates was an interplay between sizes, van der Waals volumes, dipole moments and more importantly the molecular geometries of the promoters.

### **3.3 Thermodynamic Promoters Studied in the Literature**

Callanan and Sloan (1983) investigated heat capacities and heats of dissociation for three hydrate formers at moderate conditions; Tetrahydrofuran (sII), Ethyleneoxide (sI) and Cyclopropane (sI and sII depending on temperature and pressure conditions). It was found that a significant amount of subcooling was needed to form the tetrahydrofuran hydrates at ambient pressure. No solidification was observed until temperatures about 250K (more than 20 K below the normal hydrate dissociation temperature).

Ripmeester and Ratcliffe (1990) presented a short summary of the discovery of sI and sII hydrates and the determination of these structures in the early 1950's. Ripmeester and Ratcliffe also mentioned tert-butylamine as a hydrate former. In their work, Ripmeester and Ratcliffe presented about 25 newly found sH and sII hydrate formers. Structures had been confirmed by <sup>129</sup>Xe and <sup>2</sup>H NMR measurements. Among the sII hydrate formers were; benzene, cyclohexane, isobutylene, n-butane, acetonitrile, neopentane and seven other components. The sH components included; methylcyclopentane, methylcyclohexane, cycloheptene, cyclooctane, tert-butyl methyl ether and many others. Investigated compounds that were found not to form hydrates were; iodine, n-pentane, n-hexane, toluene, trans-1,2-dimethyl-cyclohexane, diethyl ether and 8 others. Ripmeester and Ratcliffe concluded that not only size, but also space filling inside the cavities (shape of the guest compared to shape of the cavity) were important factors for the found hydrate formers.



Dyadin et al. (1991) reported phase diagrams measured for the binary system of water and tri-methyleneoxide (TMO) at pressures ranging from 0.1 MPa to 600 MPa. Results were compared to similar measurements of cyclic ethers (ethyleneoxide (EO), 1,3-dioxane, 1,4-dioxane, 1,3-dioxolane and tetrahydrofuran (THF)). TMO was reported as both an sI and sII hydrate former and observed a structural change in the TMO hydrate phase from the cubic sI hydrate at low pressures (0.1 MPa) to the cubic sII at high pressures.

Dyadin et al. (1991) concluded that the smallest ethers EO and TMO both stabilised sI hydrates at low pressures, however when increasing ether size, the hydrate formers began to stabilise sII hydrates rather than sI hydrates. However, even large hydrate formers such as tetrahydrofuran, 1,3-dioxolane and 1,4-dioxane were claimed to stabilise the sI hydrate at pressures above 200 MPa.

Danesh et al. (1993) reported measurements of benzene hydrate formation. Equilibrium-pressure data for a three-component system (methane-benzene-water) at four-phase equilibrium were presented in the temperature interval from 275 K to 288 K. The hydrate dissociation pressures of the mixed benzene/methane hydrate were considerably lowered compared to the dissociation pressure of the pure sI hydrate of methane.

Mixed hydrate equilibrium data for the sH hydrate formed by methyl cyclopentane with either methane or nitrogen as help gas was reported by Danesh et al. (1994). Excess of all components was utilised such that four-phase (H-L-L-V) equilibrium was always obtained, thereby eliminating the influence of feed concentration (univariant system according to the Gibbs Phase Rule). The formed hydrates were dissociated by stepwise heating, allowing equilibrium to settle between each temperature manipulation. The equilibrium temperature/pressure conditions for the mixtures were determined at the dissociation of the last hydrate crystal. It was shown that even though intermediate equilibrium stages were not considered in the final summary of equilibrium points, they were in fact true equilibrium points due to the uni-variance of the system. The experimental data for the mixed gas hydrates clearly showed a reduction in pressure when compared to the dissociation pressures of the pure gas hydrates of methane and nitrogen respectively.

Ng and Robinson (1996) presented acetone as a potential gas hydrate promoter at low to moderate concentrations. At concentrations in the aqueous phase higher than 75% wt., acetone however had an inhibiting effect.

Saito et al. (1996) reported equilibrium and kinetic data for mixed hydrates of acetone plus methane and tetrahydrofuran plus methane. The purpose of this study was to form hydrates suitable for methane storage at mild conditions.

Promoter concentrations in the aqueous phase were reported to affect the equilibrium pressures. From a thermodynamic point of view, tetrahydrofuran was

clearly the most efficient promoter (in terms of pressure reduction) of the investigated additives. It was concluded that the selectivity in the hydrate phase was towards the tested promoters. Low molar ratios of 1/30 methane over water were reported for the hydrate phase.

Tohidi et al. (1996) presented gas hydrate equilibria for three promoted gas hydrate systems. The promoter was cyclohexane and the help gases were either methane, nitrogen or a mixture of methane and nitrogen.

Cyclohexane lowered the dissociation pressures considerably compared to the pure gas hydrate systems of the pure gases. The formed hydrates were assumed sII where cyclohexane occupied the large cavities.

Mainusch et al. (1997) carried out an extensive study of the acetone-methane mixed gas hydrate system. The work was inspired by the unexplained findings of Ng and Robinson. Equilibrium data were reported in the temperature interval from appr. 275 K to 291 K at eight concentrations of acetone ranging from 1.7 to 48 mole percent. The presented data compared well with the data of Ng and Robinson. Mainusch et al. concluded that acetone at concentrations lower than 5 mole percent acted as a hydrate promoter, while it at higher concentrations had an inhibiting effect on the hydrate formation.

Sum et al. (1997) reported hydrate structure investigations of several single- and mixed gas hydrates including components such as methane, propane, nitrogen, carbon dioxide and also tetrahydrofuran. Raman spectroscopy was presented as a powerful tool for identifying crystal structures of formed hydrates. In the binary mixture, methane – carbon dioxide, it was found that the large cavities of the formed sI hydrate were almost fully occupied by both methane and carbon dioxide, while only methane was found in the small cavities.

Sum et al. (1997) commented on the distribution between cavities of small and large sizes in the pure hydrates of carbon dioxide. No signs of carbon dioxide presence in the small cavities of the sI hydrate were seen. Methane however appeared to distribute evenly between the small and large cages of the pure methane sI hydrate.

In the binary hydrate of methane and tetrahydrofuran, Sum et al. observed a high cage occupancy of tetrahydrofuran in the large cavities of the sII hydrate, however some methane was also found in the large cavities. Only methane was seen in the small cavities of the mixed sII hydrate. Sum et al. explained this by the fact that tetrahydrofuran is too large to enter the small cavities.

Tohidi et al. (1997) were (among) the first to report phase equilibrium data for binary and ternary sII gas hydrates formed by either cyclopentane or neopentane at pressurised conditions (gas phase containing methane or/and nitrogen). It was discovered that cyclopentane was capable of stabilising the sII hydrate structure

without the presence of a help gas, whereas neopentane needed a help gas to stabilise the hydrate structure.

By comparing benzene, cyclohexane, neopentane and cyclopentane, it was clear that out of the four, cyclopentane was the thermodynamically most stable hydrate former – independently of the choice of “help” gas (study limited to methane and nitrogen).

Khokhar et al. (1998) investigated the possibility for storing methane gas in sH hydrates as well as methods for improving the methane storage potential.

Four-phase hydrate equilibrium data for the ternary system, water-1,3-dimethylcyclohexane-methane was presented. It was concluded that sH hydrates were formed in this system at pressure conditions milder than those found for sI methane hydrates. However the promoting effect was not dramatic.

Subramanian and Sloan (1999) utilised Raman spectroscopy to investigate methane hydrate formation kinetics and cage occupancy in-situ at the presence of poly N-vinylcaprolactam (PVCap) and deuterated tetrahydrofuran. Subramanian and Sloan were able to follow the methane transport from dissolved state to adsorbed state. The relative occupancies of the small and large cavities were investigated.

In the case of mixed THF/methane hydrate, it was shown that hardly any methane was adsorbed in the large sII hydrate cavities. These cavities were mainly occupied by the larger THF molecules.

Jager et al. (1999) measured hydrate phase equilibrium conditions in the ternary mixture methane+1,4-dioxane+water. The investigated pressure interval ranged from 2 MPa to 14 MPa. Mole concentrations of 1,4-dioxane in the aqueous liquid phase was varied from one mole percent to 30 mole percent. Jager et al. (1999) concluded that adding 1,4-dioxane to the liquid phase had a promoting effect (pressure reduction) up to a concentration of approximately six mole percent (close to the stoichiometric concentration in the hydrate phase 1,4-dioxane·17H<sub>2</sub>O). When increasing concentrations above six percent, the addition of more 1,4-dioxane lowered the promoting effect.

Due to the large physical extension of the 1,4-dioxane molecule, Jager et al. (1999) assumed that the formed hydrates were sII. However no analysis was performed to support this.

Mooijer-van den Heuvel et al. (2000) presented hydrate equilibrium data for promoted methane hydrates. Three cyclic, organic compounds and two fluoroalkanes were tested as promoters, these included; tetrahydropyran (THP), cyclobutanone (CB) – both sII hydrate formers - , methylcyclohexane (MCH) – sH hydrate former – and fluoropropane (CHF<sub>3</sub>) and tetrafluoromethane (CF<sub>4</sub>) – both sI and sII hydrate formers.

A pressure reducing effect, when compared to the pure methane hydrate, was observed on the hydrate equilibrium pressure for all additives except CF<sub>4</sub>. THP was the most efficient promoter, lowering the hydrate dissociation pressure by 79% when compared to pure methane hydrate. CB was second, lowering the dissociation pressure by 77%. Mooijer-van den Heuvel et al. (2000) finally concluded that the promoted hydrates were unsuitable for methane storage purposes, since the storage capacity was considerably decreased, when compared to the pure methane hydrate phase.

De Deugd et al. (2001) reported experimental data and modeling results for mixed gas hydrates formed by methane and water-soluble hydrocarbons such as acetone, tetrahydrofuran, tetrahydropyran and 1,3-dioxolane.

Of the investigated hydrocarbons, THF and 1,3-dioxolane were the most and second most efficient promoters respectively. De Deugd et al. (2001) concluded that the five-membered ring structure obtained lower hydrate dissociation pressures than the six-membered ring. Similarly, a low number of oxygen atoms in the ring structure resulted in low dissociation pressures. Hence size and polarities were considered important factors in the hydrate formation mechanism.

A final remark was made that the strongest pressure reducing promoter (THF) also had the largest negative effect on methane content (selectivity) in the hydrate phase.

Østergaard et al. (2001) measured the effect of cyclopentane, cyclohexane, neopentane, isopentane, methyl cyclopentane and methyl cyclohexane on the hydrate phase boundary of a gas mixture, a natural gas and a model oil. Experimental equilibrium data were reported. The first three were known to form sII hydrates whereas the latter three form sH hydrates.

In their experimental work, Østergaard et al. investigated a system of a model oil, where two heavy hydrate formers (10.35 mole percent cyclopentane and 9.88 mole percent neopentane) were added to the system. This system showed less promoting effect on the hydrate formation than that seen when adding only cyclopentane (17.87 mole percent). Cyclopentane was demonstrated to have the largest (promoting) impact on the measured hydrate phase boundaries.

Sun et al. (2002) reported four-phase hydrate-liquid water-liquid hydrocarbon-vapour equilibrium data for methane hydrates promoted with cyclohexane or cyclopentane. Promoting effects of cyclohexane were also investigated for the case of gas mixtures including methane, ethane and propane. At high temperatures, cyclohexane acted as a thermodynamic inhibitor rather than a promoter.

It was shown that cyclopentane was a more powerful promoter than cyclohexane.

Ohmura et al. (2005) investigated the thermodynamic promoting effects on methane hydrate equilibrium pressures in the presence of 2-methyltetrahydrofuran or 3-methyltetrahydropyran. These promoters were chosen due to their relatively high water solubilities as well as strong thermodynamic effects on hydrate formation. In previous studies, it had been shown that high water solubility improved formation kinetics.

3-methyltetrahydropyran had the largest thermodynamic promoting effect on the hydrate formation pressures. 2-methyltetrahydrofuran provided inhibiting effects at temperatures below 278 K and a small promoting effect at temperatures above. A comparison with other known sH hydrate formers (methylcyclopentane and methylcyclohexane) showed 3-methyltetrahydropyran as the thermodynamically most efficient sH hydrate promoter of the four.

Anderson et al. (2007) reviewed the divergent findings on hydrogen storage capacities in the binary tetrahydrofuran (THF) – hydrogen (H<sub>2</sub>) hydrate reported elsewhere in literature. Storage capacities ranging from 1 mass percent up to 4 mass percent had been reported through several independent studies.

New three-phase (H-L<sub>w</sub>-V) hydrate equilibrium data were presented for the ternary system of water-THF-H<sub>2</sub> in the temperature interval from 270 K to 290 K.

Only single occupancy of hydrogen in the small sII hydrate cavities and almost complete occupancy of THF in the large cavities was found.

Mohammadi and Richon (2009a) reported experimental hydrate dissociation data for the ternary systems of water + carbon dioxide + either methylcyclopentane, methylcyclohexane, cyclopentane or cyclohexane.

It was shown that the promoting effect of the four investigated gas hydrate promoters on carbon dioxide gas hydrates could be classified as follows; cyclopentane > cyclohexane > methylcyclohexane ≈ methylcyclopentane.

Mohammadi and Richon (2009b) similarly reported experimental hydrate dissociation pressure data for the mixed hydrates of cyclopentane and hydrogen sulphide and cyclopentane and methane. Clear promoting effects were determined for both gasses.

Shin et al. (2009) reported hydrate dissociation pressures for carbon dioxide hydrates promoted by 3-methyl-1-butanol (3M1B), tetrahydrofuran (THF) and 1,4-dioxane (DXN). Hydrate structures were analysed by D/max-RB diffraction. Cage occupancies were analysed by Raman spectroscopy under liquid nitrogen temperature at ambient pressure.

3M1B is known to form sH hydrates with methane, however with CO<sub>2</sub> the sH hydrate did not form. In this system 3M1B acted as a mild inhibitor on the pure sI carbon dioxide hydrate.

For the 1,4-dioxane system, it was shown that the “promoter” had an inhibiting effect (compared to the pure sI hydrate of CO<sub>2</sub>) on the dissociation pressure of the

hydrate for a DXN concentration of 1 mole percent and a promoting effect for a concentration of 5.56 mole percent. With 3 mole percent DXN, the measured data showed promoting effect at low temperatures but crossed the conditions for pure CO<sub>2</sub> hydrate at approximately 280 K and had an inhibiting effect at higher temperatures. With 5.56 mole percent DXN in the liquid phase, the system showed promoting effect up to approximately 282 K. It was not investigated whether the hydrates formed in the “inhibited” region were in fact sII mixed hydrates or pure CO<sub>2</sub> sI hydrates.

Raman spectroscopy for the mixed hydrates of CO<sub>2</sub>/THF and CO<sub>2</sub>/DXN showed presence of CO<sub>2</sub> only in the small cavities of the sII hydrate.

Komatsu et al. (2010) reported experimental dissociation pressures of hydrogen hydrate promoted by tetrahydrofuran (THF) or cyclopentane. The enclathration characteristics of hydrogen was found similar for the two promoted hydrate systems.

In the pressure range from 2 to 14 MPa, the cyclopentane promoted hydrates were generally shifted approximately 2 Kelvin up in temperature compared to the THF promoted hydrates (5.3 mole percent THF), indicating a stronger promoting effect of hydrate formation by cyclopentane.

Equilibrium pressures and hydrate structures were investigated for methane hydrates at the presence of six heavy hydrocarbons by Lee et al. (2010a). All hydrocarbons were cyclic compounds with ring sizes of 5 to 6 atoms. Among the additives were both heterocyclic ethers (3-methyltetrahydrofuran, 2-methyltetrahydrofuran) heterocyclic acetals (4-methyl-1,3-dioxolane, 4-methyl-1,3-dioxane), an ester ( $\gamma$ -butyrolactone) and a cyclic ketone (cyclohexanone).

All systems were initiated with stoichiometric amounts of hydrate former compared to water content (approximately 5.6 mole percent promoter). All additives had reasonable miscibility in water.

The results were compared to THF as a reference. The promoting effects of the tested additives were significantly lower than that of THF.

The differences in promoting effect between compounds with similar structures were explained as follows; the addition of the methyl group to the tetrahydrofuran ether structure increases the molecular size of the compound and it therefore fits less well in the large sII hydrate cavity. 2-methyltetrahydrofuran becomes physically larger than 3-methyltetrahydrofuran due to repulsive forces between the close located methyl group and oxygen atom, making it further unsuited for the sII hydrate.

The thermodynamic promoting effect on nitrogen and ethane hydrates respectively caused by the presence of cyclopentane, cyclohexane and methyl cyclohexane was investigated by Mohammadi and Richon (2011). It was shown that the promoting effect on the nitrogen hydrates was significant when adding

cyclopentane (pressure lowered by two orders of magnitude around  $T = 282$  K), whereas less promoting effects were found for cyclohexane and methylcyclohexane.

By comparing to similar systems presented in literature, a trend was shown in the cases including methane, carbon dioxide, hydrogen sulfide as help gas. All systems behaved similar with respect to the promoting effect of the three heavy hydrocarbons.

The case with ethane as help gas behaved different. Here all three promoters acted similar and hardly showed any promoting effect. Mohammadi and Richon explained this by ethane being too large to enter the small cavity of the hydrate structures, providing less “help” in stabilising the sII hydrate at temperatures above the upper quadruple point of the pure sII hydrate of cyclopentane.

The promoting effect on hydrate dissociation pressures of carbon dioxide by the presence of acetone was investigated by Maekawa (2011). Acetone may stabilise the sII hydrate structure by itself in a 16 mass percent solution corresponding to the stoichiometric concentration in the sII hydrate phase with all large cavities occupied by acetone (5.56 mole percent acetone).

It was shown experimentally, that adding acetone to the hydrate forming system of water and carbon dioxide inhibited the sI hydrate formation of carbon dioxide for acetone mass fractions up to 0.06. The temperature shift was approximately 1-2 K.

For acetone mass fractions of 0.10 and above, the slope of the temperature-pressure formation curve shifted, indicating a change of hydrate structure. Maekawa suggested this second structure to be the sII type, since acetone forms sII hydrates and since the most stable hydrates of this type were found at an acetone mass fraction of 0.16, approximately the stoichiometric concentration of the sII hydrate with complete filling of the large cavities.

The investigated acetone systems did not provide significant pressure reduction compared to the pure sI hydrates of carbon dioxide.

Trueba et al. (2011) reported pure hydrate dissociation pressures for a number of heavy hydrocarbon sII hydrate formers. Mixtures of water and hydrocarbon (concentrations close to that of the stoichiometric sII hydrate) were used. The heavy hydrocarbons were Furan, 2,5-dihydrofuran, tetrahydropyran, 1,3-dioxolane and cyclopentane.

It was shown that the formation temperatures of the pure sII hydrates of these heavy hydrocarbons ranged from approximately 270 K (1,3-dioxolane) to 280 K (cyclopentane) at atmospheric pressure. The stability of the pure sII hydrates were ranked as follows (most stable first); cyclopentane, furan, tetrahydropyran, 2,5-dihydrofuran, 1,3-dioxolane. cyclopentane and furan were significantly more

stable than the remaining three sII hydrate formers with a 5 Kelvin temperature difference between furan and tetrahydropyran.

Only hydrates formed by cyclopentane and furan were stable at temperatures above the normal freezing point of water.

Mixed hydrates with hydrogen showed the same trend as the pure promoter systems. By comparing to similar data in the literature for tetrahydrofuran + hydrogen hydrates, it was shown that tetrahydrofuran and furan behaved similar in terms of thermodynamic promotion of hydrogen hydrates.

By considering geometry, size, and dipole moments of the heavy hydrocarbon hydrate formers, it was deduced that the molecular geometry has more influence on the hydrate stability than the dipole moments. The most symmetrical geometry (cyclopentane and furan) provided the most stable sII hydrates.

The thermodynamic promoting effect of propan-2-ol, 2-methyl-2-propanol and 2-propanone on fluoromethane hydrate formation was investigated by Imai et al. (2012). Little promoting effect was shown for the systems with 2-methyl-2-propanol and 2-propanone, whereas propan-2-ol provide similar or slightly inhibited conditions as the pure fluoromethane hydrate (sI). Fluoromethane forms hydrates at pressures down to approximately 0.3 MPa at 273-274 K. The thermodynamic promotion caused by the two promoters shifted this temperature up by approximately 5-6 K. The hydrates formed at pressures ranging from approximately 0.1 MPa to 3.9 MPa in the temperature range from 273 K to 296 K.

Chari et al. (2012) compared the promoting effect of tetrahydrofuran and tert-butylamine (t-BuNH<sub>2</sub>) on methane hydrates. It was shown that when using similar promoter concentrations, THF was significantly more efficient in terms of pressure reduction than t-BuNH<sub>2</sub>.

Shin et al. (2012) measured phase equilibrium for methane hydrates at the presence of pyrrolidine or piperidine (secondary amines, five- and six-sided ring structures respectively).

The hydrates formed were shown to be of the sII hydrate structure. At amine concentrations lower than 5.56 mole percent (in the liquid phase) Shin et al. found evidence (by <sup>13</sup>C NMR and Raman spectroscopy) that methane competes with the amine for the occupancy in the large cavities of the sII hydrate.

From a thermodynamic point of view, these promoters were significantly less stabilising than THF (at similar concentrations). In the investigated pressure range of 3.5 MPa to 9.5 MPa, the equilibrium temperatures for the pyrrolidine promoted system were 9-10 K lower, and the piperidine promoted system 10-12 K lower than those of the THF promoted system, however still higher than those of the pure sI methane hydrate.

Sun et al. (2012a) studied hydrogen removal from a coke-oven gas (mixtures of e.g. hydrogen, methane, nitrogen, carbon dioxide, carbon monoxide). These gas



mixtures often contain about 50 percent hydrogen and therefore form hydrates at high pressure. The addition of THF allowed for hydrate formation at pressures below 4 MPa in the temperature range from 281 K to 291 K. The formed hydrates contained only little amounts of hydrogen and the captured gas was mainly composed of the remaining components. Hence, impurities in the coke-oven gas could be removed by the hydrate formation process.

Separation of methane from nitrogen by hydrate formation was investigated by Sun et al. (2012b). Tetrahydrofuran (6 mole percent) was used as a thermodynamic hydrate promoter to enable hydrate formation at moderate pressures. Experimental data were presented for systems with varying methane concentrations in the initial vapour phases ranging from 4.9 mole percent to 46.3 mole percent. The investigated temperature interval was 279.2 K to 287.2 K. It was found that methane content could be enriched by hydrate formation at the investigated conditions.

Xia et al. (2012) compared THF and TBAB as thermodynamic promoters for the separation of carbon dioxide from methane by hydrate formation.

THF was shown to be a better thermodynamic promoter than TBAB at temperatures above 286 K. At lower temperatures, TBAB provided the most stable hydrates (semi-clathrate).

Lee et al. (2012) documented the promoting effect of tetrahydrofuran on hydrates of carbon dioxide, hydrates of methane and mixed hydrates of carbon dioxide and methane. Stoichiometric concentrations of 5.56 mole percent THF were used in all systems.

By the use of Raman spectroscopy, Lee et al. (2012) showed for the unpromoted mixed sI hydrate of methane and carbon dioxide, that the hydrate phase was selective towards carbon dioxide, when an initial 50/50 (moles) gas mixture was used. Carbon dioxide was shown to occupy mainly the large cavities, but was however also found present in the small cavities. Methane mainly occupied the small cavities but was also found present in the large cavities.

When adding tetrahydrofuran to the system, THF was found occupying all the large cavities of the sII hydrate. In the mixed hydrate of THF and carbon dioxide or methane, the gas components were found present in the small cavities. However for a 50/50 initial gas mixture the hydrate phase was selective towards methane in the promoted hydrate phase.

Yang et al. (2012) investigated the formation of mixed hydrates of air + Tetrahydrofuran, air + cyclopentane and air + TBAB.

It was shown that for temperatures below 285 K and pressures below 1.5 MPa, TBAB was the most efficient thermodynamic promoter, followed by CP and finally THF. Above 286 K, the range was CP (lowest pressure) -> THF -> TBAB (highest pressure).

Zhong et al. (2012) compared the three thermodynamic hydrate promoters, cyclopentane, cyclohexane and TBAB in their ability to lower pressures of mixed hydrates formed with gas mixtures of 30 mole percent methane, 60 mole percent nitrogen and 10 mole percent oxygen. 7 weight percent promoter (in the binary mixtures with water) was added in all cases. It was shown that cyclopentane, by far, was the most efficient promoter of the three. By mass balance considerations, the methane content in the mixed hydrates with cyclopentane and cyclohexane was estimated to be approximately 50 mole percent, indicating selectivity towards methane in the promoted sII hydrates.

Partoon and Javanmardi (2012) investigated the thermodynamic promoting effect of propanone on methane hydrates. It was shown that the equilibrium pressures could be lowered by the presence of propanone, however gas uptakes decreased also. Adding SDS to the promoted system was shown to increase the gas uptakes.

Ricaurte et al. (2013) studied the effects of THF (4 weight percent) and SDS (0.3 weight percent) on gas hydrate formation from carbon dioxide and methane gas mixtures at quiescent conditions (no induced mixing). It was shown that both THF and SDS were needed for significant amounts of hydrate to form at moderate conditions of temperature and pressure. However, at the presence of these additives, the selectivity towards carbon dioxide in the hydrate phase was too low for this system to be interesting in terms of industrial gas separation purposes.

Yang et al. (2013) provided thermodynamic equilibrium data (T/P) for gas hydrates formed by mixtures of carbon dioxide and hydrogen at the presence of tetrahydrofuran, ranging from 1 to 4 mole percent THF in the aqueous phase. It was shown that increasing THF concentration decreased not only dissociation pressures but also nucleation times.

Da Silva Lirio et al. (2013) investigated the common promoting effect on carbon dioxide hydrate formation of tetrahydrofuran (THF) and sodium dodecyl sulphate (SDS). The addition of only SDS did not provide improved gas uptakes in the case of pure hydrates of carbon dioxide.

However, the mixture of thermodynamic (THF) and kinetic (SDS) promoters provided significantly improved gas uptakes compared to the unpromoted systems or the systems containing only one or the other promoter.

Zhong et al. (2013) studied methane recovery by hydrate formation from gas mixtures of methane and nitrogen at the presence of cyclopentane. It was found that the highest selectivity towards methane in the hydrate phase was obtained by applying moderate pressures (driving force of 2.3 MPa) at 283.4 K. Increasing the cyclopentane amount in the system increased the overall recovery of methane, however increasing the driving force at constant temperature lowered the selectivity towards methane in the hydrates formed.

From a gas mixture initially containing 30 mole percent methane, Zhong et al. recovered approximately 46 percent of the methane and the captured gas phase was enriched in methane to 47.2 mole percent (driving force of 2.3 MPa and  $T = 283.4$  K). The addition of a second separation stage by hydrate formation could increase the methane content in the final outlet gas to approximately 72 mole percent.

The thermodynamic promoting effect of neohexane and methyl cyclopentane on the formation of nitrogen hydrates has been studied by Mohammadi and Richon (2013). It was shown that methyl cyclopentane could shift the hydrate phase boundary 7 K up in temperature compared to the pure nitrogen hydrate at similar pressures. Neohexane correspondingly increased the phase boundary temperatures by approximately 9 K. By comparing to the system of nitrogen and cyclopentane, it was however shown that these promoters were significantly less efficient in terms of pressure reduction.

### 3.3.1 Tetrahydrofuran (THF)

Gough and Davidson (1971) reported compositional data on the sII hydrate formed by tetrahydrofuran above the normal freezing point of water. Palmer (H. A. Palmer, *Thesis*, University of Oklahoma, 1950) was mentioned as the first to report clathrate hydrate formation in the binary water-tetrahydrofuran system. Gough and Davidson reported results from five mass density measurements of liquid samples of water and THF (approximate concentration THF·17H<sub>2</sub>O) at 277 K and atmospheric pressure. Densities increased with increasing temperature and THF concentration at the measured conditions. A phase diagram for the binary THF-water mixture at the sII hydrate stoichiometric concentration, THF·17H<sub>2</sub>O, was provided. It described the congruent (melting of hydrate to a single-phase liquid) melting temperature of the sII hydrate at pressures ranging from atmospheric pressure to 305 MPa. Only the sII THF·17H<sub>2</sub>O hydrate was observed in the experimental work.

Delahaye et al. (2006) measured hydrate dissociation conditions as well as heats of dissociation for the binary, sII hydrate of tetrahydrofuran (THF) and carbon dioxide (CO<sub>2</sub>).

A T-x diagram for the sII hydrate in the binary system, water-THF, at ambient pressure was presented.

Three-phase hydrate-liquid-vapour equilibrium data were reported for systems with aqueous phases containing 5.97 weight percent, 10.16 weight percent and 10.97 weight percent THF in the temperature range from 275 K to 292 K.

Sabil et al. (2010a,b) provided phase diagrams and hydrate dissociation enthalpies for the ternary system of water, tetrahydrofuran (THF) and carbon dioxide (CO<sub>2</sub>) at different overall compositions.

It was found that the H-L<sub>w</sub>-V equilibrium curve was (within the experimental accuracy) independent of the amount of CO<sub>2</sub> present in the system and thus mainly depended on the THF concentration in the aqueous phase.

The initial concentration of THF in the liquid phase had a large influence on the measured equilibrium pressures. Up to a concentration of 5 mole percent THF, the promoting effect increased. Increasing the THF concentration to 7 mole percent lowered the promoting effect compared to the system with 5 mole percent. However systems with 7 mole percent THF (in the aqueous phase) were still more promoting than systems with 3 mole percent THF.

At overall CO<sub>2</sub> concentrations of 19 and 29 mole percent, a pseudo-retrograde behaviour in the measured hydrate equilibrium pressure was observed in the four-phase region. Here an increase in pressure could both lower and increase the four-phase equilibrium temperature. For example at 19 mole percent CO<sub>2</sub> (overall), the four-phase H-L<sub>w</sub>-L<sub>a</sub>-V equilibrium temperature at P = 2.7 MPa was determined at 290.8 K. This temperature increased to 291.3 K at a pressure of 3.6 MPa. Increasing the pressure further to 4.2 MPa then lowered the four-phase equilibrium temperature to 290.7 K.

The enthalpy of dissociation for the pure carbon dioxide hydrate was estimated (calculated from equilibrium data via the Clausius-Clapeyron equation) to 56.9 and 75.4 kJ/mole at temperatures of 282.1 K and 273.2 K respectively. The general trend was decreasing enthalpy of dissociation with increasing temperature.

Papadimitriou et al. (2011) presented proof that tetrahydrofuran could promote the gas hydrate formed by helium.

The possibility of oxygen separation from atmospheric air by promoted hydrate formation was investigated by Yang et al. (2011). Dissociation pressures for oxygen + tetrahydrofuran + water, nitrogen + tetrahydrofuran + water and air + tetrahydrofuran + water were determined experimentally. Aqueous solutions containing approximately 5 mole percent THF were used. The phase boundary of the mixed hydrate of nitrogen and tetrahydrofuran was shown to shift approximately 26 K up in temperature in the investigated pressure range of 11-30 MPa. Similar results were found for the systems with oxygen and air. Promoted hydrates of oxygen were stabilised at lower pressures than those of nitrogen at similar temperatures. This was explained by oxygen being more suitable than nitrogen to stabilise the small cavity of the sII hydrate structure due to its more favourable size ratio (greater guest diameter to cage diameter ratio).

The combined promoting effect of tetrahydrofuran (THF) and sodium dodecyl sulphate (SDS) on carbon dioxide hydrates was investigated by Torr   et al. (2012)

at quiescent conditions (no induced mixing). The investigated THF concentrations were one and four weight percent.

No hydrates formed in systems without promoters, despite the system being cooled down into the sI hydrate stable region for carbon dioxide (down to 275 K at a pressure of approximately 2.1 MPa) and kept there for more than 540 minutes. Adding four percent THF to the system resulted in hydrate formation, however the growth rate quickly slowed down and hardly any pressure drop was observed. The system with both THF (4 weight percent) and SDS (0.3 weight percent) formed hydrates quickly and gas uptakes were significant. Adding only SDS provided no hydrates, however gas dissolution into the aqueous phase was speeded up.

### 3.3.2 Cyclopentane (CP)

Fan et al. (2001) presented Hydrate-Liquid water-Vapour equilibrium data for the pure sII cyclopentane clathrate hydrate formed in pure water. The reported equilibrium pressures were below atmospheric in the temperature range from approximately 273 K to 280 K.

Zhang and Lee (2009) measured four-phase (H-L<sub>w</sub>-L<sub>a</sub>-V) hydrate equilibrium data for mixed hydrates of cyclopentane (CP) with either hydrogen (H<sub>2</sub>) or carbon dioxide (CO<sub>2</sub>). The purpose was generating a thermodynamic basis for developing CO<sub>2</sub> capture or H<sub>2</sub> enriching processes by hydrate formation promoted by cyclopentane, a well-known sII hydrate former.

Equilibrium pressures were reported for the mixed CP/CO<sub>2</sub> sII hydrate in the temperature interval from 286.7 K to 292.6 K.

The melting point of the pure CP sII hydrate at atmospheric pressure was determined at 280.2 K.

The measured binary hydrate equilibrium data were compared with similar promoted hydrate systems from literature. For the binary CP/CO<sub>2</sub> hydrate, the measured formation temperatures were higher than both the TBAB and THF promoted systems in the pressure range, where literature data were available for comparison (pressures above 1.5 MPa).

Du et al. (2010) reported hydrate dissociation pressure data measured for hydrate systems of hydrogen, nitrogen and oxygen respectively, promoted by the presence of cyclopentane. Incipient hydrate formation conditions were measured in the four-phase equilibrium region.

At pressures of approximately 19 MPa, the temperature shift related to the addition of cyclopentane was about 25 K for both the nitrogen- and the oxygen system.

Pure oxygen formed hydrates at pressures slightly lower than pure nitrogen, the same applied in the promoted system, where the cyclopentane + oxygen system formed mixed hydrates at slightly lower pressures than the cyclopentane + nitrogen system.

Chen et al. (2011) investigated the effect of NaCl addition to hydrate forming systems of cyclopentane and methane. It was shown that adding NaCl to the hydrate forming system has an inhibiting effect on the measured hydrate dissociation pressures. Increasing electrolyte concentration in the range from 3.5 weight percent to 10 weight percent provided increasing inhibition. The inhibiting effect was the most pronounced at high temperatures.

Galfré et al. (2011) presented a study on both thermodynamics and kinetics of carbon dioxide hydrate formation promoted by the presence of cyclopentane. Both a bulk liquid-liquid system and an emulsified liquid system (using the surfactant, IPE 202) was investigated. Gas hydrates were formed in the ternary system {water + cyclopentane + CO<sub>2</sub>} at pressures below 0.2 MPa at temperatures above 280 K.

For the emulsified system, it was shown that induction times decreased with increasing cyclopentane content. Similarly, the total heat development associated with the crystallisation increased with increasing cyclopentane content. Growth rates were fast in the beginning, incorporating significant amounts of carbon dioxide in the hydrate phase. The pressure drop caused by hydrate formation however quickly stagnated as the emulsion became more concentrated (slurry) and particles started agglomerating on the walls of the equilibrium cell (slowing down the cooling supply).

### **3.4 Experimental Observations on Kinetics**

Conrad et al. (2009) investigated whether hydrate formation/nucleation should be described using stochastic formation models rather than by assuming hydrate precursors. By comparing Raman measurements of liquid mixtures of tetrahydrofuran (THF) and water in the stoichiometric sII hydrate composition of 1:17, at temperatures above and below the hydrate stability temperature of 277 K at atmospheric pressure, Conrad et al. found no signs of hydrate precursors in the subcooled liquid phase and thus concluded that hydrate formation should be considered a stochastic phenomenon.

Wilson and Haymet (2010) investigated the postulations in literature about memory effects in hydrate formation and re-formation. They found no clear evidence of a memory effect in the binary system of tetrahydrofuran and water. Stoichiometric concentrations (5.6 mole percent THF) were used and several repetitions of cooling/heating were performed.

The formation process of pure cyclopentane hydrate formed in water-in-oil emulsions was studied by Karanjkar et al. (2012). A differential scanning calorimeter (DSC) was used for this analysis. Emulsions were formed by the use of the Span 80 non-ionic surfactant.

It was shown that cyclopentane hydrate formation is an interfacial process. Contact surface area plays a key role in the formation process, and an increased amount of hydrate formed in the emulsified system compared to systems with two distinct liquid phases.

It was found that without the use of surfactants, a thin hydrate layer quickly formed and covered the liquid-liquid interface, slowing down transport of cyclopentane by diffusion to the water-rich liquid phase. At the presence of oil-soluble surfactants, the growth mechanism was changed dramatically. Here hydrate crystals grew and merged into the bulk water liquid-phase, rather than covering the surface, resulting in higher water conversions and a larger range of crystal particle sizes formed.

The ternary system of water, cyclopentane and Krypton was investigated for hydrate crystal growth behavior by Ishida et al. (2012). The hydrate growth mechanism was found to depend on the applied pressures and driving forces. In gas/liquid and liquid/liquid systems at low pressures/low driving forces, hydrate crystals formed were relatively large and robust. At higher driving forces, the crystals became dendritic of type.

Ishida et al. (2012) used the above observations to explain their results. At low pressure and low driving forces (8.9 K), hydrate crystals grew on the liquid-liquid surface, ending up covering the entire water droplet, slowing down the growth. The slow-down effect was explained by the crystals being dense, blocking for transport of hydrate former into the bulk water. At higher pressures and higher driving forces, it was suggested that the porosity of the hydrate layer formed on the surface of the liquid droplet allowed for transport through the hydrate shell by capillary forces. Hence the crystal growth could continue. At very high driving forces (11.8 K), the water droplet burst due to the hydrate crystals forming on the surface. The pressure ranges investigated were typically from 0.6 MPa to 6.4 MPa.

By use of Raman spectroscopy Lo et al. (2012) investigated the mechanisms of kinetic hydrate promotion by the use of SDS.

Two systems were investigated, the THF-water system and the cyclopentane-water system. It was suggested that for the THF system, SDS reduces the interfacial tension between hydrates and liquid allowing for faster crystallisation. SDS adsorbed on the hydrate crystal surface creating a hydrophobic surface, allowing for more hydrate formers to co-adsorb.

In the case of cyclopentane hydrates, the scenario was slightly different. Here the hydrate surface was only slightly hydrophobic.

It was found by the use of Surface-Enhanced Raman Spectroscopy (SERS) that in the vicinity of the liquid-liquid interface, water arranged itself around cyclopentane as in the sII hydrate structure – even without added SDS. The addition of surfactant (SDS), increased the amount of clathrate like aggregates in the bulk aqueous phase, thereby significantly shortening the induction times. Similarly SDS increased the amount of clathrate like aggregates in the vicinity of the hydrate crystals, increasing growth rate.

Wang et al. (2012) showed that induction times for the THF hydrate formed from a stoichiometric THF solution (approximately 5.56 mole percent THF) could be shortened significantly by using zeolite nanocrystals as seed material.

Prasad et al. (2012) investigated the thermodynamic and kinetic effect of silica particles (50, 150 and 200 micrometers) on the formation, and dissociation characteristics of methane hydrates.

It was shown that the presence of the largest particles had no significant thermodynamic influence, however both nucleation and growth of the sI hydrate were accelerated compared to the pure water system. Also the methane release characteristics during hydrate dissociation were affected. Induction times increased at the presence of the smallest particles.

The kinetics of mixed hydrate formation of tetrahydrofuran and hydrogen was investigated in a stirred tank reactor by Veluswamy and Linga (2013). The effects of driving force, promoter concentration and surfactant addition (SDS) were illustrated.

Hydrate growth, calculated indirectly from reactor pressure drops, was shown to increase with increasing driving force up to a certain limit, hereafter, increasing the driving force (applied pressure at constant temperature) provided only little increases in hydrate growth. Driving force was shown to have little influence on the induction times.

For the THF concentration, it was shown that concentrations up to about 3.5 mole percent THF provided similar gas uptakes (slight decrease in growth with increasing concentration of THF), whereas 5 mole percent provided significantly higher conversion (gas uptakes). The 5 mole percent THF solution showed a two-stage growth path which was explained by a second nucleation taking place as the first growth slowed down.

No promoting effects on kinetics were found when adding SDS to this system at the investigated conditions.

Sefidroodi et al. (2013) studied the proposed “memory effect” in hydrate formation from cyclopentane-water mixtures at atmospheric pressure. Their results indicated a memory effect at low driving forces (subcooling of



approximately 2-3 degrees), where re-used water systems nucleated significantly faster than “fresh” water used for the first time to form hydrates. As subcooling increased, the memory effect became less pronounced.

### **3.5 Studies on CO<sub>2</sub> Capture by Hydrate Formation**

Tajima et al. (2004) performed an energy consumption evaluation for the process of separating carbon dioxide from nitrogen (simulated flue gas: CO<sub>2</sub>: 0.10, N<sub>2</sub>: 0.79, O<sub>2</sub>: 0.04, H<sub>2</sub>O: 0.07) using gas clathrate hydrate formation. A suggested process scheme was set up, where hydrates were formed in a hydrate reactor operating at 274 K and 14 MPa. Flue gas was supplied at 298 K and 0.1 MPa. The energy balance included compressing and cooling of flue gas, pumping of cooling fluids and heat supply to dissociate the formed hydrates in order to recover the captured carbon dioxide. Furthermore, energy was recovered from the treated off-gas through de-pressurisation in gas turbines. The actual thermodynamics and kinetics of the system were ignored, so the obtained results should be used with caution.

A 95 percent conversion of the carbon dioxide in the vapour phase to the hydrate phase was assumed. Furthermore, Tajima et al. (2004) assumed a 100 percent selectivity of carbon dioxide in the hydrate phase. When treating a flue gas flow rate of 1 million normal cubic meter per hour ( $1.0 \times 10^6 \text{ N m}^3\text{h}^{-1}$ ), corresponding to the flue gas emission from a 1000 MW thermal power plant (according to Tajima et al.), the estimated energy consumption was 158.4 MW, corresponding to 0.85 kWh/kg carbon dioxide. It was concluded that this process was not competitive with the conventional chemical solvent-based capture processes in terms of energy efficiency.

Kang and Lee (2000) investigated dissociation pressures hydrate compositions for the ternary system water-N<sub>2</sub>-CO<sub>2</sub> and the quaternary system water-THF-N<sub>2</sub>-CO<sub>2</sub>.

A simulated flue gas vapour phase containing initially 17 mole percent CO<sub>2</sub> could form hydrates at pressures of 0.475 MPa (275 K), if 1 mole percent THF was added to the aqueous liquid phase. The equilibrium pressure for this system without the addition of THF was measured to 8.35 MPa (275 K).

The CO<sub>2</sub> selectivity in the hydrate phase was lowered by the addition of THF, compared to the un-promoted system. Moreover, CO<sub>2</sub> selectivity was lowered with increasing temperature. Kang and Lee (2000) concluded that in the system with 1 mole percent THF in the aqueous phase, a simulated flue gas phase initially containing 17 mole percent CO<sub>2</sub>, would form hydrates containing appr. 35 mole percent CO<sub>2</sub> on a THF- and water-free basis. At a temperature of 280K, the flue gas would need pressurisation to 1.65 MPa for hydrates to form.

From their results, Kang and Lee (2000) proposed a capture process in three hydrate formation/dissociation stages. In the first step, 1 mole percent THF should be used as a thermodynamic hydrate promoter. In the second and third step, no promoter should be added, in order to increase CO<sub>2</sub> selectivity. Intermediate vapour phase compression between capture stages would be necessary in the proposed purification process.

Kang et al. (2001) measured three-phase hydrate-liquid-vapour (H-L-V) equilibria in the ternary system of water, carbon dioxide (CO<sub>2</sub>) and nitrogen (N<sub>2</sub>), as well as in the quaternary system of water, tetrahydrofuran (THF), CO<sub>2</sub> and N<sub>2</sub>. The work was conducted in the attempt of proposing a novel process for flue gas separation by gas hydrate formation. This process had already been proposed by Spencer (1996, 2000), however Kang et al. (2001) proposed THF as a potential hydrate promoter.

Hydrate equilibrium data from an extensive study of the ternary system. H-L-V equilibrium pressures and hydrate phase compositions were presented for a large temperature, pressure and composition range.

It was concluded that CO<sub>2</sub> selectivity in the hydrate phase at constant vapour phase composition was increased by decreasing temperature in the ternary system.

Aqueous solutions containing 1 mole percent and 3 mole percent THF were investigated for thermodynamic promotion of hydrate formation from synthetic flue gasses containing 17 and 70 (initial concentration – balanced with N<sub>2</sub>) mole percent CO<sub>2</sub> respectively. It was found that the highest concentration of THF provided the largest promoting effect.

Seo et al. (2005) presented experimental hydrate dissociation pressures and hydrate compositions measured for four mixtures of carbon dioxide and nitrogen (mole fraction of carbon dioxide; 0.10, 0.17, 0.35 and 0.50). The hydrates were formed in water-saturated silica gels with average pore sizes of approximately 30 nm. By comparison of pure carbon dioxide hydrates formed in a bulk aqueous phase with those formed in the silica gels, Seo et al. concluded that the silica gels had a minor thermodynamic inhibiting effect on the hydrate equilibrium conditions.

Forming hydrates in the silica gel from a vapour phase initially containing a 10 mole percent carbon dioxide provided a water-free hydrate carbon dioxide mole fraction of 0.46, whereas the final carbon dioxide mole fraction in the released vapour phase was approximately 0.88, when the initial mole fraction was 0.50.

A final result from their experiments was the investigation of water conversion inside the silica gels. Seo et al. (2005) concluded that hydrate formation occurred much faster inside the silica gel pores than in a bulk aqueous phase.

Linga et al. (2007a) presented results from a kinetic study of gas hydrate formation from gas mixtures of CO<sub>2</sub>/H<sub>2</sub> and CO<sub>2</sub>/N<sub>2</sub>. An operating temperature of 273.7 K was applied in their experiments.

For the ternary system of water in contact with a 0.169 mole percent CO<sub>2</sub>/0.831 mole percent N<sub>2</sub> gas mixture, Linga et al. (2007a) presented induction times, and formation rates (for the first 20 minutes of crystallisation) at three applied driving forces, 1.3, 2.3 and 3.3 MPa.

Formation rates increased with increasing driving force. However it was shown that CO<sub>2</sub> selectivity decreased with increasing driving force.

Preliminary results of CO<sub>2</sub> capture by hydrate formation utilising an aqueous phase containing 1 mole percent tetrahydrofuran (THF) were shown. While the equilibrium pressure and induction times were lowered dramatically by this additive, the gas consumption became considerably lower, when adding the thermodynamic promoter at similar applied driving forces.

Linga et al. (2007b) presented a thermodynamic and kinetic study of CO<sub>2</sub> capture, both pre- and post-combustion. Gas mixtures containing H<sub>2</sub> and CO<sub>2</sub> or N<sub>2</sub> and CO<sub>2</sub> were contacted with pure water in the attempt to establish a thermodynamic and kinetic basis for the new CO<sub>2</sub> capture process. Linga et al. (2007b) chose to form hydrates just above the normal ice point of water in order to minimise flue gas compression costs.

A gas mixture containing 16.9 mole percent CO<sub>2</sub> and 83.1 mole percent N<sub>2</sub> was used to simulate the post combustion scenario. A hydrate equilibrium pressure of 7.7 MPa at a temperature of 273.8 K was determined for this gas mixture.

In order to establish hydrate formation rate data (kinetic data), a constant driving force (over-pressure compared to the equilibrium pressure) of 2.3 and 3.3 MPa was applied. Gas consumptions at isobaric condition were recorded over a time period of 120 minutes. It was found that an increase in driving force for crystallisation lowered the overall process selectivity towards CO<sub>2</sub>. Hence even though the crystallisation rate was increased, less CO<sub>2</sub> was transferred into the hydrate phase. When dissociating the formed hydrate phases, gas mixtures containing between 55 mole% and 57 mole% CO<sub>2</sub> were released. After 120 minutes of hydrate formation the vapour phase CO<sub>2</sub> content had been lowered from the initial 16.9 mole percent to approximately 10 mole percent

In the pre- combustion CO<sub>2</sub> capture scenario, a flue gas from an integrated coal gasification cycle (IGCC) was simulated. Hydrate formation from a gas containing 39.2 mole percent CO<sub>2</sub> and 60.8 mole percent H<sub>2</sub> was investigated. This gas mixture formed hydrates with pure water at a pressure of 5.1 MPa for the chosen operating temperature of 273.8 K. In the growth rate experiments, constant driving forces of 2.4 and 3.4 MPa were applied for approximately 100 minutes. Gas hydrates containing approximately 85 mole percent CO<sub>2</sub> were formed. Like in

the post-combustion case, increasing driving force lowered CO<sub>2</sub> selectivity in the hydrate phase.

Linga et al. (2007c) reported thermodynamic equilibrium data (temperature/pressure/composition) as well as kinetics of hydrate formation for the quaternary system water-tetrahydrofuran (THF)-nitrogen (N<sub>2</sub>)-carbon dioxide (CO<sub>2</sub>). The main purpose was setting up a block flow diagram for post combustion carbon dioxide capture from power station flue gasses.

A simulated flue gas containing 16.9 mole percent carbon dioxide 83.1 mole percent nitrogen was utilised. Three concentrations of THF were tested, 0.5, 1.0 and 1.5 mole percent. Promoted hydrate equilibrium data corresponded well with those presented by Kang and Lee (2000) and Kang et al. (2001) at similar conditions. The system with 1.5 mole percent THF formed hydrates already at ambient pressure at a temperature of 273.8 K.

Kinetic experiments were conducted at a temperature of 273.8 K except for the system with 1.5 mole percent THF, where the temperature was raised to 274.3 K in order to avoid hydrate formation at ambient pressure. Driving forces ranging from 0.7 MPa to 2.3 MPa were utilised. It was shown that induction times for hydrate formation depended both on applied driving force and THF concentration in the liquid phase. Induction times between 0.3 minutes and 7 minutes were reported. By utilising a driving force of 2.3 MPa and a THF concentration of 1.5 mole percent, induction times for hydrate formation of approximately 0.3 minutes were achieved.

Linga et al. (2007c) found that hydrate formation rates (gas uptake over the first 20 minutes of crystallisation) depended on both applied driving force and THF concentration. Whereas the gas uptake was increased by increasing the applied driving force, increasing THF concentration to more than 1 mole percent resulted in a decrease in gas uptake in the initial hydrate growth. The highest gas uptakes were obtained by utilising an initial concentration of 1 mole percent THF in the aqueous phase.

Linga et al. (2007c) suggested a separation process operating at a temperature of 273.8K and a constant pressure of 2.5 MPa. It was claimed that the carbon dioxide could be purified to a composition of approximately 94 mole percent in three separation stages, if a 1 mole percent THF aqueous phase was utilised in all three steps.

Duc et al. (2007) measured hydrate formation from a simulated flue gas containing N<sub>2</sub> and CO<sub>2</sub>. The need for thermodynamic promoters in order to make this capture process financially feasible was illustrated. Tetra-n-butyl ammonium bromide (TBAB – (C<sub>4</sub>H<sub>9</sub>)<sub>4</sub>-N-Br) was suggested as a thermodynamic promoter.

Euilibrium data for the mixed TBAB/CO<sub>2</sub>/N<sub>2</sub> semi-clathrate hydrate was presented for initial liquid phase TBAB concentrations ranging from 0.29 mole

percent to 9.4 mole percent and initial CO<sub>2</sub> vapour phase concentrations ranging from 15.5 mole percent to 23.4 mole percent. The investigated temperature interval ranged from 277 K to 295 K. Lower temperatures were avoided in order to avoid entering the stable region of the pure TBAB semi-clathrate hydrate.

Based on the thermodynamic results, a CO<sub>2</sub> capture process was simulated in order to estimate energy penalties as well as equipment sizes/costs in the CO<sub>2</sub> capture plant. A flue gas from a steel making blast furnace was utilised as a case study. It was concluded that CO<sub>2</sub> capture by hydrate formation, even with the use of thermodynamic promoters, are preferably to be used in applications where the feed gas is delivered at high pressures and with high initial CO<sub>2</sub> concentrations.

Zhang et al. (2009) investigated hydrate formation in the quaternary system of water + cyclopentane + carbon dioxide + hydrogen in the temperature interval from approximately 284 K to 291K.

Increasing the relative carbon dioxide content in the vapour phase lowered the equilibrium pressure of the mixed hydrate phase. However, as temperatures approached the dissociation point of the pure cyclopentane hydrate at 0.1 MPa, this effect diminished due to the formation of the pure cyclopentane hydrate.

Lee et al. (2010b) presented experimental dissociation pressures and gas uptakes measured for mixed hydrates of hydrogen and carbon dioxide promoted with tetrahydrofuran (0.5, 1 and 3 mole percent THF).

The gas mixture was comprised of 39.9 mole percent carbon dioxide and 60.1 mole percent hydrogen.

The reported pressure reduction on the mixed hydrates was the highest in the system with 3 mole percent THF. However, already with 1 mole percent THF in the initial aqueous solution, the mixed hydrate dissociation pressure at 278.7 K was reduced from about 11 MPa (without THF) to 1.87 MPa (with THF).

Kinetic studies showed that induction times decreased with increasing THF concentration, and with increasing driving force. Gas uptakes were the highest at a THF concentration of 1 mole percent. The 0.5 mole percent THF aqueous solution provided the lowest gas uptakes. The selectivities towards carbon dioxide in all experiments with similar driving forces (0.89 MPa) were much similar. The selectivity did however vary with the applied driving force. The composition of the gas captured in the experiments applying a driving force of 0.89 MPa ranged from 74 to 77 mole percent carbon dioxide. Increasing the driving force to 1.87 MPa provided a captured gas phase containing 86-88 mole percent carbon dioxide for the experiments using 1 and 3 mole percent THF aqueous solutions.

Li et al. (2010) studied the capture of carbon dioxide from simulated power station flue gasses (16.6 mole percent carbon dioxide, 83.4 mole percent nitrogen) in the quaternary system {water + cyclopentane + nitrogen + carbon dioxide} and in the corresponding modified system with an oil/water emulsifier (Tween 80)

added to it. The focus in their study was on the hydrate formation rates and the selectivity of CO<sub>2</sub> in the hydrate phase. It was shown that upon adding an emulsifier, the crystallisation rate was increased dramatically. However, a negative effect on CO<sub>2</sub> selectivity caused by the addition of the emulsifier was also reported.

For the system without emulsifier, the estimated carbon dioxide content in the hydrate phase was 37.5 to 44 mole percent depending on the applied driving force. For the emulsified system, the estimated hydrate (or emulsion) composition was 29 to 35 mole percent in terms of carbon dioxide.

Giavarini et al. (2010) performed a compositional analysis of systems forming mixed hydrates of carbon dioxide and nitrogen. The focus of the study was on the selectivity towards carbon dioxide and simultaneously investigating decomposition kinetics of the mixed hydrates.

Li et al. (2011) investigated gas uptakes by hydrate formation for the systems CO<sub>2</sub>/H<sub>2</sub>/CP/water, CO<sub>2</sub>/H<sub>2</sub>/TBAB/water and CO<sub>2</sub>/H<sub>2</sub>/CP/TBAB/water. It was shown that the gas uptake in the cyclopentane promoted system was the lowest. The TBAB promoted system provided significantly increased gas uptake at similar T/P conditions (274.7 K and 4.0 MPa). Finally, the mixed promoter system showed a synergistic effect, providing gas uptakes higher than the sum of the two pure promoter systems.

The selectivity of CO<sub>2</sub> in the hydrate phase was shown to depend slightly on the volumetric liquid loading in the equilibrium cell (with a constant CP/TBAB solution ratio of 0.05). Similarly, the selectivity decreased with increasing initial pressure (driving force).

On the mixed promoter system of TBAB and cyclopentane applied to CO<sub>2</sub> capture from fuel gasses (CO<sub>2</sub> + H<sub>2</sub>), Li et al. (2012) claimed that a synergetic effect may occur, whereby cyclopentane does not only form distinct sII hydrates, but also takes part in the semi-clathrate hydrate structure of TBAB and displaces some of the TBA<sup>+</sup> ions allowing for the formation of larger amounts of semi-clathrate hydrate. The increased gas uptake, higher than the sum of the reference systems, were explained by this fact. The reported selectivities of CO<sub>2</sub> over hydrogen were as large as 91.6 mole percent in the mixed hydrate phase for gas mixtures containing 38.6 mole percent carbon dioxide initially. The investigated system was initiated at T = 274.7 K and P = 4 MPa. 0.29 mole percent TBAB was dissolved in the aqueous phase and 5 volume percent (of the total liquid loading) cyclopentane liquid was added.

Park et al. (2013) investigated the separation of carbon dioxide from mixtures with hydrogen by hydrate formation inside porous silica gels. It was shown that the silica gels had a thermodynamic inhibiting effect on the hydrate formation, which depended on the pore size of the gel (in the range from 6 nm to 100 nm).

The formation conditions were inhibited up to 6-7 K at constant pressure in silica gels with pore sizes of 100 nm.

Water conversion by hydrate formation was however significantly enhanced compared to the bulk water system.

### **3.6 Summary**

This chapter presents an overview of experimental studies on gas hydrate promotion presented in the literature. Focus has mainly been on determining the types of promoters investigated and their effects on hydrate thermodynamics (pressure reduction). Kinetic aspects in hydrate formation (nucleation and growth) have also been discussed.

The present survey has been limited to consider mainly the promoters forming the classical gas clathrate hydrate structures (sI, sII and sH). The cited literature applies different approaches to analyse the aspects of hydrate promotion. Most studies present experimental determinations of hydrate thermodynamics and kinetics, however a few studies have investigated the promoting mechanisms by means of molecular simulation [Alavi and Ripmeester (2012), Atamas et al. (2013)].

It has been found that the sII and sH hydrate structures incorporating both large hydrate formers (such as e.g. tetrahydrofuran, cyclopentane, cyclohexane, methyl-cyclohexane etc.) and small hydrate formers (e.g. methane, nitrogen, carbon dioxide etc.) generally stabilise at temperature and pressure conditions that are milder (lower pressures and/or higher temperatures) than the sI hydrate.

Similarly, by comparing sII and sH hydrates incorporating the same gas species (e.g. methane), but being stabilised (promoted) by different hydrate formers (e.g. cyclopentane (sII) and methyl-cyclohexane (sH)), it has been found that the sII hydrate structure generally stabilises at milder conditions than the sH structure.

While the sII hydrate has the advantage of being stabilised at milder conditions than the sH hydrate, it has the disadvantage of lower gas capacity. From a gas capacity point of view the sH hydrate structure is the better choice, since the promoter occupies fewer of the hydrate cavities, leaving more empty cavities for the gas components. Hence, the choice of promoter must always be made according to specific needs and/or desires (pressure reduction or gas capacity).

It has been shown that the sII hydrate promoters, while excellent pressure reducers in systems where the gas phase components readily enters the small cavities of the sII hydrate structure, fail at promoting hydrate formation significantly in systems where the other hydrate formers do not easily enter the small cavities. This is explained by the fact that the sII hydrate structure is more

stable, if both the small and large cavities are partially (or fully) occupied. Ethane has been mentioned as an example of such a gas species.

A large number of heavy hydrocarbons have been shown to have pressure reducing effects on the formation of mixed hydrate with methane due to formation of sII or sH hydrates. Sloan and Koh (2007) have listed many of these. Since carbon dioxide, like methane, is able to enter the small cavities of the sII and sH hydrate structures, similar promoting effects are likely to be found, and have been found, for the many of the mixed hydrates with carbon dioxide and heavy promoters. The same applies for systems with nitrogen as the co-former.

Both experimental and theoretical studies have pointed out cyclopentane and tetrahydrofuran as two efficient pressure reducing additives in classical hydrate forming systems, where the gas phase component of interest readily stabilises the small cavities of the hydrate structure. Other components with slightly lower promoting effects are acetone, propane (gas phase additive at ambient conditions) or a range of quaternary ammonium salts (tetra-n-butyl ammonium halides such as e.g. TBAB, TBACl and TBAF) which form semi-clathrate hydrates.

In some experimental studies the promoting effects of tetrahydrofuran, cyclopentane and TBAB in their pressure reducing effects for hydrate formation with small gas phase components have been compared. It has been shown that while TBAB offers the lowest hydrate equilibrium pressures at moderate temperatures (typically below 286 K), the hydrate equilibrium pressures in these system increase significantly with temperature, and above 286 K, tetrahydrofuran and cyclopentane hydrates provide more stable hydrates.

In the remaining part of this work, only the two most promising pressure reducers of the classical hydrate formers, tetrahydrofuran and cyclopentane will be treated. These two components differ in their fluid phase behaviour in aqueous systems, however have similar properties in the hydrate phase.

Table 3.1 lists the studies found in the literature, presenting experimental hydrate dissociation pressure data for tetrahydrofuran promoted gas hydrate systems relevant to post-combustion CO<sub>2</sub> capture.



**Table 3.1.** Studies found in the literature, presenting experimental hydrate dissociation pressure data for tetrahydrofuran promoted gas hydrate systems relevant to post-combustion CO<sub>2</sub> capture.

Reference	Hydrate formers.
Seo et al. (2008)	Tetrahydrofuran + Carbon dioxide
Delahaye et al. (2006)	Tetrahydrofuran + Carbon dioxide
Sabil et al. (2010a)	Tetrahydrofuran + Carbon dioxide
Sabil et al. (2010b)	Tetrahydrofuran + Carbon dioxide
Mohammadi et al. (2010)	Tetrahydrofuran + Carbon dioxide
Lee et al. (2012)	Tetrahydrofuran + Carbon dioxide
Seo et al. (2001)	Tetrahydrofuran + Nitrogen
Mohammadi et al. (2010)	Tetrahydrofuran + Nitrogen
Yang et al. (2011)	Tetrahydrofuran + Nitrogen
Kang et al. (2001)	Tetrahydrofuran + Carbon dioxide + Nitrogen
Linga et al. (2007c)	Tetrahydrofuran + Carbon dioxide + Nitrogen

Table 3.2 lists the studies found in the literature, presenting experimental hydrate dissociation pressure data for cyclopentane promoted gas hydrate systems relevant to post-combustion CO<sub>2</sub> capture.

**Table 3.2.** Studies found in the literature, presenting experimental hydrate dissociation pressure data for cyclopentane promoted gas hydrate systems relevant to post-combustion CO<sub>2</sub> capture.

Reference	Hydrate formers.
Zhang and Lee (2009)	Cyclopentane + Carbon dioxide
Mohammadi and Richon (2009a)	Cyclopentane + Carbon dioxide
Tohidi et al. (1997)	Cyclopentane + Nitrogen
Du et al. (2010)	Cyclopentane + Nitrogen
Mohammadi and Richon (2011)	Cyclopentane + Nitrogen

Tetrahydrofuran is fully miscible with water at ambient conditions, but does show liquid-liquid split at elevated temperatures and pressures. Due to the miscibility of tetrahydrofuran and water, hydrate formation conditions often depend strongly on the amount of tetrahydrofuran present in the aqueous phase. It has been shown, like for most other water-soluble sII hydrate formers, that the highest pressure reduction is obtained for systems containing 5-6 mole percent promoter in the aqueous phase. This is often explained by the fact that a stoichiometric sII hydrate

phase, completely filled with promoter in the large cavities, contains 5.56 mole percent promoter.

Cyclopentane shows little solubility (ppm order of magnitude) in water under typical conditions of hydrate formation and thus forms an additional organic liquid phase when used in excess amounts. With excess cyclopentane present, the aqueous phase is always saturated with cyclopentane. Cyclopentane solubility in water also shows limited variation in cyclopentane concentration with changing temperature and pressure. For this reason, hydrate forming conditions are often independent or depend only little on the amount of cyclopentane present in the system.

From a kinetic point of view, the two hydrate formers also act different. Since tetrahydrofuran may be evenly distributed in the aqueous phase at the stoichiometric concentration, nucleation in THF promoted systems are often quick. The hydrate crystal growth has however been shown to slow down quickly. Hydrate growth rates in these systems may to some extent be increased by increasing the applied pressure (driving force).

Cyclopentane, due to its limited solubility, is available in lower amounts in the aqueous phase. Hence, the occurrence of clathrate like aggregates in the aqueous phase, combining to form the hydrate nucleus, becomes less probable from a statistical point of view. Thus, induction times are often high for cyclopentane promoted systems. Applying high driving forces, once the cyclopentane hydrate starts to form, crystal growth has been shown to occur at high rates.

Finally, the addition of surfactants, nano-particles and silica gels have been investigated as methods to speed up crystal growth rates and water conversion in hydrate forming systems. Some work still awaits in this field, before hydrate formation can occur sufficiently fast and with sufficient gas uptakes for this conceptual process to be commercially realisable.

### 3.7 Cited Literature

S. Alavi, J. A. Ripmeester, *Effect of small cage guests on hydrogen bonding of tetrahydrofuran in binary structure II clathrate hydrates*, Journal of Chemical Physics, 137-054712 (2012), 054712-1 – 054712-7.

R. Anderson, A. Chapoy, B. Tohidi, *Phase Relations and Binary Clathrate Hydrate Formation in the System H<sub>2</sub>-THF-H<sub>2</sub>O*, Langmuir, 23 (2007), 3440-3444.

A. A. Atamas, H. M. Cuppen, M. V. Koudriachova, S. W. de Leeuw, *Monte Carlo Calculations of the Free Energy of Binary sII Hydrogen Clathrate Hydrates for Identifying Efficient Promoter Molecules*, J. Phys. Chem. B, 117 (2013), 1155-1165.

J. E. Callanan and E. D. Sloan, *Calorimetric Studies of Clathrate Hydrates*, Proceedings of the International Gas Research Conference, (1983), 1012-1021.

Z.-Y. Chen, Q.-P. Li, Z.-Y. Yan, K.-F. Yan, Z.-Y. Zeng, X.-S. Li, *Phase Equilibrium and Dissociation Enthalpies for Cyclopentane + Methane Hydrates in NaCl Aqueous Solutions*, J. Chem. Eng. Data, 55 (2010), 4444-4449.

V. D. Chari, D. V.S.G.K Sharma, P. S.R. Prasad, *Methane hydrate phase stability with lower mole fractions of tetrahydrofuran (THF) and tert-butylamine (t-BuNH<sub>2</sub>)*, Fluid Phase Equilibria, 315 (2012), 126-130.

H. Conrad, F. Lehmkuhler, C. Sternemann, A. Sakko, D. Paschek, L. Simonelli, S. Huotari, O. Feroughi, M. Tolan, K. Hämäläinen, *Tetrahydrofuran Clathrate Hydrate Formation*, Physical Review Letters, 103 (2009), 218301-1 – 218301-4.

A. Danesh, B. Tohidi, R. W. Burgass, A. C. Todd, *Benzene Can Form Gas Hydrates*, Trans. IChemE., 71 (A) (1993), 457-459.

A. Danesh, B. Tohidi, R. W. Burgass, A. C. Todd, *Hydrate Equilibrium Data of Methyl Cyclopentane With Methane or Nitrogen*, Trans IChemE, 72 Part A (1994), 197-200.

C. F. Da Silva Lirio, F. L. P. Pessoa, A. M. C. Uller, *Storage capacity of carbon dioxide hydrates in the presence of sodium dodecyl sulfate (SDS) and tetrahydrofuran (THF)*, Chem. Eng. Sci., 96 (2013), 118-123.

R. M. de Deugd, M. D. Jager, J. de Swaan Arons, *Mixed Hydrates of Methane and Water-Soluble Hydrocarbons Modeling of Empirical Results*, AIChE Journal, 47 No. 3 (2001), 693-704.

A. Delahaye, L. Fournaison, S. Marinhas, I. Chatti, J.-P. Petitet, D. Dalmazzone, W. Fürst, *Effect of THF on Equilibrium Pressure and Dissociation Enthalpy of CO<sub>2</sub> Hydrates Applied to Secondary Refrigeration*, Ind. Eng. Chem. Res., 45 (2006), 391-397.

J. Du, D. Liang, D. Li, X. Li, *Experimental Determination of the Equilibrium Conditions of Binary Gas Hydrates of Cyclopentane + Oxygen, Cyclopentane + Nitrogen, and Cyclopentane + Hydrogen*, Ind. Eng. Chem. Res., 49 (2010), 11797-11800.

N. H. Duc, F. Chauvy, J.-M. Herri, *CO<sub>2</sub> capture by hydrate crystallization – A potential solution for gas emission of steelmaking industry*, Energy Conversion and Management, 48 (2007), 1313-1322.

- Yu. A. Dyadin, F. V. Zhurko, I. V. Bondaryuk, G. O. Zhurko, *Clathrate Formation in Water – Cyclic Ether Systems at High Pressures*, J. of Inclusion Phenomena and Molecular Recognition in Chemistry, 10 (1991), 39-56.
- A. Eslimimanesh, A. H. Mohammadi, D. Richon, P. Naidoo, D. Ramjugernath, *Application of gas hydrate formation in separation processes: A review of experimental studies*, J. Chem. Thermodynamics, 46 (2012), 62-71.
- S. S. Fan, D. Q. Liang and K. H. Guo, Hydrate Equilibrium Conditions for Cyclopentane and a Quarternary Cyclopentane-Rich Mixture, J. Chem. Eng. Data, 46 (2001), 930-932.
- A. Galfré, A. Fezoua, Y. Ouabbas, A. Camairao, J.-M. Herri, *Carbon dioxide hydrates crystallisation in emulsion*, Proceedings of the 7<sup>th</sup> Int. Conf. on Gas Hydrates (2011), Paper ID 442.
- C. Giavarini, F. Maccioni, M. L. Santarelli, *CO<sub>2</sub> sequestration from coal fired power plants*, Fuel, 89 (2010), 623-628.
- S. R. Gough and D. W. Davidson, *Composition of Tetrahydrofuran Hydrate and the Effect of Pressure on the Decomposition*, Can. J. Chem, 49-16 (1971), 2691-2699.
- M. Imai, Y. Oto, S. Nitta, S. Takeya, R. Ohmura, *Phase equilibrium for structure II clathrate hydrates formed with (fluoromethane + propan-2-ol, 2-methyl-2-propanol, or 2-propanone)*, J. Chem. Thermodynamics, 47 (2012), 17-20.
- Y. Ishida, Y. Takahashi, R. Ohmura, *Dynamic Behavior of Clathrate Hydrate Growth in Gas/Liquid/Liquid System*, Cryst. Growth Des., 12 (2012), 3271-3277.
- M. D. Jager, R. M. de Deugd, C. J. Peters, J. de Swaan Arons, E. D. Sloan, *Experimental determination and modeling of structure II hydrates in mixtures of methane + water + 1,4-dioxane*, Fluid Phase Equilibria, 165 (1999), 209-223.
- S.-P. Kang and H. Lee, *Recovery of CO<sub>2</sub> from Flue Gas Using Gas Hydrate: Thermodynamic Verification through Phase Equilibrium Measurements*, Environ. Sci. Technol., 34 (2000), 4397-4400.
- S.-P. Kang, H. Lee, C.-S. Lee, W.-M. Sung, *Hydrate phase equilibria of the guest mixtures containing CO<sub>2</sub>, N<sub>2</sub> and tetrahydrofuran*, Fluid Phase Equilibria, 185 (2001), 101-109.

- P. U. Karanjkar, J. W. Lee, J. F. Morris, *Calorimetric investigation of cyclopentane hydrate formation in an emulsion*, Chemical Engineering Science, 68 (2012), 481-491.
- A. A. Khokhar, J. S. Gudmundsson, E. D. Sloan, *Gas Storage in Structure H Hydrates*, Fluid Phase Equilibria, 150-151 (1998), 383-392.
- H. Komatsu, H. Yoshioka, M. Ota, Y. Sato, M. Watanabe, R. L. Smith Jr., C. J. Peters, *Phase Equilibrium Measurements of Hydrogen – Tetrahydrofuran and Hydrogen – Cyclopentane Binary Clathrate Hydrate Systems*, J. Chem. Eng. Data, 55 (2010), 2214-2218.
- J.-W. Lee, H. Lu, I. L. Moudrakovski, C. I. Ratcliffe, J. A. Ripmeester, *Thermodynamic and Molecular-Scale Analysis of New Systems of Water-Soluble Hydrate Formers + CH<sub>4</sub>*, J. Phys. Chem. B, 114 (2010a), 13393-13398.
- H. J. Lee, J. D. Lee, P. Linga, P. Englezos, Y. S. Kim, M. S. Lee, Y. D. Kim, *Gas hydrate formation process for pre-combustion capture of carbon dioxide*, Energy, 35 (2010b), 2729-2733.
- Y.-J. Lee, T. Kawamura, Y. Yamamoto, J.-H. Yoon, *Phase Equilibrium Studies of Tetrahydrofuran (THF) + CH<sub>4</sub>, THF + CO<sub>2</sub>, CH<sub>4</sub> + CO<sub>2</sub> and THF + CO<sub>2</sub> + CH<sub>4</sub> Hydrates*, J. Chem. Eng. Data, 57 (2012), 3543-3548.
- S. Li, S. Fan, J. Wang, X. Lang, Y. Wang, *Clathrate Hydrate Capture of CO<sub>2</sub> from simulated Flue Gas with Cyclopentane/Water Emulsion*, Chinese Journal of Chemical Engineering, 18, 2 (2010), 202-206.
- X.-S. Li, C.-G. Xu, Z.-Y. Chen, H.-J. Wu, *Hydrate-based pre-combustion carbon dioxide capture process in the system with tetra-n-butyl ammonium bromide solution in the presence of cyclopentane*, Energy, 36 (2011), 1394-1403.
- X.-S. Li, C.-G. Xu, Z.-Y. Chen, J. Cai, *Synergic effect of cyclopentane and tetra-n-butyl ammonium bromide on hydrate-based carbon dioxide separation from fuel gas mixture by measurements of gas uptake and X-ray diffraction patterns*, International Journal of Hydrogen Energy, 37 (2012), 720-727.
- P. Linga, R. Kumar, P. Englezos, *Gas hydrate formation from hydrogen/carbon dioxide and nitrogen/carbon dioxide gas mixtures*, Chemical Engineering Science, 62 (2007a), 4268-4276.
- P. Linga, R. Kumar, P. Englezos, *The clathrate hydrate process for post and pre-combustion capture of carbon dioxide*, J. of Hazardous Materials, 149 (2007b), 625-629.

- P. Linga, A. Adeyemo, P. Englezos, *Medium-Pressure Clathrate Hydrate/Membrane Hybrid Process for Postcombustion Capture of Carbon Dioxide*, Environ. Sci. Technol., 42 (2007c), 315-320.
- C. Y. Lo, P. Somasundaran, J. W. Lee, *Quick Assessment of Potential Hydrate Promoters for Rapid Formation*, Geomaterials, 2 (2012), 63-69.
- T. Maekawa, *Equilibrium conditions of clathrate hydrates formed from carbon dioxide and aqueous acetone solutions*, Fluid Phase Equilibria, 303 (2011), 76-79.
- S. Mainusch, C. J. Peters, J. de Swaan Arons, *Experimental Determination and Modeling of Methane Hydrates in Mixtures of Acetone and Water*, J. Chem Eng. Data, 42 (1997), 948-950.
- A. H. Mohammadi, D. Richon, *Phase equilibria of clathrate hydrates of methyl cyclopentane, methyl cyclohexane, cyclopentane or cyclohexane + carbon dioxide*, Chemical Engineering Science, 64 (2009a), 5319-5322.
- A. H. Mohammadi, D. Richon, *Phase Equilibria of Clathrate Hydrates of Cyclopentane + Hydrogen Sulfide and Cyclopentane + Methane*, Ind. Eng. Chem. Res., 48 (2009b), 9045-9048.
- A. H. Mohammadi, J. F. Martinez-López, D. Richon, *Determining phase diagrams of tetrahydrofuran+methane, carbon dioxide or nitrogen clathrate hydrates using an artificial neural network algorithm*, Chem. Eng. Sci., 65 (2010), 6059-6063.
- A. H. Mohammadi, D. Richon, *Phase equilibria of binary clathrate hydrates of nitrogen + cyclopentane/cyclohexane/methyl cyclohexane and ethane + cyclopentane/cyclohexane/methyl cyclohexane*, Chem. Eng. Science, 66 (2011), 4936-4940.
- A. H. Mohammadi, D. Richon, *Phase equilibria of neohexane/methyl cyclopentane + nitrogen clathrate hydrates*, Fluid Phase Equilibria, 348 (2013), 79-82.
- M. M. Mooijer-van den Heuvel, C. J. Peters, J. de Swaan Arons, *Influence of water-insoluble organic components on the gas hydrate equilibrium conditions of methane*, Fluid Phase Equilibria, 172 (2000), 73-91.
- H.-J. Ng and D. B. Robinson, *New Developments in the Measurement and Prediction of Hydrate Formation for Processing Needs*, Ann. N. Y. Acad. Sci., 715 (1996), 450-462.

R. Ohmura, S. Matsuda, S. Takeya, T. Ebinuma, H. Narita, *Phase Equilibrium for Structure-H Hydrates Formed with Methane and Methyl-Substituted Cyclic Ether*, Int. J. of Thermophysics, 26 No. 5 (2005), 1515-1523.

N. I. Papadimitriou, I. N. Tsimpanogiannis, A. K. Stubos, A. Martin, L. J. Rovetto, L. J. Florusse, C. J. Peters, *Experimental and Computational Investigation of the sII Binary He-THF Hydrate*, J. Phys. Chem. B, 115 (2011), 1411-1415.

S. Park, S. Lee, Y. Lee, Y. Lee, Y. Seo, *Hydrate-based pre-combustion capture of carbon dioxide in the presence of a thermodynamic promoter and porous silica gels*, International Journal of Greenhouse Gas Control, 14 (2013), 193-199.

B. Partoon, J. Javanmardi, *Effect of Mixed Thermodynamic and Kinetic Hydrate Promoters on Methane Hydrate Phase Boundary and Formation Kinetics*, J. Chem. Eng. Data, 58 (2013), 501-509.

P. S. R. Prasad, V. D. Chari, D. V. S. G. K. Sharma, S. R. Murthy, *Effect of silica particles on the stability of methane hydrates*, Fluid Phase Equilibria, 318 (2012), 110-114.

M. Ricaurte, C. Dicharry, D. Broseta, X. Renaud, J.-P. Torr , *CO<sub>2</sub> Removal from a CO<sub>2</sub>-CH<sub>4</sub> Gas Mixture by Clathrate Hydrate Formation Using THF and SDS as Water-Soluble Hydrate Promoters*, Ind. Eng. Chem. Res., 52 (2013), 899-910.

J. A. Ripmeester, C. I. Ratcliffe, *<sup>129</sup>Xe NMR Studies of Clathrate Hydrates: New Guests for Structure II and Structure H*, J. Phys. Chem, 94 (1990), 8773-8776.

K. M. Sabil, G.-J. Witkamp, C. J. Peters, *Estimations of enthalpies of dissociation of simple and mixed carbon dioxide hydrates from phase equilibrium data*, Fluid Phase Equilibria, 290 (2010a), 109-114.

K. M. Sabil, G.-J. Witkamp, C. J. Peters, *Phase equilibria in ternary (carbon dioxide + tetrahydrofuran + water) system in hydrate-forming region: Effects of carbon dioxide concentration and the occurrence of pseudo-retrograde hydrate phenomenon*, J. Chem. Thermodynamics, 42 (2010b), 8-16.

Y. Saito, T. Kawasaki, T. Okui, T. Kondo, R. Hiraoka, *Methane storage in hydrate phase with water soluble guests*, Proceedings of the 2<sup>nd</sup> International Conference on Natural Gas Hydrates, (1996), 459-465.

H. Sefidroodi, E. Abrahamsen, M. A. Kelland, *Investigation into the strength and source of the memory effect for cyclopentane hydrate*, Chem. Eng. Sci., 87 (2013), 133-140.

Y.-T. Seo, S.-P. Kang, H. Lee, *Experimental determination and thermodynamic modeling of methane and nitrogen hydrates in the presence of THF, propylene oxide, 1,4-dioxane and acetone*, Fluid Phase Equilibria, 189 (2001), 99-110.

Y.-T. Seo, I. L. Moudrakovski, J. A. Ripmeester, J.-W. Lee, H. Lee, *Efficient Recovery of CO<sub>2</sub> from Flue Gas by Clathrate Hydrate Formation in Porous Silica Gels*, Environ. Sci. Technol., 39 (2005), 2315-2319.

Y. Seo, S.-P. Kang, S. Lee, H. Lee, *Experimental Measurements of Hydrate Phase Equilibria for Carbon Dioxide in the Presence of THF, Propylene Oxide, and 1,4-Dioxane*, J. Chem. Eng. Data, 52 (2008), 2833-2837.

J. J. Shin, Y.-J. Lee, J.-H. Im, K. W. Han, J.-W. Lee Y. Lee, J. D. Lee, W.-Y. Jang, J.-H. Yoon, *Thermodynamic stability, spectroscopic identification and cage occupation of binary CO<sub>2</sub> clathrate hydrates*, Chem. Eng. Sci., 64 (2009), 5125-5130.

W. Shin, S. Park, H. Ro, D.-Y. Koh, J. Seol, H. Lee, *Phase equilibrium measurements and the tuning behavior of new sII clathrate hydrates*, J. Chem. Thermodynamics, 44 (2012), 20-25.

E. D. Sloan, C. A. Koh, *Clathrate Hydrates of Natural Gases* 3<sup>rd</sup> Ed., CRC Press, Boca Raton, 2007.

D. F. Spencer, US Patent 5700311 (1996).

D. F. Spencer, U. S. Patent 6106595 (2000).

S. Subramanian, E. D. Sloan Jr., *Molecular Measurements of Methane Hydrate Formation*, Fluid Phase Equilibria, 158-160 (1999), 813-820.

A. K. Sum, R. C. Burruss, E. D. Sloan, Jr., *Measurement of Clathrate Hydrates via Raman Spectroscopy*, J. Phys. Chem. B, 101 (1997), 7371-7377.

Z.-G. Sun, S.-S. Fan, K.-H. Guo, L. Shi, Y.-K. Guo, R.-Z. Wang, *Gas Hydrate Phase Equilibrium Data of Cyclohexane and Cyclopentane*, J. Chem. Eng. Data, 47 (2002), 313-315.

C. Sun, W. Li, X. Yang, F. Li, Q. Yuan, L. Mu, J. Chen, B. Liu, G. Chen, *Progress in Research of Gas Hydrate*, Chinese Journal of Chemical Engineering, 19, 1 (2011), 151-162.



- Q. Sun, J. Dong, X. Guo, A. Liu, J. Zhang, *Recovery of Hydrogen from Coke-Oven Gas by Forming Hydrate*, Ind. Eng. Chem. Res., 51 (2012a), 6205-6211.
- Q. Sun, X. Guo, A. Liu, J. Dong, B. Liu, J. Zhang, G. Chen, *Experiment on the Separation of Air-Mixed Coal Bed Methane in THF Solution by Hydrate Formation*, Energy Fuels, 26 (2012b), 4507-4513.
- H. Tajima, A. Yamasaki, F. Kiyono, *Energy consumption estimation for greenhouse gas separation processes by clathrate hydrate formation*, Energy, 29 (2004), 1713-1729.
- B. Tohidi, A. Danesh, A. C. Todd, R. W. Burgass, *Equilibrium data and thermodynamic modeling of cyclohexane gas hydrates*, Chem. Eng. Sc., 51, 1 (1996), 159-163.
- B. Tohidi, A. Danesh, A. C. Todd, R. W. Burgass, K. K. Østergaard, *Equilibrium data and thermodynamic modelling of cyclopentane and neopentane hydrates*, Fluid Phase Equilibria, 138 (1997), 241-250.
- J.-P. Torré, M. Ricaurte, C. Dicharry, D. Broseta, *CO<sub>2</sub> enclathration in the presence of water-soluble hydrate promoters: Hydrate phase equilibria and kinetic studies in quiescent conditions*, Chem. Eng. Sci., 82 (2012), 1-13.
- A. T. Trueba, L. J. Rovetto, L. J. Florusse, M. C. Kroon, C. J. Peters, *Phase equilibrium measurements of structure II clathrate hydrates of hydrogen with various promoters*, Fluid Phase Equilibria, 307 (2011), 6-10.
- H. P. Veluswamy, P. Linga, *Macroscopic kinetics of hydrate formation of mixed hydrates of hydrogen/tetrahydrofuran for hydrogen storage*, Int. J. of Hydrogen Energy, 38 (2013), 4587-4596.
- Y. Wang, X. Lang, S. Fan, *Accelerated nucleation of tetrahydrofuran (THF) hydrate in presence of ZIF-61*, Journal of Natural Gas Chemistry, 21 (2012), 299-301.
- P. W. Wilson, S. D. J. Haymet, *Hydrate formation and re-formation in nucleating THF/water mixtures show no evidence to support a "memory" effect*, Chemical Engineering Journal, 161 (2010), 146-150.
- Z.-M. Xia, Z.-Y. Chen X.-S. Li, Y. Zhang, K.-F. Yan, Q.-N. Lv, G.-G. Xu, J. Cai, *Thermodynamic Equilibrium Conditions for Simulated Landfill Gas Hydrate Formation in Aqueous Solutions of Additives*, J. Chem. Eng. Data, 57 (2012), 3290-3295.

H. Yang, S. Fan, X. Lang, Y. Wang, *Phase Equilibria of Mixed Gas Hydrates of Oxygen + Tetrahydrofuran, Nitrogen + Tetrahydrofuran, and Air + Tetrahydrofuran*, J. Chem. Eng. Data, 56 (2011), 4152-4156.

H. Yang, S. Fan, X. Lang, Y. Wang, X. Sun, *Hydrate Dissociation Conditions for Mixtures of Air + Tetrahydrofuran, Air + Cyclopentane, and Air + Tetra-n-butyl Ammonium Bromide*, J. Chem. Eng. Data, 57 (2012), 1226-1230.

M. Yang, W. Liu, Y. Song, X. Ruan, X. Wang, J. Zhao, L. Jiang, Q. Li, *Effects of Additive Mixture (THF/SDS) on the Thermodynamic and Kinetic Properties of CO<sub>2</sub>/H<sub>2</sub> Hydrate in Porous Media*, Ind. Eng. Chem. Res., 52 (2013), 4911-4918.

J. S. Zhang, J. W. Lee, *Equilibrium of Hydrogen + Cyclopentane and Carbon Dioxide + Cyclopentane Binary Hydrates*, J. Chem. Eng. Data, 54 (2009), 659-661.

J. Zhang, P. Yedlapalli, J. W. Lee, *Thermodynamic analysis of hydrate-based pre-combustion capture of CO<sub>2</sub>*, Chemical Engineering Science, 64 (2009), 4732-4736.

D.-I. Zhong, K. Ding, C. Yang, Y. Bian, J. Ji, *Phase Equilibria of Clathrate Hydrates Formed with CH<sub>4</sub> + N<sub>2</sub> + O<sub>2</sub> in the Presence of Cyclopentane or Cyclohexane*, J. Chem. Eng. Data, 57 (2012), 3751-3755.

D.-L. Zhong, N. Daraboina, P. Englezos, *Recovery of CH<sub>4</sub> from coal mine model gas mixture (CH<sub>4</sub>/N<sub>2</sub>) by hydrate crystallization in the presence of cyclopentane*, Fuel, 106 (2013), 425-430.

K. K. Østergaard, B. Tohidi, R. W. Burgass, A. Danesh, A. C. Todd, *Hydrate Equilibrium Data of Multicomponent Systems in the Presence of Structure-II and Structure-H Heavy Hydrate Formers*, J. Chem. Eng. Data, 46 (2001), 703-708.

## 4 Experimental Work

Two experimental studies have been conducted as part of the present work. The first study was conducted in cooperation with and in the laboratories of the Centre Sciences des Processus Industriels et Naturels (SPIN) at l'Ecole Nationale Supérieure des Mines de Saint-Etienne, France. For the details of this study, please see Herslund et al. (2013) [Appendix 2]. The second study was conducted in the laboratories of the Center for Energy Resources Engineering (CERE), Department of Chemical and Biochemical Engineering at the Technical University of Denmark. The results obtained in this study are currently in preparation for publication in a journal.

Both studies investigated the thermodynamic promoting effect of tetrahydrofuran and cyclopentane respectively on the formation pressures of the carbon dioxide hydrate. In addition to the individually studied promoters (studied mainly to validate experimental equipment and procedures), a new thermodynamic promoter system has been proposed, incorporating the presence of both thermodynamic promoters simultaneously.

The reasoning behind the proposed system of mixed promoters is as follows; tetrahydrofuran is a potent thermodynamic promoter in terms of its pressure reducing capabilities. Due to its miscibility with water in the aqueous phase, it may be added to the aqueous phase to form a stoichiometric (hydrate phase) mixture. The high contents of tetrahydrofuran in the aqueous phase have been shown to provide short induction times for hydrate nucleation. The downside to using this promoter is that it often provides a slow hydrate growth once nucleation has occurred.

Cyclopentane is a hydrophobic compound, resulting in low mutual miscibility with water. Since the cyclopentane content in the aqueous phase is low, induction times become high in systems forming cyclopentane hydrates. Once the initial hydrate crystals have formed, the hydrate growth rate has been shown to be high, provided the overall system is sufficiently mixed.

By adding the two promoters simultaneously, a system providing the best of the two promoters is hoped for. The mixed promoter system should preferably provide similar or improved pressure reduction capabilities, short induction times and high crystal growth rates.

It has been shown experimentally that tetrahydrofuran in the aqueous phase acts as a co-solvent for cyclopentane, increasing its solubility in the aqueous phase [Appendix 2]. It is suspected that this can provide a thermodynamically more favourable system, resulting in lower pressure requirements for hydrate formation.

It can be argued that an increased promoter concentration in the aqueous phase lowers the water activity and thereby decreases the thermodynamic stability of the hydrate phase. In the cases of the water-soluble promoters such as e.g. tetrahydrofuran, increased pressure reduction is obtained for increasing promoter concentration up to approximately 5 mole percent.

Thus in the mixed promoter system, as we are only adding further amounts of promoter (both tetrahydrofuran and cyclopentane) to the aqueous phase, it is expected to provide a thermodynamically more favourable system. Obviously, an optimum will occur, where the addition of more tetrahydrofuran will start decreasing the thermodynamic stability of the hydrates.

Due to the differences mainly in the experimental techniques applied at the two research laboratories, the following sections are devoted to describing and discussing the experimental set-up's and procedures.

## **4.1 Experimental Set-up and Procedure #1**

Set-up #1 is located at Centre SPIN, l'Ecole des Mines de Saint-Etienne, France. This in fact consists of three equilibrium cells ranging in internal volumes from 1.35 dm<sup>3</sup> to 2.46 dm<sup>3</sup>. The cells are all operated with similar procedures, as described briefly in the following. For the complete and detailed descriptions of the individual set-ups, please see Appendix 2.

Hydrate equilibrium data are obtained by performing an isochoric temperature cycle manipulation. The system is initially evacuated and purged three times before loaded with the desired components and the cell is closed.

In the preparation of the initial aqueous liquid phase, a tracer is added. The tracer is added in the form of an electrolyte that will not be incorporated in the hydrate phase. In this work lithium nitrate or potassium nitrate are utilised for this purpose. The initial tracer concentration in the loaded aqueous phase is approximately 10 mg/dm<sup>3</sup>. At this concentration, the thermodynamic inhibiting effect on the hydrate formation is negligible. The tracer concentration is analysed by means of an ion exchange column for either Li<sup>+</sup> or NO<sub>3</sub><sup>-</sup>.

The cell is initially allowed to equilibrate in terms of temperature and pressure. Gas dissolution in the liquid phase(s) is seen as an initial decrease in pressure. The cell content is then cooled to conditions well inside the expected hydrate stability zone. Once hydrates form and the system equilibrates, three phases, a hydrate (H), an aqueous Liquid (L<sub>w</sub>) and a vapour (V) phase are typically present in the case of promoters being miscible with water. In the case of hydrophobic promoters which, upon mixing with water, exhibit liquid-liquid phase separation, four phases (hydrate (H), aqueous liquid (L<sub>w</sub>), organic liquid (L<sub>a</sub>), and vapour (V)) should be present in equilibrium at the desired hydrate forming conditions.

Cooling and stirring are activated until the system pressure and temperature have attained their equilibrium values. The time for system equilibration depends on the amount of sub-cooling for the system at the respective initial composition as well as on the particular system investigated.

Experiments in this set-up are carried out as “blind” experiments. Thus, the first hydrate formation is observed as a sudden temperature increase. This temperature rise is caused by the hydrate crystallisation process, which is an exothermic phase transition. The intensity of the temperature peak depends on the nature of the hydrate formation process (reaction rate and specific heat of crystallisation), which are system specific and also depend on the amount of hydrate former present in the aqueous phase. The crystallisation heat is rapidly removed by the cooling system, and the system continues to form hydrates. After some time, ranging from hours to days, the system attains its equilibrium state at the given temperature set-point.

At the initial equilibrium state, temperature and pressure are noted, and a liquid sample of approximately 1 mL is extracted from the aqueous liquid phase. If tetrahydrofuran is present, the tetrahydrofuran concentration in the liquid sample is determined by refractive index measurements at 298.2 K. Aqueous phases are always assumed to be saturated with cyclopentane, whenever cyclopentane is present. However, due to the low solubility of cyclopentane in the aqueous phase, its effect on the refractive index of the {H<sub>2</sub>O + tetrahydrofuran} system is assumed to be negligible. The tracer concentration in the extracted liquid sample is measured by ion exchange chromatography. The concentration of the tracer is used to estimate the amount of water converted into solids in the hydrate phase. The total amount of tracer lost in each extracted liquid sample is considered negligible when compared to the initial amount loaded into the reactor.

After extraction of the liquid sample, the temperature set-point on the cooling system is increased by 1 K and the system is allowed to reach the corresponding equilibrium state at this new temperature. In this way multiple equilibrium stages are recorded as the hydrates are progressively dissociated. Complete dissociation of hydrates is assumed once the pressure increase between each equilibrium stage becomes insignificant. Recorded temperatures and pressures from a complete hydrate dissociation run are illustrated in Figure 4.1. The system is a ternary mixture of water, tetrahydrofuran (approximately 5 mole percent in the initial aqueous phase) and carbon dioxide.

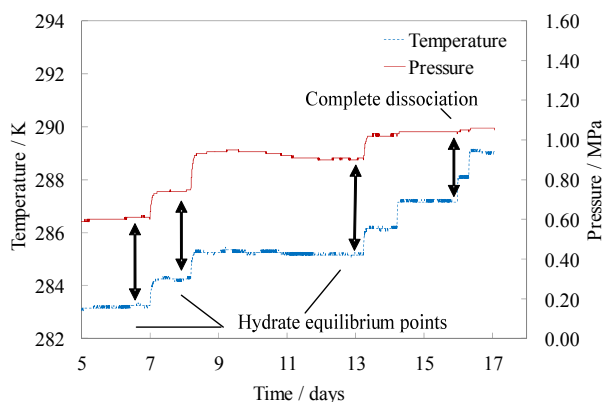


**Figure 4.1.** Typical recording of temperature and pressure as functions of time during hydrate dissociation. The dissociated hydrate is a mixed tetrahydrofuran/carbon dioxide hydrate. (Dotted line) Temperature / K, (Full line) Pressure / MPa.

The example of a typical hydrate dissociation illustrated in Figure 4.1 provides temperature/pressure conditions for three hydrate-liquid-vapour equilibrium stages. The exact position of the incipient hydrate formation pressure (last remaining crystal) for the ternary system with known feed composition is not accurately determined by this experimental procedure, since temperature increments of approximately 1 K are applied between each equilibrium stage.

## 4.2 Experimental Set-up and Procedure #2

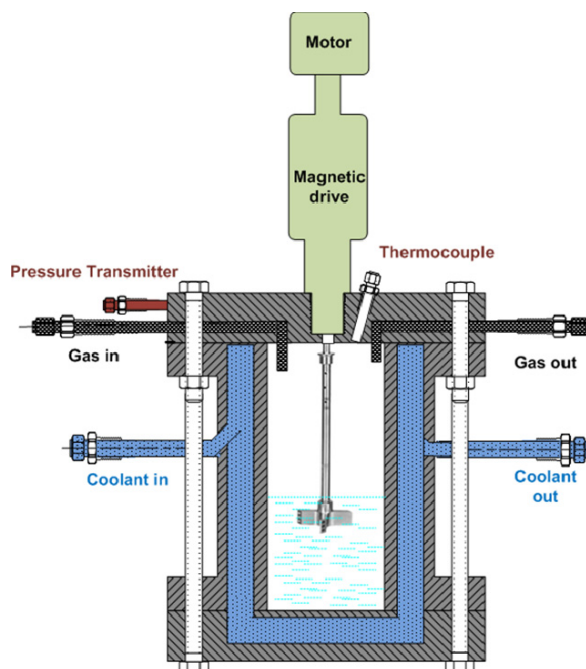
The experimental set-up #2 is located at the Department of Chemical and Biochemical Engineering at the Technical University of Denmark. Since this set-up and the experimental procedure have not yet been published outside of this thesis, it is described in detail in the following.

Figure 4.2 illustrates a schematic of the equilibrium cell utilised. It consists of a jacketed crystalliser, which is a cylindrical cell made of 316 stainless steel with an internal volume of 0.0665 dm<sup>3</sup>. The equilibrium cell has a maximum operative pressure of 15 MPa. The crystalliser is equipped with a magnetic stirrer (designed for maximum of 1500 rpm) with a stainless steel shaft (8 mm diameter) and impeller to enable proper mixing of gas and liquid(s) inside the cell.

The temperature of the equilibrium cell is controlled by continuous circulation of a water/glycol mixture (coolant) in a steel jacket surrounding the cell. The temperature of the coolant is controlled by an external cryostat in order to maintain constant temperature.

A pressure transducer with a maximum uncertainty of 0.075 percent in the working range up to 15 MPa is employed to monitor the pressure inside the cell. The temperature inside the cell is measured using a platinum resistance probe with an uncertainty of 0.01 K.

Two sapphire windows, mounted oppositely on the walls of the cell allow for visual inspection of crystal formation/decomposition inside the cell. The data acquisition system (Agilent Instruments) is coupled to a personal computer to record the data throughout the experimental procedure.



**Figure 4.2.** Schematic of the equilibrium cell in set-up #2. Drawing kindly supplied by Dr. Nagu Daraboina, Technical University of Denmark.

The isochoric temperature search method is applied to determine incipient hydrate formation conditions (formation/dissociation of first hydrate crystal). The cell is loaded with approximately 0.020 dm<sup>3</sup> of liquid and subsequently flushed three times with the experimental gas mixture to remove air from the cell. The system is pressurised by use of the experimental gas to a pressure of 1-2 MPa above to the expected incipient hydrate equilibrium pressure. The magnetic stirrer is activated to mix the solution throughout the experiment.

Once hydrate crystals have formed, the temperature is slowly increased, to the point where the crystals completely disappear. The temperature is then lowered to

form crystals again. This process is repeated several (three to four) times to remove the hysteresis associated with hydrate formation. Moreover, the initial equilibrium temperature and pressure is roughly estimated by this process.

After these temperature manipulations, the temperature in the equilibrium cell is decreased to approximately 0.1 K below the initially estimated dissociation point and small amounts of hydrate are allowed to form. If only traces of hydrate crystals are observed, the temperature is increased again by 0.1 K. If the hydrate crystals disappear, the low temperature point and the corresponding pressure is noted as an equilibrium point. If no hydrate crystals have formed 2 hours after the first equilibrated temperature and pressure, the temperature is decreased further 0.1 K. This process is repeated until an infinitesimal amount of hydrate is found to exist in equilibrium with the liquid and gas phases, and which dissociate upon heating by 0.1 K.

### **4.3 Discussion of Experimental Procedures**

The experimental procedure #1 of this work diverges from the isochoric temperature cycle procedure #2. Typically, when utilising the “traditional” isochoric temperature search method for hydrate formation experiments, only the last equilibrium stage, where the incipient hydrate crystal dissociates, is considered a true equilibrium stage. Nevertheless, Danesh et al. (1994) showed experimentally that intermediate heating stages may be regarded as true equilibrium pressures on the hydrate dissociation curve for univariant systems. Hence, the experimental procedure presented here is justified by their findings for the cyclopentane promoted system, provided that only the four-phase H-L<sub>w</sub>-L<sub>a</sub>-V equilibrium region is analysed.

In the case of the tetrahydrofuran promoted system, the H-L<sub>w</sub>-V equilibrium additionally depends on a second independent intensive variable, such as for example the concentration of tetrahydrofuran in the aqueous phase. Therefore, in these experiments, the tetrahydrofuran concentration in the liquid phase needs to be monitored and reported for each equilibrium stage, since this concentration may change during hydrate crystallisation/dissociation.

Under the assumption that all phases are allowed to equilibrate in terms of temperature, pressure and composition, the experimental procedure #1 should provide identical results to procedure #2, for the hydrate dissociation pressures. In addition to hydrate dissociation pressure, procedure #1 allows for a simultaneous estimation of hydrate composition by use of mass balance considerations, provided that suitable methods are available for analysing compositions and amounts of substance in the co-existing fluid phases.



Applying experimental procedure #1 for hydrate composition estimates should be done with caution. One has to make sure, all phases are fully equilibrated. Equilibration of the solid hydrate phase in terms of composition is expected to be a time consuming process due the slow characteristics of solid diffusion.

It is known that hydrates formed in some di-variant or multi-variant systems may obtain much different compositions depending on the compositions of the co-existing fluid phases. For this reason, in such systems the formed hydrates are expected to progressively change composition during the formation period, since the co-existing phases will continuously change compositions. If large amounts of hydrate are formed, it cannot be excluded that a concentration gradient will build up in the solid phase. The core of the hydrate particles may have significantly different composition than the outer shell. Thus at equilibrium, the “outer” part of the hydrate phase may be in equilibrium with the co-existing fluid phases, however the core may not necessarily, if the concentration gradient has not been aligned. Thus extra care must be taken, if hydrate composition is estimated using this approach. The fluid phase compositions should be continuously monitored to ensure fully stable conditions.

The possibility of a composition gradient in the hydrate phase is however expected to have negligible influence on the measured dissociation pressures, which are the only hydrate-related data reported in this work. As will be shown, results from this work compare well with those reported in the literature, coming from other experimental set-up's and techniques.

## 4.4 Cited Literature

A. Danesh, B. Tohidi, R. W. Burgass, A. C. Todd, *Hydrate Equilibrium Data of Methyl Cyclopentane With Methane or Nitrogen*, Trans IChemE, 72 Part A (1994), 197-200.

P. J. Herslund, K. Thomsen, J. Abildskov, N. von Solms, A. Galfré, P. Brântuas, M. Kwaterski, J.-M. Herri, *Thermodynamic promotion of carbon dioxide-clathrate hydrate formation by tetrahydrofuran, cyclopentane and their mixtures*, Int. J. Greenhouse Gas Control, 17 (2013), 397-410.



## 5 Thermodynamic Model

Early attempts of estimating gas hydrates equilibrium conditions (pressure, temperature and composition) were based mainly on experimental work conducted from the 1940's and 1950's. These methods have been described and reviewed in detail by Sloan and Koh (2007).

Since the sH hydrate structure had not yet been discovered at this time, the early empirical models only apply to the sI and sII hydrates.

The “Gas Gravity Method” is the simplest method for predicting hydrate formation at three-phase hydrate-liquid water-vapour equilibrium. This method was presented by Katz in 1945. As the work of Katz mainly considered hydrates formed from natural gasses, the gas gravity method should be used only for systems of natural gasses with low contents of non-combustible compounds (such as e.g. carbon dioxide, nitrogen etc.) [Sloan and Koh (2007)].

The use of the gas gravity method is simple. Katz developed charts providing hydrate formation pressures as function of temperature and gas gravity (molecular mass of gas relative to the molecular mass of air). By calculating the gravity of the gas under investigation and specifying temperature, the hydrate formation pressure could be read off the charts presented by Katz. Predicted formation pressures were however approximate at best, due to the limited amount of experimental data available at that time [Sloan and Koh (2007)].

Another method was developed a few years earlier, called the “distribution coefficient method” or in short, the “K-value method”. The K-value method assumes ideal solution of gas phase constituents in the solid hydrate phase. Under this assumption, a distribution coefficient of each hydrate former is defined as

$$K_{v-s,i} = \frac{y_i}{Y_i} \quad (5.1)$$

Where  $y_i$  is the vapour phase mole fraction of component  $i$  and  $Y_i$  is the water-free hydrate mole fraction of component  $i$ . Water-free in this context means the mole fraction is calculated only on basis of the hydrate phase guest contents.

Again, charts were produced, presenting K-values as function of temperature and pressure for individual hydrate formers. By use of these charts, and the constraint that

$$\sum_{i=1}^n \frac{y_i}{K_{v-s,i}} = 1 \quad (5.2)$$

hydrate formation conditions could be estimated by an iterative solution approach combining chart read-offs and satisfying equation (5.2).

The K-value method provides accurate temperature/pressure conditions for light gases found in typical natural gases. It has however been shown to perform less accurate for mixtures with high ethane, propane or butane contents. Similarly, accuracy is poor for the two gases of main interest in the present work, carbon dioxide and nitrogen [Sloan and Koh (2007)]. A possible explanation for the limitations to the K-value method could be that it, in its original form, did not account for differences in hydrate structures formed from systems with significant amounts of heavy compounds.

## 5.1 The van der Waals-Platteeuw Hydrate Model

The van der Waals-Platteeuw hydrate theory was proposed by J. H. van der Waals and J. C. Platteeuw in 1958 [Platteeuw and van der Waals (1958)]. This model treats the solid phase only and is typically combined with an equation of state and an activity coefficient model for the description of co-existing fluid phases. The solid phase is treated as a solid solution of hydrate formers in a crystalline host lattice.

The basic theory behind the model presented by van der Waals and Platteeuw is often claimed to come from statistical mechanics. Sloan and Koh (2007) have shown a detailed derivation of the model equations by the use of statistical mechanics. However, the model can similarly be derived by use of chemical reaction theory and classical thermodynamic relations. This has been shown by Hendriks and Meijer (2004).

In 1972 William R. Parrish and John M. Prausnitz presented an algorithm that made the van der Waals-Platteeuw hydrate model suitable for computer calculations [Parrish and Prausnitz (1972)].

The basic assumption in the Van der Waals-Platteeuw model concerns the chemical potential of water. At equilibrium, this potential must be equal in all phases present. As an example of hydrate(H) - liquid water(L<sub>w</sub>) - vapour(V) equilibrium, the equilibrium assumption states

$$\mu_w^H = \mu_w^{L_w} = \mu_w^V \quad (5.1.1)$$

Instead of evaluating absolute chemical potentials of water in the hydrate phase, van der Waals and Platteeuw defined a meta-stable, crystalline water phase that constituted the same structure of water as in the actual hydrate. This phase was noted the meta-stable  $\beta$ -phase.

The  $\beta$ -phase was called meta-stable, since it cannot exist without the presence of guest molecules. It is the interaction between the guest molecule and its surrounding water molecules that stabilises the actual hydrate structure. However, from a modelling point of view, it was convenient to use this definition of a meta-stable solid phase.

The difference in chemical potential between the actual hydrate phase and the meta-stable  $\beta$ -phase may be described by equation (5.1.2).

$$\Delta\mu_w^H = \mu_w^\beta - \mu_w^H \quad (5.1.2)$$

The following assumptions regarding the presence of the guest molecule in the water cavity allowed for the guest-host interaction to be described by an approach similar to the Langmuir adsorption theory [Parrish and Prausnitz (1972)].

- 1) All cavities are assumed spherical.
- 2) Each cavity can contain one guest at most.
- 3) Guest-guest interactions are negligible.
- 4) The guest molecule does not distort the structural properties of the water lattice.
- 5) The internal partition function of the guest is considered to be identical to that of the gas in its ideal state.
- 6) Only London forces are considered in the guest-host interaction.

Assumption 4) in particular is one important, yet questionable for some cases, assumption in the van der Waals-Platteeuw model, as it is presented here.

The difference in chemical potential of water between a theoretical empty hydrate water lattice (empty cavities) and the actual hydrate may now be described by the presence of guest molecules in the water cavities, according to monolayer Langmuir adsorption theory.

$$\Delta\mu(T, P, \theta)_w^H = -R \cdot T \cdot \sum_m \left[ v_m \cdot \ln(1 - \sum_j \theta(T, P, \bar{y})_{m,j}) \right] \quad (5.1.3)$$

Where  $v_m$  is the number of cavities type  $m$  per water molecule in the hydrate structure.  $\theta_{m,j}$  is the fractional occupancy of component  $j$  in cavity type  $m$ . This occupancy is described by

$$\theta(T, P, \bar{y})_{m,j} = \frac{C(T)_{m,j} \cdot f(T, P, \bar{y})_j}{1 + \sum_l C(T)_{m,l} \cdot f(T, P, \bar{y})_l} \quad (5.1.4)$$

Where the fugacity,  $f$ , of the hydrate former is given by:

$$f(T, P, \bar{y})_j = \varphi(T, P, \bar{y})_j \cdot y_j \cdot P \quad (5.1.5)$$

$C_{m,j}$  is the Langmuir constant for gas component  $j$  in cavity type  $m$ .  $\varphi_j$  is the fugacity coefficient of component  $j$  in the coexisting vapour phase.  $y_j$  is the mole fraction of component  $j$  in the vapour phase.

Substitution of equation (5.1.4) into equation (5.1.3) obtains the following expression for the change in chemical potential of water caused by the presence of the guest molecules.

$$\Delta\mu(T, P, \theta)_w^H = R \cdot T \cdot \sum_m \left[ v_m \cdot \ln \left( 1 + \sum_j C(T)_{m,j} \cdot f(T, P, \bar{y})_j \right) \right] \quad (5.1.6)$$

In the following, we consider the specific case, where the hydrate is formed in a co-existing liquid phase. Hence a combination of equation (5.1.1) and equation (5.1.2) may obtain

$$\Delta\mu(T, P, \theta)_w^H = \mu(T, P)_w^\beta - \mu(T, P, \bar{x})_w^{L_w} \quad (5.1.7)$$

At equilibrium, the chemical potential of water in the liquid phase may be described by

$$\mu(T, P, \bar{x})_w^{L_w} = \mu(T, P)_w^* + R \cdot T \cdot \ln \left[ \alpha(T, P, \bar{x})_w^{L_w} \right] \quad (5.1.8)$$

Where superscript  $(*)$  denotes a pure phase.  $\alpha$  is the activity of water in the non-ideal liquid phase including other species. The water activity accounts for the highly non-ideal behaviour of water at the presence of hydrogen bonding or electrolyte components in the liquid phase. The solubilities of gas phase components are often low in the aqueous liquid phase and the activity of water in this phase may in these cases be assumed unity. Nevertheless, the activity is rigorously calculated in this work.

The water activity may be described either in terms of a symmetric activity coefficient,  $\gamma$ , from an activity coefficient model or in terms of fugacity coefficients,  $\varphi$ , from an equation of state.

$$\alpha(T, P, \bar{x})_w^{L_w} = x_w^{L_w} \cdot \gamma(T, P, \bar{x})_w^{L_w} = x_w^{L_w} \cdot \frac{\varphi(T, P, \bar{x})_w^{L_w}}{\varphi(T, P)_w^*} \quad (5.1.9)$$

Where  $x_w$  denotes liquid phase composition of water.

We may now define a difference in chemical potential of water between the meta-stable  $\beta$ -phase and water in the co-existing liquid phase

$$\Delta\mu(T, P)_w^{L_w} = \mu(T, P)_w^\beta - \mu(T, P)_w^{L_w} \quad (5.1.10)$$

Combining equations (5.1.6), (5.1.7), (5.1.8), (5.1.9) and (5.1.10) obtains an explicit expression for the difference in chemical potential between the empty hydrate and the pure liquid phase at specified temperature,  $T$ , and pressure,  $P$

$$\begin{aligned} \Delta\mu(T, P)_w^{L_w} = & R \cdot T \cdot \sum_m \left[ \nu_m \cdot \ln \left( 1 + \sum_j C(T)_{m,j} \cdot f(T, P, \bar{y})_j \right) \right] \\ & + R \cdot T \cdot \ln \left[ x_w^{L_w} \cdot \frac{\varphi(T, P, \bar{x})_w^{L_w}}{\varphi(T, P)_w^*} \right] \end{aligned} \quad (5.1.11)$$

Equation (5.1.11) is hereafter named the theoretical chemical potential difference.

All fugacities and the water activity may be obtained from the CPA EOS. The last parameters to be specified are the Langmuir adsorption coefficient,  $C(T)$ . Van der Waals and Platteeuw (1958) suggested that the Langmuir adsorption coefficients may be approximated using Lennard-Jones-Devonshire cell theory with e.g. a Lennard-Jones 12-6 cell potential. They proposed the following expression for the Langmuir adsorption coefficient

$$C(T)_{m,j} = 4 \cdot \pi \cdot (k_B \cdot T)^{-1} \cdot \int_0^\infty \exp \left[ -w(r)_{m,j} \cdot (k_B \cdot T)^{-1} \right] \cdot r^2 \cdot dr \quad (5.1.12)$$

Where  $k_B$  is the Boltzmann constant and  $w(r)_{m,j}$  is the spherical core cell potential of component  $j$  in cavity type  $m$ .  $r$  is linear distance.

McKoy and Sinanoglu (1963) investigated three cell potentials for use in hydrate dissociation pressure calculations. They concluded that the Kihara cell potential is the most suitable for this kind of calculations, and proposed a method for including this cell potential in the hydrate dissociation pressure calculation. McKoy and Sinanoglu evaluated the interactions between the guest molecule and all its surrounding first layer of water molecules, and summed up the contributions in one expression for the spherical core cell potential. Parrish and Prausnitz (1972) presented the final expression for the cell potential of gas constituent  $j$  in cavity type  $m$ , in a slightly modified form. Here the expression of Parrish and Prausnitz is shown.

$$w(r)_{m,j} = 2 \cdot z_m \cdot \varepsilon_j \cdot \left[ \frac{\sigma_j^{12}}{R_m^{11} \cdot r} \cdot \left( \delta(N=10)_{m,j} + \frac{a_j}{R_m} \cdot \delta(N=11)_{m,j} \right) - \frac{\sigma_j^6}{R_m^5 \cdot r} \cdot \left( \delta(N=4)_{m,j} + \frac{a_j}{R_m} \cdot \delta(N=5)_{m,j} \right) \right] \quad (5.1.13)$$

$z_m$  is the coordination number for the guest in cavity type  $m$ ,  $\varepsilon_j$  is the characteristic energy of guest molecule  $j$ ,  $a_j$  is the core radius of molecule  $j$ ,  $\sigma_j + 2a_j$  is the collision diameter of molecule  $j$  and  $R_m$  is the radius of cavity type  $m$ .  $\delta(N)_{m,j}$  is defined by

$$\delta(N)_{m,j} = \frac{1}{N} \cdot \left[ \left( 1 - r \cdot R_m^{-1} - a_j \cdot R_m^{-1} \right)^{-N} - \left( 1 + r \cdot R_m^{-1} - a_j \cdot R_m^{-1} \right)^{-N} \right] \quad (5.1.14)$$

From equation (5.1.13) it is seen that the Kihara spherical core cell potential is undefined at  $r = 0$ . However if one looks at the limiting value of the cell potential when approaching this from  $r$ -values greater than zero, it may be shown that this point in the Kihara potential is a removable singularity [M. Kwaterski (2011)]. Also at  $r = R_m - a_j$  a discontinuity with a change of sign occurs. Approaching  $r = R_m - a_j$  from  $r$ -values greater than this results in the cell potential approaching minus infinity making the behaviour of the Langmuir adsorption coefficient divergent. Thus care should be taken, when integrating the Kihara cell potential.

In this work the Kihara potential is evaluated from  $r = 0$  to the singularity point at  $r = R_m - a_j$ . Thus equation (5.1.12) is rewritten

$$C(T)_{m,j} = 4 \cdot \pi \cdot (k_B \cdot T)^{-1} \cdot \int_0^{R_m - a_j} \exp \left[ -w(r)_{m,j} \cdot (k_B \cdot T)^{-1} \right] \cdot r^2 \cdot dr \quad (5.1.15)$$

Sloan and Koh (2007) and Mooijer-van den Heuvel et al (2000) have previously reported the same observations and adopted the same solution.

Numerical approximation of the integral in equation (5.1.15) may be performed using integration schemes such as the Gauss-Legendre Quadrature method or the Composite Simpson 3/8 rule. Applying 20 evaluation points in the Gauss-Legendre method and 200 internal sections in the Composite Simpson 3/8 rule (each with four evaluation points), the two methods obtain similar results for equation (5.1.15). However since the Gauss-Legendre method, unlike the Simpson 3/8 method, does not need to evaluate the function values in the integration limits, the Gauss-Legendre method avoids the problems of evaluating the undefined point at  $r = 0$  and the singularity point at  $r = R_m - a_j$ . Due to the lower number of evaluation points, the Gauss-Legendre method also has the



advantage of shorter computation time. Hence this method has been chosen in the present work.

Parrish and Prausnitz (1972) proposed a simpler way of calculating the Langmuir adsorption coefficients, where an explicit expression is given for the coefficients

$$C(T)_{m,j} = A_{m,j} \cdot T^{-1} \cdot \exp[B_{m,j} \cdot T^{-1}] \quad (5.1.16)$$

$A_{m,j}$  and  $B_{m,j}$  are fitting parameters related to guest type  $j$  in cavity type  $m$  only. Hence in the case where a guest molecule may enter both cavities in both sI and sII hydrates, a total of eight fitting parameters must be determined for this one guest. In the cell potential approach three parameters are needed to perform the same type of calculation, only two of them are utilised as fitting parameters in this work ( $\varepsilon_j$  and  $\sigma_j$ ). While the Parrish and Prausnitz approach provides a simpler method for calculating Langmuir constants, it requires a greater number of adjustable parameters to be regressed.

With the theoretical chemical potential difference in place, an experimental reference hydrate was introduced by Parrish and Prausnitz (1972). The difference in chemical potential between the meta-stable  $\beta$ -phase and pure water at specified temperature and pressure may be derived thermodynamically in terms of measurable quantities. These quantities could be determined indirectly from existing hydrate equilibrium data.

Knowing that the chemical potential is a state function, Parrish and Prausnitz proposed a method for transforming the chemical potential difference determined for a reference hydrate at reference temperature,  $T_0$ , and reference pressure,  $P_0$ , to the actual hydrate at temperature,  $T$ , and pressure,  $P$ . This was done in two steps according to equation (5.1.17)

$$\begin{aligned} \frac{\Delta\mu(T, P_R)_{w}^{L_w}}{R \cdot T} &= \frac{\Delta\mu(T_0, P_0)_{w}^{L_w}}{R \cdot T_0} \\ &- \int_{T_0}^T \frac{\Delta H(T_0, P_0)_{w}^{\beta/Ice} + \Delta H(T)_{w}^{Ice/L_w}}{R \cdot T^2} dT \\ &+ \int_{T_0}^T \frac{\Delta V_{w}^{\beta/Ice} + \Delta V_{w}^{Ice/L_w}}{R \cdot T} \cdot \frac{dP_R}{dT} dT \end{aligned} \quad (5.1.17)$$

and equation (5.1.18)

$$\Delta\mu(T, P)_{w}^{L_w} = \Delta\mu(T, P_R)_{w}^{L_w} + (\Delta V_{w}^{\beta/Ice} + \Delta V_{w}^{Ice/L_w}) \cdot (P - P_R) \quad (5.1.18)$$

where  $\Delta\mu(T, P_R)_w^{L_w}$  is the chemical potential difference for water at temperature,  $T$  and at the dissociation pressure of the reference hydrate,  $P_R(T)$ .  $\Delta\mu(T_0, P_0)_w^{L_w}$  is the chemical potential difference of water between the  $\beta$ -phase and liquid water, measured for the reference hydrate at reference temperature  $T_0$  and reference pressure  $P_0$ .  $\Delta H(T_0, P_0)_w^{\beta/Ice}$  and  $\Delta H(T)_w^{Ice/L_w}$  are the differences in molar enthalpy for water between the meta-stable  $\beta$ -phase measured for the reference hydrate and ice, and ice and liquid water respectively.  $\Delta H(T)_w^{Ice/L_w}$  consists of two contributions, first the phase change enthalpy from ice to liquid at the reference temperature, then a heat capacity contribution from the heating of the liquid from the reference temperature to the actual temperature.

$$\Delta H(T)_w^{Ice/L_w} = \Delta H(T_0, P_0)_w^{Ice/L_w} + \Delta C_p(T) \cdot (T - T_0) \quad (5.1.19)$$

$\Delta V_w^{\beta/Ice}$  and  $\Delta V_w^{Ice/L_w}$  are the differences in molar volume of the  $\beta$ -phase measured for the reference hydrate and ice and ice and liquid water respectively. All values are determined at reference temperature  $T_0$  and reference pressure,  $P_0$ .  $P_0$  is the vapour pressure of ice at temperature,  $T_0$ . Since this pressure is small compared to the hydrate dissociation pressure, it is assumed zero.  $T_0$  is chosen at 273.15 K

$dP_R/dT$  is the gradient of the experimentally determined dissociation pressure-temperature curve for the reference hydrate. Parrish and Prausnitz (1972) presented a three parameter expression for the temperature dependence of the reference hydrate dissociation pressure.

Recalling assumption 4) of this model, that the water lattice properties are independent of the guest molecule (for a given hydrate structure), the theoretical chemical potential difference provided in equation (5.1.11) must be equal to the reference potential difference given by equation (5.1.18) at identical temperature and pressure conditions. Hence, by equating these two expressions, and specifying either temperature or pressure, it is possible to calculate the corresponding equilibrium condition (pressure or temperature respectively).

Holder et al. (1980) suggested a combined and simplified form of equations (5.1.17) and (5.1.18). In their expression, the use of a reference pressure,  $P_R$ , was removed providing a simpler expression that could easier be evaluated analytically.

$$\begin{aligned} \frac{\Delta\mu(T, P)_w^{L_w}}{R \cdot T} &= \frac{\Delta\mu(T_0, P_0)_w^{L_w}}{R \cdot T_0} \\ &- \int_{T_0}^T \frac{\Delta H(T_0, P_0)_w^{\beta/Ice} + \Delta H(T)_w^{Ice/L_w}}{R \cdot T^2} dT \quad (5.1.20) \\ &+ \int_0^P \frac{\Delta V_w^{\beta/Ice} + \Delta V_w^{Ice/L_w}}{R \cdot T} \cdot dP \end{aligned}$$

In a previous work [Herslund et al. (2012) – Appendix 1], we used the original expression of Parrish and Prausnitz (equation (5.1.17) and (5.1.18)) for the chemical potential difference of the reference hydrate. However, to simplify the model, the expression of Holder et al. (1980), shown in equation (5.1.20), is used in the present work. Holder et al. (1980) argued that equation (5.1.20) provides similar results compared to the before mentioned expression used by Parrish and Prausnitz. The version of Holder et al. (1980) has been applied successfully in more recent uses of the van der Waals-Platteeuw gas clathrate hydrate theory [Sloan (1998)].

Once equilibrium conditions have been established in the model, the hydrate composition may be calculated from the fractional occupancies of the individual guests in each hydrate cavity. A water-free hydrate composition is defined according to equation (5.1.21).

$$Y_j = \sum_m v_m \cdot \frac{\theta(T, P, \bar{y})_{m,j}}{\left( \sum_m v_m \sum_l \theta(T, P, \bar{y})_{m,l} \right)} \quad (5.1.21)$$

The water-free composition accounts only for the guests present in the hydrate cavities. The water lattice is ignored in the composition calculation.

## 5.2 Attempts of Improving the Hydrate Model Theory

The main contribution to the development of the original hydrate model presented by Platteeuw and van der Waals (1958) must be Parrish and Prausnitz (1972) who presented a detailed algorithm for ice-hydrate-vapour and liquid water-hydrate-vapour phase equilibrium calculations in multi-component systems. The suggested two-parameter expression for the calculation of Langmuir constants also greatly simplified the calculation of the Langmuir constants.

Holder et al. (1980) later eliminated the need for the reference pressure and thus simplified the calculations. The remaining part of their model was identical to that of Parrish and Prausnitz.

Klauda and Sandler (2000) presented a new explicit fugacity based method for calculating gas hydrate equilibrium conditions. Their model was still based on the original van der Waals-Platteeuw theory for the description of gas enclathration in the solid phase, however the need for reference properties such as  $\Delta\mu$ ,  $\Delta H$  and  $\Delta C_p$  was removed in this new approach. Large uncertainties in these reference properties are expected, as these cannot be determined directly for the empty hydrate lattice. Instead of calculating reference chemical potential differences between a meta-stable hydrate lattice and actual hydrate lattices (as in the “standard” versions), Klauda and Sandler calculated an actual fugacity of water in the hydrate lattice. This fugacity was defined as the product of the water fugacity in the empty hydrate lattice, and the exponential to the (theoretical) chemical potential difference between the actual hydrate and the (pure) liquid water phase.

$$f_w^H = f_w^\beta \cdot \exp \left[ \frac{-\Delta\mu_w^H}{R \cdot T} \right] \quad (5.2.1)$$

where the fugacity of the empty hydrate lattice was defined by properties such as its saturated water vapour pressure and its molar volume. Both of these properties were assumed temperature- and pressure dependent. Moreover, the saturated water vapour pressures of the hydrate lattices were assumed component dependent.

Klauda and Sandler (2000) included contributions from the second and third water shells surrounding the guest in each cavity, when calculating Langmuir constants. They argued that these shells contributed significantly to the potential function. Later, in a more advanced model, Klauda and Sandler (2003) included guest-guest interactions as well as allowed for dual occupancy in cavities.

Whereas Klauda and Sandler (2000) emphasised that their model had not been “tuned” by fitting Langmuir parameters to actual hydrate dissociation pressure data, such kinds of data were included indirectly elsewhere in the model. Langmuir constants were originally calculated from the Kihara cell potential with parameters found in the literature, where these had been estimated from gas phase viscosity data or second virial coefficients. Later, Klauda and Sandler (2003) used Lennard-Jones 12-6 parameters estimated from quantum mechanics considerations.

Accurate descriptions of pure hydrate dissociation pressures were presented for methane, ethane, propane, cyclopropane, iso-butane, carbon dioxide, nitrogen and hydrogen sulfide [Klauda and Sandler (2000)]. Using their more advanced model, Klauda and Sandler (2003) also presented accurate descriptions of certain natural gas mixtures.

It should be mentioned, that even though Klauda and Sandler (2000 and 2003) obtained impressive “predicted” results, their hydrate model did contain an increased number of component specific, adjustable parameters, compared to the classical van der Waals-Platteeuw based models. Whereas the adjustable parameters in the classical van der Waals-Platteeuw based models are used in some extent to cancel out “errors” occurring elsewhere in the model, this was not the case of the model of Klauda and Sandler. Here the adjustable parameters were regressed separately, without the inclusion of the complete model. However, dissociation pressure data were still needed for the pure component hydrate systems to complete the model. In gas mixtures, classical mixing rules were applied to determine the saturated vapour pressure of the mixed hydrate water lattice.

Ballard (2002), attempted to improve the hydrate theory by including guest specific distortion of the water lattice in the hydrate phase. Unlike Klauda and Sandler (2000, 2003), Ballard (2002) kept the classical van der Waals-Platteeuw/Parrish-Prausnitz approach, but expanded the theory by including lattice distortion in the form of an activity correction of the chemical potential of water in the hydrate lattice. By including guest specific lattice distortion, Ballard added a significant number of adjustable parameters compared to the classical approach. Moreover, two parameters in the Kihara cell potential were still regressed to match the model with actual hydrate dissociation pressures and hydrate composition data. All adjustable parameters were obtained by multivariate optimisation using a large database of experimental data for hydrate dissociation pressures and hydrate composition/fractional occupancies. Finally, information was built into the model, restricting large molecules from entering hydrate cavities, which they were physically too large to stabilise.

The change of the original theory (and the increased number of adjustable parameters) provided a significant gain in accuracy compared to the classical van der Waals-Platteeuw model. The model and the parameters presented by Ballard (2002) are included in the CSMGem software provided by Sloan and Koh (2007).

Folas et al. (2007) applied a simplified version of the model presented by Klauda and Sandler. Saturated vapour pressures and molar volumes of the empty hydrate lattice were assumed only temperature dependent. By doing so, Folas et al. still needed to tune their model by regressing Langmuir constants to match the model with experimental data for dissociation pressures of hydrates. However the reference properties for the empty hydrate lattice,  $P^{sat}$  and  $V^{\beta}$ , in their model could be determined experimentally more easily than those of the classical models. The two-parameter expression proposed by Parrish and Prausnitz (1972) was used to calculate the Langmuir constants.

### 5.3 The Cubic-Plus-Association Equation of State

In this work, the van der Waals-Platteeuw hydrate model, applied with the algorithm proposed by Parrish and Prausnitz, has been modified such that the Cubic-Plus-Association (CPA) equation of state (EoS) supplies the hydrate model with all the needed inputs related to the co-existing fluid phases.

The Cubic-Plus-Association (CPA) equation of state presented by Kontogeorgis *et al.* (1996) combines the physical term from the cubic Soave-Redlich-Kwong (SRK) EoS with an association term similar to that found in the Statistical Associating Fluid Theory (SAFT) models. This model has been proven to provide accurate descriptions of complex systems involving water and other complex chemicals of hydrogen bonding character [Kontogeorgis and Folas (2010)].

On pressure explicit form, the CPA EoS may be expressed [Michelsen and Hendriks (2001), Kontogeorgis *et al.* (2006)]:

$$P = \frac{R \cdot T}{V_m - b} - \frac{\alpha(T)}{V_m \cdot (V_m + b)} - \frac{R \cdot T}{2 \cdot V_m} \cdot \left[ 1 + \frac{1}{V_m} \cdot \frac{\partial \ln g}{\partial (1/V_m)} \right] \times \sum_i x_i \sum_{A_i} (1 - X_{A_i}) \quad (5.3.1)$$

Where  $R$  is the gas constant and  $T$  is temperature.  $V_m$  denotes the molar volume,  $\alpha(T)$  is the temperature dependent SRK energy parameter and  $b$  is the SRK co-volume parameter.  $g$  is the hard sphere radial distribution function.  $A_i$  denotes association site  $A$  on component  $i$ .  $x_i$  is the mole fraction of component  $i$ ,  $X_{A_i}$  is the fraction of sites, type  $A$  on component  $i$ , not bonded to other sites. CPA simplifies to the SRK EoS for non-associating systems.

The fraction of non-bonded sites,  $X_{A_i}$ , is estimated by solving equation (5.3.2) and (5.3.3) below.

$$X_{A_i} = \left[ 1 + V_m^{-1} \cdot \sum_j x_j \sum_{B_j} X_{B_j} \cdot \Delta^{A_i B_j} \right]^{-1} \quad (5.3.2)$$

Equation (5.3.2) is evaluated for all site types on all associating components. The summation over  $B_j$  in equation (5.3.2) indicates summation over all association sites.

$\Delta^{A_i B_j}$  is the association strength between site  $A$  on molecule  $i$  and site  $B$  on molecule  $j$ . It may be estimated by

$$\Delta^{A_i B_j} = g(V_m)^{ref} \cdot \left[ \exp(\varepsilon^{A_i B_j} \cdot (R \cdot T)^{-1}) - 1 \right] \cdot b_{ij} \cdot \beta^{A_i B_j} \quad (5.3.3)$$

$\epsilon^{AiBj}$  and  $\beta^{AiBj}$  are the association energy and -volume respectively between site  $A$  on molecule  $i$  and site  $B$  on molecule  $j$ .  $g(V_m)^{\text{ref}}$  is the contact value of the radial distribution function for the reference hard sphere fluid system.

The radial distribution function,  $g(V_m)$  was presented in a simplified form by Kontogeorgis *et al.* (1999) (sCPA). Whereas earlier versions of CPA utilised the Carnahan-Starling expression for the hard-sphere radial distribution function, sCPA uses the expression shown in equation (5.3.4) for the simplified hard-sphere radial distribution function.

$$g(V_m) = \left[ 1 - 1.9 \cdot b \cdot (4 \cdot V_m)^{-1} \right]^{-1} \quad (5.3.4)$$

This work utilises the simplified form of CPA.

The temperature dependent energy parameter,  $\alpha_i(T)$  for pure component  $i$ , in the SRK term is calculated by means of equation (5.3.5).

$$\alpha_i(T) = a_{0,i} \cdot \left[ 1 + c_{1,i} \cdot \left( 1 - \sqrt{T \cdot T_{c,i}^{-1}} \right) \right]^2 \quad (5.3.5)$$

Where  $a_{0,i}$  and  $c_{1,i}$  are pure component parameters and  $T_{c,i}$  is the critical temperature for component  $i$ . For associating components, the CPA EoS utilises five pure component parameters,  $a_{0,i}$ ,  $b_i$ ,  $c_{1,i}$ ,  $\epsilon^{AiBi}$  and  $\beta^{AiBi}$ . Non-associating components are described by three pure component parameters,  $a_{0,i}$ ,  $b_i$  and  $c_{1,i}$  in a manner similar to that of the “standard” SRK EoS. Pure component parameters for associating components are obtained by fitting the model to experimental vapour pressures and saturated liquid densities of the pure component. The three pure component parameters for non-associating compounds may also be obtained from critical temperature,  $T_{c,i}$ , critical pressure,  $P_{c,i}$ , and the acentric factor,  $\omega_i$ .

In binary systems, the van der Waals one-fluid mixing rules are used for evaluating the SRK parameters,  $\alpha(T)$  and  $b$ . This is done according to equation (5.3.6) and (5.3.7) [Kontogeorgis *et al.* (2006)].

$$\alpha(T) = \sum_i \sum_j x_i \cdot x_j \cdot \alpha_{ij}(T) \quad (5.3.6)$$

$$b = \sum_i x_i \cdot b_i \quad (5.3.7)$$

Where the “classical” combining rules are applied for the binary  $\alpha_{ij}(T)$  in the SRK term and the binary  $b_{ij}$  in the association term.

$$\alpha_{ij}(T) = \sqrt{\alpha_i(T) \cdot \alpha_j(T)} \cdot (1 - k_{ij}) \quad (5.3.8)$$

$$b_{ij} = (b_i + b_j) \cdot 2^{-1} \quad (5.3.9)$$

$k_{ij}$  in equation (5.3.8) is the binary interaction parameter (BIP) between component,  $i$ , and component,  $j$ .  $k_{ij}$  may be temperature-dependent, e.g. according to equation (5.3.10)

$$k_{ij} = a_{kij} + b_{kij} \cdot T^{-1} \quad (5.3.10)$$

No mixing rules are needed for the association parameters of CPA. Only for cross associating systems, combining rules must be applied to obtain the two association parameters  $\epsilon^{AiBj}$  and  $\beta^{AiBj}$ . This work utilises the CR1 combining rules according to equations (5.3.11) and (5.3.12).

$$\epsilon^{AiBj} = (\epsilon^{AiBi} + \epsilon^{AjBj}) \cdot 2^{-1} \quad (5.3.11)$$

$$\beta^{AiBj} = \sqrt{\beta^{AiBi} \cdot \beta^{AjBj}} + \gamma^{AiBj} \quad (5.3.12)$$

The combining rule for  $\beta^{AiBj}$ , equation (5.3.12), has been formulated in a general form, which handles both cross-association between two self-associating molecules as well as cross-association between one self-associating and one non self-associating molecule (solvation). In the case of cross-association between two self-associating molecules,  $\gamma^{AiBj}$  may either be set to zero, in order to allow model prediction according to the standard CR1 combining rule, or it can be used as an adjustable parameter on the cross association interactions. In cases with cross-association involving one non self-associating molecule, a non-zero  $\gamma^{AiBj}$  is needed to provide cross-association interactions.

For systems containing three or more components CPA becomes predictive, since only binary interactions may be accounted for (directly) in the process of parameter estimation.

The methodology presented her, for handling cross-association between self-associating and non self-association compounds corresponds to using the modification of the CR1 combining rule presented by Folas *et al.* (2006). The advantage of expressing the CR1 combining rule in the present form is that it is general and easily handles all scenarios treated.

In this work the notation for association schemes is  $[\{X^+\};\{Y^-\}]$ , where X and Y are number of sites. Superscript (+) and (-) denotes whether the sites are electron accepting (+) or electron donating (-). Water is modeled as a self-associating compound with a total of four associating sites. Two sites are electron donating



(two sets of oxygen atom lone pair electrons) and two are electron accepting (two hydrogen atoms). Hence, the association scheme for water in the above defined notation becomes  $[2^+;2^-]$ , corresponding to the 4C association scheme as defined by Huang and Radosz (1990).

Self-association between two water molecules is modeled by allowing electron donating sites on one molecule to interact (hydrogen bond) with electron accepting sites on another molecule of the same type. The self-association strength is defined by the pure component association parameters,  $\epsilon^{AiBi}$  and  $\beta^{AiBi}$ .

## 5.4 Algorithm Applied in the Present Work

The classical van der Waals-Platteeuw hydrate model as presented in section 5.1 above has been implemented in the form of a FORTRAN program. This section describes the numerical methods and solution procedures utilised in the model set-up as well as an overview of the overall model algorithm.

The parameters required for the two models, van der Waals-Platteeuw and CPA, may be found in section 5.5.1 and 5.5.2 respectively.

This work utilises an algorithm for the hydrate dissociation pressure calculation similar to that presented by Parrish and Prausnitz (1972). Note that the algorithm and the hydrate model as presented above is valid only for describing equilibrium conditions for hydrate systems above the ice point temperature of water. In order to describe hydrate formation below the ice point temperature of water, the water activity correction term in equation (5.1.11) must be omitted. Moreover, new reference parameters are needed for equation (5.1.20).

Hydrate formation below the ice point temperature of water has not been considered in this work.

The applied procedure for hydrate dissociation pressure calculations is provided below.

- 1) Specify molar feeds of all components in the initial system.
- 2) Specify system temperature.
- 3) Evaluate Langmuir constants for all hydrate formers at the specified temperature in (for all cavities in the sI and sII hydrates).
- 4) Set an initial guess for pressure according to the reference pressure expressions provided by Parrish and Prausnitz (1972).
- 5) Perform an isothermal-isobaric multi-phase flash calculation (Gibbs energy minimisation) at the specified temperature and pressure, using the feed from 1).
- 6) Using the results from step 3) - 5), evaluate equation (5.1.11)

- 7) Evaluate equation (5.1.20) for the reference hydrate at the specified temperature and pressure.
- 8) Keeping compositions and fugacity coefficients constant, solve equation (5.1.11) and equation (5.1.20) for pressure.
- 9) If the new pressure is different from the previously assumed, return to step 5) and repeat calculations until convergence of pressure.

The above calculation procedure is performed for both structure I and structure II hydrates. The program then chooses the most stable structure according to the criteria of lowest equilibrium pressure. Incipient hydrate equilibrium pressure, and phase composition of all phases for the specified feed and temperature is finally returned to the user. Figure 5.1 provides a graphical illustration of the calculation procedure.

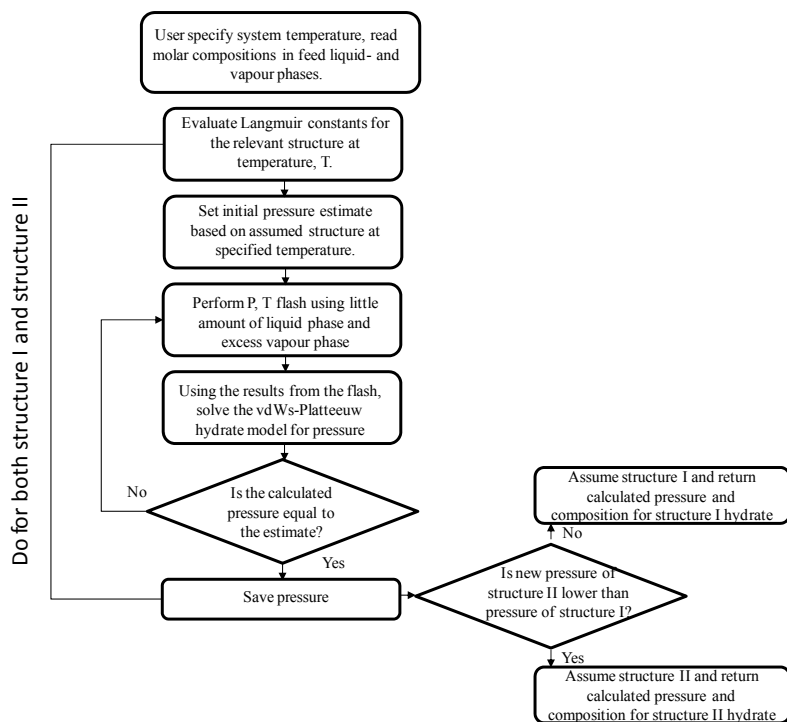


**Figure 5.1.** Algorithm used for incipient hydrate dissociation pressure calculations for a hydrate forming system of specified composition and temperature.

The main program in the developed module concerns the van der Waals-Platteeuw hydrate model. The flash routine is used to obtain the inputs required for the hydrate model at the specified temperature and pressure.

The program may be described in a very simplified manner as a program that solves equation (5.1.11) and equation (5.1.20) for the equilibrium pressure at a specified temperature. The integrals in equation (5.1.20) are evaluated analytically (as presented by Herri et al. (2011)), whereas the integral in equation (5.1.15) is evaluated numerically by the use of a 20 point Gauss-Legendre quadrature method.

By subtracting equation (5.1.11) from equation (5.1.20), the resulting equation may be solved for pressure by the use of the first-order Newton-Raphson method. Keeping fugacity coefficients and fluid phase compositions constant (in the van der Waals-Platteeuw model) while solving for pressure, the first order derivative of the function to be minimised may be approximated by:

$$\frac{df}{dP} = \Delta V_w^{\beta/Ice} + \Delta V_w^{Ice/L_w} - R \cdot T \cdot \sum_m \left[ v_m \cdot \frac{\sum_j C(T)_{m,j} \cdot \phi(T, \bar{y})_j \cdot y_j}{1 + \sum_j C(T)_{m,j} \cdot \phi(T, \bar{y})_j \cdot y_j \cdot P} \right] \quad (5.4.1)$$

Where the fugacity coefficients and fluid phase compositions are those obtained in the most recently executed flash calculation.

Overall pressure convergence is obtained by successive substitution, where the pressure is substituted back and forth between the flash and the van der Waals-Platteeuw model. The convergence may be accelerated to increase the sometimes slow convergence behaviour of the successive substitution method.

## 5.5 Model Parameters

### 5.5.1 Hydrate Model

The van der Waals-Platteeuw hydrate model contains a number of parameters. Most of these parameters are model specific, and have been found available in the literature. Among these are the structural parameters for the hydrate lattice. These include the average cell radii for each cavity, coordination numbers for specific cavities, number of cavities and water molecules for each hydrate unit cell etc. Such parameters are provided in Table 5.1.

**Table 5.1.** Water lattice and unit cell parameters for the van der Waals-Platteeuw hydrate model.

Structure	sI		sII	
Cavity	5 <sup>12</sup>	5 <sup>12</sup> 6 <sup>2</sup>	5 <sup>12</sup>	5 <sup>12</sup> 6 <sup>4</sup>
No. cavities per unit cell	2	6	16	8
Avg. cavity radius·10 <sup>10</sup> / m	3.95 <sup>a</sup>	4.33 <sup>a</sup>	3.91 <sup>a</sup>	4.73 <sup>a</sup>
Coordination number	20	24	20	28
No. water molecules per unit cell	46		136	
<sup>a</sup> Data from Sloan (1998)				

Other model specific parameters for the hydrate model are the thermodynamic properties of the reference hydrate. These parameters are given in Table 5.2.

**Table 5.2.** Thermodynamic properties for the reference hydrate in the van der Waals-Platteeuw hydrate model.

	sI	sII	Ref.
$\Delta\mu(T_0, P_0)_w^{\beta/L_w} / \text{J}\cdot\text{mole}^{-1}$	1297	937	A
$\Delta H_w^{\beta/Ice} / \text{J}\cdot\text{mole}^{-1}$	1389	1025	A
$\Delta H(T_0, P_0)_w^{Ice/L_w} / \text{J}\cdot\text{mole}^{-1}$	-6011	-6011	B
$\Delta C_p(T) / \text{J}\cdot\text{mole}^{-1}\cdot\text{K}^{-1}$	-38.12+0.141·(T-273.1)	-38.12+0.141·(T-273.1)	C
$\Delta V_w^{\beta/Ice} + \Delta V_w^{Ice/L_w} / \text{m}^3\cdot\text{mole}^{-1}$	4.6·10 <sup>-6</sup>	5.0·10 <sup>-6</sup>	C
A: From Dharmawardhana et al. (1980) , B: Herri et al. (2011) , C: From Sloan (1998)			

The thermodynamic properties of the reference hydrates are determined indirectly from experimental investigations of gas hydrate systems. These properties have been investigated by a large number of authors through time. As these thermodynamic properties are not readily measured, the reported values often differ significantly from each other. Herri et al. (2011) discussed this issue and emphasised the difficulty in comparing model results presented in literature by different authors. Often an insufficient amount of information is provided about the parameters used in hydrate models. Moreover, the models are often presented in different forms, making it even more difficult to compare them.

In the present work, the thermodynamic reference properties for the hydrate structures are almost identical to those used by Sloan (1998), who (at that time) successfully applied a similar version of the van der Waals-Platteeuw hydrate

theory. Sloan (1998) however slightly modified the  $\Delta\mu(T_0, P_0)$  for the reference hydrate.

The final parameters needed in the hydrate model are the Kihara cell potential parameters. These are the final parameters to be determined in the model, once everything else (including the equation of state) is in place.

The van der Waals-Platteeuw hydrate model, as presented here, has no real predictive capabilities without *a priori* knowledge of the gas hydrate formers of interest. Kihara parameters must be determined by fitting the complete model to existing data for dissociation pressures and/or hydrate phase compositions. When doing so, the hydrate structures should preferably be known. The use of Kihara parameters determined independently from data for the pure hydrate formers (such as viscosity data and second virial coefficients) will provide unsatisfactory results, if used in this model. The Kihara parameters regressed as part of this work are presented in Table 5.3.

**Table 5.3.** Kihara cell potential parameters regressed as a part of this work. Only  $\sigma$  and  $\varepsilon$  have been correlated. The core radii,  $a$ , are taken from elsewhere, where they have been determined typically from pure component viscosity data and/or second virial coefficients.

Component	$a \cdot 10^{10} / m$	$\sigma \cdot 10^{10} / m$	$\varepsilon / k_B / K$
Carbon dioxide	0.6805 *	2.9643	171.70
Nitrogen	0.3526 *	3.1723	128.07
Tetrahydrofuran	0.9013 **	3.5398	291.48
Cyclopentane	0.8968 ***	3.1480	250.89

\* Sloan and Koh (2007) , \*\* Strobel et al. (2009) , \*\*\* Takeuchi et al. (2009)

For the complete details of which experimental data have been used as references, please see Appendix 4 and Appendix 5.

## 5.5.2 Equation of State (CPA)

The cubic-plus-association (CPA) equation of state needs three pure component parameters for non-associating compounds and five pure component parameters for self-associating compounds. Compounds that are non self-associating, but may cross-associate with other self-associating compounds still have only three pure component parameters. In this work, carbon dioxide and tetrahydrofuran are treated in this way.

Pure component parameters for non self-associating and non cross-associating compounds are described by their critical properties in a manner identical to the Soave-Redlich-Kwong equation of state (critical temperature, critical pressure and acentric factor). Self-associating and cross-associating compounds obtain pure

component parameters by correlation of CPA to vapour pressure and saturated liquid density data. The pure component parameters used in this work for the total of five components considered (water, tetrahydrofuran, cyclopentane, carbon dioxide and nitrogen) are provided in Table 5.4.

**Table 5.4.** Cubic-Plus-Association (CPA) equation of state pure component parameters for; water (H<sub>2</sub>O), tetrahydrofuran (THF), cyclopentane (c-C<sub>5</sub>), carbon dioxide (CO<sub>2</sub>) and nitrogen (N<sub>2</sub>). Association schemes according to definition presented in section 5.3.

Comp.	Assoc. scheme	$a_0 \cdot 10^1$ Pa·m <sup>6</sup> ·mole <sup>-2</sup>	$b \cdot 10^5$ m <sup>3</sup> ·mole <sup>-1</sup>	$c_1$	$\beta^{AIBj}$	$\epsilon^{AIBj} \cdot 10^{-4}$ Pa·m <sup>3</sup> ·mol <sup>-1</sup>	Ref.
H <sub>2</sub> O	[2 <sup>+</sup> ;2 <sup>-</sup> ]	1.2277	1.4515	0.6736	0.0692	1.6655	A
THF	[0 <sup>+</sup> ;2 <sup>-</sup> ]	15.5228	6.7670	0.7773	N/A	N/A	B
c-C <sub>5</sub>	N/A	$T_c = 511.7 \text{ K}$ , $P_c = 4.51 \text{ MPa}$ , $\omega = 0.19487$					DIPPR
CO <sub>2</sub>	[0 <sup>+</sup> ;1 <sup>-</sup> ]	3.5079	2.7200	0.7602	N/A	N/A	C
N <sub>2</sub>	N/A	$T_c = 126.2 \text{ K}$ , $P_c = 3.40 \text{ MPa}$ , $\omega = 0.03772$					DIPPR

A [Kontogeorgis et al. (2006)] , B This work [Appendix 3] , C [Tsivintzelis et al. (2011)]

Water is the only component treated as self-associating in this work. Two other components, tetrahydrofuran and carbon dioxide are allowed to cross-associate (solvate) with water, however these two components do not cross-interact with each other. Cyclopentane and nitrogen are treated as non self-associating and non cross-associating.

All possible binary combinations of the above five components have been investigated for their fluid phase equilibria as a part of this work. Non-zero binary interaction parameters ( $k_{ij}$ ) and binary cross-association parameters ( $\gamma^{AIBj}$ ) have been adjusted where needed by correlating CPA to available fluid phase equilibria data found in the literature. For the complete details of this work, please see Appendix 3, Appendix 4 and Appendix 5.

**Table 5.5.** Adjusted parameters for all binary pairs formed by the five components; water, tetrahydrofuran, cyclopentane, carbon dioxide and nitrogen. Up to three binary parameters ( $a_{kij}$ ,  $b_{kij}$ ,  $\gamma^{AIBj}$ ) may be adjusted for binary pairs showing cross-association. A maximum of two binary parameters ( $a_{kij}$ ,  $b_{kij}$ ) may be adjusted in pairs with no cross-association.  $a_{kij}$  and  $b_{kij}$  are related to the binary interaction parameter,  $k_{ij}$ , as shown in equation (5.3.10).  $\gamma^{AIBj}$  enters in the combining rule for the binary cross-association volume according to equation (5.3.12).

Binary Pair	Adj. Parameters.	$k_{ij}$	$\gamma^{AIBj}$
Water-Carbon dioxide	$a_{kij}$ , $b_{kij}$ , $\gamma^{AIBj}$	0.4719 - 112.5/T	0.1707
Water-Nitrogen	$a_{kij}$ , $b_{kij}$	0.9999 - 368.4/T	N/A
Water-Tetrahydrofuran	$a_{kij}$ , $b_{kij}$ , $\gamma^{AIBj}$	0.4084 - 154.7/T	0.2543
Water-Cyclopentane	$a_{kij}$	0.0211	N/A
Carbon dioxide-Nitrogen	$a_{kij}$	-0.0856	N/A
Carbon dioxide-Tetrahydrofuran		0.00	N/A
Carbon dioxide-Cyclopentane	$a_{kij}$	0.1574	N/A
Nitrogen-Tetrahydrofuran		0.00	N/A
Nitrogen-Cyclopentane		0.00	N/A
Tetrahydrofuran-Cyclopentane	$a_{kij}$	0.1070	N/A

All binary parameters presented in Table 5.5 have been adjusted in this work. For the case of water-carbon dioxide, Tsivintzelis et al. (2011) have presented a detailed study comparing several modelling approaches for this pair. When applying the solvation approach, Tsivintzelis et al. proposed a linear temperature dependence for  $k_{ij}$  of the type:  $a_{kij} + b_{kij} \cdot T$ .

In this work, the application of a non-linear temperature dependence has however been found more appropriate in the cases, where a temperature dependence was needed.

## 5.6 The Gibbs Phase Rule

Considering the Gibbs phase rule is important when investigating equilibrium conditions for systems of multi-phase behaviour. This implies both for experimental and theoretical investigations. For this reason, this section provides a

short introduction to the Gibbs phase rule and explains how this rule applies to the hydrate forming systems, investigated as part of this work.

According to the Gibbs phase rule, the number of degrees of freedom ( $F$ )<sup>1</sup> for a simple system<sup>2</sup> in the absence of chemical reactions under the conditions of thermodynamic equilibrium, equals the number of components ( $C$ ) minus the number of phases ( $P$ ) plus two, i.e.  $F = C - P + 2$  [Callen (1985)]. Beltran et al. (2012) recently re-visited the derivation of this rule and showed how this applies to gas hydrate forming systems. Common misconceptions found in the literature were outlined.

The present work focuses mainly on three-phase hydrate(H)-liquid water ( $L_w$ )-vapour(V) equilibria or four-phase hydrate(H)-liquid water( $L_w$ )-liquid organic( $L_a$ )-vapour(V) equilibria in multi-component systems.

The simplest case is H- $L_w$ -V with only one hydrate former (e.g. water and carbon dioxide). In this case the Gibbs phase rule provides a single degree of freedom. If temperature is as the free intensive variable, the equilibrium condition may be represented as a line (often seen as P vs T diagrams). If one more hydrate former is added, without adding an equilibrium phase (as e.g. the water-carbon dioxide-nitrogen system), the degrees of freedom increase by one, and the complete set of equilibrium conditions may be visualised in the form of a plane. In the literature, these systems are often illustrated graphically in the form of several lines in a P vs. T diagram. Each line then represents a given equilibrium composition, typically reported for one of the equilibrium phases (often the vapour or the aqueous liquid phase). When finally adding one more component to the three-phase system (e.g. water-tetrahydrofuran-carbon dioxide-nitrogen), we get three degrees of freedom. In this case, temperature and phase compositions of two phases may be specified. These two phases could be the aqueous liquid and the vapour phase. Graphical illustration of the complete set of equilibrium states becomes complicated.

If one liquid phase is added to the system, with only one hydrate former (e.g. binary system of water-cyclopentane) no degrees of freedom are available, meaning H- $L_w$ - $L_a$ -V equilibrium can occur only in a single point (quadruple point). By removing e.g. the vapour phase, we obtain one degree of freedom and may again represent equilibrium conditions in the form of a line in e.g. a T vs. P diagram. For the specific case of water-tetrahydrofuran, H- $L_w$  equilibrium may occur with two degrees of freedom. This may be illustrated in a T vs. x diagram at

---

<sup>1</sup> The number of degrees of freedom  $F$  is the number of intensive properties such as e.g. temperature, pressure, or phase composition variables, that, without changing the number of phases, are capable of independent variation.

<sup>2</sup> A simple system is a system which is macroscopically homogeneous, isotropic, uncharged, for which surface area phenomena can be neglected and which is not acted on by electric, magnetic or gravitational fields.



constant (specified) pressure, where  $x$  is the mole fraction of tetrahydrofuran in the (equilibrium) aqueous phase.

Going back to the four-phase (H-L<sub>w</sub>-L<sub>a</sub>-V) equilibrium system, with three components (such as e.g. water-cyclopentane-carbon dioxide), we have a single degree of freedom, and this may be represented as a line (e.g. T vs. P diagram). By addition of one more component to the system (e.g. the system water-cyclopentane-carbon dioxide-nitrogen), a di-variant system is obtained.

Another system of this type is the water-tetrahydrofuran-cyclopentane-carbon dioxide quaternary system, showing four-phase equilibrium. In this case the equilibrium state may be determined by specification of e.g. temperature and equilibrium composition of the aqueous liquid phase.

Due to the applied algorithm in the above presented hydrate model, temperature is always chosen as the controlled variable for uni-variant hydrate forming systems (except for the specific case of the pure tetrahydrofuran hydrate). In di-variant or multi-variant systems, things become more complex. In the model only temperature and feed composition may be specified. However, the Gibbs rule does not consider feed compositions, but equilibrium phase compositions. This represents a problem in the cases, where feed compositions are not provided in context with experimental data. In the model, the feed must always be specified such that the number of equilibrium phases corresponds to that reported with the data. However within this region an infinite number of feed compositions may satisfy equilibrium of the given number of phases. If the composition of one equilibrium phase is provided with the experimental data, the feed must be adjusted in the model, such that the model provides the right composition of this phase in the final equilibrium state. In cases where the equilibrium vapour phase composition is provided, as often seen in the system of water-carbon dioxide-nitrogen, the feed may be specified with only sufficient water content to form the aqueous liquid phase, and the remaining carbon dioxide and nitrogen content should then correspond to the composition provided in the data for the equilibrium vapour phase composition. In this way, little gas will dissolve in the liquid phase, and the relative composition in the gas phase will remain constant (for all practical purposes).

## 5.7 Cited Literature

A. L. Ballard, *A Non-Ideal Hydrate Solid Solution Model for a Multiphase Equilibria Program*, Ph.D. Thesis, Colorado School of Mines, Golden, CO (2002).

J. G. Beltran, H. Bruusgaard, P. Servio, *Gas hydrate phase equilibria measurement techniques and phase rule considerations*, J. Chem. Thermodynamics, 44 (2012), 1-4.

H. B. Callen, *Thermodynamics and an introduction to thermostatistics*, John Wiley and sons Inc., New York, Chichester, Brisbane, Toronto, Singapore, 1985.

P. B. Dharmawardhana, W. R. Parrish, E. D. Sloan, *Experimental Thermodynamic Parameters for the Prediction of Natural Gas Hydrate Dissociation Conditions*, Ind. Eng. Chem. Fundam., 19 (1980), 410-414.

DIPPR, Design Institute for Physical Property Data (DIPPR 801). Diadem Pro.

G. K. Folas, G. M. Kontogeorgis, M. L. Michelsen, E. H. Stenby, *Application of the Cubic-Plus-Association (CPA) Equation of State to Complex Mixtures with Aromatic Hydrocarbons*, Ind. Eng. Chem. Res., 45 (2006), 1527–1538.

G. K. Folas, E. W. Froyna, J. Lovland, G. M. Kontogeorgis, E. Solbraa, *Data and prediction of water content of high pressure nitrogen, methane and natural gas*, Fluid Phase Equilibria, 252 (2007), 162-174.

E. Hendriks, H. Meijer, *Computer Aided Property Estimation for Process and Product Design*, 1<sup>st</sup> Ed., Chptr. 11, Edited by G. M. Kontogeorgis and R. Gani, Computer-Aided Chemical Engineering, Vol. 19, Elsevier Science, 2004.

J.-M. Herri, A. Bouchemoua, M. Kwaterski, A. Fezoua, Y. Ouabbas, A. Cameirao, *Gas hydrate equilibria for CO<sub>2</sub>-N<sub>2</sub> and CO<sub>2</sub>-CH<sub>4</sub> gas mixtures – Experimental studies and thermodynamic modeling*, Fluid Phase Equilibria, 301 (2011), 171-190.

P. J. Herslund, K. Thomsen, J. Abildskov, N. von Solms, *Phase equilibrium modeling of gas hydrate systems for CO<sub>2</sub> capture*, J. Chem. Thermodynamics, 48 (2012), 13-27.

P. J. Herslund, K. Thomsen, J. Abildskov, N. von Solms, *Application of the cubic-plus-association (CPA) equation of state to model the fluid phase behaviour of binary mixtures of water and tetrahydrofuran*, Fluid Phase Equilibria, 356 (2013), 209-222.

G. D. Holder, G. Corbin, K. D. Papadopoulos, *Thermodynamic and Molecular Properties of Gas Hydrates from Mixtures Containing Methane, Argon, and Krypton*, Ind. Eng. Chem. Fundam., 19 (1980), 282-286.

S. H. Huang, M. Radosz, *Equation of State for Small, Large, Polydisperse and Associating Molecules*, Ind. Eng. Chem. Res., 29,11 (1990), 2284–2294.

J. B. Klauda, S. I. Sandler, *A Fugacity Model for Gas Hydrate Phase Equilibria*, Ind. Eng. Chem. Res., 39 (2000), 3377-3386.

J. B. Klauda, S. I. Sandler, *Phase behaviour of clathrate hydrates: a model for single and multiple gas component hydrates*, Chem. Eng. Sci., 58 (2003), 27-41.

G. M. Kontogeorgis, E. C. Voutsas, I. V. Yakoumis, D. P. Tassios, *An Equation of State for Associating Fluids*, Ind. Eng. Chem. Res., 35 (1996), 4310-4318.

G. M. Kontogeorgis, I. V. Yakoumis, H. Meijer, E. Hendriks, T. Moorwood, *Multicomponent phase equilibrium calculations for water-methanol-alkane mixtures*, Fluid Phase Equilibria, 158-160 (1999), 201-209.

G. M. Kontogeorgis, M. L. Michelsen, G. K. Folas, S. Derawi, N. von Solms, E. H. Stenby, *Ten Years with the CPA (Cubic-Plus-Association) Equation of State. Part 1. Pure Compounds and Self-Associating Systems*, Ind. Eng. Chem. Res., 45 (2006), 4855-4868.

G. M. Kontogeorgis, G. K. Folas, *Thermodynamic Models for Industrial Applications. From Classical and Advanced Mixing Rules to Association Theories*, John Wiley and Sons, United Kingdom, 2010.

M. Kwaterski, Ecole Nationale Supérieure des Mines de Saint-Etienne, France, *Personal communication*, June 2011.

V. McKoy, O. Sinanoglu, *Theory of Dissociation Pressures of Some Gas Hydrates*, J. Chem. Phys., 38,12 (1963), 2946-2956.

M. L. Michelsen, E. M. Hendriks, *Physical Properties from association models*, Fluid Phase Equilibria, 180 (2001), 165-174.

M.M. Mooijer-van den Heuvel, C.J. Peters, J. de Swaan Arons, *Influence of water-insoluble organic components on the gas hydrate equilibrium conditions of methane*, Fluid Phase Equilibria, 172 (2000), 73-91.

W.R. Parrish, J.M. Prausnitz, *Dissociation Pressures of Gas Hydrates Formed by Gas Mixtures*, Ind. Eng. Chem. Process Des. Develop., 11,1 (1972), 26-35.

J. C. Platteeuw, J. H. van der Waals, *Thermodynamic properties of gas hydrates*, Mol. Phys. 1,1 (1958), 91-95.

- E. D. Sloan, *Clathrate Hydrates of Natural Gases* 2<sup>nd</sup> Ed., Marcel Dekker, New York, 1998.
- E. D. Sloan, C. A. Koh, *Clathrate Hydrates of Natural Gases* 3<sup>rd</sup> Ed., CRC Press, Boca Raton, 2007.
- T. A. Strobel, C. A. Koh, E. D. Sloan, *Thermodynamic predictions of various tetrahydrofuran and hydrogen clathrate hydrates*, Fluid Phase Equilibria, 280 (2009), 61-67.
- F. Takeuchi, R. Ohmura, K. Yasuoka, *Statistical-Thermodynamics Modeling of Clathrate-Hydrate-Forming Systems Suitable as Working Media of a Hydrate-Based Refrigeration System*, Int. J. Thermophys., 30 (2009), 1838-1852.
- I. Tsivintzelis, G. M. Kontogeorgis, M. L. Michelsen, E. H. Stenby, *Modeling phase equilibria for acid gas mixtures using the CPA equation of state. Part II: Binary mixtures with CO<sub>2</sub>*, Fluid Phase Equilibria, 306 (2011), 38-56.

## 6 Experimental Results

Two experimental studies have been carried out as part of this work. The first study was conducted in cooperation with Ecole Nationale Supérieure des Mines de Saint-Etienne. Results from this work have been published and the journal paper [Herslund et al. (2013)] is appended in Appendix 2. Only the main results are presented in the following, the reader is referred to Appendix 2 for the complete set of details from this work.

The second study was planned in cooperation with and executed by Dr. Nagu Daraboina at the Department of Chemical and Biochemical Engineering, Technical University of Denmark. This work was in preparation for publication at the time of writing this thesis and has therefore not been appended in the form of a completed manuscript. The main results from this study are however presented in this thesis.

Three thermodynamically promoted gas hydrate systems have been investigated. All systems operated with pure carbon dioxide gas phases. The first system is the well-known ternary system of water-tetrahydrofuran-carbon dioxide with approximately 5 mole percent tetrahydrofuran in the initial liquid phase. Hydrate-liquid water-vapour equilibrium pressures are presented for this system in section 6.1.

The second system is the ternary system of water-cyclopentane-carbon dioxide. Hydrate-liquid water-liquid organic-vapour equilibrium pressures are reported for this system in section 6.2.

The third system is the mixed promoter system of water-tetrahydrofuran-cyclopentane-carbon dioxide. Hydrate-liquid water-liquid organic-vapour equilibrium pressures are reported for this system in section 6.3.

### 6.1 *The Tetrahydrofuran Promoted System*

Equilibrium pressures as function of temperature for the tetrahydrofuran promoted system, obtained using the experimental equipment and procedure #1 (Section 4.1) are presented along with the experimentally determined tetrahydrofuran concentrations in the equilibrium liquid phase in Table 6.1.

**Table 6.1.** H-Lw-V equilibrium conditions for the ternary system of water-tetrahydrofuran-carbon dioxide obtained by (Procedure #1).  $x(\text{THF})$  is the liquid phase mole fraction of tetrahydrofuran at the equilibrium condition [Data from Appendix 2].

Temperature / K	Pressure / MPa	$x(\text{THF})$
283.3	0.61	0.057
284.3	0.75	0.050
285.2	0.91	0.053

The tetrahydrofuran mole fractions reported in Table 6.1 are in fact compositions from the equilibrium liquid phase, unlike those concentrations reported elsewhere, which are most often mole fractions of tetrahydrofuran in the initial liquid phase prior to loading.

Similar results to those presented for Procedure #1 have been obtained in the second experimental study (Procedure #2 described in section 4.2). Here an initial tetrahydrofuran mole fraction of 0.050 was used. The equilibrium mole fractions of tetrahydrofuran in the liquid phase were not determined but are expected to remain unchanged (for all practical purposes). Equilibrium pressures for this system are presented in Table 6.2.

**Table 6.2.** H-Lw-V equilibrium conditions for the ternary system of water-tetrahydrofuran-carbon dioxide obtained by (Procedure #2).  $x(\text{THF})$  is the initial liquid phase mole fraction of tetrahydrofuran.

Temperature / K	Pressure / MPa	$x(\text{THF})^a$
282.35	0.58	0.05
284.15	0.85	0.05
287.45	1.62	0.05
289.15	2.14	0.05
291.65	3.70	0.05

<sup>a</sup> Initial liquid composition – not equilibrium data.

Results from the two investigations are compared internally as well as compared to a selection of results presented in the literature for similar systems in Figure 6.1.

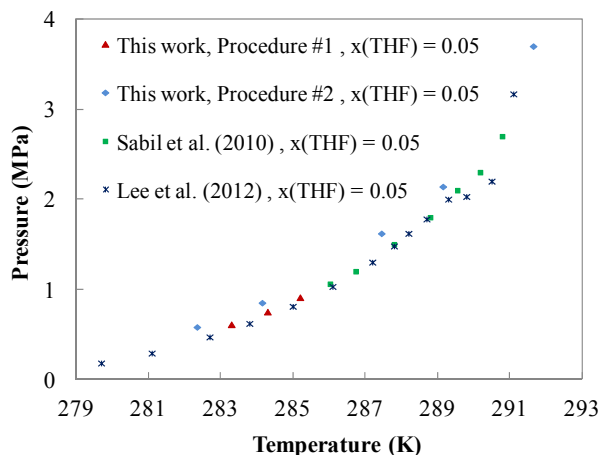


**Figure 6.1.** Hydrate-Liquid water-Vapour equilibrium pressures as function of temperature for the ternary system of water-tetrahydrofuran-carbon dioxide.  $x(\text{THF})$  denotes mole fraction of tetrahydrofuran in the initial liquid phase.

It is seen that the obtained results compare reasonably well internally as well as to the data from the literature. The data from study#2 does however appear to be slightly elevated in terms of pressure compared to the remaining data. The above results serve to confirm the validity of both experimental set-up's and procedures for the investigation of hydrate-liquid-vapour equilibrium pressures in the present system.

This work has added further data to the temperature range below 285 K, where only few data were available prior to these studies.

## 6.2 The Cyclopentane Promoted System

The cyclopentane promoted system is different from a fluid phase behaviour point of view compared to the tetrahydrofuran promoted system due to the additional cyclopentane-rich bulk phase added to the system. Thus, four-phase hydrate-liquid water-liquid organic-vapour equilibrium pressures are reported for this system.

The data from the first study (Procedure #1 - Appendix 2) has previously been shown to compare well with the available literature data at the highest temperatures investigated (approximately 285 K), however the trend in the data does not follow the trends seen at temperatures above 285 K. The dissociation pressure of the mixed cyclopentane-carbon dioxide hydrate was shown to lower only by 0.1 MPa (from 0.52 MPa to 0.42 MPa) in the temperature range from 284 K to 275 K. The complete set of data may be found in Appendix 2.

Originally this was explained by possible mass-transfer limitations in the system [Herslund et al. (2013)], preventing the system to fully equilibrate.

Further analyses of this system have however resulted in another, equally plausible explanation. Cyclopentane and carbon dioxide show high mutual miscibilities at the applied conditions of high pressure and low temperature. The system under investigation was initiated with a cyclopentane-rich liquid bulk phase corresponding to approximately 10 volume percent of the total liquid loading. Thus sufficient bulk cyclopentane was present in the equilibrium cell to saturate both the aqueous and the carbon dioxide-rich vapour phase, without the bulk-phase disappearing. However as crystallisation occurred, and cyclopentane was consumed, the amount of the cyclopentane bulk phase diminished. By following the amount of water left in the system, it was suggested by Herslund et al. (2013) that more than half of the initial cyclopentane content in the system had been converted into hydrate at a temperature of 284.3 K and a pressure of 5.2 MPa. Thus it is considered likely, that an insufficient amount of cyclopentane has been present to saturate the vapour phase at low temperatures while simultaneously forming the bulk liquid phase. This might have resulted in the disappearance of the cyclopentane-rich bulk liquid phase. All data presented at temperatures below 285 K could therefore represent hydrate-liquid water-vapour equilibrium and not hydrate-liquid water-liquid organic-vapour equilibrium as they were originally presented. If this is the case, these data are of little value according to the Gibbs phase rule, since no fluid phase composition was monitored during the experiments. By removing one phase from the uni-variant system, we move into a region, where the system becomes di-variant (composition dependence of pressure with the chosen set-up and procedure).

Only temperatures above 285 K was investigated in study #2 (Procedure #2), and the above problematic was avoided. The obtained results are presented in Table 6.3 and illustrated in Figure 6.2, where they are compared with data reported at similar conditions for this ternary system.

**Table 6.3.** H-L<sub>w</sub>-L<sub>a</sub>-V equilibrium conditions for the ternary system of water-cyclopentane-carbon dioxide obtained by (Procedure #2).

Temperature / K	Pressure / MPa
284.6	0.49
286.8	0.97
288.5	1.44
290.2	1.89
291.6	2.58



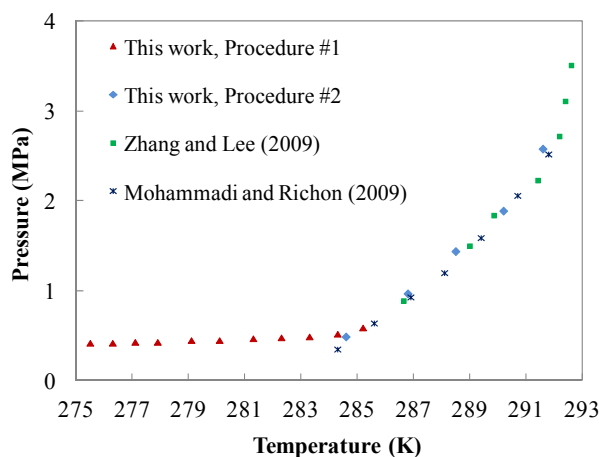


**Figure 6.2.** Hydrate-Liquid water-Liquid organic-Vapour four-phase equilibrium pressures as function of temperature for the ternary system of water-cyclopentane-carbon dioxide. Note that the data measured in this work (Procedure #1) at temperatures below 285 K could represent Hydrate-Liquid water-vapour three-phase equilibrium.

The reported data from study #2 compare well with the literature data, confirming this setup and procedure also for the cyclopentane promoted system.

The investigation of this ternary system has suggested one shortcoming in set-up and procedure #1. The missing possibility of visual inspection of the cell contents complicates the final analysis of the obtained results. When working with multi-phase systems, it is not possible to verify the actual number of phases present in the system at a given equilibrium stage.

### 6.3 The Mixed Promoter System

The mixed tetrahydrofuran-cyclopentane promoter system has, to our knowledge, been presented for the first time in the literature as a part of this work [Appendix 2]. Therefore, no other data can be used for comparison to validate the results obtained for this system. The quaternary system of water-tetrahydrofuran-cyclopentane-carbon dioxide has been investigated for equilibrium pressures in the four-phase hydrate-liquid water-liquid organic-vapour region.

The results presented in study #1 indicated a synergistic effect, where the pressure reduction (thermodynamic promotion) was enhanced compared to the two individual promoter systems. These results may be found in Figure 10 of Appendix 2.

The mixed promoter system however also showed little pressure decrease with decreasing temperature for temperatures below 283 K. For this reason, it is suspected, that the cyclopentane bulk liquid phase, like in the pure cyclopentane promoted system, might have been eliminated in the low temperature region during hydrate formation.

Thus, the mixed promoter system was further investigated in study #2. A higher tetrahydrofuran concentration in the initial aqueous phase was applied to investigate if an increased amount of tetrahydrofuran would enhance the synergistic effect observed in the first study. A two-phase liquid promoter solution was prepared by mixing a 5.5 mole percent aqueous solution of tetrahydrofuran with pure cyclopentane liquid. The molar ratio of aqueous liquid to cyclopentane liquid in the feed was approximately 19/1. The two-phase promoter liquid had a final composition of {0.894; 0.052; 0.054} in mole fractions of water, tetrahydrofuran and cyclopentane respectively.

The obtained four-phase equilibrium pressures are listed in Table 6.4.

**Table 6.4.** H-L<sub>w</sub>-L<sub>a</sub>-V equilibrium conditions for the quaternary system of water-tetrahydrofuran-cyclopentane-carbon dioxide obtained by (Procedure #2).

Temperature / K	Pressure / MPa	x(THF) <sup>a</sup>	x(Cyclopentane) <sup>b</sup>
285.2	0.42	0.055	0.054
288.2	1.05	0.055	0.054
291.0	1.77	0.055	0.054
292.1	2.26	0.055	0.054
293.2	2.92	0.055	0.054

<sup>a</sup> Initial mole fraction of tetrahydrofuran in the aqueous liquid before mixing with cyclopentane – not equilibrium data.

<sup>b</sup> Initial liquid mole fraction of cyclopentane (in the form of a separate bulk phase) – not equilibrium data.

Figure 6.3 compares the obtained results with those reported from study #1 for the mixed hydrate system, using a 1 mole percent tetrahydrofuran aqueous solution as well as the pure cyclopentane promoter system investigated in study #2.

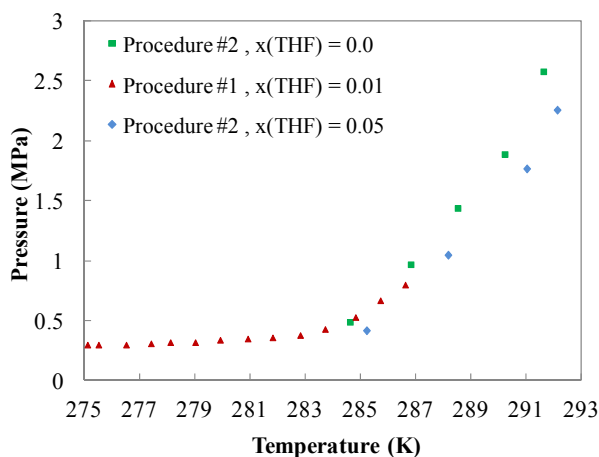


**Figure 6.3.** Hydrate-Liquid water-Liquid organic-Vapour four-phase equilibrium pressures as function of temperature for the quaternary system of water-tetrahydrofuran-cyclopentane-carbon dioxide.  $x(\text{THF})$  denotes initial mole fraction of tetrahydrofuran in the aqueous phase feed.  $x(\text{THF}) = 0.0$  represents the pure cyclopentane promoted system (water-cyclopentane-carbon dioxide). Note that the data measured in this work (Procedure #1) at temperatures below 284 K could represent Hydrate-Liquid water-vapour three-phase equilibrium.

Figure 6.3 clearly illustrates the synergistic effect occurring in the mixed promoter system. The phase boundary of the mixed promoter hydrate is shifted approximately 1.5 K up in temperature compared to the pure cyclopentane promoted hydrate pressures measured in this work (Procedure #2). The pressures reported for the mixed hydrate system in the high temperature region (291 K - 292 K) are reduced by approximately 20 percent compared to the pure cyclopentane promoted system. The synergistic effect becomes less pronounced at low temperatures.

Interestingly, the high-temperature results from study #1 are placed in between the pure cyclopentane promoted system and the 5 mole percent tetrahydrofuran plus cyclopentane mixed promoter system. This suggests that the synergy effect depends on the amount of tetrahydrofuran present in the system. A direct quantitative comparison of the two sets of data for the mixed promoter system can however not be done, since the two systems were initialised with different relative amounts of cyclopentane bulk liquid. Upon mixing, tetrahydrofuran is expected to distribute between the aqueous phase and the organic phase. Exactly how this distribution occurs has not been quantified. Hence, at the equilibrium condition, the tetrahydrofuran concentration in the aqueous phase may have changed significantly compared to that of the aqueous feed liquid.

## 6.4 Summary of Experimental Results

The present work has confirmed the thermodynamic promoting effects reported in the literature for the two classical slI hydrate formers, tetrahydrofuran and cyclopentane.

Low temperature data have been added for the mixed hydrates of tetrahydrofuran and carbon dioxide formed in 5 mole percent aqueous solutions of tetrahydrofuran. The presented data compared well with the few other data available in the literature in this temperature and composition range.

An attempt was made to measure four-phase hydrate-liquid water-liquid organic-vapour equilibria for the ternary system of water-cyclopentane-carbon dioxide. It is suspected that this system reduces to three phases (hydrate-liquid water-vapour) at low temperature and low pressures. Large amounts of cyclopentane are expected to transfer to the vapour phase. Thus, less than the expected amount of bulk liquid is present to form the desired hydrate phase. As hydrates form, the organic bulk phase is quickly consumed. The suspected three-phase hydrate-liquid water-vapour equilibrium pressures were shown to decrease little with decreasing temperature.

Finally, it was shown that the addition of tetrahydrofuran to the ternary system of water-cyclopentane-carbon dioxide provided an enhanced thermodynamic promotion of the hydrate phase. Four-phase hydrate equilibrium pressures were reduced by approximately 20 percent compared to the pure cyclopentane promoted system, considered a reference prior to this study. Though not shown in the present work, subsequent studies, investigating the kinetics of the mixed promoter system, have shown that this system does provide the short induction times of the tetrahydrofuran promoted system and furthermore the fast crystal growth of the cyclopentane promoted system [Dr. Nagu Daraboina, Technical University of Denmark]. This makes the mixed promoter hydrate system more favourable than the two pure promoter systems from a capture process point of view.

## 6.5 Cited Literature

N. Daraboina, Department of Chemical and Biochemical Engineering, Technical University of Denmark, Denmark, *Personal communication* September 2013.

P. J. Herslund, K. Thomsen, J. Abildskov, N. von Solms, A. Galfré, P. Brântuas, M. Kwaterski, J.-M. Herri, *Thermodynamic promotion of carbon dioxide-clathrate hydrate formation by*

*tetrahydrofuran, cyclopentane and their mixtures*, Int. J. Greenhouse Gas Control, 17 (2013), 397-410.

Y.-J. Lee, T. Kawamura, Y. Yamamoto, J.-H. Yoon, *Phase Equilibrium Studies of Tetrahydrofuran (THF) + CH<sub>4</sub>, THF + CO<sub>2</sub>, CH<sub>4</sub> + CO<sub>2</sub> and THF + CO<sub>2</sub> + CH<sub>4</sub> Hydrates*, J. Chem. Eng. Data, 57 (2012), 3543-3548.

A. H. Mohammadi, D. Richon, *Phase equilibria of clathrate hydrates of methyl cyclopentane, methyl cyclohexane, cyclopentane or cyclohexane + carbon dioxide*, Chemical Engineering Science, 64 (2009), 5319-5322.

K. M. Sabil, G.-J. Witkamp, C. J. Peters, *Estimations of enthalpies of dissociation of simple and mixed carbon dioxide hydrates from phase equilibrium data*, Fluid Phase Equilibria, 290 (2010a), 109-114.

J. S. Zhang, J. W. Lee, *Equilibrium of Hydrogen + Cyclopentane and Carbon Dioxide + Cyclopentane Binary Hydrates*, J. Chem. Eng. Data, 54 (2009), 659-661.



## 7 Modeling Results

The algorithm of the above presented model, providing fluid phase equilibrium conditions from the CPA multi-phase flash calculation (Gibbs energy minimisation) as inputs to the van der Waals-Platteeuw hydrate model, ensures a consistent calculation of equilibrium conditions in systems with both hydrate forming and non-hydrate forming components.

Often in the literature, models are presented, where the van der Waals-Platteeuw hydrate model is coupled with an equation of state for the vapour phase, a Gibbs excess energy model or an activity coefficient model for the activity of water in the liquid phase, and finally correlations for solubilities of gas phase components in the liquid phase (e.g. the Krichevsky and Kasarnovsky equation [Krichevsky and Kasarnovsky (1935)]).

In the present model, the CPA equation of state, with a limited number of parameters, provides all the required inputs for the hydrate model in a straightforward and consistent manner.

Being consistent in all fluid phases, this model may not only be used to describe or predict conditions of incipient gas hydrate formation, it also accurately describes or predicts the number and type of co-existing fluid phases and the distribution of feed components in the fluid phases at equilibrium conditions. For this reason, emphasis has been put on “tuning” the fluid phase description to create an accurate and reliable framework for the complete model (including the hydrate model).

CPA fluid phase modeling results are presented in the following for binary and ternary sub-systems within the five component system of water, tetrahydrofuran, cyclopentane, carbon dioxide and nitrogen. These results serve as a validation of the inputs supplied later to the van der Waals-Platteeuw gas clathrate hydrate model.

Hydrate modeling results are finally presented both for the unpromoted hydrate systems and the promoted hydrate systems containing tetrahydrofuran, cyclopentane or their mixtures.

When comparing model results to experimental data, the term Average Absolute (relative) Deviation (AAD) is used. AAD is defined according to equation (7.1).

$$AAD = \frac{1}{N} \sum_{i=1}^N \left| \frac{s_{calc,i} - s_{exp,i}}{s_{exp,i}} \right| \quad (7.1)$$

Where  $s_{calc}$  is the calculated property of interest ( $s$  may be temperature, pressure, composition etc.) and  $s_{exp}$  is the experimental reference data.  $N$  is the total number of data points.

Generally (both for fluid phase modeling and hydrate modeling), in cases, where correlation of parameters is needed, optimisation is done by minimising the sum of absolute relative deviations between model descriptions and experimental data. The objective function has been defined as equation (7.2).

$$Obj = \sum_{i=1}^N \left| \frac{s_{calc,i} - s_{exp,i}}{s_{exp,i}} \right| \quad (7.2)$$

Where  $s_{calc}$  again is the calculated property of interest ( $s$  may be temperature, pressure, composition etc.) and  $s_{exp}$  is the experimental reference data.  $N$  is the total number of data points used as reference. Other definitions of the objective function, such as the sum of squared differences or the sum of squared relative differences, have been tested for some systems without noticeable improvements.

Optimisation of parameters in this work has been performed by use of an optimisation algorithm based on a FORTRAN implementation of the simulated annealing (SA) global optimisation algorithm and implementation presented by Goffe *et al.* (1994) (source code available via [SIMANN.F]). The simulated annealing algorithm has the disadvantage of being slow (large number of function evaluations), however being based on stochastic principles, it may be used in cases, where the objective function is discontinuous due to user-defined constraints. Such a case was studied as part of this work in the binary system of water and tetrahydrofuran. More information on this may be found in Appendix 3.

## 7.1 Fluid Phase Modeling

The system of five components forms a total of 10 binary pairs, for which it is possible to improve descriptions, in case the CPA predictions are unsatisfactory. 9 binary pairs have been modelled as a part of this study. No experimental data were found for the 10<sup>th</sup> pair, comprised of tetrahydrofuran and cyclopentane.

Fluid phase equilibrium data have been retrieved from the literature, be it vapour-liquid-equilibrium (VLE), liquid-liquid-equilibrium (LLE) or vapour-liquid-liquid equilibrium (VLLE). By comparing CPA predictions with such data, it has been investigated whether or not correlation of binary parameters ( $k_{ij}$  and/or  $\gamma^{A|Bj}$ ) in CPA was needed.



### 7.1.1 Water-Carbon dioxide

Tsivintzelis et al. (2011) have presented a thorough study on the modelling of binary systems of water and carbon dioxide using CPA. It was concluded that this binary system can successfully be modelled if cross-association (solvation) between water and carbon dioxide is accounted for. Water is treated as a self-associating compound applying an association scheme with two electron donating and two electron accepting sites [ $2^+$ ;  $2^-$ ]. CO<sub>2</sub> is modelled as a non self-associating compound in its pure state, but is allowed to cross-associate (solvate) with water via a single association site. Tsivintzelis et al. assigned the notation “electron acceptor” to this association site (positive charge).

Using this approach, accurate descriptions of both the water-rich and carbon dioxide-rich fluid phases are obtained over extended ranges of temperature and pressure.

In the work of Tsivintzelis et al., a temperature dependent binary interaction parameter (among others) is proposed. Tsivintzelis et al. applied a linear, two-parameter dependence of the type;  $a_{kij} + b_{kij} \cdot T$ .

The present work uses the proposed approach and the three pure component parameters presented by Tsivintzelis et al. However, new binary parameters for the system water-carbon dioxide have been regressed in this work, using the same reference data as suggested by Tsivintzelis et al. A non-linear temperature dependence on the binary interaction parameter ( $k_{ij}$ ) has been applied according equation (5.2.10). For the details of this work, the reader is referred to Appendix 4.

Figure 7.1 a), b), c) and d) illustrate the model performances for the binary system of water and carbon dioxide at two temperatures, 288 K and 308 K. Comparisons are made with a selection of the experimental data available at the two temperatures [Wiebe and Gaddy (1940), Gillespie and Wilson (1982), Valtz et al. (2004)]. CPA results are obtained by performing a two-phase P/T flash on an equimolar (50/50) feed of the two components.

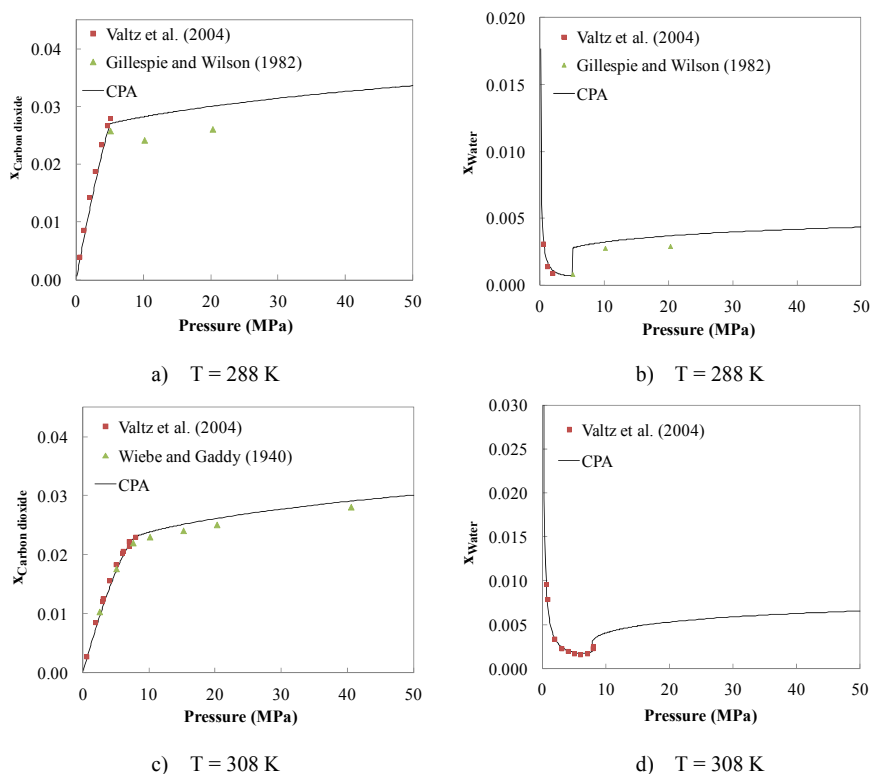


**Figure 7.1.** Fluid phase equilibria in the binary system of water and carbon dioxide. **a)** Carbon dioxide mole fraction in the water-rich phase at  $T = 288 \text{ K}$ . **b)** Water mole fraction in the carbon dioxide-rich phase at  $T = 288 \text{ K}$ . **c)** Carbon dioxide mole fraction in the water-rich phase at  $T = 308 \text{ K}$ . **d)** Water mole fraction in the carbon dioxide-rich phase at  $T = 308 \text{ K}$ .

Excellent agreement between CPA and the experimental data are found at both temperatures. As reported by Tsivintzelis et al., applying this modelling approach enables an accurate description of the minimum solubility of water occurring in the carbon dioxide-rich phase around the phase transition of this phase from vapour-like at low pressures to liquid-like at high pressures.

Average absolute deviations (AAD's) of 9.1 percent are obtained for both the description of the carbon dioxide mole fractions in the water-rich phase and the water mole fractions in the carbon dioxide-rich phase.

### 7.1.2 Water-Nitrogen

Nitrogen is treated as a non-associating compound. For simplicity, the three pure component parameters for this component are calculated from the critical temperature, critical pressure and acentric factor ( $T_c$ ,  $P_c$ ,  $\omega$ ) in a manner identical

to that applied for the cubic Soave-Redlich-Kwong (SRK) equation of state. The pure component critical properties are taken from the DIPPR database.

The predictions of CPA for the binary system of water and nitrogen are unsatisfactory, hence a non-zero binary interaction parameter ( $k_{ij}$ ) is applied. In order to obtain accurate description of both the water-rich and the nitrogen-rich fluid phases over extended ranges of temperature, a non-linear, temperature-dependent BIP has been incorporated in the model.

Figure 7.2 illustrates the model performance for the binary system of water and nitrogen at two temperatures, 273 K and 298 K. Comparisons are made with a selection of experimental data available at these two temperatures [Goodman and Krase (1931), Rigby and Prausnitz (1968), Althaus (1999), Chapoy et al. (2004)].

The water content in the vapour phase (nitrogen-rich phase) is well described by the model at both temperatures. Whereas the accuracy of the CPA model in terms of describing the nitrogen content in the water-rich phase is only acceptable at 273 K, CPA performs very well for these types of data at 298 K.

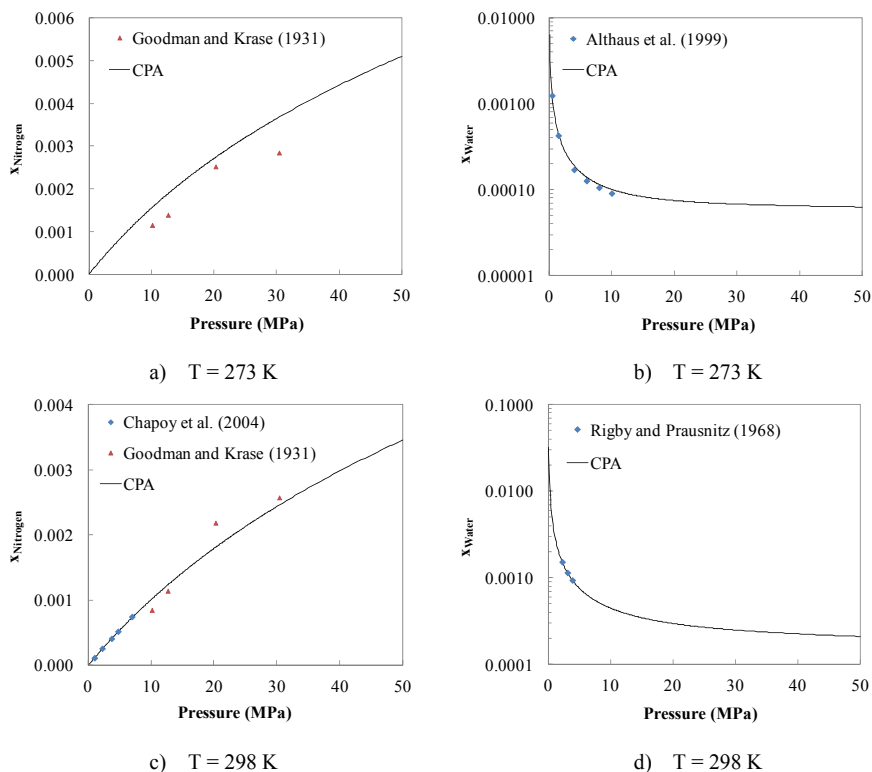


**Figure 7.2.** Vapour-liquid equilibria in the binary system of water and nitrogen. **a)** Nitrogen mole fraction in the water-rich phase at  $T = 273 \text{ K}$ . **b)** Water mole fraction in the nitrogen-rich phase at  $T = 273 \text{ K}$ . **c)** Nitrogen mole fraction in the water-rich phase at  $T = 298 \text{ K}$ . **d)** Water mole fraction in the nitrogen-rich phase at  $T = 298 \text{ K}$ .

The water content in the vapour phase (nitrogen-rich phase) is well described by CPA at both temperatures.

The obtained binary parameters provide an accurate description of this binary system in the temperature interval, which is expected to be the working range for the hydrate model.

### 7.1.3 Water-Tetrahydrofuran

A detailed study on the CPA modelling of this binary system has been presented as part of this work [Herslund et al. (2013) - Appendix 3]. Water is treated as a self-associating compound applying an association scheme with two electron donating and two electron accepting sites.

Tetrahydrofuran has been modelled as a non self-associating compound in its pure state but is allowed to cross-associate (solvate) with water via two

association sites (electron donating). This is consistent with the physical picture of this mixture.

Applying this approach provides accurate descriptions of both low-pressure vapour-liquid equilibria (VLE) and high-pressure/high temperature liquid-liquid equilibria (LLE) using a single set of CPA parameters (three binary parameters adjusted).

No fluid phase equilibrium data has been found in the literature, at conditions of temperature and pressure, where the structure II hydrates of THF form. Hence, no validation of the CPA parameters at these conditions has been possible. However, the fact that CPA correctly describes the complex behaviour of this complex binary system over extended ranges of temperature and pressure ( $T = 298 \text{ K} - 406 \text{ K}$  and  $P = 0.003 \text{ MPa} - 6.1 \text{ MPa}$ ) suggests the validity of the model parameters over an extended range of conditions.

The fluid phase behaviour of the binary THF/water system is highly non-ideal and displays some uncommon phenomena. At low to ambient pressures and temperatures, THF and water are fully miscible in their liquid states. The miscibility of these components is expected to be a result of hydrogen bonding occurring between the oxygen atom on THF and hydrogen atoms on water. Due to the cyclic structure of THF, the oxygen atom becomes more “exposed” than what is normally the case for linear ethers. THF thereby displays some degree of polarity, which could explain the greatly enhanced miscibility of THF in water, compared to linear ethers in water.

A sign of the highly non-ideal behaviour of THF/water mixtures is found in the low pressure VLE reported in the literature. Here, a low boiling azeotrope occurs at high THF concentrations, indicating strong negative deviations from Raoult’s law. Generally, with increasing temperature, the position of the azeotropic mixture composition moves towards lower THF concentrations. This phenomenon may be observed in Figure 7.3. The fact that the azeotropic behaviour is of the low-boiling type, supports the theory that THF and water cross interacts possibly by hydrogen bonding.

Despite THF and water being fully miscible at low pressures, a closed-loop miscibility gap occurs at temperatures above 345 K and elevated pressures. The formation of a closed-loop miscibility gap in binary mixtures may be explained in terms of a competition between entropic and energetic effects. For an explanation on this, please refer to [Garcia-Lisbona et al. (1998)].

Wallbruch and Schneider (1995) showed experimentally that the closed loop miscibility gap shrinks with increasing pressure and the binary system finally reaches a hypercritical point at  $T = 365 \text{ K}$ ,  $P = 24.7 \text{ MPa}$  and  $x_{\text{THF}} = 0.22$ . Riesco and Trusler (2005) confirmed the pressure effect found by Wallbruch and Schneider.

Figure 7.3 compares CPA descriptions of the azeotropic VLE for the binary system of tetrahydrofuran and water at three temperatures (298.15 K, 323.15 K and 343.15 K) with a selection of available experimental data at these conditions [Shnitko and Kogan (1968), Signer et al. (1969), Matous et al. (1972), Treiner (1973)].

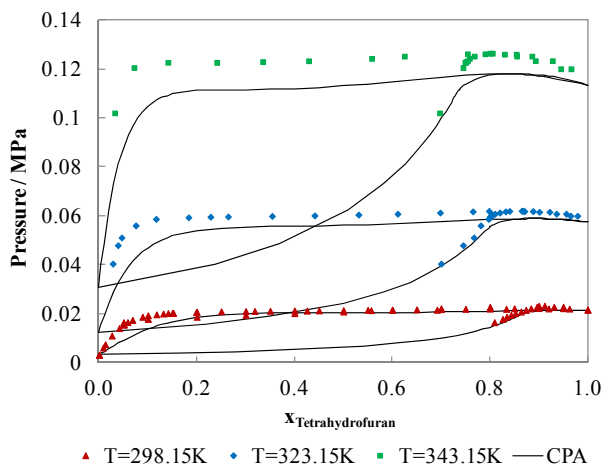


**Figure 7.3.** Comparison of correlated and experimental boiling point and dew point pressures as functions of the tetrahydrofuran (THF) mole fraction in the binary system of water and THF. Results at three temperatures are presented. Pure component parameters for CPA are those listed in Experimental data from [Shnitko and Kogan (1968), Signer et al. (1969), Matous et al. (1972), Treiner (1973)].

The azeotrope is well described at 298 K. Similarly, the experimentally documented tendency of the azeotrope to move to lower concentrations with increasing temperature is likewise described by CPA. At atmospheric pressure, the azeotrope occurs at a tetrahydrofuran mole fraction of approximately 0.82 [Matsuda et al. (2011)]. CPA places the azeotrope at a THF mole fraction of approximately 0.85. Generally, CPA underestimates the boiling point pressure of the liquid mixtures. This effect is most pronounced at high temperatures, where the boiling point pressures are underestimated by approximately 0.01 MPa (approximately 8 percent) in the THF mole fraction range from 0.2 - 0.8. The largest deviations compared to the experimental data are found in the THF mole fraction range from 0.05 - 0.2.

Figure 7.4 illustrates predicted liquid-liquid equilibrium at elevated pressures. Comparisons are made with experimental data reported by Riesco and Trusler (2005).

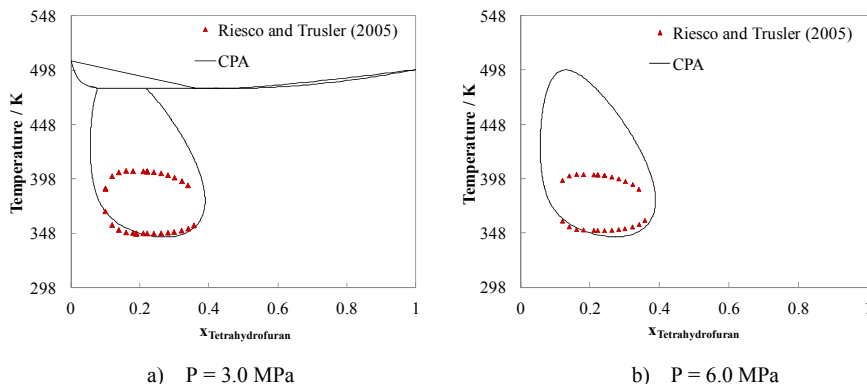


**Figure 7.4.** Comparison of CPA predictions and experimental data for liquid-liquid equilibrium at high temperature and elevated pressures for the binary system of tetrahydrofuran and water. **a)**  $P = 3.0$  MPa, **b)**  $P = 6.0$  MPa.

At a pressure of 3 MPa, CPA extends the LLE region up in temperature until the upper critical VLLE point. However, the composition range of the LLE region is accurately predicted. The closed-loop LLE behaviour is predicted by CPA, when pressure is increased to 6.0 MPa. The upper critical solution temperature is however significantly overestimated. For further details and comments on the modeling of this system, please see Appendix 3.

#### 7.1.4 Water-Cyclopentane

A detailed CPA modeling study on this binary pair is presented in Appendix 5. Only the final modeling results are presented here, the reader is referred to Appendix 5 for the details.

Cyclopentane is assumed a non self-associating compound and thus has three pure component parameters in CPA. These parameters are calculated from the critical properties of the pure component as done for the SRK equation of state. It was found that this approach provided unsatisfactory descriptions of the pure component liquid density. However, modeling cyclopentane with SRK pure component parameters provided better predictions of LLE in the binary system with water than if the pure component parameters had been correlated. A binary interaction parameter was however still needed to correct the description of cyclopentane content in the water-rich phase at low temperatures.

CPA Prediction ( $k_{ij} = 0.0$ ) and final, correlated CPA results for LLE in the binary pair of water and cyclopentane are illustrated in Figure 7.5.

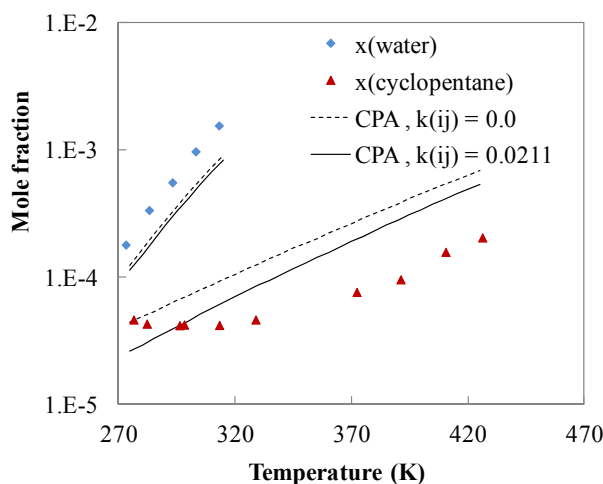


**Figure 7.5.** Comparison of predicted ( $k_{ij} = 0.0$ ) and final ( $k_{ij} = 0.0211$ ) modeling results for liquid-liquid equilibrium in the binary system of water and cyclopentane.  $X(\text{water})$  is the water mole fraction in the oil-rich liquid phase.  $x(\text{cyclopentane})$  is the cyclopentane mole fraction in the water-rich liquid phase. Experimental data from [Englin et al. (1965), Price (1976), Groves (1988), Chapoy et al. (2008)].

The water in oil content is not very well described by CPA for this binary pair. The reason for this was investigated and it was concluded that these experimental data may be questionable. For the full analysis of this, please see Appendix 5.

### 7.1.5 Tetrahydrofuran-Carbon dioxide

Both tetrahydrofuran and carbon dioxide are modelled as non self-associating compounds in their pure states. In the binary system comprised of these compounds, both species are similarly assumed not to associate. CPA accurately predicts the fluid phase equilibria of this system. An attempt was made to improve the high-temperature description of this binary system by applying a non-zero  $k_{ij}$ . However, an adjustment of the model (using a non-zero  $k_{ij}$ ) could hardly be justified due to the insignificant improvements obtained.



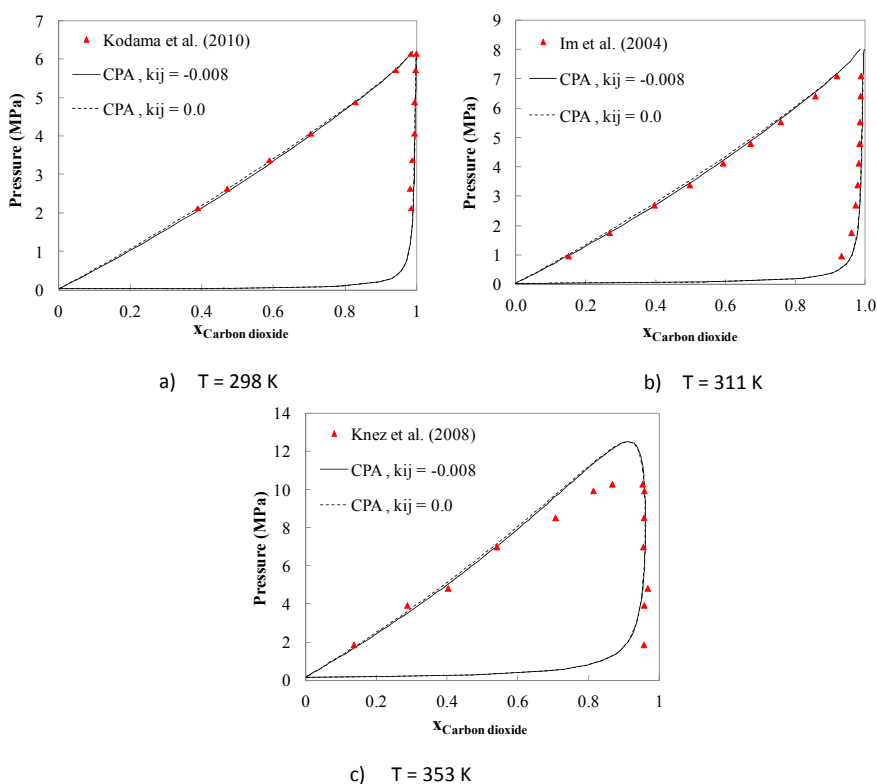


**Figure 7.6.** Fluid phase equilibria in the binary system of tetrahydrofuran and carbon dioxide. Comparison of experimental data (red triangles), CPA prediction with  $k_{ij} = 0.0$  (dashed lines) and CPA with  $k_{ij} = -0.008$  (solid lines). **a)**  $T = 298 \text{ K}$ . **b)**  $T = 311 \text{ K}$ . **c)**  $T = 353 \text{ K}$ .

CPA overestimates the upper pressure limit of the two-phase region seen at  $T = 353 \text{ K}$  (Figure 7.6 c) by roughly 20 percent. However, the low temperature description of the system is sufficiently accurate for the purpose of this model.

### 7.1.6 Tetrahydrofuran-Nitrogen

Only a single data set has been found for the fluid phase equilibria of the binary system of tetrahydrofuran and nitrogen. Five equilibrium data points for the composition of the tetrahydrofuran-rich liquid phase are presented by Gibanel et al. (1993).

CPA predictions of the solubility of nitrogen in liquid tetrahydrofuran at 0.1 MPa are compared to these experimental data in Figure 7.7.

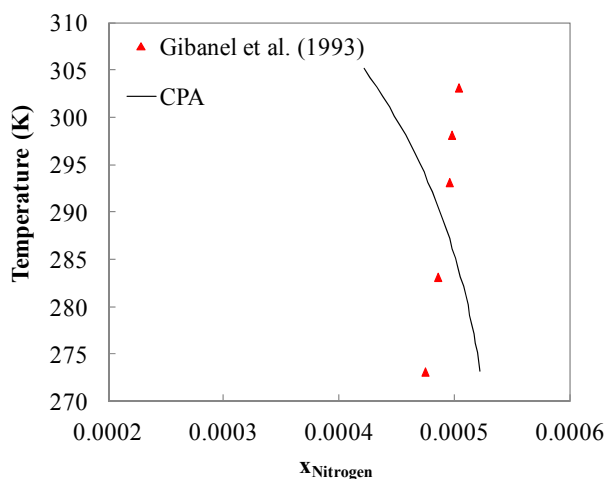


**Figure 7.7.** Solubility of nitrogen in liquid tetrahydrofuran at  $P = 0.1$  MPa. Comparison of experimental data and CPA predictions ( $k_{ij} = 0.0$ ).

CPA correctly predicts the order of magnitude of the nitrogen solubility in liquid tetrahydrofuran. However, the temperature dependence of the solubility is not captured by the model. Gibanel et al. found that the solubility of nitrogen increased with increasing temperature, whereas CPA predicts a decrease in the solubility with increasing temperature.

The application of a non-zero BIP does not enable CPA to describe this opposite tendency. Applying a temperature dependent BIP can improve the description in the temperature interval shown, however this can hardly be justified considering the limited number of data points available for only one phase in this system.

Hence we use CPA predictions for the fluid phase behaviour of this binary pair in the model development that follows.

### 7.1.7 Cyclopentane-Carbon dioxide

Both cyclopentane and carbon dioxide are treated as non self-associating compounds in their binary mixtures. Only experimental VLE data at temperatures below 400 K have been considered in this work. More data exists at higher temperatures.

A high value for the binary interaction parameter ( $k_{ij}$ ) of this pair is needed to correlate the VLE data of this system. Figure 7.8 a) compares the VLE predictions of CPA ( $k_{ij} = 0.0$ ) with the final correlated results ( $k_{ij} = 0.1574$ ) at a temperature of 293 K. The depicted experimental data are from Shah et al. (1991).

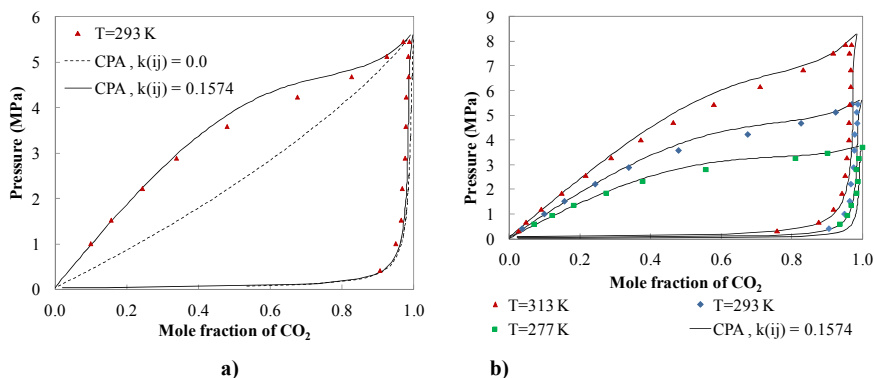


**Figure 7.8.** Comparison of model results and experimental data for VLE in the binary system of cyclopentane and carbon dioxide. Solid lines: CPA description with  $k_{ij} = 0.1574$ . **a)**  $T = 293$  K. Experimental data from [Shah et al. (1991)]. Dashed lines: CPA predictions ( $k_{ij} = 0.0$ ). **b)**  $T = 277$  K,  $293$  K and  $313$  K. Experimental data from [Shah et al. (1991)].

CPA tends to overestimate the solubility of carbon dioxide in the liquid cyclopentane phase. A significant gain in accuracy in the description of this phase composition is obtained by applying a positive  $k_{ij}$ .

### 7.1.8 Cyclopentane-Nitrogen

No association is allowed in the binary pair of cyclopentane and nitrogen. Both components are treated as non self-associating and pure component parameters are calculated from critical temperatures, critical pressures and acentric factors. In this specific binary system, CPA simplifies to the standard SRK equation of state.

Only VLE data at temperatures above  $366$  K have been found in the literature [Marathe and Sandler (1991)]. Figure 7.9 compares the model predictions,  $k_{ij} = 0.0$  and model correlations,  $k_{ij} = 0.019$  with the available reference data.

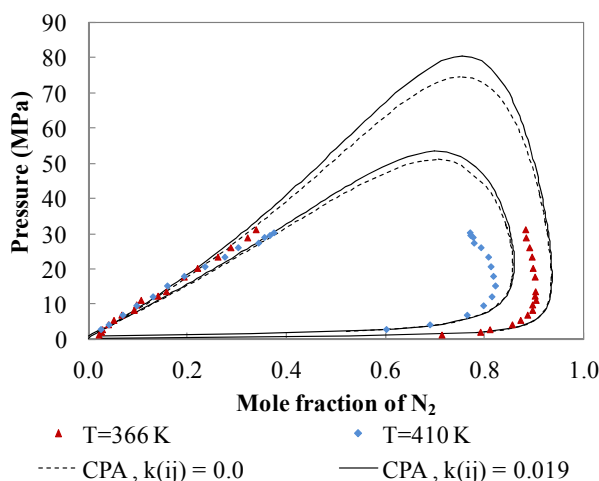


**Figure 7.9.** Comparison of model results and experimental data for VLE in the binary system of cyclopentane and nitrogen. Red triangles: VLE data at 366 K. Blue diamonds: VLE data at 410 K. Dashed lines: CPA predictions ( $k_{ij} = 0.0$ ). Solid lines: CPA description with  $k_{ij} = 0.019$ . Experimental data from [Marathe and Sandler (1991)].

The application of a non-zero  $k_{ij}$  does not provide significant improvements of the model descriptions in the  $T/P$  range covered by the experimental data. However, the application of a positive  $k_{ij}$  seems to lower the predicted upper pressure limits seen in the phase envelopes at both temperatures. Since the available experimental data are measured at conditions far from the working conditions of the developed hydrate model, and the improvements are considered insignificant, it is chosen to allow CPA to predict ( $k_{ij} = 0.0$ ) the behaviour of this binary pair in the following.

### 7.1.9 Carbon dioxide-Nitrogen

Low temperature vapour-liquid equilibria data have been modelled for this binary pair. Both components are treated as non self-associating and no cross-association occurs in this binary system.

Figure 7.10 a) and b) illustrate how CPA predicts ( $k_{ij} = 0.0$ ) the VLE of this system. The upper phase envelope pressure limit is overestimated by the model. By applying a non-zero  $k_{ij}$  of -0.086, the description is significantly improved at the low temperature (220 K). However, CPA still overestimates the upper two-phase pressure limits compared to the experimental data at 240 K.

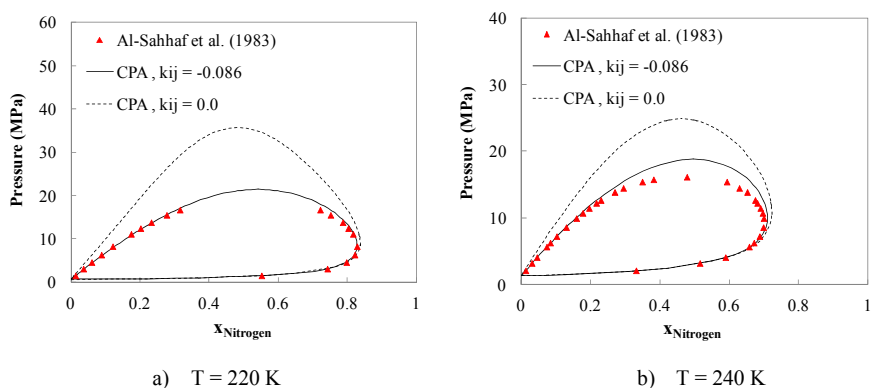


**Figure 7.10.** Fluid phase equilibria in the binary system of carbon dioxide and nitrogen. Comparison of experimental data (red triangles), CPA prediction with  $k_{ij} = 0.0$  (dashed lines) and CPA with  $k_{ij} = -0.086$  (solid lines). **a)**  $T = 220$  K. **b)**  $T = 240$  K.

No further attempts have been made to improve the high-temperature description of this binary pair, since these experimental data lie far from the expected operating temperatures of the hydrate model.

### 7.1.10 Water-Tetrahydrofuran-Cyclopentane

No experimental data for the fluid phase equilibria of the binary system comprised of tetrahydrofuran and cyclopentane have been found as part of this work.

However, LLE equilibrium conditions for the ternary system of water, tetrahydrofuran and cyclopentane have been investigated elsewhere [Appendix 2]. The addition of THF to the aqueous phase was shown to have a significant effect on the solubility of cyclopentane in the aqueous solution. THF acted as a co-solvent and enhanced the solubility of cyclopentane in the mixed solvent phase. The composition of a ternary aqueous mixture saturated in cyclopentane was determined by titration. Experiments were carried out at “ambient conditions” which are here modeled as 298 K and a pressure of 0.1 MPa. It was shown that a ternary aqueous phase with an overall THF mole fraction of  $x_{\text{THF}} = 0.2182$  could dissolve approximately 0.39 mole percent cyclopentane ( $x_{\text{cyclopentane}} = 0.0039$ ). These concentrations are an average of three compositions presented in the original work [Appendix 2].

A binary CPA interaction coefficient for the pair of tetrahydrofuran and cyclopentane has been adjusted such that CPA describes the aqueous phase of the ternary LLE system the closest possible to the above concentrations at 298 K and 0.1 MPa.

In a two-phase P-T flash calculation with an equimolar feed (equal amounts of all three components), the application of a  $k_{ij} = 0.107$  provides a saturated aqueous

liquid phase with a mole fraction of THF of  $x_{\text{THF}} = 0.2168$  and  $x_{\text{cyclopentane}} = 0.0014$ . Hence, for the given THF concentration, CPA underestimates the ability of the mixed solvent to dissolve cyclopentane compared to the experimental data. Deviations from the experimental concentrations are 0.7 percent for THF and 64 percent for cyclopentane. If CPA is allowed to predict the phase distribution of the three components ( $k_{ij} = 0.0$ ), the tetrahydrofuran mole fraction becomes 0.0900 and the cyclopentane mole fraction becomes 0.0003, significantly further away from the experimental data. Thus,  $k_{ij} = 0.109$  is used for the binary pair of tetrahydrofuran and cyclopentane in the following.

The predicted LLE phase compositions for the before mentioned P-T flash calculation are provided in Table 7.1.

**Table 7.1.** Experimental and “predicted” LLE phase compositions for the ternary system of water, tetrahydrofuran and cyclopentane. AAD in mole fractions according to eq. (7.1)

	Experimental	CPA	CPA	AAD (Aq. Phase)
	Aqueous Phase	Aqueous Phase	Organic Phase	
$x_{\text{H}_2\text{O}}$	0.7779	0.7818	0.0152	0.01
$x_{\text{Tetrahydrofuran}}$	0.2182	0.2168	0.4160	0.01
$x_{\text{Cyclopentane}}$	0.0039	0.0014	0.5688	0.64

An interesting observation here is that CPA predicts the majority of the added tetrahydrofuran to be located in the organic liquid phase.

Going back to the mixed promoter system presented in section 6.3, where a ternary mixture of water, tetrahydrofuran and cyclopentane was prepared with molar fractions of  $x_{\text{H}_2\text{O}} = 0.901$ ,  $x_{\text{Tetrahydrofuran}} = 0.051$  and  $x_{\text{Cyclopentane}} = 0.048$ . Upon mixing these two liquid phases, CPA predicts the aqueous liquid phase composition to remain unchanged (for all practical purposes) at hydrate forming conditions of e.g. 288 K and 2.0 MPa.

CPA thereby predicts tetrahydrofuran to remain in the aqueous phase of the mixed promoter system. How this distribution is affected by the later presence of carbon dioxide has not been investigated. The cyclopentane concentration in the aqueous phase of the above mentioned mixed promoter system is predicted to be 93 ppm (molar). This corresponds to approximately double the solubility of cyclopentane in pure water at this temperature.

### 7.1.11 Water-Tetrahydrofuran-Carbon dioxide

The performance of CPA in describing the ternary system of water, tetrahydrofuran and carbon dioxide has been investigated. Since these three compounds show highly non-ideal behaviour in their respective binary pairs, it is expected that the ternary system behaviour is of similar complexity.

No ternary adjustable parameters are available in CPA, hence the model relies on the ability of the model to extend from binaries to the ternary system.

Lazzaroni et al. (2004) have reported compositional data for the ternary system of carbon dioxide-tetrahydrofuran-water in temperature and pressure ranges, where this system shows three-phase vapour(V)-aqueous liquid(L<sub>w</sub>)-organic liquid(L<sub>a</sub>) equilibria. Compositions from the two liquid phases along with the density of the vapour phase are provided for a total of 16 conditions of temperature (T) and pressure (P).

The 16 T/P conditions investigated experimentally by Lazzaroni et al. have here been modelled using the Gibbs energy minimisation flash approach on a feed comprised of 10 mole percent water, 10 mole percent tetrahydrofuran and 80 mole percent carbon dioxide.

Whereas CPA predicts three-phase VLLE equilibria at the conditions reported by Lazzaroni et al., the phase composition of the aqueous phase in particular is predicted with considerable deviations compared to the reported compositions.

Figure 7.11 a) and b) compare experimental phase compositions of the co-existing liquid phases reported by Lazzaroni et al. with the phase compositions predicted by CPA.

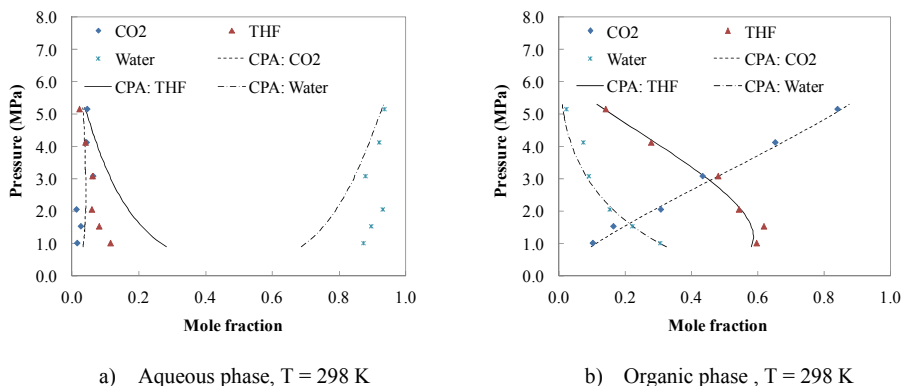


**Figure 7.11.** Compositions of co-existing liquid phases at conditions of three-phase vapour-liquid-liquid equilibrium for the ternary system of carbon dioxide, tetrahydrofuran (THF) and water. Comparison of experimental data from [Lazzaroni et al. (2004)] and CPA predictions. Blue diamonds: carbon dioxide mole fraction. Red triangles: Tetrahydrofuran (THF) mole fraction. Blue cross: Water mole fraction. Dashed line: Carbon dioxide mole fraction (CPA). Solid line: Tetrahydrofuran (THF) mole fraction (CPA). Dash dot dashed line: Water mole fraction (CPA). **a)** Aqueous liquid phase at T = 298 K. **b)** Organic liquid phase at T = 298 K.

The tetrahydrofuran concentrations in the aqueous liquid phase are predicted to be roughly twice as high as the concentrations reported by Lazzaroni et al. For this reason, the carbon dioxide solubility in the aqueous phase is also overestimated, since tetrahydrofuran acts as a co-solvent. The organic liquid phase composition is

well predicted in terms of composition at 298 K and pressures ranging from 1 to 5 MPa. Similar observations are found for the data sets at 311 K and 333 K (not shown here).

Similarly, the model has been validated against ternary data reported by Sabil et al. (2010c). Whereas Lazzaroni et al. report phase compositions in the three phase V-L<sub>w</sub>-L<sub>a</sub> equilibria region at fixed temperatures and pressures, Sabil et al. report T/P conditions of fluid phase transitions for ternary mixtures of carbon dioxide-tetrahydrofuran-water systems with various initial compositions. Upper and lower phase boundaries for the three-phase V-L<sub>w</sub>-L<sub>a</sub> region are determined experimentally for systems with constant initial compositions.

When crossing the upper phase boundary from the low pressure side to the high pressure side at specified temperature, a transition from three phases (V-L<sub>w</sub>-L<sub>a</sub>) to two phases (L<sub>w</sub>-L<sub>a</sub>) occurs. At the lower phase boundary, the system moves from V-L<sub>w</sub>-L<sub>a</sub> equilibrium for pressures above the phase boundary to V-L<sub>w</sub> equilibrium for pressures below the boundary.

The initial compositions reported for each data set presented by Sabil et al. (2010c) are specified in a manner that may be misleading. Here it is assumed that the reported compositions for carbon dioxide ( $x_1$ ) are mole fractions in the ternary mixture, whereas the compositions reported for tetrahydrofuran ( $x_2$ ) are binary mole fractions in the initial aqueous liquid phase. Hence, when modelling the systems, the initial composition of tetrahydrofuran in the ternary mixture has been corrected under the assumption that the initial system consists of  $x(\text{CO}_2) = x_1$  moles of carbon dioxide and  $x(\text{THF}) = (1-x_1)*x_2$  moles of tetrahydrofuran. In the model, the ternary system is balanced with water according to;  $x(\text{water}) = 1 - x(\text{CO}_2) - x(\text{THF}) = 1 - x_1 - ((1-x_1)*x_2)$ . This is in agreement with a separate publication of Sabil et al. (2010b), where a selection of the same data is presented alongside the measured hydrate equilibrium data.

Figure 7.12 a) illustrates a comparison of the CPA predictions with a selection of the experimental data for the upper phase boundary for the phase envelope (V-L<sub>w</sub>-L<sub>a</sub> to L<sub>w</sub>-L<sub>a</sub>) for three systems of various feed compositions. Figure 7.12 b) illustrates a comparison of the CPA predictions and experimental phase boundaries for both the upper (V-L<sub>w</sub>-L<sub>a</sub> to L<sub>w</sub>-L<sub>a</sub>) and lower (V-L<sub>w</sub>-L<sub>a</sub> to L<sub>w</sub>-V) boundaries for the phase envelope. Note that the compositions provided in these figures are the corrected feed compositions of the ternary mixtures.



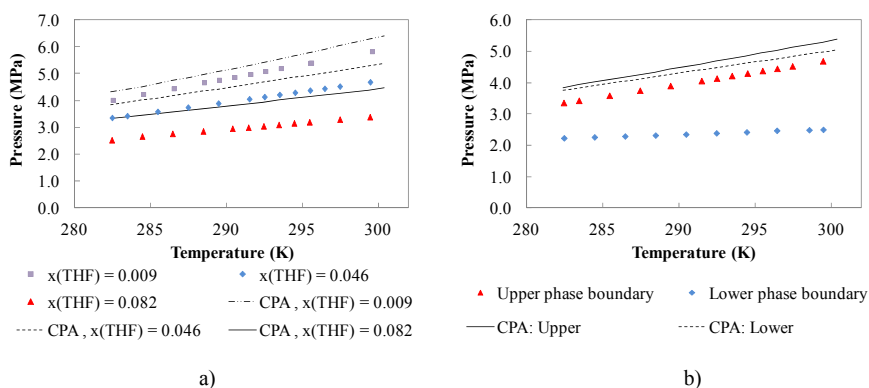


**Figure 7.12.** Comparison of calculated and experimental phase envelope boundaries for the ternary system of carbon dioxide-tetrahydrofuran (THF)-water. Experimental data are from Sabil et al. (2010c). **a)** High-pressure boundaries for phase envelope in systems with 9 mole percent carbon dioxide and varying mole fraction of tetrahydrofuran,  $x(\text{THF})$ . **b)** Lower and upper phase envelope boundaries for ternary system with  $x(\text{CO}_2) = 0.09$ ,  $x(\text{THF}) = 0.046$ ,  $x(\text{H}_2\text{O}) = 0.864$ .

The upper phase boundary is calculated by specifying initial T/P conditions that are in the two-phase  $L_w$ - $L_a$  region for the system with specified feed composition. A flash calculation then separates the feed into two liquid phases followed by a boiling point pressure calculation performed for one of the two liquid phases. The new T/P conditions are subsequently returned to the flash algorithm and this procedure is continued until the calculated boiling point pressure no longer changes within a given tolerance.

The calculation procedure for the lower phase boundary is more complex since both vapour and liquid phases co-exist on both sides of the phase boundary. Hence, here it is not possible to search for the boundary by a combination of flash- and bubble-/dew point calculations. A trial and error search method has been applied, starting at pressure conditions below the phase boundary and then increasing pressure in steps of 0.001 MPa until the phase boundary is reached (phase number and types are monitored by multi-phase T/P flash calculations).

From Figure 7.12 a) it becomes clear that CPA predicts the upper phase boundaries of the VLLE region with significant deviations compared to the experimental data. For the system with  $x(\text{THF}) = 0.082$ , the calculated pressures are approximately 30 percent higher than those measured by Sabil et al. (2010c). Deviations decrease with decreasing initial concentration of tetrahydrofuran. With an overall mole fraction of tetrahydrofuran of 0.009, the calculated boundary pressures are approximately 8 percent above the experimental data.

Figure 7.12 b) compares the measured [Sabil et al. (2010c)] and predicted (CPA) upper and lower phase envelope boundaries for the ternary system comprised of 9 mole percent carbon dioxide, 4.6 mole percent tetrahydrofuran and balance water. The upper phase boundary is predicted by CPA with deviations of

approximately 14 percent. For the lower phase boundary, CPA overestimates the pressures by approximately 69 percent at the low temperatures and 100 percent at the high temperatures.

CPA, with the obtained binary parameters, predicts the ternary system of carbon dioxide-tetrahydrofuran-water with significant deviations compared to experimental data available in the regions where this system shows three-phase V-L<sub>w</sub>-L<sub>a</sub> equilibrium. Since no experimental composition data have been found for this system in the two-phase regions, it has not been possible to investigate the accuracy of the model in the description of these regions.

## **7.2 The Un-promoted Gas Hydrate System**

As a simplification of the specific case of carbon dioxide capture from power station flue gases, it is assumed that the flue gas phase may be modelled in the form of binary mixtures of nitrogen and carbon dioxide. In actual flue gases, significant amounts of other components such as e.g. oxygen and water may also be present. With respect to hydrate formation, oxygen acts similarly to nitrogen [van Cleeff and Diepen (1960), Du et al. (2010)], thus when simulating the flue gas, it is reasonable to replace the oxygen content with nitrogen in the model gas phase. The initial water content in the flue gas phase may also be neglected since, at equilibrium, the vapour phase will be saturated with water. Hence, the simplified, un-promoted gas hydrate system consists of ternary mixtures of nitrogen, carbon dioxide and water.

Kihara parameters have been regressed for both nitrogen and carbon dioxide as part of this work. When regressing the Kihara parameters, both the pure hydrates of the two hydrate formers (sI hydrate for carbon dioxide and sII hydrate for nitrogen) have been considered together with the data for the mixed hydrates (both dissociation pressures and hydrate composition). Table 7.2 lists the data used as references. Only hydrate(H)- Liquid water(L<sub>w</sub>)-vapour(V) equilibrium data have been included as reference for the pure hydrates of carbon dioxide. The mixed hydrates of carbon dioxide and nitrogen have been assumed structure I hydrates for all the available data on the mixed hydrates. To ensure the validity of the obtained Kihara parameters for carbon dioxide in sII hydrates, a few data for the mixed hydrates of carbon dioxide and tetrahydrofuran (3 mole percent and 5 mole percent tetrahydrofuran in the aqueous liquid phase) have been included in the regression of parameters. Even though the un-promoted gas hydrate system is presented in this section without the use of promoters, regression of Kihara parameters for the four hydrate formers studied in this work (carbon dioxide, nitrogen, tetrahydrofuran and cyclopentane) has been done in an iterative procedure, to ensure internal consistency of the obtained parameters in all possible

combinations and hydrate structures. Emphasis has been put on ensuring that the model predicts the right hydrate structures in all systems.

**Table 7.2.** Reference data for optimising Langmuir constants (Kihara parameters) along with final model accuracy. P denotes equilibrium pressure. Y denotes water-free hydrate composition.  $y(\text{CO}_2)$  is vapour phase mole fraction of carbon dioxide. AAD calculated according to eg. (7.1).

Ref.	Comp.	No Points	Temp. / K	Composition	AAD (P)	AAD (Y)
[1]	CO <sub>2</sub>	P: 10	275.1 – 282.9	$y(\text{CO}_2) = 1$	0.039	N/A
[2]	CO <sub>2</sub>	P: 10	275.0 – 282.8	$y(\text{CO}_2) = 1$	0.034	N/A
[3]	N <sub>2</sub>	P: 8	273.2 – 281.1	$y(\text{N}_2) = 1$	0.036	N/A
[4]	N <sub>2</sub>	P: 23	273.2 – 283.3	$y(\text{N}_2) = 1$	0.040	N/A
[5]	CO <sub>2</sub> / N <sub>2</sub>	P: 48 Y: 20	272.9 – 284.3	$0.05 \leq y(\text{CO}_2) \leq 0.97$	0.085	0.162
[6]	CO <sub>2</sub> / N <sub>2</sub>	P: 9	278.1 – 285.3	$0.27 \leq y(\text{CO}_2) \leq 0.81$	0.16	N/A
[7]	CO <sub>2</sub> / N <sub>2</sub>	P: 24	275.3 – 283.1	$0.00 \leq y(\text{CO}_2) \leq 1.00$	0.14	N/A
[8]	CO <sub>2</sub> / N <sub>2</sub>	P: 9	273.1 – 280.2	$0.91 \leq y(\text{CO}_2) \leq 0.97$	0.06	N/A
[9]	CO <sub>2</sub> / N <sub>2</sub>	P: 15	274.0 – 281.9	$0.16 \leq y(\text{CO}_2) \leq 0.72$	0.12	N/A
[10]	CO <sub>2</sub> / N <sub>2</sub>	P: 1	273.7	$y(\text{CO}_2) = 0.17$	0.037	N/A
[11]	CO <sub>2</sub> / N <sub>2</sub>	P: 16 Y: 16	273.4 – 281.1	$0.16 \leq y(\text{CO}_2) \leq 0.59$	0.24	0.08
[12]	CO <sub>2</sub> / N <sub>2</sub>	P: 33 Y: 33	273.6 – 281.7	$0.13 \leq y(\text{CO}_2) \leq 0.75$	0.17	0.20
[13]	CO <sub>2</sub> / N <sub>2</sub>	P: 33	276.9 – 285.4	$0.81 \leq y(\text{CO}_2) \leq 0.96$	0.17	N/A

[1] Sabil et al. (2010b), [2] Ruffine and Trusler (2010), [3] Jhaveri and Robinson (1965),  
[4] van Cleeff and Diepen (1960), [5] Kang et al. (2001), [6] Ben Attouche Sfaxi et al. (2012),  
[7] Bruusgaard et al. (2008), [8] Fan and Guo (1999), [9] Olsen et al. (1999),  
[10] Linga et al. (2007a), [11] Herri et al. (2011), [12] Belandria et al. (2011),  
[13] Kim et al. (2011)

According to the Gibbs phase rule ( $f = c - p + 2$ ), in systems with two components (pure hydrates of carbon dioxide or nitrogen) and three phases in equilibrium, the system is uni-variant (one degree of freedom). Hence, when fixing e.g. the system temperature, a single equilibrium state will be valid for any feed composition that provides three phases at this temperature.

When moving to the ternary system of carbon dioxide, nitrogen and water, still considering the H-L<sub>w</sub>-V equilibrium region, the system becomes divariant due to the addition of one component. Hence, at specified temperature, multiple H-L<sub>w</sub>-V

equilibrium states exist for this system. Specifying a second intensive variable “locks” the system into a single equilibrium state. In the model, this is done artificially by setting the vapour feed composition to that of the desired equilibrium state and then feeding only sufficient amount of water to form a liquid water phase. By doing so, the vapour phase at equilibrium will be (almost) identical to the feed vapour phase composition.

Calculated equilibrium conditions for the mixed hydrates of carbon dioxide and nitrogen depend not only on the initial vapour phase composition of the feed, but also on the amount of liquid fed into the system. This is explained by the large differences in solubility of carbon dioxide and nitrogen in water. The final equilibrium composition of the vapour phase may change significantly depending on the amount of water in the feed. Hence, when comparing the model to experimental data, it is necessary to simulate the reported experimental conditions as accurately as possible. If the experimental feed composition (overall) is reported directly, this feed is used in the model. If only the vapour phase composition at equilibrium is reported, this composition should be used as vapour feed composition and the modelled system should be initiated with a low liquid to vapour feed ratio (e.g.  $L_w/(V+L_w) = 0.05$  on molar basis). If the initial vapour phase composition is reported without an exact feed composition, the model results should be used with caution, since results may vary several percent depending on the liquid to vapour feed ratio set in the feed. Of the reference data provided in Table 7.2, Kang et al. (2001), Bruusgaard et al. (2008), Fan and Guo (1999), Olsen et al. (1999) and Linga et al. (2007a) provide initial vapour phase composition and initial volume of liquid fed into the system. Hence, the overall model feed compositions have been approximated (roughly) according to reported vapour phase compositions and liquid volumes. Table 7.2 provides the average absolute relative deviations (AAD according to eq. (7.1)) in equilibrium pressure (P) and water free hydrate composition (Y), where available, for each reference data set. The water-free hydrate composition has been calculated according to equation (5.1.21).

With the regressed Kihara cell potential parameters ( $\epsilon/k$  and  $\sigma$ ) the model describes the experimental reference data for the pure hydrates of both carbon dioxide and nitrogen within an average accuracy of 4 percent in the temperature interval from approximately 273 K to 283 K. Figure 7.13 a) and b) illustrate the model description of the two pure hydrates. Comparisons are made with experimental data.

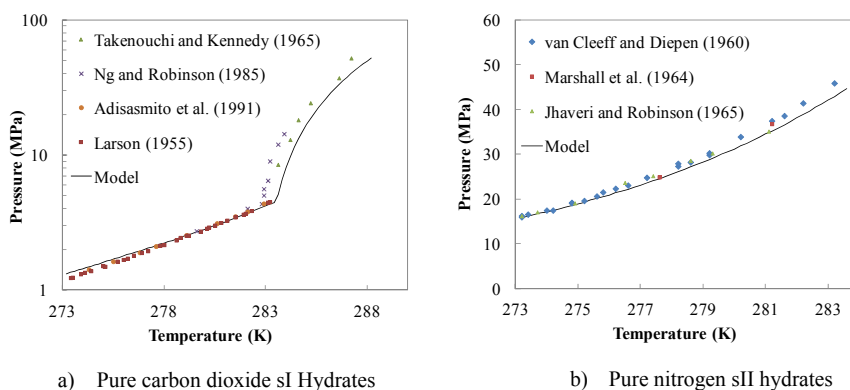


**Figure 7.13.** Comparison of model performance (solid lines) and experimental data for the pure hydrates of carbon dioxide and nitrogen. **a)** Dissociation pressures for carbon dioxide sI hydrate as function of temperature. **b)** Dissociation pressures for nitrogen sII hydrate as function of temperature.

It is seen that the model describes both of the pure hydrate forms with reasonable accuracy in the low pressure region. The sudden change of slope in the hydrate data for carbon dioxide is due to the fluid phase transition from vapour to liquid for the carbon dioxide rich phase (upper quadruple point). The model slightly overestimates this temperature, which is seen by the entire H-L<sub>w</sub>-L<sub>CO2</sub> region being shifted up in temperature by approximately half a degree.

Nitrogen hydrates are described accurately up to temperatures of approximately 278 K. At higher temperatures, the model underestimates the hydrate pressures of the pure nitrogen sII hydrate. Extending to the mixed hydrates increases complexity and absolute deviations between model descriptions and experimental data increase.

Equilibrium pressures reported by Kang et al. (2001), Fan and Guo (1999) and Linga et al. (2007a) are well described by the model with AAD's below 0.1 in terms of pressure. However, the composition data reported by Kang et al. are less accurately described. The largest deviations are found in the pressure data presented by Herri et al. (2011), Blandria et al. (2011) and Kim et al. (2011). The compositions reported by Herri et al. are described with a low AAD of 0.08, however the model fails at describing the pressures reported by these authors (AAD of 0.24). The model deviates from both the pressure- and composition data reported by Blandria et al. with AAD's of 0.17 and 0.20 respectively. Pressure data reported by Kim et al. are described with an AAD of 0.17.

Figure 7.14 compares reported dissociation pressures for various vapour phase compositions with model results. All modelling results are obtained assuming a liquid feed ratio,  $L_w/(L_w+V)$ , of 0.8 since Kang et al. (2001) conducted their experiments with high liquid to vapour molar ratios.

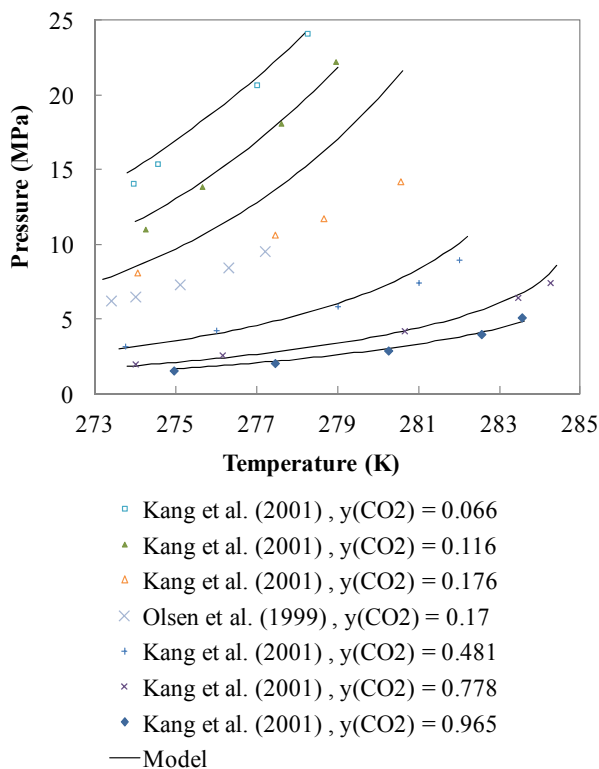


**Figure 7.14.** Comparison of model performance (solid lines) for the mixed hydrate of carbon dioxide and nitrogen and experimental data measured by Kang et al. (2001) and Olsen et al. (1999).  $y(\text{CO}_2)$  denotes vapour phase composition of carbon dioxide reported by the authors.

It is seen that the model performs well in the composition limits near pure carbon dioxide in the low-pressure region and near nitrogen in the high-pressure regions. Generally the dissociation pressure of the mixed hydrate decreases with increasing carbon dioxide content in the vapour phase. The model accurately describes five out of the six data sets reported by Kang et al., however it fails at describing the temperature-dependence for the data set at 17.6 mole percent carbon dioxide. The high-temperature experimental data of this set could be questioned for this reason, however as shown in Figure 7.14, the temperature trend in the data reported by Kang et al. at these conditions correspond well with the trend of the data reported by Olsen et al. (1999) for a similar gas phase composition.

What is difficult to see in Figure 7.14 is that whereas the model predicts the formed mixed gas hydrates to be of the sI structure type for all conditions with

carbon dioxide vapour phase compositions of 11 percent and higher, a structural transition occurs for the system with 6.7 mole percent carbon dioxide. At temperatures below 275.6 K, the predicted structure is sI, however above this temperature the model predicts the sII hydrate to be the thermodynamically most stable form.

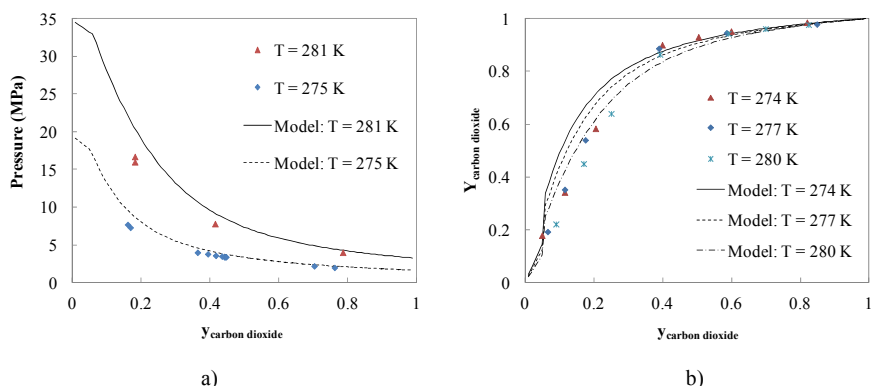


**Figure 7.15. a)** Hydrate equilibrium pressure for the mixed hydrate of carbon dioxide and nitrogen as function of vapour phase compositions. Experimental data from Bruusgaard et al. (2008). Solid line: Model at 281 K. Dashed line: Model at 275 K. **b)** Hydrate composition ( $Y_{\text{carbon dioxide}}$ ) on water-free basis (eq. (5.1.21)) for the mixed hydrate of carbon dioxide and nitrogen as function of mole fraction of carbon dioxide in the vapour phase ( $y_{\text{carbon dioxide}}$ ). Experimental data from Kang et al. (2001). Solid line: Model at 274 K. Dashed line: Model at 277 K. Dash-dot-dashed line: Model at 280 K.

Figure 7.15 a) illustrates the effect of the initial vapour phase composition on the dissociation pressure of the mixed hydrate of carbon dioxide and nitrogen. The experimental data are those reported by Bruusgaard et al. (2008). The model results are obtained assuming a liquid feed ratio,  $L_w/(L_w+V)$ , of 0.2. Note the change in slope of the model curves at approximately 5-6 mole percent carbon dioxide in the vapour phase. Despite the fact that all reference data for the mixed hydrate system were assumed sI hydrates, the model predicts sII hydrates to form for gas mixtures with less than five mole percent carbon dioxide and sI hydrates for gas mixtures with more than five mole percent carbon dioxide. This boundary is valid for the system fed with 20 mole percent liquid. It is not surprising though, that a structural change occurs in the mixed hydrate system, since the two pure hydrates form different structures. The compositional position of the structural change from sI hydrates to sII hydrates depend on the obtained Kihara parameters which are influenced by the assumed structure during the parameter regression. The difference in the composition for the structural transition observed in Figure 7.14 (6.7 mole percent carbon dioxide at 275.6 K) and that observed in Figure 7.15 a) (approximately 5-6 mole percent carbon dioxide at 275.3 K) is explained

mainly by the differences in the simulated liquid to vapour feed ratios. Hence, the presented results illustrate the importance of knowing exact feed composition, or as a minimum the equilibrium vapour phase composition for this ternary system, when comparing modelling results with experimental data.

A final and equally important aspect of the hydrate modelling for this carbon dioxide capture process is the ability of the developed model to describe the composition of the gas phase physically adsorbed inside the solid hydrate phase. Not only is it important for the model to accurately describe hydrate formation temperature/pressure conditions to enable a thermodynamic evaluation of the necessary flue gas compression, the hydrate composition is as important since it is needed to investigate the efficiency of the process to selectively remove carbon dioxide from the mixed flue gas.

Figure 7.15 b) illustrates modelling results for the water-free hydrate composition as function of the equilibrium vapour phase composition in the H-L<sub>w</sub>-V region. The model results are compared with experimental data reported by Kang et al. (2001). The vapour phase composition reported by Kang et al. for these data are actual vapour phase compositions at equilibrium, hence the model has been initiated by feeding only 5 mole percent liquid and 95 mole percent vapour to ensure that the equilibrium vapour phase composition corresponds to that reported by Kang et al.. It is seen that the model describes the data well in the composition limits, however the model overestimates the selectivity towards carbon dioxide in the region by 10 to 30 mole percent carbon dioxide in the vapour phase. The model correctly shows the trend of decreasing selectivity in the hydrate phase with increasing temperature.

### **7.3 Tetrahydrofuran Promoted Gas Hydrate Systems**

With the model in place for both the fluid phase description and the hydrate description of the un-promoted hydrate systems, only the Kihara parameters for tetrahydrofuran are needed in order to describe the promoted gas hydrates. The Kihara parameters were partly optimised along with those of carbon dioxide, to ensure correct description of carbon dioxide presence in the sII hydrate phase.

Kihara parameters ( $\epsilon/k$  and  $\sigma$ ) for tetrahydrofuran have subsequently been finally “tuned” using experimental data for the mixed hydrates of tetrahydrofuran + carbon dioxide and tetrahydrofuran + nitrogen. Only experimental data from the H-L<sub>w</sub>-V three-phase region have been used as reference. Initial concentrations of tetrahydrofuran in the liquid phase up to five mole percent have been considered. Since more data were available for the tetrahydrofuran + carbon dioxide system, the objective function to be minimised (the sum of all absolute relative deviations)



has been modified such that the two systems are weighted equally (total deviation is normalised according to the number of data points for each system).

It has been shown experimentally that, for a given temperature, the corresponding H-L<sub>w</sub>-V equilibrium pressure for the ternary system of water, tetrahydrofuran and carbon dioxide mainly depends on the concentration of tetrahydrofuran in the aqueous liquid phase [Sabil et al. (2010b)]. Hence, unless exact feed compositions are provided for the literature data, the model feed liquid is specified at the reference composition and calculations are initiated with a 90 mole percent liquid fraction (10 mole percent gas). Table 7.3 contains a list of references and conditions for the data used as reference. Comparisons of experimental data and model results in terms of equilibrium pressures are included in the form of absolute average relative deviations (AAD).

**Table 7.3.** Reference data used when regressing Kihara cell potential parameters for tetrahydrofuran (THF).  $x(\text{THF})$  denotes mole fraction of THF in the feed liquid phase. AAD (P) is absolute average relative deviation of calculated pressures compared to the reference data.

Ref.	Comp.	No Points	Temp. / K	Composition	AAD (P)
[1]	THF / CO <sub>2</sub>	13	278.3 – 289.9	$0.016 \leq x(\text{THF}) \leq 0.028$	0.17
[2]	THF / CO <sub>2</sub>	7	280.4 – 291.1	$x(\text{THF}) = 0.05$	0.21
[3]	THF / CO <sub>2</sub>	28	279.9 – 291.3	$0.012 \leq x(\text{THF}) \leq 0.05$	0.10*
[4]	THF / CO <sub>2</sub>	6	283.8 – 289.8	$x(\text{THF}) = 0.011$	0.26**
[5]	THF / N <sub>2</sub>	23	280.9 – 293.8	$0.01 \leq x(\text{THF}) \leq 0.05$	0.09
[4]	THF / N <sub>2</sub>	5	281.4 – 289.4	$x(\text{THF}) = 0.011$	0.02

\* Data at  $x(\text{THF}) = 0.012$  and  $T > 288.55$  K disregarded since model predicts H-L<sub>w</sub>-L<sub>CO<sub>2</sub></sub> equilibria.

\*\* Data for  $T > 287.4$  K disregarded since model predicts H-L<sub>w</sub>-L<sub>CO<sub>2</sub></sub> equilibria.

[1] Delahaye et al. (2006), [2] Seo et al. (2008), [3] Sabil et al. (2010a), [4] Mohammadi et al. (2010), [5] Seo et al. (2001).

With the obtained parameters, the model overestimates equilibrium pressures for the mixed hydrate of tetrahydrofuran and carbon dioxide at liquid phase concentrations of tetrahydrofuran below three mole percent. Accurate descriptions of the promoted hydrates of carbon dioxide are obtained for concentrations of tetrahydrofuran in the aqueous liquid phase at or above three mole percent.

The mixed hydrates of nitrogen and tetrahydrofuran are described with AAD's below 0.1 for both reference data sets. Figure 7.16 a) and b) compares model results with a selection of the reference data for both the mixed hydrates of carbon dioxide + tetrahydrofuran and nitrogen + tetrahydrofuran.

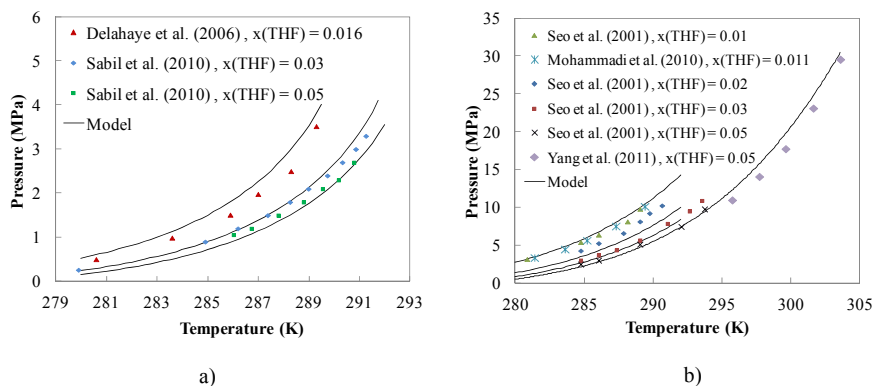


**Figure 7.16.** Dissociation pressures as function of temperature for mixed hydrates of carbon dioxide or nitrogen with tetrahydrofuran (THF).  $x(\text{THF})$  is the initial mole fraction of tetrahydrofuran in the liquid phase. Model results (solid lines) are obtained using feed liquid molar ratios,  $L_w/(L_w+V)$  of 0.9. **a)** Carbon dioxide-tetrahydrofuran hydrates. **b)** Nitrogen-tetrahydrofuran hydrates.

Figure 7.16 a) clearly illustrates how the model overestimates the dissociation pressure of the mixed carbon dioxide + tetrahydrofuran hydrate at a THF mole fraction of 0.016. The data sets at 3 and 5 mole percent THF are more accurately described by the model.

The mixed hydrates of nitrogen and tetrahydrofuran are accurately described in general. The model deviates only significantly compared to the data set at 2 mole percent THF. At this concentration, the model underestimates the dissociation pressures compared to the experimental data reported by Seo et al. (2001).

Figure 7.17 a) and b) illustrates how the equilibrium pressures for the two promoted hydrate systems, at constant temperature, depend on the THF concentration in the liquid phase. The model predictions are compared with experimental data extracted from the above reference data sets.

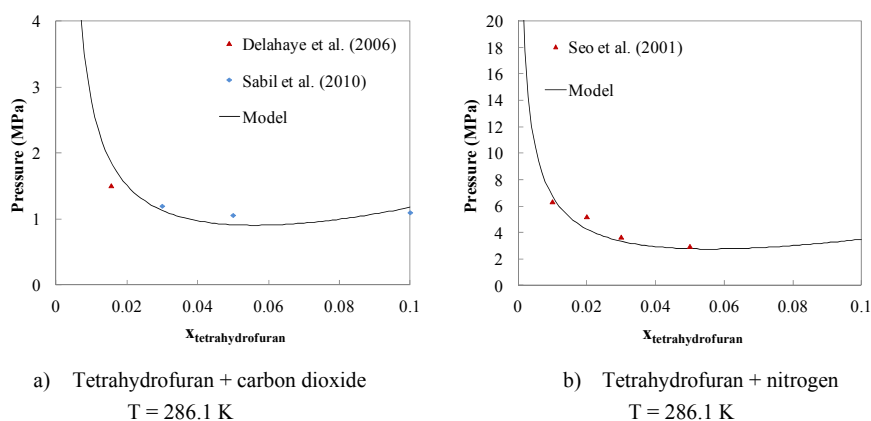


**Figure 7.17.** Dissociation pressures for the mixed sII hydrate of tetrahydrofuran and carbon dioxide (a) or nitrogen (b) as function of the initial liquid phase mole fraction of tetrahydrofuran ( $x_{\text{tetrahydrofuran}}$ ) at T = 286.1 K. Solid lines are model results using a liquid feed ratio  $L_w/(L_w+V)$  of 0.9. a).

The data extracted for the carbon dioxide + tetrahydrofuran hydrate system are not all given exactly at a temperature of 286.1 K. The temperatures for these data vary from 285.9 K to 286.2 K. Hence, a small uncertainty in the experimental data must be expected due to these temperature variations. The data for the nitrogen + tetrahydrofuran system are all measured at a temperature of 286.1 K.

The presented model results in Figure 7.17 a) and b) are calculated for a constant temperature of 286.1 K. The model clearly shows the promoting effect of tetrahydrofuran, which has also been experimentally documented. The estimated equilibrium pressures, at constant temperature, decrease with increasing concentrations of tetrahydrofuran in the liquid phase up to a concentration of approximately 5 - 6 mole percent. For concentrations above this, the promoting effect decreases.

When looking closer it is found that the model predicts an optimum in the promoting effect at approximately 5.6 mole percent tetrahydrofuran in the aqueous phase. This concentration is identical for both systems. The predicted optimum in the aqueous THF concentration thus lies at the theoretical, stoichiometric concentration of an sII hydrate with complete filling of its large cavities by THF ( $x_{\text{THF,stoich}} = 0.056$ ). An investigation of the predicted fractional occupancies of THF in the large cavities also showed occupancies higher than 0.99 for both systems.

Tetrahydrofuran acts in two opposite directions in hydrate forming systems: Tetrahydrofuran stabilises the sII hydrate structure by its presence in the large cavities of the solid hydrate phase. Simultaneously, tetrahydrofuran lowers the activity of water in the aqueous liquid phase by forming hydrogen bonds with

water. Hence, the promoting effect of THF is a competing effect of hydrate stabilisation and water de-stabilisation in the liquid phase. At concentrations lower than 5.6 mole percent, stabilisation of the solid structure is the dominating effect. At higher concentrations, the de-stabilisation of water in the aqueous liquid phase increases its effect, and the overall promoting effect on the hydrate phase decreases.

Figure 7.18 shows the same competition between hydrate stabilisation and liquid water de-stabilisation only here for the pure sII hydrate of tetrahydrofuran (binary system of tetrahydrofuran and water).

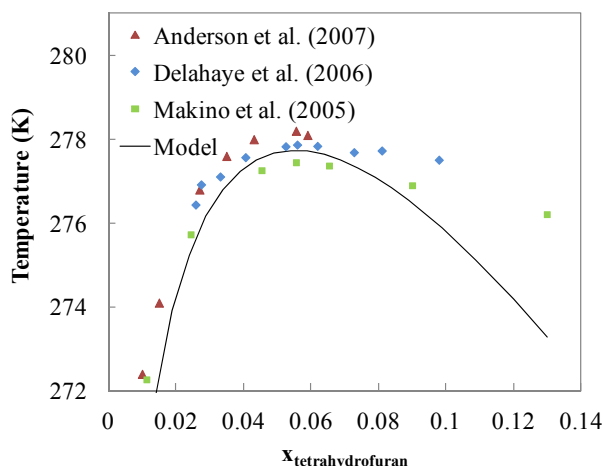


**Figure 7.18.** Dissociation temperature for the pure sII hydrate of tetrahydrofuran as function of the liquid phase mole fraction of tetrahydrofuran ( $x_{\text{tetrahydrofuran}}$ ).  $P = 0.10$  MPa. The solid line represents model predictions.

Hydrate dissociation temperatures are shown as a function of mole fraction of THF in the aqueous liquid phase. Both the experimental data and the model results are obtained at a fixed pressure of 0.1 MPa. Again an optimum is found at approximately 5.5 – 6.0 mole percent. The results indicate that the model tends to underestimate the stabilising effect of THF at low liquid phase concentrations. In the concentration range from approximately 2.5 – 7 mole percent, the model accurately describes the pure THF hydrate equilibrium temperatures. Above 7 mole percent THF, the model seems to overestimate the de-stabilising effect on the liquid phase.

The above results provide an explanation for the models more accurate performance in the mixed hydrates of THF plus gas in the concentration range from approximately 3 – 5 mole percent. This is the region where the model

provides the most accurate description of the balance between THF hydrate stabilisation and liquid water de-stabilisation.

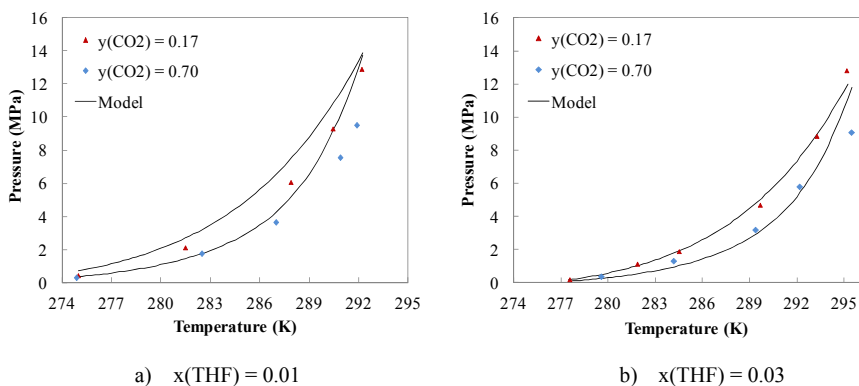


**Figure 7.19.** Hydrate dissociation pressure for the mixed hydrate of carbon dioxide-nitrogen-tetrahydrofuran as function of temperature.  $y(\text{CO}_2)$  denotes initial mole fraction of carbon dioxide in the vapour phase.  $x(\text{THF})$  is the initial mole fraction of tetrahydrofuran in the aqueous liquid phase. Solid lines are model prediction obtained using a liquid feed ratio  $L_w/(L_w+V)$  of 0.9. **a)**  $x(\text{THF}) = 0.01$ . **b)**  $x(\text{THF}) = 0.03$ . Experimental data from Kang et al. (2001).

Kang et al. (2001) report experimental data for promoted gas hydrate systems of gas mixtures containing carbon dioxide and nitrogen. The thermodynamic promoter is tetrahydrofuran and Kang et al. investigate the promoting effect at liquid phase concentrations of 1 and 3 mole percent THF. Two gas mixtures are used, initially containing 17 and 70 mole percent carbon dioxide. These conditions have been investigated using the developed model. Vapour phase and liquid phase initial compositions are those indicated by Kang et al. and the model feed liquid ratio,  $(L_w/(L_w+V))$ , is set at 0.9. Figure 7.19 a) and b) compare the model predictions with the data reported by Kang et al. As expected, the model overestimates the dissociation pressures of the mixed carbon dioxide-nitrogen-tetrahydrofuran hydrate at a liquid phase containing 1 mole percent tetrahydrofuran (Figure 7.19 a). For the system with 3 mole percent tetrahydrofuran in the liquid phase (Figure 7.19 b), the model predicts hydrate equilibrium pressures very well both for the carbon dioxide lean and carbon dioxide rich system. The model predicts all 21 data points with an AAD of 0.17 in terms of dissociation pressure. The systems with 1 mole percent THF are described with an AAD of 0.21 and the systems with 3 mole percent THF are described with an AAD of 0.14.

Both Figure 7.19 a) and b) show that the model predicts the equilibrium pressure for the gas mixture comprised of 70 mole percent carbon dioxide to increase steeply with temperature in the high temperature region. At temperatures

above the ones shown in the figures, the model predicts higher dissociation pressures for the carbon dioxide rich system than the carbon dioxide lean system.

Linga et al. (2007c) similarly report equilibrium pressures for mixed gas hydrates of carbon dioxide and nitrogen, promoted by the presence of tetrahydrofuran. A total of 9 data points are presented for liquid phase THF mole fractions ranging from 0.005 to 0.015 and vapour phase mole fractions of carbon dioxide ranging from 0.15 to 0.17. The low temperature data reported by Linga et al. (2007c) for a THF liquid mole fraction of 0.01 and a vapour phase mole fraction of 0.17 continue the trend in the data reported by Kang et al. (2001) at similar conditions. The data reported by Linga et al. (2007c) have been modelled using the present model with a liquid feed molar ratio of 0.9. The data are described with an AAD of 0.43. Again these experimental data show that the model overestimates hydrate equilibrium pressures for the promoted systems with low liquid phase mole fractions of tetrahydrofuran.

So far only hydrate-liquid water-vapour (H-L<sub>w</sub>-V) three-phase equilibrium has been modeled for the THF promoted systems with three or more components. Sabil et al. (2010b) reported hydrate equilibrium pressures for systems of known initial composition in the ternary system of water, tetrahydrofuran and carbon dioxide. These data covered not only the hydrate-liquid water-vapour (H-L<sub>w</sub>-V) three-phase region, but also the hydrate-liquid water-liquid vapour (H-L<sub>w</sub>-L<sub>v</sub>) and the hydrate-liquid water-liquid organic-vapour (H-L<sub>w</sub>-L<sub>a</sub>-V) region. These regions were found in systems comprised of aqueous phases with 5 mole percent THF and varying amounts of carbon dioxide vapour.

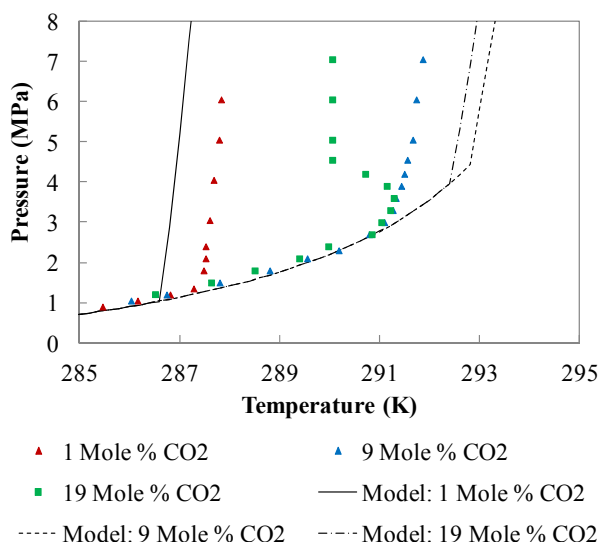


**Figure 7.20.** Hydrate stability boundaries in the ternary system of water, tetrahydrofuran and carbon dioxide. Systems with overall 1, 9 and 19 mole percent carbon dioxide and balance aqueous liquid solution containing initially 5 mole percent tetrahydrofuran. Comparison of model descriptions (predictions) and experimental data from Sabil et al. (2010b).

Figure 7.20 compares a selection of data reported by Sabil et al. (2010b) with the model descriptions. In these mixtures, once the system moves out of the three-phase (H-L<sub>w</sub>-V) region, the model is forced to predict the outcome according to the predicted fluid phase behaviour.

For the system with overall 1 mole percent carbon dioxide (red triangles), a sharp change of slope is found in the experimental data at approximately 287.5 K. This is due to a disappearance of the vapour phase, which is incorporated in the aqueous liquid phase. Hence, at temperatures above this, the system represents two-phase (H-L<sub>w</sub>) equilibrium. The model predicts this to occur at a slightly lower temperature (difference of approximately 0.8 K) than the experimentally reported.

With more carbon dioxide in the system (9 mole percent - blue diamonds), the experimental data show (H-L<sub>w</sub>-V) three-phase equilibria up to approximately 290 K. From 290 K to 291.5 K Sabil et al. reported (H-L<sub>w</sub>-L<sub>a</sub>-V) four-phase equilibria. Above these temperatures, the system changed to (H-L<sub>w</sub>-L<sub>v</sub>) three-phase equilibria. The model predicts (H-L<sub>w</sub>-V) three-phase equilibria up to approximately 293 K and then transfers directly into the (H-L<sub>w</sub>-L<sub>v</sub>) three-phase region.

With 19 mole percent carbon dioxide in the system (green squares) Sabil et al. (2010b) measured (H-L<sub>w</sub>-V) three-phase equilibria up to approximately 290 K.

From here a pseudo-retrograde behaviour was reported for the (H-L<sub>w</sub>-L<sub>a</sub>-V) four-phase region, keeping the temperature between 290.7 K and 291.3 K, as pressures increased to approximately 4.2 MPa. Above this pressure, the system changed to (H-L<sub>w</sub>-L<sub>v</sub>) three-phase equilibria. The model again predicts (H-L<sub>w</sub>-V) equilibrium up to temperatures of approximately 292.5 K and then again goes directly into the (H-L<sub>w</sub>-L<sub>v</sub>) three-phase region.

The above results show that the model, despite being accurate in the three-phase (H-L<sub>w</sub>-V) three-phase region, provides less accurate description of the other regions of the phase diagram for this ternary mixture. The failure of the hydrate model is explained by the fact that CPA has troubles describing the complex fluid phase equilibria of this system. The L<sub>w</sub>-L<sub>a</sub>-V three-phase (fluid) region is described with insufficient accuracy.

Figure 7.21 compares experimental data and modeling results for both fluid phase- and hydrate equilibrium in the specific ternary system of 9 mole percent carbon dioxide, 4.6 mole percent tetrahydrofuran and 86.4 mole percent water. The fluid phase data and modeling results are identical to those presented in Figure 7.12 b). Here the hydrate data are included along with model results.

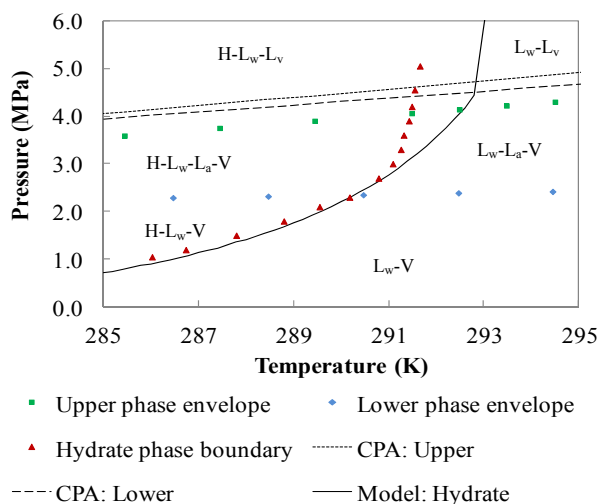


**Figure 7.21.** Selected section of the phase diagram for the ternary system comprised of 9 mole percent carbon dioxide, 4.6 mole percent tetrahydrofuran and 86.4 mole percent water. Indications of Hydrate(H), Aqueous liquid(L<sub>w</sub>), Organic liquid(L<sub>a</sub>), Liquid vapour(L<sub>v</sub>) and Vapour(V) are related to phase regions contained by the experimental data. Comparison of experimental data from Sabil et al. (2010b) and modeling results.



It is seen that the model does in fact predict four-phase hydrate(H)-aqueous liquid(L<sub>w</sub>)-organic liquid(L<sub>a</sub>)-vapour(V) equilibrium to occur for this system, despite this was not discovered previously. The four-phase region was not found when constructing Figure 7.20 due to the temperature increments (0.2 K) being too large. It is seen that the model does predict the right behaviour from a qualitative point of view.

### 7.3.1 The Tetrahydrofuran Promoted Capture Process

Up to this point, the model has been validated against available experimental data mainly for sub-systems relevant to the THF-promoted, post-combustion carbon dioxide capture process. It has been shown that significant amounts of tetrahydrofuran must be added to the process liquid phase, in order to lower the pressure requirements sufficiently for this process to become realisable in large-scale gas separation processes.

Furthermore, it is the conclusion of the previous sections, that the present model is the most reliable for systems with three or more mole percent tetrahydrofuran in the aqueous liquid phase.

Hence, the following section considers and analyses the example of carbon dioxide capture from a simulated flue gas comprised of 10 mole percent carbon dioxide and 90 mole percent nitrogen. Two process conditions are simulated, one uses a promoter solution with three mole percent THF and the other uses a promoter solution with five mole percent THF.

The investigated aspects of the capture process are the flue gas pressure requirements, process efficiency and selectivity and finally the environmental impact of this process. The latter in particular is an aspect which is often ignored.

Figure 7.22 a) illustrates the minimum pressure requirements (incipient hydrate dissociation pressures) as function of temperature for a flue gas comprised of 10 mole percent carbon dioxide and 90 mole percent nitrogen. Two cases are simulated, the first using 3 mole percent THF in the aqueous phase and the second using 5 mole percent THF in the aqueous phase. The process is simulated using a 50 mole percent liquid feed ratio.

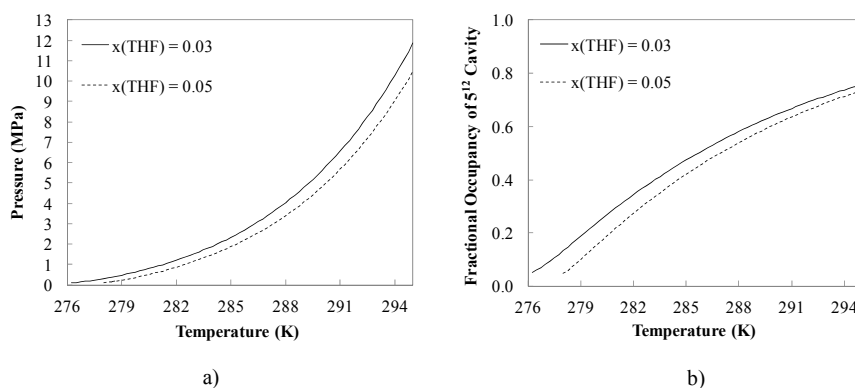


**Figure 7.22.** Mixed hydrate equilibrium pressures (a) and fractional occupancies of gas in the small  $5^{12}$  cavities of the sII hydrate (b) as functions of temperature for the quaternary system of water-tetrahydrofuran-carbon dioxide-nitrogen. Initial vapour phase comprised of 10 mole percent carbon dioxide and 90 mole percent nitrogen. Initial liquid phase consists of water and  $x(\text{THF})$  mole fraction of tetrahydrofuran. Model predictions obtained using a liquid feed ratio  $L_w/(L_w + V)$  of 0.5.

At all temperatures investigated, the minimum pressure requirement for the process using a 3 mole percent THF solution is higher than that for the process using a 5 mole percent THF solution. In the investigated temperature interval from 276 K to 295 K, equilibrium pressures vary from approximately 0.1 MPa to 12 MPa. According to the model, both systems reach an equilibrium pressure of 0.10 MPa if the process temperature is lowered sufficiently for the (almost) pure THF hydrate to form. The 3 mole percent system reaches an equilibrium pressure of 0.10 MPa at approximately 276.3 K. In the case of the 5 mole percent THF system, this temperature is approximately 277.9 K. If one compares with the T-x diagram of Figure 7.18, these temperatures are marginally higher than the equilibrium temperatures estimated for the pure THF hydrate in the binary system of tetrahydrofuran and water. The explanation for this is given in Figure 7.22 b). Even in the low temperature limits of the shown data, the hydrate phase incorporates small amounts of flue gas in the small  $5^{12}$  cavities of the hydrate structure. The presence of this gas helps stabilising the hydrate phase above the dissociation temperature of the pure THF hydrate.

Both systems in equilibrium at a pressure of 0.10 MPa, obtain a fractional occupancy of the small hydrate cavities of approximately 0.05 (seen in Figure 7.22 b)).

Even though not depicted, for all the investigated systems the fractional occupancy of tetrahydrofuran in the large  $5^{12}6^4$  cavity is predicted to be higher than 0.994 indicating complete occupancy of the large cavities by THF. The fractional occupancy of THF in the large cavities decreases slightly from

approximately 0.9994 at the low temperatures to approximately 0.995 in the high temperature limits. This is valid for both systems.

The model correctly predicts THF to only enter the large cavities. The fractional occupancy of THF in the small cavities is always predicted to be zero. Similarly, only negligible amounts of gas enter the large cavities (order of magnitude is  $10^{-3}$ ).

The information provided in the combination of Figure 7.22 a) and b) is discouraging in the context of designing a process for post-combustion carbon dioxide capture from power station flue gases using THF promoted gas hydrates. If flue gas pressurisation is considered the crucial issue in this process, low operating temperatures must be applied. Operating the 5 mole percent THF process below 0.5 MPa requires cooling the system to temperatures below 280 K. At these conditions, only 5 to 18 percent of the hydrate gas capacity (occupancy of the small cavities) is used. This means much hydrate may form, however little gas is transferred from the vapour phase into the solid phase. If the design criterion is high gas uptake in the solid phase, say 50 percent of the full capacity, the temperature must be raised to 287 K, where the minimum pressure requirement becomes 2.8 MPa. Generally, the two investigated systems behave similarly with regard to pressure and gas uptake. Hence, the 3 mole percent THF system will need pressurisation to approximately 2.7 MPa, to obtain 50 percent cage occupancy of gas in the small cavities.

Figure 7.23 a) illustrates the water- and promoter-free mole fraction of carbon dioxide in the gas phase adsorbed in the incipient hydrate crystal formed from a 10 mole percent carbon dioxide vapour phase. It is shown how this mole fraction decreases with increasing temperature/pressure. At identical temperatures, the 5 mole percent THF system turns out to be a little more selective towards carbon dioxide than the three mole percent system. The reason for this is that, for identical temperatures, this system operates at lower pressures, which in turn increases selectivity. Again, modelling results are obtained using a 50 mole percent liquid feed ratio.

Figure 7.23 b) compares the selectivity of the promoted process with 5 mole percent THF to that of the un-promoted system. Both systems are modelled using a 50 mole percent liquid feed ratio.

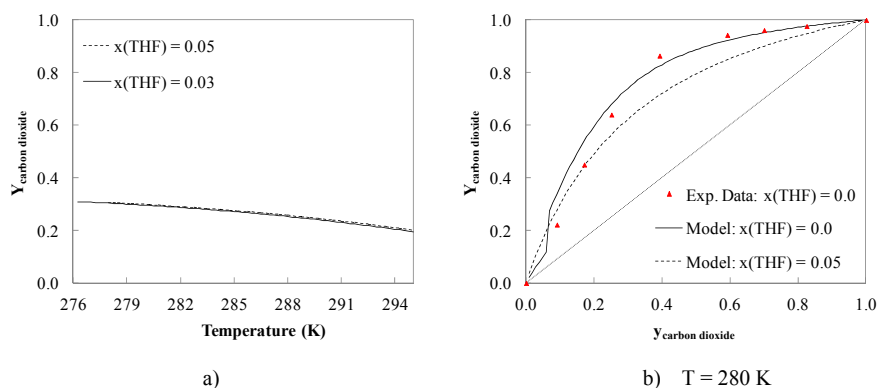


**Figure 7.23.** a) Model predictions of water- and promoter free hydrate composition of carbon dioxide as function of temperature. Initial vapour phase consists of 10 mole percent carbon dioxide and 90 mole percent nitrogen. b) Carbon dioxide content in hydrate phase on water- and promoter free basis as function of initial vapour phase composition at  $T = 280$  K. Red triangles: experimental data for the un-promoted hydrate system [Kang et al. (2001)].  $x(\text{THF})$  is mole fraction of tetrahydrofuran in the feed liquid phase.

It is seen that the selectivity towards carbon dioxide in the hydrate phase is lowered compared to the un-promoted system (ternary system of water-carbon dioxide-nitrogen). Neither the un-promoted, nor the promoted system produces a hydrate phase that is sufficiently rich in carbon dioxide to enable a single stage carbon dioxide capture process. Whereas the un-promoted system requires 3 theoretical hydrate formation/dissociation stages to reach a final vapour phase mole fraction of carbon dioxide above 0.95, the promoted system will require a total of four stages.

Table 7.4 presents predicted stage conditions for two multi-stage capture processes – one un-promoted and one promoted using 5 mole percent aqueous THF solutions. Both processes operate at a temperature of 280 K (all stages). The feed into the first stage of each process is comprised of 10 mole percent carbon dioxide and 90 mole percent nitrogen. All stages operate at a 50 mole percent liquid feed ratio and are assumed to operate at the incipient hydrate equilibrium pressure of the gas input (to the individual stages).

The un-promoted process uses pure water as liquid phase. Hence the first stage operates at a pressure of 24.9 MPa. It is assumed that the stage pressure is constant throughout the entire stage and the all hydrates formed have a composition similar to the incipient hydrate crystal. The hydrates formed in stage 1 are then dissociated at constant pressure and the released vapour phase, now containing 36 mole percent carbon dioxide is transferred to stage 2. In stage 2, hydrates will form at a pressure of 9.17 MPa and the water-free hydrate composition here becomes 80 mole percent in carbon dioxide. Passing this vapour phase (after dissociating the hydrates of stage 2) to stage 3, where hydrates will

form at a pressure of 3.65 MPa, provides a final outlet gas at a temperature of 280 K and a pressure of 3.65 MPa containing 97 mole percent carbon dioxide.

The promoted capture process operates at significantly lower pressures. The pressure of the first stage becomes 0.41 MPa and the water- and promoter-free hydrate composition of carbon dioxide is 30 mole percent. The promoted capture process requires a total of four theoretical stages to reach a final outlet gas containing 96 mole percent carbon dioxide. This outlet gas is supplied at 280 K and 0.17 MPa.

**Table 7.4.** Simulated incipient hydrate conditions for the un-promoted and promoted ( $x(\text{THF}) = 0.05$ ) capture processes.  $T = 280$  K. Initial vapour phase mole fraction of CO<sub>2</sub> in feed to stage 1 is 0.10.  $P_{\text{eq}}$  is incipient hydrate equilibrium pressure for each stage.  $Y_{\text{CO}_2}$  is mole fraction of CO<sub>2</sub> in the incipient hydrate crystal (water- and promoter-free basis). Hydrate phase composition ( $Y_{\text{CO}_2}$ ) in stage 1 is used as feed to stage 2 and so forth. All stages in both processes operate at a 50 mole percent liquid feed ratio.

Stage	Unpromoted		Promoted	
	$P_{\text{eq}}$ (MPa)	$Y_{\text{CO}_2}$	$P_{\text{eq}}$ (MPa)	$Y_{\text{CO}_2}$
1	24.9	0.36	0.41	0.30
2	9.17	0.80	0.29	0.62
3	3.65	0.97	0.21	0.86
4	N/A	N/A	0.17	0.96

The results presented above outline both the benefits and the drawbacks of using tetrahydrofuran as a thermodynamic hydrate promoter in the hydrate-based carbon dioxide capture process. The main benefit is the fact that the pressure requirement in the first separation stage of the process is reduced from 24.9 MPa to 0.41 MPa by the addition of 5 mole percent THF to the aqueous liquid. The drawback of the promoted system is not only the fact that this process requires an additional separation stage, the promoted system also delivers the final carbon dioxide rich stream at a low pressure. Hence, this process requires a final compression of the carbon dioxide product, before this stream is ready for transportation and/or storage (assuming liquid carbon dioxide is the preferred form for transportation). Compressing the outlet stream of the final separation stage is however significantly less energy consuming than compression of the original flue gas, since the final outlet gas represents only a small fraction of the original flue gas stream.

Furthermore, since the promoted hydrates provide low gas uptakes at the proposed process temperature, large amounts of liquid and hydrate slurries must be circulated in the promoted hydrate system to remove significant amounts of carbon dioxide from the original flue gas.

An interesting and often ignored aspect of the promoted hydrate based carbon dioxide capture process is the promoter slip from the aqueous liquid phase to the vapour phase. Figure 7.24 illustrates the predicted THF mole fraction in the equilibrium vapour phase (incipient hydrate forming conditions) of the promoted hydrate processes.

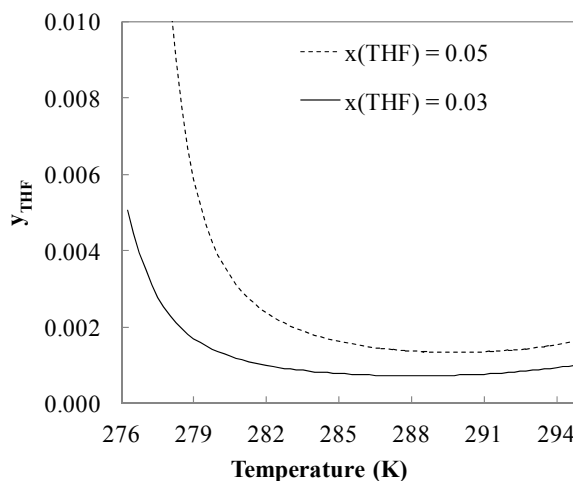


**Figure 7.24.** Equilibrium Mole fraction of tetrahydrofuran,  $y_{\text{THF}}$ , in the vapour phase leaving stage 1 of the simulated carbon dioxide capture process. Solid line: model predictions for system using a 3 mole percent THF aqueous solution. Dashed line: model predictions for system using a 5 mole percent THF aqueous solution.

As can be seen, the gas phase of stage 1 contains significant amounts of THF. For the simulated 4-stage capture process ( $x(\text{THF}) = 0.05$ ), operating at 280 K, the gas phase of stage 1 would contain 0.39 mole percent THF at equilibrium. This promoter content would have to be recovered, before the off-gas can be emitted to the atmosphere. The following stages would emit similar or higher concentrations of THF to the atmosphere, since these stages operate at lower pressures. Hence, the present model predicts furthermore one challenge in the promoted hydrate process. Significant amounts of promoter will slip from the liquid phase to the vapour phase and this content must be re-generated subsequently for both environmental and economic reasons.

## 7.4 Cyclopentane Promoted Gas Hydrate Systems

To enable incipient hydrate equilibrium calculations for systems containing cyclopentane, Kihara cell potential parameters have been regressed for this

component by matching the model to experimental data for mixed hydrates of cyclopentane + carbon dioxide and cyclopentane + nitrogen.

The spherical hard core radius,  $a$ , of cyclopentane has been calculated by Takeuchi et al. (2009) from second virial coefficient data. The calculated core radius has been used here as presented in the original work.

Table 7.5 lists the experimental hydrate dissociation pressure data found in the literature for the mixed hydrates of cyclopentane + carbon dioxide [Zhang and Lee (2009), Mohammadi and Richon (2009)] and cyclopentane + nitrogen [Tohidi et al. (1997), Du et al. (2010), Mohammadi and Richon (2011)]. All data supposedly represent hydrate(H) – liquid water(L<sub>w</sub>) – liquid organic(L<sub>a</sub>) – vapour(V) equilibria. These data have been used as reference data when correlating the two Kihara potential parameters used as adjustable parameters in the van der Waals-Platteeuw hydrate model ( $\sigma$  and  $\varepsilon/k_B$ ).

Since the modelled systems are univariant in the four-phase, hydrate forming region, all systems are modelled using an equimolar feed stock ( $x_{\text{water}} = 1/3$ ,  $x_{\text{cyclopentane}} = 1/3$ ,  $x_{\text{gas}} = 1/3$ ).

**Table 7.5.** Four-phase hydrate equilibrium data in the ternary systems of water + cyclopentane + carbon dioxide (CO<sub>2</sub>) and water + cyclopentane + nitrogen (N<sub>2</sub>). AAD in P is absolute average deviation when comparing the present model to the available reference data. AAD according to Eq. (7.1).

Reference	System	Data Points	Temp. / K	Press. / MPa	AAD (P)
[1]	Cyclopentane + CO <sub>2</sub>	7	286.7 – 292.6	0.89 – 3.51	0.20
[2]	Cyclopentane + CO <sub>2</sub>	7	284.3 – 291.8	0.35 – 2.52	0.13
[3]	Cyclopentane + N <sub>2</sub>	4	282.9 – 289.1	0.64 – 3.50	0.13
[4]	Cyclopentane + N <sub>2</sub>	8	285.9 – 302.0	1.68 – 24.5	0.04
[5]	Cyclopentane + N <sub>2</sub>	5	281.7 – 290.2	0.25 – 4.06	0.16
[1] Zhang and Lee (2009), [Mohammadi and Richon (2009)], [3] Tohidi et al. (1997), [4] Du et al. (2010), [5] Mohammadi and Richon (2011)					

The absolute average deviations (AAD) when comparing the final model performance with the experimental reference data are provided for each pressure data set. Despite the fact that the reference data for the mixed hydrates of cyclopentane and carbon dioxide only cover a narrow temperature interval of approximately 8 Kelvin, AAD's to these data are considerable. The data for the mixed hydrates of cyclopentane and nitrogen cover a larger temperature interval of approximately 20 Kelvin. Figure 7.25 a) and b) compare the model descriptions and the experimental data for the mixed hydrates of cyclopentane + carbon dioxide and cyclopentane + nitrogen respectively.

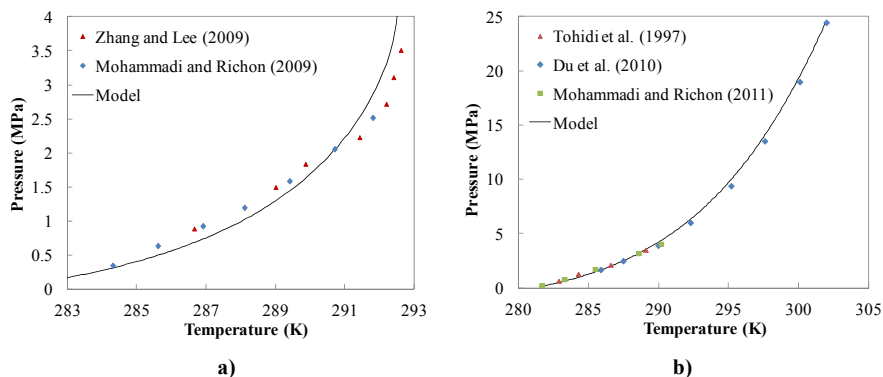


**Figure 7.25.** Hydrate dissociation pressure as function of temperature for the mixed hydrate of cyclopentane and carbon dioxide (a) or nitrogen (b). Comparison of model descriptions and experimental data.

The model description of the mixed hydrates of cyclopentane and carbon dioxide appears to contain more curvature than is seen in the experimental data. The equilibrium pressure data of the mixed hydrate increases almost linearly with increasing temperature for temperatures lower than 292 K. Above this temperature the pressures reported by Zhang and Lee (2009) increase more steeply with increasing temperature. The model seems to underestimate the dissociation pressure in the temperature range from 284 to 291 K due to the curvature in the model. Above 291 K, the model description becomes very steep with increasing temperature.

The fluid phase behaviour for this system has been tracked during all calculations. It was found that the carbon dioxide-rich vapour phase becomes incorporated in the organic liquid phase at temperatures above 292.5 K (for the given equi-molar feed). Hence, above 292.5 K, the calculated conditions represent three-phase hydrate(H) – liquid water ( $L_w$ ) – liquid organic ( $L_a$ ) equilibria. The calculated pressures increase almost vertically in this range due to the disappearance of the most compressible phase. However, below 292.5 K the steep pressure increase is likely imposed by the Kihara parameters of carbon dioxide. It is possible that the regressed Kihara parameters for carbon dioxide provide little stabilising effect of the small cavity in the sII hydrate structure at elevated temperatures.

The high AAD's reported in Table 7.5 for the data of Zhang and Lee (2009) are mainly due to the model description increasing at a temperature approximately 0.5 K lower than the experimental data. The model deviates significantly from the data point at 292.6 K, since the model “predicts” hydrate(H) - liquid water( $L_w$ ) – liquid organic( $L_a$ ) equilibria at this temperature.



Accurate descriptions of the mixed hydrate of cyclopentane and nitrogen are obtained considering the large temperature interval covered by the experimental data. Even though difficult to see, AAD's in the low-temperature range are however comparable for this system to those in the cyclopentane + carbon dioxide system. The modelled equilibrium pressures in this system do not increase suddenly as seen in the system with carbon dioxide, hence the sudden rise in pressure is ascribed the Kihara parameters for carbon dioxide.

Figure 7.26 illustrates the predicted pure sII hydrate of cyclopentane. The model predictions are compared to data reported by Fan et al. (2001) in the hydrate (H) – liquid water (L<sub>w</sub>) – vapour (V) region and data reported by Trueba et al. (2011) in the hydrate (H) – liquid water (L<sub>w</sub>) – liquid organic (L<sub>a</sub>) region.

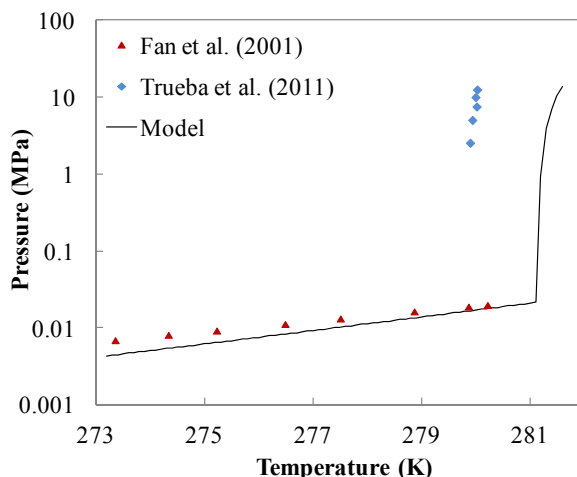


**Figure 7.26.** Hydrate dissociation pressure as function of temperature for the pure sII hydrate of cyclopentane Comparison of model prediction and experimental data.

Even though these data were not included as reference data when regressing Kihara parameters for cyclopentane, the model accurately predicts the data reported by Fan et al. (2001). AAD for these data is 0.25. The data reported by Trueba et al. (2011) are less accurately described. The developed model predicts the upper quadruple point for this binary system at a temperature approximately 1.5 K higher than the experimental data suggests.

Since the pure hydrate of cyclopentane is of little interest to the present work, no attempts have been made to improve the accuracy of the description in this sub-system.

As a final note, it is worth mentioning that the model results presented in Figure 7.26 represent the model prediction for the pure sII cyclopentane hydrate

as function of temperature. However, whereas the model does predict the sII hydrate structure to be the most stable form of the cyclopentane hydrate at temperatures below 281.2 K, the model predicts the sI hydrate structure to be the most stable form of the pure cyclopentane hydrate at temperatures above 281.2 K (not shown in Figure 7.26).

### 7.4.1 The Cyclopentane Promoted Capture Process

The model has been validated against available experimental data mainly for sub-systems relevant to the cyclopentane-promoted, post-combustion carbon dioxide capture process.

The following considers and analyses the example of carbon dioxide capture from a simulated flue gas comprised of 10 mole percent carbon dioxide and 90 mole percent nitrogen.

The investigated aspects of the capture process are the minimum flue gas pressure requirements, process efficiency and selectivity and finally the environmental impact of this process. The latter in particular turns out to be a major challenge in the cyclopentane promoted capture process.

Figure 7.27 illustrates the predicted minimum pressure requirement in the cyclopentane promoted carbon dioxide capture process, treating a flue gas initially containing 10 mole percent carbon dioxide and 90 mole percent nitrogen. The minimum pressure requirement is given by the thermodynamic equilibrium pressure of the incipient hydrate crystal. In the real process, a higher pressure must be applied to ensure sufficient driving force for the hydrate nucleation and growth to take place.

The capture process is simulated by mixing equi-molar amounts of gas (V) and liquid ( $L_w + L_a$ ), thus  $V/(V+L_w+L_a) = 0.5$ . The total amount of feed liquid is comprised of 95 mole percent water and 5 mole percent cyclopentane. Assuming the formed hydrates are of the sII type and cyclopentane fully occupies the large cavities, the cyclopentane feed alone is sufficient to convert 90 percent of the liquid water feed to solid hydrate (a “stoichiometric” hydrate phase with complete filling of large cavities contain 5.56 mole percent cyclopentane). Since the present model only allows for calculation of incipient hydrate formation conditions, actual conversion of the liquid phase at a given temperature/pressure ( $T/P$ ) condition cannot be simulated.

The modelled system is di-variant in the four-phase equilibrium region, hence the calculated equilibrium pressure is not only temperature dependent, but also composition dependent.

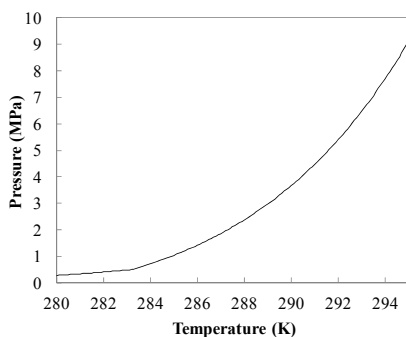


**Figure 7.27.** Predicted hydrate dissociation pressure as function of temperature for the quaternary system of water + cyclopentane + carbon dioxide + nitrogen. Feed is 47.5 mole percent water, 2.5 mole percent cyclopentane, 5 mole percent carbon dioxide and 45 mole percent nitrogen.

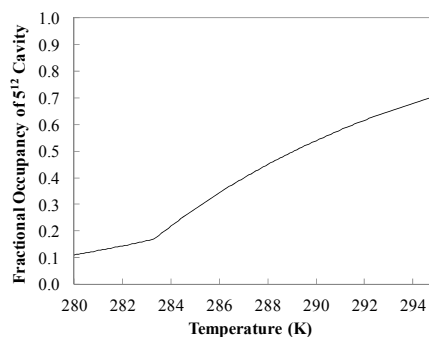


**Figure 7.28.** Predicted fractional occupancy of gas in the small 5<sup>12</sup> cavity of the sII hydrate as function of temperature for the quaternary system of water + cyclopentane + carbon dioxide + nitrogen. Feed is 47.5 mole percent water, 2.5 mole percent cyclopentane, 5 mole percent carbon dioxide and 45 mole percent nitrogen.

Only temperatures down to 280 K are considered in the process simulations, since the sII hydrate phase may be stabilised by cyclopentane alone at temperatures much lower than this. In the model this is indicated by a low fractional occupancy of gas in the small 5<sup>12</sup> cavities of the sII hydrate structure and simultaneously complete occupancy by cyclopentane in the large cavities. The model predicts the fractional occupancy of cyclopentane in the large cavities to be higher than 0.99 at all the simulated conditions. This occupancy decreases with increasing temperature from 0.999 at 280 K to 0.994 at 295 K. The predicted amount of gas present in the large cavities is negligible as is the predicted amount of cyclopentane in the small cavities.

Figure 7.28 illustrates the predicted fractional gas occupancy of the small cavities. The enclosed gas is a mixture of carbon dioxide and nitrogen. This information provides an indication of the efficiency of the gas capture process. Only the small cavities of the sII hydrate structure are available for gas uptake, since the large cavities are fully occupied by cyclopentane. Hence, Figure 7.28 illustrates how much of the full storage capacity of the formed hydrate is exploited at a given  $T/P$  condition. This along with the predicted selectivity (Figure 7.31) of carbon dioxide in the hydrate phase determines the overall efficiency of the capture process.

Generally, both the minimum pressure requirement and the gas uptake increase with increasing temperature. The minimum pressure requirement for the capture process operating at 280 K is approximately 0.28 MPa. At this condition only 11 percent of the storage capacity in the hydrate phase is exploited, since

cyclopentane almost self-stabilises the solid phase. An increase in temperature to 289.0 K results in an increase in gas uptake to a fractional occupancy of 50 percent in the small cavities. At this temperature the minimum pressure requirement becomes 2.97 MPa.

The model shows a change of slope in both the predicted minimum pressure requirement (Figure 7.27) and the predicted gas uptake (Figure 7.28) occurring at a temperature of approximately 283.4 K. Below this temperature both the dissociation pressure and the gas uptake decreases only little with lowering temperature. The explanation for this behaviour is found in the predicted fluid phase behaviour. CPA predicts a disappearance of the bulk cyclopentane liquid phase, ( $L_a$ ), occurring at a temperature of approximately 283.4 K and a pressure of approximately 0.54 MPa. These conditions are valid for the given system and will change with changing feed composition. At temperatures below 283.4 K, the cyclopentane liquid phase is incorporated in the vapour phase.

Figure 7.29 illustrates the cyclopentane mole fraction in the vapour phase for the simulated carbon dioxide capture system operating at incipient hydrate equilibrium conditions. The feed gas contains 10 mole percent carbon dioxide and the feed liquid consists of 5 mole percent cyclopentane.

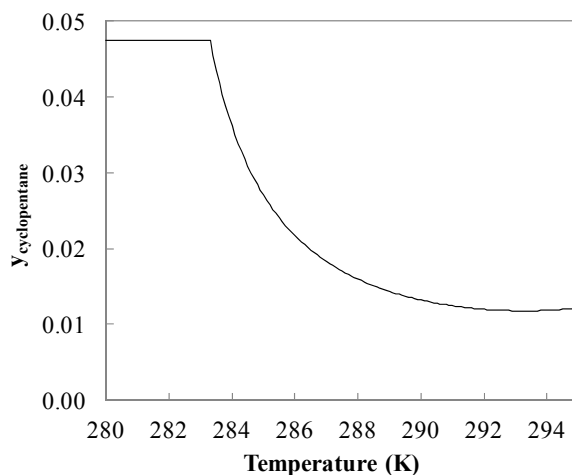


**Figure 7.29.** Mole fraction of cyclopentane in the outlet vapour phase leaving the simulated carbon dioxide capture process as function of operating temperature. Pressure the incipient hydrate formation pressure at any given temperature.

The vapour phase mole fraction of cyclopentane is the highest at low temperatures, despite the fact that the vapour pressure of the cyclopentane liquid phase increases with increasing temperature. The reason for this is that the

incipient hydrate pressure increases with increasing temperature. This compensates for the increase in vapour pressure of cyclopentane. At temperatures below 283.4 K, the curve flattens out. This is an indication that an insufficient amount of cyclopentane is present in the system to saturate the vapour phase at the given conditions of temperature and pressure while still retaining the bulk liquid phase. Thus, all bulk cyclopentane has transferred to the vapour phase. At higher temperatures, the vapour phase is saturated with cyclopentane, indicating the presence of a bulk cyclopentane liquid phase co-existing with the vapour phase. Only negligible amounts of cyclopentane transfer to the aqueous liquid phase. At no point does the cyclopentane content in the vapour phase become lower than 1 mole percent. At an operating temperature of 285 K the cyclopentane content in the outlet gas will be 2.7 mole percent. This indicates a major drawback of using this thermodynamic hydrate promoter. A significant promoter loss to the vapour phase must be expected. This organic content must be regenerated and possible re-cycled before the carbon dioxide lean outlet gas can be emitted to the atmosphere.

The present modeling results support the theory presented in section 6.2 for the experimental study of the cyclopentane promoted system (Procedure #1). Here, it was suggested that the cyclopentane bulk phase might have vapourised, resulting in a system that showed little pressure decrease with decreasing temperature. A change of slope was similarly found at higher temperatures. Since the exact composition of the experimentally studied system is unknown (dynamic study with hydrate formation), no attempts have been made to model that system.

Figure 7.30 and Figure 7.31 show equilibrium pressures and hydrate composition (water- and promoter free basis) respectively as function of the initial vapour phase composition for a cyclopentane promoted system operating at a constant temperature of 285 K. This temperature is chosen to avoid that cyclopentane transfers completely to the vapour phase. For comparison, similar results are provided for the unpromoted system operating at a constant temperature of 280 K. Data for the unpromoted system operating at a temperature of 280 K are those reported by Kang et al. (2001). Both systems are simulated using a 50/50 (molar) vapour/liquid feed with 5 mole percent of the liquid being cyclopentane and 95 mole percent being water.

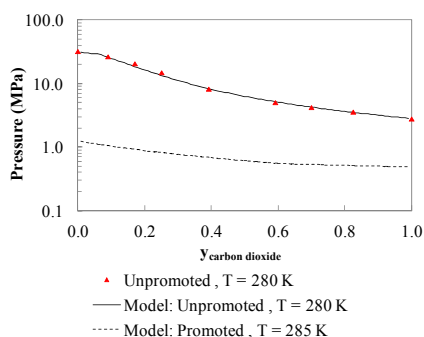


**Figure 7.30.** Mixed hydrate dissociation pressure as function of carbon dioxide mole fraction in the vapour phase (binary vapour phase with nitrogen). The unpromoted system is the ternary system of CO<sub>2</sub>, N<sub>2</sub> and H<sub>2</sub>O. The promoted system is the quaternary system of CO<sub>2</sub>, N<sub>2</sub>, H<sub>2</sub>O and Cyclopentane. Experimental data from Kang et al. (2001).

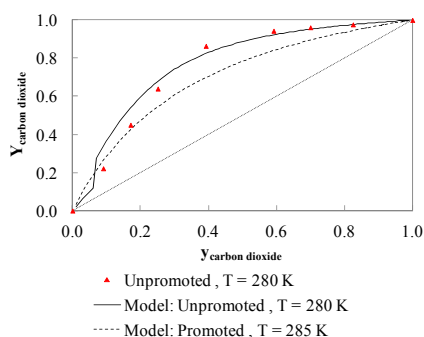


**Figure 7.31.** Mixed hydrate composition on water- and promoter-free basis as function of carbon dioxide mole fraction in the vapour phase (binary vapour phase with nitrogen). The unpromoted system is the ternary system of CO<sub>2</sub>, N<sub>2</sub> and H<sub>2</sub>O. The promoted system is the quaternary system of CO<sub>2</sub>, N<sub>2</sub>, H<sub>2</sub>O and Cyclopentane. Experimental data from Kang et al. (2001).

The pressure reducing effect of the cyclopentane additions is clearly seen in Figure 7.30. At a temperature of 285 K, the capture process operates at pressures ranging from 0.5 MPa to 1.2 MPa for the entire initial vapour phase concentration span. Even though operating at a lower temperature, the unpromoted process operates at much higher pressures ranging from 2.9 MPa to 31 MPa.

One of the drawbacks of the cyclopentane addition is seen in Figure 7.31, comparing the selectivity of carbon dioxide in the hydrate phase for the unpromoted- and the cyclopentane promoted systems. The selectivity towards carbon dioxide becomes lower by the addition of cyclopentane. However, the hydrate phase still has a clear selectivity towards carbon dioxide, providing the possibility of separating this component from nitrogen in the flue gas. An aspect not shown in the investigated isothermal systems is the gas uptake. At 285 K, this uptake range from approximately 28 to 35 percent of the full storage capacity of the sII hydrate phase, depending on the initial vapour phase composition.

The information provided in Figure 7.30 and Figure 7.31 may be combined to make a simplified capture process evaluation (thermodynamics). Neither the unpromoted, nor the promoted system produces a hydrate phase that is sufficiently rich in carbon dioxide to enable a single stage capture process. Whereas, for a flue gas initially containing 10 mole percent carbon dioxide, the unpromoted system requires 3 theoretical hydrate formation/dissociation stages to reach a final vapour phase with more than 95 mole percent carbon dioxide, the promoted system will require a total of four stages.

Table 7.6 presents predicted stage conditions for two multi-stage capture processes – one un-promoted and one promoted using cyclopentane. The unpromoted process operates at a temperature of 280 K and the promoted process at 285 K. The feed into the first stage of each process is comprised of 10 mole percent carbon dioxide and 90 mole percent nitrogen. All stages operate at a 50 mole percent liquid feed ratio. 5 mole percent of the liquid feed is pure cyclopentane. All stages are assumed to operate at the incipient hydrate equilibrium pressure of the inlet gas.

**Table 7.6.** Simulated incipient hydrate conditions for the unpromoted and cyclopentane promoted capture processes. T = 280 K for the unpromoted and 285 K for the promoted system. Initial vapour phase mole fraction of CO<sub>2</sub> in feed to stage 1 is 0.10.  $P_{eq}$  is incipient hydrate equilibrium pressure for each stage.  $Y_{CO_2}$  is mole fraction of CO<sub>2</sub> in the incipient hydrate crystal (water- and promoter-free basis). Hydrate phase composition ( $Y_{CO_2}$ ) in stage 1 is used as feed to stage 2 and so forth. All stages in both processes operate at a 50 mole percent liquid feed ratio.

Stage	Unpromoted: T = 280 K		Promoted: T = 285 K	
	$P_{eq}$ (MPa)	$Y_{CO_2}$	$P_{eq}$ (MPa)	$Y_{CO_2}$
1	24.9	0.36	1.04	0.28
2	9.17	0.80	0.79	0.58
3	3.65	0.97	0.56	0.83
4	N/A	N/A	0.51	0.95

The un-promoted process is identical to that presented in 7.3.1.

The cyclopentane promoted capture process operates at significantly lower pressures. The pressure of the first stage becomes 1.04 MPa and the water- and promoter-free hydrate composition of carbon dioxide is 28 mole percent. The promoted capture process requires a total of four theoretical stages to reach a final outlet gas containing 95 mole percent carbon dioxide. This outlet gas is supplied at 285 K and 0.51 MPa. Note that since the pressure in the final stage of the promoted process is low, the complete cyclopentane bulk phase will transfer directly to the vapour phase at the inlet of this stage.

The present investigation has shown that whereas cyclopentane is a very potent thermodynamic hydrate promoter in terms of its capability of reducing the incipient hydrate formation pressure, it does bring several drawbacks in the form of low gas uptakes in the hydrate phase, lowered selectivity towards carbon dioxide and finally high miscibility with the vapour phase compounds resulting in a significant promoter loss from the feed liquid.

Compared to the tetrahydrofuran promoted capture process, the cyclopentane promoted process has a great disadvantage in terms of the very large promoter

slip. This process cannot be operated at low pressures, since that will result in vapour phase outlet streams containing several mole percent cyclopentane. Even though cyclopentane is the more potent promoter in terms of pressure reduction, it may become the less attractive of the two promoters due to the large promoter slip and with corresponding process limitations at low temperature/low pressure conditions.

## **7.5 Mixed Promoter Gas Hydrate Systems**

With the complete model in place for all five components; water, tetrahydrofuran, cyclopentane, carbon dioxide and nitrogen, it has been possible to investigate the mixed promoter hydrate system (without nitrogen). To model this system, we have to rely on the ability of the model to predict the outcome of both the fluid phase behaviour in this quaternary system of water, tetrahydrofuran, cyclopentane and carbon dioxide and the hydrate phase behaviour with these three hydrate formers present.

The mixed promoter system from experimental study#2 was previously reported to have an overall liquid composition of {0.894; 0.052; 0.054} in terms of mole fractions of water, tetrahydrofuran and cyclopentane respectively. This composition has been used in the model along with the assumption of an overall feed liquid mole fraction of 0.9 ( $(L_w + L_a)/(V + L_w + L_a) = 0.9$ ). Figure 7.32 compares the experimental data with the model predictions. The pure cyclopentane promoted system is included as reference (both model results and experimental data).



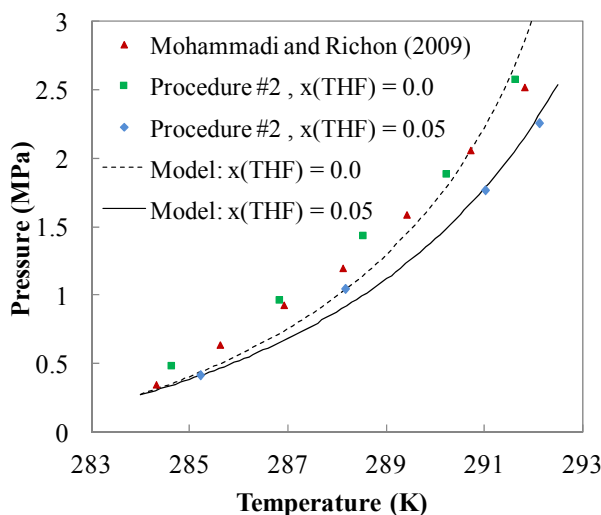


**Figure 7.32.** Comparison of experimental data and model results for hydrate formation in the ternary system of water, cyclopentane, carbon dioxide ( $x(\text{THF}) = 0.0$ ) and the quaternary system of water, cyclopentane, tetrahydrofuran and carbon dioxide ( $x(\text{THF}) = 0.05$ ).

The model accurately predicts the synergistic effect which has been documented experimentally. When looking at the model results, it becomes obvious that the synergy effect is the largest at high temperatures. At approximately 285 K, the enhanced promotion can hardly be seen in Figure 7.32. It appears that cyclopentane dominates in the large cavities, thereby stabilising the sII hydrate. When investigating temperatures below 284 K, the presence of tetrahydrofuran in the aqueous acted inhibiting (thermodynamically) on the hydrate phase compared to the pure cyclopentane promoted hydrate.

The use of a 5 mole percent tetrahydrofuran concentration in the aqueous phase in the experimental work is explained by this representing an optimum concentration in the pure tetrahydrofuran promoted system. This is however not necessarily the case in the mixed promoter system. To investigate this, the system has been analysed at isothermal conditions of 285 K and 290 K. Using still 5 mole percent cyclopentane (relative to overall feed liquid) and a vapour feed mole fraction of 10 percent, the tetrahydrofuran concentration in the aqueous phase has been varied from 0.1 mole percent to 10 mole percent. Results are illustrated in Figure 7.33.

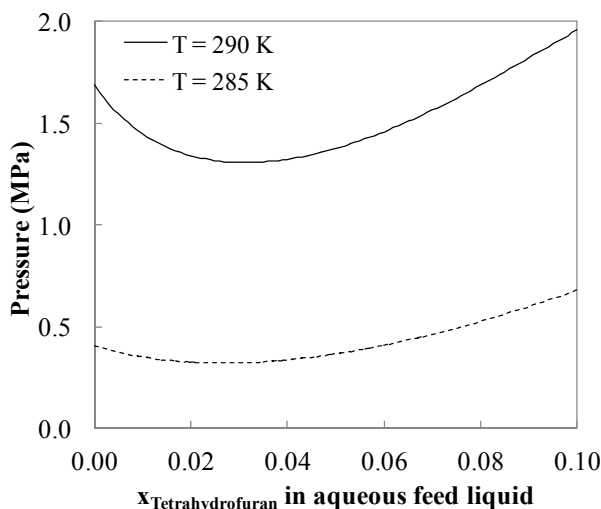


**Figure 7.33.** Model predictions of hydrate equilibrium conditions in the quaternary system of water, cyclopentane, tetrahydrofuran and carbon dioxide as function of the initial concentration of tetrahydrofuran in the aqueous liquid feed.

Figure 7.33 provides a clear picture of the synergistic effect occurring when tetrahydrofuran is added to the ternary system of water, cyclopentane and carbon dioxide. Furthermore, this analysis reveals that there is an optimum in the initial tetrahydrofuran concentration in the aqueous phase, and this optimum is no longer at 5.6 mole percent. The optimum concentration has shifted towards lower THF mole fractions. At 290 K the optimum (initial) concentration is 3.1 mole percent in the aqueous phase. At 285 K an optimum is found at 2.7 mole percent tetrahydrofuran in the initial aqueous liquid. Thus, no general conclusion is drawn about the optimum tetrahydrofuran concentration. It varies slightly around a concentration of 3 mole percent depending on the applied temperature/pressure. The equilibrium pressure is reduced from 1.69 MPa (pure cyclopentane promoted system) to approximately 1.31 MPa (mixed promoter system at optimum concentration) at a temperature of 290 K. At 285 K the pressure is reduced from 0.41 MPa to 0.32 MPa. This corresponds to a maximum predicted pressure reduction of approximately 22 percent for both temperature conditions.

Even though the temperature shift of approximately 1 K at high temperatures may seem insignificant, the synergy effect is considerable, if one considers equilibrium pressures rather than temperatures.

The model has finally been used to analyse the mechanism behind the synergy effect. The first analysis investigated if the synergy effect could be explained alone by the enhanced solubility of cyclopentane in the aqueous phase. This was

investigated by excluding tetrahydrofuran from the hydrate forming compounds in the model, but still allowing it to interfere with the fluid phases. By doing so, tetrahydrofuran acted only inhibiting on the hydrate formation due to its hydrogen bonding with water. Hence, it is clear that the synergy effect occurs in the hydrate phase.

Thus, a second analysis investigated the fractional occupancies in the hydrate phase at isothermal conditions of 290 K and varying THF concentrations in the initial aqueous phase. Results from this analysis are provided in Figure 7.34. The feed conditions applied in the model are identical to those used in the system of Figure 7.32.

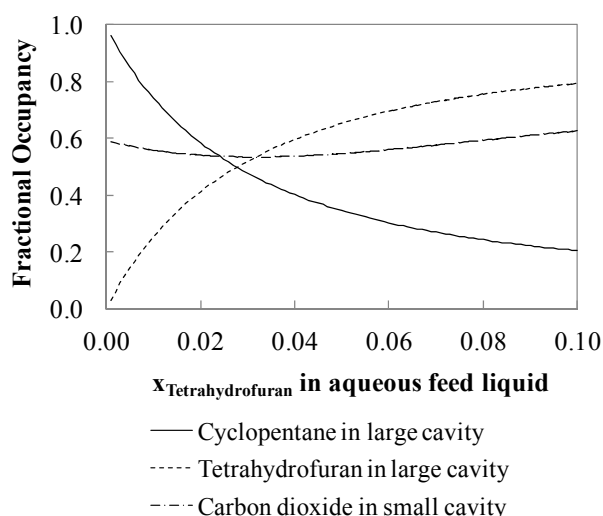


**Figure 7.34.** Model predictions of fractional occupancies of hydrate formers in the mixed hydrate formed in the quaternary system of water, cyclopentane, tetrahydrofuran and carbon dioxide as function of the initial concentration of tetrahydrofuran in the aqueous liquid feed.

It is clearly seen that the model explains the synergy effect by tetrahydrofuran displacing cyclopentane from the large cavities of the sII hydrate phase. At low THF concentrations, cyclopentane dominates in the large cavities. However as the tetrahydrofuran concentration in the (initial) liquid phase increases, THF starts displacing cyclopentane. At a THF concentration approximately 2.8 mole percent, the fractional occupancies of the two promoters in the large cavities are approximately 50/50. At the optimum concentration of 3.1 mole percent, the fractional occupancies are 53/47 in favour of tetrahydrofuran. Performing the same analysis at a lower temperature (285 K) provides slightly different results. Here the optimum liquid phase concentration is 2.7 mole percent and at this

condition cyclopentane occupies 54 percent of the large cavities and tetrahydrofuran 46 percent. This observation partly explains why the mixed promoter system shows little differences compared to the pure cyclopentane promoted system at low temperatures. Here cyclopentane dominates in the hydrate phase even at high liquid phase THF concentrations.

As a final result, Figure 7.34 shows the fractional occupancy of carbon dioxide in the small cavity of the mixed hydrate. At the investigated temperature of 290 K this occupancy is approximately 54-60 percent depending on the amount of THF present in the system. The gas uptake decreases towards the optimum concentration due to the decrease in pressure. Thus the mixed promoter system shows the same disadvantages as the pure promoter systems. As the system moves towards low temperatures and low pressures, the gas uptake decreases. The fractional occupancy of carbon dioxide gas in the small cavities at 285 K and a liquid phase THF mole fraction of 0.027 (optimum conditions at this temperature) is only 0.25.

Generally, it is found that the mixed promoter system has the same advantages and disadvantages in terms of thermodynamics as the pure cyclopentane promoted system. Significant pressure reduction is obtained, however large amounts of cyclopentane are evaporated to the vapour phase. Setting up a simplified carbon dioxide capture process as it has been done for the two pure promoter systems is unnecessary, as this system acts very similar to the cyclopentane promoted system, only at slightly elevated temperatures (0.8 – 1 K higher). Four capture stages would still be needed in this system and the outlet vapour phases of each stage would contain significant amounts of cyclopentane.

## **7.6 Summary of Modeling Results**

A modeling study of both fluid- and hydrate phase behaviour was presented. Five components were studied, water, tetrahydrofuran, cyclopentane, carbon dioxide and nitrogen. Of the 10 possible binary pairs formed by this system, 9 were studied for their fluid phase behaviour and CPA descriptions were improved when needed by correlation of binary parameters in the applied mixing- and combining rules. A maximum of three adjustable parameters were applied for binary pairs involving induced cross-association (solvation) and a maximum of two adjustable parameters were applied for pairs without cross-association. CPA predicted the fluid phase behaviour with sufficient accuracy for three of the nine binary pairs (none of them involved self- or cross-association). All binary pairs involving water needed some form of binary correction to provide satisfactory results over extended ranges of temperature and pressure.

In this work, CPA has proven its qualities as an advanced equation of state both in systems involving hydrogen bonding with resulting complex fluid phase behaviour and in systems, where CPA could be simplified to the SRK equation of state with satisfactory results.

The binary system of water and tetrahydrofuran represented a challenge from a fluid phase modeling point of view. This system shows both azeotropic vapour-liquid equilibrium (VLE) at ambient conditions and closed-loop liquid-liquid miscibility gaps at elevated temperatures and pressures. Modelling this system accurately was found to be important when later extending the model to include other components such as e.g. carbon dioxide. Whereas CPA, from a qualitative point of view, predicted the correct fluid phase behaviour in this ternary system, the phase composition of the aqueous phase in particular was described with significant deviations compared to available experimental data. The inaccuracy of the fluid phase description propagated into the later hydrate modeling results, where the predicted hydrate phase boundary in the hydrate(H)-aqueous liquid(L<sub>w</sub>)-organic liquid(L<sub>a</sub>)-vapour four-phase region was found to deviate by 1-2 K compared to the experimental data.

Cyclopentane, like other cycloalkanes ranging from cyclopropane to cyclohexane, represented a challenge for CPA, both for the description of the pure component densities and for liquid-liquid equilibrium (LLE) in the binary systems with water. It was concluded that an insufficient amount of reliable LLE data exist for the binary system of water and cyclopentane. Additional water-in-oil data in particular are needed for this system.

With CPA forming a solid framework for the fluid phase description of this system of five components, the van der Waals Platteeuw hydrate model was applied to enable calculations of incipient gas hydrate formation conditions. The application of an algorithm, supplying fluid phase compositions, fugacities of hydrate formers and water activity coefficients (all obtained from a multi-phase isothermal/isobaric flash calculation), to the hydrate model ensured a consistent model, which was applicable in all hydrate forming regions above the ice point of water.

Gas hydrate formation was successfully modeled in the four subsystems forming pure hydrates with water; the pure sI hydrate of carbon dioxide, the sII hydrate of nitrogen, the sII hydrate of tetrahydrofuran and the sII hydrate of cyclopentane. Furthermore, five binary hydrates were modeled: the sI/sII hydrates of carbon dioxide and nitrogen, the sII hydrates of carbon dioxide and tetrahydrofuran, the sII hydrate of carbon dioxide and cyclopentane, the sII hydrate of nitrogen and tetrahydrofuran and finally the sII hydrate of nitrogen and cyclopentane. Three systems with three hydrate formers were studied; the sII hydrates formed by tetrahydrofuran, carbon dioxide and nitrogen, the sII hydrates

formed by cyclopentane, carbon dioxide and nitrogen and finally the mixed promoter system forming sII hydrates with tetrahydrofuran, cyclopentane and carbon dioxide. Finally, the complete system of five components was investigated for hydrate formation. sII hydrate were predicted to form, however no actual results were presented since this system behaved very similar to the quaternary system of water, cyclopentane, carbon dioxide and nitrogen, only at slightly elevated temperatures (more stable hydrate). An interesting observation was that the model predicted the synergistic effect occurring in hydrate forming systems with simultaneous presence of tetrahydrofuran and cyclopentane.

The developed model has been applied to simulate three simplified processes for post-combustion carbon dioxide capture from power station flue gases.

All three processes applied hydrate formation to selectively remove carbon dioxide from the flue gas. The first process was named the unpromoted process. The unpromoted process operated isothermally at a temperature of 280 K. The feed into the first stage of the process was a flue gas comprised of 10 mole percent carbon dioxide and 90 mole percent nitrogen, delivered at 280 K. In the hydrate forming vessel, pure water and pressurised flue gas was mixed at a 50/50 molar feed ratio. The hydrate forming stage was assumed to operate isobarically at the incipient hydrate equilibrium pressure of the inlet gas. The pressure requirement of the first stage was estimated to be 24.9 MPa. The captured gas would contain 36 mole percent carbon dioxide. After three consecutive hydrate formation/dissociation stages (three-stage capture process), a carbon dioxide rich product (97 mole percent) could be delivered at a temperature of 280 K and a pressure of 3.65 MPa. It was concluded that this process was not economically feasible due to the large pressure requirement of the first capture stage.

The second carbon dioxide capture processes used a thermodynamic promoter to reduce the pressure requirements in all stages. The pure water liquid phase of the unpromoted process was substituted with a 5 mole percent aqueous solution of tetrahydrofuran. By doing so the pressure requirement of the first stage (still operating at 280 K) could be lowered to 0.41 MPa. Selectivity towards carbon dioxide in the hydrate phase was however lower than in the unpromoted process. Therefore the tetrahydrofuran promoted capture process needed four consecutive hydrate formation/dissociation stages to produce a 96 mole percent carbon dioxide-rich product stream. This stream was delivered at 280 K and a pressure of 0.17 MPa.

The third capture process used cyclopentane as thermodynamic promoter. Pure water was used with the addition of 5 mole percent (fraction of liquid feed) cyclopentane bulk liquid. By doing so the pressure requirement of the first stage (operating now at 285 K) could be lowered to 1.04 MPa. Selectivity towards carbon dioxide in the hydrate phase was similar to the tetrahydrofuran process.

Therefore, this process also needed four consecutive hydrate formation/dissociation stages to produce a 95 mole percent carbon dioxide-rich product stream. This stream was delivered at 285 K and a pressure of 0.51 MPa.

The cyclopentane promoted process operated at slightly elevated temperatures and pressures compared to the tetrahydrofuran promoted process. This was due to the high volatility of cyclopentane in the bulk organic liquid phase. Whereas the promoter content in the equilibrium vapour phases of the tetrahydrofuran promoted systems would be approximately 0.4 mole percent, vapour phases in the cyclopentane promoted process could contain several mole percent cyclopentane. At temperatures below 284 K, the entire cyclopentane bulk phase could evaporate completely at hydrate forming conditions (pressures below approximately 0.55 MPa).

It was concluded that despite the fact that cyclopentane is the most potent thermodynamic promoter in terms of pressure reduction capabilities, it has the disadvantage of being highly volatile. The mixed promoter system showed similar behaviour as that found in the cyclopentane promoted system. Due to the enhanced thermodynamic promotion, this system could operate at slightly elevated temperatures (approximately 1 K) compared to the cyclopentane promoted system.

## 7.7 Cited Literature

- S. Adisasmito, R. J. Frank III, E. D. Sloan Jr., *Hydrates of carbon-dioxide and methane mixtures*, J. Chem. Eng. Data 36, 1 (1991) 68-71.
- K. Althaus, Fortschritt-Berichte VDI 3 (1999), 350.
- R. Anderson, A. Chapoy, B. Tohidi, *Phase Relations and Binary Clathrate Hydrate Formation in the System H<sub>2</sub> – THF – H<sub>2</sub>O*, Langmuir, 23 (2007), 3440-3444.
- A. Bamberger, G. Sieder, G. Maurer, *High-pressure (vapor + liquid) equilibrium in binary mixtures of (carbon dioxide + water or acetic acid) at temperatures from 313 to 353 K*, Journal of Supercritical Fluids, 17 (2000), 97-110.
- V. Belandria, A. Eslamimanesh, A. H. Mohammadi, D. Richon, *Gas Hydrate Formation in Carbon Dioxide + Nitrogen + Water System: Compositional Analysis of Equilibrium Phases*, Ind. Eng. Chem. Res., 50 (2011), 4722-4730.

I. Ben Attouche Sfaxi, V. Belandria, A. H. Mohammadi, R. Lugo, D. Richon, *Phase equilibria of CO<sub>2</sub> + N<sub>2</sub> and CO<sub>2</sub> + CH<sub>4</sub> clathrate hydrates: Experimental measurements and thermodynamic modelling*, Chem. Eng. Sci., 84 (2012), 602-611.

H. Bruusgaard, J. G. Beltrán, P. Servio, *Vapor-Liquid Water-Hydrate Equilibrium Data for the System N<sub>2</sub> + CO<sub>2</sub> + H<sub>2</sub>O*, J. Chem. Eng. Data, 53 (2008), 2594-2597.

A. Chapoy, A. H. Mohammadi, B. Tohidi, D. Richon, *Gas Solubility Measurement and Modeling for the Nitrogen + Water System from 274.18 K to 363.02 K*, J. Chem. Eng. Data, 49 (2004), 1110-1115.

A. Chapoy, H. Haghighi, B. Tohidi, *Development of a Henry's constant correlation and solubility measurements of n-pentane, i-pentane, cyclopentane, n-hexane and toluene in water*, J. Chem. Thermodynamics, 40 (2008), 1030-1037.

A. Delahaye, L. Fournaison, S. Marinhas, I. Chatti, J.-P. Petitet, D. Dalmazzone, W. Fürst, *Effect of THF on Equilibrium Pressure and Dissociation Enthalpy of CO<sub>2</sub> Hydrates Applied to Secondary Refrigeration*, Ind. Eng. Chem. Res., 45 (2006), 391-397.

DIPPR, Design Institute for Physical Property Data (DIPPR 801). Diadem Pro.

J. Du, D. Liang, D. Li, X. Li, *Experimental Determination of the Equilibrium Conditions of Binary Gas Hydrates of Cyclopentane + Oxygen, Cyclopentane + Nitrogen, and Cyclopentane + Hydrogen*, Ind. Eng. Chem. Res., 49 (2010), 11797-11800.

B. A. Énglin, A. F. Platé, V. M. Tugolukov, M. A. Pryanishnikova, *Service Properties of Fuels and Oils. Solubility of Water in Individual Hydrocarbons*, Khimiya i tekhnologiya Topliv i Masel, 9 (1965), 42-46.

S.-S. Fan, T.-M. Guo, *Hydrate Formation of CO<sub>2</sub>-Rich Binary and Quaternary Gas Mixtures in Aqueous Sodium Chloride Solutions*, J. Chem. Eng. Data, 44 (1999), 829-832.

S. S. Fan, D. Q. Liang, K. H. Guo, *Hydrate Equilibrium Conditions for Cyclopentane and a Quaternary Cyclopentane-Rich Mixture*, J. Chem. Eng. Data, 46 (2001), 930-932.

M. N. Garcia-Lisbona, A. Galindo, G. Jackson, A. N. Burgess, *Predicting the high-pressure phase equilibria of binary aqueous solutions of 1-butanol, n-butoxyethanol and n-decylpentaoxyethylene ether (C<sub>10</sub>E<sub>5</sub>) using the SAFT-HS approach*, Molecular Physics, 93,1 (1998), 57-71.



- F. Gibanel, M. C. López, F. M. Royo, J. Santafé, J. S. Urieta, *Solubility of Nonpolar Gases in Tetrahydrofuran at 0 to 30°C and 101.33 kPa Partial Pressure of Gas*, J. of Solution Chemistry, 22,3 (1993), 221-217.
- P. C. Gillespie, G. M. Wilson, GPA Research Report RR-48.
- W. L., Goffe, G. D., Ferrier, J., Rogers, *Global Optimization of Statistical Functions with Simulated Annealing*, Journal of Econometrics, 60, 1/2 (1994), 65–99.
- J. B. Goodman, N. W. Krase, *Solubility of Nitrogen in Water at High Pressures and Temperatures*, Ind. Eng. Chem., 23,4 (1931), 401-404.
- F. R. Groves Jr., *Solubility of Cycloparaffins in Distilled Water and Salt Water*, J. Chem. Eng. Data, 33 (1988), 136-138.
- J.-M. Herri, A. Bouchemoua, M. Kwaterski, A. Fezoua, Y. Ouabbas, A. Cameirao, *Gas hydrate equilibria for CO<sub>2</sub>-N<sub>2</sub> and CO<sub>2</sub>-CH<sub>4</sub> gas mixtures – Experimental studies and thermodynamic modelling*, Fluid Phase Equilibria, 301 (2011), 171-190.
- J. Im, W. Bae, J. Lee, H. Kim, *Vapor-Liquid Equilibria of the Binary Carbon Dioxide-Tetrahydrofuran Mixture System*, J. Chem. Eng. Data, 49 (2004), 35-37.
- J. Jhaveri, D. B. Robinson, *Hydrates in the Methane-Nitrogen System*, Can. J. Chem. Eng., 43, 2 (1965), 75-78.
- S.-P. Kang, H. Lee, C.-S. Lee, W.-M. Sung, *Hydrate phase equilibria of the guest mixtures containing CO<sub>2</sub>, N<sub>2</sub> and tetrahydrofuran*, Fluid Phase Equilibria, 185 (2001), 101-109.
- S. H. Kim, M. D. Seo, J. W. Kang, C. S. Lee, *Hydrate-containing phase equilibria for mixed guests of carbon dioxide and nitrogen*, Fluid Phase Equilibria, 306 (2011), 229-233.
- Z. Knez, M. Skerget, L. Ilic, C. Lütge, *Vapor-liquid equilibrium of binary CO<sub>2</sub>-organic solvent systems (ethanol, tetrahydrofuran, ortho-xylene, meta-xylene, para-xylene)*, J. of Supercritical Fluids, 43 (2008), 383-389.
- D. Kodama, T. Yagihashi, T. Hosoya, M. Kato, *High pressure vapor-liquid equilibria for carbon dioxide-tetrahydrofuran mixtures*, Fluid Phase Equilibria, 297 (2010), 168-171.
- I. R. Krichevsky, J. S. Kasarnovsky, *Thermodynamical Calculations of Solubilities of Nitrogen and Hydrogen in Water at High Pressures*, J. Am. Chem. Soc., 57 (1935), 2168-2171.

S. D. Larson, Phase studies of the two-component carbon dioxide-water system, involving the carbon dioxide hydrate, University of Illinois, Urbana, IL (1955).

M. J. Lazzaroni, D. Bush, R. Jones, J. P. Hallett, C. L. Liotta, C. A. Eckert, *High-pressure phase equilibria of some carbon dioxide-organic-water systems*, Fluid Phase Equilibria, 224 (2004), 143-154.

P. Linga, R. Kumar, P. Englezos, *Gas hydrate formation from hydrogen/carbon dioxide and nitrogen/carbon dioxide gas mixtures*, Chem. Eng. Sci., 62 (2007a), 4268-4276.

P. Linga, A. Adeyemo, P. Englezos, *Medium-Pressure Clathrate Hydrate/Membrane Hybrid Process for Postcombustion Capture of Carbon Dioxide*, Environ. Sci. Technol., 42 (2007c), 315-320.

T. Makino, T. Sugahara, K. Ohgaki, *Stability Boundaries of Tetrahydrofuran + Water System*, J. Chem. Eng. Data, 50 (2005), 2058-2060.

P. Marathe, S. I. Sandler, *High-Pressure Vapor-Liquid Equilibrium of some Binary Mixtures of Cyclopentane, Argon, Nitrogen, n-Butane and Neopentane*, J. Chem. Eng. Data, 36 (1991), 192-197.

D. R. Marshall, S. Saito, R. Kobayashi, *Hydrates at high pressures 2. Application of statistical mechanics to the study of the hydrates of methane, argon and nitrogen*, AIChE J. 10 (1964) 202-205.

J., Matous, J. P., Novak, J., Sobr, J., Pick, *Phase equilibria in the system tetrahydrofuran(1)-water(2)*, Collection Szechoslov. Chem. Commun., 37 (1972), 2653-2663.

H., Matsuda, N., Kamihama, K., Kurihara, K., Tochigi, K., Yokoyama, *Measurement of Isobaric Vapor-Liquid Equilibria for Binary Systems Containing Tetrahydrofuran Using and Automatic Apparatus*, Journal of Chemical Engineering of Japan, 41, 3 (2011), 131-139.

A. H. Mohammadi, D. Richon, *Phase equilibria of clathrate hydrates of methyl cyclopentane, methyl cyclohexane, cyclopentane or cyclohexane + carbon dioxide*, Chem. Eng. Sci., 64 (2009), 5319-5322.

A. H. Mohammadi, J. F. Martinez-López, D. Richon, *Determining phase diagrams of tetrahydrofuran+methane, carbon dioxide or nitrogen clathrate hydrates using an artificial neural network algorithm*, Chem. Eng. Sci., 65 (2010), 6059-6063.

- A. H. Mohammadi, D. Richon, *Phase equilibria of binary clathrate hydrates of nitrogen + cyclopentane/cyclohexane/methyl cyclohexane and ethane + cyclopentane/cyclohexane/methyl cyclohexane*, Chem. Eng. Sci., 66 (2011), 4936-4940.
- H.-J. Ng, D. B. Robinson, *Hydrate formation in systems containing methane, ethane, propane, carbon-dioxide or hydrogen-sulfide in the presence of methanol*, Fluid Phase Equilibria, 21, 1-2 (1985), 145-155.
- M. B. Olsen, A. Majumdar, P. R. Bishnoi, *Experimental Studies on Hydrate Equilibrium – Carbon Dioxide and its Systems*, Int. J. of The Soc. Of Mat. Eng. For Resources, 7, 1 (1999), 17-23.
- L. C. Price, *Aqueous Solubility of Petroleum as Applied to its Origin and Primary Migration*, The American Association of Petroleum Geologists Bulletin, 60, 2 (1976), 213-244.
- N., Riesco, J. P. M., Trusler, *Novel optical flow cell for measurements of fluid phase behaviour*, Fluid Phase Equilibria, 228-229 (2005), 233–238.
- M. Rigby, J. M. Prausnitz, *Solubility of Water in Compressed Nitrogen, Argon and Methane*, J. Phys. Chem., 72,1 (1968), 330-334.
- L. Ruffine, J. P. M. Trusler, *Phase Behaviour of mixed-gas hydrate systems containing carbon dioxide*, J. Chem. Thermodynamics, 42 (2010), 605-611.
- K. M. Sabil, G.-J. Witkamp, C. J. Peters, *Estimations of enthalpies of dissociation of simple and mixed carbon dioxide hydrates from phase equilibrium data*, Fluid Phase Equilibria, 290 (2010a), 109-114.
- K. M. Sabil, G.-J. Witkamp, C. J. Peters, *Phase equilibria in ternary (carbon dioxide + tetrahydrofuran + water) system in hydrate-forming region: Effects of carbon dioxide concentration and the occurrence of pseudo-retrograde hydrate phenomenon*, J. Chem. Thermodynamics 42 (2010b) 8-16.
- K. M. Sabil, G.-J. Witkamp, C. J. Peters, *Measurement and Modeling of Bubble and Dew Points of the Carbon Dioxide + Tetrahydrofuran + Water System*, J. Chem. Eng. Data 55 (2010c) 813-818.
- Y.-T. Seo, S.-P. Kang, H. Lee, *Experimental determination and thermodynamic modeling of methane and nitrogen hydrates in the presence of THF, propylene oxide, 1,4-Dioxane*, Fluid Phase Equilibria, 189 (2001), 99-110.

Y. Seo, S.-P. Kang, S. Lee, H. Lee, *Experimental Measurements of Hydrate Phase Equilibria for Carbon Dioxide in the Presence of THF, Propylene Oxide, and 1,4-Dioxane*, J. Chem. Eng. Data, 53 (2008), 2833-2837.

N. N. Shah, J. A. Zollweg, W. B. Streett, *Vapor-Liquid Equilibrium in the System Carbon Dioxide + Cyclopentane from 275 to 293 K at Pressures to 12.2 MPa*, J. Chem. Eng. Data, 36 (1991), 189-192.

V. A., Shnitko, V. B., Kogan, *Liquid-Vapor equilibrium in the system tetrahydrofuran-water and tetrahydrofuran-ethylene glycol, and a method for dehydration of tetrahydrofuran*, Journal of Applied Chemistry of the USSR (Zhurnal Prikladnoi Khimii), 41, 6 (1968), 1235-1242.

R., Signer, H., Arm, H., Daeniker, *Dampfdrücke, Dichten, Thermodynamische Mischungsfunktionen und Brechungsindices der binären systeme Wasser-Tetrahydrofuran und Wasser-Kiäthyläther bei 25°*, Helvetica Chimica Acta, 52, 8 (1969), 2347-2351.

SIMANN.F, <http://www.netlib.no/netlib/opt/simann.f> (Acquired July 2012).

S. Takenouchi, G. C. Kennedy, *Dissociation pressures of phase CO<sub>2</sub>.5 3/4H<sub>2</sub>O*, The Journal of Geology, 73, 2 (1965), 383-390.

F. Takeuchi, R. Ohmura, K. Yasuoka, *Statistical-Thermodynamics Modeling of Clathrate-Hydrate-Forming Systems Suitable as Working Media of a Hydrate-Based Refrigeration System*, Int. J. Thermophys, 30 (2009), 1838-1852.

B. Tohidi, A. Danesh, A. C. Todd, R. W. Burgass, K. K. Østergaard, *Equilibrium data and thermodynamic modeling of cyclopentane and neopentane hydrates*, Fluid Phase Equilibria, 138 (1997), 241-250.

C., Treiner, *Solvation Ionique dans les mélanges de solvant a partir de mesures de tension de vapeur en solutions électrolytiques. II. Enthalpies libres de transfert de NaCl entre l'eau et des mélanges eau-tétrahydrofurane a 25°C*, Journal de Chimie Physique, 70, 9 (1973), 1183-1187.

A. T. Trueba, L. J. Rovetto, L. J. Florusse, M. C. Kroon, C. J. Peters, *Phase equilibrium measurements of structure II clathrate hydrates of hydrogen with various promoters*, Fluid Phase Equilibria, 307 (2011), 6-10.

I. Tsivintzelis, G. M. Kontogeorgis, M. L. Michelsen, E. H. Stenby, *Modeling phase equilibria for acid gas mixtures using the CPA equation of state. Part II: Binary mixtures with CO<sub>2</sub>*, Fluid Phase Equilibria 306 (2011) 38-56.

- A. Valtz, A. Chapoy, C. Coquelet, P. Paricaud, D. Richon, *Vapour-liquid equilibria in the carbon dioxide-water system, measurement and modeling from 278.2 to 318.2 K*, Fluid Phase Equilibria, 226 (2004), 333-344.
- A. van Cleeff, G. A. M. Diepen, *Gas Hydrates of Nitrogen and Oxygen*, Recueil des travaux chimiques des Pays-Bas, 79, 5 (1960) 582-586.
- A. Wallbruch, G. M. Schneider, *(Liquid + liquid) phase equilibria at high pressures. Pressure-limited closed-loop behaviour of  $\{x\text{-}(\text{CH}_2)_4\text{O} + (1-x)\text{H}_2\text{O}\}$  and the effect of dissolved ammonium sulfate*, J. Chem. Thermodynamics, 27 (1995), 377-382.
- R. Wiebe, V. L. Gaddy, *The Solubility of Carbon Dioxide in Water at Various Temperatures from 12 to 40° and at Pressures to 500 Atmospheres. Critical Phenomona.*, J. of the American Chemical Society 62 (1940) 815-817.
- H. Yang, S. Fan, X. Lang, Y. Wang, *Phase Equilibria of Mixed Gas Hydrates of Oxygen + Tetrahydrofuran, Nitrogen + Tetrahydrofuran, and Air + Tetrahydrofuran*, J. Chem. Eng. Data, 56 (2011), 4152-4156.
- J. S. Zhang, J. W. Lee, *Equilibrium of Hydrogen + Cyclopentane and Carbon Dioxide + Cyclopentane Binary Hydrates*, J. Chem. Eng. Data, 54 (2009), 659-661.



## 8 Conclusion and Perspectives

A novel gas separation technique based on gas hydrate formation (solid precipitation) was investigated by means of thermodynamic modeling and experimental investigations. Important parameters in this process are the hydrate formation conditions (temperature and pressure). Moreover, the selectivity towards carbon dioxide in the hydrate phase was investigated.

A literature study was conducted focusing mainly on thermodynamic gas hydrate promotion by hydrate formers stabilising the classical gas clathrate hydrate structures (sI, sII and sH). Much literature is available on this subject. Most of this literature presents experimental determinations of hydrate thermodynamics and kinetics, however a few studies have also investigated the promoting mechanisms by means of molecular simulation.

It has been found that the sII and sH hydrate structures incorporating both large hydrate formers (such as e.g. tetrahydrofuran, cyclopentane, cyclohexane, methyl-cyclohexane etc.) and small hydrate formers (e.g. methane, nitrogen, carbon dioxide etc.) generally stabilise at temperature and pressure conditions that are milder (lower pressures and/or higher temperatures) than the sI hydrate.

Similarly, by comparing sII and sH hydrates incorporating the same gas species (e.g. methane), but being stabilised (promoted) by different hydrate formers (e.g. cyclopentane (sII) and methyl-cyclohexane (sH)), it has been found that the sII hydrate structure generally forms at milder conditions than the sH structure.

While the sII hydrate has the advantage of being stabilised at milder conditions than the sH hydrate, the sII structure has the disadvantage of lower gas capacity. From a gas capacity point of view the sH hydrate structure is the better choice, since the promoter occupies fewer of the hydrate cavities, leaving more empty cavities for the gas components. Hence, the choice of promoter must always be made according to specific needs and/or desires (pressure reduction or gas capacity).

Both experimental and theoretical studies presented in the literature have pointed out cyclopentane and tetrahydrofuran as the two most efficient pressure reducing additives in classical hydrate forming systems, where the gas phase component of interest readily stabilises the small cavities of the hydrate structure. Other components with slightly lower promoting effects are acetone, propane (gas phase additive at ambient conditions) or a range of quaternary ammonium salts (tetra-n-butyl ammonium halides such as e.g. TBAB, TBACl and TBAF) which form semi-clathrate hydrates.

In some experimental studies the promoting effects of tetrahydrofuran, cyclopentane and TBAB have been compared in their pressure reducing effects

for hydrate formation with small gas phase components. It has been shown that TBAB offers the lowest hydrate equilibrium pressures at moderate temperatures (typically below 285 K to 286 K), however the hydrate equilibrium pressures in these system increase significantly with temperature. At temperatures above 286 K, tetrahydrofuran and cyclopentane provide more stable hydrates.

The thermodynamic promoting effects reported in the literature for the two classical sII hydrate formers, tetrahydrofuran and cyclopentane have been experimentally confirmed in the present work.

Low temperature data have been measured for the mixed hydrates of tetrahydrofuran and carbon dioxide formed in 5 mole percent aqueous solutions of tetrahydrofuran. The presented data compared well with the few other data available in the literature in this temperature and composition range.

An attempt was made to measure four-phase hydrate-liquid water-liquid organic-vapour equilibria at low temperatures for the ternary system of water-cyclopentane-carbon dioxide. It was suspected that this system reduces to three phases (hydrate-liquid water-vapour) at low temperature and low pressures. The suspected three-phase hydrate-liquid water-vapour equilibrium pressures were shown to decrease little with decreasing temperature from approximately 284 K down to 275 K.

In two separate studies, it was shown that the addition of tetrahydrofuran to the ternary system of water-cyclopentane-carbon dioxide provided an enhanced thermodynamic promotion of the gas hydrate phase. Hydrate equilibrium pressures were reduced by approximately 20 percent compared to the pure cyclopentane promoted system. Since cyclopentane prior to this study was considered a reference in terms of its pressure reducing abilities, the proposed system of mixed promoters represents a new state-of-the-art within thermodynamic promotion of gas hydrates in the framework of the classical hydrate structures. Though not shown in the present work, studies investigating the kinetics of the mixed promoter system have shown that this system of mixed promoters provides the short induction times of the tetrahydrofuran promoted system and furthermore the fast crystal growth rates of the cyclopentane promoted system. This makes the mixed promoter hydrate system interesting from a gas capture process point of view.

A thermodynamic model based on the Cubic-Plus-Association equation of state and the van der Waals-Platteeuw hydrate model was implemented as a computer-based simulation tool. This model enabled the performance of a thermodynamic evaluation of gas hydrate forming systems relevant for post-combustion carbon dioxide capture.

A modeling study of both fluid phase behaviour and hydrate phase behaviour was presented. Five components were studied, water, tetrahydrofuran,



cyclopentane, carbon dioxide and nitrogen. Of the 10 possible binary pairs formed by this five-component system, 9 pairs were studied for their fluid phase behaviour. CPA descriptions were improved when needed by correlation of binary parameters in the applied mixing- and combining rules. A maximum of three adjustable parameters were applied for binary pairs involving induced cross-association (solvation) and a maximum of two adjustable parameters were applied for pairs without cross-association. CPA predicted the fluid phase behaviour with sufficient accuracy for three of the nine binary pairs (none of them involved self- or cross-association). All binary pairs involving water needed some form of binary correction to provide satisfactory results over extended ranges of temperature and pressure.

In this work, CPA has proven its qualities as an advanced equation of state both in systems involving hydrogen bonding, resulting in complex fluid phase behaviour, and in systems where CPA could be simplified to the SRK equation of state while still providing satisfactory results.

The binary system of water and tetrahydrofuran represented a challenge from a fluid phase modeling point of view, as this system shows both azeotropic vapour-liquid equilibrium (VLE) at ambient conditions and closed-loop miscibility gaps at elevated temperatures and pressures. Accurate modeling of this system was found to be important when later extending the model to include other components such as e.g. carbon dioxide. Whereas CPA, from a qualitative point of view, predicted the correct fluid phase behaviour in this ternary system, the phase composition of the aqueous phase in particular was described with significant deviations compared to available experimental data. The inaccuracy of the fluid phase description propagated into the later hydrate modeling results, where the predicted hydrate phase boundary in the hydrate(H)-aqueous liquid(L<sub>w</sub>)-organic liquid(L<sub>a</sub>)-vapour four-phase region was found to deviate by 1-2 K compared to available experimental data.

Cycloalkanes ranging from cyclopropane to cyclohexane, represented a challenge for CPA, both for the description of the pure component densities and for liquid-liquid equilibrium (LLE) in the binary systems with water. It was concluded that an insufficient amount of reliable LLE data exist for the binary system of water and cyclopentane. Additional water-in-oil data in particular are desired for this system.

With CPA forming a solid framework for the fluid phase description of this system of five components, the van der Waals Platteeuw hydrate model was applied to enable calculations of incipient gas hydrate formation conditions. The application of an algorithm, supplying fluid phase compositions, fugacities of hydrate formers and water activity coefficients to the hydrate model (all obtained from a multi-phase isothermal/isobaric flash calculation) ensured a consistent

calculation procedure, which was applicable in all hydrate forming systems formed by the five compounds above the freezing point of water.

Gas hydrate formation was successfully modeled in the four subsystems forming pure hydrates with water; the pure sI hydrate of carbon dioxide, the sII hydrate of nitrogen, the sII hydrate of tetrahydrofuran and the sII hydrate of cyclopentane. Furthermore, five binary hydrates were modeled: the sI/sII hydrates of carbon dioxide and nitrogen, the sII hydrates of carbon dioxide and tetrahydrofuran, the sII hydrate of carbon dioxide and cyclopentane, the sII hydrate of nitrogen and tetrahydrofuran and finally the sII hydrate of nitrogen and cyclopentane. Three systems with three hydrate formers were studied; the sII hydrates formed by tetrahydrofuran, carbon dioxide and nitrogen, the sII hydrates formed by cyclopentane, carbon dioxide and nitrogen and finally the mixed promoter system forming sII hydrates with tetrahydrofuran, cyclopentane and carbon dioxide. The complete system of five components was finally investigated for hydrate formation. sII hydrates were predicted to form, however no actual results were presented since this system behaved very similar to the quaternary system of water, cyclopentane, carbon dioxide and nitrogen, only at slightly elevated temperatures (more stable hydrate). Generally, the model predicted the right hydrate structures in all possible combinations of hydrate formers. An interesting observation was that the model predicted the synergistic effect occurring in hydrate forming systems with simultaneous presence of tetrahydrofuran and cyclopentane.

The developed model has been applied to simulate three simplified processes for post-combustion carbon dioxide capture from power station flue gases. All three processes applied hydrate formation to selectively remove carbon dioxide from the flue gas.

The first process, an unpromoted hydrate process, operated isothermally at a temperature of 280 K. The flue gas feed into the first stage of the process was comprised of 10 mole percent carbon dioxide and 90 mole percent nitrogen. In the hydrate forming vessel, pure water and pressurised flue gas was mixed at a 50/50 molar feed ratio. The hydrate forming stage was assumed to operate isobarically at the incipient hydrate equilibrium pressure of the inlet gas. The pressure requirement of the first stage was estimated to be 24.9 MPa. The captured gas contained 36 mole percent carbon dioxide suggesting the need for a multi-stage capture design. After three consecutive hydrate formation/dissociation stages (three-stage capture process), a carbon dioxide-rich product (97 mole percent) could be delivered at a temperature of 280 K and a pressure of 3.65 MPa. It was concluded that this process was not economically feasible due to the high pressure requirement of the first capture stage.

The second carbon dioxide capture process used tetrahydrofuran as thermodynamic promoter to reduce the pressure requirements in all stages. A 5 mole percent aqueous solution of tetrahydrofuran was circulated in the second process. By doing so the pressure requirement of the first stage (still operating at 280 K) could be lowered to 0.41 MPa. Selectivity towards carbon dioxide in the hydrate phase was however lower than in the unpromoted process. Therefore the tetrahydrofuran promoted capture process needed four consecutive hydrate formation/dissociation stages to produce a 96 mole percent carbon dioxide-rich product stream. This stream was delivered at 280 K and a pressure of 0.17 MPa.

The third capture process used cyclopentane as thermodynamic promoter. In this system, 5 mole percent (fraction of liquid feed) cyclopentane bulk liquid was added to the pure water system. By doing so the pressure requirement of the first stage (operating at 285 K) could be lowered to 1.04 MPa. Selectivity towards carbon dioxide in the hydrate phase was similar to the tetrahydrofuran process. Therefore, this process also needed four consecutive hydrate formation/dissociation stages to produce a 95 mole percent carbon dioxide-rich product stream. The product stream was delivered at 285 K and a pressure of 0.51 MPa.

The cyclopentane promoted process operated at slightly elevated temperatures and pressures compared to the tetrahydrofuran promoted process. This was due to the high volatility of cyclopentane in the bulk organic liquid phase. The vapour phases in the cyclopentane promoted process contained several mole percent cyclopentane at hydrate equilibrium conditions. At temperatures below 284 K, the entire cyclopentane bulk phase would evaporate completely at hydrate forming conditions. For comparison, the vapour phase promoter content in the tetrahydrofuran promoted process was only 0.4 mole percent.

Despite the fact that the mixed promoter system provided enhanced pressure reduction and favourable kinetics, this system still showed significant promoter slip (cyclopentane mainly) to the vapour phase.

This work has developed a powerful tool for the thermodynamic evaluation of gas hydrate forming systems relevant for post-combustion carbon dioxide capture. All model details and complete lists of model parameters have been provided, enabling full reproduction of the presented results.

The results obtained when applying the model are discouraging for the post-combustion carbon dioxide capture process under development. Classical gas hydrates generally form at high pressures and/or low temperatures. These are opposite conditions of those found in power station flue gases. Known hydrate promoters such as cyclopentane and tetrahydrofuran enable hydrate formation at conditions close to ambient pressure and temperatures above the normal ice-point of water. The present study has however pointed out several drawbacks of using

these additives, when applied in low-pressure processes. Due to their high volatilities, they readily transfer to the vapour phase. Furthermore, they lower the selectivity towards carbon dioxide in the hydrate phase compared to the unpromoted system.

Thus, hydrate formation as a means of performing gas phase separation is an interesting alternative to existing separation techniques. With the currently known thermodynamic promoters, this separation can be performed at pressure conditions making the overall separation more economical. In systems supplying the initial gas phase at moderate to high pressure, this technology may prove itself an interesting alternative. With the new mixed promoter system presented in this work, it is possible to lower pressures even further compared to previously known systems. However, the present study has shown this concept to be unsuitable for the specific case of post-combustion carbon dioxide capture from power station flue gases, where pressures should preferably remain close to atmospheric.

It is not in the nature of species such as carbon dioxide and nitrogen to form the classical gas hydrates at conditions close to atmospheric pressure. Therefore, even though these hydrate structures become available at low pressure conditions, carbon dioxide may not necessarily enter the solid phase in significant amounts. It is thermodynamically more favourable for this component to remain in the co-existing fluid phases.

*You can lead a horse to water, but you can't make it drink.*

## 9 List of Symbols and Abbreviations

### Abbreviations

3M1B	3-methyl-1-butanol
AAD	Average Absolute Deviation (defined in equation (7.1))
BIP	Binary Interaction Parameter
CB	Cyclobutanone
CCS	Carbon Capture and Sequestration
CERE	Center for Energy Resources Engineering
CF <sub>4</sub>	Tetrafluoromethane
CHF <sub>3</sub>	Fluoroform
CP	Cyclopentane
CPA	Cubic-Plus-Association
DIPPR	Design Institute for Physical Property Data
DSC	Differential Scanning Calorimeter (Calorimetry)
DXN	1,4-dioxane
EO	Ethyleneoxide
EOS	Equation of State
H-L <sub>w</sub>	Hydrate-Liquid water
H-L-V	Hydrate-Liquid (water)-Vapour
H-L <sub>w</sub> -V	Hydrate-Liquid water-Vapour
H-L <sub>w</sub> -L <sub>v</sub>	Hydrate-Liquid water-Liquid vapour
H-L <sub>w</sub> -L <sub>a</sub> -V	Hydrate-Aqueous liquid-Organic liquid-Vapour
IEA	International Energy Agency
LLE	Liquid Liquid Equilibrium
L <sub>w</sub> -V	Liquid water-Vapour
L <sub>w</sub> -L <sub>a</sub> -V	Aqueous liquid-Organic liquid-Vapour
MCH	Methylcyclohexane
MEA	Monoethanolamine
NMR	Nuclear Magnetic Resonance
PPM	Parts per million
PVCap	Poly-N-vinylcaprolactam
SAFT	Statistical Associating Fluid Theory
SDS	Sodium dodecyl Sulfate
sI	Structure I hydrate
sII	Structure II hydrate
sH	Structure H hydrate
SERS	Surface Enhanced Raman Spectroscopy
SPIN	Sciences des Processus Industriels et Naturels
SRK	Soave-Redlick-Kwong (equation of state)
t-BUNH <sub>2</sub>	Tert-butylamine
TBAB	Tetra-n-butyl-ammonium bromide
THF	Tetrahydrofuran

THP	Tetrahydropyran
TMO	Tri-methyleneoxide
VLE	Vapour Liquid Equilibrium
VLLE	Vapour Liquid Liquid Equilibrium

## CPA Related Symbols

### Normal Characters

$A_i$	Association site type “A” on component $i$ [unit less]
$a_{kij}$	Constant in temperature expression for $k_{ij}$ [unit less]
$a_0$	CPA pure component parameter [ $\text{Pa} \cdot \text{m}^6 \cdot \text{mol}^{-2}$ ]
$B_j$	Association site type “B” on component $j$ [unit less]
$b$	CPA co-volume parameter [ $\text{m}^3 \cdot \text{mol}^{-1}$ ]
$b_{kij}$	Constant in temperature expression for $k_{ij}$ [Kelvin]
$c_l$	CPA pure component parameter [unit less]
$g$	Hard sphere radial distribution function [unit less]
$k_{ij}$	Binary interaction parameter [unit less]
$P$	Pressure [Pa]
$T$	Temperature [Kelvin]
$R$	Gas constant [ $\text{m}^3 \cdot \text{Pa} \cdot \text{mole}^{-1} \cdot \text{K}^{-1}$ ]
$V$	Volume [ $\text{m}^3$ ]
$x$	Liquid phase mole fraction [unit less]
$X_{Ai}$	Fraction of non-bonded association sites of type “A” on component $i$ [unit less]
$y$	Vapour phase mole fraction [unit less]

### Greek letters

$\alpha(T)$	CPA temperature dependent attractive parameter [ $\text{Pa} \cdot \text{m}^6 \cdot \text{mol}^{-2}$ ]
$\beta^{AiBj}$	CPA association volume [unit less]
$\gamma^{AiBj}$	CPA binary adjustable in combining rule for $\beta^{AiBj}$ [unit less]
$\Delta^{AiBj}$	CPA association strength []
$\varepsilon^{AiBj}$	CPA association energy [ $\text{Pa} \cdot \text{m}^3 \cdot \text{mol}^{-1}$ ]
$\omega$	Acentric factor [unit less]

### Subscripts

$i$	Component $i$ [unit less]
$j$	Component $j$ [unit less]

## Van der Waals-Platteeuw Hydrate Model Related Symbols

### Normal Characters

$a_j$	Spherical core radius of component $j$ in the Kihara cell potential [m]
-------	---

$A_{m,j}$	A parameter for calculation of Langmuir constant of specie $j$ in cavity $m$ [Pa <sup>-1</sup> ·K]
$B_{m,j}$	B parameter for calculation of Langmuir constant of specie $j$ in cavity $m$ [K]
$C_{m,j}$	Langmuir Constant component $j$ in cavity type $m$ [Pa <sup>-1</sup> ]
$\Delta C_p(T)$	Reference heat capacity difference between the meta-stable empty hydrate phase and liquid water at temperature $T$ [J·mole <sup>-1</sup> ]
$f_j$	Fugacity of component $j$ [Pa]
$\Delta H(T_0, P_0)_w^{\beta/Ice}$	Reference hydrate enthalpy difference between water in the meta-stable empty hydrate phase and water in ice at reference temperature and pressure conditions [J·mole <sup>-1</sup> ]
$\Delta H(T)_w^{Ice/L_w}$	Enthalpy difference between water in ice and Liquid water at temperature, $T$ [J·mole <sup>-1</sup> ]
$\Delta H(T_0, P_0)_w^{Ice/L_w}$	Reference enthalpy difference between water in ice and Liquid water at reference temperature and pressure conditions [J·mole <sup>-1</sup> ]
$k_B$	The Boltzmann constant [J·K <sup>-1</sup> ]
$P$	Pressure [Pa]
$P_0$	Pressure at reference condition [Pa]
$P_R$	Pressure of reference hydrate [Pa]
$r$	Linear distance [m]
$R$	Universal gas constant [m <sup>3</sup> ·Pa·mole <sup>-1</sup> ·K <sup>-1</sup> ]
$R_m$	Radius of cavity type $m$ [m]
$T$	Temperature [K]
$T_0$	Temperature at reference condition [K]
$\Delta V_w^{\beta/Ice}$	Molar volume difference between empty hydrate structure and ice [m <sup>3</sup> ·mole <sup>-1</sup> ]
$\Delta V_w^{Ice/L_w}$	Molar volume difference between ice and liquid water [m <sup>3</sup> ·mole <sup>-1</sup> ]
$w(r)_{m,j}$	Spherical core cell potential [J]
$x$	liquid phase mole fraction [unit less]
$y$	Vapour phase mole fraction [unit less]
$Y_j$	Water free hydrate composition of guest $j$ [unit less]
$z_m$	Coordination number of cavity type $m$ [unit less]

### Greek letters

$\alpha_w^{Lw}$	Activity of water in the liquid phase [unit less]
$\varepsilon_j$	Maximum attractive potential of specie $j$ in the Kihara cell potential [J]
$\varphi_j$	Fugacity coefficient of specie $j$ [unit less]
$\gamma$	Symmetric activity coefficient [unit less]

$v_m$	Number of cavities type $m$ , per water molecule in the hydrate unit cell [unit less]
$\mu$	Chemical potential [J·mole <sup>-1</sup> ]
$\mu_w^H$	Chemical potential of water in filled hydrate phase [J·mole <sup>-1</sup> ]
$\mu_w^{L_w}$	Chemical potential of water in Liquid phase [J·mole <sup>-1</sup> ]
$\mu_w^V$	Chemical potential of water in vapour phase [J·mole <sup>-1</sup> ]
$\mu_w^\beta$	Chemical potential of water in meta-stable hydrate phase [J·mole <sup>-1</sup> ]
$\mu_w^*$	Chemical potential of water in pure water phase at standard state [J·mole <sup>-1</sup> ]
$\Delta\mu_w^H$	Chemical potential difference between water in the meta-stable empty hydrate phase and the actual hydrate phase [J·mole <sup>-1</sup> ]
$\Delta\mu_w^{L_w}$	Chemical potential difference between water in the meta-stable empty hydrate phase and water in the co-existing liquid phase [J·mole <sup>-1</sup> ]
$\Delta\mu_w^{\beta/L_w}$	Reference hydrate chemical potential difference between water in the meta-stable empty hydrate phase and water in the co-existing liquid phase [J·mole <sup>-1</sup> ]
$\Delta\mu(T_0, P_0)_{L_w}^{L_w}$	Reference hydrate chemical potential difference between water in the meta-stable empty hydrate phase and liquid water at reference temperature and pressure conditions [J·mole <sup>-1</sup> ]
$\pi$	Pi [unit less]
$\sigma_j$	Cores distance at zero potential for specie $j$ in Kihara cell potential [m]
$\theta_{m,j}$	Fractional occupancy of component $j$ in cavity type $m$ [unit less]

## Subscripts

$j$	Component $j$ [unit less]
$m$	Cavity type $m$ [unit less]
$w$	Water [unit less]



## Appendix 1





# Phase equilibrium modeling of gas hydrate systems for CO<sub>2</sub> capture<sup>☆</sup>

Peter Jørgensen Herslund<sup>a</sup>, Kaj Thomsen<sup>a</sup>, Jens Abildskov<sup>b</sup>, Nicolas von Solms<sup>a,\*</sup>

<sup>a</sup> Centre for Energy Resources Engineering (CERE), Department of Chemical and Biochemical Engineering, Technical University of Denmark, Kgs. Lyngby DK2800, Denmark

<sup>b</sup> Computer Aided Process Engineering Center (CAPEC), Department of Chemical and Biochemical Engineering, Technical University of Denmark, Kgs. Lyngby DK2800, Denmark

## ARTICLE INFO

### Article history:

Available online 8 January 2012

### Keywords:

Gas hydrates  
Carbon dioxide  
Modeling  
van der Waals–Platteeuw  
CPA  
Thermodynamics  
CO<sub>2</sub> capture

## ABSTRACT

Two thermodynamic models capable of describing dissociation pressures of mixed gas clathrate hydrates formed from ternary mixtures of CO<sub>2</sub>, N<sub>2</sub> and liquid water, are presented. Both of the models utilize the Cubic-Plus-Association (CPA) equation of state (EOS) for the thermodynamic description of the non-solid phases (vapor and liquid). The solid hydrate phase is described by the van der Waals–Platteeuw model as presented by Parrish and Prausnitz. An algorithm for combining the CPA EOS with the van der Waals–Platteeuw model in a calculation of hydrate dissociation pressure is presented.

Two models are described in this work. They differ in their method for describing the Langmuir adsorption coefficients in the van der Waals–Platteeuw model. These models are named Model I and Model II. Model I utilizes a statistical thermodynamics approach based on Lennard-Jones–Devonshire theory, using the spherical core Kihara cell potential. Model II uses a two-parameter explicit expression for the Langmuir adsorption coefficient, based on Langmuir adsorption theory. With two hydrate formers, four parameters in the Kihara cell potentials are fitted for Model I. Sixteen parameters are required to be fitted for Model II. The two model parameter sets are fitted to pure hydrate dissociation pressures and mixed hydrate dissociation pressures found in literature. In the fitting process, vapor phases with initial mole fractions of CO<sub>2</sub> below 0.15 are assumed to form structure II hydrates, while structure I hydrates are assumed to form from vapor phases with initial mole fractions of CO<sub>2</sub> at or above 0.15.

The two models are validated against mixed hydrate equilibrium data found in literature. Both dissociation pressures and hydrate compositions are considered in the validation process.

With the fitted parameters, Model I predicts a hydrate structure transition from structure II hydrates at vapor phase mole fractions of CO<sub>2</sub> below 0.12 to 0.16 (depending on temperature) to structure I hydrates at mole fractions of CO<sub>2</sub> above this concentration range. The exact transition concentration is shown to increase with increasing temperature. Model II predicts structure I hydrates to be stable in concentrations down to vapor phase mole fractions of CO<sub>2</sub> in the order of 0.001 to 0.02, depending on temperature. Model II predicts the transition concentration to decrease with increasing temperature.

Since there is disparity amongst the different literature data for this system, it was not possible to determine unequivocally, which of the two models perform better.

© 2012 Published by Elsevier Ltd.

## 1. Introduction

In post-combustion CO<sub>2</sub> capture from power station flue gases, chemical absorption has been considered the most mature of the carbon capture technologies. There are however problems associated with it, the main ones being high capital costs and energy demanding solvent handling. Nevertheless this is still an active field of research. This work considers an alternative capture process, where CO<sub>2</sub> may be separated from flue gasses by gas clathrate hydrate formation.

### 1.1. Gas clathrate hydrates

Gas clathrate hydrates, hereafter named gas hydrates, are ice-like, solid inclusion bodies of hydrogen bonded water and small guest molecules. Hydrogen bonded water clusters may form cavities, where small guest molecules are encapsulated. The three most commonly occurring hydrate crystal structures are; structure I (sI), structure II (sII) and structure H (sH). The three structures are formed by a total of five different water cavities, the 5<sup>12</sup>, 5<sup>12</sup>6<sup>2</sup>, 5<sup>12</sup>6<sup>4</sup>, 5<sup>12</sup>6<sup>8</sup> and the 4<sup>3</sup>5<sup>6</sup>6<sup>3</sup> [1]. A schematic of these cavities may be found in figure 1.

The physical properties of the hydrate cavities and unit cells are provided in table 1.

In its pure form, the unit cell of the sI hydrate contains two small 5<sup>12</sup> and six large 5<sup>12</sup>6<sup>2</sup> cavities while a unit cell of the sII

<sup>☆</sup> Paper for gas hydrate initiative.

\* Corresponding author. Tel.: +45 4525 2867; fax: +45 4588 2258.

E-mail address: [nvs@kt.dtu.dk](mailto:nvs@kt.dtu.dk) (N. von Solms).

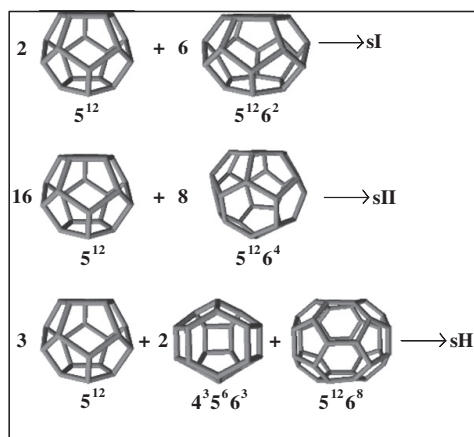


**FIGURE 1.** Water molecules forming cages corresponding to hydrate structures, sI, sII and sH.

hydrate contains sixteen small  $5^{12}$  and eight large  $5^{12}6^4$  cavities. Both of these unit cell lattice structures belong to the cubic type. The sH hydrate structure is more complex and contains three  $5^{12}$ , two  $4^35^66^3$  and one  $5^{12}6^8$  cavities [1]. This hydrate structure forms a hexagonal unit cell.

A given hydrate structure is typically determined by the size and shape of the guest molecule. Each cavity may encapsulate one or in rare cases more guest molecules of proper sizes. It is the presence of the guest molecule that stabilizes the crystalline water structure at temperatures well above the normal freezing point.

### 1.2. CO<sub>2</sub> capture process

In the capture process considered here, CO<sub>2</sub> is physically adsorbed in solid gas hydrate crystals, rather than chemically bonded to a solvent such as in the amine process. Since the two main constituents of power station flue gasses, N<sub>2</sub> and CO<sub>2</sub> are both known to form gas hydrates with water at low temperatures and high pressures, a mixed hydrate containing H<sub>2</sub>O, N<sub>2</sub> and CO<sub>2</sub> is expected to form. Pure CO<sub>2</sub> hydrates are known to form at lower pressures than pure N<sub>2</sub> hydrates, hence a selectivity towards CO<sub>2</sub> in the mixed hydrate is expected.

From a process point of view, this capture process resembles that of the chemical absorption. The flue gas is contacted with a liquid phase in which selective removal of CO<sub>2</sub> takes place. The main advantage of this process over the amine process is that the solid hydrate particles may readily be separated from the remaining liquid phase before the CO<sub>2</sub> is released by hydrate dissociation. Thus only the CO<sub>2</sub> rich phase needs to be treated in the CO<sub>2</sub> release process, which in turn results in lowered energy demands in the release unit operation.

**TABLE 1**  
Physical properties of cavities and unit cells of sI, sII and sH hydrates.

Structure	sI		sII		sH		
Cavity	$5^{12}$	$5^{12}6^2$	$5^{12}$	$5^{12}6^4$	$5^{12}$	$4^35^66^3$	$5^{12}6^8$
No. cavities per unit cell	2	6	16	8	3	2	1
Avg. cavity diameter · 10 <sup>10</sup> /m	7.95 <sup>a</sup>	8.60 <sup>a</sup>	7.82 <sup>a</sup>	9.46 <sup>a</sup>	7.82 <sup>b</sup>	8.12 <sup>b</sup>	11.4 <sup>b</sup>
Coordination number	20	24	20	28	20	20	36
No. water molecules per unit cell	46		136		34		

<sup>a</sup> Data from Parrish and Prausnitz [7].

<sup>b</sup> Data from Koh et al. [2].

The disadvantage of this process, when compared to the chemical absorption process, is that the flue gas must be compressed and cooled, in order for the hydrates to form. Since compression is an expensive unit operation, low pressure selective hydrate formation is needed, in order for this capture process to be competitive from an economic point of view.

### 1.3. Purpose of this work

In order to evaluate the energy efficiency of this process, accurate thermodynamic models are required over a wide range of temperatures and pressures. In this work a thermodynamic model, capable of predicting the phase equilibrium behavior of N<sub>2</sub>/CO<sub>2</sub> mixed hydrates, has been implemented and validated against experimental data found in literature. The parameter of main interest is the equilibrium pressure, at which the mixed hydrates form at a given temperature and flue gas composition. This pressure sets the minimum requirement for the flue gas compression stage in the capture process.

## 2. Model theory

The classical van der Waals and Platteeuw model [3] for the solid hydrate phase is combined with a state of the art equation of state – the Cubic-Plus-Association (CPA) EOS [4]. The van der Waals and Platteeuw model is utilized in the form presented by Parrish and Prausnitz [7]. Van der Waals and Platteeuw described the physical adsorption of guest molecules in the solid hydrate structure by an approach similar to that of Langmuir adsorption and utilized statistical mechanics to estimate Langmuir adsorption coefficients for the encapsulated gas molecules in the crystalline water structures. In the specific case of CO<sub>2</sub> capture by hydrate formation, CPA is utilized to describe the chemical equilibrium between the flue gas phase and the liquid water phase. This is done by performing a two-phase flash calculation. CPA accurately accounts for the presence of water as well as other components in the aqueous liquid phase, which may be hydrogen bonding. An accurate description of the activity of water in the liquid phase is of great importance, since this activity is a key parameter in the solid hydrate phase model.

### 2.1. The CPA equation of state

The CPA equation of state presented by Kontogeorgis et al. [4,6] combines the physical term from the cubic Soave–Redlich–Kwong (SRK) EOS with an association term similar to that found in the Statistical Associating Fluid Theory (SAFT) models. The pressure-explicit form of the CPA EOS may be expressed [5]:

$$P = \frac{R \cdot T}{V_m - b} - \frac{\alpha(T)}{V_m \cdot (V_m + b)} - \frac{R \cdot T}{2 \cdot V_m} \cdot \left[ 1 + \frac{1}{V_m} \cdot \frac{\partial \ln g}{\partial (1/V_m)} \right] \times \sum_i x_i \sum_{A_i} (1 - X_{A_i}) \quad (1)$$

where  $R$  is the gas constant and  $T$  is temperature;  $V_m$  denotes the molar volume,  $\alpha(T)$  is the temperature dependent SRK energy parameter and  $b$  is the SRK co-volume parameter. The  $g$  is the radial distribution function;  $A_i$  denotes association site  $A$  on component  $i$ ,  $x_i$  is the mole fraction of component  $i$ ,  $X_{Ai}$  is the fraction of sites, type  $A$  on component  $i$ , not bonded to other sites. Note that CPA simplifies to the SRK EOS for non-associating systems.

The fraction of non-bonded sites,  $X_{Ai}$ , is estimated by solving equations (2) and (3).

$$X_{Ai} = \left[ 1 + V_m^{-1} \cdot \sum_j x_j \sum_{B_j} X_{Bj} \cdot \Delta^{A_i B_j} \right]^{-1} \quad (2)$$

Equation (2) is evaluated for all site types on all associating components. The summation over  $B_j$  in equation (2) indicates summation over all association sites.

The  $\Delta^{A_i B_j}$  is the association strength between site  $A$  on molecule  $i$  and site  $B$  on molecule  $j$ . It may be estimated by

$$\Delta^{A_i B_j} = g(V_m)^{\text{ref}} \cdot [\exp(\epsilon_{CPA}^{A_i B_j} \cdot (R \cdot T)^{-1}) - 1] \cdot b_{ij} \cdot \beta^{A_i B_j} \quad (3)$$

$\epsilon_{CPA}^{A_i B_j}$  and  $\beta^{A_i B_j}$  are the association energy and volume, respectively, between site  $A$  on molecule  $i$  and site  $B$  on molecule  $j$ . The  $g(V_m)^{\text{ref}}$  is the contact value of the radial distribution function for the reference hard sphere fluid system.

The radial distribution function,  $g(V_m)$  was presented in a simplified form by Kontogeorgis *et al.* (sCPA [6]). Whereas earlier versions of CPA utilized the Carnahan–Starling expression for the hard-sphere radial distribution function, sCPA uses the expression shown in equation (4) for the simplified hard-sphere radial distribution function.

$$g(V_m) = [1 - 1.9 \cdot b \cdot (4 \cdot V_m)^{-1}]^{-1} \quad (4)$$

This work utilizes the simplified form of CPA.

The temperature dependent energy parameter in the SRK term is calculated by means of equation (5).

$$\alpha(T) = a_0 \cdot \left[ 1 + c_1 \cdot \left( 1 - \sqrt{T \cdot T_c^{-1}} \right) \right]^2 \quad (5)$$

where  $a_0$  and  $c_1$  are pure component parameters and  $T_c$  is the critical temperature. For associating components, the CPA EOS utilizes five pure component parameters,  $a_0$ ,  $b$ ,  $c_1$ ,  $\epsilon_{CPA}^{A_i B_j}$  and  $\beta$ . Non-associating components are described by three pure component parameters,  $a_0$ ,  $b$  and  $c_1$  in a manner similar to that of the “standard” SRK EOS. Pure component parameters for associating components are obtained by fitting the model to experimental vapor pressures and saturated liquid densities of the pure component. The three pure component parameters for non-associating compounds may also be estimated by this approach, however in this work they are obtained from critical temperature,  $T_c$ , critical pressure,  $P_c$ , and the acentric factor,  $\omega$ .

In binary systems, the van der Waals one-fluid mixing rules are used for evaluating the SRK parameters,  $\alpha$  and  $b$ . This is done according to equations (6) and (7) [5].

$$\alpha = \sum_i \sum_j x_i \cdot x_j \cdot \alpha_{ij} \quad (6)$$

$$b = \sum_i x_i \cdot b_i \quad (7)$$

where the “classical” combining rules are applied.

$$\alpha_{ij} = \sqrt{\alpha_i \cdot \alpha_j} \cdot (1 - k_{ij}) \quad (8)$$

$$b_{ij} = (b_i + b_j) \cdot 2^{-1} \quad (9)$$

and  $k_{ij}$  in equation (8) is the binary interaction parameter between component,  $i$ , and component,  $j$ .

No mixing rules are needed for the association parameters of CPA. Only for cross associating systems, combining rules must be applied to the two association parameters,  $\epsilon_{CPA}^{A_i B_j}$  and  $\beta^{A_i B_j}$ . No combining rules are needed in this work, since water is the only associating component considered. The utilized CPA package does however incorporate the CR1 combining rules according to equations (10) and (11). Hence it is possible to extend the existing model to cross associating systems.

$$\epsilon_{CPA}^{A_i B_j} = (\epsilon_{CPA}^{A_i B_i} + \epsilon_{CPA}^{A_j B_j}) \cdot 2^{-1} \quad (10)$$

$$\beta^{A_i B_j} = \sqrt{\beta^{A_i B_i} \cdot \beta^{A_j B_j}} \quad (11)$$

For systems containing three or more components sCPA becomes predictive, since only binary interactions may be accounted for in the process of parameter estimation.

## 2.2. The van der Waals–Platteeuw hydrate model

This model was presented by van der Waals and Platteeuw in 1958 [3]. The van der Waals–Platteeuw model handles the solid phase only and is typically combined with an equation of state and an activity coefficient model for the co-existing phases. In 1972 William R. Parrish and John M. Prausnitz presented an algorithm that made the van der Waals–Platteeuw hydrate model suitable for computer calculations [7]. In this work, the algorithm of Parrish and Prausnitz is modified such that the CPA EOS supplies the hydrate model with all needed inputs.

The basic assumption in the van der Waals–Platteeuw model concerns the chemical potential of water. At equilibrium, this potential must be balanced in all phases present, e.g.

$$\mu_{\text{water}}^{\text{HydratePhase}} = \mu_{\text{water}}^{\text{LiquidPhase}} = \mu_{\text{water}}^{\text{VaporPhase}} \quad (12)$$

Instead of evaluating the actual chemical potential of water in the hydrate phase, van der Waals and Platteeuw defined a theoretical, solid water phase that constituted the same structure of water as in the actual hydrate. This phase is here denoted the meta-stable  $\beta$ -phase. The meta-stable  $\beta$ -phase is a crystalline configuration of empty water cavities as illustrated in figure 1.

Since it is the interaction between the guest molecule and its surrounding water molecules that stabilizes the actual hydrate structure, van der Waals and Platteeuw chose to consider this interaction, rather than actual chemical potentials.

The difference in chemical potential between the actual hydrate phase and the meta-stable  $\beta$ -phase may thus be described by equation (13).

$$\Delta \mu_{\text{water}}^{\beta\text{-Phase} \rightarrow \text{HydratePhase}} = \mu_{\text{water}}^{\beta\text{-Phase}} - \mu_{\text{water}}^{\text{HydratePhase}} = \Delta \mu_{\text{water}}^{\text{H}} \quad (13)$$

The following assumptions regarding the presence of the guest molecule in the water cavity allowed for the guest–host interaction to be described by an approach similar to Langmuir adsorption theory using Lennard–Jones–Devonshire theory for the description of the Langmuir adsorption coefficients [7].

- (1) All cavities are assumed spherical.
- (2) Each cavity can contain one guest at most.
- (3) No guest–guest interactions are considered.
- (4) The guest molecule does not distort the physical properties of the water lattice.
- (5) The internal partition function of the guest is considered to be identical to that of its ideal state.
- (6) Only London forces are considered in the guest–host interaction.

Assumption (4) in particular is one very important assumption in the van der Waals–Platteeuw model, as it is presented here.

The difference in chemical potential of water between a theoretical empty hydrate water lattice (empty cavities) and the actual hydrate may now be described by the presence of guest molecules in the water cavities, according to Langmuir adsorption theory.

$$\Delta\mu(T, P, \theta)_{\text{water}}^H = -R \cdot T \cdot \sum_m \left[ v_m \cdot \ln \left( 1 - \sum_j \theta(T, P, \bar{y})_{mj} \right) \right], \quad (14)$$

where  $v_m$  is the number of cavities type  $m$  per water molecule in the hydrate structure. The  $\theta_{mj}$  is the fractional occupancy of component  $j$  in cavity type  $m$ . This occupancy is described by

$$\theta(T, P, \bar{y})_{mj} = C(T)_{mj} \cdot f(T, P, \bar{y})_j \cdot \left( 1 + \sum_l C(T)_{ml} \cdot f(T, P, \bar{y})_l \right)^{-1}, \quad (15)$$

where the fugacity  $f$  is given by:

$$f(T, P, \bar{y})_j = \phi(T, P, \bar{y})_j \cdot y(T, P)_j \cdot P. \quad (16)$$

The  $C_{mj}$  is the Langmuir constant for gas component  $j$  in cavity type  $m$ ,  $\phi_j$  is the fugacity coefficient of component  $j$  in the vapor phase and  $y_j$  is the mole fraction of component  $j$  in the vapor phase.

Combining equations (14) and (15) leads to the following expression for the change in chemical potential of water caused by the presence of the guest molecules.

$$\Delta\mu(T, P, \theta)_{\text{water}}^H = R \cdot T \cdot \sum_m \left[ v_m \cdot \ln \left( 1 + \sum_j C(T)_{mj} \cdot f(T, P, \bar{y})_j \right) \right]. \quad (17)$$

In the following, we consider the specific case, where the hydrate is formed in a co-existing liquid phase. Hence a combination of equations (12) and (13) leads to

$$\Delta\mu(T, P, \theta)_{\text{water}}^{\beta\text{-Phase} \rightarrow \text{HydratePhase}} = \mu(T, P)_{\text{water}}^{\beta\text{-Phase}} - \mu(T, P, \bar{x})_{\text{water}}^{\text{LiquidPhase}}. \quad (18)$$

At equilibrium, the chemical potential of water in the liquid phase may be described by

$$\mu(T, P, \bar{x})_{\text{water}}^{\text{LiquidPhase}} = \mu(T, P)_{\text{water}}^* + R \cdot T \cdot \ln \left[ \alpha(T, P, \bar{x})_{\text{water}}^{\text{LiquidPhase}} \right], \quad (19)$$

where superscript  $*$  denotes a pure phase,  $\alpha$  is the activity of water in the non-ideal liquid phase. The water activity accounts for the highly non-ideal behavior of water at the presence of hydrogen bonding components in the liquid phase. In the case of hydrocarbon gases or in this specific case of carbon dioxide and nitrogen, the solubility values of the gasses are low and the activity of water in the liquid phase may be assumed unity. Nevertheless, the activity is rigorously calculated in this work. This is relevant when the model is extended to include other solvents and/or salts. The water activity may be described either in terms of a symmetric activity coefficient,  $\gamma$ , or in terms of fugacity coefficients,  $\phi$ .

$$\alpha(T, P, \bar{x})_{\text{water}}^{\text{LiquidPhase}} = \frac{\bar{x}_{\text{water}}^{\text{LiquidPhase}}}{\bar{x}_{\text{water}}} \cdot \gamma(T, P, \bar{x})_{\text{water}}^{\text{LiquidPhase}} = \bar{x}_{\text{water}}^{\text{LiquidPhase}} \cdot \phi(T, P, \bar{x})_{\text{water}}^{\text{LiquidPhase}} \cdot (\phi(T, P)_{\text{water}}^*)^{-1}, \quad (20)$$

where  $x$  denotes liquid phase composition.

We may now define a difference in chemical potential between the meta-stable  $\beta$ -phase and a pure water liquid phase

$$\Delta\mu(T, P)_{\text{water}}^{\beta\text{-Phase} \rightarrow \text{WaterPhase}} = \mu(T, P)_{\text{water}}^{\beta\text{-Phase}} - \mu(T, P)_{\text{water}}^* = \Delta\mu(T, P)_{\text{water}}^L. \quad (21)$$

Substituting first equation (18) and then equation (16) into equation (20), we obtain an explicit expression for the difference in chemical potential between the empty hydrate and the pure liquid phase at specified temperature,  $T$ , and pressure,  $P$

$$\Delta\mu(T, P)_{\text{water}}^L = R \cdot T \cdot \sum_m \left[ v_m \cdot \ln \left( 1 + \sum_j C(T)_{mj} \cdot f(T, P, \bar{y})_j \right) \right] + R \cdot T \cdot \ln \left[ \phi_{\text{water}}^{\text{LiquidPhase}}(T, P, \bar{x}) \right]. \quad (22)$$

Equation (22) is hereafter noted the theoretical chemical potential difference. Note that all values of fugacity and the water activity may be obtained from the CPA EOS. The last parameters to be specified are the Langmuir adsorption coefficient,  $C(T)$ . Van der Waals and Platteeuw [3] showed that the Langmuir adsorption coefficients may be estimated from Lennard-Jones–Devonshire cell theory with e.g. a Lennard-Jones 12-6 cell potential. They proposed the following expression for the Langmuir adsorption coefficient

$$C(T)_{mj} = 4 \cdot \pi \cdot (k_B \cdot T)^{-1} \cdot \int_0^\infty \exp[-w(r)_{mj} \cdot (k_B \cdot T)^{-1}] \cdot r^2 \cdot dr, \quad (23)$$

where  $k_B$  is the Boltzmann constant and  $w(r)_{mj}$  is the spherical core cell potential of component  $j$  in cavity type  $m$ .  $r$  is the linear distance from the center of the cell.

McKoy and Sinanoglu [8] investigated three cell potentials for use in hydrate dissociation pressure calculations. They concluded that the Kihara cell potential is the most suitable for this kind of calculations, and proposed a method for including this cell potential in the hydrate dissociation pressure calculation. McKoy and Sinanoglu evaluated the interactions between the guest molecule and all its surrounding first layer of water molecules, and summed up the contributions in one expression for the spherical core cell potential. Parrish and Prausnitz [7] presented the final expression for the cell potential of gas constituent  $j$  in cavity type  $m$ , in a slightly modified form. Here the expression of Parrish and Prausnitz is utilized.

$$w(r)_{mj} = 2 \cdot z_m \cdot \epsilon_j \cdot \left[ \frac{\sigma_j^{12}}{R_m^{11}} \cdot \left( \delta(N=10)_{mj} + \frac{a_j}{R_m} \cdot \delta(N=11)_{mj} \right) - \frac{\sigma_j^6}{R_m^5 \cdot r} \cdot \left( \delta(N=4)_{mj} + \frac{a_j}{R_m} \cdot \delta(N=5)_{mj} \right) \right]. \quad (24)$$

The  $z_m$  is the coordination number for the guest in cavity type  $m$ ,  $\epsilon_j$  is the characteristic energy of guest molecule  $j$ ,  $a_j$  is the core radius of molecule  $j$ ,  $\sigma_j + 2a_j$  is the collision diameter of molecule  $j$  and  $R_m$  is the radius of cavity type  $m$ .  $\delta(N)_{mj}$  is defined by

$$\delta(N)_{mj} = N^{-1} \cdot \left[ (1 - r \cdot R_m^{-1} - a_j \cdot R_m^{-1})^{-N} - (1 + r \cdot R_m^{-1} - a_j \cdot R_m^{-1})^{-N} \right]. \quad (25)$$

From equation (24), it is seen that the Kihara spherical core cell potential is undefined in the cavity center. However if one looks at the limiting value of the cell potential when approaching this position from positive side, it may be shown that this point in the Kihara potential is a removable singularity. Also at a distance from the cavity center of  $r = R_m - a_j$  a discontinuity with a change of sign occurs. Approaching  $r = R_m - a_j$  from  $r$ -values greater than this results in the cell potential approaching minus infinity making the behavior of the Langmuir adsorption coefficient divergent. Thus care should be taken, when integrating the Kihara cell potential.

In this work, the Kihara potential is evaluated from the cavity center to the singularity point at  $r = R_m - a_j$ . Thus equation (23) is rewritten as

$$C(T)_{mj} = 4 \cdot \pi \cdot (k_B \cdot T)^{-1} \cdot \int_0^{R_m - a_j} \exp[-w(r)_{mj} \cdot (k_B \cdot T)^{-1}] \cdot r^2 \cdot dr. \quad (26)$$

Sloan and Koh [14] and Mooijer-van den Heuvel et al. [9] have reported the same observations and adopted a similar solution.

Two methods have been investigated for the numerical approximation of the integral in equation (26), the Gauss–Legendre Quadrature method and the Composite Simpson 3/8 rule. Using 20 evaluation points in the Gauss–Legendre method and 200 internal sections in the Composite Simpson 3/8 rule (each with four evaluation points), the two methods obtain similar results for the integral. However since the Gauss–Legendre method, unlike the Simpson 3/8 method, does not need to evaluate the function values in the integration limits, the Gauss–Legendre method avoids the problems of evaluating the undefined point at  $r = 0$  and the singularity point at  $r = R_m - a_j$ . Due to the lower number of evaluation points, the Gauss–Legendre method also has the advantage of shorter computation time. Hence this method is chosen.

Parrish and Prausnitz [7] proposed a simpler way of calculating the Langmuir adsorption coefficients, where an explicit expression is given for the coefficients

$$C(T)_{mj} = A_{mj} \cdot T^{-1} \cdot \exp[B_{mj} \cdot T^{-1}], \quad (27)$$

where  $A_{mj}$  and  $B_{mj}$  are fitting parameters related to guest type  $j$  in cavity type  $m$  only. Hence in the case where a guest molecule may enter both cavities in both sl and sll hydrates, a total of eight fitting parameters must be determined for this one guest. In the cell potential approach, three parameters are needed to perform the same type of calculation, only two of them are utilized as fitting parameters in this work ( $\epsilon_j$  and  $\sigma_j$ ). Thus while the Parrish and Prausnitz approach results in a simpler expression, it requires a much greater number of fitting parameters to be used.

With the theoretical chemical potential difference in place, an experimental reference hydrate is introduced. The difference in chemical potential between the meta-stable  $\beta$ -phase and pure water at specified temperature and pressure may be derived thermodynamically in terms of measurable quantities. Knowing that the chemical potential is a state function, Parrish and Prausnitz [7] proposed a method for transforming the chemical potential difference measured for the reference hydrate at reference temperature,  $T_0$ , and reference pressure,  $P_0$ , to the actual temperature,  $T$ , and pressure,  $P$ . This is done in two steps. First, the measured chemical potential difference is transformed from reference temperature,  $T_0$ , to the actual temperature,  $T$ , and from reference pressure,  $P_0$ , at reference temperature,  $T_0$ , to the reference pressure,  $P_R$ , at the actual temperature,  $T$ , giving:

$$\begin{aligned} \frac{\Delta\mu(T, P_R)_{\text{water}}^{L, \text{Ref}}}{R \cdot T} &= \frac{\Delta\mu(T_0, P_0)_{\text{water}}^{\beta/\text{LiqWater}}}{R \cdot T_0} - \\ &\int_{T_0}^T \frac{\Delta H(T_0, P_0)_{\text{water}}^{\beta/\text{LiqWater}} + \Delta H(T)_{\text{water}}^{\text{Ice/LiqWater}}}{R \cdot T^2} dt + \\ &\int_{T_0}^T \frac{\Delta V_{\text{water}}^{\beta/\text{LiqWater}} + \Delta V_{\text{water}}^{\text{Ice/LiqWater}}}{R \cdot T} \cdot \frac{dP_R}{dt} dt, \end{aligned} \quad (28)$$

where  $\Delta\mu(T, P_R)_{\text{water}}^{L, \text{Ref}}$  is the chemical potential difference for water at temperature,  $T$  and at the dissociation pressure of the reference pressure,  $P_R$ . The  $\Delta\mu(T_0, P_0)_{\text{water}}^{\beta/\text{LiqWater}}$  is the chemical potential difference of water between the  $\beta$ -phase and liquid water, measured for the reference hydrate at reference temperature  $T_0$  and reference pressure  $P_0$ . The  $\Delta H(T_0, P_0)_{\text{water}}$  and  $\Delta H(T)_{\text{water}}$  are the differences in molar enthalpy for water between the meta-stable  $\beta$ -phase measured for the reference hydrate and ice and ice and liquid water respectively. The  $\Delta H(T)_{\text{water}}^{\text{Ice/LiqWater}}$  consists of two contributions, first the phase change enthalpy from ice to liquid at the reference temperature, then a heat capacity contribution from the heating of the liquid from the reference temperature to the actual temperature.

$$\Delta H(T)_{\text{water}}^{\text{Ice/LiqWater}} = \Delta H(T_0, P_0)_{\text{water}}^{\text{Ice-Liquid}} + \Delta C_p(T) \cdot (T - T_0). \quad (29)$$

$\Delta V_{\text{water}}^{\beta/\text{LiqWater}}$  and  $\Delta V_{\text{water}}^{\text{Ice/LiqWater}}$  are the differences in molar volume of the  $\beta$ -phase measured for the reference hydrate and ice and ice and

liquid water respectively. All values are measured at reference temperature  $T_0$  and reference pressure,  $P_0$ ;  $P_0$  is the vapor pressure of ice at temperature,  $T_0$ . Since this pressure is small compared to the hydrate dissociation pressure, it is assumed zero. The  $dP_R/dT$  is the slope of the measured dissociation pressure–temperature curve for the reference hydrate. Parrish and Prausnitz [7] presented a three parameter expression for the temperature dependence of the reference hydrate dissociation pressure:

$$\ln[P_R/\text{atm}] = A_R + B_R \cdot T^{-1} + C_R \cdot \ln T. \quad (30)$$

In the second step, the chemical potential difference for the reference hydrate is transformed from the reference pressure,  $P_R$ , to the actual pressure,  $P$ .

$$\Delta\mu(T, P)_{\text{water}}^{L, \text{Ref}} = \Delta\mu(T, P_R)_{\text{water}}^{L, \text{Ref}} + (\Delta V_{\text{water}}^{\beta/\text{LiqWater}} + \Delta V_{\text{water}}^{\text{Ice/LiqWater}}) \cdot (P - P_R). \quad (31)$$

Recalling assumption (4) of this model, that the water lattice properties are independent of the guest molecule (for a given hydrate structure), the theoretical chemical potential difference provided in equation (22) must be identical to the reference potential difference given by equation (31). Hence, by equating these two expressions, and specifying either temperature or pressure, it is possible to determine the corresponding equilibrium condition (pressure or temperature respectively).

### 2.3. Model implementation – numerical methods and algorithm

The hydrate model as presented above is implemented in a FORTRAN95 module. This section presents the numerical methods and solution procedures utilized in the model set-up as well as an overview of the used parameters and the overall model algorithm. The parameters required for the two models (CPA and van der Waals–Platteeuw) may be found in table 1.

This work utilizes an algorithm for the hydrate dissociation pressure calculation similar to that presented by Parrish and Prausnitz [7]. Note that the algorithm and the hydrate model as presented above is valid only for describing equilibrium conditions for hydrate systems above the ice point temperature of water. In order to describe hydrate formation below the ice point temperature of water, the water activity correction term in equation (22) must be omitted while new reference parameters for equations (28), (29), and (31) are needed. Moreover, the CPA equation of state approach for determining the input parameters for the van der Waals–Platteeuw model is no longer valid since CPA (like all equations of state) does not account for solid phases (ice). Hydrate formation below the ice point temperature of water was not considered in this work.

A two phase isothermal/isobaric flash calculation has been implemented, utilizing CPA for the thermodynamic description of the non-solid phase(s). The algorithm and solution procedures utilized are those proposed by Michelsen and Møllerup [10]. Since the pressure inputs for the flash calculation are controlled by the hydrate model, emphasis has been put on robustness in the choice of flash algorithm. All flash calculations in this algorithm are “blind” calculations, hence no *a priori* assumptions can be made regarding the number (one or two) or type of phases present.

Pure component parameters for the CPA model are provided in table 2. In this work, water is considered an associating component and is modeled using the 4C association scheme. This means that a water molecule has four possible points where it can hydrogen-bond. For a discussion of association schemes, see Huang and Radosz [11]. Carbon dioxide and nitrogen are considered to be non-associating components. Hence, five pure component parameters are needed for water, whereas only three are needed for carbon dioxide and nitrogen. The pure component parameters for water



are those reported by Kontogeorgis *et al.* [5]. Carbon dioxide and nitrogen are described by their critical data and acentric factor. These are taken from the DIPPR database [12].

Experimental solubility data for carbon dioxide in liquid water and nitrogen in liquid water at various temperatures and pressures have been used to estimate binary interaction parameters for the binary pairs water–carbon dioxide and water–nitrogen. Experimental solubility data for CO<sub>2</sub> in pure water were obtained from [15–18]. A total of 45 data points have been considered when fitting the binary interaction parameter. Similarly, solubility data for N<sub>2</sub> in pure water [19,20] have been used to fit the binary interaction parameter for N<sub>2</sub> in pure water. Here 15 reference data points were utilized. The binary interaction parameter for carbon dioxide–nitrogen is assumed zero.

The objective function minimized in the procedure of determining the optimal binary interaction parameters is provided in equation (32).

$$OBJ = \sum_i^N \frac{abs(x_i^{calc} - x_i^{exp})}{x_i^{exp}}, \quad (32)$$

where subscript *i* indicates data point *i*. *N* is the number of data points. Superscripts *calc* and *exp* denote calculated and measured solubility respectively. The binary interaction parameters obtained are presented in table 3. Note that a high absolute value of the binary interaction parameter is chosen to obtain best possible accuracy in low temperature regions.

The main program in the developed module concerns the van der Waals–Platteeuw hydrate model. The flash routine is used to obtain the inputs required for the hydrate model at the specified temperature and pressure.

The hydrate module may be described in a very simplified manner as a program that solves equations (22) and (31) for the equilibrium pressure at a specified temperature. Integrals in equations (26) and (28) are evaluated numerically by the use of a 20 point Gauss–Legendre quadrature method. When subtracting equation (31) from equation (22), the resulting equation may be solved by a Newton–Raphson method.

Reference hydrate properties are taken from the work of Parrish and Prausnitz [7] and the work of Munck *et al.* [13]. These are provided in table 4.

Parameters for the description of the Langmuir adsorption coefficients have been obtained by fitting the model to hydrate dissociation pressures of pure nitrogen and carbon dioxide hydrates as well as mixed hydrates containing both gasses in the three phase equilibrium region (liquid water, vapor, hydrate). An objective function similar to that of equation (32) has been utilized to minimize the error between calculated and experimental dissociation pressures. Nitrogen and carbon dioxide are assumed to occupy both the small and large cavities of sI and sII hydrates. The obtained parameter sets for a description of the Langmuir adsorption coefficients both by equations (26) and (27) are provided in tables 5 and 6 respectively.

Note that only  $\epsilon$  and  $\sigma$  in the Kihara potential have been fitted as a part of this work. The core radii,  $a$ , of the molecules are taken from Sloan and Koh [14].

**TABLE 2**  
Pure component parameters for the CPA EOS.

	$a_0 \cdot 10^{-11}/(\text{Pa} \cdot \text{m}^{-6} \cdot \text{mol}^{-2})$	$b \cdot 10^5/(\text{m}^3 \cdot \text{mol}^{-1})$	$c_1$	$\beta$	$\epsilon_{CPA}^{AB} \cdot 10^{-4}/(\text{Pa} \cdot \text{m}^3 \cdot \text{mol}^{-1})$	Reference
H <sub>2</sub> O	1.2277 $T_c/K$	1.451 $P_c \cdot 10^{-6}/\text{Pa}$	0.67359	0.0692	1.6655	[5]
N <sub>2</sub>	126.2	3.400	0.03772			[12]
CO <sub>2</sub>	304.2	7.383	0.22362			[12]

**TABLE 3**

Fitted binary interaction parameters for the CPA EOS. The binary interaction parameters for H<sub>2</sub>O–CO<sub>2</sub> were obtained by fitting CPA flash results to 62 liquid phase solubility points. Thirteen data points were used for the binary interaction parameter of H<sub>2</sub>O–N<sub>2</sub>. Modeling results are presented in section 3.1.

$k_{ij}$	H <sub>2</sub> O	N <sub>2</sub>	CO <sub>2</sub>
H <sub>2</sub> O		–0.344	–0.078
N <sub>2</sub>	–0.344		0.000
CO <sub>2</sub>	–0.078	0.000	

Note how six parameters are sufficient to describe the two hydrate structures of nitrogen and carbon dioxide with the Kihara cell potential approach, whereas a total of 16 parameters are needed when using the simple, explicit expression for the Langmuir adsorption coefficient.

Parrish and Prausnitz [7] noted that the explicit expression for the Langmuir adsorption coefficient is only suitable in the temperature range from (260 to 300) K. At temperatures below or above this interval, the cell potential approach should be used.

The algorithm used for dissociation pressure calculations is provided below. This algorithm assumes that the hydrate structure formed (sI or sII) is known. Note that the algorithm indicated below is modified in a later stage, to assure thermodynamic consistency in model predictions: The modification removes the assumed hydrate structure transition at a mole fraction of CO<sub>2</sub> of 0.15 in the vapor phase. Instead the model chooses the most stable structure according to the lowest equilibrium pressure. However the illustrated algorithm is utilized in the parameter fitting process. The algorithm is illustrated schematically by the flowchart in figure 2.

### 3. Results and discussion

The model parameters provided in tables 3 to 6, have been fitted as part of this work. Sections 3.1 and 3.2 describe the process of fitting model parameters and illustrate modeling results compared to the utilized reference data. Section 3.3 presents model predictions.

#### 3.1. CPA flash calculation – parameter fitting results

Solubility data for CO<sub>2</sub> in pure water [15–18] have been used to fit the binary interaction parameter between water and CO<sub>2</sub>. Similarly, solubility data for N<sub>2</sub> in pure water [19,20] have been used to fit the binary interaction parameter for N<sub>2</sub>/water binaries. In general, fitting binary EOS parameters, using liquid phase compositions only, results in loss of accuracy in the vapor phase description. However in this work it has been chosen to consider the liquid phase only, when determining binary interaction parameters for CPA. Calculated solubilities are compared to a selection of the reference data utilized in figures 3 and 4.

Values of the solubility in figures 3 and 4 are illustrated as total pressures as a function of equilibrium solubility at constant temperature. Results are illustrated for various temperatures. Note how the temperature dependency of the CO<sub>2</sub> solubility is well



TABLE 4

Data for reference hydrate in van der Waals–Platteeuw model.  $T_0/K = 273.15$ ,  $P_0/\text{Pa} = 0$ .

	sl hydrate	sII hydrate	Reference
$\Delta\mu(T_0, P_0)^{\beta/\text{LiqWater}}/(\text{J} \cdot \text{mol}^{-1})$	1264	882.8	[7]
$\Delta H_{\text{water}}^{\beta/\text{Ice}}/(\text{J} \cdot \text{mol}^{-1})$	1151	807.5	[7]
$\Delta H(T_0)^{\text{Ice-Liquid}}/(\text{J} \cdot \text{mol}^{-1})$	–6009	–6009	[7]
$\Delta C_p(T)/(\text{J} \cdot \text{K}^{-1} \cdot \text{mol}^{-1})$	$38.11 - 0.1406(T - 273.1)$	$38.11 - 0.1406(T - 273.1)$	[7]
$(\Delta V_{\text{water}}^{\beta/\text{Ice}} + \Delta V_{\text{water}}^{\text{Ice-LiqWater}}) \cdot 10^6/(\text{m}^3 \cdot \text{mol}^{-1})$	4.6	5.0	[13]
$P_R/\text{atm}$ , $T/K < 291$			
$A_R$	–1212.2	–1023.14	[7]
$B_R$	44344.0	34984.3	[7]
$C_R$	187.719	159.923	[7]
$P_R/\text{atm}$ , $T/K > 291$			
$A_R$	–1212.2	4071.64	[7]
$B_R$	44344.0	–193428.8	[7]
$C_R$	187.719	–599.755	[7]

TABLE 5

Kihara cell potential parameters for hydrate formers.

	$a \cdot 10^{10}/\text{m}$	$(a/k_B)/\text{K}$	$\sigma \cdot 10^{10}/\text{m}$
$\text{N}_2$	0.3526 <sup>a</sup>	125.2968	2.99000
$\text{CO}_2$	0.6805 <sup>a</sup>	166.7304	2.99134

<sup>a</sup> Data from Sloan and Koh [14].

described using a constant value of  $k_{ij} = -0.078$ . Solubility lowers with increasing temperature. This is seen as an increase in total pressure at constant liquid phase composition and increasing temperature.

Nitrogen solubility is less accurately described by CPA, and a high absolute value of the binary interaction parameter is needed to obtain an accurate description of the solubility in the low temperature region.  $k_{ij} = -0.344$  was chosen thus obtaining high accuracy at a temperature of 273.15 K, however accuracy diminishes at higher temperatures. The high absolute value of the binary interaction parameter depresses the effect of temperature on the calculated solubilities. At high temperatures and high pressures, CPA, with the given parameters, predicts a higher solubility than what is found in the literature data. In this work, the chosen binary interaction parameter for water/ $\text{N}_2$  provides good low temperature description of the liquid phase. Choosing a lower absolute value of the binary interaction parameter can improve the high temperature description, the price being loss of accuracy at low temperatures. Since the low temperature region is of highest interest to this work, emphasis is put on accuracy at low temperatures.

### 3.2. Hydrate model – parameter fitting results

Two hydrate models have been set up. The difference between the two is the method used for describing the Langmuir adsorption coefficient. The first model, Model I, utilizes the Kihara cell potential approach for the description of the Langmuir adsorption

coefficients. Model II, utilizes the simple, explicit two-parameter expression for the description of the Langmuir adsorption coefficient.

- Model I: Kihara cell potential (equations (23) to (25)).
- Model II: Two-parameter explicit expression (equation (27)).

Since both approaches consider the Langmuir adsorption coefficient to be a function of temperature only, pressure/temperature curves have been utilized as reference data in the parameter fitting process: This kind of data illustrates the effect of temperature on the hydrate dissociation (equilibrium) pressure at constant vapor phase composition. Reference data for the pure hydrates of  $\text{N}_2$  [21,22] and  $\text{CO}_2$  [23,24] have been used along with reference data for the mixed hydrates of  $\text{N}_2$  and  $\text{CO}_2$  [25]. Table 7 shows how the reference data are utilized for fitting the Langmuir parameters.  $\text{CO}_2$  and  $\text{N}_2$  are assumed to enter both small and large cavities in both hydrate structures.

Initial estimates for the Kihara parameters of Model I are taken from Sloan and Koh [14]. Initial estimates for parameters,  $A_{mj}$  and  $B_{mj}$  in Model II are taken from Parrish and Prausnitz [7]. Note that the fitted Langmuir adsorption coefficients in the van der Waals–Platteeuw hydrate model depend highly on the choice of reference hydrate parameters and, to a lesser extent, the equation of state. This is the main reason for the variation in parameters presented in literature.

In this work, the four fitting parameters of Model I are fitted simultaneously using all the reference data in table 7. In Model II, the 16 fitting parameters are hydrate structure specific. Hence a selection of relevant data must be performed for each set of  $A_{mj}$  and  $B_{mj}$  parameters. From experimental work in the literature, it has been found that nitrogen forms sII hydrate [21,22], while carbon dioxide forms sl [23,24]. Mixtures of the two gasses may be expected for form either one or the other of these two structures, depending on the gas phase composition. There is a disagreement

TABLE 6

Parameters for Langmuir adsorption coefficients required in equation (27).

Guest type	$A_{mj} \cdot 10^3/(\text{K} \cdot \text{Pa}^{-1})$	$B_{mj} \cdot 10^{-3}/\text{K}$	$A_{mj} \cdot 10^7/(\text{K} \cdot \text{Pa}^{-1})$	$B_{mj} \cdot 10^{-3}/\text{K}$
	Small cavity		Large cavity	
		<i>sl hydrate</i>		
N <sub>2</sub>	3.00712	2.13934	2.18150	2.24147
CO <sub>2</sub>	1.15849	2.86050	0.78920	3.28085
		<i>sII hydrate</i>		
N <sub>2</sub>	2.83936	2.17500	7.48338	1.86060
CO <sub>2</sub>	1.26507	2.78974	4.04863	2.82898

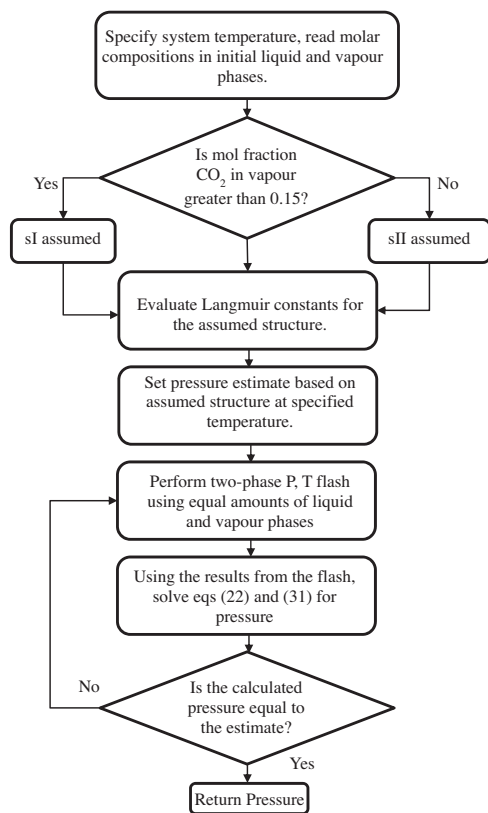


**FIGURE 2.** Algorithm for calculating hydrate dissociation pressure for a given gas mixture and temperature. At a subsequent stage the assumption of structure sI or sII is removed: the pressure for both structures is calculated and the structure for which the lowest equilibrium pressure is obtained is then determined to be the most stable.

in literature concerning the exact cut-off concentration between the two structures. Kang *et al.* [25] report a cut-off concentration of approximately 16 mol% CO<sub>2</sub>. The sI hydrates will form at higher CO<sub>2</sub> concentrations, while sII hydrates form at lower CO<sub>2</sub> concentrations.

Seo and Lee [26] report findings of sI mixed hydrates at vapor phase concentrations down to 1 mol% CO<sub>2</sub> and thus report the cut-off concentration to be 1 mol% CO<sub>2</sub>. As previously mentioned, the work presented here assumes the cut-off concentration to be 15 mol% CO<sub>2</sub> in the vapor phase. The objective function minimized in the parameter fitting procedure is:

$$OBJ = \sum_i^N \frac{abs(p_i^{calc} - p_i^{exp})}{p_i^{exp}}, \quad (33)$$

where  $P$  is dissociation pressure. Subscript  $i$  denotes data point  $i$  and superscripts *calc* and *exp* denote calculated and experimental data points respectively. The  $N$  is the total number of reference data points used for estimating the parameter sets.

Figures 5 to 8 illustrate the performances of the two hydrate models compared with the reference data used to estimate the Langmuir adsorption coefficient parameters.

Figures 5 and 6 compare the two model performances for the pure CO<sub>2</sub> hydrate and the pure N<sub>2</sub> hydrate respectively. Note the

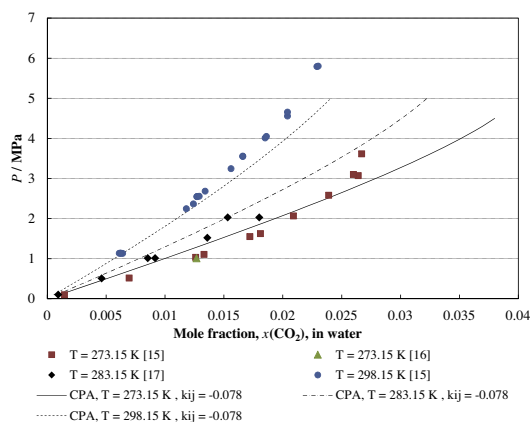


**FIGURE 3.** Equilibrium pressures of binary CO<sub>2</sub>/H<sub>2</sub>O liquid mixtures as a function of mole fraction of CO<sub>2</sub> at constant temperature. Comparison of experimental data and CPA flash results. Squares: experimental data at  $T = 273.15$  K [15], triangles: experimental data at  $T = 273.15$  K [16], diamonds: experimental data at  $T = 273.15$  K [17], circles: experimental data at  $T = 298.15$  K [15]. Solid line: CPA results at  $T = 273.15$  K. Dash-dot-dash line: CPA results at  $T = 273.15$  K, dash-dash line: CPA results at  $T = 298.15$  K. A single temperature-independent  $k_{ij} = -0.078$  was used to fit the data.

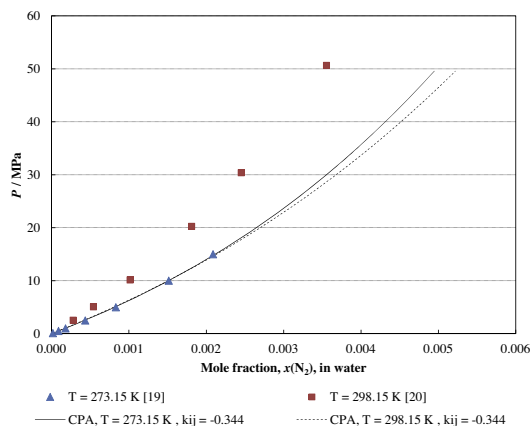


**FIGURE 4.** Equilibrium pressures of binary N<sub>2</sub>/H<sub>2</sub>O liquid mixtures as a function of mole fraction of N<sub>2</sub> at constant temperature. Comparison of experimental data and CPA flash results. Triangles: modeling data at  $T = 273.15$  K [19], squares: experimental data at  $T = 298.15$  K [20], solid line: CPA results at  $T = 273.15$  K, dash-dash line: CPA results at  $T = 298.15$  K. A single temperature-independent  $k_{ij} = -0.344$  was used to fit the data. Using a constant  $k_{ij}$  value however means the model is unable to capture the temperature dependence of the nitrogen solubility adequately.

10-fold difference in equilibrium pressures between pure N<sub>2</sub> sII hydrates and pure CO<sub>2</sub> sI hydrates. This large difference in equilibrium pressures is what the CO<sub>2</sub> capture process exploits. The CO<sub>2</sub> is expected to enter the mixed hydrates more readily than N<sub>2</sub>, hence creating a selective removal of CO<sub>2</sub> from the flue gas phase. Both Model I and Model II perform well in the case of the pure hydrates. Both models return AAD below 3% (AAD below 0.03) when compared to the reference data in the illustrated temperature interval. AAD here is defined as

**TABLE 7**

Reference data utilized for fitting Langmuir adsorption coefficients.  $y(\text{CO}_2)$  denotes initial vapor phase composition of  $\text{CO}_2$ . The available reference data are divided into relevant structures, because all Model II fitting parameters are structure specific. Fitting parameters in Model I are universal and thus valid for both structures.

Model parameters	Reference data
<i>Model I</i>	
$\text{N}_2$ sl/sII	Pure $\text{N}_2$ hydrates [21,22]
$\text{CO}_2$ sl/sII	Mixed $\text{N}_2/\text{CO}_2$ hydrates [25]
	Pure $\text{CO}_2$ hydrates [23,24]
	Mixed $\text{N}_2/\text{CO}_2$ hydrates [25]
<i>Model II</i>	
$\text{N}_2$ sl	Mixed $\text{N}_2/\text{CO}_2$ hydrates with $y(\text{CO}_2) \geq 0.15$ [25]
$\text{N}_2$ sII	Pure $\text{N}_2$ hydrates [21,22]
$\text{CO}_2$ sl	Pure $\text{CO}_2$ hydrates [23,24]
$\text{CO}_2$ sII	Mixed $\text{N}_2/\text{CO}_2$ hydrates with $y(\text{CO}_2) < 0.15$ [25]

$$\text{AAD} = \sum_i^N \frac{\text{abs}(P_i^{\text{calc}} - P_i^{\text{exp}})}{P_i^{\text{exp}}} \cdot \frac{1}{N} \quad (34)$$

where  $N$  is total the number of data points considered. Equation (34) differs from equation (33) in the way that equation (33) is the total of all absolute relative errors, whereas equation (34) represents the average absolute deviation per data point. Generally, Model II performs better than Model I. This is however also expected, considering the difference in the number of fitting parameters in the two models (4 versus 16). The difference between the two model performances becomes clear when considering mixed hydrates. These results are illustrated in Figures 7 and 8.  $y(\text{CO}_2)$  and  $y(\text{N}_2)$  denotes vapor phase mole fraction of  $\text{CO}_2$  and  $\text{N}_2$  respectively.

The two models perform comparably in the composition region close to the pure  $\text{CO}_2$  vapor phase. Model II does however describe the experimental data with higher accuracy especially in the high pressure region with low  $\text{CO}_2$  concentrations. A hydrate structure phase transition is imposed in both models at a  $\text{CO}_2$  concentration of 0.15. Kang *et al.* [25] comment on the slopes of the two upper reference data curves being similar to the slope of the pure  $\text{N}_2$  hydrate curve. They conclude that this is as an indication of sII hydrates forming under these conditions. Hence the two upper

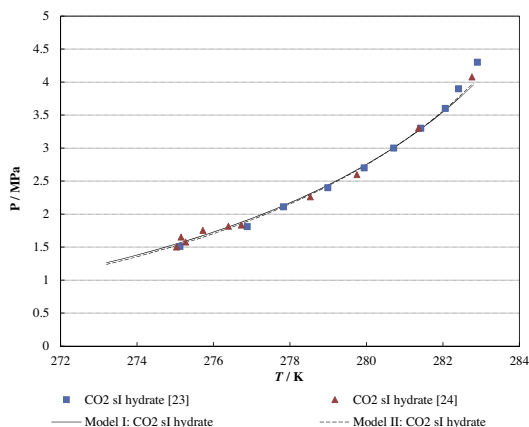


**FIGURE 5.** Dissociation pressures of pure  $\text{CO}_2$  structure I hydrates as a function of temperature. Comparison of experimental data and modeling results. Squares: experimental data [23], triangles: experimental data [24], solid line: Model I, dash-dash-dash line: Model II. Model I and Model II perform similar for the case of the pure  $\text{CO}_2$  hydrates. AAD defined by equation (34) is below 3% for both models. Binary interaction parameters in CPA were fitted only to two-phase equilibrium data and were not adjusted further in order to capture the hydrate dissociation pressure.

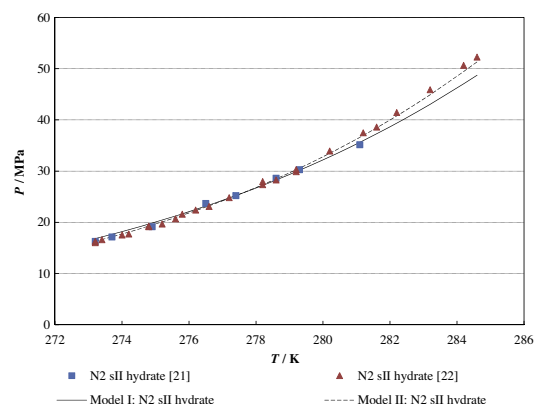


**FIGURE 6.** Dissociation pressures of pure  $\text{N}_2$  structure II hydrates as a function of temperature. Comparison of experimental data and modeling results. Squares: experimental data [21], triangles: experimental data [22], solid line: Model I, dash-dash-dash line: Model II. Model II is more accurate than Model I for the case of the pure  $\text{N}_2$  hydrates. AAD defined by equation (34) is below 3% for Model I and below 2% for Model II. Binary interaction parameters in CPA were fitted only to two-phase equilibrium data and were not adjusted further in order to capture the hydrate dissociation pressure.

hydrate  $P/T$  curves are modeled as sII hydrates whereas the four lower curves are modeled as sl hydrates. This is in accordance with the assumption mentioned previously about the cut-off concentration between the two structures. Both models lose accuracy when describing hydrate equilibrium at  $\text{CO}_2$  concentrations between of 10 and 50 mol%. Average absolute deviations between the model results and the 28 reference data points are 10.8% and 6.9% for Model I and Model II respectively.

### 3.3. Hydrate model – predictions

In addition to the mixed hydrate dissociation pressures, used for parameter fitting, Kang *et al.* [25] have measured mixed  $\text{N}_2/\text{CO}_2$  hydrate/vapor phase equilibrium data at constant temperature. They present data illustrating how both the dissociation pressure and the hydrate phase composition depend on the vapor phase composition. In this work, these data are utilized to validate the performances of the two models.

In order to calculate pressure-composition diagrams of the type shown in figures 9, 10, 13, 14 and 18, a dew-point pressure type calculation is performed – for a given temperature and concentration of  $\text{CO}_2$  in the vapor phase, the pressure at which the first hydrate just starts to form, is calculated. In a calculation of this type the initial gas phase composition is therefore also the equilibrium gas phase composition.

The hydrate phase composition is presented on a water free basis (in other words, the composition of the released gas, when the hydrate is dissociated). In the van der Waals–Platteeuw model, this composition may be calculated from the estimated fractional occupancies,  $\theta_{m,j}$ , at the converged pressure. The hydrate phase composition is calculated as:

$$Y_j = \sum_m v_m \cdot \theta(T, P, \bar{y})_{m,j} \cdot \left( \sum_m v_m \sum_l \theta(T, P, \bar{y})_{m,l} \right)^{-1} \quad (35)$$

where  $Y_j$  is the composition of hydrate former  $j$  in the hydrate phase on a water free basis.

Figure 9 compare model predictions with the constant temperature data of Kang *et al.* [25]. Figures 9 and 10 show how the mixed

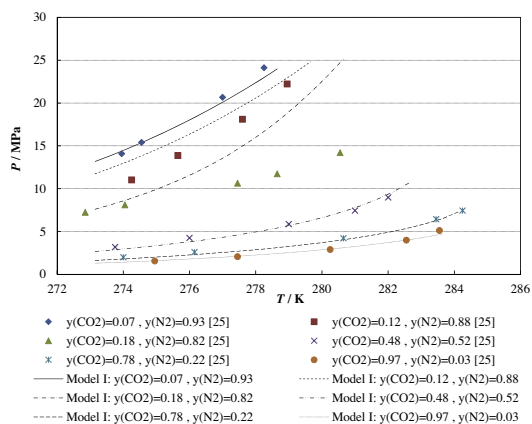


**FIGURE 7.** Dissociation pressures of mixed  $N_2/CO_2$  hydrates as a function of temperature for various vapor phase compositions. Comparison of experimental data by Kang *et al.* [25] and fitted modeling results for Model I.  $y(CO_2)$  and  $y(N_2)$  denotes vapor phase compositions of  $CO_2$  and  $N_2$  respectively. Vapor phases with  $CO_2$  mole fractions at or above 0.15 are modeled as sl hydrates. Vapor phases with  $CO_2$  mole fractions below 0.15 are modeled as sll hydrates. Diamonds: experimental data,  $y(CO_2)=0.07$ ,  $y(N_2)=0.93$ , squares: experimental data,  $y(CO_2)=0.12$ ,  $y(N_2)=0.88$ , triangles: experimental data,  $y(CO_2)=0.18$ ,  $y(N_2)=0.82$ , crosses: experimental data,  $y(CO_2)=0.48$ ,  $y(N_2)=0.52$ , crosses with line: experimental data,  $y(CO_2)=0.78$ ,  $y(N_2)=0.22$ , circles: experimental data,  $y(CO_2)=0.97$ ,  $y(N_2)=0.03$ , Solid line: Model I,  $y(CO_2)=0.07$ ,  $y(N_2)=0.93$ , short dashed line: Model I,  $y(CO_2)=0.12$ ,  $y(N_2)=0.88$ , dash-dot-dash line: Model I,  $y(CO_2)=0.18$ ,  $y(N_2)=0.82$ , dashdot-dot-dash line: Model I,  $y(CO_2)=0.48$ ,  $y(N_2)=0.52$ , long dashed line: Model I,  $y(CO_2)=0.78$ ,  $y(N_2)=0.22$ , dotted line: Model I,  $y(CO_2)=0.97$ ,  $y(N_2)=0.03$ . Binary interaction parameters in CPA were fitted only to two-phase equilibrium data and were not adjusted further in order to capture the hydrate dissociation pressure.

hydrate dissociation pressure varies with the equilibrium vapor phase composition at constant temperature. Kang *et al.* [25] provide data at three temperatures, 274, 277, and 280 K.

Performing this kind of calculation reveals a problem caused by the combination of algorithm (as presented in section 2.3) and fitted parameters. The imposed hydrate structure transition at a  $CO_2$  mole fraction of 0.15 (approximate equilibrium mole fraction of 0.14) results in a discontinuity in the calculated dissociation pressures at this composition. Extending the allowed composition regions for the two structures, reveals that both models predict sl hydrate to be the most stable structure even at vapor phase mole fractions of  $CO_2$  lower than 0.15 in all cases except for Model I at  $T=280$  K. This is seen by the calculated sl dissociation pressures being lower than the calculated sll dissociation pressures.

Figures 11 and 12 illustrate the calculated hydrate phase composition as a function of the equilibrium vapor phase composition. This kind of data has not been considered in the parameter fitting process, yet both models predict the temperature dependence of the composition correctly.

Model I seems to perform better than Model II in the composition calculations at concentrations close to the two pure hydrates, seen by lower absolute deviations from the reference data. However in the problematic concentration region with  $CO_2$  concentrations between 10 and 50 mol%, Model II performs better than Model I. However the assumption regarding structures renders both models thermodynamically inconsistent. This is clearly indicated by the discontinuities in the predicted composition dependencies.

In order to make the two models thermodynamically consistent, their common algorithm is changed, such that the dissociation pressure at any given temperature and vapor phase composition is calculated for both structure I and structure II.

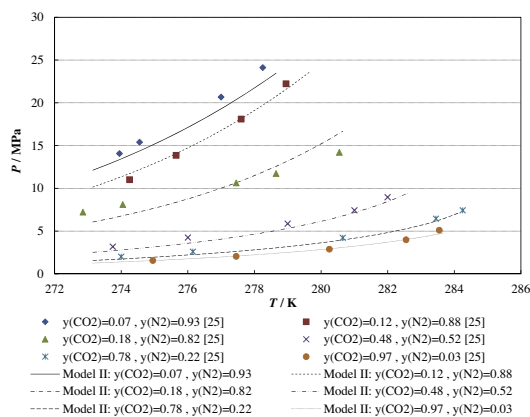


**FIGURE 8.** Dissociation pressures of mixed  $N_2/CO_2$  hydrates as a function of temperature for various vapor phase compositions. Comparison of experimental data by Kang *et al.* [25] and fitted modeling results for Model II.  $y(CO_2)$  and  $y(N_2)$  denotes vapor phase compositions of  $CO_2$  and  $N_2$  respectively. Vapor phases with  $CO_2$  mole fractions at or above 0.15 are modeled as sl hydrates. Vapor phases with  $CO_2$  mole fractions below 0.15 are modeled as sll hydrates. Diamonds: experimental data,  $y(CO_2)=0.07$ ,  $y(N_2)=0.93$ , squares: experimental data,  $y(CO_2)=0.12$ ,  $y(N_2)=0.88$ , triangles: experimental data,  $y(CO_2)=0.18$ ,  $y(N_2)=0.82$ , crosses: experimental data,  $y(CO_2)=0.48$ ,  $y(N_2)=0.52$ , crosses with line: experimental data,  $y(CO_2)=0.78$ ,  $y(N_2)=0.22$ , circles: experimental data,  $y(CO_2)=0.97$ ,  $y(N_2)=0.03$ , Solid line: Model II,  $y(CO_2)=0.07$ ,  $y(N_2)=0.93$ , short dashed line: Model II,  $y(CO_2)=0.12$ ,  $y(N_2)=0.88$ , dash-dot-dash line: Model II,  $y(CO_2)=0.18$ ,  $y(N_2)=0.82$ , dashdot-dot-dash line: Model II,  $y(CO_2)=0.48$ ,  $y(N_2)=0.52$ , long dashed line: Model II,  $y(CO_2)=0.78$ ,  $y(N_2)=0.22$ , dotted line: Model II,  $y(CO_2)=0.97$ ,  $y(N_2)=0.03$ . Binary interaction parameters in CPA were fitted only to two-phase equilibrium data and were not adjusted further in order to capture the hydrate dissociation pressure.

The model then chooses the result with the lowest dissociation pressure, hence the thermodynamically most stable structure is chosen.

The data by Kang *et al.* [25] are re-modeled with this new algorithm. The results obtained are shown in figures 13 to 16 where the structural transition points have been located and are indicated by clear tendency changes of the slopes on the calculated dissociation pressure curves.

The data shown in figures 13 to 16 represent the two-phase hydrate-vapor (HV) data of Kang *et al.* [25]. In order to model these data, a dew-point pressure type calculation is performed for a given temperature. This calculation gives the dissociation pressure and hydrate phase composition for a given vapor phase composition. It is possible to compare the Kang *et al.* [25] two-phase data (for example presented in figure 9) with the Kang *et al.* [25] three-phase hydrate-liquid-vapor (HLV) flash data (for example as presented in figure 7). We give a single example here: In figure 7, there is a three-phase data point for an initial  $CO_2$  concentration (loading) of 0.0663 at a temperature of 277 K, giving a pressure of 20.68 MPa. In figure 9, the same concentration and temperature give a similar (two-phase) pressure of 19.174 MPa. Since the  $CO_2$  loading (initial composition) in the  $P$ - $T$  diagram does not correspond exactly to the equilibrium  $CO_2$  composition (although it will be close), an exact comparison cannot be made between the HV and the HLV data.

Figures 13 and 14 illustrate how Model I gains accuracy in the calculated dissociation pressures, when using the thermodynamically consistent algorithm, while Model II loses accuracy. Model I predicts the structural transition point between sll hydrates and sl hydrates at an equilibrium vapor phase mole fraction of  $CO_2$  ranging from 0.11 to 0.15, depending on temperature. This

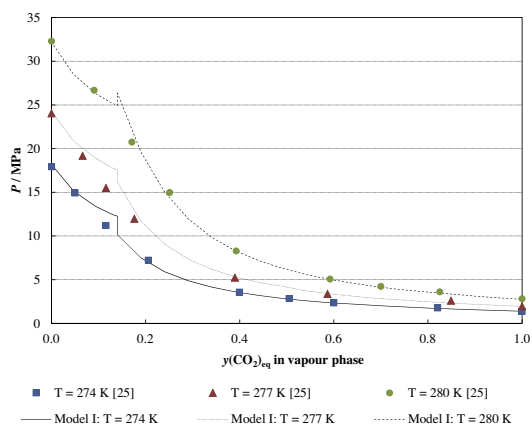


**FIGURE 9.** Dissociation pressures of mixed  $N_2/CO_2$  hydrates as a function of equilibrium vapor phase compositions at constant temperature using Model I. Comparison of experimental data by Kang *et al.* [25] and predicted results by Model I.  $y(CO_2)_{eq}$  denotes equilibrium vapor phase composition of  $CO_2$  after contact with the liquid phase. Vapor phases with  $CO_2$  mole fractions at or above 0.15 are modeled as sl hydrates. Vapor phases with  $CO_2$  mole fractions below 0.15 are modeled as sll hydrates. Squares: experimental data at  $T = 274$  K, triangles: experimental data at  $T = 277$  K, circles: experimental data at  $T = 280$  K. Solid line: Model I,  $T = 274$  K, dotted line: Model I,  $T = 277$  K, dashed line: Model I,  $T = 280$  K. The assumed structural transitions occur at an equilibrium vapor phase mole fraction of  $CO_2$  of approximately 0.14 and are seen as discontinuities in the predicted pressures. These results may be considered predictive, since the presented reference data have not been used in the parameter fitting. Note how the predictions of Model I at a temperature of 280 K seem to support the assumption regarding the position of the cutoff concentration between the two structures. From the illustrated modeling results for the lower temperatures it is difficult to tell the position of predicted cut-off concentration.

corresponds to vapor phase mole fractions of  $CO_2$  ranging from 0.12 to 0.16. The structure change is displaced to higher vapor phase concentrations with increasing temperature.

Model II behaves differently and predicts the transition point at equilibrium vapor phase fractions of  $CO_2$  ranging from approximately 0.001 to 0.02. In Model II, increasing temperature displaces the transition point to lower equilibrium vapor phase concentrations of  $CO_2$ .

Figures 15 and 16 illustrate the calculated hydrate phase compositions of  $CO_2$  using the thermodynamically consistent models. The changes when compared to the original algorithm are most obvious for Model II, which has increased accuracy in this kind of calculations.

With this knowledge, the mixed hydrate data utilized for the parameter fitting of Model II is re-modeled using the new algorithm. This is done in order to see the real performance of Model II. Model I results for these data remain unchanged, since this model predicts the structural transition point just above the vapor phase composition of the lower sll  $P/T$  curve.

The new results for Model II are illustrated in figure 17. Note that the vapor phase mole fractions of  $CO_2$  in figure 17 are initial compositions.

The two high pressure curves with initial vapor phase mole fractions of  $CO_2$  below 0.15 are now predicted to be sl hydrates and the predicted dissociation pressures are significantly lower than the reference data.

Comparing the two thermodynamically consistent models with all the data of Kang *et al.* [25], it appears that Model I is the most accurate model for the mixed  $N_2/CO_2$  hydrate systems.

In order to determine which of the models gives the most reliable predictions, three additional publications [26–28], presenting

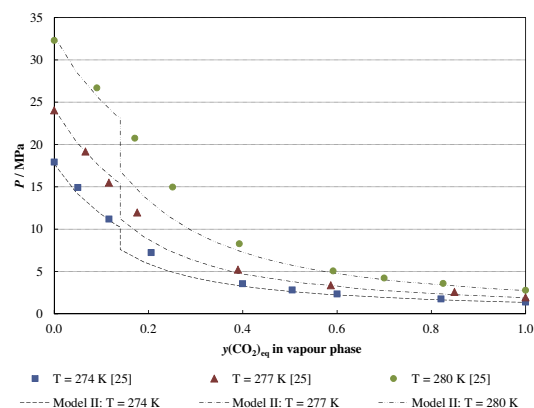


**FIGURE 10.** Dissociation pressures of mixed  $N_2/CO_2$  hydrates as a function of equilibrium vapor phase compositions at constant temperature using Model II. Comparison of experimental data by Kang *et al.* [25] and predicted results by Model II.  $y(CO_2)_{eq}$  denotes equilibrium vapor phase composition of  $CO_2$  after contact with the liquid phase. Vapor phases with  $CO_2$  mole fractions at or above 0.15 are modeled as sl hydrates. Vapor phases with  $CO_2$  mole fractions below 0.15 are modeled as sll hydrates. Squares: experimental data at  $T = 274$  K, triangles: experimental data at  $T = 277$  K, circles: experimental data at  $T = 280$  K. Dashed line: Model II,  $T = 274$  K, dash-dot-dash line: Model II,  $T = 277$  K, dash-dot-dot line: Model II,  $T = 280$  K. The assumed structural transitions occur at an equilibrium vapor phase mole fraction of  $CO_2$  of approximately 0.14 and are seen as discontinuities in the predicted pressures. These results may be considered predictive, since the presented reference data have not been used in the parameter fitting. Note how the predictions of Model II seem to undermine the assumption regarding the position of the cut-off concentration between the two structures for all temperatures. Model II seem to predict sl hydrates to be the most stable down to very low concentrations of  $CO_2$ . From the illustrated modeling results it is difficult to tell the precise position of predicted cut-off concentration.

experimental equilibrium data for mixed  $N_2/CO_2$  hydrate systems were considered.

Seo and Lee [26] present hydrate/vapor equilibrium data similar to Kang *et al.* [25]. However these data are measured below the ice point temperature of water. Hence this model is incapable of modeling these data.

Linga *et al.* [27] present three dissociation pressures at a temperature of 273.7 K for three initial vapor phase compositions. The two models of this work have been tested against these data. Results are provided in table 8. Figure 18 illustrates the results and compare the experimental data of Linga *et al.* [27] with those of Kang *et al.* [25].

$$AD = \frac{abs(p_i^{calc} - p_i^{exp})}{p_i^{exp}} \quad (36)$$

Average absolute deviations (equation (34)) of Model I and Model II, when compared to the three data points of Linga *et al.* [27], are 4.2% and 6.4% respectively. All the data are placed in the region, where both models predict sl to be the thermodynamically most stable structure. Thus no clear answer is obtained from these data. The data points of Linga *et al.* [27] correspond well with the data of Kang *et al.* [25], although in the case of Linga *et al.* [27] the data are reported as initial mole fraction of  $CO_2$ , since the equilibrium vapor phase compositions were not reported. This is not expected to result in large differences because of the low solubility of the gases in water.

Herri *et al.* [28] present phase equilibrium data from an experimental study of the mixed  $N_2/CO_2$  hydrate system. Both hydrate composition and dissociation pressures are reported for various temperatures and equilibrium vapor phase compositions. The data

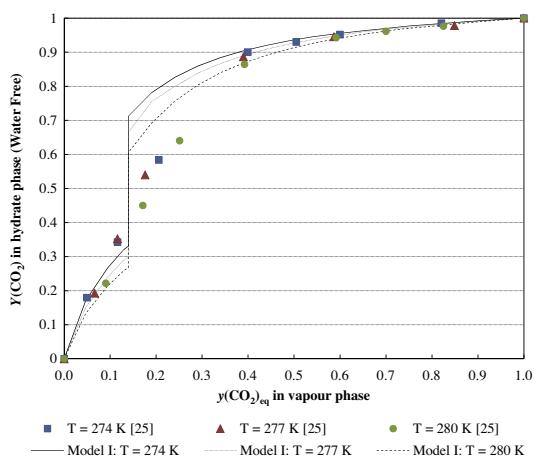


**FIGURE 11.** Mole fraction of  $\text{CO}_2$  in the mixed  $\text{N}_2/\text{CO}_2$  hydrates as a function of equilibrium vapor phase composition at constant temperature. Comparison of experimental data by Kang *et al.* [25] and predicted results by Model I.  $y(\text{CO}_2)_{\text{eq}}$  denotes equilibrium vapor phase composition of  $\text{CO}_2$  after contact with the liquid phase.  $Y(\text{CO}_2)$  denotes hydrate phase mole fraction of  $\text{CO}_2$  on a water free basis. All compositions are balanced with  $\text{N}_2$ . Vapor phases with  $\text{CO}_2$  mole fractions at or above 0.15 are modeled as sl hydrates. Vapor phases with  $\text{CO}_2$  mole fractions below 0.15 are modeled as sll hydrates. Squares: experimental data at  $T = 274$  K, triangles: experimental data at  $T = 277$  K, circles: experimental data at  $T = 280$  K. Solid line: Model I,  $T = 274$  K, dotted line: Model I,  $T = 277$  K, dashed line: Model I,  $T = 280$  K. The assumed structural transitions occur at an equilibrium vapor phase mole fraction of  $\text{CO}_2$  of approximately 0.14 and are seen as discontinuities in the predicted compositions.

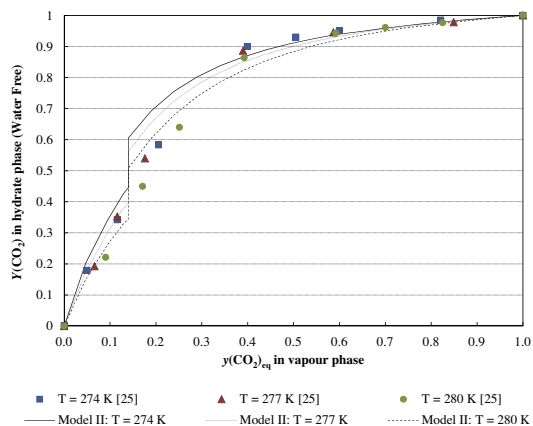


**FIGURE 12.** Mole fraction of  $\text{CO}_2$  in the mixed  $\text{N}_2/\text{CO}_2$  hydrates as a function of equilibrium vapor phase composition at constant temperature. Comparison of experimental data by Kang *et al.* [25] and predicted results by Model II.  $y(\text{CO}_2)_{\text{eq}}$  denotes equilibrium vapor phase composition of  $\text{CO}_2$  after contact with the liquid phase.  $Y(\text{CO}_2)$  denotes hydrate phase mole fraction of  $\text{CO}_2$  on a water free basis. All compositions are balanced with  $\text{N}_2$ . Vapor phases with  $\text{CO}_2$  mole fractions at or above 0.15 are modeled as sl hydrates. Vapor phases with  $\text{CO}_2$  mole fractions below 0.15 are modeled as sll hydrates. Squares: experimental data at  $T = 274$  K, triangles: experimental data at  $T = 277$  K, circles: experimental data at  $T = 280$  K. Solid line: Model II,  $T = 274$  K, dotted line: Model II,  $T = 277$  K, dashed line: Model II,  $T = 280$  K. The assumed structural transitions occur at an equilibrium vapor phase mole fraction of  $\text{CO}_2$  of approximately 0.14 and are seen as discontinuities in the predicted compositions.

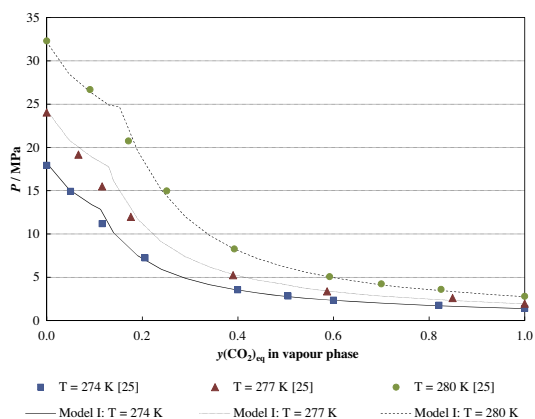


**FIGURE 13.** Dissociation pressures of mixed  $\text{N}_2/\text{CO}_2$  hydrates as a function of equilibrium vapor phase compositions at constant temperature using model I. Comparison of experimental data by Kang *et al.* [25] and predicted results by Model I.  $y(\text{CO}_2)_{\text{eq}}$  denotes equilibrium vapor phase composition of  $\text{CO}_2$  after contact with the liquid phase. Squares: experimental data at  $T = 274$  K, triangles: experimental data at  $T = 277$  K, circles: experimental data at  $T = 280$  K. Solid line: Model I,  $T = 274$  K, dotted line: Model I,  $T = 277$  K, dashed line: Model I,  $T = 280$  K. The predicted structural transitions occur at equilibrium vapor phase mole fractions of  $\text{CO}_2$  of approximately 0.11 to 0.15, depending on temperature. Phase transitions are seen as tendency changes in the predicted pressures.

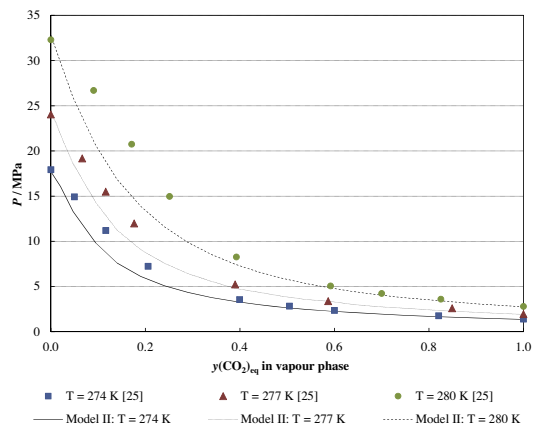


**FIGURE 14.** Dissociation pressures of mixed  $\text{N}_2/\text{CO}_2$  hydrates as a function of equilibrium vapor phase compositions at constant temperature using model II. Comparison of experimental data by Kang *et al.* [25] and predicted results by Model II.  $y(\text{CO}_2)_{\text{eq}}$  denotes equilibrium vapor phase composition of  $\text{CO}_2$  after contact with the liquid phase. Squares: experimental data at  $T = 274$  K, triangles: experimental data at  $T = 277$  K, circles: experimental data at  $T = 280$  K. Dashed line: Model II,  $T = 274$  K, dash-dot-dot line: Model II,  $T = 277$  K, dash-dot-dot-dot line: Model II,  $T = 280$  K. The predicted structural transitions occur at equilibrium vapor phase mole fractions of  $\text{CO}_2$  below 0.02.

have been modeled using the two models of this work. Results are compared with the data of Herri *et al.* [28] in tables 9 and 10.

Note that tables 9 and 10 present equilibrium pressure and equilibrium composition respectively from 16 experimental data sets. Model predictions are included for comparison.

It is clear from the results in tables 9 and 10 that Model II describes the experimental results of Herri *et al.* [28] with



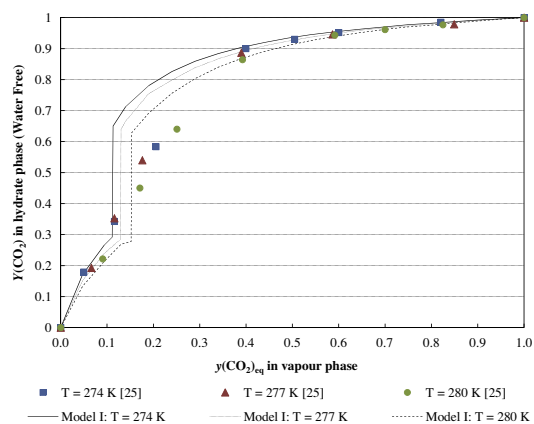


**FIGURE 15.** Mole fraction of CO<sub>2</sub> in the mixed N<sub>2</sub>/CO<sub>2</sub> hydrates as a function of equilibrium vapor phase composition at constant temperature. Comparison of experimental data by Kang *et al.* [25] and predicted results by Model I.  $y(\text{CO}_2)_{\text{eq}}$  denotes equilibrium vapor phase composition of CO<sub>2</sub> after contact with the liquid phase.  $Y(\text{CO}_2)$  denotes hydrate phase mole fraction of CO<sub>2</sub> on a water free basis. All compositions are balanced with N<sub>2</sub>. Squares: experimental data at  $T = 274$  K, triangles: experimental data at  $T = 277$  K, circles: experimental data at  $T = 280$  K. Solid line: Model I,  $T = 274$  K, dotted line: Model I,  $T = 277$  K, dashed line: Model I,  $T = 280$  K. The predicted structural transitions occur at equilibrium vapor phase mole fractions of CO<sub>2</sub> of approximately 0.11 to 0.15, depending on temperature. Phase transitions are seen as tendency discontinuities in the predicted compositions.

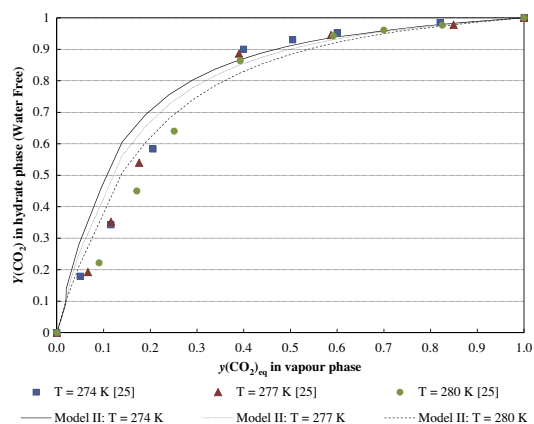


**FIGURE 16.** Mole fraction of CO<sub>2</sub> in the mixed N<sub>2</sub>/CO<sub>2</sub> hydrates as a function of equilibrium vapor phase composition at constant temperature. Comparison of experimental data by Kang *et al.* [25] and predicted results by Model II.  $y(\text{CO}_2)_{\text{eq}}$  denotes equilibrium vapor phase composition of CO<sub>2</sub> after contact with the liquid phase.  $Y(\text{CO}_2)$  denotes hydrate phase mole fraction of CO<sub>2</sub> on a water free basis. All compositions are balanced with N<sub>2</sub>. Squares: experimental data at  $T = 274$  K, triangles: experimental data at  $T = 277$  K, circles: experimental data at  $T = 280$  K. Solid line: Model II,  $T = 274$  K, dotted line: Model II,  $T = 277$  K, dashed line: Model II,  $T = 280$  K. The predicted structural transitions occur at equilibrium vapor phase mole fractions of CO<sub>2</sub> below 0.02.

significantly higher accuracy than Model I. Dissociation pressures and hydrate compositions of the 16 data sets are predicted with average absolute deviations of 14% and 4.3% respectively by Model II. Model I fails to describe the dissociation pressures measured by Herri *et al.* [28] and an average absolute deviation of 33% is

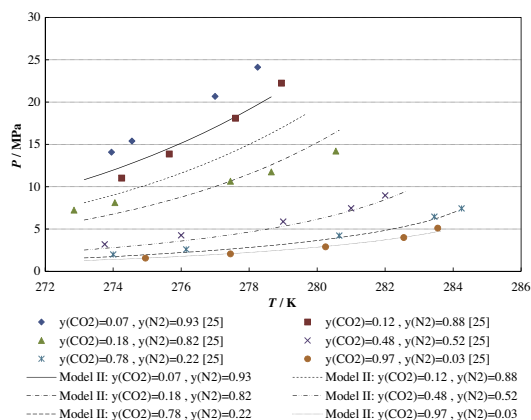


**FIGURE 17.** Dissociation pressures of mixed N<sub>2</sub>/CO<sub>2</sub> hydrates as a function of temperature for various vapor phase compositions. Comparison of experimental data by Kang *et al.* [25] and fitted modeling results for Model II.  $y(\text{CO}_2)$  and  $y(\text{N}_2)$  denotes vapor phase compositions of CO<sub>2</sub> and N<sub>2</sub> respectively. Diamonds: experimental data,  $y(\text{CO}_2) = 0.07$ ,  $y(\text{N}_2) = 0.93$ , squares: experimental data,  $y(\text{CO}_2) = 0.12$ ,  $y(\text{N}_2) = 0.88$ , triangles: experimental data,  $y(\text{CO}_2) = 0.18$ ,  $y(\text{N}_2) = 0.82$ , crosses: experimental data,  $y(\text{CO}_2) = 0.48$ ,  $y(\text{N}_2) = 0.52$ , crosses with line: experimental data,  $y(\text{CO}_2) = 0.78$ ,  $y(\text{N}_2) = 0.22$ , circles: experimental data,  $y(\text{CO}_2) = 0.97$ ,  $y(\text{N}_2) = 0.03$ . Solid line: Model II,  $y(\text{CO}_2) = 0.07$ ,  $y(\text{N}_2) = 0.93$ , short dashed line: Model II,  $y(\text{CO}_2) = 0.12$ ,  $y(\text{N}_2) = 0.88$ , dash-dot line: Model II,  $y(\text{CO}_2) = 0.18$ ,  $y(\text{N}_2) = 0.82$ , dash-dot-dot line: Model II,  $y(\text{CO}_2) = 0.48$ ,  $y(\text{N}_2) = 0.52$ , long dashed line: Model II,  $y(\text{CO}_2) = 0.78$ ,  $y(\text{N}_2) = 0.22$ , dotted line: Model II,  $y(\text{CO}_2) = 0.97$ ,  $y(\text{N}_2) = 0.03$ . Binary interaction parameters in CPA were fitted only to two-phase equilibrium data and were not adjusted further in order to capture the hydrate dissociation pressure. Cut-off concentration between sl and slI hydrates is predicted by Model II.

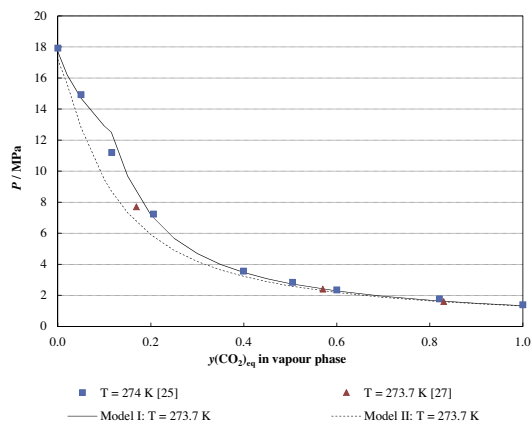


**FIGURE 18.** Dissociation pressures of mixed N<sub>2</sub>/CO<sub>2</sub> hydrates as a function of equilibrium vapor phase compositions at constant temperature. Comparison of experimental data by Linga *et al.* [27], Kang *et al.* [25] and predicted results by Model I and Model II.  $y(\text{CO}_2)_{\text{eq}}$  denotes equilibrium vapor phase composition of CO<sub>2</sub> after contact with the liquid phase. Squares: experimental data at  $T = 274$  K [25], triangles: experimental data at  $T = 273.7$  K [27]. Solid line: Model I,  $T = 273.7$  K, dashed line: Model II,  $T = 273.7$  K. Note that even though there is a small difference in the temperatures of the two reference data sets, their values seem to correspond. It should be noted that the data of Linga *et al.* [27] is initial composition of CO<sub>2</sub> (before loading), whereas the data of Kang *et al.* [25] (and the model results) represent the CO<sub>2</sub> composition in the vapor at equilibrium.

obtained. For the hydrate phase compositions, Model I obtains an average absolute deviation of 11%. All data are predicted as sl hydrates by both models. These predictions are confirmed by the

**TABLE 8**

Comparison of Model I and Model II predictions with data from Linga *et al.* [27].  $y(\text{CO}_2)$  denotes initial vapor phase mole fraction of  $\text{CO}_2$ . Initial vapor phase is balanced with  $\text{N}_2$  gas. Absolute deviation (AD) is defined in equation (36).

$T/\text{K}$	$y(\text{CO}_2)$	$P(\text{exp})/\text{MPa}$	$P/\text{MPa}$ Model I	AD Model I	$P/\text{MPa}$ Model II	AD Model II
273.7	0.17	7.70	8.57	0.11	6.71	0.13
273.7	0.57	2.40	2.40	0.00	2.28	0.05
273.7	0.83	1.60	1.62	0.01	1.58	0.01

**TABLE 9**

Comparison of Model I and Model II dissociation pressure predictions with data from Herri *et al.* [28].  $y(\text{CO}_2)_{\text{eq}}$  denotes equilibrium vapor phase mole fraction of  $\text{CO}_2$ . Vapor phase is balanced with  $\text{N}_2$  gas. Absolute deviation (AD) is defined in equation (36).

$T/\text{K}$	$y(\text{CO}_2)_{\text{eq}}$ Vapor	$P/\text{MPa}$ Exp	$P/\text{MPa}$ Model I	$P/\text{MPa}$ Model II	AD Model I	AD Model II
273.4	0.16	6.10	8.26	6.55	0.35	0.07
274.5	0.16	6.20	9.68	7.54	0.56	0.22
275.4	0.19	6.40	9.27	7.43	0.45	0.16
276.5	0.20	6.60	10.3	8.24	0.56	0.25
273.9	0.25	5.90	5.65	4.91	0.04	0.17
274.7	0.26	5.90	6.04	5.25	0.02	0.11
276.0	0.26	5.90	7.21	6.22	0.22	0.05
276.9	0.27	6.00	7.90	6.78	0.32	0.13
277.8	0.29	6.30	8.34	7.18	0.32	0.14
278.1	0.30	6.40	8.38	7.25	0.31	0.13
278.4	0.30	6.40	8.78	7.57	0.37	0.18
278.6	0.30	6.50	9.43	7.79	0.45	0.20
275.4	0.20	6.10	8.79	7.12	0.44	0.17
276.0	0.22	6.20	8.63	7.14	0.39	0.15
280.1	0.56	5.30	5.47	5.22	0.03	0.02
281.1	0.59	5.60	5.97	5.71	0.07	0.02

**TABLE 10**

Comparison of Model I and Model II hydrate phase composition predictions with data from Herri *et al.* [28].  $y(\text{CO}_2)_{\text{eq}}$  denotes equilibrium vapor phase mole fraction of  $\text{CO}_2$ . Vapor phase is balanced with  $\text{N}_2$  gas.  $Y(\text{CO}_2)$  denotes hydrate phase mole fraction of  $\text{CO}_2$  on a water free basis. Absolute Deviation (AD) is defined in equation (36).

$T/\text{K}$	$y(\text{CO}_2)_{\text{eq}}$ Vapor	$Y(\text{CO}_2)$ Hydrate	$Y(\text{CO}_2)$ Model I	$Y(\text{CO}_2)$ Model II	AD Model I	AD Model II
273.4	0.16	0.66	0.73	0.62	0.11	0.06
274.5	0.16	0.66	0.72	0.60	0.09	0.09
275.4	0.19	0.66	0.74	0.64	0.12	0.03
276.5	0.20	0.58	0.73	0.63	0.26	0.09
273.9	0.25	0.75	0.80	0.74	0.07	0.01
274.7	0.26	0.73	0.80	0.74	0.10	0.01
276.0	0.26	0.70	0.78	0.72	0.11	0.03
276.9	0.27	0.70	0.78	0.71	0.11	0.01
277.8	0.29	0.67	0.78	0.72	0.16	0.07
278.1	0.30	0.69	0.78	0.72	0.13	0.04
278.4	0.30	0.72	0.77	0.71	0.07	0.01
278.6	0.30	0.70	0.76	0.71	0.09	0.01
275.4	0.20	0.67	0.74	0.65	0.10	0.03
276.0	0.22	0.65	0.75	0.67	0.15	0.03
280.1	0.56	0.85	0.82	0.81	0.04	0.05
281.1	0.59	0.82	0.81	0.78	0.01	0.05

observations of Herri *et al.* [28]. It should be noted that Herri *et al.* [28] conclude that their experimental data differ from those data found elsewhere in literature, especially with respect to hydrate composition. Hence it is expected that the two models performances change when comparing with these reference data.

If all the experimental hydrate data found in literature are considered, it is not possible to determine which of the two models is more reliable in general, when it comes to the predicted hydrate structure transition. However Model I confirms the conclusions made by Kang *et al.* [25].

A more recent attempt to determine the structure of mixed  $\text{N}_2/\text{CO}_2$  hydrates, presented by Seo and Lee [26], concludes that sl hydrates are formed as soon as the vapor phase mole fraction of  $\text{CO}_2$  exceeds 0.01. Below this concentration, sII hydrates are formed. Seo and Lee [26] performed X-ray diffraction and  $^{13}\text{C}$  NMR measurements on the mixed hydrates in order to determine the structure of the mixed hydrates. Their conclusions confirm the predictions by Model II.

The above results indicate that more experimental data on mixed hydrate equilibrium pressures and compositions are needed. Especially the low  $\text{CO}_2$  concentration region needs to be more thoroughly investigated, in order to determine the hydrate structure formed under these conditions.

Assumptions regarding structures play an important role in the process of fitting parameters in the van der Waals–Platteeuw model. For the case of mixed  $\text{N}_2/\text{CO}_2$  hydrates, the two models of this work could be re-fitted under the assumption that sl hydrates are formed from all vapor phase mixtures with more than one mole percent of  $\text{CO}_2$ . Here it would be interesting to see how the predicted structure transitions would be affected in the two cases. This has however not been done as a part of this work.

#### 4. Conclusions

Two thermodynamic models capable of describing dissociation pressures of mixed gas clathrate hydrates formed from ternary mixtures of  $\text{CO}_2$ ,  $\text{N}_2$  and liquid water, have been set up. Both models utilized the Cubic-Plus-Association (CPA) equation of state for the thermodynamic description of the non-solid phases (vapor and liquid). The solid hydrate phase was described by the van der Waals–Platteeuw model as presented by Parrish and Prausnitz.

The two models differed only in their method for describing the Langmuir adsorption coefficients in the van der Waals–Platteeuw model.

The two models were validated against available hydrate equilibrium pressure and composition data found in literature. Data from three publications were utilized.

When allowing the two models to predict the structural phase transition of the mixed hydrates, Model I predicted a hydrate structure transition from structure II hydrates at vapor phase mole fractions of  $\text{CO}_2$  below 0.12 to 0.16 to structure I hydrates at mole fraction of  $\text{CO}_2$  above this range. The exact transition concentration was shown to increase with increasing temperature. Model II predicted structure I hydrates to be stable in concentrations down to vapor phase mole fractions of  $\text{CO}_2$  in the order of 0.001 to 0.02, depending on temperature. Model II predicted the transition concentration to lower with increasing temperature.

Due to a large diversity in the literature data found for this system, it was not possible to determine, which of the two models perform better. Model I exceeded the performance of Model II when comparing the two model predictions against equilibrium data presented by Kang *et al.* [25] and Linga *et al.* [27], whereas Model II by far performed better when comparing to the data presented by Herri *et al.* [28]. This may be explained by the fact that the reference data of Herri *et al.* [28] differ from the data of Kang and Linga. Finally, the importance of knowing the structure of the formed hydrates when fitting parameters in the van der Waals–Platteeuw models was emphasized.

#### Acknowledgements

This work was supported by the European iCap project (EU FP7) and the Department of Chemical and Biochemical Engineering (MP2T) at the Technical University of Denmark.



## References

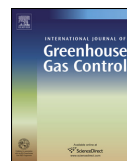
- [1] A.K. Sum, C.A. Koh, E.D. Sloan, *Ind. Eng. Chem. Res.* 48 (2009) 7457–7465.
- [2] C.A. Koh, A.K. Sum, E.D. Sloan, *J. Appl. Phys.* 106 (2009) 061101.
- [3] J.C. Platteeuw, J.H. van der Waals, *Mol. Phys.* 1 (1) (1958) 91–95.
- [4] G.M. Kontogeorgis, E.C. Voutsas, I.V. Yakoumis, D.P. Tassios, *Ind. Eng. Chem. Res.* 35 (1996) 4310–4318.
- [5] G.M. Kontogeorgis, M.L. Michelsen, G.K. Folas, S. Derawi, N. von Solms, E.H. Stenby, *Ind. Eng. Chem. Res.* 45 (2006) 4855–4868.
- [6] G.M. Kontogeorgis, I.V. Yakoumis, H. Meijer, E. Hendriks, T. Moorwood, *Fluid Phase Equilib.* 158–160 (1999) 201–209.
- [7] W.R. Parrish, J.M. Prausnitz, *Ind. Eng. Chem. Process Des. Develop.* 11 (1) (1972) 26–35.
- [8] V. McKoy, O. Sinanoglu, *J. Chem. Phys.* 38 (12) (1963) 2946–2956.
- [9] M.M. Mooijer-van den Heuvel, C.J. Peters, J. de Swaan Arons, *Fluid Phase Equilib.* 172 (2000) 73–91.
- [10] M.L. Michelsen, J.M. Møllerup, *Thermodynamic Models: Fundamentals & Computational Aspects*, second ed., Tie-Line Publications, Denmark, 2007.
- [11] S.H. Huang, M. Radosz, *Ind. Eng. Chem. Res.* 29 (11) (1990) 2284–2294.
- [12] DIPPR, Design Institute for Physical Properties, Diadem 801, 2011.
- [13] J. Munck, S. Skjold-Jørgensen, P. Rasmussen, *Chem. Eng. Sc.* 43 (10) (1988) 2661–2672.
- [14] E.D. Sloan, C.A. Koh, *Clathrate Hydrates of Natural Gases*, third ed., CRC Press, Boca Raton, 2008.
- [15] Y.D. Zelvenskii, *J. Chem. Ind.* 14 (1937) 1250–1257.
- [16] P.B. Stewart, P. Munjal, *J. Chem. Eng. Data* 15 (1970) 67–71.
- [17] E. Bartholomé, H. Friz, *Chem. Ing. Tech.* 28 (1956) 706–708.
- [18] H.S. Harned, R. Davis, *J. Am. Chem. Soc.* 65 (1943) 2030–2037.
- [19] R. Sun, W. Hu, Z. Duan, *J. Sol. Chem.* 30 (6) (2001) 561–673.
- [20] R. Wiebe, V.L. Gaddy, C. Heins Jr., *Ind. Eng. Chem.* 24 (1932) 927.
- [21] J. Jhaveri, D.B. Robinson, *Can. J. Chem. Eng.* 43 (2) (1965) 75–78.
- [22] A. Van Cleeff, G.A.M. Diepen, *Recl. Trav. Chim. Pay. B* 79 (5) (1960) 582–586.
- [23] K.M. Sabil, G.-J. Witkamp, C.J. Peters, *J. Chem. Thermodyn.* 42 (2010) 8–16.
- [24] L. Ruffine, J.P.M. Trusler, *J. Chem. Thermodyn.* 42 (2010) 605–611.
- [25] S.-P. Kang, H. Lee, C.-S. Lee, W.-M. Sung, *Fluid Phase Equilib.* 185 (2001) 101–109.
- [26] Y.-T. Seo, H. Lee, *J. Phys. Chem. B* 108 (2004) 530–534.
- [27] P. Linga, R. Kumar, P. Englezos, *J. Hazard. Mater.* 149 (2007) 625–629.
- [28] J.-M. Herri, A. Bouchemoua, M. Kwaterski, A. Fezoua, Y. Ouabbas, A. Cameirao, *Fluid Phase Equilib.* 301 (2011) 171–190.

JCT -11-432



## Appendix 2





# Thermodynamic promotion of carbon dioxide–clathrate hydrate formation by tetrahydrofuran, cyclopentane and their mixtures

Peter Jørgensen Herslund<sup>a</sup>, Kaj Thomsen<sup>a</sup>, Jens Abildskov<sup>b</sup>, Nicolas von Solms<sup>a,\*</sup>, Aurélie Galfré<sup>c</sup>, Pedro Brântuas<sup>c</sup>, Matthias Kwaterski<sup>c</sup>, Jean-Michel Herri<sup>c</sup>

<sup>a</sup> Department of Chemical and Biochemical Engineering, Center for Energy Resources Engineering (CERE), Technical University of Denmark, Kgs. Lyngby DK2800, Denmark

<sup>b</sup> Department of Chemical and Biochemical Engineering, Computer Aided Process Engineering Center (CAPEC), Technical University of Denmark, Kgs. Lyngby DK2800, Denmark

<sup>c</sup> Ecole Nationale Supérieure des Mines de St-Etienne, 158 Cours Fauriel, 42023 St-Etienne, France

## ARTICLE INFO

### Article history:

Received 10 December 2012

Received in revised form 21 May 2013

Accepted 24 May 2013

### Keywords:

Gas hydrates

Carbon dioxide capture

Tetrahydrofuran

Cyclopentane

Thermodynamic promoter

## ABSTRACT

Gas clathrate hydrate dissociation pressures are reported for mixtures of carbon dioxide, water and thermodynamic promoters forming structure II hydrates.

Hydrate (H)–aqueous liquid ( $L_w$ )–vapour (V) equilibrium pressures for the ternary system composed of water, tetrahydrofuran (THF), and carbon dioxide ( $CO_2$ ), with 5.0 mole percent THF in the initial aqueous phase, are presented in the temperature range from 283.3 K to 285.2 K. At 283.3 K, the three-phase equilibrium pressure is determined to be 0.61 MPa (absolute pressure).

Four-phase hydrate (H)–aqueous liquid ( $L_w$ )–organic liquid ( $L_o$ )–vapour (V) equilibrium data are presented for the ternary system of water–cyclopentane–carbon dioxide at temperatures ranging from 285.2 K down to 275.5 K.

New four-phase H– $L_w$ – $L_o$ –V equilibrium data for the quaternary system water–THF–cyclopentane–carbon dioxide are presented in the temperature range from 275.1 K to 286.6 K. It is shown that upon adding THF to the pure aqueous phase to form a 4 mass percent solution, the equilibrium pressure of the formed hydrates may be lowered compared to the ternary system of water, cyclopentane and carbon dioxide.

© 2013 Elsevier Ltd. All rights reserved.

## 1. Introduction

Gas clathrate hydrates, more commonly known as gas hydrates, are solid solutions of small guest molecules physically adsorbed into cavities formed by hydrogen bonded water clusters. These solid compounds form when the constituents come into contact at conditions of low temperature and/or high pressure (Sloan, 2003). Temperature and pressure conditions, at which the hydrates form, depend on the physical and chemical properties of the guest molecule, assuming that the water phase is pure. Impurities or additives dissolved in the aqueous phase may also affect the gas hydrate equilibrium conditions as well as the formation kinetics.

Gas hydrates are often referred to as non-stoichiometric solid inclusion bodies, where water (host) forms a lattice by hydrogen bonding (Koh et al., 2009; Sloan, 2003; Sum et al., 2009). The lattice formation generates a number of empty cavities, in which small molecules (guests) may be encapsulated. Several structures are

known, the most common being structures sI, sII and sH. The pure, empty hydrate water lattice itself is a thermodynamically unstable structure, and it is the interactions between water and guest molecules stabilise the lattice structure (Sum et al., 2009).

### 1.1. Gas hydrate formation with thermodynamic promotion

When the occurrence of gas hydrates in the petroleum industry was discovered, an increased effort was made to map their structures and to find ways of avoiding their formation in oil and gas pipelines.

Recently, gas hydrates have received new interest due to their relatively high gas/energy density. Whereas most previous efforts were directed towards looking for ways to avoid hydrate formation (hydrate inhibition), the focus is now also on finding ways to promote their formation at moderate temperatures and pressures (hydrate promotion). Sun et al. (2011) and Eslamimanesh et al. (2012) have reviewed recent advances in gas hydrate research including applications of promoted gas hydrate formation in processes for methane/natural gas storage, fuel gas (hydrogen) storage and gas separation (e.g. carbon dioxide capture).

\* Corresponding author. Tel.: +45 4525 2867; fax: +45 4588 2258.

E-mail address: [nvs@kt.dtu.dk](mailto:nvs@kt.dtu.dk) (N. von Solms).

## 1.2. Thermodynamic gas hydrate promoters

A thermodynamic promoter is here defined as a component that participates actively in the hydrate formation process and readily enters the hydrate structure at higher temperature and lower pressure than in the unpromoted hydrate.

Whereas the mechanism for thermodynamic inhibition of hydrate formation is a consequence of a change in water activity due to hydrogen bonding between hydrate inhibitors (mainly methanol, monoethylene glycol or diethylene glycol) and water, thermodynamic promotion of gas hydrates is a consequence of the active formation of mixed promoter/gas hydrates under moderate conditions of temperature and pressure. The hydrates formed in that way then serve as a storage medium for gas-like components but may also contain significant amounts of the added promoter.

In this work, only hydrate promoters forming classical hydrate structures (mainly sII and sH, where the promoter molecules partly enter the appropriately sized cavities), have been considered. Hydrate promoters such as the tetra-*n*-butyl ammonium halides (TBAB, TBACl, TBAF etc.) which form semi-clathrates, where the promoter actively takes part in the formation of the lattice structure of water molecules, have not been considered.

Over the years many heavy hydrocarbon compounds have been investigated for their ability to form gas hydrates in the presence of small gas molecules. A summary including hydrate dissociation pressure data for most of the binary methane-/heavy hydrocarbon-based hydrate systems (mainly sH forming systems) investigated was presented by Sloan and Koh (2008). Most of these heavy hydrocarbons are – due to their hydrophobic characteristics – only partially miscible with water, giving rise to liquid–liquid phase separation. Hence, the experimental data represent hydrate (H)–aqueous liquid ( $L_w$ )–organic liquid ( $L_a$ )–vapour (V) four-phase equilibria.

Several hydrophilic, organic compounds are also known for forming hydrates at moderate temperatures and pressures. Saito et al. (1996) investigated the possibility of storing natural gas in the form of hydrates by using either tetrahydrofuran (THF) or acetone to lower the equilibrium pressure of the mixed hydrates. They showed how the three-phase H– $L_w$ –V equilibrium pressure depends on the promoter concentration in the liquid phase co-existing with the hydrate phase. A minimum in the observed hydrate dissociation pressures was detected at a promoter concentration in the aqueous liquid phase of approximately 5 mole percent, close to the stoichiometric concentration of the sII hydrate structure with complete occupation of the large cavity by the promoter molecules.

De Deugd et al. (2001) compared the promoting effect of three water-soluble hydrate formers constituting mixed hydrates with methane. The three hydrate formers were THF, 1,3-dioxolane and tetrahydropyran. From their results, De Deugd et al. concluded that five sided cyclo-ether structures (THF) are more efficient sII hydrate stabilisers than six sided cyclo-ether structures (tetrahydropyran). Furthermore, they inferred from their data that one oxygen atom in the five sided ring structure (THF) stabilises the sII hydrate better than five sided ring structures with two oxygen atoms (1,3-dioxolane). De Deugd et al. explained these findings by the differences in physical size and polarity of the three compounds and suggested cyclopentane as a possible promoter for the formation of sII hydrate. Tohidi et al. (1997) had already shown this by measuring the promoting effect on the dissociation pressures of methane or nitrogen hydrates by adding cyclopentane to binary systems of water and gas.

Ohmura et al. (2005) measured hydrate dissociation pressures for two methyl-substituted cyclic ethers (2-methyltetrahydrofuran and 3-methyltetrahydropyran) with methane. These ethers were soluble in water to some extent, but not fully miscible with water,

like THF. Even though these methyl-substituted cyclic ethers were more interesting promoters for hydrate-based gas storage applications from an environmental impact point of view, they were unfortunately less efficient hydrate promoters in comparison with their non-substituted counterparts.

Tsuji et al. (2004) showed the importance of water solubility in order to obtain high formation rates of hydrates. They measured formation rates of mixed promoter/methane hydrates by spraying an aqueous phase into a methane gas phase at constant pressure. It was concluded that the gas uptake into the sH hydrate phase was promoter dependent but they also found that, in their process configuration, the largest gas uptakes were generally obtained in systems with high promoter concentrations in the aqueous phase.

In this work the specific case of capturing carbon dioxide ( $\text{CO}_2$ ) using thermodynamically promoted gas hydrate formation is investigated. The two hydrate promoters, cyclopentane and THF were chosen for the study. They differ in their fluid phase behaviour in aqueous systems, but have similar properties in the hydrate phase. THF appears to be the most efficient of the known water-soluble sII hydrate promoters and cyclopentane appears to be the most efficient of all known sII hydrate promoters. Hence, THF and cyclopentane are the hydrate promoters selected in this work.

### 1.2.1. Tetrahydrofuran—A hydrophilic hydrate promoter

Tetrahydrofuran is a five-sided cyclic ether structure that has received much attention in the literature not only due to its properties as an organic solvent, but also due to the fact that it forms structure II hydrates with water. At ambient conditions, THF and water are completely miscible in the liquid state, i.e., upon mixing THF and water, homogeneous liquid mixtures are formed over the whole composition range. However, closed loop miscibility gaps (liquid–liquid phase splits) have been observed at temperatures above 345 K and slightly elevated pressures (Riesco and Trusler, 2005).

Several publications are available in the literature, presenting THF as a possible promoter in pre- (Lee et al., 2010; Linga et al., 2007a, 2007b; Zhang et al., 2009) or post combustion (Giavarini et al., 2010; Kang and Lee, 2000; Kang et al., 2001; Linga et al., 2007b, 2008, 2010) hydrate-based  $\text{CO}_2$  capture processes. However, only a few publications provide detailed phase equilibrium data for the ternary system of water, THF, and  $\text{CO}_2$ , especially at low temperatures and THF concentrations of approximately 17.4 mass percent (5 mole percent) in the aqueous phase (Delahaye et al., 2006; Sabili et al., 2010; Seo et al., 2008). Such data can provide information on the true ability of THF promoted sII hydrates to incorporate sufficient amounts of  $\text{CO}_2$  in order to establish a feasible capture process operating at temperatures close to the freezing point of water.

In separation attempts applied to gas mixtures containing  $\text{CO}_2$  and nitrogen, one of the main conclusions was that the selectivity of  $\text{CO}_2$  over  $\text{N}_2$  in the hydrate phase is lowered by the presence of THF compared to the non-promoted systems (Kang and Lee, 2000). The highest  $\text{CO}_2$  selectivities were obtained when operating at low temperatures. Hence it is of interest to investigate how binary hydrate systems of THF and  $\text{CO}_2$  behave in the low temperature region, not only with respect to the inclusion of  $\text{CO}_2$  in the solid phase but also with respect to the pressure requirements needed to form mixed hydrates at these conditions.

Delahaye et al. (2006) measured hydrate dissociation  $P$ – $T$  conditions as well as heats of dissociation for the ternary system of water, THF and  $\text{CO}_2$ . In addition, the  $T$ – $x$  diagram for the binary sub-system of water and THF was experimentally determined at atmospheric pressure for reference and for modelling purposes. In the binary system {water+THF}, the melting point (dissociation temperature) of the THF sII hydrate formed from a 19.17 mass percent (approximately 5.9 mole percent) THF aqueous solution was determined to be 277.9 K.

Delahaye et al. presented mixed THF–CO<sub>2</sub> hydrate dissociation pressures for systems of three THF mass fractions in the liquid phase ranging from 0.06 to 0.11 (approximately 1.6 to 3.0 mole percent). Dissociation pressures of the mixed THF/CO<sub>2</sub> hydrate were shown to decrease with increasing THF concentration.

Likewise, Seo et al. (2008) presented hydrate dissociation pressure data for the ternary system {water+THF+CO<sub>2</sub>} with four different THF mass fractions in the aqueous phase ranging from 0.034 to 0.174 (approximately 1 to 5 mole percent). Their data proved that the hydrate dissociation pressure decreases with increasing THF concentration in the aqueous phase, up to a concentration of 5 mole percent THF. However, their results also showed that increasing THF concentration in the aqueous solution from 3 to 5 mole percent provided only a small additional promoting effect on the dissociation pressure of the mixed THF–CO<sub>2</sub> hydrate system.

Sabil et al. (2010) provided detailed *P–T* phase diagrams for the ternary system of water, THF, and CO<sub>2</sub> at seven different compositions, all with THF mass fractions of 0.174 (5 mole percent) in the initial aqueous solution. Hence, Sabil et al. varied only the initial CO<sub>2</sub> gas to liquid ratio. Sabil et al. measured H–L<sub>w</sub>–V three-phase equilibrium pressures at temperatures down to approximately 285 K. It was concluded that the H–L<sub>w</sub>–V equilibrium curve was (within the experimental accuracy) independent of the amount of CO<sub>2</sub> in the system and thus mainly depended on the THF concentration in the aqueous phase. The upper quadruple point (point at H–L<sub>w</sub>–L<sub>g</sub>–V four-phase equilibrium, where L<sub>g</sub> stands for the liquefied gas phase, i.e., the liquid phase being rich in CO<sub>2</sub>) did however depend on the overall composition, and hence, the hydrate (H)–aqueous liquid (L<sub>w</sub>)–liquefied gas (L<sub>g</sub>) equilibrium line was shifted towards higher temperatures with increasing overall CO<sub>2</sub> concentrations. Sabil et al. discovered a four-phase equilibrium region in some systems with three fluid phases (two liquids and one vapour) and one solid phase. Generally, these scenarios were found at temperatures above 290 K and pressures above 2.0 MPa. At overall CO<sub>2</sub> concentrations of 19 and 29 mole percent, a pseudo-retrograde behaviour in the measured hydrate equilibrium pressure was observed in this four-phase region. Here an increase in pressure could both lower and increase the four-phase equilibrium temperature. For example at 19 mole percent CO<sub>2</sub> (overall), the four-phase H–L<sub>w</sub>–L<sub>g</sub>–V equilibrium temperature at *P* = 2.7 MPa was determined at 290.8 K. This temperature increased to 291.3 K at a pressure of 3.6 MPa. Increasing the pressure further to 4.2 MPa then lowered the four-phase equilibrium temperature to 290.7 K.

### 1.2.2. Cyclopentane—A hydrophobic hydrate promoter

Cyclopentane is a cycloalkane and thus a hydrophobic compound. Therefore, due to its molecular characteristics, it is almost insoluble in liquid water over wide ranges of state conditions. For example, at ambient temperature and pressure, the binary system {water+cyclopentane} exhibits liquid–liquid phase separation into a water-rich and a cyclopentane-rich liquid phase, respectively, over a wide interval of composition. Fan et al. (2001) were the first to experimentally document the occurrence of pure sII cyclopentane hydrates, formed without the simultaneous presence of small gas molecules. Hydrates were formed at pressures below the dew point pressure of cyclopentane in the temperature interval examined. The quadruple point at which additionally a cyclopentane-rich liquid phase (L<sub>a</sub>) coexists with the three phases H, L<sub>w</sub>, and V, was determined at a temperature of 280.2 K and a pressure of 0.0198 MPa. At a temperature of 273.4 K, the hydrate–liquid water–vapour equilibrium pressure of the pure cyclopentane sII hydrate was measured at 0.0069 MPa.

Recently, Trueba et al. (2011) measured hydrate (H)–aqueous liquid (L<sub>w</sub>)–cyclopentane-rich liquid (L<sub>a</sub>) phase equilibrium pressures for the binary {water+cyclopentane} system at high pressures. Trueba et al. found that the hydrate dissociation

temperature for this univariant three-phase equilibrium was almost independent of pressure due to the low compressibility of the two fluid phases and the one solid phase. At a pressure of 2.55 MPa the corresponding hydrate dissociation temperature was 279.9 K. Increasing the pressure to 12.55 MPa increased the dissociation temperature by only 0.09 K.

The ternary system {water+cyclopentane+CO<sub>2</sub>} was investigated by Zhang and Lee (2009a, b) in the sII mixed hydrate stability region. Four-phase (hydrate–liquid water–organic liquid–vapour) equilibrium pressures were determined in the temperature interval from 286.7 K to 292.6 K. The hydrate dissociation pressures varied from 0.89 MPa to 3.15 MPa at the low and high temperatures respectively.

Mohammadi and Richon (2009) presented similar data from the ternary system of water, cyclopentane, and CO<sub>2</sub> in the temperature interval from 284.3 K to 291.8 K. Their data corresponded well with the pressures measured by Zhang and Lee (2009a, b). However, Mohammadi and Richon extended the low end of the temperature interval compared to Zhang and Lee by approximately 2 K. At 284.3 K, Mohammadi and Richon determined the mixed hydrate equilibrium pressure at 0.35 MPa. Neither Zhang and Lee (2009a, b) nor Mohammadi and Richon (2009) commented on the CO<sub>2</sub> gas uptake in the hydrate phase during their experiments.

Li et al. (2010) studied the capture of CO<sub>2</sub> from simulated power plant flue gases (16.6 mole percent CO<sub>2</sub>, 83.4 mole percent N<sub>2</sub>) in the quaternary system {water+cyclopentane+N<sub>2</sub>+CO<sub>2</sub>} and in the corresponding modified system with an oil/water emulsifier (Tween 80) added to it. The focus in their study was on the hydrate formation rates and the selectivity of CO<sub>2</sub> in the hydrate phase. It was shown that upon adding an emulsifier, the crystallisation rate was increased dramatically. However, a negative effect on CO<sub>2</sub> selectivity caused by the addition of the emulsifier was also reported.

Galfré et al. (2011) reported findings similar to those presented by Li et al. (2010), only here pure CO<sub>2</sub> gas phases and another emulsifier (IPE 202) were utilised. Gas hydrates were formed in the ternary system {water+cyclopentane+CO<sub>2</sub>} at pressures below 0.2 MPa at temperatures above 280 K.

Karanjkar et al. (2012) performed a kinetic study on the cyclopentane sII hydrate formation from emulsified mixtures with water (water droplets in oil). Karanjkar et al. found that in their system hydrate formation was primarily an interfacial phenomenon taking place between the fluid phases present. Hydrate crystals formed rapidly on the water droplet surface and additionally, in the absence of surfactants, a shell was quickly formed by agglomerated hydrate particles. Hence the transport of hydrate former into the remaining water quickly became limited by the hydrate shell.

In a recent kinetic study combined with morphological observations, Lim et al. (2013) showed that the presence of cyclopentane enhances hydrate formation kinetics and results in higher gas uptake for CO<sub>2</sub> capture.

Aman et al. (2013) studied the effect of interfacial tension and adsorption on formation of cyclopentane hydrates.

### 1.3. Mixed promoter systems

Few studies of mixed promoter systems have been presented in the literature. Li et al. (2011) and Li et al. (2012) presented CO<sub>2</sub> capture from fuel gases (gas mixtures of carbon dioxide and hydrogen) by hydrate formation in systems containing both tetra-*n*-butyl ammonium bromide (TBAB) and cyclopentane. The focus in their work was on improving the gas uptake and CO<sub>2</sub> selectivity in the hydrate phase(s) as well as shortening the induction times compared to the single promoter systems. Li et al. (2011) showed enhanced gas uptakes compared to known promoter systems at similar conditions and induction times as short as 15 s. Li

et al. (2012) claimed that a synergetic effect may occur, whereby cyclopentane does not only form sII hydrates but also takes part in the semi-clathrate hydrate structure and displaces some of the TBA<sup>+</sup> molecules allowing for the formation of larger amounts of semi-clathrate hydrate. The reported selectivities of CO<sub>2</sub> over hydrogen were as large as 91.6 mole percent in the mixed hydrate phase for gas mixtures containing 38.6 mole percent carbon dioxide initially (Li et al., 2012).

#### 1.4. Purpose of this work

It is the purpose of this work to investigate the thermodynamic effect of two hydrate promoters, THF and cyclopentane, on the dissociation pressures of CO<sub>2</sub> hydrates. THF was chosen as the model for a water-soluble hydrate former, since it is reasonably well-studied and easy to obtain for laboratory studies. For possible industrial applications less toxic alternatives would likely be considered. Mixed CO<sub>2</sub>/promoter hydrate dissociation pressures in the low temperature region are determined individually for the two promoter systems as well as a third mixed promoter system containing both promoters together. The qualitative behaviour of the systems with regard to the CO<sub>2</sub> uptake in the hydrate phase is discussed, although no hydrate composition data have been determined in the framework of this investigation.

When working with promoters that are essentially insoluble in the aqueous liquid phase, proper mixing of the fluid and solid phases is vital in order to arrive at reliable equilibrium conditions. Insufficient mixing may result in the formation of complex multi-phase systems which appear to be in thermodynamic equilibrium, but which more likely constitute unequilibrated phases that are kinetically limited by mass transfer through the solid phase formed.

## 2. Experimental

The experimental part of this work was carried out in three high-pressure equilibrium cells, named C1, C2 and C3 in the following sections. The basic principles behind each set-up are identical for the three cells. Some differences in the set-ups are noted where relevant. A schematic and a detailed description of the experimental set-up (equilibrium cell C2) are provided elsewhere (Herri et al., 2011).

#### 2.1. Experimental procedure

Hydrate equilibrium data are obtained by performing an isochoric temperature cycle manipulation of the two- or three-phase fluid mixtures inside the batch reactors. A detailed description of the experimental procedure used in this work is provided elsewhere (Herri et al., 2011). Once hydrate forms and the system equilibrates, three phases, a hydrate (H), an aqueous liquid (L<sub>w</sub>), and a vapour (V) phase will typically be present in the case of promoters being miscible with water over the whole composition range. In the case of hydrophobic promoters which, upon mixing with water, exhibit liquid–liquid phase-separation over more or less extended composition ranges, four phases (hydrate (H)–aqueous liquid (L<sub>w</sub>)–organic liquid (L<sub>o</sub>)–vapour (V)) will usually be present in equilibrium under hydrate forming conditions. According to the Gibbs phase rule, the number of degrees of freedom (*F*)<sup>1</sup> for a simple

<sup>1</sup> The number of degrees of freedom *F* is the number of intensive properties such as e.g. temperature, pressure, or phase composition variables, that, without changing the number of phases, are capable of independent variation.

**Table 1**  
Chemicals utilised in this work.

Component	Supplier	Purity grade
Water	Milli-Q Plus 185	Organic content <5 ppb Salinity: conductivity of $\sigma = 0.055 \mu\text{S}/\text{cm}$ >99.9% (anhydrous) Stabilised with 250 ppm butylhydroxytoluene (BHT)
Tetrahydrofuran	Sigma-Aldrich	>95%
Cyclopentane	Chimie Plus Laboratoires	>95%
Carbon dioxide	Air Liquide	C <sub>4</sub> H <sub>8</sub> ( <i>n</i> > 2) <5 ppm CO <2 ppm H <sub>2</sub> O < 7 ppm O <sub>2</sub> < 10 ppm H <sub>2</sub> < 1 ppm N <sub>2</sub> <25 ppm 1001 ± 5 mg dm <sup>-3</sup> Li <sup>+</sup> LiNO <sub>3</sub> in 0.5 mol dm <sup>-3</sup> HNO <sub>3</sub> aqueous solution
Li <sup>+</sup> Tracer	Merck	1000 ± 5 mg dm <sup>-3</sup> NO <sub>3</sub> <sup>-</sup> KNO <sub>3</sub> in 0.5 mol dm <sup>-3</sup> HNO <sub>3</sub> aqueous solution
NO <sub>3</sub> <sup>-</sup> Tracer	Merck	

system<sup>2</sup> in the absence of chemical reactions under the conditions of thermodynamic equilibrium, equals the number of components (*C*) minus the number of phases (*P*) plus two, i.e.  $F = C - P + 2$  (Callen, 1985). Therefore, for a hydrate forming system of three components, among which one is a water-miscible promoter, and three equilibrium phases, two degrees of freedom are available. For such a system, e.g. initial composition and temperature are variables that may be varied experimentally. In the case of ternary systems containing a hydrophobic promoter which is miscible with water over a small composition range only, four phases are often encountered in equilibrium under hydrate forming state conditions. Here, only one degree of freedom is available. Due to the design of the experimental set-up, the temperature has been chosen as the controlled variable. In the special case where both THF and cyclopentane are used, the system is comprised of four components and typically exhibits four phases under hydrate forming conditions. Under these conditions, the system possesses an additional degree of freedom, leading to  $F=2$ . Hence, fixing the mole fraction of one arbitrarily selected component in one of the phases (experimentally, this is achieved by choosing a fixed, overall, initial composition) and the temperature determines the equilibrium conditions.

#### 2.2. Chemicals

The chemicals utilised in this work are presented in Table 1. Both tetrahydrofuran and cyclopentane were obtained specifically for this investigation, and are assumed to comply with the claimed purities and to contain no considerable amount of impurities or oxidation products as e.g. peroxides in the case of THF.

#### 2.3. Loading of equilibrium cells

The system using THF as the thermodynamic promoter was investigated in equilibrium cell C1. C1 is the smallest of the three equilibrium cells and has a net volume of 1.35 dm<sup>3</sup>. It is equipped with one Keller pressure transducer located at the top of the cell (accuracy of ±0.01 MPa) and one Prosenor Pt-100 temperature sensor (accuracy of ±0.1 K) placed at the bottom of the cell. The temperature in the cell is controlled by a LAUDA Edition 2000

<sup>2</sup> A simple system is a system which is macroscopically homogeneous, isotropic, uncharged, for which surface area phenomena can be neglected and which is not acted on by electric, magnetic or gravitational fields.



cryostat allowing for controlling the temperature both below and above the normal freezing point of water.

A solution containing a mass fraction of THF of approximately 0.175 (5.0 mole percent) in distilled water and with an initial tracer concentration of approximately  $10.0 \text{ mg dm}^{-3}$  (determined gravimetrically assuming a liquid density of  $1000 \text{ kg m}^{-3}$ ) was prepared.

According to data found in the literature, a thermodynamic optimum with respect to hydrate promotion is found for THF mole fractions between 0.05 and 0.06 (Saito et al., 1996). The lowest possible equilibrium pressures for the mixed hydrate are generally obtained at this promoter concentration, hence the choice of the THF concentration made in this work.

An amount of 802.9 g of the prepared solution was placed in equilibrium cell C1, which was subsequently closed, evacuated and purged once before being pressurised with pure  $\text{CO}_2$  gas to an absolute pressure of 1.49 MPa.

The system with cyclopentane as hydrate promoter was investigated in equilibrium cell C3. C3 has a net volume of  $2.46 \text{ dm}^3$ . It is equipped with one Keller pressure transducer in the top of the cell (uncertainty of  $\pm 0.01 \text{ MPa}$ ) and two Prosensor Pt-100 temperature sensors (uncertainty of  $\pm 0.1 \text{ K}$ ), one placed at the bottom and one at the top of the cell. The cell temperature is controlled by a HUBER CC3-K6 cryostat allowing for temperature control both above and below the normal freezing point of water. A VARIAN model 450GC gas chromatograph is connected to the cell. However, since only  $\text{CO}_2$  is in the feed gas, it is not utilised in this experiment.

The equilibrium cell was initially pressurised to an absolute pressure of 0.99 MPa at a temperature of 275.9 K. Subsequently, 57.8 g of cyclopentane was pumped into the cell, followed by the injection of 759.1 g of an aqueous solution containing a  $\text{NO}_3^-$  tracer amount of  $9.9 \text{ mg dm}^{-3}$  (determined gravimetrically). (The solution had previously been prepared from distilled water and a pre-prepared reference solution of  $\text{LiNO}_3$ .) The injected liquid amounts correspond to a volumetric ratio between the aqueous solution and cyclopentane liquid of approximately 9:1.

The experiment using both THF and cyclopentane in a mixed promoter solution was performed in equilibrium cell C2. C2 has a net volume of  $2.36 \text{ dm}^3$ . It is equipped with one Keller pressure transducer in the top of the cell (accuracy of  $\pm 0.01 \text{ MPa}$ ) and two Prosensor Pt-100 temperature sensors (accuracy of  $\pm 0.1 \text{ K}$ ) one placed in the bottom of the cell and one in the top. The cell temperature is controlled by a Lauda edition 2000 cryostat allowing for temperature control both above and below the normal freezing point of water. A VARIAN CP 3800 gas chromatograph is connected to the cell, however since only  $\text{CO}_2$  is in the feed gas, it is not utilised in this experiment.

The equilibrium cell was pressurised to an absolute pressure of 0.99 MPa at a temperature of 276.2 K. An amount of 56.3 g cyclopentane was then pumped into the cell followed by 730.2 g solution of 4.0 mass percent (1.0 mole percent) THF in distilled water with a tracer ( $\text{NO}_3^-$ ) concentration of  $10.0 \text{ mg dm}^{-3}$  (determined by weighing). The liquid masses injected into the cell corresponded to a volumetric ratio of the aqueous liquid to cyclopentane liquid of approximately 9:1, which was similar to the ratio in the system using only cyclopentane as promoter.

#### 2.4. Data recording and analysis

The evolution of temperature and pressure recorded for a typical experimental run covering the formation of a hydrate phase are provided in Fig. 1.

Since all experiments are carried out as “blind” experiments, during the initial cooling, the first hydrate formation is observed as a sudden temperature rise. This rise is caused by the hydrate crystallisation process which is an exothermic phase transition. The intensity of the temperature peak depends on the nature of

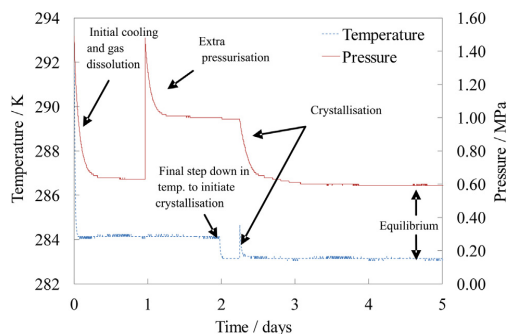


**Fig. 1.** Typical recording of temperature and pressure as functions of time during experimental start-up and hydrate crystallisation. Recording from experimental run in equilibrium cell C1. Formed hydrate is a mixed THF/ $\text{CO}_2$  hydrate. (Dotted line) Temperature (K), (full line) pressure (MPa).

the hydrate formation process (reaction rate and specific heat of crystallisation), which are system specific and also depend on the amount of hydrate former present in the aqueous phase. In the example shown in Fig. 1, the crystallisation heat is rapidly removed by the cooling system, and the system temperature continues to drop while, progressively, more hydrates are formed. After some time, ranging from hours to days, the system attains its equilibrium state at the given temperature set-point.

At the initial equilibrium state, temperature and pressure are noted, and a liquid sample of approximately 1 mL is extracted from the remaining aqueous liquid phase. The THF concentration in the liquid sample is determined by refractive index measurements at 298.2 K using a refractive index apparatus, model 16275 from Carl Zeiss. Aqueous phases are always assumed to be saturated with cyclopentane, whenever cyclopentane is present. However, due to the very low solubility of cyclopentane in the aqueous phase, its effect on the refractive index of the  $\{\text{H}_2\text{O} + \text{THF}\}$  system is assumed to be negligible. Hence, the results of the refractive index measurements performed on the liquid samples should not be significantly distorted. The tracer concentration in the extracted liquid sample is measured by ion exchange chromatography in a DIONEX apparatus. The concentration of the tracer is used to estimate the amount of water consumed in the hydrate phase. The total amount of tracer lost in each extracted liquid sample is considered negligible when compared to the initial amount loaded into the reactor.

After extraction of the liquid sample, the temperature set-point on the cryostat is increased by 1 K and the system is allowed to reach the corresponding equilibrium state. A complete hydrate dissociation run is illustrated in Fig. 2.

The experimental procedure described and illustrated above diverges from the isochoric temperature cycle procedure presented elsewhere in the literature (Sloan and Koh, 2008). Typically, when utilising the isochoric temperature cycle procedure for hydrate formation experiments, only the last equilibrium stage, where the last remaining hydrate crystal dissociates, is considered a true equilibrium stage. Nevertheless, Danesh et al. (1994) showed experimentally that intermediate heating stages may be regarded as true equilibrium points on the hydrate dissociation curve for univariant systems. Hence, the experimental procedure presented here is justified by their findings.

In the case of the THF promoted hydrate formation, the  $\text{H-L}_{\text{w-V}}$  equilibrium additionally depends on a second independent intensive variable, such as for example the concentration of THF in the aqueous phase. Therefore, in these experiments, the THF concentration in the liquid phase needs to be followed closely, since it may change during hydrate crystallisation/dissociation. The amount of

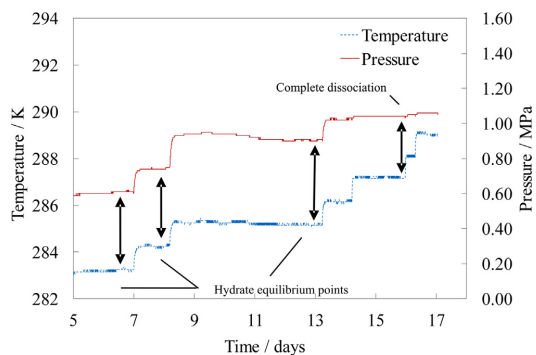


**Fig. 2.** Typical recording of temperature and pressure as functions of time during hydrate dissociation. Recording from experimental run in equilibrium cell C1. Dissociated hydrate is a mixed THF/CO<sub>2</sub> hydrate. (Dotted line) Temperature (K), (Full line) Pressure (MPa).

water consumed in the hydrate phase is indirectly calculated by using the electrolyte tracer concentration. It is assumed that at all times the tracer is only present in the bulk liquid phase; however, it cannot be excluded that some liquid has been entrained inside the formed hydrate crystals. It is expected that this will have only a minor influence on the presented results.

#### 2.4.1. Tetrahydrofuran concentration in the aqueous phase

For systems where THF is present in the feed, the concentration of tetrahydrofuran in the aqueous phase is estimated via refractive index measurements performed on each extracted liquid sample. The analytical method assumes that the presence of THF in the aqueous phase has an effect on the refractive index of the solution and that at constant temperature this effect is linear with respect to composition.

In order to calibrate the refractive index apparatus utilised in the experiments, 15 liquid samples ranging from pure, distilled water to binary mixtures with a mass fraction of THF of 0.45, were prepared and analysed. Refractive indices of all samples were measured, and a mathematical expression for the concentration dependence of the refractive index was obtained by linear regression.

The detection limit of the analysis equipment was determined to a mass fraction of THF of approximately 0.02. At concentrations below this limit, the presence of THF in the aqueous phase could not be identified with sufficient accuracy. THF mass fractions between 0.02 and 0.10 could be detected, however the calibration curve returned large uncertainties in this concentration range (max deviation of  $\pm 22\%$  in calculated THF mass fractions compared to the reference solutions). For THF mass fractions above 0.1 the uncertainty in the calculated mass fraction values amounted to  $\pm 6\%$ , when THF concentrations obtained from the calibration curve were compared to the actual reference concentrations.

The calibration curve relating the mass fraction of THF to the corresponding refractive index could be described by Eq. (1).

$$w_{\text{THF}} = \frac{n_R - 1.332518}{9.555629 \times 10^{-2}} \quad (1)$$

where  $w_{\text{THF}}$  is the THF mass fraction and  $n_R$  is the measured refractive index. The refractive index measured for pure distilled water was 1.333000; hence Eq. (1) cannot be used to describe pure water. Thus, for all measurements returning refractive indices of approximately 1.3330, the concentration of THF is assumed zero, even though the calibration curve returns a THF mass fraction of

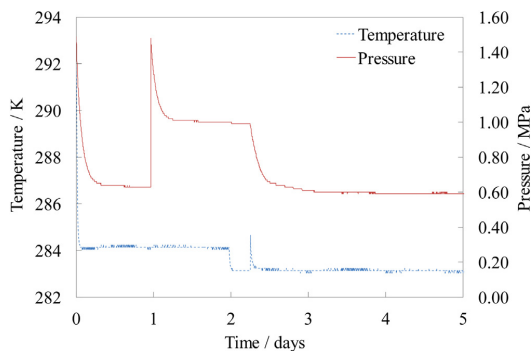


**Fig. 3.** Temperature and pressure as functions of time during experimental start-up and hydrate crystallisation. Recording from experimental run in equilibrium cell C1. The hydrate formed in the cell is a mixed THF/CO<sub>2</sub> hydrate. (Dotted line) Temperature (K), (full line) pressure (MPa).

approximately 0.005. Further details about the calibration procedure can be found in [Appendix A.1](#).

#### 2.5. Aqueous phase converted into solids

By assuming that the tracer is present in the bulk aqueous phase only, the volume of the aqueous phase (water and possibly water soluble promoters) consumed during the hydrate crystallisation, may be estimated indirectly from the tracer concentration measured at each equilibrium stage. The calculation procedure for this estimated water consumption is presented in [Appendix A.2](#).

In the case where cyclopentane is the only promoter, the consumed amount of aqueous phase is assumed to be pure water due to the very low solubility of cyclopentane in the aqueous phase. In the case where THF is present in the aqueous phase in a considerable amount, the water consumption is obtained by correcting the consumed aqueous phase by the measured THF concentration at a given equilibrium stage. In this way, both consumed water and THF may be estimated.

### 3. Results and discussion

#### 3.1. The tetrahydrofuran promoted system

**Fig. 3** illustrates the recorded reactor temperature and pressure during the cooling procedure. The reactor was allowed to attain equilibrium for one day, followed by a re-pressurisation to a pressure of 1.48 MPa. The initial pressure drop, due to CO<sub>2</sub> dissolution in the liquid phase is quite large since CO<sub>2</sub> is more soluble in THF solutions than in water. From a gas separation process point of view, this is beneficial as long as other gas phase components (such as nitrogen) do not experience similarly enhanced solubility. Further dissolution of CO<sub>2</sub> was observed until day two, where the reactor pressure had dropped to 1.00 MPa. The reactor temperature was lowered further by 1 K and crystallisation initiated shortly after, identified in **Fig. 3** by a temperature peak (exotherm) at approximately 2.2 days. The system was fully stabilised after approximately six days at a temperature of 283.2 K and a pressure of approximately 0.6 MPa.

During the heating procedure the system was heated in steps of approximately one Kelvin and allowed to achieve equilibrium with regard to both temperature and pressure between each temperature step. A total of seven equilibrated stages were obtained. Measured and calculated results obtained in the hydrate dissociation run are listed in [Table 2](#). All hydrates had dissociated at

**Table 2**

Measured temperature, absolute pressure, refractive index and tracer concentration of liquid phase along with calculated mass fraction of tetrahydrofuran (THF) and calculated mass of aqueous phase converted into hydrate. Data from equilibrium stages obtained in equilibrium cell C1.

Measured					Calculated		
Sample	T (K)	P (MPa)	Refractive index	$\rho_{\text{Li}}^a$ (mg dm <sup>-3</sup> )	W <sub>THF</sub>	$m_{\text{aq,consumed}}$ (g)	$n_{\text{water,consumed}} \times (n_{\text{THF,consumed}})^{-1}$
0	N/A	N/A	1.347095	11.34	0.153	N/A	N/A
1 <sup>b</sup>	283.3	0.61	1.351124	12.48	0.195	104.1	97 <sup>a</sup>
2 <sup>b</sup>	284.3	0.75	1.349110	12.20	0.174	88.3	18 <sup>a</sup>
3 <sup>b</sup>	285.2	0.91	1.350115	11.50	0.184	45.0	297 <sup>a</sup>
4	286.2	1.03	1.348105	10.95	0.163	0.0	N/A
5	287.2	1.04	1.349114	10.91	0.174	0.0	N/A
6	288.2	1.05	1.348102	10.73	0.163	0.0	N/A
7	289.1	1.06	1.350115	10.84	0.184	0.0	N/A

<sup>a</sup> Assuming molar masses of 18.02 g mol<sup>-1</sup> and 72.11 g mol<sup>-1</sup> for water and THF, respectively.

<sup>b</sup> Only samples 1, 2 and 3 are hydrate equilibrium points. Samples 4 to 7 are fluid phase equilibria and sample 0 is initial aqueous liquid phase.

equilibrium stage 4. This was concluded from the fact that the pressure rise at each subsequent temperature increase was very low for stages 5, 6 and 7. Moreover, upon heating at these temperatures, the measured tracer concentrations turned out to be constant within the limits of the experimental accuracy. Equilibrium stages at temperatures higher than 285 K are thus expected to be vapour–liquid equilibrium points. Liquid samples were extracted and analysed for THF- and tracer concentration at all stages. Liquid samples were de-pressurised (“CO<sub>2</sub> boil-off”) before being analysed.

The THF mass fraction in the initial liquid (sample 0) obtained from the refractive index measurement is underestimated compared to the prepared feed solution. The initial liquid contained a mass fraction of THF of 0.175, but the refractive index measurement indicates a fraction of 0.153. Also, the tracer concentration in the feed is overestimated. The initial tracer concentration should be approximately 10.0 mg dm<sup>-3</sup> according to the individual masses of each component added to the prepared aqueous solution (see Section 2.3). However, in sample 0 the measured tracer concentration is 11.34 mg dm<sup>-3</sup>. Sample 0 was extracted shortly after the second pressurisation to a pressure of 1.48 MPa at a temperature of 284.2 K (day one in Fig. 3). The high tracer concentration could indicate that crystallisation has already occurred at this point, however since no temperature peak was observed, it is rather regarded as a faulty analysis result. However, since the conditions of 284.2 K and 1.48 MPa are well within the hydrate stability zone for the mixed THF/CO<sub>2</sub> hydrate, it cannot be excluded, that the increased tracer concentration in sample 0 is due to unseen hydrate formation. In order to obtain an estimate of the initial feed tracer concentration (measured), the average of the final four liquid samples is utilised. This average amounts to 10.9 mg dm<sup>-3</sup>. The following analyses are based on this value for the feed tracer concentration as well as the calculated initial THF concentration.

Assuming that the hydrates formed from THF and CO<sub>2</sub> are all hydrates and that the THF molecules enter all the large cavities only, i.e., that the occupation of THF in the small cavities can be neglected, the consumption of THF and water should occur in a molar ratio of 1:17 respectively (8 large cavities to 136 water molecules), corresponding to a gas-free mole fraction of THF in the hydrate phase of  $x_{\text{THF}}^{\text{H}} = n_{\text{THF}}^{\text{H}} / (n_{\text{THF}}^{\text{H}} + n_{\text{H}_2\text{O}}^{\text{H}}) = 0.059$ . Since in this experiment, the THF concentration in the feed liquid is lower than the stoichiometric concentration in the hydrate phase (with respect to a complete filling of the large cavities by THF molecules exclusively), we expect a small decrease in THF concentration as the hydrates form, and thus, an increase in the THF concentration in the liquid phase as the hydrates are dissociated. The THF concentration should hereafter remain unchanged (within the experimental accuracy) once all hydrates have dissociated.

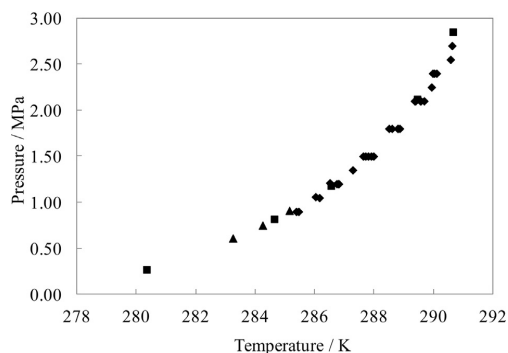
The three equilibrium stages in the temperature interval from 283 K to 285 K seem to experience little variation in the calculated liquid phase THF concentration, indicating that the dissociated

hydrate composition in terms of water and THF is close to the co-existing liquid phase composition. The calculated THF concentrations at the four highest temperatures are close to constant, when considering the experimental uncertainty.

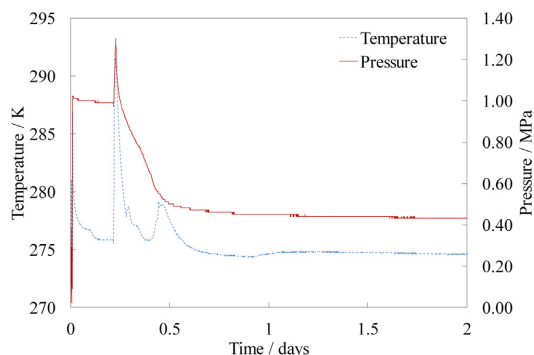
The calculated ratios of water to THF consumed in the hydrate phase are likewise provided in Table 2. In the “ideal case”, i.e., in the case of a complete filling of the large cavities by THF molecules only, this number would be 17. However in the three established hydrate equilibrium points, it varies from 18 to 297. This number is highly sensitive to the estimated THF concentration, which explains the large variation.

Fig. 4 compares the three identified hydrate equilibrium stages with those reported for similar systems by Seo et al. (2008) and Sabil et al. (2010) using similar compositions in the liquid phase. Sabil et al. concluded from their results, that even though this ternary three-phase equilibrium system is composition dependent according to the Gibbs phase rule, the initial (overall) composition of CO<sub>2</sub> had little, if any (within the experimental uncertainty), impact on the position of the three-phase (H–L<sub>w</sub>–V) phase boundary. This phase boundary was mainly governed by the initial THF concentration in the aqueous phase. Thus, even though the initial concentration of CO<sub>2</sub> (overall) in our work may vary from that of Sabil et al. and Seo et al., the initial THF concentrations in the aqueous solution are identical.

The three data points obtained in this work follow the trend observed in the data of Sabil et al. (2010). Data measured in this work corresponds well with the data presented by Seo et al. (2008)



**Fig. 4.** Comparison of three-phase (H–L<sub>w</sub>–V) equilibrium pressure (absolute) as a function of temperature for mixed hydrates of tetrahydrofuran (THF) and CO<sub>2</sub>. Hydrates formed from an aqueous THF solution initially containing 5 mol% THF. The initial vapour phase consists of pure CO<sub>2</sub>. (▲) this work, (◆) Sabil et al. (2010), (■) Seo et al. (2008). The data from Sabil et al. include six individual experiments with initial overall CO<sub>2</sub> mole fractions ranging from 0.01 to 0.29.



**Fig. 5.** Temperature and absolute pressure as functions of time during experimental start-up and hydrate crystallisation. Recording from experimental run in equilibrium cell C3. The formed hydrate is a mixed cyclopentane/CO<sub>2</sub> hydrate. (Dotted line) Temperature (K), (full line) pressure (MPa).

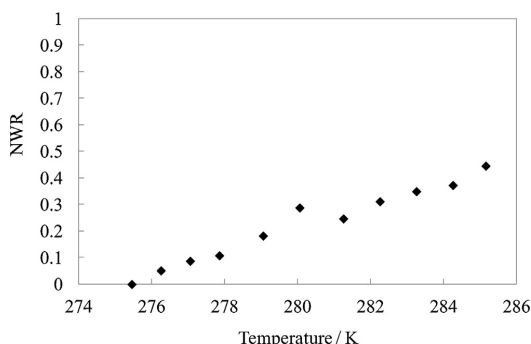
and form a connection towards the low temperature data point measured by Seo et al. Note also that the liquid phase composition vary slightly between the three data points obtained in this work. Data from Seo et al. (2008) and Sabil et al. (2010) are all measured at a constant THF mole fraction in the initial aqueous solution of 0.05 (mass fraction of 0.175). In the comparison of data points in

Fig. 4 it should be borne in mind that the three equilibrium points obtained in this work refer to different values for the calculated mole fraction of THF in the aqueous phase at equilibrium varying between 5.0 and 5.8 mol%. However, the fact that variations in the THF concentration in this range have little influence on the dissociation pressure of the mixed THF/CO<sub>2</sub> hydrate justifies the comparison made here.

### 3.2. The cyclopentane promoted system

Fig. 5 shows the temperature and pressure recorded as functions of time during reactor cooling. The peaks in temperature and pressure in Fig. 5 at approximately 0 and 0.25 days are due to the liquid loading (cyclopentane first, followed by aqueous phase). Crystallisation is first observed as a small temperature peak at 0.3 days (shoulder on the large temperature decline) and again as a larger peak at 0.5 days. The first crystallisation peak corresponds to the formation of a mixed cyclopentane/CO<sub>2</sub> hydrate. This explains the decline in pressure in connection with the first temperature peak. The second crystallisation occurs at a temperature close to 281 K. At these conditions of temperature and pressure, we are within the stable zone for the mixed cyclopentane/CO<sub>2</sub> hydrate and at the proximity of the phase boundary for the pure cyclopentane hydrate. At the second crystallisation peak, hardly any pressure drop occurs, indicating the formation of the pure cyclopentane hydrate only. The small decline in pressure after  $t = 0.5$  days is as likely due to the temperature decrease as it could be ascribed to the inclusion of CO<sub>2</sub> in the hydrate phase.

The cyclopentane promoted system stabilised in terms of temperature and pressure within three days. After three days the system set-point temperature was increased by one degree, which did not have any effect on the reactor pressure. Since the equilibrium cell was operating at conditions within the stable zone for the pure cyclopentane hydrate, it is possible that most if not all of the bulk cyclopentane phase has been converted into hydrate, and the hydrate system was sub cooled. A total of 11 heating stages in the temperature interval from 275.5 K to 285.2 K were recorded during the hydrate dissociation run.



**Fig. 6.** Normalised water release (NWR—according to Eq. (2)) as function of temperature during the dissociation of the mixed cyclopentane/CO<sub>2</sub> hydrates. Note the near constant water release rate despite the non-linear behaviour in the recorded pressure increase.

Measured and calculated data for all equilibrium stages are provided in Table 3. Sample 0 was taken from the initial aqueous liquid phase prior to reactor loading.

Assuming cyclopentane enters all large cavities in the formed sII hydrates, the added amount of cyclopentane is sufficient to convert approximately one-third of the aqueous phase into hydrates. If only a fraction of the large cavities are occupied by cyclopentane, a larger amount of the initial aqueous phase may be converted into hydrates. The present system is univariant only if four phases are present in all hydrate equilibrium stages. Since this is a closed reactor experiment, the measured tracer concentration may be used as an indicator for the number of phases present. If the tracer concentration indicates more than one-third of the water being converted, it is possible that the bulk cyclopentane phase has been completely converted into the hydrate phase.

The final column in Table 3 provides the estimated ratio of consumed water over the initial loading of cyclopentane. For sample 1 this ratio is above 17 indicating the possibility of complete conversion of the bulk cyclopentane phase. At the second stage (sample 2), the ratio is below 17 suggesting the presence of the cyclopentane bulk phase and thus four phases in equilibrium.

An interesting observation is made when looking at the pressure behaviour of the system. The increase in temperature from 275.5 K to 283.3 K provides an increase in pressure of only 0.05 MPa. However when looking at the estimated water consumption provided in Table 3, this appears to decrease continuously.

Fig. 6 illustrates the normalised water release during dissociation of formed hydrates. The normalised water release (NWR) is defined according to Eq. (2).

$$\text{NWR} = \frac{m_{\text{aq, consumed, max}} - m_{\text{aq, consumed}}(T)}{m_{\text{aq, consumed, max}}} \quad (2)$$

where  $m_{\text{aq, consumed}}(T)$  is the mass of water consumed in the hydrate phase at temperature,  $T$ ,  $m_{\text{aq, consumed, max}}$  is the maximum amount of consumed aqueous phase occurring at the lowest recorded equilibrium temperature.

Fig. 6 clearly shows that water is continuously released during the heating process, indicating an almost constant rate of hydrate dissociation caused by the stepwise increase in temperature. Even for the three stages at temperatures between 283.3 K and 285.2 K the water release seems to be constant despite the fact that the observed pressure increase becomes significant under these conditions.

The results indicate that the ability of cyclopentane to form pure sII promoter hydrates at low temperatures becomes a disadvantage

**Table 3**

Measured temperature, absolute pressure, refractive index and tracer concentration in the aqueous liquid phase along with calculated mass of water converted into hydrate. Data from equilibrium stages obtained in equilibrium cell C3.

Measured				Calculated	
Sample	T (K)	P (MPa)	$\rho_{\text{NO}_3}$ (mg dm <sup>-3</sup> )	$m_{\text{aq,consumed}}$ (g)	$n_{\text{water,consumed}}(n_{\text{cyclopentane,initial}})^{-1}$
0	N/A	N/A	8.85 <sup>a</sup>	N/A	
1	275.5	0.42	13.47	260.2	17.5
2	276.3	0.42	13.12	246.9	16.6
3	277.1	0.43	12.88	237.5	16.0
4	277.9	0.43	12.75	232.1	15.6
5	279.1	0.45	12.30	212.8	14.3
6	280.1	0.45	11.71	185.2	12.5
7	281.3	0.47	11.93	196.0	13.2
8	282.3	0.48	11.58	179.1	12.1
9	283.3	0.49	11.39	169.3	11.4
10	284.3	0.52	11.27	163.2	11.0
11	285.2	0.59	10.93	144.3	9.7

<sup>a</sup> Average of two analyses obtaining 8.79 mg dm<sup>-3</sup> and 8.90 mg dm<sup>-3</sup>.

from a gas capture point of view. This work suggests that pure cyclopentane sII hydrates mainly form at temperatures below 281 K. This conclusion is thermodynamically confirmed by the stability limit for pure cyclopentane hydrates the temperature of which is located at approximately 280 K.

An explanation for the low gas uptake could be that only the small 5<sup>12</sup> cavities of the sII hydrates are available for CO<sub>2</sub> molecules which, at low pressures, have only a low affinity for this cavity. Sum et al. (1997) measured compositions of pure CO<sub>2</sub> sI hydrates by Raman spectroscopy. They found no signs indicating the presence of CO<sub>2</sub> in the small (5<sup>12</sup>) cavities of the sI hydrate structure and concluded that CO<sub>2</sub> enters only the large cavities. In the mixed hydrate, cyclopentane is expected to occupy most of the large sII hydrate cavities leaving mainly the small cavities available for CO<sub>2</sub>. Another explanation may be slow gas diffusion from the bulk gas phase to the hydrate forming regions.

Even though the mixed hydrate phase is the thermodynamically most stable hydrate form at temperatures between 281 K and 285 K, it is considered possible that the diffusion of carbon dioxide through the liquid and solid phases does not proceed fast enough to be noticed when using this experimental procedure. Hence there is a risk that the equilibrium stages which are assumed to exist at these temperatures are rather kinetically inhibited systems which do only appear to be stable.

Fig. 7 compares the results of this work with mixed cyclopentane/CO<sub>2</sub> hydrate dissociation pressures measured by Zhang and Lee (2009a, b) and Mohammadi and Richon (2009).

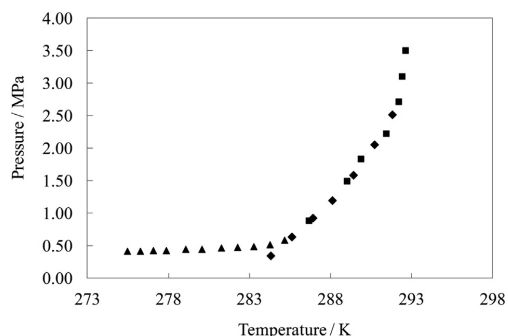


**Fig. 7.** Comparison of four-phase (H–L<sub>w</sub>–L<sub>s</sub>–V) equilibrium pressures (absolute) as function of temperature for mixed hydrates of cyclopentane/CO<sub>2</sub>. Hydrates formed from a two-liquid phase system, initially containing pure water and pure cyclopentane, and an initial vapour phase consisting of pure CO<sub>2</sub>. (▲) this work, (◆) Mohammadi and Richon (2009), (■) Zhang and Lee (2009a, b).

No equilibrium stages were measured at temperatures above 285.2 K in this work. However in the low temperature region, data from this work show a different trend than those reported by Mohammadi and Richon (2009). We cannot exclude the possibility that the system measured here has been mass transfer limited in the low temperature region due to the large amounts of hydrates formed and possibly also due to insufficient mixing.

### 3.3. The tetrahydrofuran and cyclopentane mixed promoter system

A system containing two thermodynamic promoters, cyclopentane and THF, was investigated for efficiency of thermodynamic promotion of CO<sub>2</sub> hydrates. Utilising this system in a single-phase promoter solution would be ideal, since the elimination of one liquid phase (cyclopentane bulk phase) would simplify process design and control. Hence attempts were made to increase the solubility of cyclopentane in the aqueous phase from the normal 40–50 ppm (molar) at atmospheric conditions to approximately 0.5 mol% by adding tetrahydrofuran to the aqueous phase.

#### 3.3.1. Cyclopentane solubility in ternary mixtures with water and tetrahydrofuran

Titration experiments were carried out at atmospheric conditions in order to determine the amount of THF necessary to increase the solubility of cyclopentane in aqueous solutions roughly by a factor of 100 compared to its solubility in pure water.

Initially a two-phase feed mixture was prepared with distilled water and cyclopentane. This initial mixture was approximately 0.5 mol% cyclopentane and 99.5 mol% water. THF was then added to the system at constant stirring until a single-phase mixture was obtained. The system was kept closed in order not to lose volatile components (cyclopentane and THF). It was opened only when adding THF. Three attempts were made to prepare solutions of different total volumes. Whereas two of these solutions possessed volumes of approximately 0.06 dm<sup>3</sup>, the preparation of the third mixture aimed at achieving a total solution volume of around 1 dm<sup>3</sup>. The solutions were prepared by weighing, whereby the masses of all components were noted when being added to the solution. The results are provided in Table 4.

The solutions were left overnight without stirring in order to test phase stability. All solutions proved to be stable over time. Mixture three was also stable down to a temperature of 275.2 K. Lower temperatures were not tested.

Generally it required more than 20 mol% of THF in the ternary mixture to allow the dissolution of approximately 0.4 mol% cyclopentane. This corresponds to having more than 50 mass% THF in the system. Having this quantity of THF in the system lowers



**Table 4**  
Single-phase liquid ternary mixtures of water (H<sub>2</sub>O), tetrahydrofuran (THF) and cyclopentane prepared at ambient conditions. All mixtures are saturated in cyclopentane. Further addition of cyclopentane will result in a split into two liquid phases.

Solution	1		2		3	
	Mass (g)	Mole fraction	Mass (g)	Mole fraction	Mass (g)	Mole fraction
H <sub>2</sub> O	27.11	0.7942	27.10	0.7705	434.87	0.7689
Tetrahydrofuran	27.55	0.2016	31.77	0.2257	514.82	0.2274
Cyclopentane	0.56	0.0042	0.523	0.0038	8.17	0.0037

the activity of water in the solution dramatically, since THF forms hydrogen bonds with water. A lowering of water activity results in the need for a pressure increase in order to stabilise the hydrates. Hence, in the above promoter solutions, it is likely that the benefits of having higher cyclopentane concentrations will be lost due to the large amount of THF.

The above solutions were never tested in hydrate experiments, since they proved to be unstable in the presence of CO<sub>2</sub> at moderate pressures. The initial single-phase solution splits up into two liquid phases, an organic phase (L<sub>3</sub>), and an aqueous phase (L<sub>w</sub>), respectively, when being mixed with CO<sub>2</sub> in the pressurised reactor (to a pressure of approximately 1.0 MPa). A possible explanation for this behaviour could be that CO<sub>2</sub>, due to its local polarity, may solvate and form hydrogen bonds with water. Having a mass fraction of THF larger than 0.5 in the liquid solution, the solubility of CO<sub>2</sub>, and thereby CO<sub>2</sub>–water interactions, become significant, which further lowers the water activity and thereby the solvent properties of the aqueous phase. The resulting two liquid phases are likely to be an organic THF rich phase containing some water and most of the original cyclopentane content, and an aqueous phase rich in water with some THF and traces of cyclopentane.

### 3.3.2. Mixed promoter system—Hydrate equilibrium

Due to the instability of the single-phase mixed promoter solution in the quaternary system with CO<sub>2</sub>, it was decided to investigate the mixed promoter system as a two-phase promoter system with an aqueous phase containing small amounts of THF, traces of cyclopentane and a bulk cyclopentane phase.

Adding one further component (THF) to the previous (H–L<sub>w</sub>–L<sub>3</sub>–V) univariant ternary system {H<sub>2</sub>O+cyclopentane+CO<sub>2</sub>} adds one degree of freedom to the experiment, since no additional phases form. Hence temperature and furthermore one intensive variable, like e.g. the concentration of THF in any of the co-existing phases, determine uniquely the state conditions at equilibrium provided that four phases are present in this state. In practice, the variable that can easily be influenced by the experimenter is the concentration of THF in the initial liquid and thereby the overall composition of the mixture in general. In order to avoid large changes in composition of the initial aqueous phase inside the reactor when fluid phase equilibrium is attained (before hydrate formation), it was chosen to carry out the experiments on a system prepared with an initial binary sub-mixture {H<sub>2</sub>O+THF} possessing a low concentration of THF.

Fig. 8 shows the temperature and pressure as a function of time for the mixed promoter system measured during reactor cooling. From Fig. 8, it becomes clear that the qualitative crystallisation behaviour of the mixed promoter system is similar to the one encountered in the cyclopentane promoted system. Crystallisation occurs in two steps. The first step takes place at a similar pressure of approximately 1.0 MPa. Whereas the pure cyclopentane promoted system crystallised at a temperature of approximately 278 K (Fig. 5), the mixed THF/cyclopentane promoted system required cooling to approximately 276.8 K. However, as crystallisation is a stochastic phenomenon, one cannot draw any conclusions with regard to the thermodynamics of the system solely based upon

the above observation due to the need for sub cooling, stochastic behaviour in induction times, etc. After the system had stabilised within 5.8 days, heating was initiated. Table 5 provides recorded and calculated data for a total of 18 heating stages obtained during the heating procedure.

Sample 0 is the analysis of the aqueous feed phase prior to being loaded into the reactor. This value differs significantly from the tracer concentrations measured in the final two stages, where all hydrates are dissociated. These three values should be similar. In order to obtain an estimate of the consumed aqueous phase, the feed tracer concentration is calculated as an average of sample 0, 17 and 18. This provides a feed tracer concentration of 8.69 mg dm<sup>−3</sup>.

Due to some instability in temperature recordings in the low temperature region, the stage at 274.0 K (stage 1) is disregarded in the following analysis. Stage 16 is the final equilibrium stage with the possibility of hydrate presence. However with the large uncertainty in feed tracer concentration, it cannot be verified, that hydrates are still present in the system. Hence, this stage is also discarded from the expected hydrate equilibrium points.

When looking at the calculated THF concentrations in the aqueous phase provided in Table 5, it is worth noting that the THF mass fraction is below the detection level of the analysis method at temperatures below 283.2 K. Above this temperature, THF is detected in low concentrations in some of the samples and not in others. For samples 16, 17 and 18, the feed THF concentration is found, supporting the suspicion that no hydrates are present at these stages anymore. The fact that the THF mass fraction remains constant in these three samples also supports this theory. For the intermediate recordings indicating THF mass fractions of 0.016 (samples 11, 12 and 14), the calculated THF concentrations should be used with caution since these values are close to the lower detection limit of the experimental apparatus used for measuring refractive indices. Samples 13 and 15 showed no traces of THF (within the uncertainty of the analysis method) despite the fact that both sample 12, 14 and 16 contained THF. It is possible that some THF has been lost

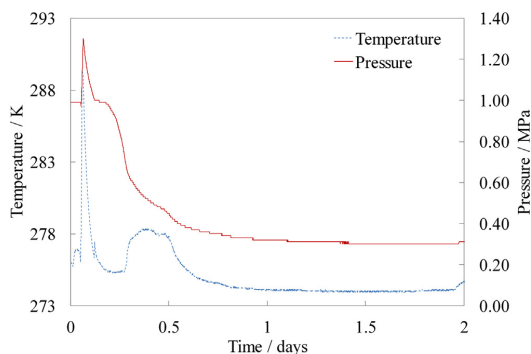


**Fig. 8.** Temperature and absolute pressure as functions of time during experimental start-up and hydrate crystallisation. Recording from experimental run in equilibrium cell C2. Formed hydrate is a mixed cyclopentane/THF/CO<sub>2</sub> hydrate. (Dotted line) Temperature (K), (full line) pressure (MPa).

**Table 5**

Measured temperature, absolute pressure, refractive index and tracer concentration of aqueous liquid phase along with calculated THF mass fraction and calculated mass of water converted into hydrate. Data from heating stages obtained in equilibrium cell C2.

Measured					Calculated	
Sample	T (K)	P (MPa)	Refractive index	$\rho_{\text{NO}_3^-}$ (mg dm <sup>-3</sup> )	w <sub>THF</sub>	<sup>a</sup> m <sub>aq,consumed</sub> (g)
0	N/A	N/A	1.335017	9.89	0.026	N/A
<sup>b</sup> 1	274.0	0.29	1.333001	23.43	0.0	459.5
2	275.1	0.30	1.333005	21.06	0.0	428.9
3	275.5	0.30	1.333004	17.71	0.0	372.0
4	276.5	0.30	1.333003	19.10	0.0	398.0
5	277.4	0.31	1.333004	17.53	0.0	368.2
6	278.1	0.32	1.333001	17.92	0.0	376.2
7	279.0	0.32	1.333000	17.84	0.0	374.6
8	279.9	0.34	1.333001	17.21	0.0	361.6
9	280.9	0.35	1.333000	17.33	0.0	364.1
10	281.8	0.36	1.333002	16.91	0.0	355.1
11	282.8	0.38	1.334007	17.03	0.016	357.6
12	283.7	0.43	1.334010	16.04	0.016	334.7
13	284.8	0.53	1.333000	14.24	0.0	284.6
14	285.7	0.67	1.334010	12.93	0.016	239.7
15	286.6	0.80	1.333002	10.67	0.0	135.8
<sup>b</sup> 16	287.6	0.95	1.335015	9.31	0.026	48.6
<sup>b</sup> 17	288.6	0.96	1.335015	8.07	0.026	-56.4
<sup>b</sup> 18	289.6	0.97	1.335016	8.11	0.026	-52.3

<sup>a</sup> Calculated using an average of sample 0, 17 and 18 for tracer concentration in the feed.

<sup>b</sup> Only samples 2–15 are expected hydrate equilibrium stages. Samples 1, 16, 17 and 18 are suspected either subcooled solid–liquid–vapour equilibrium or only fluid phase equilibria.

due to vaporisation in the time the samples were extracted until the time at which they were analysed for refractive index. From a qualitative point of view, these results suggest that all THF is consumed in the hydrate phase at temperatures below 283.2 K. THF is then released by hydrate dissociation in the temperature range from approximately 283.2 K to 287.2 K.

Fig. 9 illustrates the normalised water release (NWR—according to Eq. (2)) between heating stages 2 and 15.

The normalised water release for the mixed promoter system is interesting in the sense that water is slowly released at temperatures below 283.2 K. At higher temperatures, the water release increases rapidly, indicating an increase in amount of dissociated hydrates for each temperature step. Hence, even though the qualitative behaviour of the recorded reactor pressure during hydrate dissociation for this system is similar to that of the pure cyclopentane promoted system, the dissociation mechanism appears to be different. The normalised water release rate is low at temperatures below 283.2 K and then increases steeply at temperatures above.

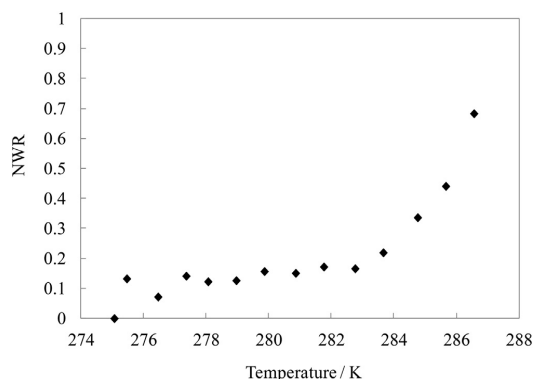


**Fig. 9.** Normalised water release (NWR—according to Eq. (2)) as function of temperature during dissociation of mixed cyclopentane/tetrahydrofuran/CO<sub>2</sub> hydrates. Note the highly non-linear water release rate.

In the cyclopentane promoted system, the water release rate was close to linear with increasing temperature.

It is well known that THF and cyclopentane both stabilise the sII hydrate structure. Hence they are expected to compete for the large cavities of the hydrate structure, since the molecules of both compounds are, with regard to their geometrical characteristics, too large to enter the small cavities. According to the pressure-, water consumption- as well as the THF mass fraction data provided in Table 5, the mixed hydrate phase containing remarkable amounts of THF is stable below temperatures of 283.2 K (or present in concentrations below the detection limit of this experimental method). As in the case of pure cyclopentane promoted hydrates, this observation indicates that the hydrate phase being dissociated in this temperature region does mainly contain cyclopentane guest molecules and is correspondingly low in gas content.

Fig. 10 compares the measured dissociation pressures of the pure cyclopentane promoted system with those of the mixed THF/cyclopentane promoted system.

Since the mixed promoter system is divariant and the cyclopentane promoted system is univariant, a quantitative comparison cannot be made due to the changes in aqueous phase composition (mainly THF concentration) between each data point representing the divariant system.

Fig. 10 illustrates an interesting conclusion drawn from this experiment. Adding THF to the aqueous phase allows for a significant pressure reduction of the promoted hydrate system when compared to the pure cyclopentane promoted system. The reduction in absolute pressures is in the order of 25–30% at low temperatures. Why should this mixed promoter system be superior to the single promoter system? Tetrahydrofuran (THF) is an example of a molecule that is soluble in water but has also been shown to be a structure II hydrate promoter (Kang et al., 2001) with increasing effect up to concentrations of 5 to 6 mol% in the aqueous phase. This concentration is consistent with a single THF molecule occupying and stabilising the large cage of sII hydrate (a ratio of 17 water molecules to one THF molecule). So up to this overall concentration the aqueous phase is nearly pure water (since the THF is in the hydrate). Above this concentration, there is an excess of THF (with respect to formation

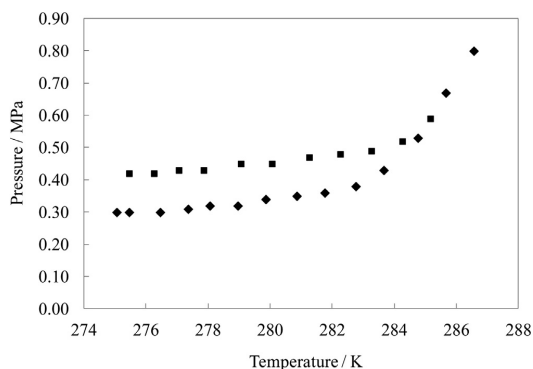


**Fig. 10.** Four-phase (H–L<sub>w</sub>–L<sub>a</sub>–V) equilibrium pressures (absolute) as functions of temperature for mixed hydrates of cyclopentane/tetrahydrofuran/CO<sub>2</sub>. Hydrates formed from a two-liquid phase system prepared from an aqueous solution containing 4 mass% tetrahydrofuran and an organic phase containing pure cyclopentane. For comparison, (H–L<sub>w</sub>–L<sub>a</sub>–V) hydrate equilibrium data exhibiting a mixed cyclopentane/CO<sub>2</sub> hydrate phase of the ternary system (H<sub>2</sub>O + cyclopentane + CO<sub>2</sub>) are included. The initial vapour phase consists of pure CO<sub>2</sub> in both cases. (♦) cyclopentane/THF/CO<sub>2</sub>, this work, (■) cyclopentane/CO<sub>2</sub>, this work, note the significant reduction in equilibrium pressures caused by the addition of 4 mass% tetrahydrofuran to the aqueous phase.

of sII large cages) and the THF in the aqueous phase reduces the water chemical potential, increasing the hydrate formation pressure. A similar effect was observed by Jäger et al. (1999) for 1,4-dioxane.

Adding cyclopentane to this system (water–THF–CO<sub>2</sub>) will result in the formation of more stable sII hydrates, with cyclopentane molecules now stabilising the large cages, forcing the THF molecules into the aqueous phase. Here they will form more sII hydrates, as long as the concentration in this phase does not exceed about 6 mol% (1 THF molecule to 17 water molecules). In our experiments the concentration of THF was 4 mass%, or about 1 mol%, so we do not approach this limit.

So to some extent the THF and cyclopentane are not competing for the same hydrates (the formation mechanisms are different) and there is consequently the synergistic effect observed.

The data presented in this work indicate some disadvantages of using cyclopentane as a thermodynamic promoter for CO<sub>2</sub> hydrate formation in gas separation processes operating at low temperatures and low pressures. Having a self-stability temperature of the pure promoter hydrate at approximately 280 K, the system quickly starts forming significant amounts of the pure promoter hydrate, if mixing is insufficient. These results indicate the need for emulsifiers and possibly anti agglomeration agents, if successful carbon capture should be obtained in systems containing water in-soluble promoters. The addition of emulsifiers and anti-agglomeration agents will not prevent the formation of the promoter hydrate, but it will ease the transport of gas into the hydrate forming regions. Even though hydrates do form in the systems shown in this work, the CO<sub>2</sub> uptake in the hydrate phase is low. Similar behaviour is expected for THF promoted systems at lower temperatures than those investigated here, since THF may also self-stabilise the sII hydrate structure at low temperatures. However since THF is water soluble, mixing in this system is easier and more hydrates may form before mass transfer limitations occur.

The main goal of this work was to study thermodynamic promotion of CO<sub>2</sub> capture with hydrates, and kinetic and mass transfer aspects have not been addressed here. These areas have previously been covered by Li et al. (2011, 2012); Linga et al. (2012); Babu et al. (2013); Daraboina et al. (2013); Kang et al. (2013); Adeyemo et al.

(2010); Zhang and Lee (2009a, b). A kinetic study combined with morphological observations has also recently appeared (Lim et al., 2013).

#### 4. Conclusion

Gas hydrate dissociation pressures were measured for systems of water, one (or two different) structure II hydrate promoter(s) and carbon dioxide. In this investigation, tetrahydrofuran (THF), cyclopentane and a mixture of the two were investigated for their potential for thermodynamically promoting the formation of carbon dioxide hydrate in the low pressure/low temperature region. For the ternary mixture {water + THF + carbon dioxide}, prepared from an initial aqueous solution containing 5.0 mol% THF, H–L<sub>w</sub>–V equilibrium pressures were measured in the temperature range from 283.3 K to 285.2 K. At 283.3 K, the hydrate equilibrium pressure was determined at 0.61 MPa (absolute pressure) for this system. Data from this work compared well with data reported elsewhere in the literature.

For the ternary system of water–cyclopentane–carbon dioxide, four-phase hydrate–aqueous liquid–organic liquid–vapour (H–L<sub>w</sub>–L<sub>a</sub>–V) equilibrium data was presented at temperatures ranging from 275.5 K to 285.2 K. It was suggested that despite the fact that cyclopentane is one of the most efficient sII hydrate promoters known at intermediate/high temperatures (283 K), it is efficiency as a thermodynamic gas hydrate promoter for carbon dioxide hydrate formation becomes limited at temperatures below 281 K due to the stability of the pure promoter hydrate. The data presented in this study suggested that almost pure cyclopentane sII hydrates rather than mixed carbon dioxide–cyclopentane hydrates formed at temperatures below 281 K and pressures above 0.4 MPa. The measured dissociation pressures compared well with data reported elsewhere in the high temperature region, but deviated from other data in the low temperature region.

Finally, new four-phase (H–L<sub>w</sub>–L<sub>a</sub>–V) equilibrium data for the quaternary system {water + THF + cyclopentane + carbon dioxide} were presented in the temperature range from 275.1 K to 286.6 K. It was shown that adding THF to water to form a 4 mass% aqueous solution lowered the equilibrium pressure by 25–30% compared to the ternary system of water, cyclopentane and carbon dioxide. However, as in the pure cyclopentane promoted system, almost pure promoter hydrates were formed at low temperatures. Further studies are needed to explain the qualitative behaviour of the mixed promoter system. It is suggested that the synergistic effect is the result of different formation mechanisms for the polar and the non-polar hydrate former, whereby in a system where cyclopentane in hydrates is in equilibrium with cyclopentane in the aqueous phase, some further formation of hydrates with THF can still occur resulting in an overall reduction in formation pressure.

#### Acknowledgements

This work was financially supported partly by the European iCap research project (EU FP7) and partly by the Department of Chemical and Biochemical Engineering (MP<sub>2</sub>T) at the Technical University of Denmark (DTU). The authors wish to thank Fabien Chauvy, Alain Lallemand, Richard Drogo, Albert Boyer, Jean-Pierre Poyet (the technical staff at Centre SPIN, Ecole Nationale Supérieure des Mines de Saint-Etienne) for their help and technical support. We also acknowledge the initiative and work Erling H. Stenby and Philip L. Fosbøl put into establishing the funding for DTU, as part of the iCap project.



## Appendix A.

### A.1. Refractive index measurements for water/tetrahydrofuran solutions—calibration curve

Refractive index measurements have been performed for 14 solutions of THF in distilled water as well as one sample of pure distilled water. THF concentrations are known (gravimetrically) for all solutions. By performing a regression on the measured refractive indices over the known THF mass fraction, an expression for the linear concentration dependence of the refractive index is obtained. All measurements are performed at atmospheric pressure and a temperature of 298.2 K on a Carl Zeiss model 16275 refractive index apparatus. Measured refractive indices and calculated THF mass fractions are provided in Table A.1. The calibration curve is shown Fig. A.1.

The refractive index method, when using the Carl Zeiss apparatus for estimating THF concentrations in aqueous solutions, has insufficient resolution at THF mass fractions 0.02. Hence, in this work, the obtained calibration curve is valid only for concentrations above this value. When performing the linear regression, a constraint could have been set, such that the linear regression describes the refractive index of pure water correctly. However in order to increase accuracy in the in the concentration interval from 0.02 to 0.10, no constraint has been set. Thus, it is noted that this calibration

**Table A.1**

Refractive indices of THF solutions in distilled water. Data measured at atmospheric pressure and 298.2 K.

Ref. THF mass fraction	Measured refractive index	Calculated THF mass fraction	AD in calculated THF concentration (%)
0.000	1.333000	0.005	N/A
0.004	1.333001	0.005	26.1
0.008	1.333005	0.005	36.4
0.020	1.334010	0.016	22.2
0.033	1.335015	0.026	19.6
0.077	1.340050	0.079	2.9
0.099	1.341058	0.089	9.8
0.159	1.348104	0.163	2.4
0.174	1.350118	0.184	5.9
0.224	1.354141	0.226	1.0
0.293	1.361184	0.300	2.2
0.308	1.363197	0.321	4.3
0.341	1.365206	0.342	0.4
0.392	1.369230	0.384	2.1
0.459	1.375263	0.447	2.4

Calculated using the linear regression from Fig. A.1: refractive index =  $9.555629 \times 10^{-2} w_{\text{THF}} + 1.332518$ , where  $w_{\text{THF}}$  is mass fraction of THF in percent.

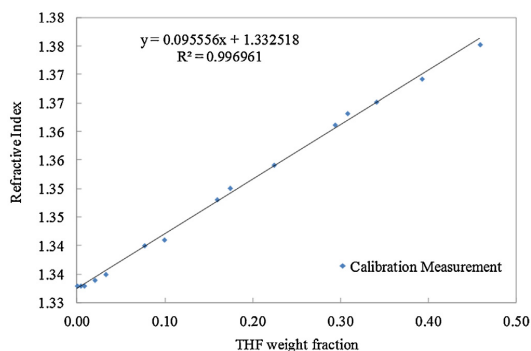


**Fig. A.1.** Measured refractive indices for solutions of tetrahydrofuran (THF) in distilled water. Measurements carried out at atmospheric pressure and 298.2 K.

should be used only for mass fractions above 0.02 and preferably above 0.10.

### A.2. Calculation of mass of aqueous phase converted into solids

The mass of aqueous phase converted into solid hydrate is calculated according to

$$V_{\text{aq}, 0} \cdot \rho_{\text{tracer}, 0} = V_{\text{aq}}(t) \cdot \rho_{\text{tracer}}(t) \quad (\text{A.1})$$

where  $\rho_{\text{tracer}, 0} \equiv \rho_{\text{tracer}}(t=0)$  is the initial tracer concentration in the aqueous phase (here the mass concentration  $\rho_{\text{tracer}}$  with  $[\rho_{\text{tracer}}] = \text{mg dm}^{-3}$  is used), before it is loaded into the equilibrium cell.  $\rho_{\text{tracer}}(t)$  is the tracer concentration at a given equilibrium stage detected at time  $t$ .  $V_{\text{aq}, 0} \equiv V_{\text{aq}}(t=0)$  is the initial volume of aqueous liquid and  $V_{\text{aq}}(t)$  is the remaining volume of the aqueous liquid phase at time  $t$  not converted into hydrate phase at time  $t$ . Using Eq. (A.1), the change in volume of the liquid phase due to the formation of the hydrate phase at any given equilibrium stage at  $t > 0$ ,  $V_{\text{aq}, \text{consumed}}(t) = \Delta V_{\text{aq}, \text{consumed}}(t)$ , can be expressed as

$$\begin{aligned} V_{\text{aq}, \text{consumed}}(t) &= \Delta V_{\text{aq}}(t) = V_{\text{aq}, 0} - V_{\text{aq}}(t) \\ &= V_{\text{aq}, 0} \cdot \left( 1 - \frac{\rho_{\text{tracer}, 0}}{\rho_{\text{tracer}}(t)} \right) \end{aligned} \quad (\text{A.2})$$

The infinitesimal change in mass of the aqueous phase at instant  $t$ ,  $dm_{\text{aq}}(t)$ , is related to the corresponding infinitesimal volume change  $dV_{\text{aq}}(t)$  through the density of the liquid phase at that time  $\rho_{\text{aq}}(t)$  according to

$$dm_{\text{aq}}(t) = \rho_{\text{aq}}(t) \cdot dV_{\text{aq}}(t) \quad (\text{A.3})$$

If the density of the liquid phase is assumed to be unaffected by the small temperature- and composition changes occurring during the experimental run and thus assumed to be approximately constant and taken as the value of the initial liquid solution, i.e.  $\rho_{\text{aq}}(t) = \rho_{\text{aq}, 0}$ , the mass of consumed aqueous phase is calculated by

$$\begin{aligned} m_{\text{aq}, \text{consumed}}(t) &= \Delta m_{\text{aq}}(t) = \rho_{\text{aq}, 0} \Delta V_{\text{aq}}(t) \\ &= (V_{\text{aq}, 0} - V_{\text{aq}}(t)) \rho_{\text{aq}, 0} \end{aligned} \quad (\text{A.4})$$

By combining Eq. (A.2) with Eq. (A.4), the mass consumed for the formation of the hydrate phase at the equilibrium stage at  $t > 0$  is given by the following relation:

$$\begin{aligned} m_{\text{aq}, \text{consumed}}(t) &= \Delta m_{\text{aq}}(t) = \rho_{\text{aq}, 0} V_{\text{aq}, 0} \left( 1 - \frac{\rho_{\text{tracer}, 0}}{\rho_{\text{tracer}}(t)} \right) \\ &= m_{\text{aq}, 0} \left( 1 - \frac{\rho_{\text{tracer}, 0}}{\rho_{\text{tracer}}(t)} \right) \end{aligned} \quad (\text{A.5})$$

where  $m_{\text{aq}, 0}$  denotes the initial mass of the loaded solution, i.e., its mass at  $t=0$ . In experimental investigations using a digital vibrating-tube densimeter, Blandria et al. (2009) showed that in the temperature range from 293.15 K up to 333.15 K, the change in density of water-THF solutions as a function of composition for THF mass fractions of up to approximately 0.2 (corresponding to approximately 6 mol%) is lower than 1% when compared to the density of pure water at similar temperatures. Similarly, the density of pure water varies less than 0.2% in the temperature interval from 278.15 K to 293.15 K (NIST). Hence, in this work, it is considered a reasonable approximation to assume a constant value for the density of the aqueous phase despite variations in temperature, pressure and THF concentration. As the initial mass of the loaded aqueous liquid is known, the actual density of the solution then becomes unimportant, since it cancels out in subsequent calculations when considered constant.

Knowing the mass fraction of THF in the aqueous phase initially,  $w_{\text{THF},0}$ , and at a given equilibrium point,  $w_{\text{THF}}(t)$ , the masses of consumed water,  $m_{w,\text{consumed}}(t)$ , and THF,  $m_{\text{THF},\text{consumed}}(t)$ , may be estimated individually. Eq. (A.6) is used for estimating the THF consumption

$$\begin{aligned} m_{\text{THF},\text{consumed}}(t) &= m_{\text{aq},0} w_{\text{THF},0} - m_{\text{aq}}(t) w_{\text{THF}}(t) \\ &= m_{\text{aq},0} w_{\text{THF},0} - m_{\text{aq},0} \frac{\rho_{\text{tracer},0}}{\rho_{\text{tracer}}} w_{\text{THF}}(t) \\ &= m_{\text{aq},0} \left( w_{\text{THF},0} - \frac{\rho_{\text{tracer},0}}{\rho_{\text{tracer}}} w_{\text{THF}}(t) \right) \end{aligned} \quad (\text{A.6})$$

where  $m_{\text{aq},0}$  is the mass of the loaded aqueous phase at time 0 and  $m_{\text{aq}}(t)$  is the mass of the residual aqueous phase at time,  $t$ . Eq. (A.7) is utilised for the calculation of the corrected water consumption.

$$m_{w,\text{consumed}}(t) = m_{\text{aq},\text{consumed}}(t) - m_{\text{THF},\text{consumed}}(t) \quad (\text{A.7})$$

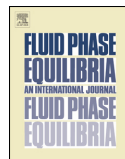
The equations shown here assume that water and THF initially present in the aqueous liquid phase is only transferred into the hydrate phase. The water content in the vapour and possible organic liquid phases are assumed negligible.

## References

- Adeyemo, A., Kumar, R., Linga, P., Ripmeester, J., Englezos, P., 2010. Capture of carbon dioxide from flue or fuel gas mixtures by clathrate crystallization in a silica gel column. *International Journal of Greenhouse Gas Control* 4, 478–485.
- Aman, Z.M., Olcott, K., Pfeiffer, K., Sloan, E.D., Sum, A.K., Koh, C.A., 2013. Surfactant adsorption and interfacial tension investigations on cyclopentane hydrate. *Langmuir* 29, 2676–2682.
- Babu, P., Kumar, R., Linga, P., 2013. Pre-combustion capture of carbon dioxide in a fixed bed reactor using the clathrate hydrate process. *Energy* 50, 364–373.
- Belandria, V., Mohammadi, A.H., Richon, D., 2009. Volumetric properties of the (tetrahydrofuran + water) and (tetra-*n*-butyl ammonium bromide + water) systems: experimental measurements and correlations. *Journal of Chemical Thermodynamics* 41, 1382–1386.
- Callen, H.B., 1985. *Thermodynamics and an Introduction to Thermostatistics*. John Wiley and Sons Inc, New York, Chichester, Brisbane, Toronto, Singapore.
- Daraboina, N., Ripmeester, J., Englezos, P., 2013. The impact of  $\text{SO}_2$  on post combustion carbon dioxide capture in bed of silica sand through hydrate formation. *International Journal of Greenhouse Gas Control* 15, 97–103.
- Danesh, A., Tohidi, B., Burgass, R.W., Todd, A.C., 1994. Hydrate equilibrium data of methyl cyclopentane with methane or nitrogen. *Chemical Engineering Research and Design* 72 (Part A), 197–200.
- De Deugd, R.M., Jager, M.D., de Swaan Arons, J., 2001. Mixed hydrates of methane and water-soluble hydrocarbons modeling of empirical results. *AIChE Journal* 47 (3), 693–704.
- Delahaye, A., Fournaison, L., Marinhas, S., Chatti, I., Petitot, J.-P., Dalmazzone, D., Fürst, W., 2006. Effect of THF on equilibrium pressure and dissociation enthalpy of  $\text{CO}_2$  hydrates applied to secondary refrigeration. *Industrial and Engineering Chemistry Research* 45, 391–397.
- Eslamimanesh, A., Mohammadi, A.H., Richon, D., Naidoo, P., Ramjugernath, D., 2012. Application of gas hydrate formation in separation processes: a review of experimental studies. *Journal of Chemical Thermodynamics* 46, 62–71.
- Fan, S., Liang, D.Q., Guo, K.H., 2001. Hydrate equilibrium conditions for cyclopentane and a quaternary cyclopentane-rich mixture. *Journal of Chemical and Engineering Data* 46, 930–932.
- Galfre, A., Fezoua, A., Ouabbas, Y., Cameirao, A., Herri, J.-M., 2011. Carbon dioxide hydrates crystallisation in emulsion. In: *Proceedings of the 7th International Conference on Gas Hydrates*, Paper ID 442.
- Giavarini, C., Maccioni, F., Santarelli, M.L., 2010.  $\text{CO}_2$  sequestration from coal fired power plants. *Fuel* 89, 623–628.
- Herri, J.-M., Bouchemoua, A., Kwaterski, M., Fezoua, A., Ouabbas, Y., Cameirao, A., 2011. Gas hydrate equilibria for  $\text{CO}_2$ - $\text{N}_2$  and  $\text{CO}_2$ - $\text{CH}_4$  gas mixtures—experimental studies and thermodynamic modelling. *Fluid Phase Equilibria* 301, 171–190.
- Jager, M.D., de Deugd, R.M., Peters, C.J., de Swaan Arons, J., Sloan, E.D., 1999. Experimental determination and modeling of structure II hydrates in mixtures of methane + water + 1,4-dioxane. *Fluid Phase Equilibria* 165, 209–223.
- Kang, S.-P., Lee, H., 2000. Recovery of  $\text{CO}_2$  from flue gas using gas hydrate, thermodynamic verification through phase equilibrium measurements. *Environmental Science and Technology* 34, 4397–4400.
- Kang, S.-P., Lee, H., Lee, C.-S., Sung, W.-M., 2001. Hydrate phase equilibria of the guest mixtures containing  $\text{CO}_2$ ,  $\text{N}_2$  and tetrahydrofuran. *Fluid Phase Equilibria* 185, 101–109.
- Kang, S.-P., Lee, J., Seo, Y., 2013. Pre-combustion capture of  $\text{CO}_2$  by gas hydrate formation in silica gel pore structure. *Chemical Engineering Journal* 218, 126–132.
- Karanjkar, P.U., Lee, J.W., Morris, J.F., 2012. Calorimetric investigation of cyclopentane hydrate formation in an emulsion. *Chemical Engineering Science* 68, 481–491.
- Koh, C.A., Sum, A.K., Sloan, E.D., 2009. Gas hydrates: unlocking the energy from icy cages. *Journal of Applied Physics* 106, 061101-1–061101-14.
- Lee, H.J., Lee, J.D., Linga, P., Englezos, P., Kim, Y.S., Lee, M.S., Kim, Y.D., 2010. Gas hydrate formation process for pre-combustion capture of carbon dioxide. *Energy* 35, 2729–2733.
- Li, S., Fan, S., Wang, J., Lang, X., Wang, Y., 2010. Clathrate hydrate capture of  $\text{CO}_2$  from simulated flue gas with cyclopentane/water emulsion. *Chinese Journal of Chemical Engineering* 18 (2), 202–206.
- Li, X.-S., Xu, C.-G., Chen, Z.-Y., Wu, H.-J., 2011. Hydrate-based pre-combustion carbon dioxide capture process in the system with tetra-*n*-butyl ammonium bromide solution in the presence of cyclopentane. *Energy* 36, 1394–1403.
- Li, X.-S., Xu, C.-G., Chen, Z.-Y., Cai, J., 2012. Synergic effect of cyclopentane and tetra-*n*-butyl ammonium bromide on hydrate-based carbon dioxide separation from fuel gas mixture by measurements of gas uptake and X-ray diffraction patterns. *International Journal of Hydrogen Energy* 37, 720–727.
- Lim, Y.-A., Babu, P., Kumar, R., Linga, P., 2013. Morphology of carbon dioxide-hydrate-cyclopentane hydrates with or without sodium dodecyl sulfate. *Crystal Growth and Design* 13, 2047–2059.
- Linga, P., Kumar, R., Englezos, P., 2007a. Gas hydrate formation from hydrogen/carbon dioxide and nitrogen/carbon dioxide gas mixtures. *Chemical Engineering Science* 62, 4268–4276.
- Linga, P., Kumar, R., Englezos, P., 2007b. The clathrate hydrate process for post and pre-combustion capture of carbon dioxide. *Journal of Hazardous Materials* 149, 625–629.
- Linga, P., Adeyemo, A., Englezos, P., 2008. Medium-pressure clathrate hydrate/membrane hybrid process for postcombustion capture of carbon dioxide. *Environmental Science and Technology* 42, 315–320.
- Linga, P., Kumar, R., Lee, J.D., Ripmeester, J.A., Englezos, P., 2010. A new large scale apparatus to enhance the rate of gas hydrate formation: application to capture of carbon dioxide. *International Journal of Greenhouse Gas Control* 4, 630–637.
- Linga, P., Daraboina, N., Ripmeester, J.A., Englezos, P., 2012. Enhanced rate of gas hydrate formation in a fixed bed column filled with sand compared to a stirred vessel. *Chemical Engineering Science* 68, 617–623.
- Mohammadi, A.H., Richon, D., 2009. Phase equilibria of clathrate hydrates of methyl cyclopentane, methyl cyclohexane, cyclopentane or cyclohexane + carbon dioxide. *Chemical Engineering Science* 64, 5319–5322.
- Ohmura, R., Matsuda, S., Takeya, S., Ebinuma, T., Narita, H., 2005. Phase equilibrium for structure-H hydrates formed with methane and methyl-substituted cyclic ether. *International Journal of Thermophysics* 26 (5), 1515–1523.
- Riesco, N., Trusler, J.P.M., 2005. Novel optical flow cell for measurements of fluid phase behavior. *Fluid Phase Equilibria* 228–229, 233–238.
- Sabil, K.M., Witkamp, G.-J., Peters, C.J., 2010. Phase equilibria in ternary (carbon dioxide + tetrahydrofuran + water) system in hydrate-forming region: effects of carbon dioxide concentration and the occurrence of pseudo-retrograde hydrate phenomenon. *Journal of Chemical Thermodynamics* 42, 8–16.
- Saito, Y., Kawasaki, T., Okui, T., Kondo, T., Hiraoka, R., 1996. Methane storage in hydrate phase with water soluble guests. In: *Proceedings of the Second International Conference on Natural Gas Hydrates*, pp. 459–465.
- Seo, Y., Kang, S.-P., Lee, S., Lee, H., 2008. Experimental measurements of hydrate phase equilibria for carbon dioxide in the presence of THF, propylene oxide, and 1,4-dioxane. *Journal of Chemical and Engineering Data* 53, 2833–2837.
- Sloan Jr., E.D., 2003. Fundamental principles and applications of natural gas hydrates. *Nature* 426, 353–359.
- Sloan, E.D., Koh, C.A., 2008. *Clathrate Hydrates of Natural Gases*, third ed. CRC Press, Taylor & Francis Group, Boca Raton, London, New York.
- Sum, A.K., Burruss, R.C., Sloan Jr., E.D., 1997. Measurement of clathrate hydrates via Raman spectroscopy. *Journal of Physical Chemistry B* 101, 7371–7377.
- Sum, A.K., Koh, C.A., Sloan, E.D., 2009. Clathrate hydrates: from laboratory science to engineering practice. *Industrial Chemistry Research* 48, 7457–7465.
- Sun, C., Li, W., Yang, X., Li, F., Yuan, Q., Mu, L., Chen, J., Liu, B., Chen, G., 2011. Progress in research of gas hydrate. *Chinese Journal of Chemical Engineering* 19 (1), 151–162.
- Tohidi, B., Danesh, A., Todd, A.C., Burgass, R.W., 1997. Equilibrium data and thermodynamic modelling of cyclopentane and neopentane hydrates. *Fluid Phase Equilibria* 138, 241–250.
- Trueba, A.T., Rovetto, L.J., Florusse, L.J., Kroon, M.C., Peters, C.J., 2011. Phase equilibrium measurements of structure II clathrate hydrates of hydrogen with various promoters. *Fluid Phase Equilibria* 307, 6–10.
- Tsuiji, H., Ohmura, R., Mori, Y.H., 2004. Forming structure-H hydrates using water spraying in methane gas: effects of chemical species of large-molecule guest substances. *Energy and Fuels* 18, 418–423.
- Zhang, J.S., Lee, J.W., 2009a. Equilibrium of hydrogen + cyclopentane and carbon dioxide + cyclopentane binary hydrates. *Journal of Chemical and Engineering Data* 54, 659–661.
- Zhang, J.S., Lee, J.W., 2009b. Enhanced kinetics of  $\text{CO}_2$  hydrate formation under static conditions. *Industrial and Engineering Chemistry Research* 48, 5934–5942.
- Zhang, J.S., Yedlapalli, P., Lee, J.W., 2009. Thermodynamic analysis of hydrate-based pre-combustion capture of  $\text{CO}_2$ . *Chemical Engineering Science* 64, 4732–4736.

## **Appendix 3**





# Application of the cubic-plus-association (CPA) equation of state to model the fluid phase behaviour of binary mixtures of water and tetrahydrofuran



Peter Jørgensen Herslund<sup>a,c</sup>, Kaj Thomsen<sup>a,c</sup>, Jens Abildskov<sup>b,c</sup>, Nicolas von Solms<sup>a,c,\*</sup>

<sup>a</sup> Center for Energy Resources Engineering (CERE), Technical University of Denmark, DK2800 Kongens Lyngby, Denmark

<sup>b</sup> Computer Aided Process Engineering Center (CAPEC), Technical University of Denmark, DK2800 Kongens Lyngby, Denmark

<sup>c</sup> Department of Chemical and Biochemical Engineering, Technical University of Denmark, DK2800 Kongens Lyngby, Denmark

## ARTICLE INFO

### Article history:

Received 21 December 2012

Received in revised form 9 July 2013

Accepted 15 July 2013

Available online 26 July 2013

### Keywords:

Fluid phase behaviour

Aqueous

Tetrahydrofuran

Modelling

Cubic-plus-association (CPA)

Thermodynamics

## ABSTRACT

The complex fluid phase behaviour, of the binary system comprised of water and tetrahydrofuran (THF) is modelled by use of the cubic-plus-association (CPA) equation of state. A total of seven modelling approaches are analysed, differing only in their way of describing THF and its interactions (hydrogen bonding) with water.

The qualitative behaviour of the fluid phase equilibria in this system can only be described by CPA when cross-association between water and THF is allowed.

Six of the seven tested modelling scenarios allow for cross-association between the two compounds. These scenarios are named Case 2 to Case 7. Case 2 treats THF as non self-associating, but applies a single association site on the THF oxygen atom, that allows for cross-linking with a single water molecule. Case 3 is identical to Case 2 but applies two association sites on THF, allowing for simultaneous cross-association with two water molecules. Case 4 treats THF as self-associating and cross-associating according to an association scheme with two electron accepting sites and a single electron donating site. Case 5 also considers both self- and cross-association by THF, but applies an association scheme with two electron accepting- and two electron donating sites.

Cases 6 and 7 are similar to Cases 4 and 5, respectively, however the binary cross-association volume between electron accepting sites on water and electron donating sites on THF is adjusted to match the CPA descriptions with available experimental VLE data.

It is found that Cases 2, 3, 6 and 7 (when applying three adjustable binary parameters), are the only cases, which can describe both VLE and LLE using a single set of parameters. With a total of three binary parameters correlated to available VLE data, these data may be described with average absolute deviations of approximately 5–7 percent. The LLE is well predicted by both model Cases 2 and 3, with a slightly better phase composition prediction by Case 3.

While Cases 6 and 7 describe VLE data better than the cases treating THF as solvating, the LLE is less accurately described.

Based on the results presented in this work, it is suggested to model this binary system considering THF as cross-associating only, with two cross-association sites. The use of a temperature dependent binary interaction parameter and a correlated binary cross-association volume then allows for both accurate VLE and LLE descriptions in large ranges of temperature and pressure.

© 2013 Elsevier B.V. All rights reserved.

## 1. Introduction

The fluid phase behaviour of binary systems containing tetrahydrofuran (THF) and water was intensively studied from the late 1960s to the beginning of the 1980s [1–9]. Most studies have

focused on the vapour–liquid equilibrium (VLE) of this system, which is highly non-ideal and exhibits an azeotrope in the high THF concentration region.

THF is a cyclic ether with the chemical formula  $c-(CH_2)_4O$ , which is widely used as a precursor in polymer production, a solvent for polymers (e.g. poly vinyl chloride–PVC) and a cleaning agent for semi-conductors [9].

In chemical processes where THF is used as a solvent, the solvent phase is easily polluted with water due to the hygroscopic

\* Corresponding author. Tel.: +45 4525 2867; fax: +45 4588 2258.  
E-mail address: [NVS@kt.dtu.dk](mailto:NVS@kt.dtu.dk) (N. von Solms).

**List of symbols***Normal characters*

$A_i$	association site type “A” on component $i$ [unit less]
$a_{k_{ij}}$	constant in temperature expression for $k_{ij}$ [unit less]
$a_0$	CPA pure component parameter [ $\text{Pa m}^6 \text{mol}^{-2}$ ]
$B_j$	association site type “B” on component $j$ [unit less]
$b$	CPA co-volume parameter [ $\text{m}^3 \text{mol}^{-1}$ ]
$b_{k_{ij}}$	constant in temperature expression for $k_{ij}$ [K]
$c_1$	CPA pure component parameter [unit less]
$g$	hard sphere radial distribution function [unit less]
$k_{ij}$	binary interaction parameter [unit less]
$P$	pressure [Pa]
$T$	temperature [K]
$R$	gas constant [ $\text{m}^3 \text{Pa mole}^{-1} \text{K}^{-1}$ ]
$V$	volume [ $\text{m}^3$ ]
$x$	liquid phase mole fraction [unit less]
$X_{A_i}$	fraction of non-bonded association sites of type “A” on component $i$ [unit less]
$y$	vapour phase mole fraction [unit less]

*Greek letters*

$\alpha(T)$	CPA temperature dependent attractive parameter [ $\text{Pa m}^6 \text{mol}^{-2}$ ]
$\beta$	CPA association volume [unit less]
$\Delta$	CPA association strength [ ]
$\varepsilon$	CPA association energy [ $\text{Pa m}^3 \text{mol}^{-1}$ ]
$\omega$	acentric factor [unit less]

*Subscripts*

$i$	component $i$ [unit less]
$j$	component $j$ [unit less]

*Superscripts*

Ref	reference system [unit less]
-----	------------------------------

properties of THF and the mutual miscibility of THF and water in the liquid state (at ambient pressure and temperature). One of the main motivations behind the before mentioned VLE studies of this binary system, was the attempt of establishing efficient purification processes for THF solvent phases contaminated with water. Since the proposed processes were often based on distillation, VLE data were measured mainly at or below atmospheric pressure. Matsuda et al. [9] listed some of the most recent separation processes based on distillation. Most processes apply modifications such as pressure swing, addition of salt or polymers in order to overcome the distillation barrier caused by the azeotrope occurring at approximately 82 mole percent THF at atmospheric pressure [9].

The fluid phase behaviour of the binary THF/water system is highly non-ideal and displays some uncommon phenomena. At low to ambient pressures and temperatures, THF and water are fully miscible in their liquid states. The miscibility of these components is expected to be a result of hydrogen bonding occurring between the oxygen atom on THF and hydrogen atoms on water. Due to the cyclic structure of THF, the oxygen atom becomes more “exposed” than what is normally the case for linear ethers. THF thereby displays some degree of polarity, which could explain the greatly enhanced miscibility of THF in water, compared to linear ethers in water.

A sign of the highly non-ideal behaviour of THF/water mixtures is found in the low pressure VLE reported in the literature. Here, a low boiling azeotrope occurs at high THF concentrations, indicating strong negative deviations from Raoult's law. Generally, with increasing temperature, the position of the azeotropic mixture

**Table 1**

Selected experimental vapour–liquid equilibrium data reported in the literature for the binary system of tetrahydrofuran and water.

Reference	Type	No data points	Temp. (K)	Pressure (MPa)
[1]	Txy/Pxy	40	298.15–373.15	0.0165–0.1013
[2]	Px	21	298.15	0.0032–0.0216
[3]	Txy	4	334.55–335.85	0.0973
[4]	Pxy	34	323.15–343.15	0.0404–0.1264
[5]	Txy	7	336.95–338.85	0.1013
[6]	Px	22	298.15	0.0032–0.0221
[7]	Txy	12	336.70–337.70	0.1013
[8]	Txy	10	336.75–339.10	0.1013
[9]	Tx	102	311.80–373.20	0.0400–0.1013

moves towards lower THF concentrations. This phenomenon may be observed in Fig. 3. The fact that the azeotropic behaviour is of the low-boiling type, supports the theory that THF and water cross interacts possibly by hydrogen bonding.

Table 1 presents a selection of the available VLE data found in the literature. These data are utilised as reference data in the modelling of this work. The binary compositions in most of the experimental investigations listed in Table 1 range from pure THF to pure water.

Shnitko and Kogan [1] pointed towards the fact that the concentration independence of the measured boiling point temperatures in the concentration interval from approximately 10–60 mole percent is similar to that found in systems with liquid–liquid splits, however Shnitko and Kogan observed no liquid splits during their experimental work. Similar observations and conclusions have been reported recently by Matsuda et al. [9].

Matous et al. [4,11] were the first to present findings of a circular miscibility gap for the binary THF/water system. This split was found to occur in the liquid phase region above atmospheric pressure. Their investigations were inspired by the diverging conclusions in previously reported data.

The findings of Matous et al. [4] have later been confirmed by others. Table 2 provides a list of authors reporting experimental data for the closed loop miscibility gap occurring in the THF/water system above atmospheric pressure.

Despite THF and water being fully miscible at low pressures, a closed-loop miscibility gap occurs at temperatures above 345 K and elevated pressures. The formation of a closed-loop miscibility gap in binary mixtures may be explained in terms of a competition between entropic and energetic effects [13]. At temperatures below the lower critical solution temperature (LCST) hydrogen bonding between THF and water molecules are sufficient to overcome unfavourable orientational entropy and enthalpic contributions to the overall energy of the system. Hence, the liquid phase is stable. By increasing the temperature enthalpic contributions begin to dominate. Weak van der Waals forces between unlike species force the mixture to separate into two immiscible phases in order to minimise the overall system energy. Increasing further in temperature, to above the upper critical solution temperature (UCST), entropic effects dominate, and the system may minimise its overall energy by maximising its compositional and orientational entropy. Hence a single phase re-appears [13].

For the THF/water system, the LCST at  $P=3.0$  MPa is approximately 348 K. The UCST is found at 405 K. Increasing pressure

**Table 2**

Selected experimental liquid–liquid equilibrium data reported in the literature for the binary system of tetrahydrofuran and water.

Reference	Type	No data points	Temp. (K)	Pressure (MPa)
[4]	Tx	38	344.95–410.25	N/A
[10]	PT	51	350.00–401.50	2.7000–24.7000
[12]	Tx	82	345.45–405.63	0.4830–6.0600

increases the LCST and lowers the UCST, thereby shrinking the size of the miscibility gap.

Wallbruch and Schneider [10] showed experimentally that the closed loop miscibility gap shrinks with increasing pressure and the binary system finally reaches a hypercritical point at  $T = 365$  K,  $P = 24.7$  MPa and  $x_{\text{THF}} = 0.22$ . Riesco and Trusler [12] confirmed the pressure effect found by Wallbruch and Schneider.

Several models have been applied through time to enable a description of the complex VLE and LLE behaviour of the binary THF/Water systems. Early attempts of modelling the fluid phase behaviour in the binary system of THF and water have mainly been based on approaches, combining Gibbs excess energy models such as the Redlich–Kister equation [14] and later the more advanced local composition models such as the non-random two-liquid (NRTL) [15] and the UNiversal QUasi-Chemical (UNIQUAC) [16]. The UNiversal Functional Activity Coefficient (UNIFAC) group contribution model [17] has also been applied recently. Most often the above models are combined with either the assumption of a coexisting ideal gas or with cubic equations of state such as the Soave–Redlich–Kwong (SRK) [18] or the Peng–Robinson (PR) [19] for the vapour phase. Using an equation of state for modelling the vapour phase enables phase equilibrium calculations at high pressures, where the assumption of ideality in the vapour phase becomes questionable.

In more recent modelling attempts, advanced equations of state such as the cubic-plus-association (CPA) [20,21] have been applied or the simpler cubic PR and SRK have been combined with advanced mixing rules such as the Huron–Vidal types (MHV-1 [22], MHV-2 [23] and HVOS [24]), incorporating activity coefficient models typically in the form of UNIQUAC, NRTL, UNIFAC etc. A short summary of presented applications of the above mentioned models to the model the binary water–THF system is presented in the following.

Few of the authors listed in Table 1 also present attempts of modelling their data. Matous et al. [4] utilised a modified Redlich–Kister equation in order to describe liquid phase activity coefficients of water and THF in their binary mixtures. A total of four binary parameters (three in the Redlich–Kister polynomial and one concentration related) were correlated in order to obtain a satisfactory description of the VLE data. These parameters were highly temperature dependent and two parameter sets were presented (for 50 °C and 70 °C). Matous et al. emphasised the importance of investigating the physical meaning of obtained parameters such that a thermodynamically consistent model was obtained. It was illustrated how simply correlating VLE data could result in binary parameters predicting unstable liquid phases in the stable liquid phase region of this system. Matous et al. presented means of avoiding this, when using the modified Redlich–Kister equation.

Lampa et al. [8] presented modelling attempts also using a variation of the Redlich–Kister equation based on mole fractions. They concluded that four binary parameters (all in the Redlich–Kister polynomial) were sufficient to correlate activity coefficients and VLE data in this system while still respecting the stability of the liquid phase at temperatures below the normal boiling point temperature. The approach presented by Matous et al. [4] was followed in order to obtain physically meaningful parameters. Model parameters were correlated and results compared to isobaric experimental VLE data measured only at a single pressure of 1 atm.

Rehak et al. [25] compared performances of modified Wilson [26] and modified NRTL models in terms of their ability to describe both the VLE and LLE of the binary THF/water system. The modifications to both models were made by super-imposing the Redlich–Kister polynomial as an additional residual term on the models. Hence both the Wilson or NRTL and the Redlich–Kister models contributed to calculated Gibbs excess energies. Eight binary parameters were correlated in the modified NRTL model

in order to get an accurate description of both the VLE and LLE. Nine binary parameters were needed in the modified Wilson model. According to Rehak et al., both models had been tested with higher numbers of correlated parameters without a significant gain in accuracy. Whereas the two models performed comparable for the VLE description, a clear difference was observed in the LLE description. Here the modified Wilson model outperformed the modified NRTL model in describing the circular LLE region.

Brovchenko and Guillot [27] performed molecular simulations using the NPT (fixed number of molecules, pressure and temperature) Gibbs ensemble in order to describe the liquid–liquid co-existence in the binary THF/water system. Systems of various compositions, all containing a total of 500 molecules (approximately) were simulated. The TIP4P force field model was used for water and a five-site force field model for THF. Using only one binary correction factor, Brovchenko and Guillot were able to describe the upper critical temperature reported by Matous et al. [4] with an accuracy of approximately 20 K and a concentration close to the experimentally determined. However the model was unable to describe the lower critical temperature. By investigating the structural properties of the simulated phases, Brovchenko and Guillot found that, on average, between one and two water molecules were always hydrogen bonded to the oxygen atom of each THF molecule, indicating a high temperature stability of this hydrogen bond.

Lazzaroni et al. [28] modelled the binary system using the Peng–Robinson equation of state (EoS) with the modifications of Stryjek and Vera (PRSV) [29]. Correlation results when using different mixing rules for the alpha parameter were presented. Among others, three variations of the Huron–Vidal mixing rules (MHV1, MHV2 and HVOS) were applied. Both the NRTL and the UNIQUAC Gibbs excess energy models were tested in these modified Huron–Vidal mixing rules. The simple linear concentration dependence was used for the  $b$  parameter of the PRSV EoS. Lazzaroni et al. put emphasis on the ability to correlate VLE data without falsely predicting LLE, when evaluating the tested mixing rules. The HVOS mixing rule combined with the NRTL model provided the best correlation of boiling point pressures in the temperature range from 298 K to 343 K. An absolute average deviation (AAD) less than 1 percent in terms of calculated pressures at three temperatures (298 K, 323 K and 343 K) was obtained by correlating two binary parameters in the model for each temperature, plus a third correlation parameter, that was held constant at all three temperatures. Hence, a total of seven binary parameters were needed in order to describe the boiling point curves of the binary system in the above mentioned temperature interval. No comments were made on the accuracy in the predicted vapour phase compositions or the accuracy of the model of describing the azeotrope or the LLE occurring at higher temperatures.

Browarzik [30] presented both VLE and LLE modelling results for the binary system of THF and water using an advanced Gibbs excess energy model based on continuous thermodynamics. The model used a continuous distribution function for describing associating compounds as mixtures of chain associates. This distribution function was temperature and composition dependent. Despite the fact that water forms three-dimensional rather than chain associates, the model performed well in describing aqueous systems.

Three binary parameters were correlated to the experimental LLE data of Matous et al. [4]. Accurate descriptions of the circular LLE behaviour were obtained. The developed model predicted the azeotrope in the VLE data reported by Matous et al. [4] at 323 K and 343 K. However, predicted boiling point pressures were generally lower than the experimental data, especially in the water-rich composition region.

Susilo et al. [31] claimed to be able to model VLE of mixtures of THF and water using the SRK EoS combined with the MHV-2 mixing rule obtaining activity coefficients from the modified UNIFAC



model. The model was combined with the van der Waals–Platteeuw gas clathrate hydrate model [32] in order to model phase boundaries of the solid hydrate phase formed in aqueous THF mixtures in contact with methane. No fluid phase modelling results were presented. Parameters for the modified UNIFAC model were taken from elsewhere in the literature [33].

When modelling mixed THF/hydrogen gas clathrate hydrates, Martin and Peters [34] claimed to be able to model fluid phase behaviour of binary mixtures of THF and water in the temperature interval from 298 K to 373 K using the CPA equation of state. Water was modelled using an association scheme with two electron donating and two electron accepting sites, THF was assumed non self-associating. Pure component parameters for THF were obtained from critical data ( $T$ ,  $P$ ,  $\omega$ ) and a constant binary interaction parameter ( $k_{ij}$ ) of  $-0.35$  was utilised. According to the authors, equilibrium data presented elsewhere [35] were modelled with an absolute average accuracy of 10.1 percent in terms of calculated pressures, however no actual fluid phase modelling results were presented.

Sabil et al. [36] modelled the ternary system of carbon dioxide, THF and water using the PRSV EoS with the HVOS mixing rule incorporating the UNIQUAC Gibbs excess energy model. Four binary parameters in the UNIQUAC model for the THF/water binary pair were fitted to experimental data presented by Lazzaroni et al. [28]. No modelling results for the binary THF/water system were presented, but good accuracy in the description of the liquid water ( $L_w$ ) – liquid organic ( $L_o$ ) → liquid water ( $L_w$ ) – liquid organic ( $L_o$ ) – vapour ( $V$ ) phase transition (boiling point) was obtained for various compositions in the temperature range from 282 K to 298 K and pressures up to approximately 6 MPa.

Matsuda et al. [9] modelled VLE in the binary THF/water system using the NRTL model for the liquid phase combined with the assumption of ideal gas for the vapour phase. Boiling point temperatures were successfully modelled in the pressure range from 0.04 MPa to 0.1 MPa. Three binary NRTL parameters were correlated in order to match the model with their own experimental data (boiling point temperatures). An average absolute deviation of 0.2 K was obtained for a total of 102 data points. The maximum absolute deviation in the calculated boiling point temperatures compared to the measured data was 1.7 K. No LLE modelling was presented.

Lee et al. [37] combined the Wilson equation with the assumption of ideal gas behaviour at pressures at or below 1 atm and the PR equation at pressures above 1 atm, in order to model VLE behaviour of the THF/water system. Two binary parameters were correlated in the Wilson model to get accurate VLE description at a pressure of 1 atm. Lee et al. made no comments on whether a binary interaction parameter in the PR EoS had been correlated or not. Largest deviations between calculated and experimental data were found in the concentration region around 10 mole percent THF, where boiling point temperatures were over estimated by approximately 2 K.

Ben Attouche Sfaxi [38] modelled VLE behaviour for the binary system using the advanced Cubic-Plus-Association (CPA) equation of state (EoS). A four-site association scheme was used for water (self-associating with two electron donating and two electron accepting sites) and THF was treated as non self-associating. In order to account for the expected interactions between the two species, Ben Attouche Sfaxi defined two association sites (electron donating sites) on the THF oxygen molecule and made these available for cross association with hydrogen atoms on the surrounding water molecules. The approach of Folas et al. [39] was first followed in order to obtain binary association parameters. However this approach was found inappropriate for the THF/water system. Ben Attouche Sfaxi finally correlated both the binary cross association parameters ( $\epsilon^{A_i B_j}$  and  $\beta^{A_i B_j}$ ) and a constant  $k_{ij}$  to available VLE data. The final VLE modelling results presented did however still indicate an undesired liquid–liquid split occurring in the VLE region

at temperatures around 343 K. No LLE modelling results were presented.

Pahlavanzadeh et al. [40] recently used the UNIFAC group contribution model to describe activity coefficients of THF and water in their binary mixtures in the attempt of modelling gas clathrate hydrates containing THF. However, no UNIFAC model parameters or fluid phase modelling results were presented.

In recent attempts of modelling the fluid phase behaviour of the binary system of THF and water [23,27], an advanced equation of state, the cubic-plus-association (CPA) [20,21] has been applied. While only few results have been presented on the VLE description by this model at low to moderate pressures [27], no results have been presented for the liquid phase behaviour predicted by this model at higher temperatures and pressures.

Some of the referenced attempts of modelling the fluid phase behaviour of binary systems of water and THF have been motivated by the need for developing thermodynamic models capable of describing the formation of gas clathrate hydrates containing THF. In such models, an accurate description of both the water activity in the liquid phase and the fugacity of THF is of great importance, as these are key factors, that play important roles in gas hydrate models such as e.g. the van der Waals–Platteeuw gas clathrate hydrate model [32]. The development of such a model in order to enable thermodynamic evaluations of gas separation processes based on gas hydrate formation is also the main motivator behind this work. THF may form structure II gas hydrates at mild conditions of temperature and pressure and has been proposed as a potential thermodynamic hydrate promoter e.g. in carbon dioxide capture processes.

In this work the CPA equation of state is applied to model both the VLE and the LLE of the binary system. CPA has the advantage of being able to account for the strong polar interactions (hydrogen bonds) occurring between THF and water. Results from several attempts of correlating the binary VLE behaviour while respecting the high temperature/high pressure liquid–liquid phase behaviour are presented. The main differences between the presented modelling attempts lie in the treatment of THF in CPA as being either non-associating, cross-associating (solvating) or self- and cross-associating.

## 2. Model

### 2.1. The cubic-plus-association equation of state

The CPA equation of state presented by Kontogeorgis et al. [19,20] combines the physical term from the cubic Soave–Redlich–Kwong (SRK) EoS with an association term similar to that found in the statistical associating fluid theory (SAFT) models.

On pressure explicit form, the CPA EoS may be expressed [41]:

$$P = \frac{R \cdot T}{V_m - b} - \frac{\alpha(T)}{V_m \cdot (V_m + b)} - \frac{R \cdot T}{2 \cdot V_m} \cdot \left[ 1 + \frac{1}{V_m} \cdot \frac{\partial \ln g}{\partial (1/V_m)} \right] \times \sum_i x_i \sum_{A_i} (1 - X_{A_i}) \quad (1)$$

where  $R$  is the gas constant and  $T$  is temperature.  $V_m$  denotes the molar volume,  $\alpha(T)$  is the temperature dependent SRK energy parameter and  $b$  is the SRK co-volume parameter.  $g$  is the hard sphere radial distribution function.  $A_i$  denotes association site A on component  $i$ .  $x_i$  is the mole fraction of component  $i$ ,  $X_{A_i}$  is the fraction of sites, type A on component  $i$ , not bonded to other sites. CPA simplifies to the SRK EoS for non-associating systems.



The fraction of non-bonded sites,  $X_{A_i}$ , is estimated by solving Eqs. (2) and (3).

$$X_{A_i} = \left[ 1 + V_m^{-1} \cdot \sum_j x_j \sum_{B_j} X_{B_j} \cdot \Delta^{A_i B_j} \right]^{-1} \quad (2)$$

Eq. (2) is evaluated for all site types on all associating components. The summation over  $B_j$  in Eq. (2) indicates summation over all association sites.

$\Delta^{A_i B_j}$  is the association strength between site A on molecule  $i$  and site B on molecule  $j$ . It is given by

$$\Delta^{A_i B_j} = g(V_m)^{\text{ref}} \cdot [\exp(\varepsilon^{A_i B_j} \cdot (R \cdot T)^{-1}) - 1] \cdot b_{ij} \cdot \beta^{A_i B_j} \quad (3)$$

$\varepsilon^{A_i B_j}$  and  $\beta^{A_i B_j}$  are the association energy and volume, respectively between site A on molecule  $i$  and site B on molecule  $j$ .  $g(V_m)^{\text{ref}}$  is the contact value of the radial distribution function for the reference hard sphere fluid system.

The radial distribution function,  $g(V_m)$  was presented in a simplified form by Kontogeorgis et al. (sCPA [21]). Whereas earlier versions of CPA utilised the Carnahan–Starling expression for the hard-sphere radial distribution function, sCPA uses the expression shown in Eq. (4) for the simplified hard-sphere radial distribution function.

$$g(V_m) = [1 - 1.9 \cdot b \cdot (4 \cdot V_m)^{-1}]^{-1} \quad (4)$$

This work utilises the simplified form of CPA.

The temperature-dependent energy parameter,  $\alpha_i(T)$  for pure component  $i$ , in the SRK term is calculated by means of Eq. (5).

$$\alpha_i(T) = a_{0,i} \cdot \left[ 1 + c_{1,i} \cdot \left( 1 - \sqrt{T \cdot T_{c,i}^{-1}} \right) \right]^2 \quad (5)$$

where  $a_{0,i}$  and  $c_{1,i}$  are pure component parameters and  $T_{c,i}$  is the critical temperature for component  $i$ . For associating components, the CPA EoS utilises five pure component parameters,  $a_{0,i}$ ,  $b_i$ ,  $c_{1,i}$ ,  $\varepsilon^{A_i B_i}$  and  $\beta^{A_i B_i}$ . Non-associating components are described by three pure component parameters,  $a_{0,i}$ ,  $b_i$  and  $c_{1,i}$  in a manner similar to that of the “standard” SRK EoS. Pure component parameters for associating components are obtained by fitting the model to experimental vapour pressures and saturated liquid densities of the pure component. The three pure component parameters for non-associating compounds may also be obtained from critical temperature,  $T_{c,i}$ , critical pressure,  $P_{c,i}$ , and the acentric factor,  $\omega_i$ .

In binary systems, the van der Waals one-fluid mixing rules are used for evaluating the SRK parameters,  $\alpha(T)$  and  $b$ . This is done according to Eqs. (6) and (7) [41].

$$\alpha(T) = \sum_i \sum_j x_i \cdot x_j \cdot \alpha_{ij}(T) \quad (6)$$

$$b = \sum_i x_i \cdot b_i \quad (7)$$

where the “classical” combining rules are applied for the binary  $\alpha_{ij}(T)$  in the SRK term and the binary  $b_{ij}$  in the association term.

$$\alpha_{ij}(T) = \sqrt{\alpha_i(T) \cdot \alpha_j(T)} \cdot (1 - k_{ij}) \quad (8)$$

$$b_{ij} = (b_i + b_j) \cdot 2^{-1} \quad (9)$$

$k_{ij}$  in Eq. (8) is the binary interaction parameter (BIP) between component,  $i$ , and component,  $j$ .  $k_{ij}$  may be temperature-dependent, e.g. according to the equation  $k_{ij} = a_{kij} + b_{kij}/T$ . No mixing rules are needed for the association parameters of CPA. Only for cross associating systems, combining rules must be applied to the two

association parameters  $\varepsilon^{A_i B_j}$  and  $\beta^{A_i B_j}$ . This work utilises the CR1 combining rules according to Eqs. (10) and (11).

$$\varepsilon^{A_i B_j} = (\varepsilon^{A_i B_i} + \varepsilon^{A_j B_j}) \cdot 2^{-1} \quad (10)$$

$$\beta^{A_i B_j} = \sqrt{\beta^{A_i B_i} \cdot \beta^{A_j B_j}} + \gamma^{A_i B_j} \quad (11)$$

The combining rule for  $\beta^{A_i B_j}$ , Eq. (11), has been written in a general form, which handles both cross-association between two self-associating molecules as well as cross-association between one self-associating and one non self-associating molecule (solvation). In the case of cross-association between two self-associating molecules,  $\gamma^{A_i B_j}$  may either be set to zero, in order to allow model prediction according to the standard CR1 combining rule, or it can be used as a handle on the deviation of the cross association interactions from the arithmetic mean. In cases with cross-association involving one non self-associating molecule,  $\gamma^{A_i B_j}$  is needed to provide cross-association interactions. For systems containing three or more components sCPA becomes predictive, since only binary interactions may be accounted for (directly) in the process of parameter estimation.

### 3. Parameterisation of the model

#### 3.1. Pure component parameters and association schemes

In this work the general notation for association schemes is  $\{ \{X^+ \}; \{Y^- \} \}$ , where  $X$  and  $Y$  are number of sites. Superscripts (+) and (−) denote whether the sites are electron accepting (+) or electron donating (−). Water is always modelled as a self-associating compound with a total of four associating sites. Two sites are electron donating (two sets of oxygen atom lone pair electrons) and two are electron accepting (two hydrogen atoms). Self-association between two water molecules is modelled by allowing electron donating sites on one molecule to interact (hydrogen bond) with electron accepting sites on another molecule of the same type. The association strength is defined by the pure component association parameters,  $\varepsilon^{A_i B_i}$  and  $\beta^{A_i B_i}$ . Hence, the association scheme for water in the above defined notation becomes  $[2^+; 2^-]$ , corresponding to the 4C association scheme as defined by Huang and Radosz [42]. The five pure component parameters for water are available elsewhere in the literature [41] and these have been adopted here.

Since no authors in the literature have presented successful attempts of modelling both VLE and LLE for the binary system of water and THF using the CPA equation of state, a screening of potential modelling approaches for THF has been performed in this work. Scenarios including THF as non-associating, only cross-associating (solvating), self- and cross-associating have been investigated. When THF is modelled as non-associating or cross-associating only, the three pure component CPA parameters ( $a_0$ ,  $b$  and  $c_1$ ) are obtained by correlating vapour pressure and saturated liquid densities. Similarly, these data are used when the five pure component parameters ( $a_0$ ,  $b$ ,  $c_1$ ,  $\varepsilon^{A_i B_i}$  and  $\beta^{A_i B_i}$ ) for THF as self-associating are regressed. The “Design Institute for Physical Property Data (DIPPR)” correlations [43] in the reduced temperature range from  $0.30 < T/T_c < 0.93$  have been used as reference data in both approaches.

In the cases where THF is assumed to cross-associate only, two cases with different association schemes have been tested. These cases differ in their number of electron donating sites on the THF molecule. The first case applies a single electron donating site on the THF oxygen atom. In the general notation, this type of association scheme becomes  $[0^+; 1^-]$  The site is allowed to associate only with electron accepting sites (hydrogen atoms) on water molecules.

The second case applies two electron lone-pairs (donating sites) on THF. This association scheme is noted  $[0^+; 2^-]$ . Both of the sites

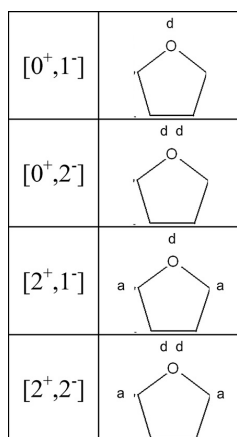


**Fig. 1.** Graphical illustration of investigated association schemes for THF. (a) denotes electron accepting site, (d) denotes electron donating site.

are allowed to cross-associate with the electron accepting sites on water.

When THF is considered both a self- and a cross-associating compound, two association schemes have been investigated. The first is a  $[2^+; 1^-]$  scheme with two electron accepting sites (the two carbon groups directly connected to the oxygen atom) and one electron donating site (the two electron lone-pairs on the oxygen atom, “lumped” into one site). The second test scenario applies a  $[2^+; 2^-]$  scheme with two electron accepting sites and two electron donating sites. In the self-associating cases, electron donating- and accepting sites on THF molecules are allowed to self-associate in a similar way as they are allowed to cross-associate with water. Fig. 1 illustrates the investigated association schemes for THF. a is an electron accepting site and d is an electron donating site. Fig. 2 illustrates the investigated scenarios in the binary mixtures with water as well as the allowed types of association in each case. In addition to the illustrated association types, water is always allowed to self-associate.

In the following, the different scenarios will be named according to the case numbers illustrated in Fig. 2.

The pure component parameters utilised in this work are provided in Table 3.

The three parameters,  $a_0$ ,  $b$  and  $c_1$  for THF are identical in Cases 1–3, where THF is considered non self-associating. This implies that the description of the pure THF system is unchanged even for the cases where THF is allowed to cross-associate (solvate) with water. The differences between THF-cases of no association and only cross-associating are seen in the binary mixture with water.

When no association or only cross-association is allowed (Cases 1–3), the pure THF system is described by the CPA equation of state with average absolute deviations (AAD) of 1.4 percent compared to the reference data in both vapour pressures and saturated liquid densities (in the temperature interval  $0.30 < T/T_c < 0.93$ ). If self-association is allowed (Case 4 to Case 7), two additional pure component parameters are added to the CPA model, and the AAD is lowered to 1.1 percent in both vapour pressure and saturated liquid density description for both the  $[2^+; 1^-]$  and the  $[2^+; 2^-]$  association scheme.

Average absolute deviations are defined according to Eq. (12).

$$\text{AAD} = \frac{1}{N} \sum_{i=1}^N \left| \frac{s_{\text{calc},i} - s_{\text{exp},i}}{s_{\text{exp},i}} \right| \quad (12)$$

Case	Assoc Scheme for THF	Allowed association
1	N/A	N/A
2A and 2B	$[0^+; 1^-]$	
3A and 3B	$[0^+; 2^-]$	
4, 6A and 6B	$[2^+; 1^-]$	
5, 7A and 7B	$[2^+; 2^-]$	

**Fig. 2.** Modelled cases for tetrahydrofuran (THF). In addition to the illustrated scenarios of cross-association with water, water is also allowed to self-associate.

where  $s_{\text{calc}}$  is the calculated property of interest ( $s$  may be temperature, pressure, composition etc.) and  $s_{\text{exp}}$  is the experimental reference data.  $N$  is the total number of data points.

For Cases 2 and 3, applying the CR-1 combining rule to obtain the water–THF cross association parameters, will return a binary association energy,  $\epsilon^{A_i B_j}$ , corresponding to half the self-association energy of water, and a binary association volume,  $\beta^{A_i B_j}$ , of  $\gamma^{A_i B_j}$ . Hence, in cases involving solvation,  $\gamma^{A_i B_j}$  must take a non-zero value in order to allow cross-association.

The methodology presented her, for handling cross-association between self-associating and non self-association compounds corresponds to using the modification of the CR-1 combining rule presented by Folas et al. [39]. The advantage of expressing the CR-1

**Table 3**

CPA equation of state pure component parameters for water and tetrahydrofuran (THF). Case numbering according to scenarios illustrated in Fig. 2.

Component	Assoc scheme	$a_0 \times 10^{-11}$ (Pa m <sup>6</sup> mol <sup>-2</sup> )	$b \times 10^5$ (m <sup>3</sup> mol <sup>-1</sup> )	$c_1$	$\beta^{AB}$	$\varepsilon^{AB} \times 10^{-4}$ (Pa m <sup>3</sup> mol <sup>-1</sup> )	Ref.
Water	[2 <sup>+</sup> ; 2 <sup>-</sup> ]	1.2277	1.451	0.6736	0.0692	1.6655	[41]
THF Cases 1, 2A, 2B, 3A, 3B	[0 <sup>+</sup> ; 1 <sup>-</sup> ] and [0 <sup>+</sup> ; 2 <sup>-</sup> ]	15.5228	6.767	0.7773	N/A	N/A	This work
THF Cases 4, 6A, 6B	[2 <sup>+</sup> ; 1 <sup>-</sup> ]	14.9512	6.859	0.7621	0.0654	0.3579	This work
THF Cases 5, 7A, 7B	[2 <sup>+</sup> ; 2 <sup>-</sup> ]	15.0561	6.859	0.7654	0.0410	0.2662	This work

combining rule in the present form is that it is general and easily handles all the investigated cases.

### 3.2. Data fitting and parameter optimisation algorithm

A constrained optimisation algorithm has been implemented in order to adjust binary parameters in CPA and thereby to correlate the available VLE data. Constraints were implemented in the optimisation algorithm, in order to assure stability of the liquid phase, when needed.

The optimisation algorithm utilised in this work is based on a FORTRAN implementation of the simulated annealing (SA) global optimisation algorithm presented by Goffe et al. [44] (source code available via [45]). The function, to which the SA algorithm is applied, is defined by the sum of absolute differences between calculated and experimental boiling point temperatures, or boiling point pressures as well as calculated and experimental vapour phase compositions (if available). As an example, when correlating Pxy data, the objective function is defined by Eq. (13).

$$OBJ = \sum_i \left( \left| \frac{P_{calc,i} - P_{exp,i}}{P_{exp,i}} \right| + \left| \frac{y_{calc,i} - y_{exp,i}}{y_{exp,i}} \right| \right) \quad (13)$$

If Txy data are available, the pressure residuals in Eq. (13) are replaced by temperature residuals. If only Tx or Px data are available, the second term of Eq. (13) is omitted.

In order to assure low pressure liquid phase stability, constraints have been applied in all optimisations. These constraints have been implemented in the form of stability tests (Gibbs energy minimisation) on the liquid phase in temperature and pressure regions close to the experimental boiling point data. A penalty function has been applied such that any findings of liquid–liquid phase splits, where the experimental data show a single liquid phase, result in a large relative step increase, in the objective function.

Finally the experimental liquid–liquid equilibrium data at approximately 0.5 MPa presented by Riesco and Trusler [12] have been considered. A constraint has been set assuring liquid phase stability at 0.5 MPa up to temperatures of approximately 345 K. Again, this has been implemented in the form of stability tests for multiple compositions at the above conditions of temperature and pressure.

For each parameter set proposed by the SA algorithm, the objective function consists of contributions from the liquid phase stability tests followed by the boiling point calculations. In this way, the objective function is defined over the entire allowed parameter space. The fact that the penalty function makes the objective function discontinuous is not a problem, since the simulated annealing algorithm is based on stochastic principles rather than gradients.

The binary parameters available for correlation are the binary interaction parameter,  $k_{ij}$ , in all cases and additionally  $\gamma^{A_i B_j}$  in the binary association volume,  $\beta^{A_i B_j}$ .

Since the obtained  $k_{ij}$ s in Cases 2 and 3 turned out to be highly temperature dependent, attempts were made applying a  $1/T$  temperature dependency on the correlated  $k_{ij}$ s. By doing this, a total of three binary parameters were finally adjusted simultaneously. In the following, Case 2 with a constant value for  $k_{ij}$  is denoted as

Case 2A. When a temperature dependent  $k_{ij}$  is used, the notation is changed to Case 2B. The same goes for Case 3A and 3B.

In Cases 4 and 5, where THF is treated as self-associating, no further accuracy was gained by introducing a temperature dependency on the binary interaction parameter,  $k_{ij}$ . Hence these scenarios are not treated in the following.

In order to make a fair comparison of cases treating THF as self-associating with cases treating THF as solvating, Cases 6 and 7 are included in this study, treating THF as self-associating. These cases apply two or three binary adjustable parameters for the self-associating cases. Hence, they are similar to Cases 2A, 2B and 3A and 3B in terms of adjustable parameters and are named Cases 6A, 6B, 7A and 7B. A and B again mean constant  $k_{ij}$  (A) or temperature dependent  $k_{ij}$  (B). Case 6A and 6B assigns the [2<sup>+</sup>; 1<sup>-</sup>] association scheme to THF and Case 7A and 7B assigns the [2<sup>+</sup>; 2<sup>-</sup>] scheme. The six and seven cases leave  $\gamma^{A_i B_j}$  in the combining rule for the binary cross-association volume between electron donating sites on THF and electron accepting sites on water as an adjustable parameter (similar to the solvating cases). The binary association volume for cross-association between electron accepting sites on THF and electron donating sites on water is still predicted by the standard CR-1 combining rule with ( $\gamma^{A_i B_j} = 0$ ). Attempts were made for both Cases 6 and 7 to model all types of cross-association with one correlated binary cross-association volume (unique  $\gamma^{A_i B_j}$  for each case). Whereas the correlated  $\gamma^{A_i B_j}$  changed their values compared to those presented in Table 4 by doing so, the final modelling results were similar to the cases included in this work. Table 4 summarises the investigated cases as well as the parameters obtained. Table 4 presents, for all cases considered, the correlated binary parameters for the system THF–water along with their AAD's compared to the experimental data points (Px, Tx, Pxy, Txy) used as reference data. All VLE data from the authors listed in Table 1, except those measured by Matsuda et al. [9], have been used as reference data. The data measured by Matsuda et al. are reserved for later verification of the model predictions in terms of boiling point temperatures at various pressures. Even though some authors present boiling point data for the pure systems along side with the mixture data, these pure component data points have been excluded from the reference data.

## 4. Results and discussion

### 4.1. Correlated VLE

When modelling the binary system water–THF, using the pure component parameters provided in Table 3 and the “standard” mixing and combining rules ( $k_{ij} = 0$  and  $\gamma^{A_i B_j} = 0$ ), it becomes obvious that this model needs correlation of binary parameters in order to describe the experimental VLE data while simultaneously respecting the stability of the liquid phase in the low pressure region (complete miscibility of water and THF).

With no binary parameters adjusted, Cases 1, 2A/2B and 3A/3B (Cases 2A/2B and 3A/3B inhibit cross-association when using the “standard” mixing and combining rules) predicted the presence of two liquid phases with only limited miscibility at conditions of atmospheric pressure.

**Table 4**

Correlated binary CPA parameters for the system of tetrahydrofuran and water.  $k_{ij} = a_{kij} + b_{kij}/T$  is the binary interaction parameter used in the mixing rule for the binary alpha parameter in the SRK term of CPA.  $\gamma^{A,B_i}$  enters in the binary association volume of the CPA association term. Average absolute deviation (AAD) according to Eq. (12) with respect to all reference data used in the parameter regression (boiling point temperatures, pressures and corresponding vapour phase compositions).

Case	Association scheme for THF	Adj. parameters	$k_{ij}$	$\gamma^{A,B_i}$	AAD $\times 10^2$
1	N/A	$a_{kij}$	N/A	N/A	N/A
2A	[0 <sup>+</sup> ;1 <sup>-</sup> ]	$a_{kij}, \gamma^{A,B_i}$	-0.132	0.6435	9.97
2B	[0 <sup>+</sup> ;1 <sup>-</sup> ]	$a_{kij}, b_{kij}, \gamma^{A,B_i}$	$0.132 - 92.55/T$	0.4317	6.70
3A	[0 <sup>+</sup> ;2 <sup>-</sup> ]	$a_{kij}, \gamma^{A,B_i}$	-0.104	0.3221	13.0
3B	[0 <sup>+</sup> ;2 <sup>-</sup> ]	$a_{kij}, b_{kij}, \gamma^{A,B_i}$	$0.408 - 154.65/T$	0.2543	5.82
4	[2 <sup>+</sup> ;1 <sup>-</sup> ]	$a_{kij}$	-0.083	N/A	7.10
5	[2 <sup>+</sup> ;2 <sup>-</sup> ]	$a_{kij}$	-0.063	N/A	6.70
6A	[2 <sup>+</sup> ;1 <sup>-</sup> ]	$a_{kij}, \gamma^{A,B_i}$	-0.1258	-0.0298	5.78
6B	[2 <sup>+</sup> ;1 <sup>-</sup> ]	$a_{kij}, b_{kij}, \gamma^{A,B_i}$	$0.0848 - 66.99/T$	-0.0320	5.42
7A	[2 <sup>+</sup> ;2 <sup>-</sup> ]	$a_{kij}, \gamma^{A,B_i}$	-0.1145	-0.0108	4.61
7B	[2 <sup>+</sup> ;2 <sup>-</sup> ]	$a_{kij}, b_{kij}, \gamma^{A,B_i}$	$0.0412 - 50.99/T$	-0.0225	5.13

It was found that only the cases “naturally” allowing for cross-association (Cases 4 and 5) could provide sufficient attractive forces between water and THF in order to allow liquid phase miscibility, to some extent. However, even Cases 4 and 5 predicted unstable liquid phases (liquid–liquid splits) in some concentration regions in the low pressure/low temperature regions.

For Case 1, where cross-association is neglected, even when applying a negative binary interaction parameter,  $k_{ij}$ , the contribution of the SRK term is too dominant for the two liquid phases to mix completely over the wide temperature and pressure range covered by the experimental data. Not even a temperature dependent  $k_{ij}$  could provide the necessary attractive forces over the desired temperature interval. Thus, Case 1 has been omitted from the following analysis.

The solvating cases, Cases 2A, 2B, 3A and 3B are all capable of describing the miscibility of the two compounds in the liquid state at low pressures. However of these, only Cases 2B and 3B are able to describe the liquid–liquid split at higher pressures, where experimental data document liquid–liquid separation.

The self-associating Cases 4, 5, 6A, 6B, 7A and 7B almost all describe the VLE data as well as the solvating cases with three adjustable parameters (2B and 3B). Not surprisingly, in the self-associating cases, accuracy of the VLE description is increased with increasing number of adjustable parameters. However, only Cases 6B and 7B are able at describing the LLE occurring at higher pressures.

An interesting conclusion drawn from the AAD's presented in Table 4 is that the Cases 4 and 5, treating THF as self-associating with one adjustable binary parameter, provide accuracies comparable to the cases treating THF as only cross-associating with a temperature dependent binary interaction parameter (Cases 2B and 3B). This is despite the fact that Cases 4 and 5 have only a single correlated binary parameter, whereas Cases 2B and 3B have three correlated binary parameters. Cases 4 and 5 do, however, have two additional pure component parameters for THF compared to Cases 2B and 3B. This provides a significant improvement in the description of pure component physical properties such as e.g. the vapour pressure. It is possible that the improved description of the mixed system properties is partly due to the higher accuracy of the pure component description for THF in Cases 4 and 5. Table 4 also shows that high absolute values of both the binary interaction parameter,  $k_{ij}$ , and the binary association volume ( $\gamma^{A,B_i}$ ), are needed in order to stabilise the liquid phase in the scenarios where THF is not considered a self-associating compound (Cases 2A/2B and 3A/3B).

On a general note, it is seen that the absolute value of  $k_{ij}$  is always larger in the cases where THF has only a single association site on its oxygen atom. This is a natural consequence of the fact that the contribution of the SRK term of CPA need to be reduced further in the cases with little if any cross-association. The largest absolute values

of the correlated  $k_{ij}$ s are found at low temperatures. At 298 K, the  $k_{ij}$  for Case 2B takes a value of -0.179 where in Case 3B it takes a value of -0.111. At 343 K, the  $k_{ij}$  values are increased to -0.138 and -0.043 for Cases 2B and 3B, respectively. For the self-associating Cases 6B and 7B,  $k_{ij}$ s at 298 K are -0.130 and -0.140, respectively. Also here, the absolute values of the regressed  $k_{ij}$ s decrease with increasing temperature. A similar tendency is seen in the regressed binary association volumes for the solvating cases. It seems the binary association volume is reduced by a factor of two when the number of association sites on the THF oxygen atom is doubled, i.e. when one goes from Case 2A to Case 3A or from Case 2B to Case 3B.

Figs. 3–7 compare the performances of the obtained model cases with a selection of the experimental data utilised as reference data in the binary parameter optimisation procedure.

Fig. 3 illustrates results from modelling Cases 2A and 2B. In these modelling cases THF is considered only to cross-associate with water via the single association site on the THF oxygen atom. It is seen that the low temperature data at 298 K are well described using a constant  $k_{ij}$ , however this modelling approach is unable to

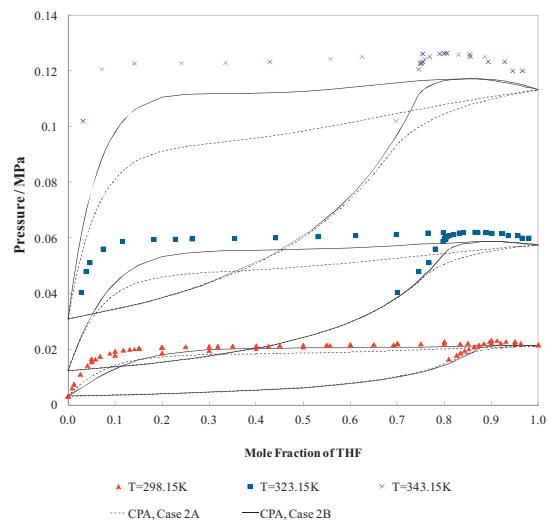


**Fig. 3.** Comparison of correlated and experimental boiling point and dew point pressures as functions of the tetrahydrofuran (THF) mole fraction in the binary system of water and THF. Results at three temperatures are presented. Pure component parameters for CPA are those listed in Table 3 and the regressed binary parameters for Case 2A and 2B may be found in Table 4. Experimental data from [1,2,4,6]. Dashed line: CPA, Case 2A. Solid line: CPA, Case 2B.

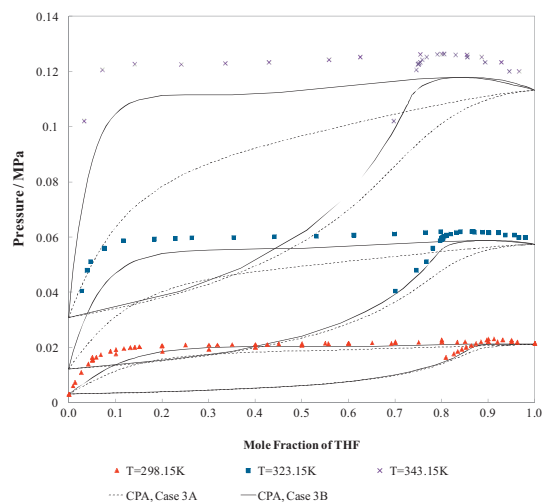


**Fig. 4.** Comparison of correlated and experimental boiling point and dew point pressures as functions of the tetrahydrofuran (THF) mole fraction in the binary system of water and THF. Results at three temperatures are presented. Pure component parameters for CPA are those listed in Table 3 and the regressed binary parameters for Case 3A and 3B may be found in Table 4. Experimental data from [1,2,4,6]. Dashed line: CPA, Case 3A. Solid line: CPA, Case 3B.

describe the azeotrope, if the high temperature data and liquid stability is also considered when regressing binary parameters. If the VLE data at higher temperatures are discarded in the parameter optimisation, the azeotrope at 298 K may be described accurately using a constant value for  $k_{ij}$ .

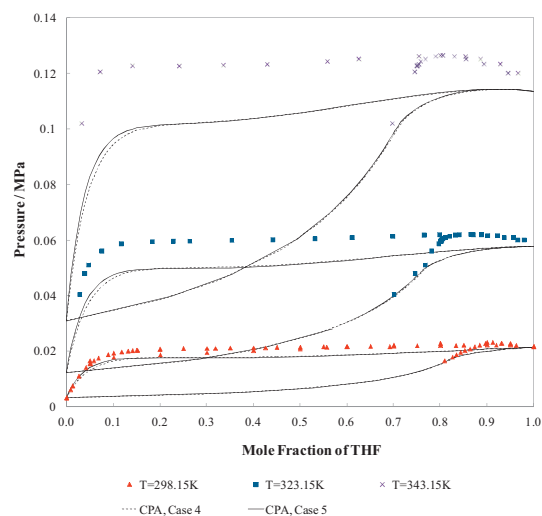


**Fig. 5.** Comparison of correlated and experimental boiling point and dew point pressures as functions of the tetrahydrofuran (THF) mole fraction in the binary system of water and THF. Results at three temperatures are presented. Pure component parameters for CPA are those listed in Table 3 and the regressed binary parameters for Cases 4 and 5 may be found in Table 4. Experimental data from [1,2,4,6]. Dashed line: CPA, Case 4. Solid line: CPA, Case 5. Cases 4 and 5 provide almost identical results for these properties, hence it may be difficult to distinguish between solid and dashed lines in most parts of this figure.

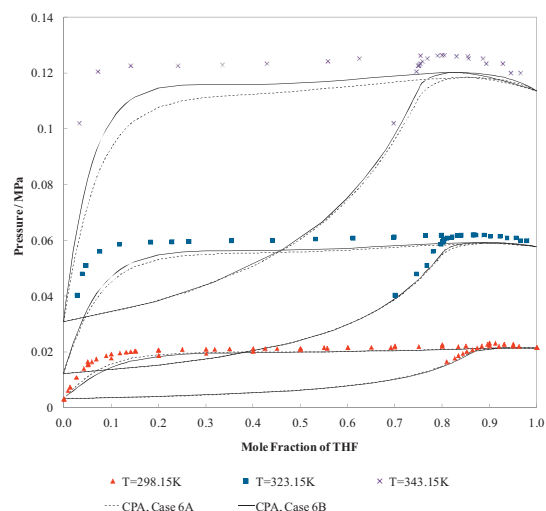


**Fig. 6.** Comparison of correlated and experimental boiling point and dew point pressures as functions of the tetrahydrofuran (THF) mole fraction in the binary system of water and THF. Results at three temperatures are presented. Pure component parameters for CPA are those listed in Table 3 and the regressed binary parameters for Case 6A and 6B may be found in Table 4. Experimental data from [1,2,4,6]. Dashed line: CPA, Case 6A. Solid line: CPA, Case 6B. Case 6A and 6B provide similar results for these properties, hence it may be difficult to distinguish between solid and dashed lines in most parts of this figure.

Introducing the temperature dependency on the regressed  $k_{ij}$  greatly enhances the model accuracy. The azeotrope is well described at 298 K and the high temperature descriptions, in particular, are improved. The experimentally documented tendency of the azeotrope to move to lower THF concentrations with increasing temperature is likewise described in model Case 2B. However the azeotrope at high temperatures is slightly higher in THF concentration than those determined experimentally. At atmospheric pressure, the azeotrope occurs at a THF mole fraction of approximately 0.82 [9]. Model Case 2B places the azeotrope at a THF mole fraction of approximately 0.85 (cannot be seen in Fig. 3). Generally, model Case 2A and 2B underestimates the boiling point pressure of the liquid mixtures. This effect is most pronounced at high temperatures, where the boiling point pressures are underestimated by approximately 0.1 bar (approximately 8 percent) in the THF mole fraction range from 0.2 to 0.8. The largest deviations compared to the experimental data are found in the THF mole fraction range from 0.05 to 0.2. Attempts have been made to improve the accuracy of the model at the low THF concentrations, by weighing these experimental data points heavier in the objective function, than the high concentration data. These attempts to improve the models were however unsuccessful.

It was found during the parameter optimisation work that the model 2B accuracy at high temperatures could be improved significantly by allowing for liquid–liquid splits at pressures of 0.5 MPa and temperatures below 345 K. However, the resulting liquid–liquid split turned out to propagate to lower pressures and thus interfered with the VLE data at  $T = 343$  K.

Fig. 4 compares modelling Cases 3A and 3B with the same experimental data as those shown in Fig. 3. Here THF has been assigned two association sites on its oxygen atom. The same conclusions are drawn from these results as those for Case 2A and 2B. A single value  $k_{ij}$  is insufficient to cover the entire temperature interval of available VLE data. However, by introducing a temperature dependant  $k_{ij}$ , the high temperature accuracy is improved and the model is

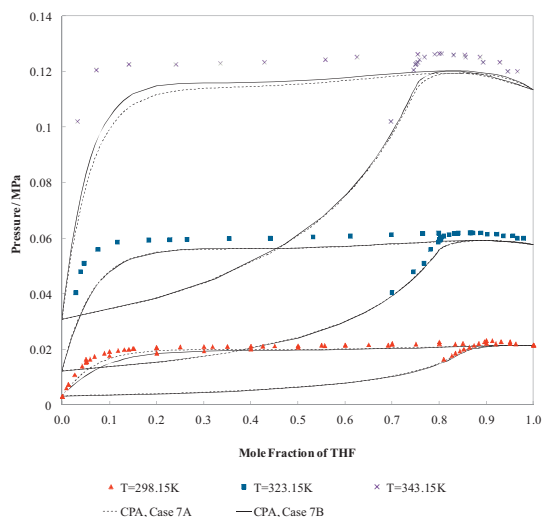


**Fig. 7.** Comparison of correlated and experimental boiling point and dew point pressures as functions of the tetrahydrofuran (THF) mole fraction in the binary system of water and THF. Results at three temperatures are presented. Pure component parameters for CPA are those listed in Table 3 and the regressed binary parameters for Case 7A and 7B may be found in Table 4. Experimental data from [1,2,4,6]. Dashed line: CPA, Case 7A. Solid line: CPA, Case 7B. Case 7A and 7B provide similar results for these properties, hence it may be difficult to distinguish between solid and dashed lines in most parts of this figure.

able to describe the azeotrope. Like model Case 2B, Case 3B places the azeotrope at 1 atm at a THF mole fraction of approximately 0.85, slightly above the experimentally determined composition. Model Case 3B results are almost identical to those of Case 2B. Model Case 3B does, however, provide slightly better descriptions in the low THF concentration range than Case 2B, indicating that the increased possibility for cross association improves the VLE description in the low THF concentration region.

Fig. 5 illustrates the performances of Cases 4 and 5, where THF is treated both as a self- and cross-associating compound. Cases 4 and 5 perform well at 298 K. However, they fail at describing the azeotrope. The accuracies of these models decrease as the temperature increases, and the azeotrope only occurs in the models in the final data set at 343 K. Here both models place the azeotrope at a THF mole fraction of approximately 0.92. An interesting observation is the higher accuracy of model Cases 4 and 5 in the low THF concentration range at 298 K compared to Cases 2B and 3B. It seems however, that these models lose the accuracy as temperature is increased. As mentioned, attempts were made, to include a temperature dependant  $k_{ij}$  in Cases 4 and 5 in order to improve the high-temperature descriptions. However, no significant improvements were found compared to the cases with constant  $k_{ij}$ s. Even with the additional degree of freedom, these models could not describe the azeotrope correctly at any of the three temperatures.

The performances of model Cases 4 and 5 are very similar, thus the curves representing these models in Fig. 5 are hardly distinguishable. Pronounced differences are found only in the low THF concentration range, where Case 5 is a little more accurate than Case 4.

Figs. 6 and 7 show results for Cases 6A/6B and 7A/7B, respectively. As can also be seen in Table 4, including two or three binary adjustable parameters in the self-associating cases can hardly be justified when considering the VLE description only. Little accuracy is gained when going from two adjustable parameters to three,

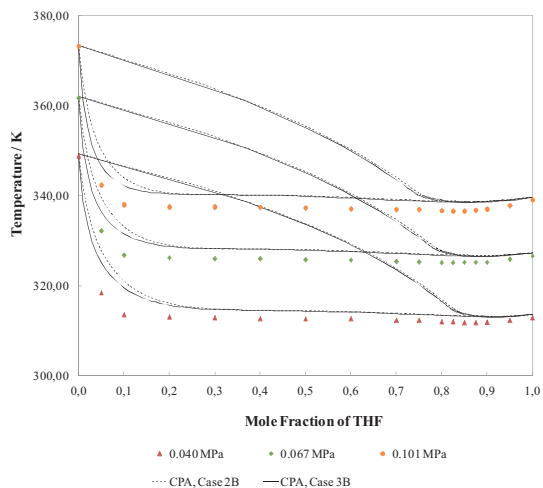


**Fig. 8.** Comparison of predicted and experimental boiling point- and dew point temperatures as functions of tetrahydrofuran (THF) mole fraction in the binary system of water and THF. Results at three pressures are presented. Pure component parameters for CPA are those listed in Table 3 and the regressed binary parameters for Cases 2B and 3B may be found in Table 4. Experimental data from [9]. Dashed line: CPA, Case 2B. Solid line: CPA, Case 3B. Cases 2B and 3B provide almost identical results for this property, hence it may be difficult to distinguish between solid and dashed lines in most parts of this figure.

however with three binary parameters, the self-associating cases also arrive at describing LLE.

From the above results, it is obvious that Cases 2B, 3B, 6B and 7B are the only modelling approaches that provide sufficient accuracy in the VLE description over the entire temperature and pressure range covered by the experimental data and succeed in describing LLE at elevated pressures. Hence, only these cases will be treated in the following.

#### 4.2. Predicted boiling point temperatures

Figs. 8 and 9 illustrate predicted boiling point temperatures at three pressures and compare with experimental data which have not been included as reference data. Only Cases 2B, 3B, 6B and 7B are included in this comparison. All other solvating or self-associating cases were considered either unable to correlate the reference data accurately or unable to describe the high pressure LLE.

Fig. 8 illustrates the boiling point temperatures predicted by model Cases 2B and 3B, and compares them with a selection of the experimental data presented by Matsuda et al. [9]. At these pressure conditions, both models describe the boiling point temperatures well. It should be noted that, even though these data were not included in the parameter optimisation algorithm, the represented conditions of temperature and pressure were covered by other data. Hence, these results are predictions, however the two models still operate well inside the conditions of temperature and pressure covered by the reference data. The improvement of Case 3B compared to Case 2B at the low THF concentration range is visible in Fig. 8. As temperature increases, the differences between the two models become more pronounced.

Fig. 9 compares model Cases 6B and 7B in their description of the boiling point temperatures measured by Matsuda et al. [9]. These two models describe the experimental data with similar accuracy as the cases treating THF as cross-associating only (Cases 2B and 3B). Hence, it seems that with three adjustable binary



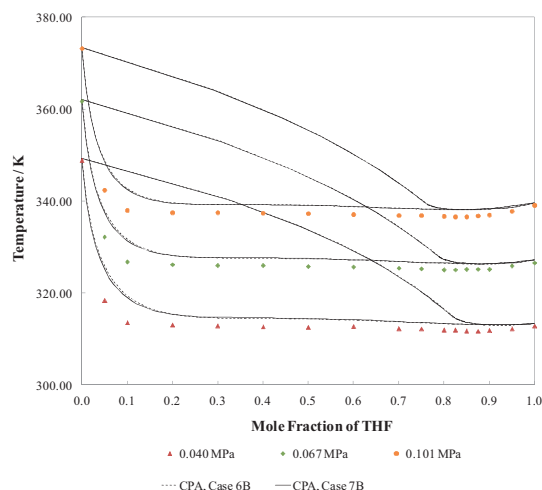


**Fig. 9.** Comparison of predicted and experimental boiling point- and dew point temperatures as functions of tetrahydrofuran (THF) mole fraction in the binary system of water and THF. Results at three pressures are presented. Pure component parameters for CPA are those listed in Table 3 and the regressed binary parameters for Cases 6B and 7B may be found in Table 4. Experimental data from [9]. Dashed line: CPA, Case 6B. Solid line: CPA, Case 7B. Cases 6B and 7B provide almost identical results for this property, hence it may be difficult to distinguish between solid and dashed lines in most parts of this figure.

parameters, treating THF as solvating or self-association provides similar performance in the VLE description of this system.

#### 4.3. Predicted LLE

No liquid–liquid equilibrium (LLE) data have been directly considered in the process of regressing binary parameters for this system. Only the experimental LCST at 0.5 MPa and 345 K has been used as an indirect means of controlling the liquid phase below the temperatures at which liquid–liquid splits have been reported in the literature.

All modelling cases have been investigated for occurrences of liquid–liquid splits in the pressure region from 0.5 MPa to 6.0 MPa. Only Cases 2B, 3B, 6B and 7B show this kind of phase behaviour. Figs. 10, 12 and 14 illustrate the liquid–liquid splits predicted by model Cases 2B and 3B at pressures of 0.5 MPa, 3.0 MPa and 6.0 MPa, respectively. Similarly, Figs. 11, 13 and 15 show the liquid–liquid splits predicted by Cases 6B and 7B. The “method of alternating tangents” as presented by von Solms et al. [46], has been utilised to search for LLE regions as well as to calculate the upper- and lower critical solution temperatures of the illustrated circular liquid–liquid split regions. This method has the advantage of considering only a single phase at a time and thus is less sensitive than traditional flash calculations, where both phases are accounted for simultaneously. As the critical point is approached, the two phases become close to identical, resulting in computational/numerical challenges that are easier overcome in the “method of alternating tangents”.

Figs. 10 and 11 show the LLE predicted by the models at a pressure of 0.5 MPa. Note how the imposed liquid phase stability criterion has resulted in a lower critical solution temperature (LCST) occurring at approximately 345 K for all cases, close to the temperature reported by Riesco and Trusler [12]. The overall composition ranges enclosed in the two-phase LLE regions predicted by the models are in fact true predictions, and these lie close to the

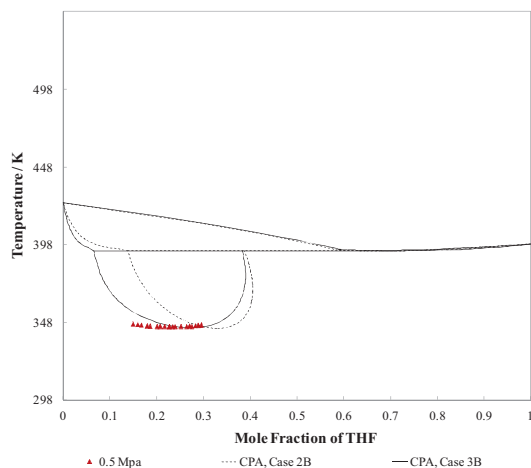


**Fig. 10.** Comparison of predicted and experimental liquid–liquid equilibrium temperatures as functions of tetrahydrofuran (THF) mole fraction in the binary system of water and THF. Pressure is 0.5 MPa. Pure component parameters for CPA are those listed in Table 3 and the regressed binary parameters for Cases 2B and 3B may be found in Table 4. Experimental data from [12]. Dashed line: CPA, Case 2B. Solid line: CPA, Case 3B. Cases 2B and 3B provide almost identical results for boiling point and dew point temperatures, hence it may be difficult to distinguish between solid and dashed lines in these parts of this figure representing these properties.

experimentally determined compositions for the solvating cases. The water rich liquid phase is less accurately described by the cases treating THF as self-associating. Cases 2B and 3B predict the LLE region to extend up in temperature until an upper three-phase critical point (VLLE) is reached. Cases 6B and 7B close the loop before the VLE region is reached.

Figs. 12 and 14 illustrate the predicted LLE at a pressure of 3.0 MPa and compare with available experimental data. The entire closed loop miscibility gap is covered by the experimental data at this pressure. Again, all models predict the LCST at approximately 345 K and the composition ranges for the cases treating THF as solvating lie close to the experimental data. An interesting difference between model Cases 2B and 3B is seen at these conditions. Whereas Case 3B still extends the LLE region up in temperature until the upper critical VLLE point, Case 2B closes the LLE loop with an upper critical solution temperature (UCST) of approximately 456 K. However, Case 3B still predicts the composition range of the LLE more accurate than Case 2B which overestimates the THF mole fractions of both liquid phases. At 3.0 MPa it becomes clear that Cases 6B and 7B underpredict the size of the miscibility gap and overestimate the THF concentration in the water rich liquid phase. Cases 2B and 3B overestimate the size of the miscibility gap, however these models are more accurate in terms of compositions of the predicted liquid phases.

The LLE predictions at 6.0 MPa are illustrated in Figs. 14 and 15. At these conditions, the predicted VLE is shifted to such high temperatures, that both of the models treating THF as solvating are capable of closing the circular LLE miscibility gap. Case 2B predicts the UCST at approximately 454 K and this critical point occurs at a THF mole fraction of 0.19. The UCST predicted by Case 3B occurs at 498 K and here the critical solution composition is approximately 0.13 in terms of THF. Thus, whereas Case 2B describes the UCST better, Case 3B is more accurate in liquid phase compositions. Cases 6B and 7B still underpredict the size of miscibility gap.

Generally, it is worth mentioning that the CPA EoS performs its best at the scenario that is the physically most meaningful

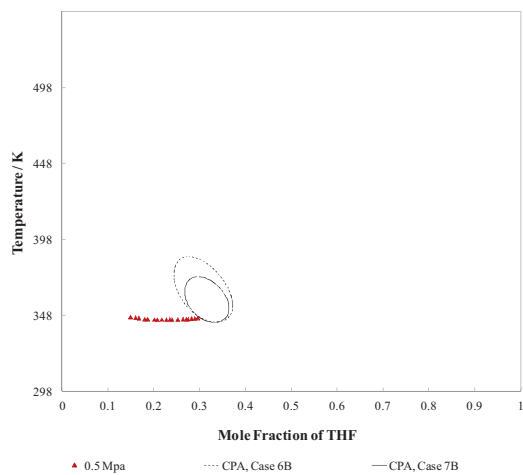


**Fig. 11.** Comparison of predicted and experimental liquid-liquid equilibrium temperatures as functions of tetrahydrofuran (THF) mole fraction in the binary system of water and THF. Pressure is 0.5 MPa. Pure component parameters for CPA are those listed in Table 3 and the regressed binary parameters for Cases 6B and 7B may be found in Table 4. Experimental data from [12]. Dashed line: CPA, Case 6B. Solid line: CPA, Case 7B.

description of THF. This somewhat confirms the theory behind the model. Two association sites on THF available for cross-association with water provide the best overall accuracy in both VLE and LLE descriptions.

A final note is made on the pressure dependency of the predicted LLE. When comparing Figs. 10 to 15 it is observed that the “shrinking” effect pressure has on the extension of the circular miscibility gap (experimental data) is larger than the effect predicted by the models. Whereas the LCST in the experimental data presented by Riesco and Trusler [12] increases from approximately 345.5 K at

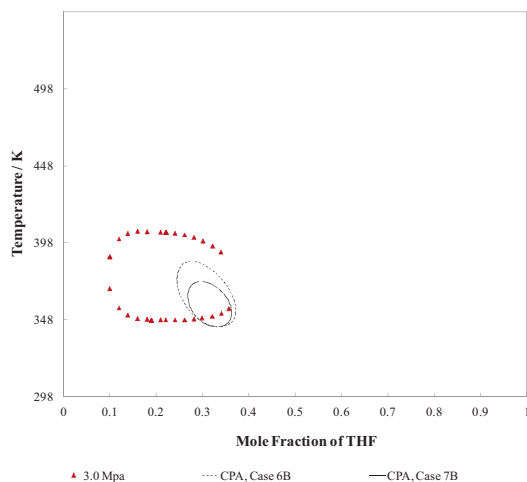


**Fig. 13.** Comparison of predicted and experimental liquid-liquid equilibrium temperatures as functions of tetrahydrofuran (THF) mole fraction in the binary system of water and THF. Pressure is 3.0 MPa. Pure component parameters for CPA are those listed in Table 3 and the regressed binary parameters for Cases 6B and 7B may be found in Table 4. Experimental data from [12]. Dashed line: CPA, Case 6B. Solid line: CPA, Case 7B.

0.5 MPa to 350.7 K at 6.0 MPa, it remains in the region of 345 K for all model cases.

Hence, whereas the temperature dependent binary parameters allows for an accurate description of the VLE and simultaneously a good prediction of the circular LLE miscibility gap, it seems the temperature dependency of the binary interaction parameter,  $k_{ij}$ , dampens the natural pressure effect on the LLE phase behaviour present in the model.

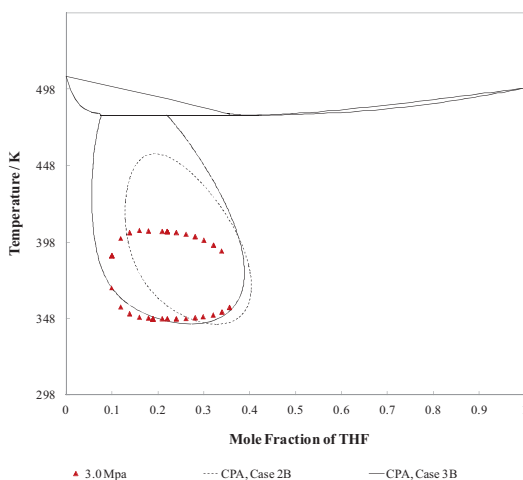


**Fig. 12.** Comparison of predicted and experimental liquid-liquid equilibrium temperatures as functions of tetrahydrofuran (THF) mole fraction in the binary system of water and THF. Pressure is 3.0 MPa. Pure component parameters for CPA are those listed in Table 3 and the regressed binary parameters for Cases 2B and 3B may be found in Table 4. Experimental data from [12]. Dashed line: CPA, Case 2B. Solid line: CPA, Case 3B.

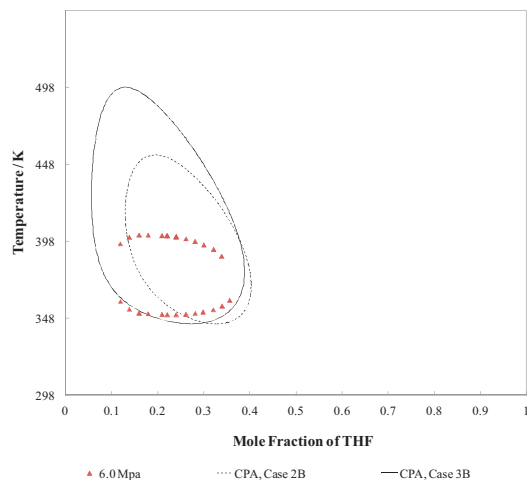


**Fig. 14.** Comparison of predicted and experimental liquid-liquid equilibrium temperatures as functions of tetrahydrofuran (THF) mole fraction in the binary system of water and THF. Pressure is 6.0 MPa. Pure component parameters for CPA are those listed in Table 3 and the regressed binary parameters for Cases 2B and 3B may be found in Table 4. Experimental data from [12]. Dashed line: CPA, Case 2B. Solid line: CPA, Case 3B.



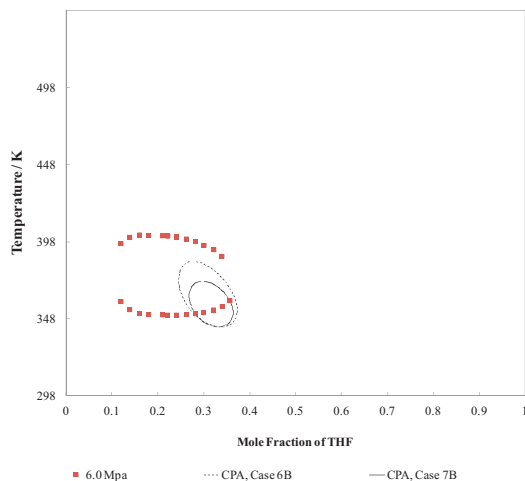


**Fig. 15.** Comparison of predicted and experimental liquid–liquid equilibrium temperatures as functions of tetrahydrofuran (THF) mole fraction in the binary system of water and THF. Pressure is 6.0 MPa. Pure component parameters for CPA are those listed in Table 3 and the regressed binary parameters for Cases 6B and 7B may be found in Table 4. Experimental data from [12]. Dashed line: CPA, Case 6B. Solid line: CPA, Case 7B.

The above observations correspond well with the findings of Kontogeorgis et al. [47], who applied the CPA EoS to model liquid–liquid equilibria of two linear ethers (di-*n*-propylether and ethyl propylether) in their binary mixtures with water. Water was assigned an association scheme with two electron donating and two electron accepting sites, while both ethers were assumed to be non self-associating. Kontogeorgis et al. concluded that CPA would wrongly predict the qualitative behaviour of the LLE systems, if cross-association between the electron accepting sites on water and electron donating sites on the ether oxygen atom were not accounted for. Similarly, it was claimed that vapour–liquid equilibria descriptions were improved when accounting for cross-association. Furthermore it was found that assigning one or two electron donating sites on the ethers provided comparable performances, though a small gain in accuracy was found when assigning two sites.

## 5. Conclusion

The complex fluid phase behaviour, of the binary system comprised of water and tetrahydrofuran (THF) was modelled by use of the cubic-plus-association (CPA) equation of state. A total of seven modelling approaches were analysed, differing only in their way of describing THF and its interactions (hydrogen bonding) with water.

Experimental data, available in the literature, documenting the fluid phase behaviour of this binary system, showed both azeotropic vapour–liquid equilibrium (VLE) behaviour and a circular liquid–liquid miscibility gap. This qualitative behaviour could only be described by CPA when cross-association between water and THF was allowed.

Six of the seven tested modelling scenarios allowed for cross-association between the two compounds. These scenarios were named Case 2 to Case 7. Case 2 treated THF as non self-associating, but applied a single association site on the THF oxygen atom, that allowed for cross-linking with a single water molecule. Case 3 was identical to Case 2 but applied two association sites on THF, allowing for simultaneous cross-association with two water molecules.

Case 4 treated THF as self-associating and cross-associating according to an association scheme with two electron accepting sites and a single electron donating site. Case 5 also considered both self- and cross-association by THF, but applied an association scheme with two electron accepting- and two electron donating sites.

Cases 6 and 7 were similar to Cases 4 and 5, respectively, however the binary cross-association volume between electron accepting sites on water and electron donating sites on THF was adjusted to match the CPA descriptions with available experimental VLE data.

It was found that Cases 2, 3, 6 and 7, providing three adjustable binary parameters, were the only cases, which could describe both VLE and LLE using a single set of parameters. With a total of three binary parameters correlated to available VLE data, these data could be described with average absolute deviations of approximately 5–7 percent. The LLE was well predicted by both model Case 2 and 3, with a slightly better phase composition prediction by Case 3.

While Cases 6 and 7 described VLE data better than the cases treating THF as solvating, the size of the circular miscibility gap at high pressures was under predicted.

Based on the results presented in this work, it is suggested to model this binary system considering THF as cross-associating only, with two cross-association sites. The use of a temperature dependent binary interaction parameter and a correlated binary cross-association volume then allows for both accurate VLE and LLE descriptions in large ranges of temperature and pressure.

## Acknowledgements

This work was financially supported partly by the European iCap project (EU FP7) and partly by the Department of Chemical and Biochemical Engineering (MP<sub>2</sub>T) at the Technical University of Denmark (DTU).

The authors wish to thank Georgios Kontogeorgis, Michael L. Michelsen and Ioannis Tsivintzelis from the Technical University of Denmark for their help and technical advice on the computational aspects of this work.

The authors also wish to thank Xiaodong Liang from the Technical University of Denmark for the many, fruitful discussions on both thermodynamics and computational aspects.

We direct our sincere gratitude towards Eric Hendriks from Shell Global Solutions, for his valuable comments and suggestions for improvements of this work.

The authors finally acknowledge the initiative and work Erling H. Stenby and Philip L. Fosbøl put into establishing the funding for DTU, as part of the iCap project.

## References

- [1] V.A. Shnitko, V.B. Kogan, *J. Appl. Chem. USSR* 41 (6) (1968) 1235–1242.
- [2] R. Signer, H. Arm, H. Daeniker, *Helv. Chim. Acta* 52 (8) (1969) 2347–2351.
- [3] H.M. Lybarger, H.L. Greene, *Adv. Chem. Ser.* 115 (1972) 148–158.
- [4] J. Matous, J.P. Novak, J. Sobr, *J. Pick, Collect. Czech. Chem. Commun.* 37 (1972) 2653–2663.
- [5] W. Hayduk, H. Laudie, O.H. Smith, *J. Chem. Eng. Data* 18 (4) (1973) 373–376.
- [6] C. Treiner, *J. Chim. Phys.* 70 (9) (1973) 1183–1187.
- [7] E. Sada, T. Morisue, K. Miyahara, *J. Chem. Eng. Data* 20 (3) (1975) 283–287.
- [8] J. Lampa, J. Matous, J.P. Novak, J. Pick, *Collect. Czech. Chem. Commun.* 45 (1980) 1159–1167.
- [9] H. Matsuda, N. Kamihama, K. Kurihara, K. Tochigi, K. Yokoyama, *J. Chem. Eng. Jpn.* 41 (3) (2011) 131–139.
- [10] A. Wallbruch, G.M. Schneider, *J. Chem. Thermodyn.* 27 (1995) 377–382.
- [11] J. Matous, J. Hrnčirik, J.P. Novak, J. Sobr, *Collect. Czech. Chem. Commun.* 35 (1970) 1904–1905.
- [12] N. Riesco, J.P.M. Trusler, *Fluid Phase Equilib.* 228–229 (2005) 233–238.
- [13] M.N. Garcia-Lisbona, A. Galindo, G. Jackson, A.N. Burgess, *Mol. Phys.* 93 (1) (1998) 57–71.
- [14] O. Redlich, A.T. Kister, C.E. Turnquist, *Chem. Eng. Prog. Symp. Ser.* 48 (2) (1952) 49–61.
- [15] H. Renon, J.M. Prausnitz, *Am. Inst. Chem. Eng. J.* 14 (1968) 135–144.
- [16] D.S. Abrams, J.M. Prausnitz, *Am. Inst. Chem. Eng. J.* 21 (1975) 116–128.

- [17] Aa. Fredenslund, R.L. Jones, J.M. Prausnitz, *Am. Inst. Chem. Eng. J.* 21 (1975) 1086–1099.
- [18] G. Soave, *Chem. Eng. Sci.* 27 (1972) 1197–1203.
- [19] D.-Y. Peng, D.B. Robinson, *Ind. Eng. Chem. Fundam.* 15 (1976) 59–64.
- [20] G.M. Kontogeorgis, E.C. Voutsas, I.V. Yakoumis, D.P. Tassios, *Ind. Eng. Chem. Res.* 35 (1996) 4310–4318.
- [21] G.M. Kontogeorgis, I.V. Yakoumis, H. Meijer, E. Hendriks, T. Moorwood, *Fluid Phase Equilib.* 158–160 (1999) 201–209.
- [22] M.L. Michelsen, *Fluid Phase Equilib.* 60 (1990) 323–327.
- [23] S. Dahl, M.L. Michelsen, *AIChE J.* 36 (12) (1990) 1829–1836.
- [24] H. Orbey, S.I. Sandler, *Fluid Phase Equilib.* 111 (1995) 53–70.
- [25] K. Rehak, J. Matous, J.P. Novak, *Fluid Phase Equilib.* 109 (1995) 113–129.
- [26] G.M. Wilson, *J. Am. Chem. Soc.* 86 (1964) 127–130.
- [27] I. Brovchenko, B. Guillot, *Fluid Phase Equilib.* 183–184 (2001) 311–319.
- [28] M.J. Lazzaroni, D. Bush, R. Jones, J.P. Hallett, C.L. Liotta, C.A. Eckert, *Fluid Phase Equilib.* 224 (2004) 143–154.
- [29] R. Stryjek, J.H. Vera, *Can. J. Chem. Eng.* 64 (1986) 323–333.
- [30] D. Browarzik, *Fluid Phase Equilib.* 230 (2005) 143–152.
- [31] R. Susilo, S. Alavi, J. Ripmeester, P. Englezos, *Fluid Phase Equilib.* 263 (2008) 6–17.
- [32] J.C. Platteeuw, J.H. van der Waals, *Mol. Phys.* 1 (1) (1958) 91–95.
- [33] R.C. Reid, J.M. Prausnitz, B.E. Poling, *The Properties of Gases and Liquids*, fourth ed., McGraw-Hill Book Company, New York, 1987.
- [34] A. Martin, C.J. Peters, *J. Phys. Chem. B* 113 (2009) 7548–7557.
- [35] R.H. Perry, D.W. Green (Eds.), *Perry's Chemical Engineers' Handbook*, seventh ed., McGraw-Hill Book Company, New York, 1997.
- [36] K.M. Sabil, G.-J. Witkamp, C.J. Peters, *J. Chem. Eng. Data* 55 (2010) 813–818.
- [37] J. Lee, J. Cho, D.M. Kim, S. Park, *Korean J. Chem. Eng.* 28 (2) (2011) 591–596.
- [38] I. Ben, Attouche Sfaxi, *Étude thermodynamique d'un procédé de captage du CO<sub>2</sub> par formation d'hydrates appliqué aux fumées de postcombustion*, Ph.D. Thesis, École nationale supérieure des mines de Paris, France, 2011.
- [39] G.K. Folas, G.M. Kontogeorgis, M.L. Michelsen, E.H. Stenby, *Ind. Eng. Chem. Res.* 45 (2006) 1527–1538.
- [40] H. Pahlavanzadeh, A. Kamran-Pirzaman, A.H. Mohammadi, *Fluid Phase Equilib.* 320 (2012) 32–37.
- [41] G.M. Kontogeorgis, M.L. Michelsen, G.K. Folas, S. Derawi, N. von Solms, E.H. Stenby, *Ind. Eng. Chem. Res.* 45 (2006) 4855–4868.
- [42] S.H. Huang, M. Radosz, *Ind. Eng. Chem. Res.* 29 (11) (1990) 2284–2294.
- [43] Design Institute for Physical Property Data (DIPPR), *Diadem Pro*.
- [44] W.L. Goffe, G.D. Ferrier, J. Rogers, *J. Econom.* 60 (1/2) (1994) 65–99.
- [45] SIMANN.F. (<http://www.netlib.no/netlib/opt/simann.f>) (acquired July 2012).
- [46] N. von Solms, I.A. Kouskoumvekaki, T. Lindvig, M.L. Michelsen, G.M. Kontogeorgis, *Fluid Phase Equilib.* 222–223 (2004) 87–93.
- [47] G.M. Kontogeorgis, G.K. Folas, N. Muro-Suñé, F. Roca Leon, M.L. Michelsen, *Oil Gas Sci. Technol.—Rev. IFP* 63 (3) (2008) 305–319.

## **Appendix 4**



# **Modelling of Tetrahydrofuran Promoted Gas Hydrate Systems for Carbon Dioxide Capture Processes**

**Peter Jørgensen Herslund<sup>a</sup>, Kaj Thomsen<sup>a</sup>, Jens Abildskov<sup>b</sup>, Nicolas von Solms<sup>a\*</sup>**

**<sup>a</sup>Center for Energy Resources Engineering (CERE)**

**<sup>b</sup>Computer Aided Process Engineering Center (CAPEC)**

**<sup>a,b</sup>Department of Chemical and Biochemical Engineering**

**Technical University of Denmark**

**DK2800, Kgs. Lyngby.**

**DENMARK**

---

\* Corresponding author: Phone: +45 4525 2867 Fax: +45 4588 2258 E-mail: NVS@kt.dtu.dk

## Abstract

A thermodynamic modelling study of both fluid phase behaviour and hydrate phase behaviour is presented for the quaternary system of water, tetrahydrofuran, carbon dioxide and nitrogen. The applied model incorporates the Cubic-Plus-Association (CPA) equation of state for the fluid phase description and the van der Waals-Platteeuw hydrate model for the solid (hydrate) phase. Six binary pairs are studied for their fluid phase behaviour. CPA descriptions are adjusted when needed by correlation of binary parameters in the applied mixing- and combining rules. Kihara cell potential parameters in the hydrate model are regressed for the three hydrate formers, tetrahydrofuran, carbon dioxide and nitrogen.

The developed model is applied to simulate two simplified, gas hydrate-based processes for post-combustion carbon dioxide capture from power station flue gases.

The first process, an unpromoted hydrate process, operates isothermally at a temperature of 280 K. Applying three consecutive hydrate formation/dissociation stages (three-stage capture process), a carbon dioxide-rich product (97 mole percent) is finally delivered at a temperature of 280 K and a pressure of 3.65 MPa. The minimum pressure requirement of the first stage is estimated to be 24.9 MPa, corresponding to the incipient hydrate dissociation pressure at 280 K for the considered flue gas.

A second simulated carbon dioxide capture process uses tetrahydrofuran as a thermodynamic promoter to reduce the pressure requirements. By doing so the minimum pressure requirement of the first capture stage is lowered to 0.41 MPa. Selectivity towards carbon dioxide in the hydrate phase is however lower than in the unpromoted process. Therefore the tetrahydrofuran promoted capture process needs four consecutive hydrate formation/dissociation stages to produce a 96 mole percent carbon dioxide-rich product stream. This stream is delivered at 280 K and a pressure of 0.17 MPa.

The present modelling study suggests several drawbacks of using tetrahydrofuran as a thermodynamic hydrate promoter, when applied in low-pressure, hydrate-based gas separation processes. Due to the high volatility of this compound, the promoter readily transfers to the vapour phase. Furthermore, tetrahydrofuran lowers the selectivity towards carbon dioxide, and the gas uptake in general, in the hydrate phase compared to the unpromoted system.

**Keywords:** Gas hydrates, Promoter, Carbon Dioxide, Tetrahydrofuran, Modelling, Thermodynamics, Cubic-Plus-Association (CPA), Van der Waals-Platteeuw.

## 1. Introduction

Carbon dioxide is a greenhouse gas. It absorbs and re-emits long-wave (infrared) radiation in the atmosphere of this planet. Part of this re-emitted radiation is sent back to the surface of the planet, helping to retain thermal balance.

During the last 200 years, the amount of carbon dioxide present in the atmosphere has increased from 280 ppm to a level of about 390 ppm in 2010 [1, 2].

Though ambiguously shown, there is growing consensus that our climate is changing due to anthropogenic emissions of greenhouse gases. Carbon dioxide from anthropogenic sources is considered to be the main contributor to the observed climate change [3].

Much focus has recently been put on reducing carbon dioxide emissions from centralised locations such as e.g. fossil fuel (coal, oil and gas) fired power stations. The International Energy Agency (IEA) estimated the global carbon dioxide emission from fossil fuel fired heat- and energy production to be 8.2 gigaton per year in 2001. This corresponded to approximately 35 percent of the total carbon dioxide emission related to combustion of fossil fuels that year [4].

Carbon dioxide capture is typically divided into two sections, pre- or post-combustion. In pre-combustion, at fossil fuel is contacted with air or oxygen to form hydrogen and carbon monoxide. The gas is hereafter contacted with steam, whereby the carbon monoxide is further oxidised to form carbon dioxide and more hydrogen. After this stage, the pre-combustion carbon dioxide capture stage is placed to remove carbon dioxide, thereby purifying the fuel (hydrogen) [5]. Post-combustion capture implies removing carbon dioxide from flue gases after combustion, before the flue gas is released to the atmosphere. The post-combustion technology offers the advantage of being easier to retro-fit to existing plants without making significant changes to the combustion technology [6].

A novel gas clathrate hydrate based separation technology forms the basis for the present study. This process has been proposed as an alternative to the existing gas separation technologies.

Gas clathrate hydrates, more commonly known as gas hydrates, are solid compounds of sufficiently small molecules and water. These solid compounds form when the constituents come into contact at conditions of low temperature and/or high pressure [7].

Gas hydrates are often referred to as non-stoichiometric solid inclusion bodies, where water (host) form a crystalline lattice by hydrogen bonding [8, 9, 10]. The lattice formation generates a number of empty cavities, in which small gas molecules (guests) may be enclathrated. The water lattice itself is a thermodynamically unstable structure, however attractive and repulsive interactions between the water and guest molecules stabilise the lattice [10]. The three most commonly encountered gas clathrate hydrate structures are the sI, the sII and the sH structures. Detailed descriptions of each hydrate structure may be found elsewhere [7]

The size of the guest molecule is often what defines the structure of a formed hydrate. Guest molecules of diameter size 4.2 – 6 Å, such as methane ( $\text{CH}_4$ ) and carbon dioxide ( $\text{CO}_2$ ) form structure I hydrates. Some guest molecules with diameters smaller than 4.2 Å form structure II hydrates when present as single guests. These include nitrogen ( $\text{N}_2$ ) and hydrogen ( $\text{H}_2$ ). Larger molecules with diameter 6 – 7 Å also form structure II. Propane ( $\text{C}_3\text{H}_8$ ) and iso-butane ( $\text{C}_4\text{H}_{10}$ ) are the most common among these. Structure H hydrates are

typically formed by large molecules of diameter 7 – 9 Å accompanied by smaller molecules such as methane, hydrogen sulfide or nitrogen [7].

Carbon dioxide may form gas hydrates with water at a pressure of approximately 1.2 MPa and temperature of 273 K [7]. The crystalline structure formed by the hydrogen bonded water molecules creates a total of 8 vacancies, so-called cavities, for each 46 water molecules. Assuming single occupancy of carbon dioxide in each of these cavities allow for a maximum carbon dioxide mole fraction of 0.15 in the solid phase. This corresponds to a mass fraction of carbon dioxide in the solid phase of approximately 0.31. Since gas hydrates are non-stoichiometric phases, full occupancy of carbon dioxide in the hydrate structure is however rarely achievable at moderate conditions of temperature and pressure.

Nitrogen and oxygen, like carbon dioxide, may form gas hydrates. However, these compounds form hydrates at significantly higher pressures. The formation pressure of the nitrogen hydrate at 273 K is approximately 16 MPa [7]. Gas mixtures of nitrogen, oxygen and carbon dioxide will form hydrates at conditions in between those of the pure gases. The hydrates formed from these mixtures will enclathrate all gas phase components with appropriate sizes. Since carbon dioxide forms hydrates at the lowest pressures of the three main constituents of the flue gas, the mixed hydrates are expected to be rich in carbon dioxide.

Assuming liquid carbon dioxide is the desired end-product, the hydrate based carbon dioxide capture process, like the chemical absorption process, will contain two sections, capture and release. In the capture part, the flue gas is compressed, cooled and mixed with water, whereby hydrates may form by crystallisation. A carbon dioxide-rich hydrate slurry is hereafter transferred to the release section, where the solid particles are dissociated (melted) by either heating or pressure release. The captured gas is released at conditions of moderate to high pressures and low temperature. The aqueous liquid phase may be re-cycled to the capture section.

Figure 1 illustrates a simplified schematic of a suggested process configuration.



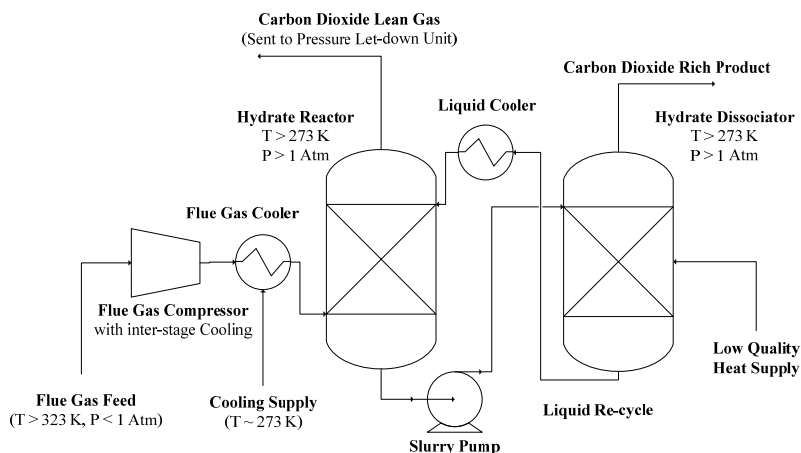


**Figure 1.** Simplified Schematic of a suggested configuration for the gas clathrate hydrate-based post-combustion carbon dioxide capture technology. The suggested conditions for temperature and pressure are not necessarily actual conditions of the process.

One of the main advantages of the hydrate based separation technology is that it operates at temperatures, where low-quality heat can be used in the release section of the process. Also, a smaller amount of excess liquid is heated in the release part, since the hydrate slurry may be concentrated before being heated. Finally, the captured gas is delivered at high pressure and low temperature, reducing costs for liquefaction of the final carbon dioxide product.

The main drawback of this process is the high pressure/low temperature requirement in the capture part. Large amounts of flue gas must be compressed in (multi-stage) compressor trains. A large amount of nitrogen is basically compressed just to be let down in pressure after the capture stage. By introducing a turbine generator downstream of the capture stage, some energy may be recovered from the carbon dioxide lean flue gas before emission to the atmosphere. This will however further increase the capital cost of the capture plant. Other challenges with this process are low kinetics of the hydrate crystallisation, low water conversion as well as handling of the particle suspension. With solid particles in the system, a high risk of plugging of process equipment is expected due to agglomeration of particles.

Recent attempts of improving this technology have looked into ways of lowering the pressure requirement in the capture stage. It has been found that the addition of low pressure/high temperature gas hydrate stabilisers, so-called thermodynamic gas hydrate promoters, may significantly lower the pressure requirement of this process. A thermodynamic gas hydrate promoter is a gas hydrate former that stabilises the hydrate structure at low pressures/high temperatures, thereby allowing for gas phase components to enter the hydrate phase at milder conditions. The result is a hydrate phase that enclathrates both the promoter and the desired gas phase constituents. If the additive is a liquid at the operating conditions of the process, it does not pollute the final gas product since it will remain with the liquid phase when the hydrates are dissociated. One disadvantage of adding these promoters is that they lower the gas storage capacity of the solid phase. Thus, a lot of

research has gone into finding the ideal gas hydrate promoter that allows for hydrate formation at near-atmospheric pressure with high gas uptake capacity.

Tetrahydrofuran, a five-sided cyclic ether, has been suggested as a potential thermodynamic gas hydrate promoter for the hydrate based carbon dioxide capture process.

Kang and Lee [11] investigated hydrate dissociation pressures and compositions for the ternary system water-N<sub>2</sub>-CO<sub>2</sub> and the quaternary system water-THF-N<sub>2</sub>-CO<sub>2</sub>.

A simulated flue gas vapour phase containing initially 17 mole percent CO<sub>2</sub> was shown to form hydrates at pressures of 0.475 MPa (275 K), if 1 mole percent THF was added to the aqueous liquid phase. The hydrate equilibrium pressure for this system without the addition of THF was 8.35 MPa (275 K).

It was found that CO<sub>2</sub> selectivity in the hydrate phase was lowered by the addition of THF, compared to the un-promoted system. Moreover, CO<sub>2</sub> selectivity was lowered with increasing temperature. A simulated flue gas phase initially containing 17 mole percent CO<sub>2</sub> could form hydrates containing approximately 35 mole percent CO<sub>2</sub> on a THF- and water-free basis.

From their results, Kang and Lee proposed a capture process in three hydrate formation/dissociation stages. In the first step, 1 mole percent THF should be used as a thermodynamic hydrate promoter. In the second and third step, no promoter should be added, in order to increase CO<sub>2</sub> selectivity. Intermediate vapour phase compression, performed between the individual capture stages, would be necessary in the proposed purification process.

Kang et al. [12] measured three-phase hydrate-liquid-vapour (H-L-V) equilibria in the ternary system of water, carbon dioxide (CO<sub>2</sub>) and nitrogen (N<sub>2</sub>), as well as in the quaternary system of water, tetrahydrofuran (THF), CO<sub>2</sub> and N<sub>2</sub>.

It was concluded that CO<sub>2</sub> selectivity in the hydrate phase was increased by decreasing temperature in the unpromoted (without THF) system.

Aqueous solutions containing 1 mole percent and 3 mole percent THF were investigated for their thermodynamic promotion of gas hydrate formation from synthetic flue gasses containing 17 and 70 mole percent CO<sub>2</sub>. Hydrate equilibrium pressure data were reported.

Linga et al. [13] presented results from a kinetic study of gas hydrate formation from gas mixtures of CO<sub>2</sub>/H<sub>2</sub> and CO<sub>2</sub>/N<sub>2</sub>.

Preliminary results of CO<sub>2</sub> capture by hydrate formation using an aqueous solution of 1 mole percent tetrahydrofuran (THF) were shown. While the equilibrium pressure and induction times were lowered dramatically by this additive, the gas consumption became considerably lower at similar applied driving forces.

A thermodynamic and kinetic study of CO<sub>2</sub> capture, both pre- and post combustion, was presented by Linga et al. [14]. Gas mixtures containing H<sub>2</sub> and CO<sub>2</sub> or N<sub>2</sub> and CO<sub>2</sub> were contacted with pure water in the attempt to establish a thermodynamic and kinetic basis for the new CO<sub>2</sub> capture process. A gas mixture containing 16.9 mole percent CO<sub>2</sub> and 83.1 mole percent N<sub>2</sub> was used to simulate the post combustion scenario. A hydrate equilibrium pressure of 7.7 MPa at a temperature of 273.8K was determined for this gas mixture.

Gas consumptions at isobaric conditions were recorded over a time period of 120 minutes. When dissociating the formed hydrate phases, gas mixtures containing between 55 mole% and 57 mole% CO<sub>2</sub> were released. After 120 minutes of hydrate formation the vapour phase

CO<sub>2</sub> content had been lowered from the initial 16.9 mole percent to approximately 10 mole percent

Thermodynamic and kinetic data for hydrate formation in the quaternary system of water-tetrahydrofuran (THF)-nitrogen (N<sub>2</sub>)-carbon dioxide (CO<sub>2</sub>) have been reported in the literature [15]. The main purpose of this work was setting up a block flow diagram for post combustion carbon dioxide capture from power station flue gasses.

A simulated flue gas containing 16.9 mole percent carbon dioxide 83.1 mole percent nitrogen was utilised. Three concentrations of THF were used, 0.5, 1.0 and 1.5 mole percent. Promoted hydrate equilibrium data corresponded well with those Kang et al. [12] at similar conditions. The system with 1.5 mole percent THF formed hydrates already at atmospheric pressure at a temperature of 273.8 K.

Kinetic experiments were conducted, applying driving forces from 0.7 MPa to 2.3 MPa. It was shown that induction times for hydrate formation depended both on applied driving force and THF concentration in the liquid phase. Induction times between 0.3 minutes and 7 minutes were reported. By applying a driving force of 2.3 MPa and a THF concentration of 1.5 mole percent, induction times for hydrate formation of approximately 0.3 minutes were achieved.

It was found that the hydrate phase gas uptake (measured as pressure drop during hydrate formation) was increased when increasing the applied driving force. Furthermore, increasing THF concentration to more than 1 mole percent resulted in a decrease in gas uptake in the initial hydrate growth period. The highest gas uptakes were obtained when using an initial concentration of 1 mole percent THF in the aqueous phase.

A separation process was proposed, operating at a temperature of 273.8K and a constant pressure of 2.5 MPa. It was suggested that the carbon dioxide could be purified to a composition of approximately 94 mole percent in three separation stages, if a 1 mole percent THF aqueous phase was utilised in all three steps.

## 2. Purpose of This Study

In order to evaluate the efficacy of CO<sub>2</sub> removal in the hydrate-based post-combustion carbon dioxide capture process, accurate thermodynamic models are required.

To enable a thorough evaluation, a generic thermodynamic model should cover wide ranges of temperature and pressure and include descriptions of both fluid and solid phases occurring in the process.

The present study focuses on modelling equilibrium conditions in the hydrate forming vessel of the capture process. An important piece of information here is the hydrate formation conditions (temperature and pressure) both for the un-promoted and the promoted hydrate systems. Moreover, since gas hydrates are non-stoichiometric phases, estimates of the hydrate composition and thereby the composition of the captured gas phase is desired for various process conditions.

A thermodynamic model presented in a previous study [16], combining the van der Waals-Plaatteuw hydrate model [17] with the Cubic-Plus-Association equation of state [18, 19] has been applied and modified to incorporate all four components present in the system of interest (water-tetrahydrofuran-carbon dioxide-nitrogen). The developed model is

validated against experimental data for both fluid phase equilibria and hydrate equilibria. A simplified post-combustion carbon dioxide capture process is simulated by use of the developed model.

### 3. Model

The van der Waals-Platteeuw hydrate model [17] as presented by Parrish and Prausnitz [20], has been modified such that the Cubic-Plus-Association (CPA) equation of state (EoS) supplies the hydrate model with all the needed inputs related to the co-existing fluid phases.

The Cubic-Plus-Association (CPA) equation of state presented by Kontogeorgis et al. [18, 19] combines the physical term from the cubic Soave-Redlich-Kwong (SRK) EoS with an association term similar to that found in the Statistical Associating Fluid Theory (SAFT) models.

Holder et al. [21] suggested a simplified (compared to that originally presented by Parrish and Prausnitz) method for transforming the reference hydrate chemical potential difference from reference temperature and pressure to the actual temperature and pressure. In their expression, the use of an experimental reference hydrate pressure,  $P_R$ , was removed providing a simpler expression.

$$\begin{aligned}
 \frac{\mu(T, P)_w^\beta}{R \cdot T} - \frac{\mu(T, P)_w^{L_w}}{R \cdot T} &= \frac{\Delta\mu(T, P)_w^{\beta/L_w}}{R \cdot T} \\
 &= \frac{\Delta\mu(T_0, P_0)_w^{\beta/L_w}}{R \cdot T_0} - \int_{T_0}^T \frac{\Delta H(T_0, P_0)_w^{\beta/L_w} + \Delta H(T)_w^{L_w}}{R \cdot T^2} dT \\
 &\quad + \int_0^P \frac{\Delta V_w^{\beta/L_w} + \Delta V_w^{L_w}}{R \cdot T} \cdot dP
 \end{aligned}
 \tag{1}$$

In a previous work [16], the van der Waals-Platteeuw hydrate model was applied using the original expression of Parrish and Prausnitz for the chemical potential difference of the reference hydrate. However the model was subsequently modified to incorporate the expression of Holder et al., shown in equation (1). Equation (1) is therefore used in the present work.

Furthermore, to enable thermodynamic calculations in systems involving the simultaneous presence of more than two fluid phases, the two-phase iso-thermal/iso-baric flash module originally used in the model [16] has been exchanged by an in-house, Gibbs energy minimisation multi-phase flash routine, allowing for the simultaneous co-existence of multiple fluid phases.

### 3.1 Hydrate Model Parameters

The van der Waals-Platteeuw hydrate model contains a number of model specific parameters. Among these are the structural parameters for the hydrate lattice. Values for these parameters are available in the literature and are provided in Table 1.

**Table 1.** sI and sII hydrate lattice and unit cell parameters for the van der Waals-Platteeuw hydrate model.

Structure	sI		sII	
Cavity	5 <sup>12</sup>	5 <sup>12</sup> 6 <sup>2</sup>	5 <sup>12</sup>	5 <sup>12</sup> 6 <sup>4</sup>
No. cavities per unit cell	2	6	16	8
Avg. cavity radius · 10 <sup>10</sup> / m	3.95 <sup>a</sup>	4.33 <sup>a</sup>	3.91 <sup>a</sup>	4.73 <sup>a</sup>
Coordination number	20	24	20	28
No. water molecules per unit cell	46		136	

<sup>a</sup> Data from Sloan (1998) [22]

Other model specific parameters for the hydrate model are the thermodynamic properties of the reference hydrate. These properties have been indirectly determined by a large number of authors over time. As these thermodynamic properties are not readily estimated, the reported values often differ significantly from each other. Table 2 lists the thermodynamic properties for the reference hydrate used in the model of this work.

**Table 2.** Thermodynamic properties for the reference hydrate in the van der Waals-Platteeuw hydrate model.

	sI	sII	Ref.
$\Delta\mu(T_0, P_0)_w^{\beta/L_w} / \text{J} \cdot \text{mole}^{-1}$	1297	937	[23]
$\Delta H_w^{\beta/Ice} / \text{J} \cdot \text{mole}^{-1}$	1389	1025	[23]
$\Delta H(T_0, P_0)_w^{Ice/L_w} / \text{J} \cdot \text{mole}^{-1}$	-6011	-6011	[22]
$\Delta C_p(T) / \text{J} \cdot \text{mole}^{-1} \cdot \text{K}^{-1}$	-38.12+0.141 · (T-273.1)	-38.12+0.141 · (T-273.1)	[22]
$\Delta V_w^{\beta/Ice} + \Delta V_w^{Ice/L_w} / \text{m}^3 \cdot \text{mole}^{-1}$	4.6 · 10 <sup>-6</sup>	5.0 · 10 <sup>-6</sup>	[22]

The van der Waals-Platteeuw hydrate model, as presented here, has no real predictive capabilities without *a priori* knowledge of the gas hydrate formers of interest. Kihara parameters must be determined by fitting the complete model to existing data for dissociation pressures and/or hydrate phase compositions. When doing so, the hydrate structures of the used reference data should preferably be known. The use of Kihara parameters determined independently from data for the pure hydrate formers (such as

viscosity data and/or second virial coefficients) will provide unsatisfactory results, if used in this model. The Kihara parameters regressed as part of this work are presented in Table 3.

**Table 3.** Kihara cell potential parameters regressed as a part of this work. Only  $\sigma_j$  and  $\varepsilon_j$  have been correlated. The core radii,  $a_j$ , are taken from other sources, where they have been determined typically from pure component viscosity data and/or second virial coefficients.

Component	$a_j \cdot 10^{10} / m$	$\sigma_j \cdot 10^{10} / m$	$\varepsilon_j / k_B / K$
Carbon dioxide	0.6805 *	2.9643	171.70
Nitrogen	0.3526 *	3.1723	128.07
Tetrahydrofuran	0.9013 **	3.5398	291.48

\* Sloan and Koh (2007) [7], \*\* Strobel et al. (2009) [24].

### 3.2 Equation of State Parameters

The cubic-plus-association (CPA) equation of state uses three pure component parameters for non-associating compounds and five pure component parameters for self-associating compounds. Compounds that are non self-associating, but may cross-associate with other self-associating compounds still have only three pure component parameters. In this work, carbon dioxide and tetrahydrofuran are treated in this way.

Pure component parameters for non self-associating and non cross-associating compounds are here obtained from critical properties (critical temperature, critical pressure and acentric factor) in a manner similar to that applied in the Soave-Redlich-Kwong equation of state. Self-associating and cross-associating compounds obtain pure component parameters by correlation of CPA to vapour pressure and saturated liquid density data. The pure component parameters used in this work for the total of four components considered (water, tetrahydrofuran, carbon dioxide and nitrogen) are provided in Table 4.

**Table 4.** Cubic-Plus-Association (CPA) equation of state pure component parameters for; water (H<sub>2</sub>O), tetrahydrofuran (THF), carbon dioxide (CO<sub>2</sub>) and nitrogen (N<sub>2</sub>). Association scheme according to definition presented elsewhere [25].

Comp.	Assoc. scheme	$a_0 \cdot 10^1$ Pa · m <sup>6</sup> · mole <sup>-2</sup>	$b \cdot 10^5$ m <sup>3</sup> · mole <sup>-1</sup>	$c_1$	$\beta^{AiBi}$	$\varepsilon^{AiBi} \cdot 10^{-4}$ Pa · m <sup>3</sup> · mol <sup>-1</sup>	Ref.
H <sub>2</sub> O	[2 <sup>+</sup> ;2 <sup>-</sup> ]	1.2277	1.4515	0.6736	0.0692	1.6655	[20]
THF	[0 <sup>+</sup> ;2 <sup>-</sup> ]	15.5228	6.7670	0.7773	N/A	N/A	[25]
CO <sub>2</sub>	[0 <sup>+</sup> ;1 <sup>-</sup> ]	3.5079	2.7200	0.7602	N/A	N/A	[26]
N <sub>2</sub>	N/A	$T_c = 126.2 \text{ K}$ , $P_c = 3.40 \text{ MPa}$ , $\omega = 0.03772$					[27]

Water is the only component treated as self-associating in this work. Two other components, tetrahydrofuran and carbon dioxide are allowed to cross-associate (solvate) with water, however these two components do not cross-interact with each other. Nitrogen is treated as non self-associating and non cross-associating.

All possible binary combinations of the above four components have been investigated for their fluid phase equilibria as a part of this work. Non-zero binary interaction parameters ( $k_{ij}$ ) and binary cross-association values ( $\gamma^{AiBj}$ ) have been adjusted where needed by correlating CPA to available fluid phase equilibria data found in the literature.

$k_{ij}$  is the binary interaction parameter (BIP) between component,  $i$ , and component,  $j$ .  $k_{ij}$  enters in the mixing rule for the binary energy parameter in the SRK term of CPA. In this work,  $k_{ij}$  may be temperature-dependent, according to equation (2).

$$k_{ij} = a_{kij} + b_{kij} \cdot T^{-1} \quad (2)$$

Both  $a_{kij}$  and  $b_{kij}$  take non-zero values if temperature dependence of  $k_{ij}$  is needed to obtain accurate fluid phase descriptions of binary pairs over extended ranges of temperature. If a constant  $k_{ij}$  suffice, only  $a_{kij}$  will take a non-zero value.

$\gamma^{AiBj}$  enters in the combining rule for the binary association volume parameter,  $\beta^{AiBj}$ . This work applies the CR1 combining rule as suggested elsewhere [25].

$$\beta^{AiBj} = \sqrt{\beta^{AiBi} \cdot \beta^{AjBj}} + \gamma^{AiBj} \quad (3)$$

In the case of cross-association between two self-associating molecules,  $\gamma^{AiBj}$  is set to zero, to allow model prediction according to the standard CR1 combining rule. In cases with cross-association involving a self associating and a non self-associating molecule, a non-zero  $\gamma^{AiBj}$  is needed to provide cross-association interactions. In the present work, this is the case for the two binary pairs of water-tetrahydrofuran and water-carbon dioxide.

Table 5 lists binary parameters regressed as part of the present work for all six possible binary combinations of the four components.

**Table 5.** Adjusted parameters for all binary pairs formed by the four components; water, tetrahydrofuran, carbon dioxide and nitrogen. Up to three binary parameters ( $a_{kij}$ ,  $b_{kij}$ ,  $\gamma^{AiBj}$ ) may be adjusted for binary pairs showing cross-association. A maximum of two binary parameters ( $a_{kij}$ ,  $b_{kij}$ ) may be adjusted in pairs with no cross-association.  $a_{kij}$  and  $b_{kij}$  are related to the binary interaction parameter,  $k_{ij}$ , as shown in equation (2).  $\gamma^{AiBj}$  enters in the combining rule for the binary cross-association volume according to equation (3).

Binary Pair	Adj. Parameters.	$k_{ij}$	$\gamma^{AiBj}$
Water-Tetrahydrofuran	$a_{kij}$ , $b_{kij}$ , $\gamma^{AiBj}$	0.4084 - 154.7/T	0.2543
Water-Carbon dioxide	$a_{kij}$ , $b_{kij}$ , $\gamma^{AiBj}$	0.4719 - 112.5/T	0.1707
Water-Nitrogen	$a_{kij}$ , $b_{kij}$	0.9999 - 368.4/T	N/A
Tetrahydrofuran-Carbon dioxide		0.00	N/A
Tetrahydrofuran-Nitrogen		0.00	N/A
Carbon dioxide-Nitrogen	$a_{kij}$	-0.0856	N/A

## 4. Results and Discussion

### 4.1 Fluid Phase Modelling

The algorithm of this model, providing fluid phase equilibrium conditions from the CPA multi-phase flash calculation (Gibbs energy minimisation) as inputs to the van der Waals-Platteeuw hydrate model, ensures a consistent calculation of equilibrium conditions in systems with both hydrate forming and non-hydrate forming components.

Often in the literature, models are presented, where the van der Waals-Platteeuw hydrate model is coupled with an equation of state for the vapour phase, a Gibbs excess energy model or an activity coefficient model for the activity of water in the liquid phase, and finally correlations for solubilities of gas phase components in the liquid phase (e.g. the Krichevsky and Kasarnovsky equation [28]). Whereas such an approach provides a large degree of freedom in terms of tuning the final results of the hydrate model, these types of model require an extensive list of input parameters.

By contrast, in the present model, the CPA equation of state, with a limited number of parameters, provides all the required inputs for the hydrate model in a straightforward and consistent manner.

Being consistent in all fluid phases, this model may not only be used to describe or predict conditions of incipient gas hydrate formation, it also accurately describes or predicts the number and type of co-existing fluid phases and the distribution of feed components in



the fluid phases at equilibrium conditions. For this reason, emphasis has been put on “tuning” the fluid phase description to create an accurate and reliable framework for the overall model.

The following sections present CPA modelling results of binary and ternary sub-systems within the quaternary system of water-tetrahydrofuran-carbon dioxide-nitrogen. These results serve as a validation of the inputs supplied later to the van der Waals-Platteeuw gas clathrate hydrate model.

When comparing model results to experimental data, the term Average Absolute (relative) Deviation (AAD) is used. AAD is defined according to equation (4).

$$AAD = \frac{1}{N} \sum_{i=1}^N \left| \frac{s_{calc,i} - s_{exp,i}}{s_{exp,i}} \right| \quad (4)$$

Where  $s_{calc}$  is the calculated property of interest ( $s$  may be temperature, pressure, composition etc.) and  $s_{exp}$  is the experimental reference data.  $N$  is the total number of data points.

Generally (both for fluid phase modelling and hydrate modelling), in cases, where correlation of parameters was needed, optimisation has been done by minimising the sum of absolute relative deviations between model descriptions and experimental data. The objective function has been defined as equation (5).

$$Obj = \sum_{i=1}^N \left| \frac{s_{calc,i} - s_{exp,i}}{s_{exp,i}} \right| \quad (5)$$

Where  $s_{calc}$  again is the calculated property of interest ( $s$  may be temperature, pressure, composition etc.) and  $s_{exp}$  is the experimental reference data.  $N$  is the total number of data points used as reference. Other definitions of the objective function, such as the sum of squared differences or the sum of squared relative differences, have been tested for some systems without noticeable improvements.

Optimisation of parameters in this work has been performed by use of an optimisation algorithm based on a FORTRAN implementation of the simulated annealing (SA) global optimisation algorithm presented by Goffe et al. [29] (source code available via [30]).

### **Water-tetrahydrofuran**

A detailed study on the CPA modelling of this binary system has been presented previously [25]. Water is treated as a self-associating compound applying an association scheme with two electron donating and two electron accepting sites.

Tetrahydrofuran has been modelled as an inert compound in its pure state but is allowed to cross-associate with water via two association sites (electron donating). This is consistent with the physical picture of this mixture.

Applying this approach provides accurate descriptions of both low-pressure vapour-liquid equilibria (VLE) and high-pressure/high temperature liquid-liquid equilibria (LLE) using a single set of CPA parameters (three binary parameters adjusted).

No fluid phase equilibrium data has been found in the literature, at conditions of temperature and pressure, where the structure II hydrates of THF form. Hence, no validation of the CPA parameters at these conditions has been performed. However, the fact that CPA correctly describes the complex behaviour of this complex binary system over extended ranges of temperature and pressure ( $T = 298 \text{ K} - 406 \text{ K}$  and  $P = 0.003 \text{ MPa} - 6.1 \text{ MPa}$ ) suggests the validity of the model parameters over an extended range of conditions.

Figure 2 illustrates the description of the (low boiling) azeotropic vapour-liquid equilibria for this binary system at a pressure of 0.1 MPa. CPA overestimates the boiling point temperatures of the binary mixture at this pressure. Herslund *et al.* [25] showed that the accuracy of the model is improved considerably at  $T = 298 \text{ K}$ , which is closer to the expected working range of the hydrate model (approximately 273 K to 300 K).

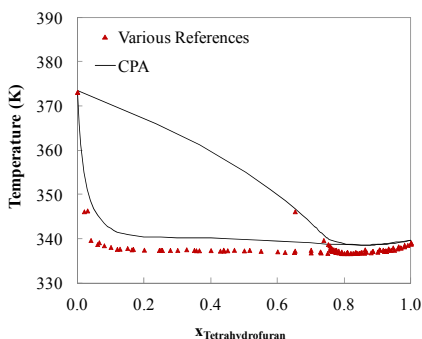


**Figure 2.** Vapour-liquid equilibria for the binary system of water and tetrahydrofuran at  $P = 0.1 \text{ MPa}$ . Red triangles: experimental data from [31-34]. Solid lines: CPA.

The fact that the binary system of water and tetrahydrofuran shows azeotropic VLE behaviour of the low-boiling type indicates positive deviations from Raoult's law. This observation suggests that while tetrahydrofuran does form hydrogen bonds with water, these bonds are not as strong as those between two water molecules. The competition between the hydrophobicity and hydrophilicity in tetrahydrofuran gives rise to the above mentioned positive deviations from Raoult's law as well as other remarkable behaviour for this binary system (e.g. the circular liquid miscibility gap at elevated pressure).

### Water-carbon dioxide

Tsivintzelis *et al.* [26] have presented a thorough study on the modelling of the binary system of water and carbon dioxide using CPA. It was concluded that this binary system can successfully be modelled when cross-association (solvation) between water and carbon dioxide is accounted for. Water is treated as a self-associating compound applying an

association scheme with two electron donating and two electron accepting sites. CO<sub>2</sub> is modelled as an inert compound in its pure state, but is allowed to cross-associate (solvate) with water via a single association site. Tsivintzelis *et al.* assigned the notation “electron acceptor” to this association site (positive charge).

Using this approach, accurate descriptions of both the water-rich and carbon dioxide-rich fluid phases are obtained over extended ranges of temperature and pressure.

In the work of Tsivintzelis *et al.*, a temperature dependent binary interaction parameter is proposed. Tsivintzelis *et al.* applied a linear, two-parameter dependence of the type;  $a_{kij} + b_{kij} \cdot T$ .

The present work also uses this approach and the pure component parameters presented by Tsivintzelis *et al.*. However, new binary parameters for the system water-carbon dioxide have been regressed in this work, using the same reference data suggested by Tsivintzelis *et al.*. A non-linear temperature dependence on the BIP ( $k_{ij}$ ) has been applied according equation (2). The reference data are those listed in Table 6.

**Table 6.** Experimental fluid phase equilibrium data used as reference data in this work for the binary system of water and carbon dioxide. x denotes compositional data from the water-rich phase. y denotes compositional data from the carbon dioxide-rich phase.

Reference	Type	No. Data Points	Temp. / K	Press. / MPa
[35]	x,y	80	288.7 – 533.2	0.69 – 20.3
[36]	x,y	77	278.2 – 318.2	0.46 – 7.96
[37]	x,y	58	323.2 – 353.1	4.05 – 10.2

A comparison of the linear-type and non-linear type temperature dependence for the binary interaction parameter showed that the non-linear dependence provided more accurate descriptions of the complete set of reference data from Table 6. Hence, this temperature dependence is applied in the following.

Wiebe and Gaddy [38] provide data for the water-rich phase at a temperature of 308 K. These data are used to validate the model parameters along with a selection of the used reference data.

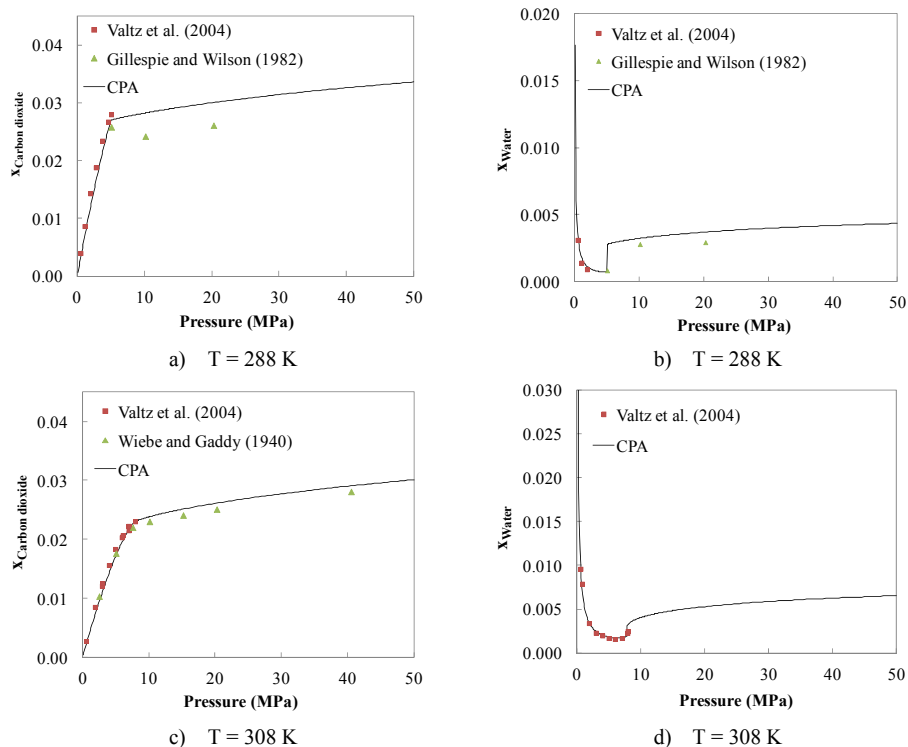


**Figure 3.** Fluid phase equilibria in the binary system of water and carbon dioxide. **a)** Carbon dioxide mole fraction in the water-rich phase at  $T = 288$  K. Experimental data from [35, 36]. **b)** Water mole fraction in the carbon dioxide-rich phase at  $T = 288$  K. Experimental data from [35, 36]. **c)** Carbon dioxide mole fraction in the water-rich phase at  $T = 308$  K. Experimental data from [36, 38]. **d)** Water mole fraction in the carbon dioxide-rich phase at  $T = 308$  K. Experimental data from [36].

Figure 3 a), b), c) and d) illustrate the model performances for the binary system of water and carbon dioxide at two temperatures, 288 K and 308 K. Comparisons are made with the selected reference data available at the two temperatures and the data reported by Wiebe and Gaddy. Excellent agreement between CPA and the experimental data are found at both temperatures. As reported by Tsivintzelis et al., applying this modelling approach enables an accurate description of the minimum solubility of water occurring in the carbon dioxide-rich phase around the phase transition of this phase from vapour-like at low pressures to liquid-like at high pressures.

Average absolute deviations (AAD's) of 9.1 percent are obtained for the description of the carbon dioxide mole fractions in the water-rich phase and the water mole fractions in the carbon dioxide-rich phase.

## Water-nitrogen

Nitrogen is treated as a non self-associating compound. For simplicity, the three pure component parameters for this component are calculated from the critical temperature, critical pressure and acentric factor ( $T_c$ ,  $P_c$ ,  $\omega$ ) in a manner identical to that applied for the cubic Soave-Redlich-Kwong (SRK) equation of state. The pure component critical properties are taken from the DIPPR database [27].

The predictions of CPA for the binary system of water and nitrogen are unsatisfactory, hence a non-zero binary interaction parameter ( $k_{ij}$ ) is applied. In order to obtain accurate description of both the water-rich and the nitrogen-rich fluid phases over extended ranges of temperature, a non-linear, temperature-dependent BIP has been incorporated in the model. The experimental data used as reference data are those listed in Table 7.

**Table 7.** Experimental fluid phase equilibrium data used as reference data in this work for the binary system of water and nitrogen. x denotes compositional data from the water-rich phase. y denotes compositional data from the nitrogen-rich phase.

Reference	Type	No. Data Points	Temp. / K	Press. / MPa
[39]	x	28	273.2 – 442.2	10.1 – 30.4
[40]	x,y	36	323.2 – 373.2	10.1 – 30.4
[41]	y	13	298.2 – 373.2	2.11 – 10.2
[42]	y	22	273.2 – 293.2	0.50 – 10.0
[43]	x	52	274.2 – 363.0	0.92 – 7.04
[44]	y	35	282.9 – 363.1	0.43 – 4.96

Figure 4 illustrates the model performance for the binary system of water and nitrogen at two temperatures, 273 K and 298 K. Comparisons are made with the reference data available at these two temperatures.

The water content in the vapour phase (nitrogen-rich phase) is well described by the model at both temperatures. Whereas the accuracy of the CPA model in terms of describing the nitrogen content in the water-rich phase is acceptable at 273 K, CPA performs very well for these types of data at 298 K.

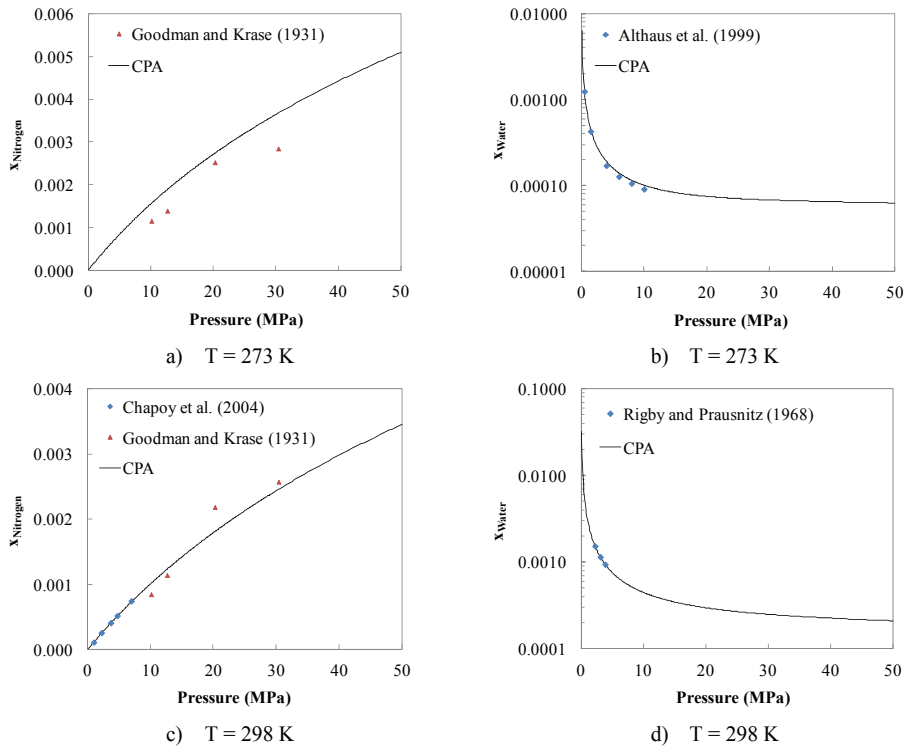


**Figure 4.** Vapour-liquid equilibria in the binary system of water and nitrogen. **a)** Nitrogen mole fraction in the water-rich phase at  $T = 273$  K. Experimental data from [39] **b)** Water mole fraction in the nitrogen-rich phase at  $T = 273$  K. Experimental data from [42] **c)** Nitrogen mole fraction in the water-rich phase at  $T = 298$  K. Experimental data from [39, 43] **d)** Water mole fraction in the nitrogen-rich phase at  $T = 298$  K. Experimental data from [41].

Figure 4 a), b), c) and d) confirm that the model is accurate in describing this binary system in the temperature interval, which is expected to be the working range for the hydrate model.

### Tetrahydrofuran-carbon dioxide

Both tetrahydrofuran and carbon dioxide are modelled as non self-associating compounds in their pure states. In the binary system comprised of these compounds, both species are similarly assumed non associating, and CPA accurately predicts the fluid phase equilibria of this system. The reference data indicated in Table 8 are described with an absolute average deviation (AAD) of 8.2 percent. An attempt has been made to improve the high-temperature description of this binary system by applying a non-zero BIP. With a BIP value of  $k_{ij} = -0.008$ , the description of the reference data may be lowered to 8.0 percent. Hence, an adjustment of the model (non-zero BIP) can hardly be justified.

**Table 8.** Experimental fluid phase equilibrium data used as reference data in this work for the binary system of tetrahydrofuran and carbon dioxide. x denotes compositional data from the tetrahydrofuran-rich phase. y denotes compositional data from the carbon dioxide-rich phase.

Reference	Type	No. Data Points	Temp. / K	Press. / MPa
[45]	x,y	85	311.0 – 331.3	0.81 – 8.14
[46]	x,y	65	313.0 – 333.0	6.51 – 9.69
[47]	x,y	68	313.2 – 353.2	0.47 – 10.3
[48]	x,y	30	298.2 – 313.2	2.06 – 7.63

Figure 5 a), b) and c) illustrate the model performances in describing the fluid phase equilibria at three temperatures, 298 K (Figure 5a), 311 K (Figure 5b) and 353 K (Figure 5c). CPA predictions ( $k_{ij} = 0.0$ ) are compared with the correlated model ( $k_{ij} = -0.008$ ).

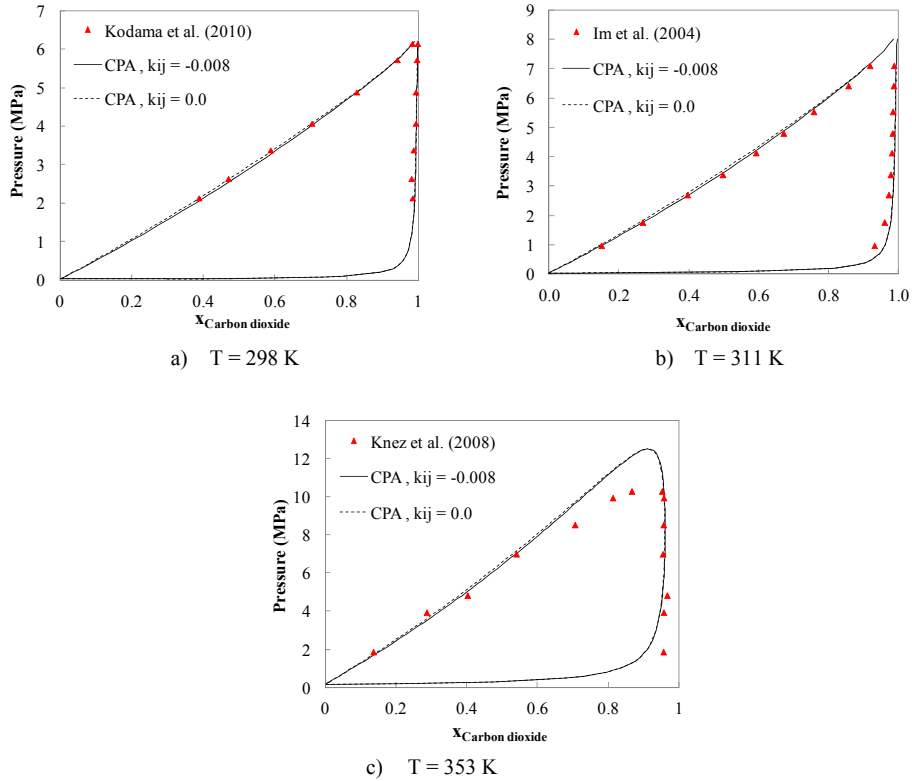


**Figure 5.** Fluid phase equilibria in the binary system of tetrahydrofuran and carbon dioxide. Comparison of experimental data (red triangles), CPA prediction with  $k_{ij} = 0.0$  (dashed lines) and CPA with  $k_{ij} = -0.008$  (solid lines). **a)** T = 298 K. Experimental data from [48]. **b)** T = 311 K. Experimental data from [45]. **c)** T = 353 K. Experimental data from [47].

No obvious differences are observed between the adjusted model and the CPA predictions, hence CPA predictions ( $k_{ij} = 0.0$ ) of the behaviour of this binary pair are used subsequently.

CPA overestimates the upper pressure limit of the two-phase envelope seen at  $T = 353$  K (Figure 5c) by roughly 20 percent. However, the low temperature description of the system is sufficiently accurate for the purpose of this model.

### Tetrahydrofuran-nitrogen

Only a single data set has been found for the fluid phase equilibria of the binary system of tetrahydrofuran and nitrogen. This data set is indicated in Table 9. Five equilibrium data points from the tetrahydrofuran-rich liquid phase are presented by Gibanel et al. [49].

**Table 9.** Experimental fluid phase equilibrium data used as reference data in this work for the binary system of Tetrahydrofuran and nitrogen.  $x$  denotes compositional data from the tetrahydrofuran-rich phase (liquid state).

Reference	Type	No. Data Points	Temp. / K	Press. / MPa
[49]	$x$	5	273.2 – 303.2	0.10

CPA predictions of the solubility of nitrogen in liquid tetrahydrofuran at 0.1 MPa are shown in Figure 6.

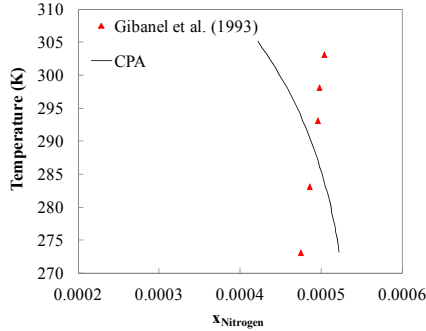


**Figure 6.** Solubility of nitrogen in liquid tetrahydrofuran at  $P = 0.1$  MPa. Comparison of experimental data and CPA predictions. Red triangles: Experimental data from [49]. Solid line: CPA prediction ( $k_{ij} = 0.0$ ).

CPA correctly predicts the order of magnitude of the nitrogen solubility in liquid tetrahydrofuran. However, the temperature dependence of the solubility is not captured by the model. Gibanel et al. found that the solubility of nitrogen increased with increasing temperature, whereas CPA predicts a decrease in the solubility with increasing temperature.



The application of a non-zero BIP does not enable CPA to describe this opposite tendency. Applying a temperature dependent BIP can improve the description in the temperature interval shown, however this can hardly be justified considering the limited number of experimental data points available for this system.

Hence we use CPA predictions for the fluid phase behaviour of this binary pair in the model development that follows.

### Carbon dioxide-nitrogen

Low temperature vapour-liquid equilibria data have been modelled for this binary pair. Table 10 lists the data used as reference.

**Table 10.** Experimental fluid phase equilibrium data used as reference data in this work for the binary system of carbon dioxide and nitrogen. x denotes compositional data from the carbon dioxide-rich phase. y denotes compositional data from the nitrogen-rich phase.

Reference	Type	No. Data Points	Temp. / K	Press. / MPa
[50]	x,y	54	220.0 – 240.0	1.29 – 16.7

Figure 7 a) and b) illustrate how CPA predicts ( $k_{ij} = 0.0$ ) the VLE of this system. The upper pressure limit of the two-phase region is overestimated by the model. By applying a non-zero  $k_{ij}$  of -0.086, the description is significantly improved at the low temperature (220 K). However, CPA still overestimates the pressure extension of the phase envelope compared to the experimental data at 240 K.

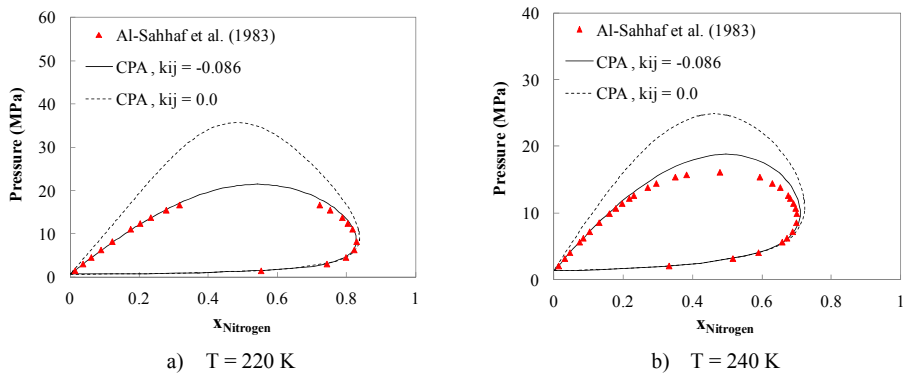


**Figure 7.** Fluid phase equilibria in the binary system of carbon dioxide and nitrogen. Comparison of experimental data (red triangles), CPA prediction with  $k_{ij} = 0.0$  (dashed lines) and CPA with  $k_{ij} = -0.086$  (solid lines). Experimental data from [50]. **a)**  $T = 220 \text{ K}$ . **b)**  $T = 240 \text{ K}$ .

No further attempts have been made to improve the high-temperature description of this binary pair, since these experimental data lie far from the expected operating temperatures of the hydrate model under development.

### Water-tetrahydrofuran-carbon dioxide

The performance of CPA in describing the ternary system of water, tetrahydrofuran and carbon dioxide is investigated. Since these three compounds show highly non-ideal behaviour in their respective binary pairs, it is suspected that the ternary system behaviour is of similar complexity.

No ternary adjustable parameters are available in CPA, hence the model relies on the ability of the model to extend from binaries to the ternary system.

Table 11 provides a selection of available equilibrium data for this ternary system.

**Table 11.** Experimental data for fluid phase equilibria in the ternary system of water-tetrahydrofuran-carbon dioxide. x denotes aqueous liquid phase, z denotes organic liquid phase.

Reference	Type	No. Data Points	Temp. / K	Press. / MPa
[51]	x,z	32	298 – 333	0.99 – 5.21
[52]	x,z	30	298.2 – 313.2	2.06 – 7.63

Lazzaroni et al. [51] have reported compositional data for the ternary system of carbon dioxide-tetrahydrofuran-water in temperature and pressure ranges, where this system shows three-phase vapour(V)-aqueous liquid(L<sub>w</sub>)-organic (or CO<sub>2</sub>-rich) liquid(L<sub>a</sub>) equilibria. Compositions from the two liquid phases along with the density of the vapour phase are provided for a total of 16 conditions of temperature (T) and pressure (P).

The 16 T/P conditions investigated experimentally by Lazzaroni et al. have here been modelled using the Gibbs energy minimisation flash approach on a feed comprised of 10 mole percent water, 10 mole percent tetrahydrofuran and 80 mole percent carbon dioxide.

Whereas CPA, with the binary parameters provided in Table 5, predicts three-phase VLLE equilibria at the conditions reported by Lazzaroni et al., the phase composition of the aqueous phase in particular is predicted with considerable deviations compared to the reported compositions. Figure 8a) and Figure 8b) compare experimental phase compositions of the co-existing liquid phases reported by Lazzaroni et al. with the phase compositions predicted by CPA.

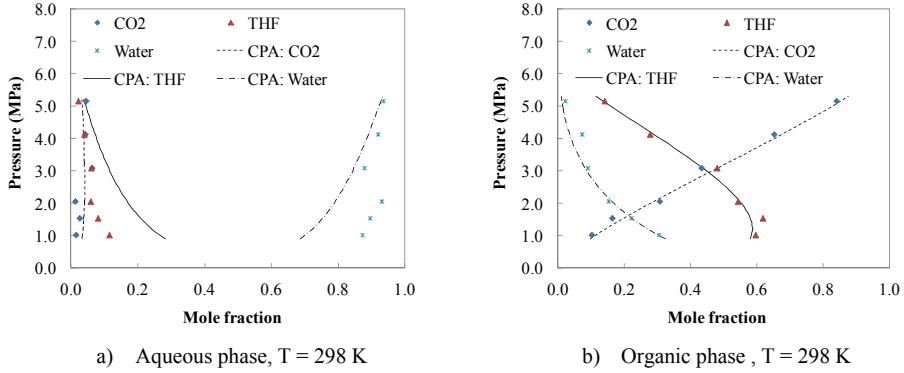


**Figure 8.** Compositions of co-existing liquid phases at conditions of three-phase vapour-liquid-liquid equilibrium for the ternary system of carbon dioxide, tetrahydrofuran (THF) and water. Comparison of experimental data from [51] and CPA predictions. Blue diamonds: carbon dioxide mole fraction. Red triangles: Tetrahydrofuran (THF) mole fraction. Blue cross: Water mole fraction. Dashed line: Carbon dioxide mole fraction (CPA). Solid line: Tetrahydrofuran (THF) mole fraction (CPA). Dash dot dashed line: Water mole fraction (CPA). **a)** Aqueous liquid phase at T = 298 K. **b)** Organic liquid phase at T = 298 K.

The tetrahydrofuran concentration in the aqueous liquid phase is predicted to be roughly twice as high as the concentrations reported by Lazzaroni et al. For this reason, the carbon dioxide solubility in the aqueous phase is also overestimated. The organic liquid phase composition is well predicted in terms of composition at 298 K and pressures ranging from 1 to 5 MPa. Similar observations are found for the data sets at 311 K and 333 K (not shown here).

Similarly, the model has been validated against the ternary data reported by Sabil et al. [52]. Whereas Lazzaroni et al. report phase compositions in the three phase V-L<sub>w</sub>-L<sub>a</sub> equilibria region at fixed temperatures and pressures, Sabil et al. report T/P conditions of fluid phase transitions for ternary mixtures of carbon dioxide-tetrahydrofuran-water systems with various initial compositions. Upper and lower phase boundaries for the three-phase V-L<sub>w</sub>-L<sub>a</sub> region are determined experimentally for systems with specified initial compositions.

When crossing the upper phase boundary from the low pressure side to the high pressure side at specified temperature, a transition from three phases (V-L<sub>w</sub>-L<sub>a</sub>) to two phases (L<sub>w</sub>-L<sub>a</sub>) occurs. At the lower phase boundary, the system moves from V-L<sub>w</sub>-L<sub>a</sub> equilibrium for pressures above the phase boundary to V-L<sub>w</sub> equilibrium for pressures below the boundary.

The initial compositions reported for each data set presented by Sabil et al. [52] are specified in a manner that may be misunderstood. Here it is assumed that the reported compositions for carbon dioxide ( $x_1$ ) are mole fractions in the ternary mixture, whereas the compositions reported for tetrahydrofuran ( $x_2$ ) are binary mole fractions in the initial aqueous liquid phase. Hence, when modelling the systems, the initial composition of tetrahydrofuran in the ternary mixture has been corrected under the assumption that the initial system consists of  $x(\text{CO}_2) = x_1$  moles of carbon dioxide and  $x(\text{THF}) = (1-x_1)*x_2$  moles of tetrahydrofuran. In the model, the ternary system is balanced with water according to;  $x(\text{water}) = 1 - x(\text{CO}_2) - x(\text{THF}) = 1 - x_1 - ((1-x_1)*x_2)$ . This is in agreement with a

separate publication of Sabil et al. [53], where a selection of the same data is presented alongside measured hydrate equilibrium data.

Figure 9 a) illustrates a comparison of the CPA predictions with a selection of the experimental data for the upper phase boundary for the phase envelope ( $V-L_w-L_a$  to  $L_w-L_a$ ) for three systems of various feed compositions. Figure 9 b) illustrates a comparison of the CPA predictions and experimental phase boundaries for both the upper ( $V-L_w-L_a$  to  $L_w-L_a$ ) and lower ( $V-L_w-L_a$  to  $L_w-V$ ) boundaries for the phase envelope. Note that the compositions provided in these figures are the corrected feed compositions of the ternary mixtures.

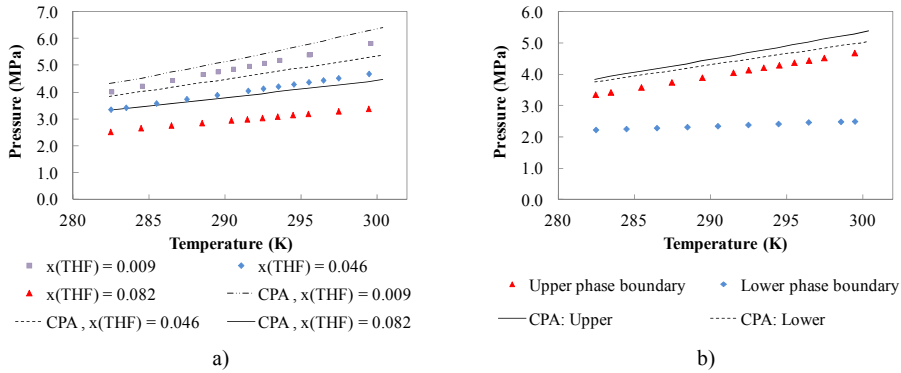


**Figure 9.** Comparison of calculated and experimental phase envelope boundaries for the ternary system of carbon dioxide-tetrahydrofuran (THF)-water. Experimental data are from Sabil et al. [52]. **a)** High-pressure boundaries for phase envelope in systems with 9 mole percent carbon dioxide and varying mole fraction of tetrahydrofuran,  $x(\text{THF})$ . **b)** Lower and upper phase envelope boundaries for ternary system with  $x(\text{CO}_2) = 0.09$ ,  $x(\text{THF}) = 0.046$ ,  $x(\text{H}_2\text{O}) = 0.864$ .

The upper phase boundary is calculated by specifying initial T/P conditions that are in the two-phase  $L_w-L_a$  region for the system with specified feed composition. A flash calculation then separates the feed into two liquid phases followed by a boiling point calculation performed for one of the two liquid phases. The new T/P conditions are subsequently returned to the flash algorithm and this procedure is continued until the calculated boiling point temperature/pressure no longer changes within a given tolerance.

The calculation procedure for the lower phase boundary is more complex since both vapour and liquid phases co-exist on both sides of the phase boundary. Hence, here it is not possible to search for the boundary by a combination of flash- and bubble-/dew point calculations. A trial and error search method has been applied, starting at pressure conditions below the phase boundary and then increasing pressure in steps of 0.001 MPa until the phase boundary is reached (phase number and types are monitored by multi-phase T/P flash calculations).

From Figure 9 a) it becomes clear that CPA predicts the upper phase boundaries of the VLE region with significant deviations compared to the experimental data. For the system with  $x(\text{THF}) = 0.082$ , the calculated pressures are approximately 30 percent higher than those measured by Sabil et al. [52]. Deviations decrease with decreasing concentration of tetrahydrofuran. With an overall mole fraction of tetrahydrofuran of 0.009, the calculated boundary pressures are approximately 8 percent above the experimental data.

Figure 9 b) compares the measured [52] and predicted (CPA) upper and lower phase envelope boundaries for the ternary system comprised of 9 mole percent carbon dioxide, 4.6 mole percent tetrahydrofuran and balance water. The upper phase boundary is predicted by CPA with deviations of approximately 14 percent. For the lower phase boundary, CPA overestimates the pressures by approximately 69 percent at the low temperatures and 100 percent at the high temperatures.

From the above analyses it is concluded that CPA, with the given parameters, predicts the ternary system of carbon dioxide-tetrahydrofuran-water with significant deviations compared to experimental data available in the regions where this system shows three-phase  $V-L_w-L_a$  equilibrium. Since no experimental data have been found for this system in the two-phase regions, it has not been possible to investigate the accuracy of the model in the description of these regions.

## 4.2 Modelling of the Un-promoted Gas Hydrate System

As a simplification of the specific case of carbon dioxide capture from power station flue gases, it is assumed that the flue gas phase may be modelled in the form of binary mixtures of nitrogen and carbon dioxide. In actual flue gases, significant amounts of other components such as e.g. oxygen and water may also be present. With respect to hydrate formation, oxygen acts similarly to nitrogen [54, 55], thus when simulating the flue gas, it is reasonable to replace the oxygen content with nitrogen in the model gas phase. The initial water content in the flue gas phase may also be neglected since, at equilibrium, the vapour phase will be saturated with water. Hence, the simplified, un-promoted gas hydrate system consists of ternary mixtures of nitrogen, carbon dioxide and water.

Several aspects of the model have been altered compared to a previously presented study of this ternary system [16]. The CPA parameters for the fluid phase description have been changed and the hydrate model equation for the reference hydrate have been changed from the form presented by Parrish and Prausnitz [18] to that of Holder et al. [21]. The calculation algorithm and numerical methods are however unchanged compared to the previous work.

New experimental studies, presenting mixed hydrate equilibrium data for the ternary system of carbon dioxide, nitrogen and water have appeared in the literature in recent years [12, 13, 56-62]. These data are not entirely consistent with the data previously used as reference data for the mixed nitrogen-carbon dioxide hydrate [12]. Eslamimanesh et al. [63] tried to establish a method for investigating the thermodynamic consistency of available gas hydrate data on the ternary system of nitrogen-carbon dioxide-water. Due to the complexity in both modelling and measuring equilibrium conditions for mixed gas hydrates in general, Eslamimanesh et al. were unable to draw clear conclusions on the thermodynamic consistency of the investigated data.

Hence, new Kihara parameters have been regressed for both nitrogen and carbon dioxide as part of this work. When regressing the Kihara parameters, both the pure hydrates of the two hydrate formers (sI hydrate for carbon dioxide and sII hydrate for nitrogen) have been considered together with the data for the mixed hydrates (both dissociation pressures and hydrate composition). Table 12 lists the data used as reference. Only hydrate(H)- Liquid water( $L_w$ )-vapour(V) equilibrium data have been included as reference for the pure hydrates of carbon dioxide. The mixed hydrates of carbon dioxide and nitrogen have been assumed

structure I hydrates for all the available data on the mixed hydrates. To ensure the validity of the obtained Kihara parameters for carbon dioxide in sII hydrates, a few data for the mixed hydrates of carbon dioxide and tetrahydrofuran (3 mole percent and 5 mole percent tetrahydrofuran in the aqueous liquid phase) have been included in the regression of parameters. Even though the un-promoted gas hydrate system is presented in this section without the use of promoters, regression of Kihara parameters for the three hydrate formers studied in this work (carbon dioxide, nitrogen, tetrahydrofuran and cyclopentane) has been done in an iterative procedure, to ensure internal consistency of the obtained parameters in all possible combinations and hydrate structures. Emphasis has been put on ensuring that the model predicts the right hydrate structures in all systems.

**Table 12.** Reference data for optimising Langmuir contents (Kihara parameters) along with final model accuracy. P denotes equilibrium pressure. Y denotes water-free hydrate composition.  $y(\text{CO}_2)$  is vapour phase mole fraction of carbon dioxide.

Ref.	Comp.	No Points	Temp. / K	Composition	AAD (P)	AAD (Y)
[53]	CO <sub>2</sub>	P: 10	275.1 – 282.9	$y(\text{CO}_2) = 1$	0.039	N/A
[64]	CO <sub>2</sub>	P: 10	275.0 – 282.8	$y(\text{CO}_2) = 1$	0.034	N/A
[12]	CO <sub>2</sub> / N <sub>2</sub>	P: 48 Y: 20	272.9 – 284.3	$0.05 \leq y(\text{CO}_2) \leq 0.97$	0.085	0.162
[13]	CO <sub>2</sub> / N <sub>2</sub>	P: 1	273.7	$y(\text{CO}_2) = 0.17$	0.037	N/A
[56]	CO <sub>2</sub> / N <sub>2</sub>	P: 9	278.1 – 285.3	$0.27 \leq y(\text{CO}_2) \leq 0.81$	0.16	N/A
[57]	CO <sub>2</sub> / N <sub>2</sub>	P: 24	275.3 – 283.1	$0.00 \leq y(\text{CO}_2) \leq 1.00$	0.14	N/A
[58]	CO <sub>2</sub> / N <sub>2</sub>	P: 9	273.1 – 280.2	$0.91 \leq y(\text{CO}_2) \leq 0.97$	0.06	N/A
[59]	CO <sub>2</sub> / N <sub>2</sub>	P: 15	274.0 – 281.9	$0.16 \leq y(\text{CO}_2) \leq 0.72$	0.12	N/A
[60]	CO <sub>2</sub> / N <sub>2</sub>	P: 16 Y: 16	273.4 – 281.1	$0.16 \leq y(\text{CO}_2) \leq 0.59$	0.24	0.08
[61]	CO <sub>2</sub> / N <sub>2</sub>	P: 33 Y: 33	273.6 – 281.7	$0.13 \leq y(\text{CO}_2) \leq 0.75$	0.17	0.20
[62]	CO <sub>2</sub> / N <sub>2</sub>	P: 33	276.9 – 285.4	$0.81 \leq y(\text{CO}_2) \leq 0.96$	0.17	N/A
[65]	N <sub>2</sub>	P: 8	273.2 – 281.1	$y(\text{N}_2) = 1$	0.036	N/A
[66]	N <sub>2</sub>	P: 23	273.2 – 283.3	$y(\text{N}_2) = 1$	0.040	N/A

According to the Gibbs phase rule ( $f = c - p + 2$ ), in systems with two components (pure hydrates of carbon dioxide or nitrogen) and three phases in equilibrium, the system is uni-variant (one degree of freedom). Hence, when fixing e.g. the system temperature, a single equilibrium state will be valid for any feed composition that provides three phases at this temperature.

When moving to the ternary system of carbon dioxide, nitrogen and water, still considering the H-L<sub>w</sub>-V equilibrium region, the system becomes di-variant due to the addition of one component. Hence, at specified temperature, multiple H-L<sub>w</sub>-V equilibrium states exist for this system. Specifying a second intensive variable “locks” the system into a single equilibrium state. In the model, this is done artificially by setting the vapour feed

composition to that of the desired equilibrium state and then feeding only sufficient amount of water to form a liquid water phase. By doing so, the vapour phase at equilibrium will be very close to the feed vapour phase composition.

Calculated equilibrium conditions for the mixed hydrates of carbon dioxide and nitrogen depend not only on the initial vapour phase composition of the feed, but also on the amount of liquid fed into the system. This is explained by the large differences in solubility of carbon dioxide and nitrogen in water. The final equilibrium composition of the vapour phase may change significantly depending on the amount of water in the feed. Hence, when comparing the model to experimental data, it is necessary to simulate the reported experimental conditions as accurately as possible. If the experimental feed (overall) composition is reported directly, this feed is used in the model. If only the vapour phase composition at equilibrium is reported, this composition should be used as vapour feed composition and the modelled system should be initiated with a low liquid to vapour feed ratio (e.g.  $L_w/(V+L_w) = 0.05$  on molar basis). If the initial vapour phase composition is reported without an exact feed composition, the model results should be used with caution, since results may vary several percent depending on the liquid to vapour feed ratio set in the feed. Of the reference data provided in Table 12, [12, 13 and 57-59] provide only initial vapour phase composition and initial volume of liquid fed into the system. Hence, the overall model feed compositions have been approximated roughly according to reported vapour phase compositions and liquid volumes. Table 12 contains the average absolute relative deviations (AAD according to equation (4)) in equilibrium pressure (P) and water free hydrate composition (Y), where available, for each reference data set.

With the regressed Kihara cell potential parameters ( $\varepsilon/k$  and  $\sigma$ ) the hydrate model describes the pure hydrates of both carbon dioxide and nitrogen within an average accuracy of 4 percent in the temperature interval from approximately 273 K to 283 K. Figure 10 illustrates the model description of the two pure hydrates. Comparisons are made with experimental data.

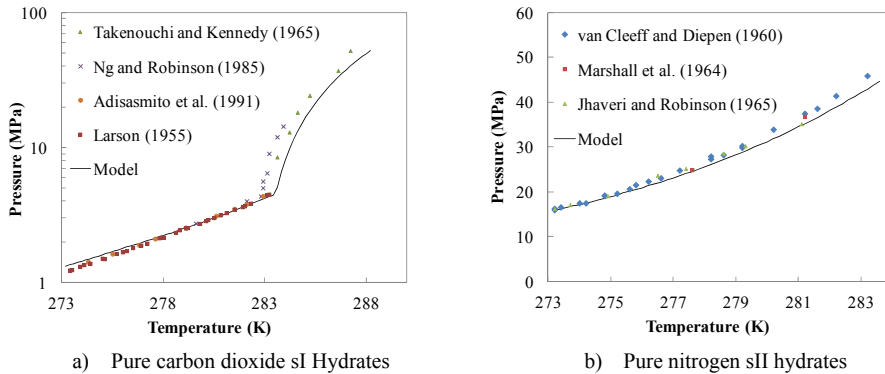


**Figure 10.** Comparison of model performance (solid lines) and experimental data for the pure hydrates of carbon dioxide and nitrogen. **a)** Dissociation pressures for carbon dioxide sI hydrate as function of temperature. Experimental data from [67-70]. **b)** Dissociation pressures for nitrogen sII hydrate as function of temperature. Experimental data from [65, 66, 71].

It is seen that the model describes both of the pure hydrate forms with reasonable accuracy in the low pressure region. The sudden change of slope in the hydrate data for carbon dioxide is due to the transition from vapour to liquid for the carbon dioxide rich phase (upper quadruple point). The model slightly overestimates this temperature, which is seen by the entire H-L<sub>w</sub>-L<sub>CO2</sub> being shifted up in temperature by approximately half a degree.

Nitrogen hydrates are described accurately up to temperatures of approximately 278 K. At higher temperatures, the model underestimates the hydrate pressures of the pure nitrogen sII hydrate.

Extending to the mixed hydrates increases complexity and pressure deviations increase.

Equilibrium pressures reported by Kang et al. [12], Fan and Guo [58] and Linga et al. [13] are well described by the model with AAD's below 0.1 in terms of pressure. However, the composition data reported by Kang et al. are less accurately described. The largest deviations are found in the pressure data presented by Herri et al. [60], Belandria et al. [61] and Kim et al. [62]. The compositions reported by Herri et al. [60] are described with a low AAD of 0.08, however the model fails at describing the pressures reported by these authors (AAD of 0.24). The model deviates from both the pressure- and composition data reported by Belandria et al. [61] with AAD's of 0.17 and 0.20 respectively. Pressure data reported by Kim et al. [62] are described with an AAD of 0.17.

Figure 11 compares reported dissociation pressures for various vapour phase compositions with model results. All modelling results are obtained assuming a liquid feed ratio,  $L_w/(L_w+V)$ , of 0.8.



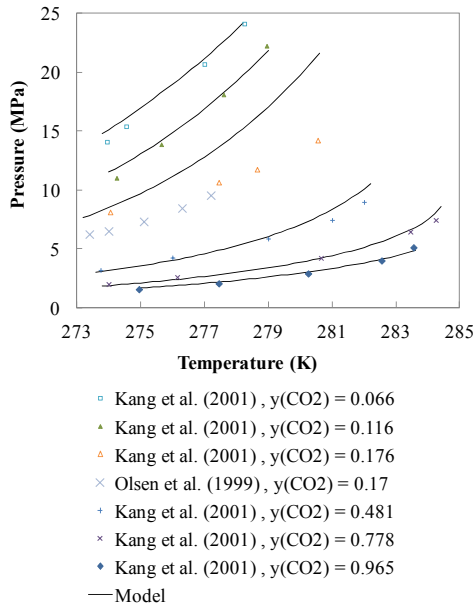


**Figure 11.** Comparison of model performance (solid lines) for the mixed hydrate of carbon dioxide and nitrogen and experimental data measured by Kang et al. [12] and Olsen et al. [59].  $y(\text{CO}_2)$  denotes vapour phase composition of carbon dioxide reported by the authors.

It is seen that the model performs well in the composition limits near pure carbon dioxide in the low-pressure region and near nitrogen in the high-pressure regions. Generally the dissociation pressure of the mixed hydrate decreases with increasing carbon dioxide content in the vapour phase. The model accurately describes five out of the six data sets reported by Kang et al. [12], however it fails at describing the temperature-dependence for the data set at 17.6 mole percent carbon dioxide. The high-temperature experimental data of this set could be questioned for this reason, however as shown in Figure 11, the temperature trend in the data reported by Kang et al. at these conditions correspond well with the trend of the data reported by Olsen et al. [59] at similar conditions.

What is difficult to see in Figure 11 is that whereas the model predicts the formed mixed gas hydrates to be of the sI structure type for all conditions with carbon dioxide vapour phase compositions of 11 percent and higher, a structural transition occurs for the system with 6.7 mole percent carbon dioxide. At temperatures below 275.6 K, the predicted structure is sI, however above this temperature the model predicts the sII hydrate to be the thermodynamically most stable form.

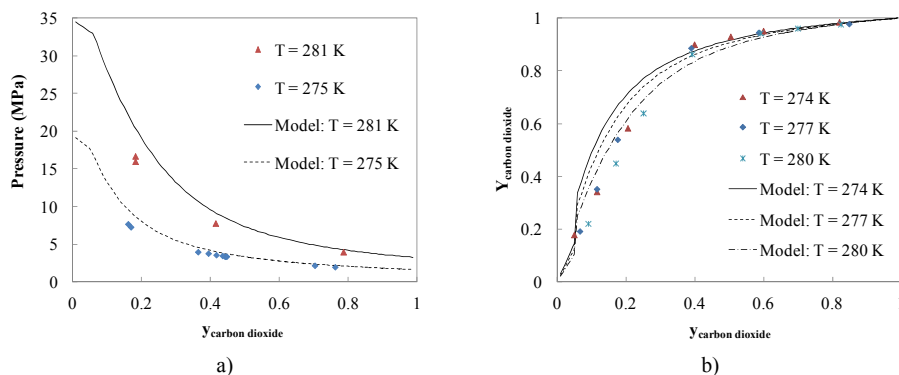


**Figure 12.** a) Hydrate equilibrium pressure for the mixed hydrate of carbon dioxide and nitrogen as function of vapour phase compositions. Experimental data from Bruusgaard et al. [57]. Solid line: Model at 281 K. Dashed line: Model at 275 K. b) Hydrate composition ( $Y_{\text{carbon dioxide}}$ ) on water-free basis for the mixed hydrate of carbon dioxide and nitrogen as function of mole fraction of carbon dioxide in the vapour phase ( $y_{\text{carbon dioxide}}$ ). Experimental data from Kang et al. [12]. Solid line: Model at 274 K. Dashed line: Model at 277K. Dash-dot-dashed line: Model at 280 K.

Figure 12 a) illustrates the effect of the initial vapour phase composition on the dissociation pressure of the mixed hydrate of carbon dioxide and nitrogen. The experimental data are reported by Bruusgaard et al. [57]. The model results are obtained assuming a liquid feed ratio,  $L_w/(L_w+V)$ , of 0.2. Note the change in slope of the model curves at approximately 5-6 mole percent carbon dioxide in the vapour phase. Despite the fact that all reference data for the mixed hydrate system were assumed sI hydrates, the model predicts sII hydrates to form for gas mixtures with less than five mole percent carbon dioxide and sI hydrates for gas mixtures with more than five mole percent carbon dioxide. This boundary is valid for the system fed with 20 mole percent liquid. It is not surprising though, that a structural change occurs in the mixed hydrate system, since the two pure hydrates form different structures. The compositional position of the structural change from sI hydrates to sII hydrates depend on the obtained Kihara parameters which are influenced by the assumed structure during the parameter regression. The difference in the composition for the structural transition observed in Figure 11 (6.7 mole percent carbon dioxide at 275.6 K) and that observed in Figure 12 a) (approximately 5-6 mole percent carbon dioxide at 275.3 K) is explained by the differences in the simulated liquid to vapour feed ratios. Hence, the presented results illustrate the importance of knowing exact feed composition, or as a minimum the equilibrium vapour phase composition for this ternary system, when comparing modelling results with experimental data.

A final and equally important aspect of the hydrate modelling for this carbon dioxide capture process is the ability of the developed model to describe the composition of the gas phase physically adsorbed inside the solid hydrate phase. Not only is it important for the model to accurately describe hydrate formation temperature/pressure conditions to enable a thermodynamic evaluation of the necessary flue gas compression, the hydrate composition is as important since it is needed to investigate the efficiency of the process to selectively remove carbon dioxide from the mixed flue gas.

Figure 12 b) illustrates modelling results for the water-free hydrate composition as function of the equilibrium vapour phase composition in the H-L<sub>w</sub>-V region. The model results are compared with experimental data reported by Kang et al. [12]. The vapour phase composition reported by Kang et al. for these data are actual vapour phase compositions at equilibrium, hence the model has been initiated by feeding only 5 mole percent liquid and 95 mole percent vapour to ensure that the equilibrium vapour phase composition corresponds to that reported by Kang et al.. It is seen that the model describes the data well in the composition limits, however the model overestimates the selectivity towards carbon dioxide in the region by 10 to 30 mole percent carbon dioxide in the vapour phase. The model correctly shows the trend of decreasing selectivity in the hydrate phase with increasing temperature.

### 4.3 Modelling the Thermodynamic Promotion Effect of Tetrahydrofuran

With the model in place for both the fluid phase description and the hydrate description of the un-promoted hydrate systems, only the Kihara parameters for tetrahydrofuran are needed in order to describe the promoted gas hydrates.

Kihara parameters ( $\varepsilon/k$  and  $\sigma$ ) for tetrahydrofuran have been regressed using experimental data for the mixed hydrates of tetrahydrofuran + carbon dioxide and tetrahydrofuran + nitrogen. Only experimental data from the H-L<sub>w</sub>-V three-phase region have been used as reference. Initial concentrations of tetrahydrofuran in the liquid phase up to five mole percent have been considered. Since more data were available for the tetrahydrofuran + carbon dioxide system, the objective function to be minimised has been modified such that the two systems are weighted equally (total deviation is normalised according to the number of data points for each system).

It has been shown experimentally that, for a given temperature, the corresponding H-L<sub>w</sub>-V equilibrium pressure for this ternary system mainly depends on the concentration of tetrahydrofuran in the aqueous liquid phase [53]. Hence, unless exact feed compositions are provided for the literature data, the model feed liquid is specified at the reference composition and calculations are initiated with a 90 mole percent liquid fraction (10 mole percent gas). Table 13 contains a list of references and conditions for the data used as reference. Comparisons of experimental data and model results in terms of equilibrium pressures are included.

**Table 13.** Reference data used when regressing Kihara cell potential parameters for tetrahydrofuran (THF).  $x(\text{THF})$  denotes mole fraction of THF in the feed liquid phase. AAD (P) is absolute average relative deviation of calculated pressures compared to the reference data.

Ref.	Comp.	No Points	Temp. / K	Composition	AAD (P)
[72]	THF / CO <sub>2</sub>	13	278.3 – 289.9	$0.016 \leq x(\text{THF}) \leq 0.028$	0.17
[73]	THF / CO <sub>2</sub>	7	280.4 – 291.1	$x(\text{THF}) = 0.05$	0.21
[74]	THF / CO <sub>2</sub>	28	279.9 – 291.3	$0.012 \leq x(\text{THF}) \leq 0.05$	0.10*
[75]	THF / CO <sub>2</sub>	6	283.8 – 289.8	$x(\text{THF}) = 0.011$	0.26**
[75]	THF / N <sub>2</sub>	5	281.4 – 289.4	$x(\text{THF}) = 0.011$	0.02
[76]	THF / N <sub>2</sub>	23	280.9 – 293.8	$0.01 \leq x(\text{THF}) \leq 0.05$	0.09

\* Data at  $x(\text{THF}) = 0.012$  and  $T > 288.55$  K disregarded since model predicts H-L<sub>w</sub>-L<sub>CO<sub>2</sub></sub> equilibria.  
\*\* Data for  $T > 287.4$  K disregarded since model predicts H-L<sub>w</sub>-L<sub>CO<sub>2</sub></sub> equilibria.

With the obtained parameters, the model overestimates equilibrium pressures for the mixed hydrate of tetrahydrofuran and carbon dioxide at liquid phase concentrations of tetrahydrofuran below three mole percent. Accurate descriptions of the promoted hydrates of carbon dioxide are obtained for concentrations of tetrahydrofuran in the aqueous liquid phase at or above three mole percent.

The mixed hydrates of nitrogen and tetrahydrofuran are described with AAD's below 0.1 for both reference data sets. Figure 13 a) and b) compares model results with a selection of the reference data for both the mixed hydrates of carbon dioxide + tetrahydrofuran and nitrogen + tetrahydrofuran.

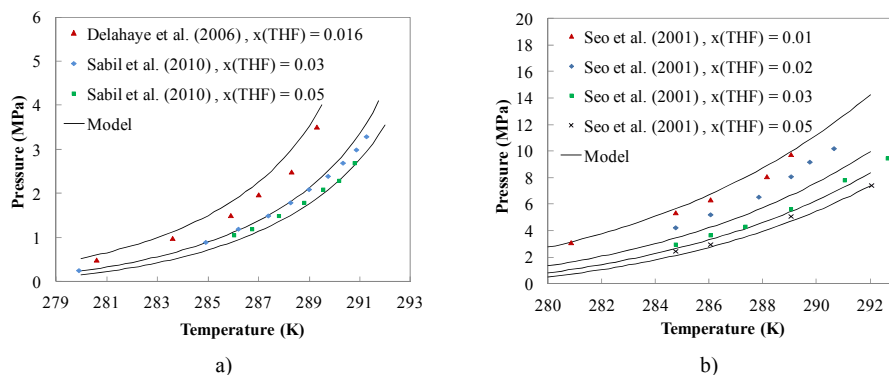


**Figure 13.** Dissociation pressures as function of temperature for mixed hydrates of carbon dioxide or nitrogen with tetrahydrofuran (THF).  $x(\text{THF})$  is the initial mole fraction of tetrahydrofuran in the liquid phase. Model results (solid lines) are obtained using feed liquid molar ratios,  $L_w/(L_w + V)$  of 0.9. **a)** Carbon dioxide-tetrahydrofuran hydrates. Experimental data from [72, 74]. **b)** Nitrogen-tetrahydrofuran hydrates. Experimental data from [75, 76].

Figure 13 a) clearly illustrates how the model overestimates the dissociation pressure of the mixed carbon dioxide + tetrahydrofuran hydrate at a THF mole fraction of 0.016. The data sets at 3 and 5 mole percent THF are accurately described by the model.

The mixed hydrates of nitrogen and tetrahydrofuran are accurately described in general. The model deviates only compared to the data set at 2 mole percent THF. At this concentration, the model underestimates the dissociation pressures compared to the experimental data reported by Seo et al. [76].

Figure 14 a) and b) illustrates how the equilibrium pressures for the two promoted hydrate systems, at constant temperature, depend on the THF concentration in the liquid phase. The model predictions are compared with experimental data extracted from the above reference data sets.

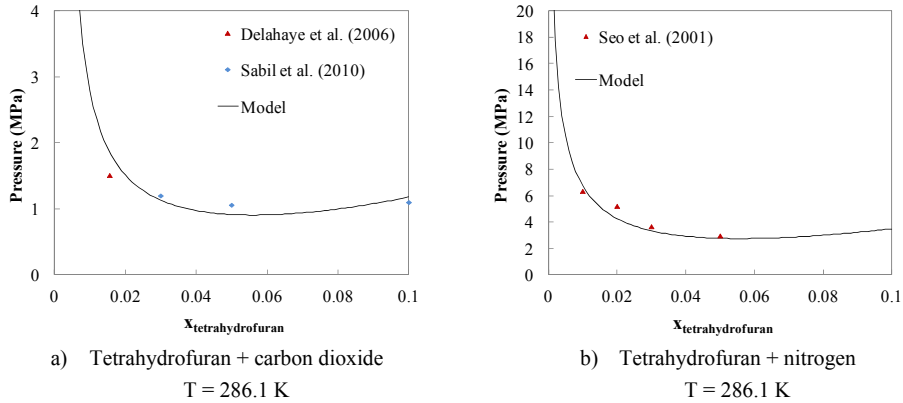


**Figure 14.** Dissociation pressures for the mixed sII hydrate of tetrahydrofuran and carbon dioxide (a) or nitrogen (b) as function of the initial liquid phase mole fraction of tetrahydrofuran ( $x_{\text{tetrahydrofuran}}$ ) at  $T = 286.1$  K. Solid lines are model results using a liquid feed ratio  $L_w/(L_w+V)$  of 0.9. a) Experimental data from [72, 74]. b) Experimental data from [76].

The data extracted for the carbon dioxide + tetrahydrofuran hydrate system are not all given exactly at a temperature of 286.1 K. The temperatures for these data vary from 285.9 K to 286.2 K. Hence, a small uncertainty in the experimental data must be expected due to these temperature variations. The data for the nitrogen + tetrahydrofuran system are all measured at a temperature of 286.1 K.

The presented model results in Figure 14 a) and b) are calculated for a constant temperature of 286.1 K. The model clearly shows the promoting effect of tetrahydrofuran, which has also been experimentally documented. The estimated equilibrium pressures, at constant temperature, decrease with increasing concentrations of tetrahydrofuran in the liquid phase up to a concentration of approximately 5 – 6 mole percent. For concentrations above this, the promoting effect decreases.

Looking closer at Figure 14 a) and b), it is found that the model predicts an optimum in the promoting effect at approximately 5.6 mole percent tetrahydrofuran in the aqueous phase. This concentration is identical for both of the systems shown in Figure 14 a) and b). The predicted optimum in the aqueous THF concentration thus lies at the theoretical, stoichiometric concentration of an sII hydrate with complete filling of its large cavities by

THF ( $x_{\text{THF,stoich}} = 0.056$ ). An investigation of the predicted fractional occupancies of THF in the large cavities also showed occupancies higher than 0.99.

Tetrahydrofuran acts in two opposite directions in hydrate forming systems: Tetrahydrofuran stabilises the sII hydrate structure by its presence in the large cavities of the solid hydrate phase. Simultaneously, tetrahydrofuran lowers the activity of water in the aqueous liquid phase by forming hydrogen bonds with water. Hence, the promoting effect of THF is a competing effect of hydrate phase stabilisation and water de-stabilisation in the liquid phase. At concentrations lower than 5.6 mole percent, stabilisation of the solid structure is the dominating effect. At higher concentrations, the de-stabilisation of water in the aqueous liquid phase increases its effect, and the overall promoting effect on the hydrate phase decreases.

Figure 15 shows the same competition between hydrate stabilisation and liquid water de-stabilisation only here for the pure sII hydrate of tetrahydrofuran (binary system of tetrahydrofuran and water).

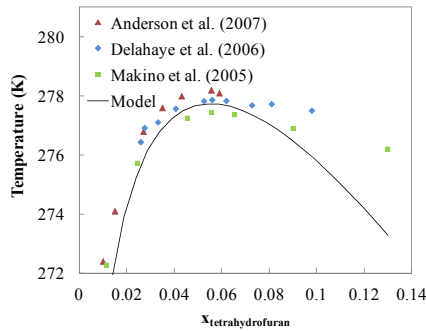


**Figure 15.** Dissociation temperature for the pure sII hydrate of tetrahydrofuran as function of the liquid phase mole fraction of tetrahydrofuran ( $x_{\text{tetrahydrofuran}}$ ).  $P = 0.10$  MPa. Experimental data from [72, 77, 78]. The solid line represents model predictions.

Hydrate dissociation temperatures are shown as a function of mole fraction of THF in the aqueous liquid phase. Both the experimental data and the model results are obtained at a fixed pressure of 0.10 MPa. Again an optimum is found at approximately 5.5 – 6.0 mole percent. The results shown in Figure 15 illustrate how the model tends to underestimate the stabilising effect of THF at low liquid phase concentrations. In the concentration range from approximately 2.5 – 7 mole percent, the model accurately describes the pure THF hydrate equilibrium temperatures. Above 7 mole percent THF, the model seems to overestimate the de-stabilising effect on the liquid phase.

The above results provide an explanation for the model's more accurate performance in the mixed hydrates of THF plus gas in the concentration range from approximately 3 – 5 mole percent. This is the region where the model provides the most accurate description of the balance between THF hydrate stabilisation and liquid water de-stabilisation.

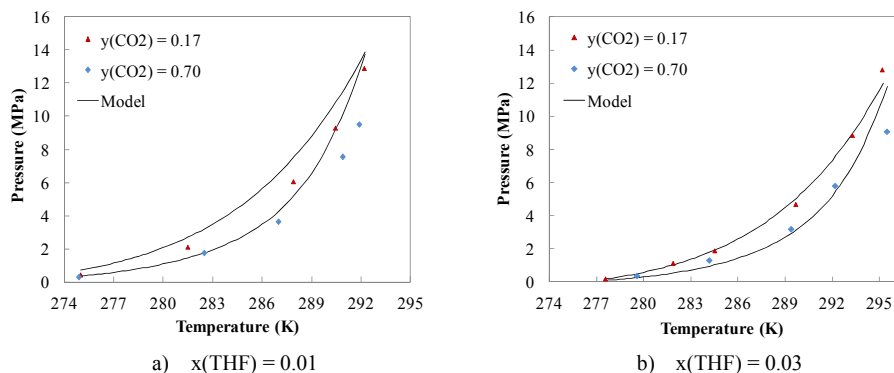


**Figure 16.** Hydrate dissociation pressure for the mixed hydrate of carbon dioxide-nitrogen-tetrahydrofuran as function of temperature.  $y(\text{CO}_2)$  denotes initial mole fraction of carbon dioxide in the vapour phase.  $x(\text{THF})$  denotes initial mole fraction of tetrahydrofuran in the aqueous liquid phase. Experimental data from [12]. Solid lines are model prediction obtained using a liquid feed ratio  $L_w/(L_w+V)$  of 0.9. **a)**  $x(\text{THF}) = 0.01$ . **b)**  $x(\text{THF}) = 0.03$ .

Kang et al. [12] report experimental data for promoted gas hydrate systems of gas mixtures containing carbon dioxide and nitrogen. The thermodynamic promoter is tetrahydrofuran and Kang et al. investigate the promoting effect at liquid phase concentrations of 1 and 3 mole percent THF. Two gas mixtures are used, initially containing 17 and 70 mole percent carbon dioxide. These conditions have been investigated using the developed model. Vapour phase and liquid phase initial compositions are those indicated by Kang et al. and the model feed liquid ratio,  $(L_w/(L_w+V))$ , is set at 0.9. Figure 16 a) and b) compare the model predictions with the data reported by Kang et al. As expected, the model overestimates the dissociation pressures of the mixed carbon dioxide-nitrogen-tetrahydrofuran hydrate at a liquid phase containing 1 mole percent tetrahydrofuran (Figure 16 a). For the system with 3 mole percent tetrahydrofuran in the liquid phase, the model predicts hydrate equilibrium pressures very well both for the carbon dioxide lean and carbon dioxide rich system. The model predicts all 21 data points with an AAD of 0.17. The systems with 1 mole percent THF are described with an AAD of 0.21 and the systems with 3 mole percent THF are described with an AAD of 0.14.

Both Figure 16 a) and b) show that the model predicts the equilibrium pressure for the gas mixture comprised of 70 mole percent carbon dioxide to increase steeply with temperature in the high temperature region. At temperatures above the ones shown in Figure 16 a) and b), the model predicts higher dissociation pressures for the carbon dioxide rich system than the carbon dioxide lean system.

Linga et al. [15] similarly report equilibrium pressures for mixed gas hydrates of carbon dioxide and nitrogen, promoted by the presence of tetrahydrofuran. A total of 9 data points are presented for liquid phase THF mole fractions ranging from 0.005 to 0.015 and vapour phase mole fractions of carbon dioxide ranging from 0.15 to 0.17. The low temperature data reported by Linga et al. [15] for a THF liquid mole fraction of 0.01 and a vapour phase mole fraction of 0.17 continue the trend in the data reported by Kang et al. at similar conditions.

The data reported by Linga et al. have been modelled using the present model with a liquid feed molar ratio of 0.9. The data are described with an AAD of 0.43. Again these experimental data show that the model overestimates hydrate equilibrium pressures for the promoted systems with low liquid phase mole fractions of tetrahydrofuran.

#### 4.4 Model predictions for the promoted carbon dioxide capture process

Up to this point, the model has been validated against available experimental data mainly for sub-systems relevant to the THF-promoted, post-combustion carbon dioxide capture process. It has been shown that significant amounts of tetrahydrofuran must be added to the aqueous liquid phase, in order to lower the pressure requirements sufficiently for this process to become realisable in large-scale gas separation processes.

Furthermore, it is the conclusion of the previous sections, that the present model is the most reliable for systems with three or more mole percent tetrahydrofuran in the aqueous liquid phase.

Hence, the following section considers and analyses the example of carbon dioxide capture from a simulated flue gas comprised of 10 mole percent carbon dioxide and 90 mole percent nitrogen. Two process conditions are simulated, one uses a promoter solution with three mole percent THF and the other uses a promoter solution with five mole percent THF.

The investigated aspects of the capture process are the flue gas minimum pressure requirements, process efficiency and selectivity and finally the environmental impact of this process. The latter in particular is an aspect which is often ignored.

Figure 17 a) illustrates the minimum pressure requirements (hydrate dissociation pressures) as function of temperature for a flue gas comprised of 10 mole percent carbon dioxide and 90 mole percent nitrogen. Two cases are simulated, the first using three mole percent THF in the aqueous phase and the second using 5 mole percent THF in the aqueous phase. The process is simulated using a 50 mole percent liquid feed ratio.

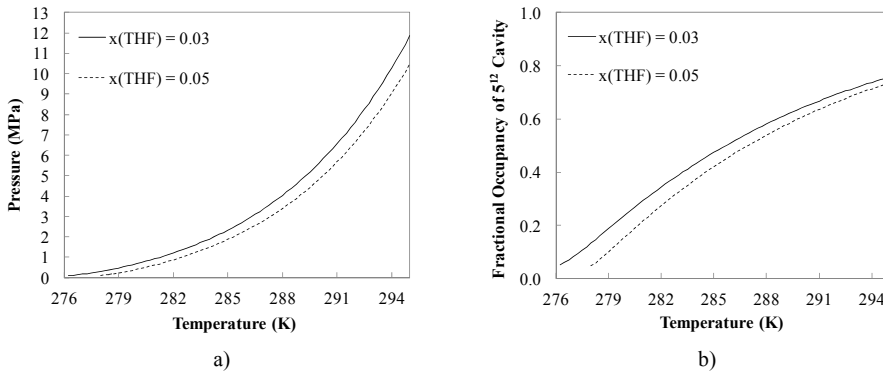


**Figure 17.** Mixed hydrate equilibrium pressures (a) and fractional occupancies of gas in the small  $5^{12}$  cavities of the sII hydrate (b) as functions of temperature for the quaternary system of water-tetrahydrofuran-carbon dioxide-nitrogen. Initial vapour phase comprised of 10 mole percent carbon dioxide and 90 mole percent nitrogen. Initial liquid phase consists of water and  $x(\text{THF})$  mole fraction of tetrahydrofuran. Model predictions obtained using a liquid feed ratio  $L_w/(L_w + V)$  of 0.5.



At all temperatures investigated, the minimum pressure requirement for the process using a 3 mole percent THF solution is higher than that for the process using a 5 mole percent THF solution. In the investigated temperature interval from 276 K to 295 K, equilibrium pressures vary from approximately 0.1 MPa to 12 MPa. According to the model, both systems reach an equilibrium pressure of 0.10 MPa if the process temperature is lowered sufficiently for the (almost) pure THF hydrate to form. The 3 mole percent system reaches an equilibrium pressure of 0.10 MPa at approximately 276.3 K. In the case of the 5 mole percent THF system, this temperature is approximately 277.9 K. If one compares with the T-x diagram of Figure 15, these temperatures are marginally higher than the equilibrium temperatures estimated for the pure THF hydrate in the binary system of tetrahydrofuran and water. The explanation for this is given in Figure 17 b). Even in the low temperature limits of the shown data, the hydrate phase incorporates small amounts of flue gas in the small  $5^{12}$  cavities of the hydrate structure. The presence of this gas helps stabilising the hydrate phase above the dissociation temperature of the pure THF hydrate.

Both systems in equilibrium at a pressure of 0.10 MPa, obtain a fractional occupancy of the small hydrate cavities of approximately 0.05 (seen in Figure 17 b)).

Even though not depicted in Figure 17, in all the investigated systems, the fractional occupancy of tetrahydrofuran in the large  $5^{12}6^4$  cavity is predicted to be higher than 0.994 indicating complete occupancy of the large cavities by THF. The fractional occupancy of THF in the large cavities decreases from approximately 0.9994 at the low temperatures to approximately 0.995 in the high temperature limits. This is valid for both systems.

The model correctly predicts THF to only enter the large cavities. The fractional occupancy of THF in the small cavities is always predicted to be zero. Similarly, only negligible amounts of gas enter the large cavities (order of magnitude is  $10^{-3}$ ).

The information provided in the combination of Figure 17 a) and b) is discouraging in the context of a process for post-combustion carbon dioxide capture from power station flue gases using THF promoted gas hydrates. If flue gas pressurisation is considered the crucial issue in this process, low operating temperatures must be applied. Operating the 5 mole percent THF process below 0.5 MPa requires cooling the system to below 280 K. At these conditions, only 5 to 18 percent of the hydrate gas capacity (occupancy of the small cavities) is used. This means much hydrate may form, however little gas is transferred from the vapour phase into the solid phase. If the design criterion is high gas uptake in the solid phase, say 50 percent of the full capacity, the temperature must be raised to 287 K, where the minimum pressure requirement becomes 2.8 MPa. Generally, the two investigated systems behave similarly with regard to pressure and gas uptake. Hence, the 3 mole percent THF system will need similar pressurisation to obtain 50 percent cage occupancy of gas in the small cavities.

Figure 18 a) illustrates the water- and promoter-free mole fraction of carbon dioxide in the gas phase adsorbed in the incipient hydrate crystal formed from a 10 mole percent carbon dioxide vapour phase. It is shown how this mole fraction decreases with increasing temperature/pressure. At identical temperatures, the 5 mole percent THF system turns out to be a little more selective towards carbon dioxide than the three mole percent system. The reason for this is that, for identical temperatures, this system operates at lower pressures,

which in turn increases selectivity. Again, modelling results are obtained using a 50 mole percent liquid feed ratio.

Figure 18 b) compares the selectivity of the promoted process with 5 mole percent THF to that of the un-promoted system. Both systems are modelled using a 50 mole percent liquid feed ratio.

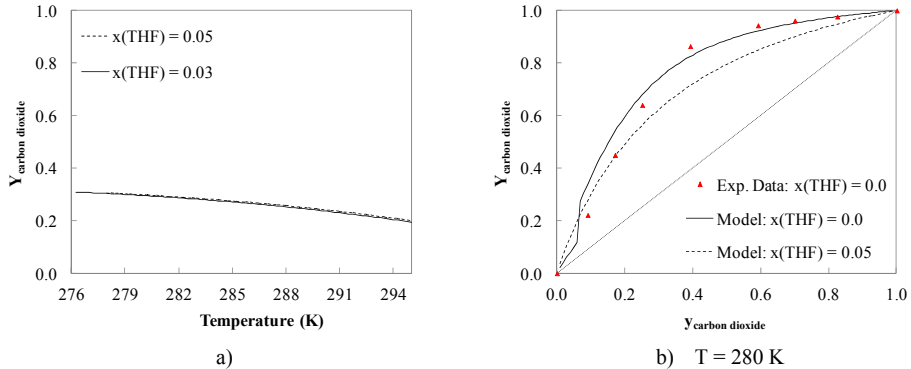


**Figure 18. a)** Model predictions of water- and promoter free hydrate composition of carbon dioxide as function of temperature. Initial vapour phase consists of 10 mole percent carbon dioxide and 90 mole percent nitrogen. **b)** Carbon dioxide content in hydrate phase on water- and promoter free basis as function of initial vapour phase composition at  $T = 280 \text{ K}$ . Red triangles: experimental data for the un-promoted hydrate system [12].  $x(\text{THF})$  is mole fraction of tetrahydrofuran in the feed liquid phase.

It is seen that the selectivity towards carbon dioxide in the hydrate phase is lowered compared to the un-promoted system (ternary system of water-carbon dioxide-nitrogen). Neither the un-promoted, nor the promoted system produces a hydrate phase that is sufficiently rich in carbon dioxide to enable a single stage carbon dioxide capture process. Whereas the un-promoted system requires 3 theoretical hydrate formation/dissociation stages to reach a final vapour phase mole fraction of carbon dioxide above 0.95, the promoted system will require a total of four stages.

Table 14 presents predicted stage conditions (incipient hydrate crystal dissociation conditions) for two multi-stage capture processes – one un-promoted and one promoted using 5 mole percent aqueous solutions. Both processes operate at a temperature of 280 K. The feed into the first stage of each process is comprised of 10 mole percent carbon dioxide and 90 mole percent nitrogen. All stages operate at a 50 mole percent liquid feed ratio. Since the minimum pressure requirements are of interest, all stages are assumed to operate at the incipient hydrate equilibrium pressure of the input gas. In the suggested process, a single capture stage comprises all the equipment illustrated in Figure 1. After the first capture stage, it is likely that only a limited amount of compression becomes necessary between stages, as the incipient hydrate dissociation pressure decreases with increasing carbon dioxide mole fraction in the vapour phase.

The un-promoted process uses pure water as liquid phase. Hence the first stage operates at a pressure of 24.9 MPa. It is assumed that the stage pressure is constant throughout the entire stage and the all hydrates formed have a composition similar to the incipient hydrate

crystal. The hydrates formed in stage 1 are then dissociated at constant pressure and the released vapour phase, now containing 36 mole percent carbon dioxide is transferred to stage 2. In stage 2, hydrates will form at a pressure of 9.17 MPa and the water-free hydrate composition here becomes 80 mole percent in carbon dioxide. Passing this vapour phase (after dissociating the hydrates of stage 2) to stage 3, where hydrates will form at a pressure of 3.65 MPa, provides a final outlet gas at a temperature of 280 K and a pressure of 3.65 MPa containing 97 mole percent carbon dioxide.

The promoted capture process operates at significantly lower pressures. The minimum pressure requirement of the first stage becomes 0.41 MPa and the water- and promoter-free hydrate composition of carbon dioxide is 30 mole percent. The promoted capture process requires a total of four theoretical stages to reach a final outlet gas containing 96 mole percent carbon dioxide. This outlet gas is supplied at 280 K and 0.17 MPa.

**Table 14.** Simulated incipient hydrate conditions for the un-promoted and promoted ( $x(\text{THF}) = 0.05$ ) capture processes.  $T = 280$  K. Initial vapour phase mole fraction of  $\text{CO}_2$  in feed to stage 1 is 0.10.  $P_{\text{eq}}$  is incipient hydrate equilibrium pressure for each stage.  $Y_{\text{CO}_2}$  is mole fraction of  $\text{CO}_2$  in the incipient hydrate crystal (water- and promoter-free basis). Hydrate phase composition ( $Y_{\text{CO}_2}$ ) in stage 1 is used as feed to stage 2 and so forth. All stages in both processes operate at a 50 mole percent liquid feed ratio.

Stage	Unpromoted		Promoted	
	$P_{\text{eq}}$ (MPa)	$Y_{\text{CO}_2}$	$P_{\text{eq}}$ (MPa)	$Y_{\text{CO}_2}$
1	24.9	0.36	0.41	0.30
2	9.17	0.80	0.29	0.62
3	3.65	0.97	0.21	0.86
4	N/A	N/A	0.17	0.96

The results presented above outline both the benefits and the drawbacks of using tetrahydrofuran as a thermodynamic hydrate promoter in the hydrate-based carbon dioxide capture process. The main benefit is the fact that the minimum pressure requirement in the first separation stage of the process is reduced from 24.9 MPa to 0.41 MPa by the addition of 5 mole percent THF to the aqueous liquid. The drawback of the promoted system is not only the fact that this process requires an additional separation stage, the promoted system also delivers the final carbon dioxide rich stream at a low pressure. Hence, this process requires a final compression of the carbon dioxide product, before this stream is ready for transportation and/or storage (assuming liquid carbon dioxide is the preferred form for transportation). Compressing the outlet stream of the final separation stage is however significantly less energy consuming than compressing the original flue gas, since the final outlet gas only represents a small fraction of the original flue gas stream.

Furthermore, since the promoted hydrates provide low gas uptakes at the proposed process temperature, large amounts of liquid and hydrate slurries must be circulated in the system to remove significant amounts of carbon dioxide from the original flue gas.

An interesting yet often ignored aspect of the promoted hydrate based carbon dioxide capture process is the promoter slip from the aqueous liquid phase to the vapour phase. Figure 19 illustrates the predicted THF mole fraction in the equilibrium vapour phase (incipient hydrate forming conditions) leaving the first stage of the promoted hydrate process.

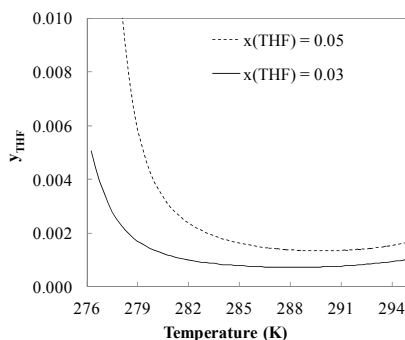


**Figure 19.** Equilibrium Mole fraction of tetrahydrofuran,  $y(\text{THF})$ , in the vapour phase leaving stage 1 of the simulated carbon dioxide capture process. Solid line: model predictions for system using a 3 mole percent THF aqueous solution. Dashed line: model predictions for system using a 5 mole percent THF aqueous solution.

As can be seen, the gas phase of stage 1 contains significant amounts of THF. For the simulated four-stage capture process ( $x(\text{THF}) = 0.05$ ), operating at 280 K, the gas phase in stage 1 would contain 0.39 mole percent THF at equilibrium. This promoter content would have to be recovered, before the off-gas can be emitted to the atmosphere. The following stages would emit similar or higher concentrations of THF to the atmosphere, since these stages operate at even lower pressures. Hence, the present model predicts furthermore one challenge in the promoted hydrate process. Significant amounts of promoter will slip from the liquid phase to the vapour phase and this content must be re-generated subsequently for both environmental and economic reasons.

## 5. Conclusion

A modelling study of both fluid phase behaviour and hydrate phase behaviour was presented. Four components were studied, water, tetrahydrofuran, carbon dioxide and nitrogen. Six binary pairs were studied for their fluid phase behaviour. CPA descriptions were improved when needed by correlation of binary parameters in the applied mixing- and combining rules.

In this work, CPA has proven its qualities as an advanced equation of state handling systems involving hydrogen bonding, resulting in complex fluid phase behaviour. Accurate descriptions were obtained for all the investigated systems.

The binary system of water and tetrahydrofuran represents a challenge from a fluid phase modelling point of view, as this system shows both azeotropic vapour-liquid equilibrium (VLE) at ambient conditions and closed-loop miscibility gaps at elevated temperatures and pressures. Accurate modelling of this system was found to be important when later extending the model to include other components such as e.g. carbon dioxide. Whereas CPA, from a qualitative point of view, predicted the correct fluid phase behaviour in this ternary

system, the phase composition of the aqueous phase in particular was described with significant deviations compared to available experimental data.

The developed model was applied to simulate two simplified processes for post-combustion carbon dioxide capture from power station flue gases.

The first process, an unpromoted hydrate process, was assumed to operate isothermally at a temperature of 280 K. The flue gas feed into the first stage of the process was comprised of 10 mole percent carbon dioxide and 90 mole percent nitrogen. In the hydrate forming vessel, pure water and flue gas was mixed at a 50/50 molar feed ratio. The hydrate forming stage was assumed to operate isobarically at the incipient hydrate equilibrium pressure of the inlet gas. This is a simplified scenario as hydrate crystallization would need further pressurisation or cooling to take place. The incipient hydrate dissociation conditions were however used as a means of determining the minimum pressure requirement of the system. The minimum pressure requirement of the first stage was estimated to be 24.9 MPa. The captured gas contained 36 mole percent carbon dioxide suggesting the need for a multi-stage capture process design. Applying three consecutive hydrate formation/dissociation stages (three-stage capture process), a carbon dioxide-rich product (97 mole percent) could be delivered at a temperature of 280 K and a pressure of 3.65 MPa. It was concluded that this process was not economically feasible due to the high pressure requirement of the first capture stage.

The second carbon dioxide capture process used tetrahydrofuran as a thermodynamic promoter to reduce the pressure requirements. A five mole percent aqueous solution of tetrahydrofuran was circulated in the second process. By doing so the minimum pressure requirement of the first capture stage could be lowered to 0.41 MPa. Selectivity towards carbon dioxide in the hydrate phase was however lower than in the unpromoted process. Therefore the tetrahydrofuran promoted capture process needed four consecutive hydrate formation/dissociation stages to produce a 96 mole percent carbon dioxide-rich product stream. This stream was delivered at 280 K and a pressure of 0.17 MPa.

The presented results are discouraging for the carbon dioxide capture process in development. The present modelling study has suggested several drawbacks of using tetrahydrofuran, when applied in low-pressure, hydrate-based gas separation processes. Due to the high volatility of this compound, the promoter readily transfers to the vapour phase. Furthermore, tetrahydrofuran lowers the selectivity towards carbon dioxide in the hydrate phase compared to the unpromoted system.

It is not in the nature of species such as carbon dioxide and nitrogen to form the classical gas hydrates at conditions close to atmospheric pressure. Therefore, even though these hydrate structures become available at low pressure, carbon dioxide may not necessarily enter the solid phase in significant amounts. This model suggests that it is thermodynamically more favourable for carbon dioxide to remain in the co-existing fluid phases at low pressure conditions.

## 6. Acknowledgements

This work was financially supported partly by the European iCap project (EU FP7) and partly by the Department of Chemical and Biochemical Engineering (MP<sub>2</sub>T) at the Technical University of Denmark (DTU).

The authors acknowledge the initiative and work Erling H. Stenby and Philip L. Fosbøl put into establishing the funding for DTU, as part of the iCap project.

## 7. List of Abbreviations and Symbols

### Abbreviations

AAD	Average Absolute Deviation
BIP	Binary Interaction Parameter
CPA	Cubic-Plus-Association
LLE	Liquid Liquid Equilibrium
Obj	Objective function
SA	Simulated Annealing
THF	Tetrahydrofuran
VLE	Vapour Liquid Equilibrium
VLLE	Vapour Liquid Liquid Equilibrium

### Symbols

#### Normal Characters

$A_i$	Association site type “A” on component $i$ [unit less]
$a_0$	CPA pure component parameter [ $\text{Pa} \cdot \text{m}^6 \cdot \text{mol}^{-2}$ ]
$a_j$	Spherical core radius of component $j$ in the Kihara cell potential [m]
$a_{kij}$	Constant in temperature expression for $k_{ij}$ [unit less]
$B_j$	Association site type “B” on component $j$ [unit less]
$b$	CPA co-volume parameter [ $\text{m}^3 \cdot \text{mol}^{-1}$ ]
$b_{kij}$	Constant in temperature expression for $k_{ij}$ [K]
$c_l$	CPA pure component parameter [unit less]
$\Delta C_p(T)$	Reference heat capacity difference between the meta-stable empty hydrate phase and liquid water at temperature $T$ [ $\text{J} \cdot \text{mole}^{-1}$ ]

$\Delta H(T_0, P_0)_w^{\beta/Ice}$	Reference hydrate enthalpy difference between water in the meta-stable empty hydrate phase and water in ice at reference temperature and pressure conditions [ $J \cdot mole^{-1}$ ]
$\Delta H(T)_w^{Ice/L_w}$	Enthalpy difference between water in ice and Liquid water at temperature, $T$ [ $J \cdot mole^{-1}$ ]
$\Delta H(T_0, P_0)_w^{Ice/L_w}$	Reference enthalpy difference between water in ice and Liquid water at reference temperature and pressure conditions [ $J \cdot mole^{-1}$ ]
$k_B$	The Boltzmann constant [ $J \cdot K^{-1}$ ]
$k_{ij}$	Binary interaction parameter [unit less]
$N$	Total number [unit less]
$P$	Pressure [Pa]
$P_0$	Pressure at reference condition [Pa]
$P_c$	Critical pressure [Pa]
$P_R$	Pressure of reference hydrate [Pa]
$R$	Gas constant [ $m^3 \cdot Pa \cdot mole^{-1} \cdot K^{-1}$ ]
$s_{calc}$	Calculated parameter value used in definition of AAD or obj
$s_{exp}$	Experimental parameter value used in definition of AAD or obj
$T$	Temperature [Kelvin]
$T_0$	Temperature at reference condition [K]
$T_c$	Critical temperature [Kelvin]
$\Delta V_w^{\beta/Ice}$	Molar volume difference empty hydrate structure and ice [ $m^3 \cdot mole^{-1}$ ]
$\Delta V_w^{Ice/L_w}$	Molar volume difference between ice and liquid water [ $m^3 \cdot mole^{-1}$ ]
$x$	Liquid phase mole fraction [unit less]
$X_{Ai}$	Fraction of non-bonded association sites of type “A” on component $i$ [unit less]
$y$	Vapour phase mole fraction [unit less]
$Y_j$	Water free hydrate composition of guest $j$ [unit less]

### Greek letters

$\beta^{AiBi}$	CPA pure component association volume [unit less]
$\beta^{AiBj}$	CPA binary association volume [unit less]
$\gamma^{AiBj}$	CPA binary adjustable in combining rule for $\beta^{AiBj}$ [unit less]
$\varepsilon_j$	Maximum attractive potential of specie $j$ in the Kihara cell potential [J]
$\varepsilon^{AiBi}$	CPA pure component association energy of specie $i$ [ $Pa \cdot m^3 \cdot mol^{-1}$ ]
$\Delta \mu_w^{\beta/L}$	Reference hydrate chemical potential difference between water in the meta-stable empty hydrate phase ( $\beta$ ) and water in the co-existing liquid phase (L) [ $J \cdot mole^{-1}$ ]
$\Delta \mu(T_0, P_0)_w^{\beta/L_w}$	Reference hydrate chemical potential difference between water in the meta-stable empty hydrate phase ( $\beta$ ) and liquid water (L) at reference temperature and pressure conditions [ $J \cdot mole^{-1}$ ]

$\omega$  Acentric factor [unit less]

### Subscripts

$i$  Component  $i$  [unit less]

$j$  Component  $j$  [unit less]

$w$  Water [unit less]

## 8. References

- [1] C. Garnier, G. Fiqueneisel, T. Zimny, Z. Pokryszka, S. Lafortune, P. D. C. Défossez, E. C. Gaucher, *Int. J. Coal Geology* 87, 2 (2011) 80-86.
- [2] J.-R. Li, Y. Ma, M. C. McCarthy, J. Sculley, J. Yu, J.-K. Jeong, P. B. Balbuena, H.-C. Zhou, *Coordination Chemistry Reviews* 255, 15-16 (2011) 1791-1823.
- [3] J. D. Figueroa, T. Fout, S. Plasynski, H. McIlvried, R. D. Srivastava, *Int. J. Greenhouse Gas Control* 2 (2008) 9-20.
- [4] IEA, CO<sub>2</sub> emissions from fuel combustion, 1971–2001, OECD/IEA, Paris, 2003.
- [5] C.-H. Yu, C.-H. Huang, C.-S. Tan, *Aerosol and Air Quality Research* 12 (2012) 745-769.
- [6] M. Wang, A. Lawal, P. Stephenson, J. Sidders, C. Ramshaw, *Chem. Eng. Res. Design* 89, 9 (2011) 1609-1624.
- [7] E. D. Sloan, C. A. Koh, *Clathrate Hydrates of Natural Gases*, 3rd Ed., CRC Press, Boca Raton, 2007.
- [8] E. D. Jr Sloan, *Nature* 426 (2003) 353-363.
- [9] C. A. Koh, A. K. Sum, E. D. Sloan, *Journal of Applied Physics* 106 (2009) 061101.
- [10] A. K. Sum, C. A. Koh, E. D. Sloan, *Ind. Chem. Res.* 48 (2009) 7457-7465.
- [11] S.-P. Kang and H. Lee, *Environ. Sci. Technol.* 34 (2000) 4397-4400.
- [12] S.-P. Kang, H. Lee, C.-S. Lee, W.-M. Sung, *Fluid Phase Equilibria* 185 (2001) 101-109.
- [13] P. Linga, R. Kumar, P. Englezos, *Chem. Eng. Sci.* 62 (2007) 4268-4276.
- [14] P. Linga, R. Kumar, P. Englezos, *J. of Hazardous Materials* 149 (2007) 625-629.
- [15] P. Linga, A. Adeyemo, P. Englezos, *Environ. Sci. Technol.* 42 (2007) 315-320.
- [16] P. J. Herslund, K. Thomsen, J. Abildskov, N. von Solms, *J. Chem. Thermodynamics* 48 (2012) 13-27.



- [17] J. C. Platteeuw, J. H. van der Waals, *Mol. Phys.* 1,1 (1958) 91-95.
- [18] W.R. Parrish, J.M. Prausnitz, *Ind. Eng. Chem. Process Des. Develop.* 11,1 (1972) 26-35.
- [19] G. M. Kontogeorgis, E. C. Voutsas, I. V. Yakoumis, D. P. Tassios, *Ind. Eng. Chem. Res.* 35 (1996) 4310–4318.
- [20] G. M. Kontogeorgis, I. V. Yakoumis, H. Meijer, E. Hendriks, T. Moorwood, *Fluid Phase Equilibria* 158-160 (1999) 201–209.
- [21] G. D. Holder, G. Corbin, K. D. Papadopoulos, *Ind. Eng. Chem. Fundam.* 19 (1980) 282-286.
- [22] E. D. Sloan, *Clathrate Hydrates of Natural Gases* 2nd Ed., Marcel Decker, New York, 1998.
- [23] P. B. Dharmawardhana, W. R. Parrish, E. D. Sloan, *Ind. Eng. Chem. Fundam.* 19 (1980) 410-414.
- [24] T. A. Strobel, C. A. Koh, E. D. Sloan, *Fluid Phase Equilibria* 280 (2009) 61-67.
- [25] P. J. Herslund, K. Thomsen, J. Abildskov, N. von Solms, *Fluid Phase Equilibria* 356 (2013) 209-222.
- [26] I. Tsivintzelis, G. M. Kontogeorgis, M. L. Michelsen, E. H. Stenby, *Fluid Phase Equilibria* 306 (2011) 38-56.
- [27] DIPPR, Design Institute for Physical Property Data (DIPPR 801). Diadem Pro.
- [28] I. R. Krichevsky, J. S. Kasarnovsky, *J. Am. Chem. Soc.* 57 (1935) 2168-2171.
- [29] W. L. Goffe, G. D. Ferrier, J. Rogers, *Journal of Econometrics* 60, 1/2 (1994) 65–99.
- [30] SIMANN.F, <http://www.netlib.no/netlib/opt/simann.f> (Acquired July 2012).
- [31] V. A. Shnitko, V. B. Kogan, *Journal of Applied Chemistry of the USSR (Zhurnal Prikladnoi Khimii)* 41, 6 (1968) 1235–1242.
- [32] W. Hayduk, H. Laudie, O. H. Smith, *Journal of Chemical and Engineering Data* 18, 4 (1973) 373–376.
- [33] E. Sada, T. Morisue, K. Miyahara, *Journal of Chemical and Engineering Data* 20, 3 (1975) 283–287.
- [34] J. Lampa, J. Matous, J. P. Novak, J., Pick, *Collection Czechoslov. Chem. Commun.* 45 (1980) 1159–1167.

- [35] P. C. Gillespie, G. M. Wilson, GPA Research Report RR-48.
- [36] A. Valtz, A. Chapoy, C. Coquelet, P. Paricaud, D. Richon, *Fluid Phase Equilibria* 226 (2004) 333-344.
- [37] A. Bamberger, G. Sieder, G. Maurer, *Journal of Supercritical Fluids* 17 (2000) 97-110.
- [38] R. Wiebe, V. L. Gaddy, *J. of the American Chemical Society* 62 (1940) 815-817.
- [39] J. B. Goodman, N. W. Krase, *Industrial and Engineering Chemistry* 23,4 (1931) 401-404
- [40] A. W. Saddington, N. W. Krase, *J. of the American Chemical Society* 56 (1934) 353-361.
- [41] M. Rigby, J. M. Prausnitz, *The Journal of Physical Chemistry* 72,1 (1968) 330-334.
- [42] K. Althaus, *Fortschritt-Berichte, VDI* 3 (1999), 350.
- [43] A. Chapoy, A. H. Mohammadi, B. Tohidi, D. Richon, *J. Chem. Eng. Data* 49 (2004) 1110-1115.
- [44] A. H. Mohammadi, A. Chapoy, B. Tohidi, D. Richon, *J. Chem. Eng. Data* 50 (2005) 541-545.
- [45] J. Im, W. Bae, J. Lee, H. Kim, *J. Chem. Eng. Data* 49 (2004) 35-37.
- [46] J. Li, M. Rodrigues, A. Paiva, H. A. Matos, E. G. de Azevedo, *J. of Supercritical Fluids* 41 (2007) 343-351.
- [47] Z. Knez, M. Skerget, L. Ilic, C. Lütge, *J. of Supercritical Fluids* 43 (2008) 383-389.
- [48] D. Kodama, T. Yagihashi, T. Hosoya, M. Kato, *Fluid Phase Equilibria* 297 (2010) 168-171.
- [49] F. Gibanel, M. C. López, F. M. Royo, J. Santafé, J. S. Urieta, *J. of Solution Chemistry* 22,3 (1993) 221-217.
- [50] T. A. Al-Sahhaf, A. J. Kidnay, E. D. Sloan, *Ind. Eng. Chem. Fundam.* 22 (1983) 372-380.
- [51] M. J. Lazzaroni, D. Bush, R. Jones, J. P. Hallett, C. L. Liotta, C. A. Eckert, *Fluid Phase Equilibria* 224 (2004) 143-154.
- [52] K. M. Sabil, G.-J. Witkamp, C. J. Peters, *J. Chem. Eng. Data* 55 (2010) 813-818.
- [53] K. M. Sabil, G.-J. Witkamp, C. J. Peters, *J. Chem. Thermodynamics* 42 (2010) 8-16.

- [54] J. Du, D. Liang, D. Li, X. Li, *Ind. Eng. Chem. Res.* 49 (2010) 11797-11800.
- [55] H. Yang, S. Fan, X. Lang, Y. Wang, *J. Chem. Eng. Data* 56 (2011) 4152-4156.
- [56] I. Ben Attouche Sfaxi, V. Belandria, A. H. Mohammadi, R. Lugo, D. Richon, *Chem. Eng. Sci.* 84 (2012) 602-611.
- [57] H. Bruusgaard, J. G. Beltrán, P. Servio, *J. Chem. Eng. Data* 53 (2008) 2594-2597.
- [58] S.-S. Fan, T.-M. Guo, *J. Chem. Eng. Data* 44 (1999) 829-832.
- [59] M. B. Olsen, A. Majumdar, P. R. Bishnoi, *Int. J. of The Soc. Of Mat. Eng. For Resources* 7, 1 (1999) 17-23.
- [60] J.-M. Herri, A. Bouchemoua, M. Kwaterski, A. Fezoua, Y. Ouabbas, A. Cameirao, *Fluid Phase Equilibria* 301 (2011) 171-190.
- [61] V. Belandria, A. Eslamimanesh, A. H. Mohammadi, D. Richon, *Ind. Eng. Chem. Res.* 50 (2011) 4722-4730.
- [62] S. H. Kim, M. D. Seo, J. W. Kang, C. S. Lee, *Fluid Phase Equilibria* 306 (2011) 229-233.
- [63] A. Eslamimanesh, S. Babaei, A. H. Mohammadi, J. Javanmardi, D. Richon, *Ind. Eng. Chem. Res.* 51 (2012) 3819-3825.
- [64] L. Ruffine, J. P. M. Trusler, *J. Chem. Thermodynamics* 42 (2010) 605-611.
- [65] J. Jhaveri, D. B. Robinson, *Can. J. Chem. Eng.*, 43, 2 (1965) 75-78.
- [66] A. van Cleeff, G. A. M. Diepen, *Recueil des travaux chimiques des Pays-Bas*, 79, 5 (1960) 582-586.
- [67] S. Takenouchi, G. C. Kennedy, *The Journal of Geology* 73, 2 (1965) 383-390.
- [68] H.-J. Ng, D. B. Robinson, *Fluid Phase Equilibria* 21, 1-2 (1985) 145-155.
- [69] S. Adisasmito, R. J. Frank III, E. D. Sloan Jr., *J. Chem. Eng. Data* 36, 1 (1991) 68-71.
- [70] S. D. Larson, *Phase studies of the two-component carbon dioxide-water system, involving the carbon dioxide hydrate*, University of Illinois, Urbana, IL (1955).
- [71] D. R. Marshall, S. Saito, R. Kobayashi, *AIChE J.* 10 (1964) 202-205.
- [72] A. Delahaye, L. Fournaison, S. Marinhas, I. Chatti, J.-P. Petitet, D. Dalmazzone, W. Fürst, *Ind. Eng. Chem. Res.* 45 (2006) 391-397.
- [73] Y. Seo, S.-P. Kang, S. Lee, H. Lee, *J. Chem. Eng. Data* 53 (2008) 2833-2837.

- [74] K. M. Sabil, G.-J. Witkamp, C. J. Peters, *Fluid Phase Equilibria* 290 (2010) 109-114.
- [75] A. H. Mohammadi, J. F. Martinez-López, D. Richon, *Chem. Eng. Sci.* 65 (2010) 6059-6063.
- [76] Y.-T. Seo, S.-P. Kang, H. Lee, *Fluid Phase Equilibria* 189 (2001) 99-110.
- [77] R. Anderson, A. Chapoy, B. Tohidi, *Langmuir* 23 (2007) 3440-3444.
- [78] T. Makino, T. Sugahara, K. Ohgaki, *J. Chem. Eng. Data* 50 (2005) 2058-2060.

## **Appendix 5**



# **Modelling of Cyclopentane Promoted Gas Hydrate Systems for Carbon Dioxide Capture Processes**

**Peter Jørgensen Herslund<sup>a</sup>, Kaj Thomsen<sup>a</sup>, Jens Abildskov<sup>b</sup>, Nicolas von Solms<sup>a\*</sup>**

<sup>a</sup>Center for Energy Resources Engineering (CERE)

<sup>b</sup>Computer Aided Process Engineering Center (CAPEC)

<sup>a,b</sup>Department of Chemical and Biochemical Engineering

Technical University of Denmark

DK2800, Kgs. Lyngby.

DENMARK

---

\* Corresponding author: Phone: +45 4525 2867 Fax: +45 4588 2258 E-mail: NVS@kt.dtu.dk

## Abstract

A thermodynamic model based on the Cubic-Plus-Association equation of state and the van der Waals-Platteeuw hydrate model is applied to perform a thermodynamic evaluation of gas hydrate forming systems relevant for post-combustion carbon dioxide capture.

A modelling study of both fluid phase behaviour and hydrate phase behaviour is presented. Cycloalkanes ranging from cyclopropane to cyclohexane, represents a challenge for CPA, both in the description of the pure component densities and for liquid-liquid equilibrium (LLE) in the binary systems with water. It is concluded that an insufficient amount of reliable LLE data exist for the binary system of water and cyclopentane. Additional water-in-oil data in particular are desired for this system.

An unpromoted hydrate-based capture process, operating isothermally at a temperature of 280 K is simulated. The minimum pressure requirement of the first stage is estimated to be 24.9 MPa. Applying three consecutive hydrate formation/dissociation stages (three-stage capture process), a carbon dioxide-rich product (97 mole percent) may be delivered at a temperature of 280 K and a pressure of 3.65 MPa.

A second capture process, where cyclopentane is incorporated as a thermodynamic hydrate promoter is simulated. At the presence of cyclopentane the minimum pressure requirement of the first stage (operating at 285 K) is lowered to 1.04 MPa. This process needs four consecutive hydrate formation/dissociation stages to produce a 95 mole percent carbon dioxide-rich product stream. The vapour phases in the cyclopentane promoted process contains several mole percent cyclopentane at hydrate equilibrium conditions. At temperatures below 284 K, the entire cyclopentane bulk phase evaporates completely at hydrate forming conditions (pressures below 0.55 MPa).

The present study suggests the hydrate-based separation technology to be unsuitable for the specific case of post-combustion carbon dioxide capture from power station flue gases, where operating pressures should preferably remain close to atmospheric. Even though the hydrate structure becomes available at low pressure conditions (by use of thermodynamic promoters), carbon dioxide may not necessarily enter the solid phase in significant amounts.

**Keywords:** Gas hydrates, Promoter, Carbon Dioxide, Cyclopentane, Modelling, Thermodynamics, Cubic-Plus-Association (CPA), Van der Waals-Platteeuw.



## 1. Introduction

Being a greenhouse gas, carbon dioxide absorbs and re-emits long-wave (infrared) radiation in the atmosphere of this planet. In the last 200 years, the concentration of carbon dioxide in the atmosphere has increased from approximately 280 ppm to a level of about 390 ppm in 2010 [1, 2].

Though not proven, it is suspected that our climate is changing due to anthropogenic emissions of greenhouse gases. Among the known greenhouse gases, carbon dioxide is suspected to be a main contributor to the observed climate change [3].

Efforts have been made to reduce carbon dioxide emissions from central locations such as e.g. fossil fuel (coal, oil and gas) fired power stations. The International Energy Agency (IEA) estimated that approximately 35 percent of the total carbon dioxide emission coming from combustion of fossil fuels in 2001 was related to heat- and energy production [4].

One way of lowering emissions of carbon dioxide from such locations is post-combustion carbon dioxide capture. Post-combustion capture is performed by removing carbon dioxide from flue gases before the gas is released to the atmosphere. These kinds of capture technologies are often easier to retro-fit to existing plants, since this can be done without making significant changes to the combustion technology [5].

A novel gas clathrate hydrate based separation technology is analysed in the present communication. This process is currently investigated as an alternative to the existing gas separation technologies.

Gas clathrate hydrates, are solid, crystalline formations of small molecules and water. Gas hydrates form when the constituents come into contact at conditions of low temperature and/or high pressure [6].

Gas hydrates are often referred to as non-stoichiometric solid inclusion bodies, where water acts as a host, forming a crystalline lattice by hydrogen bonding [7, 8, 9]. A number of empty cavities are incorporated in this lattice, in which small guest molecules may be physically adsorbed. The water lattice is a thermodynamically unstable structure, however interactions between the water and guest molecules stabilise the lattice [9]. The most commonly encountered gas clathrate hydrate structures are the sI, the sII and the sH structures. Detailed descriptions of each hydrate structure may be found elsewhere [6].

Hydrate structures are often governed by the physical sizes and shapes of the guest molecules enclathrated in the lattice cavities. Guest molecules of diameter size 4.2 – 6 Å, such as methane ( $\text{CH}_4$ ), carbon dioxide ( $\text{CO}_2$ ) and hydrogen sulfide ( $\text{H}_2\text{S}$ ) all form structure I hydrates. There are guest molecules with diameters smaller than 4.2 Å that form structure II hydrates when present as single guests. These include nitrogen ( $\text{N}_2$ ) and hydrogen ( $\text{H}_2$ ). Larger molecules with diameter 6 – 7 Å may similarly form structure II. Propane ( $\text{C}_3\text{H}_8$ ) and iso-butane ( $\text{C}_4\text{H}_{10}$ ) are the most common among these. Structure H hydrates are typically formed by large molecules of diameter 7 – 9 Å accompanied by smaller molecules such as e.g. methane [6].

The carbon dioxide hydrate forms a pressure of approximately 1.2 MPa for a temperature of 273 K [6]. The resulting sI hydrate structure creates a total of 8 cavities for each 46 water molecules. If a single carbon dioxide molecule is enclathrated in each of these cavities, the hydrate phase molar concentration of carbon dioxide becomes 15 percent. This corresponds to a mass fraction of carbon dioxide of approximately 0.31. Such a gas density is however

rarely achievable at moderate conditions of temperature and pressure since gas hydrates are non-stoichiometric formations (some cavities are left vacant).

Nitrogen and oxygen also form gas hydrates, however, these compounds form hydrates at significantly higher pressures. Gas mixtures of nitrogen, oxygen and carbon dioxide are expected to form hydrates at conditions in between those of the pure gases. The hydrates formed from such gas mixtures will enclathrate all gas phase components. As carbon dioxide forms hydrates at the lowest pressures of the three main constituents of the flue gas, the mixed hydrates are expected to be rich in carbon dioxide.

The suggested hydrate based carbon dioxide capture process contains two sections, capture and release. The flue gas is compressed, cooled and mixed with water in the capture section, whereby hydrates may form by crystallisation. A hydrate slurry may subsequently be transferred to the release section, where the solid particles are dissociated by either heating or pressure release. The carbon dioxide-rich gas is released at conditions of moderate to high pressures and low temperature. The aqueous liquid phase may be re-cycled to the capture section.

Figure 1 illustrates a simplified schematic of a suggested process configuration.

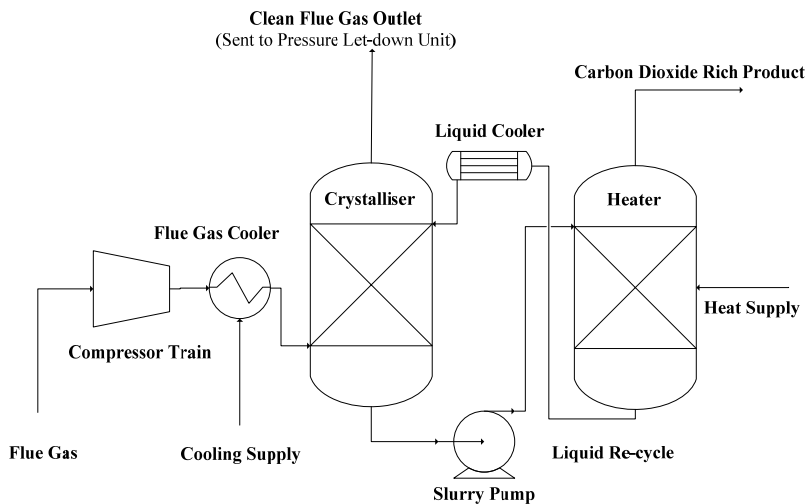


**Figure 1.** Simplified Schematic of a suggested configuration for the gas clathrate hydrate-based post-combustion carbon dioxide capture process. Modified from [10].

The hydrate based separation technology has the advantage of operating at temperatures, where low-quality heat can be used in the release section of the process. Furthermore, smaller amount of excess liquid is heated in the release part, since the hydrate slurry is a concentrated phase.

This technology has the disadvantage of requiring high pressures/low temperatures in the capture part. Very large volumes of flue gas must be compressed. By doing this, a large amount of nitrogen is compressed just to be let down in pressure after the capture stage. The

introduction of a turbine generator downstream of the capture stage may recover some energy. This will however increase the capital cost of the capture plant. Other known challenges related to this process are the slow kinetics of the hydrate crystallisation as well as handling of the particle suspension.

Previous attempts of improving this technology have investigated ways of lowering the pressure requirement in the capture stage. It has been found that the addition of low pressure/high temperature gas hydrate stabilisers (thermodynamic hydrate promoters) may significantly lower the pressure requirement of this process. A thermodynamic gas hydrate promoter is a gas hydrate former that stabilises a hydrate structure at low pressures/high temperatures, thereby allowing for gas phase components to enter the hydrate phase at milder conditions. The formed hydrate phase thereby enclathrates both the promoter and the desired gas phase constituents. If the promoter is a liquid at the operating conditions of the process, it does not pollute the final gas product since it will remain with the liquid phase when the hydrates are dissociated. One disadvantage of adding these promoters is that they lower the gas storage capacity of the solid phase, since they occupy a fraction of the lattice cavities.

Cyclopentane has been suggested in the literature as a potential thermodynamic gas hydrate promoter for the hydrate based carbon dioxide capture process, as this component is known to form sII hydrates at ambient conditions of temperature and pressure.

Hydrate-Liquid water-Vapour equilibrium data for the sII cyclopentane clathrate hydrate formed in pure water was measured by Fan et al. [11]. The reported equilibrium pressures were sub-atmospheric in the temperature range from approximately 273 K to approximately 280 K, suggesting that cyclopentane may be used as a thermodynamic hydrate promoter in processes operating at near-atmospheric pressure conditions.

The formation mechanism of pure cyclopentane hydrate formed in water-in-oil emulsions was studied by Karanjkar et al. [12]. Emulsions were formed by the use of the Span 80 non-ionic surfactant. It was shown that cyclopentane hydrate formation is an interfacial process. Contact surface area played a key role in the formation process, and an increased amount of hydrate was formed in emulsified systems compared to systems with two distinct liquid phases.

It was found that without the use of surfactants, a thin hydrate layer quickly formed and covered the liquid-liquid interface, slowing down transport of cyclopentane by diffusion to the water-rich liquid phase. At the presence of oil-soluble surfactants, the growth mechanism was changed dramatically. Hydrate crystals then grew and merged into the water liquid-phase, rather than covering the surface, resulting in higher water conversions and a larger range of crystal particle sizes.

In a recent study combining kinetic and morphological observations, Lim et al. [13] showed that the presence of cyclopentane enhances hydrate formation rates and provides high gas uptakes for systems relevant to CO<sub>2</sub> capture.

Hydrate formation in the ternary system of water-cyclopentane-carbon dioxide has been investigated by Zhang and Lee [14] and Mohammadi and Richon [15]. Cyclopentane was shown to have a significant pressure reducing effect on the hydrate formation conditions compared to the pure carbon dioxide hydrates. Four-phase equilibrium conditions, involving

hydrates, were determined in the temperature interval from 284.3 K to 292.6 K. Hydrate dissociation pressures varied from 0.35 MPa to 3.51 MPa in this temperature range.

Zhang et al. [16] investigated hydrate formation in the quaternary system of water + cyclopentane + carbon dioxide + hydrogen in the temperature interval from approximately 284 K to 291 K. Increasing the relative carbon dioxide content in the vapour phase lowered the equilibrium pressure of the mixed hydrate phase. However, as temperatures approached the dissociation point of the pure cyclopentane hydrate at 0.1 MPa, this effect diminished due to the formation of an almost pure cyclopentane hydrate.

Li et al. [17] studied carbon dioxide capture from synthetic flue gases comprised of 83.4 mole percent N<sub>2</sub> and 16.6 mole percent CO<sub>2</sub>. Mixed hydrates were formed in the presence of cyclopentane. They investigated hydrate formation rates and the selectivity of CO<sub>2</sub> in the hydrate phase. It was shown that upon adding an emulsifier to the promoted system, the crystallisation rate was increased dramatically compared to the promoted system with two bulk liquid phases (water and cyclopentane). However, the selectivity towards CO<sub>2</sub> in the hydrate phase was decreased by the addition of the emulsifier.

## **2. Purpose of This Study**

The post-combustion carbon dioxide capture process applying gas hydrate formation is investigated by means of thermodynamic modelling. The main focus is on the minimum pressure requirements in the hydrate forming vessel (crystalliser). The minimum pressure requirement is here defined as the incipient hydrate dissociation pressure for a given system at specified temperature. Since gas hydrates are non-stoichiometric phases, estimates of the water-free hydrate composition and thereby the composition of the captured gas phase is reported for various process conditions.

A thermodynamic model handling equilibrium of both fluid phases and hydrate formation in the ternary system of water, carbon dioxide and nitrogen was presented in a previous study [18]. This model combines the van der Waals-Platteeuw hydrate model [19] with the Cubic-Plus-Association (CPA) equation of state [20, 21]. The model has recently been modified [10] and accuracy has been improved for both the fluid phase and hydrate phase descriptions in the above mentioned ternary system. Furthermore, tetrahydrofuran was incorporated in the component list, enabling the performance of a thermodynamic evaluation of the post-combustion carbon dioxide capture process using tetrahydrofuran as a thermodynamic hydrate promoter.

In the present study, the component list is further expanded to include cyclopentane. The new model is validated against experimental data for both fluid phase equilibria and hydrate equilibria. A simplified post-combustion carbon dioxide capture process, including cyclopentane as a thermodynamic promoter, is simulated by use of the developed model.

## **3. Model**

The model applied in this work is described in detail elsewhere [10, 18], and will therefore not be presented here. Model specific parameters for the van der Waals Platteeuw hydrate model used in this work may be found in our most recent communication [10].

This section only presents component specific parameters applied in the present study. These parameters include CPA pure component parameters for the four components of interest in this study, water, cyclopentane, carbon dioxide and nitrogen. These parameters are provided in Table 1.

**Table 1.** Cubic-Plus-Association (CPA) equation of state pure component parameters for; water (H<sub>2</sub>O), cyclopentane(1) (CP(1)), carbon dioxide (CO<sub>2</sub>) and nitrogen (N<sub>2</sub>). Association scheme according to definition presented elsewhere [22].

Component	Assoc. scheme	$a_0 \cdot 10^1$ / Pa·m <sup>6</sup> ·mol <sup>-2</sup>	$b \cdot 10^5$ / m <sup>3</sup> ·mol <sup>-1</sup>	$c_1$	$\beta^{AiBi}$	$\epsilon^{AiBi} \cdot 10^{-4}$ / Pa·m <sup>3</sup> ·mol <sup>-1</sup>	Ref.
H <sub>2</sub> O	[2 <sup>+</sup> ;2 <sup>-</sup> ]	1.2277	1.4515	0.6736	0.0692	1.6655	[21]
CP(1)	N/A	$T_c = 511.7 \text{ K}$ , $P_c = 4.51 \text{ MPa}$ , $\omega = 0.19487$					[23]
CO <sub>2</sub>	[0 <sup>+</sup> ;1 <sup>-</sup> ]	3.5079	2.7200	0.7602	N/A	N/A	[24]
N <sub>2</sub>	N/A	$T_c = 126.2 \text{ K}$ , $P_c = 3.40 \text{ MPa}$ , $\omega = 0.03772$					[23]

In CPA, two approaches may be used to obtain pure component parameters for non-associating compounds. One is to use critical temperature, critical pressure and acentric factor for the pure component (if available) and calculate the three pure component parameters in a manner identical to that used for the SRK equation of state. The second approach is to regress the three parameters by fitting CPA to data for vapour pressures and saturated liquid densities for the pure component. Both approaches are used in this work. For non self-associating and non cross-associating compounds, critical data are used to calculate the three pure component parameters of CPA. For components that are cross-associating or self- and cross-associating, parameters are regressed by use of experimental data for vapour pressures and liquid densities.

All CPA parameters of this work that are calculated from critical data, use critical data from the DIPPR database [23].

In addition to the pure component parameters, binary parameters in CPA have previously been presented for all binary pairs formed by the ternary system of water, carbon dioxide and nitrogen [10]. The present study has expanded to include three new binary systems incorporating cyclopentane. Binary CPA parameters for all pairs formed in the quaternary system of water, cyclopentane, carbon dioxide and nitrogen are provided in Table 2.

**Table 2.** Binary parameters for all pairs formed by the four components; water, cyclopentane, carbon dioxide and nitrogen. Up to three binary parameters ( $a_{kij}$ ,  $b_{kij}$ ,  $\gamma^{AiBj}$ ) may be adjusted for binary pairs showing cross-association. A maximum of two binary parameters ( $a_{kij}$ ,  $b_{kij}$ ) may be adjusted in pairs with no cross-association.  $a_{kij}$  and  $b_{kij}$  are related to the binary interaction parameter,  $k_{ij}$ .  $\gamma^{AiBj}$  enters in the combining rule for the binary cross-association volume,  $\beta^{AiBj}$ .

Binary Pair	Adj. Parameters.	$k_{ij}$	$\gamma^{AiBj}$	Ref.
Water-Cyclopentane(1)	$a_{kij}$	0.0211	N/A	This work
Water-Carbon dioxide	$a_{kij}$ , $b_{kij}$ , $\gamma^{AiBj}$	0.4719 - 112.5/T	0.1707	[10]
Water-Nitrogen	$a_{kij}$ , $b_{kij}$	0.9999 - 368.4/T	N/A	[10]
Cyclopentane(1)-Carbon dioxide	$a_{kij}$	0.1574	N/A	This work
Cyclopentane(1)-Nitrogen	N/A	0.0000	N/A	
Carbon dioxide-Nitrogen	$a_{kij}$	-0.0856	N/A	[10]

The van der Waals-Platteeuw hydrate model, as applied here, has no real predictive capabilities without *a priori* knowledge of the gas hydrate formers of interest. Kihara parameters must be determined by fitting the complete model to existing data for dissociation pressures and/or hydrate phase compositions. When doing so, the hydrate structures of the used reference data should preferably be known. The Kihara parameters applied in this modelling study are presented in Table 3. Only the parameters ( $\sigma_j$  and  $\varepsilon_j$ ) for cyclopentane have been regressed as part of the present work.

**Table 3.** Kihara spherical cell potential parameters used in this work.  $k_B$  is the Boltzmann constant.

Component	$a_j \cdot 10^{10} / m$	$\sigma_j \cdot 10^{10} / m$	$\varepsilon_j / k_B / K$	Ref.
Carbon dioxide	0.6805 *	2.9643	171.70	[10]
Nitrogen	0.3526 *	3.1723	128.07	[10]
Cyclopentane	0.8968 **	3.1480	250.89	This work

\* From [6], \*\* From [25]

The Kihara parameters presented in Table 3 are valid only for the specific model applied here [10, 18], since these depend on the reference hydrate properties, equation of state etc. Other implementations of the van der Waals-Platteeuw hydrate model, incorporating different hydrate reference properties and/or another equation of state, may therefore not necessarily provide results that are identical to those presented in this work.

#### 4. Results and Discussion

When comparing model results to experimental data, the term Average Absolute (relative) Deviation (AAD) is used. AAD is defined according to equation (1).

$$AAD = \frac{1}{N} \sum_{i=1}^N \left| \frac{s_{calc,i} - s_{exp,i}}{s_{exp,i}} \right| \quad (1)$$

Where  $s_{calc}$  is the calculated property of interest ( $s$  may be temperature, pressure, composition etc.) and  $s_{exp}$  is the experimental reference data.  $N$  is the total number of data points.

Generally (both for fluid phase modelling and hydrate modelling), in cases, where correlation of parameters was needed, optimisation has been done by minimising the sum of absolute relative deviations between model descriptions and experimental data. The objective function has been defined as in equation (2).

$$Obj = \sum_{i=1}^N \left| \frac{s_{calc,i} - s_{exp,i}}{s_{exp,i}} \right| \quad (2)$$

Where  $s_{calc}$  again is the calculated property of interest ( $s$  may be temperature, pressure, composition etc.) and  $s_{exp}$  is the experimental reference data.  $N$  is the total number of data points used as reference.

Optimisation of parameters in this work has been performed by use of an optimisation algorithm based on a FORTRAN implementation of the simulated annealing (SA) global optimisation algorithm presented by Goffe et al. [26] (source code available via [27]).

#### 4.1 Fluid Phase Modelling

Being consistent in all fluid phases, this model may not only be used to describe/predict conditions of incipient gas hydrate formation, it also accurately describes/predicts the number and types of co-existing fluid phases and the distribution of feed components in the fluid phases at equilibrium conditions. For this reason, emphasis has been put on “tuning” the fluid phase description to create an accurate and reliable framework for the hydrate model.

The following sections present CPA modelling results of pure and binary sub-systems within the quaternary system of water, cyclopentane, carbon dioxide and nitrogen. These results serve as a validation of the inputs supplied later to the van der Waals-Platteeuw gas clathrate hydrate model.

##### CPA Pure Component parameters for cyclopentane

Cyclopentane is assumed a non self-associating compound and thus has three pure component parameters in CPA. As mentioned, these parameters may be obtained in two ways.

As an example below, CPA parameters for cyclopentane calculated from critical properties;  $T_c = 511.7$  K,  $P_c = 4.51$  MPa,  $\omega = 0.194874$  (from here on referred to as Cyclopentane(1)) are:

$$\begin{aligned}
 a_0 &= 17.155 \cdot 10^{-1} & (\text{Pa} \cdot \text{m}^6 \cdot \text{mol}^{-2}) \\
 b &= 8.173 \cdot 10^{-5} & (\text{m}^3 \cdot \text{mol}^{-1}) \\
 c_1 &= 0.7801 & (\text{Unit less})
 \end{aligned}$$

Alternatively, three pure component parameters are regressed by fitting CPA to vapour pressures and saturated liquid molar volumes of cyclopentane in the reduced temperature interval from approximately 0.5 to 0.9. Experimental data are generated from the correlations provided by the DIPPR database [23]. In this temperature interval, the correlation deviations are lower than 1 percent compared to the experimental source data behind the correlation. The regressed CPA parameters (referred to as Cyclopentane(2)) become:

$$\begin{aligned}
 a_0 &= 16.311 \cdot 10^{-1} & (\text{Pa} \cdot \text{m}^6 \cdot \text{mol}^{-2}) \\
 b &= 7.527 \cdot 10^{-5} & (\text{m}^3 \cdot \text{mol}^{-1}) \\
 c_1 &= 0.7262 & (\text{Unit less})
 \end{aligned}$$

Some results of calculations performed using the two pure component sets are shown in Figure 2.

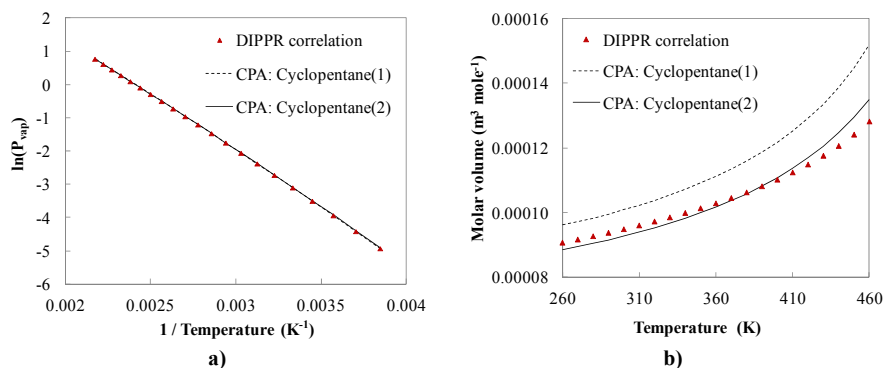


**Figure 2.** Comparison of calculated and “experimental” vapour pressure **a)** and saturated liquid molar volume **b)** of cyclopentane. “Experimental” data from [23]. Cyclopentane(1) parameters are obtained from critical data. Cyclopentane(2) parameters are obtained by fitting CPA to the shown “experimental” data along with saturated liquid volumes

Figure 2 a) and b) illustrate, respectively, the natural logarithm of the vapour pressure as function of inverse temperature and saturated liquid molar volume as function of temperature for pure cyclopentane. Data from DIPPR are shown in the two figures for comparison with the calculations using cyclopentane(1) and cyclopentane(2) parameters.

CPA: Cyclopentane(1) (critical data) and CPA: Cyclopentane(2) (regressed parameters) describe the vapour pressure of pure cyclopentane with similar accuracy. CPA: Cyclopentane(1) has an absolute average deviation (AAD) of 0.7% while for CPA: Cyclopentane(2), the AAD has decreased to 0.4%.

A more noticeable difference between the two pure component parameter sets is seen in the description of the saturated liquid volume of cyclopentane (Figure 2 b).



The AAD of parameter set 1 (critical data) in the reduced temperature interval from 0.5 to 0.9 is approximately 9.5%, while parameter set 2 (regressed parameters) obtains an AAD of approximately 2.0%. Hence, in this case a significant gain in accuracy in the description of the pure component saturated liquid volumes is obtained by regressing pure component parameters.

An AAD of 2.0 percent in the reduced temperature interval from 0.5 to 0.9 is relatively large considering cyclopentane is a non self-associating compound. It is a little surprising that CPA has trouble describing molar liquid volumes of the pure cycloalkane.

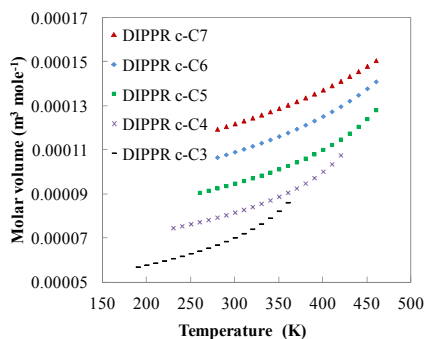


**Figure 3.** DIPPR [23] correlations of saturated liquid molar volumes of cycloalkanes. Data for cyclopropane (c-C3), cyclobutane (c-C4), cyclopentane (c-C5), cyclohexane (c-C6) and cycloheptane (c-C7).

The DIPPR data however reveal nothing unusual for cyclopentane compared to four other cycloalkanes (see Figure 3). The illustrated data (from correlations) show clear trends with increasing molar volumes as function of increasing ring size and increasing temperature.

Further attempts were made to find a reason for the low accuracy in the description of the saturated liquid volumes. By regressing CPA pure component parameters for cycloalkanes ranging from cyclopropane (c-C3) to cyclohexane (c-C6) and comparing these to the DIPPR correlations shown in Figure 3 it was found that CPA has difficulties in describing these densities for cyclobutane and cyclopentane, whereas the remaining investigated cycloalkanes (cyclopropane and cyclohexane) are well described in terms of saturated liquid volumes. The regressed CPA parameters for the four cycloalkanes have been compared to published parameters for *n*-alkanes of similar sizes. Trends in the parameters of this work compare well with those found for other compounds. Hence, no reason was found to question the present parameters. See Appendix A1 for a more detailed description of this analysis.

### Water-Cyclopentane

Cyclopentane(1) (from critical properties) and Cyclopentane(2) (regressed parameters) presented above yield significant differences in the description of the saturated liquid volume of this component. In the following, it is investigated how the two parameter sets

perform when moving to liquid-liquid equilibrium (LLE) conditions of the binary system of water and cyclopentane. Experimental reference data for this binary system are taken from [28-31]. The conditions covered by the experimental data are listed in Table 4.

**Table 4.** Liquid-Liquid equilibria (LLE) data for the binary system of cyclopentane and water. x denotes water-rich liquid phase composition data, z denotes cyclopentane-rich phase composition data. AAD is absolute average deviation according to Eq. (1) when using the Cyclopentane(1) parameter set and a binary interaction parameter,  $k_{ij}$ , of 0.0211.

Reference	Type	No. Data Points	Temp. / K	AAD
[28]	z	5	273.2 – 313.2	0.47
[29]	x	1	298.2	0.03
[30]	x	6	313.3 – 426.3	1.35*
[31]	x	3	276.5 – 296.2	0.24

\* AAD = 0.44 for the single data point measured at 313 K.

Figure 4 a) illustrates the predicted LLE (oil in water and water in oil contents) for the binary system of water and cyclopentane. Water is treated as a self-associating compound using an association scheme with two electron donating and two electron accepting sites (also known as the 4C scheme in the terms of Huang and Radosz [32]). Cyclopentane is modelled either using the Cyclopentane(1) parameters (from critical data) or with regressed Cyclopentane(2) parameters.

It is seen that the regressed CPA parameters provide a lower accuracy in the oil in water description in the binary system with water compared to the CPA parameters obtained from critical data. Both of the parameter sets overestimate the cyclopentane in water contents and under estimate the water in cyclopentane content. Whereas the differences between the two parameter sets are large for the water-rich phase, both parameter sets describe the cyclopentane-rich phase with similar deviations.

An attempt has been made to improve the LLE description of CPA for both cyclopentane parameter cases. Figure 4 b) illustrates the performances of CPA in describing LLE for the binary system of water and cyclopentane. Non-zero binary interaction parameters have been regressed by minimising model deviations compared to all the experimental reference data listed in Table 4.

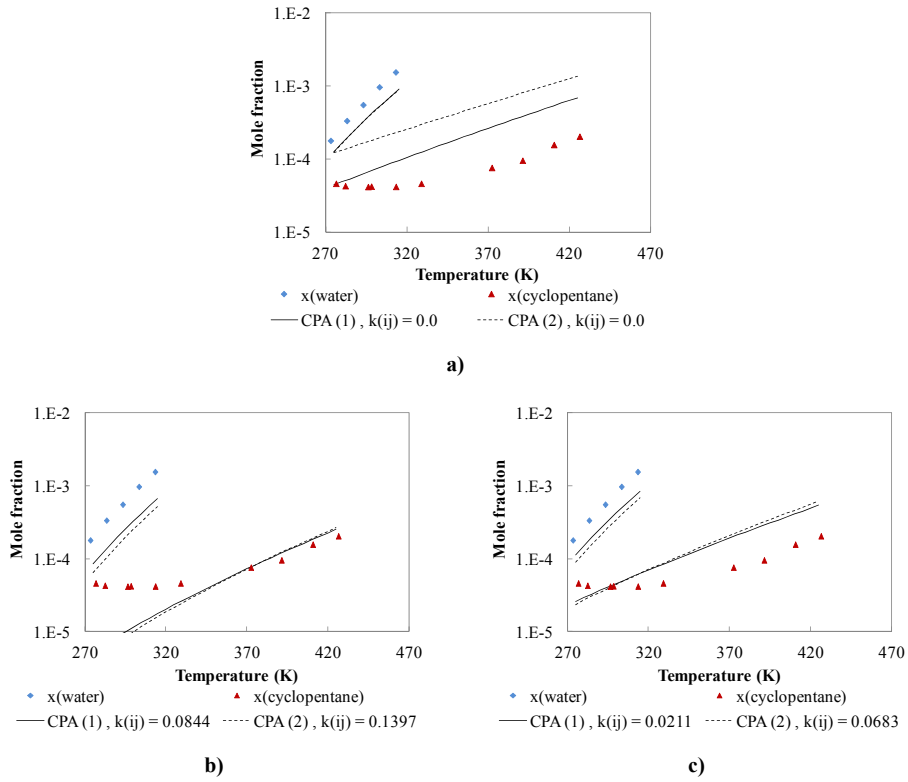


**Figure 4.** Comparison of Experimental, predicted **a)** and correlated **b), c)** LLE for the binary system of water and cyclopentane. Blue diamonds: mole fraction of water in liquid cyclopentane [28]. Red triangles: mole fraction of cyclopentane in liquid water [29-31]. Solid lines: CPA using Cyclopentane(1) parameter set. Dashed lines: CPA using Cyclopentane(2) parameter set.

Both parameter sets for cyclopentane result in an underestimation of the cyclopentane content in the water-rich phase at temperatures below 370 K. At temperatures above 370 K the oil in water content is overestimated. The water in oil description is underestimated significantly in the entire temperature interval covered by the experimental data. A binary interaction parameter (BIP) of 0.0844 was needed to correct the oil in water description in the case of parameter set (1), the regressed BIP for parameter set (2) was 0.1397, significantly larger than case (1). It becomes obvious that the application of a binary interaction parameter cannot enable an accurate description of both liquid phases simultaneously for this system. A positive BIP of approximately 0.084 is needed with the cyclopentane parameter set (1) to correlate the water-rich phase data and a negative BIP of roughly -0.126 is needed to correlate the cyclopentane-rich phase. Hence, both phases cannot be described accurately using a single, constant BIP.

Figure 4 b) shows that both model approaches for cyclopentane result in dissatisfactory descriptions of the oil in water content in the temperature range, which is the expected operating range for the hydrate model under development (273.2 K to approximately 310 K).

Hence, an attempt has been made to improve the accuracy of the model in terms of describing the shown LLE data at temperatures below 315 K. Only experimental data from the water-rich phase, below 315 K) have been considered as reference data. New BIP's have been regressed. The results are shown in Figure 4 c). The regressed BIP's for both modelling approaches are reduced significantly. The BIP for cyclopentane parameter set (1) becomes 0.0211 and for parameter set (2), the new BIP becomes 0.0683. The AAD when comparing to the four experimental data points for the water-rich phase below 315 K are 23.5 percent and 25.7 percent for set (1) and set (2) respectively. Deviations compared to the experimental data at higher temperatures become significantly larger than the parameters providing the best overall fit of the complete data set.

It is surprising that CPA cannot describe both LLE phases when applying a non-zero BIP since with a non-zero, positive BIP, CPA accurately describes both LLE phases in the binary system of water and cyclohexane [33]. An analysis of this has been appended in Appendix A2. Based on observations of trends in LLE data in similar oil/water systems, it is concluded that the experimental data reported by Englin et al. [28] may be faulty. This would explain why CPA fails at describing these data, even with the application of a non-zero, positive BIP.

Generally, the accuracy of CPA in describing the water-rich phase could be improved by applying a temperature dependent BIP. However, due to the limited amount of trusted data available for this system, it is chosen not to make further attempts of correlating the few existing data sets.

Since the calculated (from  $T_c$ ,  $P_c$  and  $\omega$ ) parameter set for cyclopentane provides the best descriptions of the experimental data with the lowest value for the regressed BIP, this parameter set has been chosen for the following work.

### **Water-carbon dioxide**

Detailed modelling results for this binary pair have been presented elsewhere [10, 24]. Water is treated as self-associating and carbon dioxide is treated as non self-associating but is allowed to cross-associate with water via a single association site. Three binary, adjustable parameters are used to describe VLE and LLE of this binary pair over extended ranges of temperature and pressure. The pure component parameters and binary parameters may be found in Table 1 and Table 2.

### **Water-nitrogen**

Nitrogen is assumed non self-associating and the three pure component parameters for this compound are calculated from the critical temperature, critical pressure and acentric factor in a manner similar to that used in the Soave-Redlich-Kwong (SRK) equation of state (EOS). VLE in the binary system of water and nitrogen has successfully been modelled previously [10] applying a non-linear, temperature dependent binary interaction parameter. The pure component parameters and binary parameters may be found in Table 1 and Table 2.

### **Cyclopentane-carbon dioxide**

Both cyclopentane and carbon dioxide are treated as non associating compounds in their binary mixtures. Table 5 lists experimental VLE data found in the literature for this binary

system. Only experimental data at temperatures below 400 K are considered. Some of the listed authors in Table 5 do however present data at temperatures up to 500 K.

**Table 5.** List of references presenting VLE data for the binary system of cyclopentane and carbon dioxide. x denotes liquid phase composition data, y denotes vapour phase composition data. Note that some references may present more data outside the T/P conditions listed here. These are not used as reference data in this work. AAD is absolute average deviation according to Eq. (1) using a binary interaction parameter,  $k_{ij}$ , of 0.1574.

Reference	Type	No. Data Points	Temp. / K	Press. / MPa	AAD
[34]	x,y	24	366.8	1.03 – 11.2	0.05
[35]	x,y	218	276.6 – 388.1	0.33 – 12.0	0.03
[36]	x	5	283.0 – 303.0	0.10	0.10

A high value for the BIP of this pair is needed to correlate the VLE data of this system. Figure 5 a) compares the VLE predictions of CPA ( $k_{ij} = 0.0$ ) with the final correlated results ( $k_{ij} = 0.1574$ ) at a temperature of 293 K. The depicted experimental data are from Shah et al. [35].

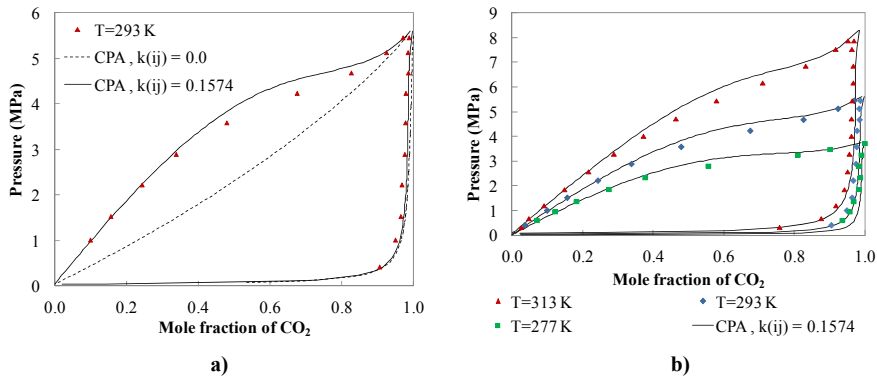


**Figure 5.** Comparison of model results and experimental data for vapour-liquid-equilibria (VLE) at various temperatures in the binary system of cyclopentane and carbon dioxide. VLE data from [35]. Dashed lines: CPA predictions ( $k_{ij} = 0.0$ ). Solid lines: CPA description with  $k_{ij} = 0.1574$ . a) T = 293 K. b) T = 277 K, T = 293 K and T = 313 K.

CPA tends to over estimate the solubility of carbon dioxide in the liquid cyclopentane phase. A significant gain in accuracy in the description of this phase is obtained by applying a positive BIP.

Only data in the expected working range for the hydrate model are depicted in Figure 5 a) and b). CPA does however describe data at higher temperatures with comparable accuracy. This can also be seen from the AAD's presented in Table 5.

### Cyclopentane-nitrogen

No association is allowed in the binary pair of cyclopentane and nitrogen. Both components are treated as non self-associating and pure component parameters are calculated from

critical temperatures, critical pressures and acentric factors. Parameters may be found in Table 1. In this specific system, CPA simplifies to the standard SRK equation of state.

**Table 6.** VLE data available for the binary system of cyclopentane and nitrogen. x denotes liquid phase composition data, y denotes vapour phase composition data. AAD is absolute average deviation according to Eq. (1) using a binary interaction parameter,  $k_{ij}$ , of 0.0.

Reference	Type	No. Data Points	Temp. / K	Press. / MPa	AAD
[34]	x,y	62	366.4 – 410.2	1.36 – 31.3	0.08

Reference VLE data for this system have been reported by Marathe and Sandler [34]. The temperature and pressure conditions covered by the data are listed in Table 6. A binary interaction coefficient (BIP) has been correlated using all the binary data reported by Marathe and Sandler. A value of  $k_{ij} = 0.019$  is obtained. Figure 6 compares the model predictions,  $k_{ij} = 0.0$  and model correlations,  $k_{ij} = 0.019$  with the available reference data.

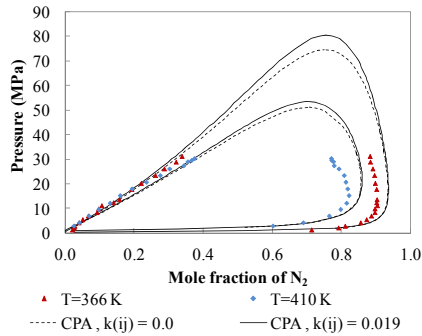


**Figure 6.** Comparison of model results and experimental data for VLE in the binary system of cyclopentane and nitrogen. Experimental data from [34]. Dashed lines: CPA predictions ( $k_{ij} = 0.0$ ). Solid lines: CPA description with  $k_{ij} = 0.019$ .

As seen in Figure 6, the application of a non-zero BIP does not provide significant improvements of the model descriptions in the  $T/P$  range covered by the experimental data. However, the application of a positive BIP seems to lower the described upper pressure limits of the phase envelope for both temperature conditions. Since the available experimental data are measured at conditions far from the working conditions of the developed hydrate model, and the improvements are considered insignificant, it is chosen to allow CPA to predict ( $k_{ij} = 0.0$ ) the behaviour of this binary pair in the following work.

### Carbon dioxide-nitrogen

Since carbon dioxide only solvates with water, both carbon dioxide and nitrogen are considered non-associating in their binary pair. Low temperature fluid phase equilibria have

been modelled previously [10] applying a constant binary interaction parameter. The pure component parameters and binary parameters may be found in Table 1 and Table 2.

#### 4.2 Modelling the Un-promoted Gas Hydrate System

The present model has been applied previously to model hydrate formation in the ternary system of water, carbon dioxide and nitrogen [10]. It has been shown that both the pure structure I (sI) hydrates of carbon dioxide and the pure structure II (sII) hydrates of nitrogen are accurately described in terms of dissociation pressures in the temperature interval from 273.2 to 283.2 K.

Since the experimental data available in the literature for the mixed hydrates of carbon dioxide and nitrogen [37-45] do not all compare well, it is uneasy to evaluate the performance of the model for the mixed hydrates. However the model compares well to most of the available data for both hydrate equilibrium pressures and mixed hydrate compositions.

The model predicts a structural transition in the formed hydrates from sI hydrates for mixed gas phases containing more than approximately 5 mole percent carbon dioxide to sII hydrates for gas phases with less than approximately 5 mole percent carbon dioxide. The exact concentration for the structural transition depends on both the water content in the system and temperature. Increasing temperature results in an increased cut-off concentration for a given system with fixed water content.

#### 4.3 Modelling the Thermodynamic Promotion Effect of Cyclopentane

To enable incipient hydrate equilibrium calculations for systems containing cyclopentane, Kihara cell potential parameters have been regressed for this component by matching the model to experimental data for mixed hydrates of cyclopentane + carbon dioxide and cyclopentane + nitrogen.

The spherical hard core radius,  $a_j$ , of cyclopentane has been calculated by Takeuchi et al. [25] from second virial coefficient data. The calculated core radius, as presented in the original work of Takeuchi et al., has been used in the present study.

Table 7 lists the experimental hydrate dissociation pressure data found in the literature for the mixed hydrates of cyclopentane + carbon dioxide [14,15] and cyclopentane + nitrogen [46-48]. All data supposedly represent hydrate(H) – liquid water( $L_w$ ) – liquid organic( $L_a$ ) – vapour(V) equilibria. These data have been used as reference data when correlating the two Kihara potential parameters used as adjustable parameters in the van der Waals-Platteeuw hydrate model ( $\sigma_j$  and  $\epsilon_j/k_B$ ).

Since the modelled systems are uni-variant in the four-phase, hydrate forming region, all systems are modelled using an equimolar feed stock ( $x_{\text{water}} = 1/3$ ,  $x_{\text{cyclopentane}} = 1/3$ ,  $x_{\text{gas}} = 1/3$ ).

**Table 7.** Four-phase hydrate equilibrium data in the ternary systems of water, cyclopentane, carbon dioxide (CO<sub>2</sub>) and water, cyclopentane, nitrogen (N<sub>2</sub>). AAD in P is absolute average deviation when comparing the present model to the available reference data. AAD according to Eq. (1).

Reference	System	No. Data Points	Temp. / K	Press. / MPa	AAD in P
[14]	Cyclopentane + CO <sub>2</sub>	7	286.7 – 292.6	0.89 – 3.51	0.20
[15]	Cyclopentane + CO <sub>2</sub>	7	284.3 – 291.8	0.35 – 2.52	0.13
[46]	Cyclopentane + N <sub>2</sub>	4	282.9 – 289.1	0.64 – 3.50	0.13
[47]	Cyclopentane + N <sub>2</sub>	8	285.9 – 302.0	1.68 – 24.5	0.04
[48]	Cyclopentane + N <sub>2</sub>	5	281.7 – 290.2	0.25 – 4.06	0.16

Table 7 lists, for each reference data set, the absolute average deviations (AAD) in terms of hydrate dissociation pressures when comparing the final model performance with the experimental reference data. Despite the fact that the reference data for the mixed hydrates of cyclopentane and carbon dioxide only cover a narrow temperature interval of approximately 8 Kelvin, AAD's to these data are considerable. The data for the mixed hydrates of cyclopentane and nitrogen cover a larger temperature interval of approximately 20 Kelvin. Figure 7 a) and b) compare the model descriptions and the experimental data for the mixed hydrates of cyclopentane + carbon dioxide (Figure 7 a) and cyclopentane + nitrogen (Figure 7 b).

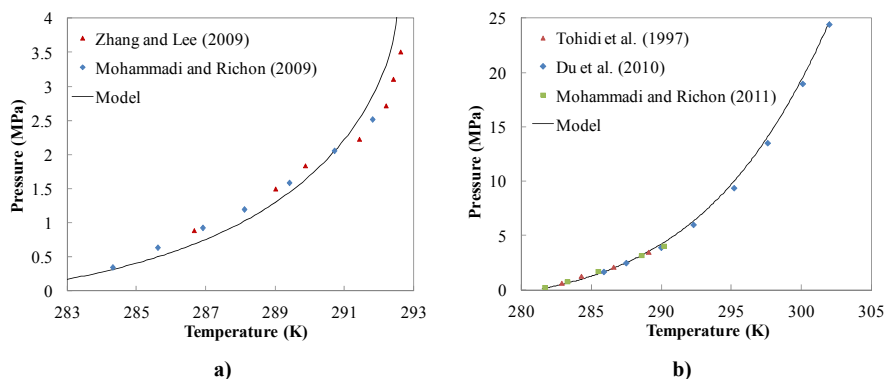


**Figure 7.** Gas hydrate dissociation pressure as function of temperature for the mixed hydrate of cyclopentane and carbon dioxide (a) and cyclopentane and nitrogen (b). Experimental data from [14,15] (a) and [46-48] (b).

The model description of the mixed hydrates of cyclopentane and carbon dioxide appears to contain more curvature than is seen in the experimental data. The equilibrium pressure data of the mixed hydrate increases almost linearly with increasing temperature for temperatures lower than 292 K. Above this temperature the pressures reported by Zhang and Lee [14] increase more steeply with increasing temperature. The model seems to underestimate the dissociation pressure in the temperature range from 284 to 291 K due to the curvature in the model. Above 291 K, the model description becomes very steep with increasing temperature.



The fluid phase behaviour for this system has been tracked during all calculations. It was found that the carbon dioxide-rich vapour phase becomes incorporated in the organic liquid phase at temperatures above 292.5 K (for the equi-molar feed). Hence, above 292.5 K, the calculated conditions represent three-phase hydrate(H) – liquid water ( $L_w$ ) – liquid organic ( $L_a$ ) equilibria. The calculated pressures increase almost vertically in this range due to the disappearance of the most compressible phase. However, below 292.5 K the steep pressure increase is likely imposed by the Kihara parameters of carbon dioxide. It is possible that the regressed Kihara parameters for carbon dioxide provide little stabilising effect of the small cavity in the sII hydrate structure at elevated temperatures.

The high AAD's reported in Table 7 for the data of Zhang and Lee [14] are mainly due to the model description increasing steeply at a temperature approximately 0.5 K lower than the experimental data. The model deviates significantly from the data point at 292.6 K, since the model predicts hydrate(H) - liquid water( $L_w$ ) – liquid organic( $L_a$ ) equilibria at this temperature.

Accurate descriptions of the mixed hydrate of cyclopentane and nitrogen are obtained considering the large temperature interval covered by the experimental data. Even though difficult to see, AAD's in the low-temperature range are however comparable for this system to those in the cyclopentane + carbon dioxide system. The modelled equilibrium pressures in this system do not increase suddenly as seen in the system with carbon dioxide, hence the sudden increase in pressure is ascribed the Kihara parameters for carbon dioxide as suggested above.

Figure 8 illustrates the predicted pure sII hydrate of cyclopentane. The model predictions are compared to data reported by Fan et al. [49] in the hydrate (H) – liquid water ( $L_w$ ) – vapour (V) region and data reported by Trueba et al. [50] in the hydrate (H) – liquid water ( $L_w$ ) – liquid organic ( $L_a$ ) region.

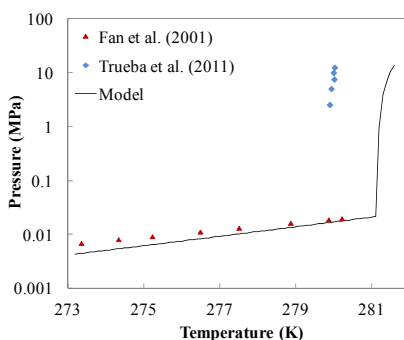


**Figure 8.** Hydrate dissociation pressure as function of temperature for the pure sII hydrate of cyclopentane. Comparison of model prediction and experimental data from [49, 50].

Even though these data were not included as reference data when regressing Kihara parameters for cyclopentane, the model accurately predicts the data reported by Fan et al. [49]. AAD for these data is 0.25. The data reported by Trueba et al. [50] are less accurately

described. The developed model predicts the upper quadruple point for this binary system at a temperature approximately 1.5 K higher than the experimental data suggests.

Since the pure hydrate of cyclopentane is of little interest to the present work, no attempts have been made to improve the accuracy of the description in this sub-system.

As a final note, it is worth mentioning that the model results presented in Figure 8 represent the model prediction for the pure sII cyclopentane hydrate as function of temperature. However, whereas the model does predict the sII hydrate structure to be the most stable form of the cyclopentane hydrate at temperatures below 281.2 K, the model predicts the sI hydrate structure to be the most stable form of the pure cyclopentane hydrate at temperatures above 281.2 K (not shown in Figure 8).

#### 4.4 Model predictions for the promoted carbon dioxide capture process

Up to this point, the model has been validated against available experimental data mainly for sub-systems relevant to the cyclopentane-promoted, post-combustion carbon dioxide capture process.

The following considers and analyses the example of carbon dioxide capture from a simulated flue gas comprised of 10 mole percent carbon dioxide and 90 mole percent nitrogen.

The investigated aspects of the capture process are the minimum flue gas pressure requirements, process efficiency and selectivity and finally the environmental impact of this process. The latter in particular turns out to be a major challenge in the cyclopentane promoted capture process.

Figure 9 a) illustrates the predicted minimum pressure requirement in the cyclopentane promoted carbon dioxide capture process, treating a flue gas initially containing 10 mole percent carbon dioxide and 90 mole percent nitrogen. The minimum pressure requirement is here described by the thermodynamic equilibrium pressure of the incipient hydrate crystal for the feed. In a real process, a higher pressure must be applied to ensure sufficient driving force for the hydrate nucleation and growth to take place.

The capture process is simulated by mixing equi-molar amounts of gas (V) and liquid ( $L_w + L_a$ ), thus  $V/(V+L_w+L_a) = 0.5$ . The total amount of feed liquid is comprised of 95 mole percent water and 5 mole percent cyclopentane. Assuming the formed hydrates are of the sII type and cyclopentane fully occupies the large cavities, the cyclopentane feed alone is sufficient to convert approximately 90 percent of the liquid water feed to solid hydrate (a “stoichiometric” hydrate phase with complete filling of large cavities contain 5.56 mole percent cyclopentane). Since the present model only allows for calculation of incipient hydrate formation conditions, actual conversion of the liquid phase at a given temperature/pressure (T/P) condition cannot be simulated.

The modelled system is di-variant in the four-phase equilibrium region, hence the calculated equilibrium pressure is not only temperature dependent, but also composition dependent.

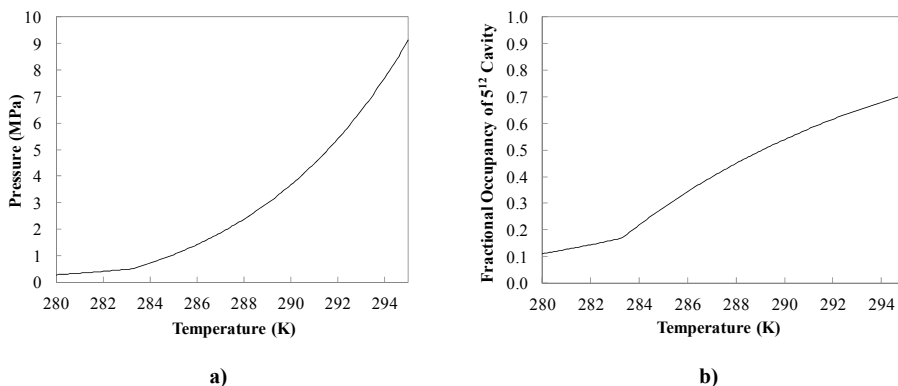


**Figure 9.** Predicted hydrate dissociation pressure (a) and fractional occupancy of gas in the small  $5^{12}$  cavity (b) as function of temperature for the quaternary system of water, cyclopentane, carbon dioxide and nitrogen. The feed is 47.5 mole percent water, 2.5 mole percent cyclopentane, 5 mole percent carbon dioxide and 45 mole percent nitrogen.

Only temperatures down to 280 K are considered in the process simulations, since the sII hydrate phase may be stabilised by cyclopentane alone at temperatures lower than this. In the model this is indicated by a low fractional occupancy of gas in the small  $5^{12}$  cavities of the sII hydrate structure and simultaneously complete occupancy by cyclopentane in the large cavities. The model predicts the fractional occupancy of cyclopentane in the large cavities to be higher than 0.99 at all the simulated conditions. This occupancy decreases from 0.999 at 280 K to 0.994 at 295 K. The predicted amount of gas present in the large cavities is negligible as is the predicted amount of cyclopentane in the small cavities.

Figure 9 b) illustrates the predicted fractional gas occupancy of the small cavities. The enclosed gas is a mixture of carbon dioxide and nitrogen. This information provides an indication of the efficiency of the gas capture process. Only the small cavities of the sII hydrate structure are available for gas uptake, since the large cavities are fully occupied by cyclopentane. Hence, Figure 9 b) illustrates how much of the full storage capacity of the formed hydrate is used at a given T/P condition. This along with the predicted selectivity (Figure 11 b) of carbon dioxide in the hydrate phase determines the efficacy of the capture process.

Both the minimum pressure requirement and the gas uptake increase with increasing temperature. The minimum pressure requirement for the capture process operating at 280 K is approximately 0.28 MPa. At this condition only 11 percent of the storage capacity in the hydrate phase is exploited, since cyclopentane almost self-stabilises the solid phase. An increase in temperature to 289.0 K results in an increase in gas uptake to a fractional occupancy of 50 percent in the small cavities. At this temperature the minimum pressure requirement becomes 2.97 MPa.

The model shows a change of slope in both the predicted minimum pressure requirement (Figure 9 a) and the predicted gas uptake (Figure 9 b) occurring at a temperature of approximately 283.4 K. Below this temperature both the dissociation pressure and the gas uptake decreases only little with lowering temperature. The explanation for this behaviour is found in the predicted fluid phase behaviour. CPA predicts a disappearance of the bulk

cyclopentane liquid phase, ( $L_a$ ), occurring at a temperature of approximately 283.4 K and a pressure of approximately 0.54 MPa. These conditions are valid for the given system and will change with changing feed composition. At temperatures below 283.4 K, the cyclopentane liquid phase is incorporated in the vapour phase.

Figure 10 illustrates the cyclopentane mole fraction in the vapour phase for the simulated carbon dioxide capture system operating at incipient hydrate equilibrium conditions. The feed gas contains 10 mole percent carbon dioxide and the feed liquid consists of 5 mole percent cyclopentane.

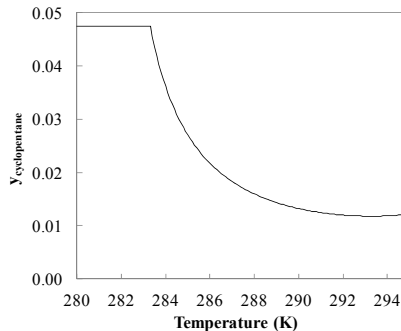


**Figure 10.** Mole fraction of cyclopentane in the outlet vapour phase leaving stage 1 of the simulated carbon dioxide capture process as function of operating temperature. Pressure the incipient hydrate formation pressure at any given temperature.

The vapour phase mole fraction of cyclopentane is the highest at low temperatures, despite the fact that the vapour pressure of the cyclopentane liquid phase increases with increasing temperature. The reason for this is that the incipient hydrate pressure increases with increasing temperature. This overcompensates for the increase in vapour pressure of cyclopentane. At temperatures below 283.4 K, the curve flattens. This is an indication that an insufficient amount of cyclopentane is present in the system to saturate the vapour phase at the given conditions of temperature and pressure. Thus, all bulk cyclopentane has transferred to the co-existing phases. At higher temperatures, the vapour phase is saturated with cyclopentane, indicating the presence of a bulk cyclopentane liquid phase co-existing with the vapour phase. Only negligible amounts of cyclopentane transfer to the aqueous liquid phase. At no point does the cyclopentane content in the vapour phase become lower than 1 mole percent. At an operating temperature of 285 K the cyclopentane content in the outlet gas will be 2.7 mole percent. This indicates a major drawback of using this thermodynamic hydrate promoter. A significant promoter loss to the vapour phase must be expected. This organic content must be regenerated and possibly re-cycled before the carbon dioxide lean outlet gas can be emitted to the atmosphere.

Figure 11 a) and Figure 11 b) show equilibrium pressures and hydrate composition (water- and promoter free basis) respectively as function of the initial vapour phase composition for a cyclopentane promoted system operating at a constant temperature of 285

K. This temperature is chosen to avoid that cyclopentane transfers completely to the vapour phase. For comparison, similar results are provided for the unpromoted system operating at a constant temperature of 280 K. Data for the unpromoted system operating at a temperature of 280 K are those reported by Kang et al. [37]. Both systems are simulated using a 50/50 (molar) vapour/liquid feed with 5 mole percent of the liquid being cyclopentane and 95 mole percent being water.

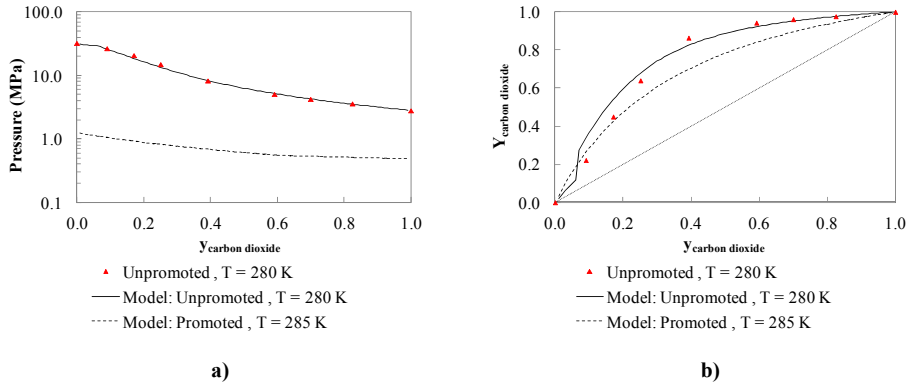


**Figure 11.** Mixed hydrate dissociation pressure (a) and hydrate gas composition (b) as function of carbon dioxide mole fraction in the vapour phase (binary vapour phase with nitrogen). The unpromoted system is the ternary system of  $\text{CO}_2$ ,  $\text{N}_2$  and  $\text{H}_2\text{O}$ . The promoted system is the quaternary system of  $\text{CO}_2$ ,  $\text{N}_2$ ,  $\text{H}_2\text{O}$  and cyclopentane. Experimental data from [37].

The pressure reducing effect of the cyclopentane addition is clearly seen in Figure 11 a). At a temperature of 285 K, the capture process operates at pressures ranging from 0.5 MPa to 1.2 MPa for the entire vapour phase concentration span. Even though operating at a lower temperature, the unpromoted process operates at much higher pressures ranging from 2.9 MPa to 31 MPa.

One of the drawbacks of the cyclopentane addition is seen in Figure 11 b), comparing the selectivity of carbon dioxide in the hydrate phase for the unpromoted- and the cyclopentane promoted systems. The selectivity towards carbon dioxide becomes lower by the addition of cyclopentane. However, the hydrate phase still has a clear selectivity towards carbon dioxide, providing the possibility of separating this component from nitrogen in the flue gas. An aspect not shown in the investigated isothermal systems is the gas uptake. At 285 K, this uptake range from approximately 28 to 35 percent of the full storage capacity of the sII hydrate phase, depending on the initial vapour phase composition.

The information provided in Figure 11 a) and Figure 11 b) may be combined to make a simplified thermodynamic process evaluation.

Neither the un-promoted, nor the promoted system produces a hydrate phase that is sufficiently rich in carbon dioxide to enable a single stage capture process. Whereas, for a flue gas initially containing 10 mole percent carbon dioxide, the un-promoted system requires 3 theoretical hydrate formation/dissociation stages to reach a final vapour phase with more than 95 mole percent carbon dioxide, the promoted system will require a total of

four stages. In the suggested process, a single capture stage comprises all the equipment illustrated in Figure 1. After the first capture stage, it is likely that only a limited amount of compression becomes necessary between stages, as the incipient hydrate dissociation pressure decreases with increasing carbon dioxide mole fraction in the vapour phase.

Table 8 presents predicted stage conditions for two multi-stage capture processes – one un-promoted and one promoted using cyclopentane. The unpromoted process operates at a temperature of 280 K and the promoted process at 285 K. The feed into the first stage of each process is comprised of 10 mole percent carbon dioxide and 90 mole percent nitrogen. All stages operate at a 50 mole percent liquid feed ratio. 5 mole percent of the liquid feed is pure cyclopentane in the promoted process. All stages are assumed to operate at the incipient hydrate equilibrium pressure of the inlet gas.

**Table 8.** Simulated incipient hydrate conditions for the un-promoted and cyclopentane promoted capture processes.  $T = 280$  K for the unpromoted and 285 K for the promoted system. Initial vapour phase mole fraction of  $\text{CO}_2$  in feed to stage 1 is 0.10.  $P_{\text{eq}}$  is incipient hydrate equilibrium pressure for each stage.  $Y_{\text{CO}_2}$  is mole fraction of  $\text{CO}_2$  in the incipient hydrate crystal (water- and promoter-free basis). Hydrate phase composition ( $Y_{\text{CO}_2}$ ) in stage 1 is used as feed composition to stage 2 and so forth. All stages in both processes operate at a 50 mole percent liquid feed ratio.

Stage	Unpromoted: $T = 280$ K		Promoted: $T = 285$ K	
	$P_{\text{eq}}$ (MPa)	$Y_{\text{CO}_2}$	$P_{\text{eq}}$ (MPa)	$Y_{\text{CO}_2}$
1	24.9	0.36	1.04	0.28
2	9.17	0.80	0.79	0.58
3	3.65	0.97	0.56	0.83
4	N/A	N/A	0.51	0.95

The un-promoted process uses pure water as liquid phase. Hence the first stage operates at a pressure of 24.9 MPa. It is assumed that the stage pressure is constant throughout the entire stage and the all hydrates formed have a composition similar to the incipient hydrate crystal. The hydrates formed in stage 1 are then dissociated at constant pressure and the released vapour phase, now containing 36 mole percent carbon dioxide is transferred to stage 2. In stage 2, hydrates will form at a pressure of 9.17 MPa and the water-free hydrate composition here becomes 80 mole percent in carbon dioxide. Passing this vapour phase (after dissociating the hydrates of stage 2) to stage 3, where hydrates will form at a pressure of 3.65 MPa, provides a final outlet gas at a temperature of 280 K and a pressure of 3.65 MPa containing 97 mole percent carbon dioxide.

The cyclopentane promoted capture process may operate at significantly lower pressures. The minimum pressure requirement of the first stage becomes 1.04 MPa and the water- and promoter-free hydrate composition of carbon dioxide is 28 mole percent. The promoted capture process requires a total of four theoretical stages to reach a final outlet gas containing 95 mole percent carbon dioxide. This outlet gas is supplied at 285 K and 0.51 MPa. Note that the model predicts that the cyclopentane bulk phase will transfer directly to the vapour phase at the inlet of last stage due to the low pressure condition.

The present investigation has shown that whereas cyclopentane is a potent thermodynamic hydrate promoter in terms of its capability of reducing the incipient hydrate formation pressure, it does bring several drawbacks in the form of low gas uptakes in the hydrate phase, lowered selectivity towards carbon dioxide. Furthermore, the high miscibility

with the vapour phase compounds results in a significant promoter loss from the process liquid(s).

## 5. Conclusion

A thermodynamic model based on the Cubic-Plus-Association equation of state and the van der Waals-Platteeuw hydrate model was applied to perform a thermodynamic evaluation of gas hydrate forming systems relevant for post-combustion carbon dioxide capture.

A modelling study of both fluid phase behaviour and hydrate phase behaviour was presented.

Cycloalkanes ranging from cyclopropane to cyclohexane, represented a challenge for CPA, both for the description of the pure component densities and for liquid-liquid equilibrium (LLE) in the binary systems with water. It was concluded that an insufficient amount of reliable LLE data exist for the binary system of water and cyclopentane. Additional water-in-oil data in particular are desired for this system.

An unpromoted hydrate-based capture process, operating isothermally at a temperature of 280 K was simulated. The flue gas feed into the first stage of the process was comprised of 10 mole percent carbon dioxide and 90 mole percent nitrogen. The hydrate forming vessel was assumed to operate isobarically at the incipient hydrate equilibrium pressure of the inlet gas. The minimum pressure requirement of the first stage was estimated to be 24.9 MPa. The captured gas contained 36 mole percent carbon dioxide, suggesting the need for a multi-stage capture process design. Applying three consecutive hydrate formation/dissociation stages (three-stage capture process), a carbon dioxide-rich product (97 mole percent) could be delivered at a temperature of 280 K and a pressure of 3.65 MPa. It was concluded that this process was not economically feasible due to the high pressure requirement of the first capture stage.

A second capture process, where cyclopentane was used as a thermodynamic hydrate promoter, operated at slightly elevated temperatures compared to the unpromoted process. In this system, 5 mole percent (fraction of liquid feed) cyclopentane bulk liquid was added to the pure water system. By doing so the minimum pressure requirement of the first stage (operating at 285 K) could be lowered to 1.04 MPa. Selectivity towards carbon dioxide in the hydrate phase was however lowered compared to the unpromoted process. Therefore, this process needed four consecutive hydrate formation/dissociation stages to produce a 95 mole percent carbon dioxide-rich product stream. The product stream was delivered at 285 K and a pressure of 0.51 MPa. The vapour phases in the cyclopentane promoted process contained several mole percent cyclopentane at hydrate equilibrium conditions. At temperatures below 284 K, the entire cyclopentane bulk phase would evaporate completely at hydrate forming conditions (pressures below 0.55 MPa).

The present study has shown the hydrate-based separation technology to be unsuitable for the specific case of post-combustion carbon dioxide capture from power station flue gases, where operating pressures should preferably remain close to atmospheric.

It is not in the nature of species such as carbon dioxide and nitrogen to form the classical gas hydrates at conditions close to atmospheric pressure. Therefore, even though these

hydrate structures become available at low pressure conditions (by use of thermodynamic promoters), carbon dioxide may not necessarily enter the solid phase in significant amounts.

## 6. Acknowledgements

This work was financially supported partly by the European iCap project (EU FP7) and partly by the Department of Chemical and Biochemical Engineering (MP<sub>2</sub>T) at the Technical University of Denmark (DTU).

The authors acknowledge the initiative and work Erling H. Stenby and Philip L. Fosbøl put into establishing the funding for DTU, as part of the iCap project.

## 7. List of Symbols

### Abbreviations

AAD	Average Absolute (relative) Deviation
BIP	Binary Interaction Parameter
CP	Cyclopentane
CPA	Cubic-Plus-Association
LLE	Liquid Liquid Equilibrium
Obj	Objective function
SA	Simulated Annealing
VLE	Vapour Liquid Equilibrium
VLLE	Vapour Liquid Liquid Equilibrium

### Symbols

#### Normal Characters

$A_i$	Association site type “A” on component $i$ [unit less]
$a_0$	CPA pure component parameter [ $\text{Pa} \cdot \text{m}^6 \cdot \text{mol}^{-2}$ ]
$a_j$	Spherical core radius of component $j$ in the Kihara cell potential [m]
$a_{kij}$	Constant in temperature expression for $k_{ij}$ [unit less]
$B_j$	Association site type “B” on component $j$ [unit less]
$b$	CPA co-volume parameter [ $\text{m}^3 \cdot \text{mol}^{-1}$ ]
$b_{kij}$	Constant in temperature expression for $k_{ij}$ [K]
$c_1$	CPA pure component parameter [unit less]
$k_B$	The Boltzmann constant [ $\text{J} \cdot \text{K}^{-1}$ ]
$k_{ij}$	Binary interaction parameter [unit less]
$N$	Total number [unit less]
$P$	Pressure [Pa]



$P_c$	Critical pressure [Pa]
$R$	Gas constant [ $\text{m}^3 \cdot \text{Pa} \cdot \text{mole}^{-1} \cdot \text{K}^{-1}$ ]
$s_{calc}$	Calculated parameter value used in definition of AAD or obj
$s_{exp}$	Experimental parameter value used in definition of AAD or obj
$T$	Temperature [Kelvin]
$T_c$	Critical temperature [Kelvin]
$x$	Liquid phase mole fraction [unit less]
$y$	Vapour phase mole fraction [unit less]
$Y_j$	Water free hydrate composition of guest $j$ [unit less]

### Greek letters

$\beta^{AiBi}$	CPA pure component association volume [unit less]
$\beta^{AiBj}$	CPA binary association volume [unit less]
$\gamma^{AiBj}$	CPA binary adjustable in combining rule for $\beta^{AiBj}$ [unit less]
$\epsilon_j$	Maximum attractive potential of specie $j$ in the Kihara cell potential [J]
$\epsilon^{AiBi}$	CPA pure component association energy of specie $i$ [ $\text{Pa} \cdot \text{m}^3 \cdot \text{mol}^{-1}$ ]
$\omega$	Acentric factor [unit less]

### Subscripts

$i$	Component $i$ [unit less]
$j$	Component $j$ [unit less]

## 8. References

- [1] C. Garnier, G. Finqueneisel, T. Zimny, Z. Pokryszka, S. Lafortune, P. D. C. Défossez, E. C. Gaucher, Int. J. Coal Geology 87, 2 (2011) 80-86.
- [2] J.-R. Li, Y. Ma, M. C. McCarthy, J. Sculley, J. Yu, J.-K. Jeong, P. B. Balbuena, H.-C. Zhou, Coordination Chemistry Reviews 255, 15-16 (2011) 1791-1823.
- [3] J. D. Figueroa, T. Fout, S. Plasynski, H. McIlvried, R. D. Srivastava, Int. J. Greenhouse Gas Control 2 (2008) 9-20.
- [4] IEA, CO2 emissions from fuel combustion, 1971–2001, OECD/IEA, Paris, 2003.
- [5] M. Wang, A. Lawal, P. Stephenson, J. Sidders, C. Ramshaw, Chem. Eng. Res. Design 89, 9 (2011) 1609-1624.
- [6] E. D. Sloan, C. A. Koh, Clathrate Hydrates of Natural Gases, 3rd Ed., CRC Press, Boca Raton, 2007.
- [7] E. D. Jr Sloan, Nature 426 (2003) 353-363.
- [8] C. A. Koh, A. K. Sum, E. D. Sloan, Journal of Applied Physics 106 (2009) 061101.

- [9] A. K. Sum, C. A. Koh, E. D. Sloan, *Ind. Chem. Res.* 48 (2009) 7457-7465.
- [10] P. J. Herslund, K. Thomsen, J. Abildskov, N. von Solms, Submitted Dec. 2013.
- [11] S. S. Fan, D. Q. Liang, K. H. Guo, *J. Chem. Eng. Data* 46 (2001) 930-932.
- [12] P. U. Karanjkar, J. W. Lee, J. F. Morris, *Chem. Eng. Sci.* 68 (2012) 481-491.
- [13] Y.-A. Lim, P. Babu, R. Kumar, P. Linga, *Cryst. Growth Des.* 13 (2013) 2047-2059.
- [14] J. S. Zhang, J. W. Lee, *J. Chem. Eng. Data* 54 (2009) 659-661.
- [15] A. H. Mohammadi, D. Richon, *Chem. Eng. Sci.* 64 (2009) 5319-5322.
- [16] J. Zhang, P. Yedlapalli, J. W. Lee, *Chem. Eng. Sci.* 64 (2009) 4732-4736.
- [17] S. Li, S. Fan, J. Wang, X. Lang, Y. Wang, *Chinese J. Chem. Eng.* 18,2 (2010) 202-206.
- [18] P. J. Herslund, K. Thomsen, J. Abildskov, N. von Solms, *J. Chem. Thermodynamics* 48 (2012) 13-27.
- [19] J. H. van der Waals, J. C. Platteeuw, *Adv. Chem. Phys.* 2, (1959) 1-57.
- [20] G. M. Kontogeorgis, E. C. Voutsas, I. V. Yakoumis, D. P. Tassios, *Ind. Eng. Chem. Res.* 35 (1996) 4310-4318.
- [21] G. M. Kontogeorgis, I. V. Yakoumis, H. Meijer, E. Hendriks, T. Moorwood, *Fluid Phase Equilibria* 158-160 (1999) 201-209.
- [22] P. J. Herslund, K. Thomsen, J. Abildskov, N. von Solms, *Fluid Phase Equilibria* 356 (2013) 209-222.
- [23] DIPPR, Design Institute for Physical Property Data (DIPPR 801). Diadem Pro.
- [24] I. Tsivintzelis, G. M. Kontogeorgis, M. L. Michelsen, E. H. Stenby, *Fluid Phase Equilibria* 306 (2011) 38-56.
- [25] F. Takeuchi, R. Ohmura, K. Yasuoka, *Int. J. Thermophys.* 30 (2009) 1838-1852.
- [26] W. L. Goffe, G. D. Ferrier, J. Rogers, *Journal of Econometrics* 60, 1/2 (1994) 65-99.
- [27] SIMANN.F, <http://www.netlib.no/netlib/opt/simann.f> (Acquired July 2012).
- [28] B. A. Énglin, A. F. Platé, V. M. Tugolukov, M. A. Pryanishnikova, *Khimiya i tekhnologiya Topliv i Masel* 9 (1965) 42-46.
- [29] F. R. Groves Jr., *J. Chem. Eng. Data* 33 (1988) 136-138.

- [30] L. C. Price, The American Association of Petroleum Geologists Bulletin 60, 2 (1976) 213-244.
- [31] A. Chapoy, H. Haghighi, B. Tohidi, J. Chem. Thermodynamics 40 (2008) 1030-1037.
- [32] S. H., Huang, M., Radosz, Ind. Eng. Chem. Res. 29,11 (1990) 2284–2294.
- [33] G. K. Folas. Modeling of Complex Mixtures Containing Hydrogen Bonding Molecules. PhD thesis, Technical University of Denmark, 2007.
- [34] P. Marathe, S. I. Sandler, J. Chem. Eng. Data 36 (1991) 192-197.
- [35] N. N. Shah, J. A. Zollweg, W. B. Streett, J. Chem. Eng. Data 36 (1991) 189-192.
- [36] F. Gironi, R. Lavecchia, Fluid Phase Equilibria 87 (1993) 153-161.
- [37] S.-P. Kang, H. Lee, C.-S. Lee, W.-M. Sung, Fluid Phase Equilibria 185 (2001) 101-109.
- [38] I. Ben Attouche Sfaxi, V. Belandria, A. H. Mohammadi, R. Lugo, D. Richon, Chem. Eng. Sci. 84 (2012) 602-611.
- [39] H. Bruusgaard, J. G. Beltrán, P. Servio, J. Chem. Eng. Data 53 (2008) 2594-2597.
- [40] S.-S. Fan, T.-M. Guo, J. Chem. Eng. Data 44 (1999) 829-832.
- [41] M. B. Olsen, A. Majumdar, P. R. Bishnoi, Int. J. of The Soc. Of Mat. Eng. For Resources 7, 1 (1999) 17-23.
- [42] P. Linga, R. Kumar, P. Englezos, Chem. Eng. Sci. 62 (2007) 4268-4276.
- [43] J.-M. Herri, A. Bouchemoua, M. Kwaterski, A. Fezoua, Y. Ouabbas, A. Cameirao, Fluid Phase Equilibria 301 (2011) 171-190.
- [44] V. Belandria, A. Eslamimanesh, A. H. Mohammadi, D. Richon, Ind. Eng. Chem. Res. 50 (2011) 4722-4730.
- [45] S. H. Kim, M. D. Seo, J. W. Kang, C. S. Lee, Fluid Phase Equilibria 306 (2011) 229-233.
- [46] B. Tohidi, A. Danesh, A. C. Todd, R. W. Burgass, K. K. Østergaard, Fluid Phase Equilibria 138 (1997) 241-250.
- [47] J. Du, D. Liang, D. Li, X. Li, Ind. Eng. Chem. Res. 49 (2010) 11797-11800.
- [48] A. H. Mohammadi, D. Richon, Chem. Eng. Sci. 66 (2011) 4936-4940.
- [49] S. S. Fan, D. Q. Liang, K. H. Guo, J. Chem. Eng. Data 46 (2001) 930-932.

- [50] A. T. Trueba, L. J. Rovetto, L. J. Florusse, M. C. Kroon, C. J. Peters, Fluid Phase Equilibria 307 (2011) 6-10.
- [51] I. V. Yakoumis, G. M. Kontogeorgis, E. C. Voutsas, D. P. Tassios, Fluid Phase Equilibria 130 (1997) 31-47.
- [52] G. M. Kontogeorgis, M. L. Michelsen, G. K. Folas, S. Derawi, N. von Solms, E. H. Stenby, Ind. Eng. Chem. Res. 45 (2006) 4855-4868.
- [53] A. Maczynski, B. Wisniewska-Gocłowska, M. Góral, J. Phys. Chem. Ref. Data 33, 2 (2004) 549-577.

## 9. Appendices

### Appendix A1

In the following analyses, CPA pure component parameters are regressed for cycloalkanes ranging from cyclopropane (c-C<sub>3</sub>) to cyclohexane (c-C<sub>6</sub>).

Pure component parameters are already available in the literature for cyclohexane [33], however these parameters provided unsatisfactory descriptions of the vapour pressure data, when comparing to the most recent DIPPR correlations (DIPPR 801 2013 database [23]). Hence, new pure component parameters have been regressed as a part of this work and these are compared with the previous parameters. All the cycloalkane parameters presented in Table A1.1 are regressed to DIPPR correlation data for vapour pressure and saturated liquid volumes in the reduced temperature interval from approximately 0.5 to 0.9.

**Table A1.1.** Regressed CPA parameters for a selection of normal- and cycloalkanes.

Compound	$a_0 \cdot 10^1$ (Pa·m <sup>6</sup> ·mol <sup>-2</sup> )	$b \cdot 10^5$ (m <sup>3</sup> ·mol <sup>-1</sup> )	$c_1$	Ref.	AAD P <sub>vap</sub>	AAD P <sub>liq</sub>
n-C <sub>3</sub>	9.114	5.78	0.6307	[51]	0.009*	0.019*
c-C <sub>3</sub>	8.144	4.84	0.6327	This work	0.004	0.012
n-C <sub>4</sub>	13.144	7.21	0.7077	[51]	0.002*	0.010*
c-C <sub>4</sub>	12.089	6.17	0.6819	This work	0.005	0.024
n-C <sub>5</sub>	18.199	9.10	0.7986	[51]	0.005*	0.010*
c-C <sub>5</sub>	16.311	7.53	0.7262	This work	0.004	0.020
n-C <sub>6</sub>	23.682	10.79	0.8313	[51]	0.005*	0.005*
c-C <sub>6</sub>	21.784	9.04	0.7426	[33]	0.072	0.012
c-C <sub>6</sub> **	21.112	9.03	0.7587	This work	0.012	0.014

\* Stated AAD's in the reduced temperature interval from 0.55 to 0.90.

\*\* New parameters for cyclohexane from this work.

For comparison, Table A1.1 also contains regressed CPA parameters for propane, n-butane, n-pentane and n-hexane. These parameters have been found in the literature [51].

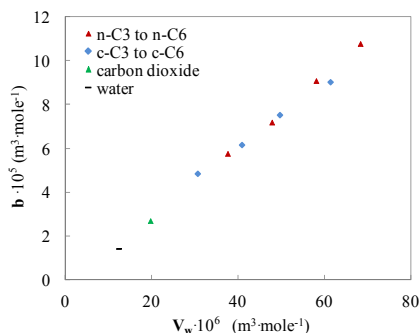
Only regressed CPA parameters are shown in Table A1.1. The performances of CPA with parameters calculated from critical data and acentric factors have been compared to the

above. Generally, both the calculated parameters (SRK) and the regressed parameters (CPA) provide accurate descriptions of vapour pressures for the pure cycloalkanes. The calculated parameters however result in an overestimation of the saturated liquid volumes, similar to that shown for cyclopentane in section 4.1.

It is seen that for both cyclobutane and cyclopentane, CPA has troubles describing the saturated liquid volumes. CPA generally underestimates the volumes at low temperatures, and overestimates at high temperatures. The cyclopropane and cyclohexane liquid volume data are described with AAD's similar to those found in the normal-alkane systems.

A trend is seen when comparing CPA parameters of normal- and cycloalkanes with equal carbon numbers. The  $a_0$  parameter increases its value by approximately 10% (9-12%) when going from cycloalkane to normal-alkane. Similarly, the  $b$  parameter increases by 20% (17-21%). A less clear trend is seen in the  $c_1$  parameters. These increase by approximately 10% when going from cycloalkane to normal-alkane in the n-pentane/cyclopentane and n-hexane/cyclohexane systems. For n-butane/cyclobutane the increase is only 4% and finally for propane/cyclopropane, the regressed  $c_1$  parameters are almost identical.

As a final validation of the regressed CPA parameters, the correlated  $b$  parameters are displayed against van der Waals volumes of the four compounds cyclopropane to cyclohexane. Van der Waals volumes are taken from the DIPPR database. Kontogeorgis et al. [52] showed that CPA  $b$ -parameters displayed against van der Waals volumes fall into a straight line for components of various types (n-alkanes, alcohols, acids, glycols, amines and water).



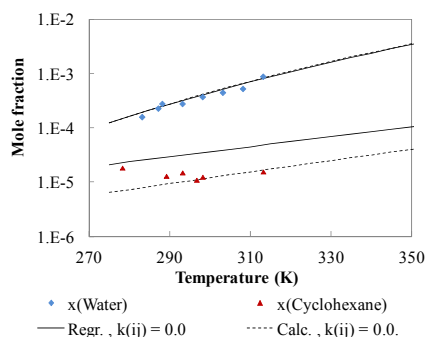
**Figure A1.1.** Correlated CPA  $b$  parameters against van der Waals volumes ( $V_w$ ) for cyclopropane (c-C3) to cyclohexane (c-C6), propane (n-C3) to n-hexane (n-C6), carbon dioxide and water.

Figure A1.1 shows a clear coherency in the obtained  $b$ -parameters for the four cycloalkanes (c-C3 to c-C6). The four compounds all fall reasonably into the straight line behaviour found in the normal-alkanes as well as carbon dioxide and water. Hence, there is no reason to question the obtained  $b$  parameters, which are known to have a significant influence on density descriptions by CPA.

## Appendix A2

To investigate how the two presented CPA parameters for cyclopentane affect descriptions of binary systems, the binary system with water has been investigated.

The system of water and cyclohexane is first modelled as a reference system, since this system is known and successfully modelled previously using CPA [33]. Predicted LLE results for the water + cyclohexane system are shown in Figure A2.1. Water is modelled using a classical association scheme with two electron donating and two electron accepting sites. Pure component parameters for water are taken from [21]. Pure component parameters for cyclohexane are those regressed in this work. For comparison, the predicted LLE using calculated parameters (from  $T_c$ ,  $P_c$  and  $\omega$ ) for cyclohexane are included in Figure A2.1. Experimental data are those recommended by Maczynski et al. [53], who performed a critical evaluation of LLE data available in the literature among others for water hydrocarbon systems.



**Figure A2.1.** LLE. Predicted solubilities of oil in water,  $x(\text{cyclohexane})$ , and water in oil,  $x(\text{water})$ , for the binary system of water and cyclohexane. Comparison of modelling results and experimental data [53]. Solid lines: CPA prediction with regressed parameters for cyclohexane. Dashed lines: CPA prediction with parameters for cyclohexane calculated from  $T_c$ ,  $P_c$  and  $\omega$ .

An interesting observation is that the calculated parameters for cyclohexane predict this binary system well. Whereas the two parameter sets predict the cyclohexane-rich phase similarly, the water-rich phase is more accurately predicted when using the calculated pure component parameters for CPA. A binary interaction parameter (BIP) has been regressed to improve the description of the experimental data illustrated in Figure A2.1. Only a BIP for the system with fitted CPA parameters for cyclohexane has been regressed. The results are shown in Figure A2.2.

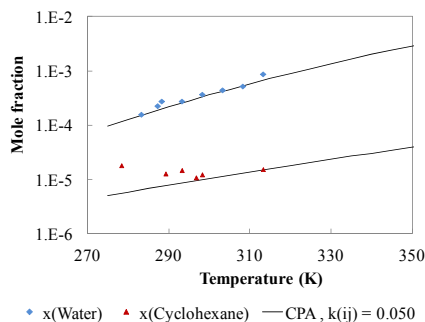


**Figure A2.2.** LLE. Oil in water,  $x(\text{cyclohexane})$ , and water in oil,  $x(\text{water})$ , for the binary system of water and cyclohexane. Comparison of modelling results and experimental data [53]. Solid lines: CPA description with regressed parameters for cyclohexane and a binary interaction coefficient of  $k_{ij} = 0.050$ .

Applying a BIP of 0.050 enables an accurate description of both LLE phases for this system. However, the model still fails at describing the low-temperature minimum solubility of cyclohexane in water occurring at approximately 296 K - 298 K.

The predicted LLE in the binary system of cyclopentane and water is different from that of cyclohexane and water in the way that both the calculated and the regressed CPA parameters underpredict the water in oil content and overpredict the oil in water content. In the cyclohexane/water system, both these contents are overpredicted.

Hence, it is suspected that the water in oil reference data reported by Englin et al. [28] could be erroneous for the cyclopentane water system. Whereas the oil in water data for the system of cyclopentane and water are among the data recommended by Maczynski et al. [53], the water in oil data used in this work are not among the recommended data. In order to investigate if the water in oil data could be faulty, LLE data for the cyclohexane-water system are compared with similar LLE data for the n-hexane-water system in Figure A2.3.

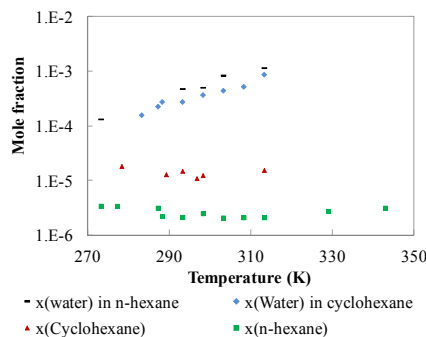


**Figure A2.3.** Comparison of LLE data for the binary systems; cyclohexane/water and n-hexane/water. Experimental data from [53]. Red triangles: cyclohexane mole fraction in water-rich phase. Green squares: n-hexane mole fraction in water-rich phase.

It is seen that a liquid water phase can dissolve more cyclohexane than n-hexane at similar temperatures. A cyclohexane liquid phase, on the other hand, can dissolve less water than a liquid n-hexane phase. Figure A2.4 illustrates the same type of LLE data for the binary systems; n-pentane/water and cyclopentane/water.

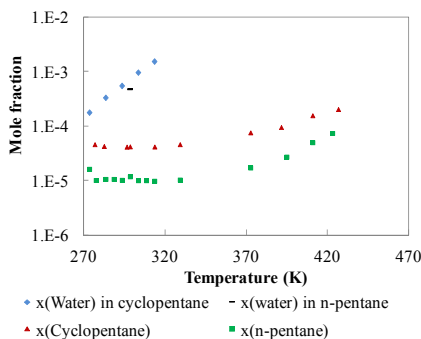


**Figure A2.4.** Comparison of LLE data for the binary systems; cyclopentane/water and n-pentane/water. Experimental data from [53]. Red triangles: cyclopentane mole fraction in water-rich phase. Green squares: n-pentane mole fraction in water-rich phase.

In the binary water-pentane systems, the aqueous liquid phase can dissolve more cycloalkane than normal alkane (like the water-hexane systems), however an interesting behaviour is found in the liquid oil phases. These data show that the normal alkane liquid



phase dissolves less water than the cycloalkane liquid phase, this being the opposite behaviour of that seen in the systems of water + normal- or cyclohexane.

Since much data is available for the binary systems of n-hexane/water and cyclohexane/water, and at all temperatures, the data show higher water contents in the normal alkane liquid phase than in the cycloalkane liquid phase, it is expected that these data are consistent.

Due to the fact that only a few data on the water content in oil phases exist for the pentane systems, it is likely that one or even both of these data sets are erroneous. The single data point for the water content in the n-pentane liquid phase is however among the recommended data of Maczynski et al. [53], whereas the data series for water content in cyclopentane is not (despite being considered by Maczynski et al.).

With the trends of the hexane systems in mind, one would have expected the water content in n-pentane to be higher than that in cyclopentane. However the few available data for these systems show the opposite.

It cannot be excluded that the experimental data for the binary system c-C5/water are erroneous. This would be a plausible explanation for the failure of CPA to describe both LLE phases in the binary system of water and cyclopentane.



Center for Energy Resources Engineering  
Department of Chemical and  
Biochemical Engineering  
Technical University of Denmark  
Søltofts Plads, Building 229  
DK-2800 Kgs. Lyngby  
Denmark

Phone: +45 4525 2800  
Fax: +45 4525 4588  
Web: [www.cere.dtu.dk](http://www.cere.dtu.dk)

ISBN : 978-87-93054-54-7